NUI MAYNOOTH

Ollscoil na hÉireann Má Nuad

Non-Radiative Calibration of Active Antenna Arrays

Justine Mc Cormack
61743252

A thesis presented in fulfillment
of the requirements for the degree of
DOCTOR OF PHILOSOPHY
in
Departement of Electronic Engineering
National University of Ireland, Maynooth,
Maynooth,
Co. Kildare,
Ireland.

Supervisor
Dr. Ronan J. Farrell
Head of Department
Dr. Sean Mcloone

26th February 2010

Abstract

Antenna arrays offer significant benefits for modern wireless communication systems but they remain difficult and expensive to produce. One of the impediments of utilising them is to maintain knowledge of the precise amplitude and phase relationships between the elements of the array, which are sensitive to errors particularly when each element of the array is connected to its own transceiver. These errors arise from multiple sources such as manufacturing errors, mutual coupling between the elements, thermal effects, component aging and element location errors. The calibration problem of antenna arrays is primarily the identification of the amplitude and phase mismatch, and then using this information for correction.

This thesis will present a novel measurement-based calibration approach, which uses a fixed structure allowing each element of the array to be measured. The measurement structure is based around multiple sensors, which are interleaved with the elements of the array to provide a scalable structure that provides multiple measurement paths to almost all of the elements of the array. This structure is utilised by comparison based calibration algorithms, so that each element of the array can be calibrated while mitigating the impact of the additional measurement hardware on the calibration accuracy. The calibration was proven in the investigation of the experimental test-bed, which represented a typical telecommunications basestation. Calibration accuracies of ±0.5dB and 5^{o} were achieved for all but one amplitude outlier of 0.55dB. The performance is only limited by the quality of the coupler design. This calibration approach has also been demonstrated for wideband signal calibration.

Table of Contents

Table of Figures

Table of Tables

List of Papers

- T. Cooper, J. M. Cormack, R. Farrell, and G. Baldwin, "Towards Scalable Automated Tower Top Phased Array Calibration," in *IEEE 65th Vehicular Technology Conference VTC-2007* Dublin, Ireland, 2007, pp. 1-5.
- J. McCormack, T. Cooper, and R. Farrell, "A Multi-Path Algorithmic Approach to Phased Array Calibration," in *Antennas and Propagation, 2007. EuCAP 2007. The Second European Conference on*, 2007, pp. 1-6.
- J. McCormack, T. Cooper, and R. Farrell, "Tower-Top Antenna Array Calibration Scheme for Next Generation Networks," *EURASIP Journal on Wireless Communications and Networking,* vol. 2007, pp. 1-13, Jan 1 2007.
- L. Barrandon, J. McCormack, T. S. Cooper, and R. Farrell, "On the Accuracy and Hardware Requirements of Cordic-Based Phased Array Calibration," in *Antennas and Propagation, 2007. EuCAP 2007. The Second European Conference on*, 2007, pp. 1-5.
- J. McCormack, L. Lengier, J. Dooley, and R. Farrell, "The Effectiveness of Non-Radiative Calibration Approaches of a Tower Top Distributed Transceiver System " in *URSI Colloquium on Wireless Communications* Dublin, 2008.
- J. McCormack, G. Corley, and R. Farrell, "Experimental results of non-radiative calibration of a tower top adaptive array," in *Antennas and Propagation, 2009. EuCAP 2009. 3rd European Conference on*, 2009, pp. 3389-3393.
- G. P. Corley, J. M. McCormack, and R. J. Farrell, "Demonstrator Platform for Antenna Array Calibration " in *China - Ireland International Conference on Information and Communications Technologies (CIICT)* Maynooth, 2009.

"Time is an illusion, lunchtime doublely so"

Douglas Adams

Acknowledgements

To Grandmummy

for never asking 'if', always saying 'when'.

This has been an interesting journey, and I have learned a lot about myself and others. I would like to take this opertunity to thank everyone who has helped me in so many ways.

I would like to thank my supervisor Dr. Ronan Farrell for his unflagging belief in me, his support and motivations. I would like to thank everyone in Institute of Microelectronics and Wireless Communications for everything. It has been an amazing experience working with you all.

I would like to thank my family for putting up with me through all of this. I would like to thank Tom McCallion, especially, for all his tireless efforts to improve my english. I would like to thank my mum for everything, pushing when I needed it and a shoulder when I didn't. My dad for always being interested. My two sisters, Louise and Niamh, for their faith and all the tea.

There are so many people to thank, and you all know who you are. I would just like to thank, Linda and John for making it fun.

Chapter 1

Introduction

Antennas when combined in groups or arrays can offer many advantages such as the ability to create directional radiation patterns. They do this by directing the gain in a particular direction and reducing it in others. This offers advantages over single antenna implementations. The individual antenna elements work together to create a directional radiation pattern, such as the one shown in figure 1-1. This figure shows the cross section of directional radiation pattern of an ideal 4 by 4 array of omnidirectional antennas and consists of a main and aft lobe; these are the large lobes pointing to 0^o and 180^o in this polar plot. They are termed the main and aft lobes because they contain the most radiation power in any single lobe. The radiation pattern also contains four sidelobes, which are the four smaller lobes. These are created by the nulls in the radiation pattern in particular pointing directions. This means that the whole coverage provided by the antenna array is not one continuous sector but it is separated into sections with varying radiation power. This provides the ability to spatially filter the radio environment. By using its low and high gain regions spatial filtering can be done by utilising the electronic steering of the radiation pattern.

Antenna arrays are an improvement over a single antenna element as they provide capacity increases because they are capable of spatially filtering the radio environment, therefore determining the location of the users in the radio link. This improvement in the use of the radio link provides the optimization needed for the ever increasing demands put upon such applications as mobile telephony. On the other hand, the implementations of antenna arrays have been to date exceedingly impractical. For antenna arrays to operate at their full potential an active array is used, where each element needs to know its amplitude and phase relationships.

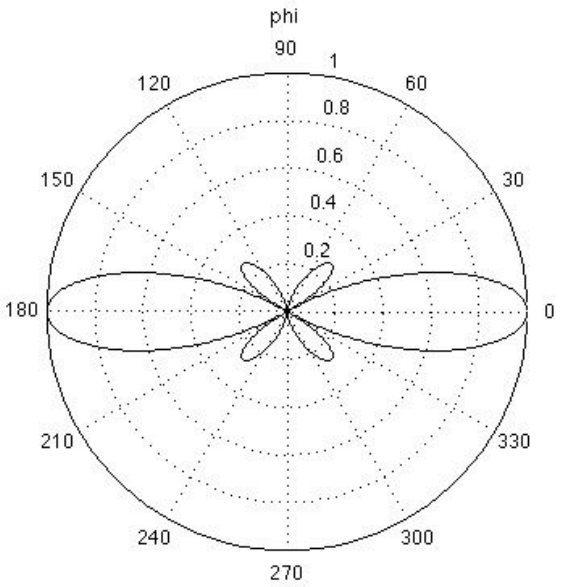

figure 1-1: Cross Section of the Ideal Radiation Pattern of a 4 by 4 Planar Antenna Array.

This ensures that when changes in these amplitude and phase relationships are applied then the radiation pattern points in the desired direction and with the correct shape. Therefore, significant alterations in these relationships will degrade the radiation pattern in its pointing direction, main lobe shape and width, and also the sidelobe sizes and locations. These changes in the radiation pattern mean that the advantages that antenna arrays offer are reduced or removed entirely in such a way as to worsen their performance when compared to that of a single antenna element. This has made their implementation impractical and has led to the calibration problem, which is the problem of calibrating the antenna arrays so that they offer the potential performance optimization.

figure 1-2: Alcatel Lucent 9116WBS Antenna Array, which contains four fixed 12 element linear arrays that are controlled seperately to create a 4 element active array.

Antenna arrays are currently being deployed in WiMax systems in Ireland. The first such operational system was in National University of Maynooth in 2007, using Alcatel Lucent's 9116 WBS which has an operating frequency of 2.3 – 2.5 GHz. This system is shown in figure 1-2 and 1-3 and uses four linear arrays together to create a four element controllable linear array for Mulitiple Input Multiple Output transmission and beamforming capabilities, which will be discussed in more detail in later chapters. This is done by having four linear arrays of 12 elements that have a fixed radiation pattern. Each of these fixed arrays have a single controllable input and are consider to be a single controllable element of a four element linear array. Currently there is another such system in operation in Dublin City University and they are being rolled out by Imagine Communication Group for telephony and mobile broadband applications.

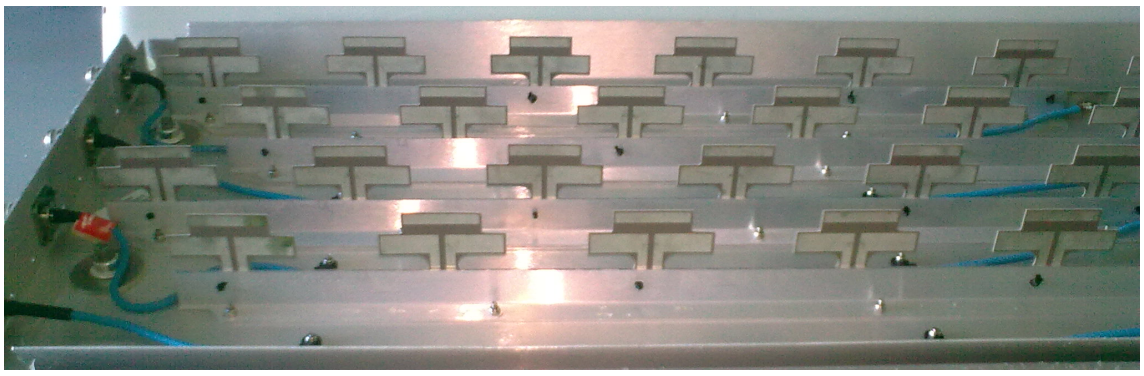

figure 1-3: Close Up of Antenna Elements of Alcatel Lucent 9116WBS Antenna Array.

1.1 Research Area

Antenna arrays are a solution to the capacity problem in mobile wireless communication systems. There is a need to overcome their implementation issues. The problem that arrises due to the need to calibrate antenna arrays is an impediment to their use in practical systems. This thesis proposes to present a calibration approach that will match the amplitude and phase relationships within the array. This is a complex problem due to the large quantity of error sources that affect antenna arrays, this is intended to be overcome with a calibration approach that will provide dynamic calibration for ever changing radio environments. This approach will be implementable in a practical system.

1.2 The Outline of this Dissertation

This thesis will continue in Chapter 2 with a discussion of antenna arrays, the ways in which they are implemented, the functionality each of these implementations offer and the different types of array structures that are used. This is followed by a discussion of the possible error sources that affect them. Then the calibration problem is presented, followed by an analysis of the possible solutions to it, in Chapter 3.

Chapter 4 presents the proposed calibration approach taken by this dissertation in detail, highlighting the advantages and proposed methods of overcoming scalability and accuracy issues. The algorithms that were developed for this calibration techniques are then discussed. Their advantages and limitations are discussed in terms of their predicted performance in Chapter 5.

The accuracy of the algorithmic simulations is tested in Chapter 6. This is done on two test-beds, which are 2 by 4 and 4 by 4 array sizes. The effectiveness of the calibration is presented here for narrowband and wideband operations. This dissertation finishes with a brief summary and conclusions, followed by the mention of possible future work in Chapter 7.

Chapter 2

Antenna Arrays and Their Properties

2.1 Introduction

After the brief discussion presented in the previous chapter of antennas, it has been mentioned that the optimization of the radio link that antenna arrays offer to cellular systems is significant when it is considered in terms of market demand. As was briefly mentioned in the previous chapter, there are implementation issues associated with antenna arrays. Before the calibration approach that is proposed by this thesis is shown in more detail, this chapter will present the properties and issues associated with antenna arrays to put this work in context. It does this by first looking at the origins of antenna arrays. This history is followed by a more detailed description of various antenna types and their application groups. These application groups dictate the performance and complexity of the antenna array. This is important, as it will be the deciding factor in the performance and challenges of their implementation. Achieving these requirements will be determined by the structure of the array. Each of these contributing factors to the performance and effectiveness of antenna arrays will be covered in this chapter. Finally, some of the capabilities of antenna arrays will be discussed in more detail in order to display the significance of antenna arrays in a clearer light and portray their importance.

2.2 A Brief History of Adaptive Antenna Arrays

Antenna arrays are not a new concept; their origins can be traced back through the research into magnetism, light and electricity. These three areas of research and their interdependency have led to the development of wireless communication and the understanding of the challenges of optimising the radio environment. A brief history of antenna arrays will be presented here, firstly to show their development through the years and secondly to show that though they have a rich history, there are still

significant challenges that need to be overcome to make sure that their potential can be fully realised.

Antenna arrays have their origins in the area of antennas and wireless communication research. It makes sense to mention a few of milestones of that research such as the advances in understanding of electromagnetics achieved by Maxwell, and in the research and the subsequent manipulation of his equations by Hertz and Heaviside. The greater understanding of the mechanism for wireless communication led to the first systems, such as those by Loomis and Marconi [1]. Though these systems do not resemble the current wireless communication systems, they did pave the way for them. This is not a comprehensive history of the origins of wireless communication, simply a starting point for the discussion of the origins of antenna arrays. They are considered to have originated in the time between 1923 and 1926, based on the research published at the time by Friis [2], which presents the use of an antenna array in short wave radio, and mention of them by Marconi [3], when discussing the properties of directional antennas. Another group of researchers were experimenting with antenna arrays around this time and showed their directional properties [4]. These works were significant in the area of antenna array research, but their true significance was not fully realised at the time. This is clearly seen from Friis *et al* who published a work much later in 1937 [5], which highlights the steering of the directional antenna arrays. Thus, some of the potential of antenna arrays were discovered with this discovery of directionality.

The understanding of the potential of a technology does not led to the ability to implement it. As was mentioned in the previous chapter, one of the advantages of antenna arrays is the steering ability. This ability is dependent upon the amplitude and phase relationships between the elements of the array. The steering of the radiation pattern is controlled by the phase relationships between the elements and requires a progressive shift across the array to create the steering of the array. These progressive phase shifts were however not available to provide matched phase shifts. The first scanning array called the Wullenweber array [1, 6], was not developed until the second world war by the Germans.

From the first scanning array, others were developed. These achieved the phase shifts in the radial signals using switched sets of transmission lines of various lengths to steer the array. This changed with the use of microwave phase shifters in the 1950s by Button

[7]. This made the implementation of antenna arrays significantly easier by providing a means of applying phase shifts for the steering of the array's radiation pattern. This does not solve the implementation and adaptability issues, which will more clearly be seen from the analysis of the approaches taken to the calibration problem in the next chapter.

The same year, 1950, Van Atta first coined the phrase *'Adaptive Arrays'* for a self-phasing array. This was an array that retransmits the signal it receives in the direction from which it receives it. This presents a method of implementing an adaptable antenna array, but it is limited to a relay action. This signified progress in the use of antenna arrays and the possibilities of optimization of the radio environment using antenna arrays. An adaptive receiving array was developed by Widrow [8, 9], which was also called an 'adaptive array'. With these advances in antenna arrays' adaptability, there were also advances in the technology that make up the antenna array, such as Barrett's development of Microwave Printed Circuits (MPC), which had the effect of making the implementation much more feasible. This was further enhanced by Barrett's realisation of the link between flattened coaxial cabling and that of low frequency printed circuit boards, between the years of 1949 and 1951 [1, 10].

These implementation advancements made the creation of antenna arrays smaller and drove research into the optimization of the radio environment using antenna arrays. This led to Howell's development of the analogue sidelobe canceller in the 1960s, and later to Applebaum's [11] development of the use of the signal to noise ratio (SNR) as a cost criterion for the optimisation of the radio environment in 1966. This was further developed by using the self optimising algorithm that had previously been used for filters, the least mean squares (LMS) algorithm in 1967 [9, 12].

The limitations of antenna arrays are more clearly seen when scalability is considered. The size of the array is limited by the implementation structures: as the number of elements in the array increases so does the complexity of implementing them. The matching of the amplitude and phase relationships gets more complicated as the number of elements rises. The implementation issue can be simplified by splitting the array into smaller arrays, but it does not eliminate the implementation issues completely. This investigation of the practical implementation issue was followed by research into other questions about practical implementations. Such were the Widrow *et al* [13] investigation into the trade off between the speed of adaptability and the quality of SNR

optimization in 1976 and Baker and Chow's investigation of the effect of sampling jitter on an adaptable array in 1978 [14]. These investigations highlight the severity of the implementation issues and the diverse sources of these errors.

Though the research into the implementation issues of antenna arrays became more prominent in the area, it did not constitute all of the research in the area into the optimization of the use of antenna arrays. In 1983, Gabriel [15, 16] presented a method of overcoming Lord Rayleigh's optical aperture resolution criteria in distinguishing two sources in close proximity, which have since been termed as superresolution methods. This was the forerunner of the subsequently widely used Direction of Arrival (DOA) approaches used in adaptive antenna systems to more fully utilise the radio environment [17-19].

Some of the implementation issues have been touched on in this discussion of the history of the investigation of the antenna array. The matching of the amplitude and phase relationships has not been addressed in any great detail in this discussion. It will be covered in much more detail in the next chapter. The points and capabilities of antenna arrays discussed. So far generally assume ideal arrays or at least idealised amplitude and phase matching for the array. This assumption is what makes these capabilities possible. Therefore when implemented upon a practical system, the capabilities that optimise the radio environment will not work as effectively or even at all in a practical implementation.

2.3 Antenna Arrays Implementations

There are two main types of array implementations that have many applications. These are passive and active arrays. The difference between the two implementations lies in the components that make up the array, the control over the elements and the capabilities.

Passive arrays use the same transceiver element to feed all of the elements of the array. This means that each element is fed with the same signals. The connections between the elements and the transceiver will dictate the kind of matching between them. The amplitude and phase relationships between the elements control the radiation pattern. If, for example in a broadside linear array, all of the elements are equally matched then the radiation pattern will be pointing normal to the array. When a progressive phase shift is

added to the element's relationship the radiation pattern will be steered proportional to the shift. By using a passive array, these relationships are fixed as the elements of the array are fed by passive structures. The advantage of such a structure is that the relationships are fixed and a simple implementation for antenna arrays.

The advantage of the passive arrays is also their greatest disadvantage. By having a simple fixed implementation all of the control over the radiation pattern is lost. With this loss of control, the ability to optimise the radio link is also lost. Therefore active arrays offer more advantages over passive ones. Active arrays consist of individual transceivers for each element of the array. This means that the amplitude and phase relationships of the array can be controlled giving the ability to adapt the radiation pattern to the scenario. By having individual transceiver elements, the matching of the antenna array becomes much more complex as each element has its own amplitude and phase errors due to the active components. The active components will also react differently to environmental conditions.

Each of the implementations has its own advantages and disadvantages. These led to the different levels of functionality in their use.

2.3.1 Functionality of Antenna Arrays

Variations of the implementations will be considered here based on their functionality in order to further understand antenna arrays, their implementations and their capabilities. The antenna array's intelligence in terms of the capabilities is based upon its choice of implementation. The distinction between the implementations is best considered in terms of their functionality. The levels of adaptability are grouped into three main types of functionality, which are:

- Switched Beam Arrays
- Direction Finding or Dynamically Phased Arrays
- Adaptive or Optimum Combining Arrays

2.3.1.1 Switched Beam Arrays

Switched Beam (SB) Arrays are an example of a passive implementation. It uses a set of fixed feeder paths that create a set of predefined beams in the radiation environment. The appropriate beam is selected generally based upon maximum SNR or signal

strength of the desired signal. Switched beam array implementation is the simplest kind. This passive array then uses different length cabling to create the different radiation patterns. By steering the radiation pattern using these predefined beam selection, the interference seen by the array can be limited in all but the pointing direction. The array can be slowly adjusted due to the angle of arrival (AOA) of the desired signal and can also use the same beam for transmit and receive [20-22]. Its advantages therefore include simplicity, the fact that it is computationally comparatively inexpensive and its ability to null interferers from all but the look direction of the array. There are however disadvantages to this approach including the inability to null out interferers close to the look direction, the inability to change the predefined pointing directions and the inability to adapt to a fast changing environment.

2.3.1.2 Direction finding or Dynamically Phased Arrays

Direction finding or dynamically phased arrays (DF) is an active array implementation. It estimates the direction of arrival (DOA) of the desired signal and steers the array accordingly. It is limited to line of sight (LOS) as it performs under the pretext that the AOA is that of the angle of incidence (AOI) of the signal. The difference between these two angles is that the angle of arrival is the angle at which the signal arrives at the antenna array, whereas the angle of incidence is the angle at which the signal would make with the array if it were to reach the array directly from the actual location of the signal source regardless of the obstacles between the two. By taking the AOA as the AOI, it means that the system assumes that the signal source is in the direction at which the signal arrives at the array. When it transmits to the source, it points in the direction at which the signal arrives at the array. Thus it can be considered to be a retrodirective implementation [21]. This kind of antenna array cannot be implemented using a passive array, as that would limit the control that the system would have over its radiation pattern manipulation. Hence the use of an active array or some combination of the two that is specifically designed for the system. By using an active array, this implementation has the ability to adapt the radiation pattern to the DOA of the desired signals. Its comparative computational expense, when compared to a switched beam implementation, is less than the adaptive array implementation, which will be discussed in the next section. This implementation does have disadvantages, which include its inability to null out interferers close to the look direction of the array, and the fact that

in a rich multipath environment its operation will be disrupted due to its assumption that AOA and AOI are the same.

2.3.1.3 Adaptive Arrays

Adaptive arrays (AA) are the final type of implementation considered and it is another active array one. It presents an antenna array whose radiation pattern is fully adaptable. It calculates the DOA of the desired signals and the interference sources. This information can be used to null out the interference sources. Adaptive arrays are capable of nulling out up to *M-1* interferers, where *M* is the number of elements in the array. In conjunction with the ability to selectively null out interferers, adaptive arrays have the ability to operate in non-line of sight (NLOS) and multipath environments, unlike the direction finding or switched beam antenna arrays implementations.

The adaptive arrays operation is too complex to be implemented using a passive antenna array, and therefore needs an active array. This adaptive array implementation is most suited to utilise the multiple input multiple output (MIMO) capabilities. This is due to the control over the radiation pattern that is offered by the individual transceiver connected to the antenna elements. Thus significant performance gains can be achieved in a rich multipath environment [22]. Another capability of this implementation is fading mitigation. This is possible by identifying and locating the interferers, as the multipath duplicates of a signal can act as interference depending upon the operation of a system.

The advantages of the adaptive array implementation include the ability to balance the nulling of interferers with the ability to receive the desired sources. They have the ability to implement full MIMO operation and therefore the ability to operate in a rich multipath environment. These advantages are balanced by disadvantages, which include the computational cost associated with these operations and the complexity of the implementation, *i.e.* the active array hardware and the required processing abilities.

2.3.2 Antenna Arrays Implementations Summary

Each of these implementations has its own advantages and disadvantages and thus the application is generally the deciding factor in the choice. However it is clear that the greatest advantage is to be gained from the use of the active array implementation and

also the greatest complexity as well. So the rest of this dissertation, active arrays will be considered, unless otherwise stated.

2.4 Antenna Array Structures

As the implementation type of the antenna array decides the intelligence, the structure of the antenna array dictates the radiation pattern. Though the weighting of the array can alter the radiation pattern generated by the array structure, it cannot completely overcome some of the fundamental properties of the array structure. For the purpose of simplicity and understanding, uniform antenna array structures will be considered here to clearly display the properties of each array structure created by the interdependence of the antenna elements. There are three main structures:

- Linear Arrays
- Planar Arrays
- Circular Arrays

Before discussing the array structures, the radiative principles of antenna arrays need to be considered as they affect all of the afore-mentioned array structures. Antenna arrays, regardless of structure, create directive patterns using the constructive and destructive interactions of antenna elements in close proximity. The contribution of each element is important as the radiation pattern and the interactions between the elements control the total radiation pattern. Thus the selection of antenna element will have considerable effect. For example the ratio of heat loss to radiative power needs to be low [23], or the scattering due to the proximity of the elements needs to be low [24]. The radiative pattern of an antenna array system can be mathematically predicted by calculating the power flow through each element and the summation in a sphere where the array is at the centre [23]. These interactions are dictated by, [25]:

1. The geometry of the array
2. The inter-element spacing
3. The amplitude of the input excitation
4. The phase of the input excitation
5. The relative patterns of the elements

For simplicity in the discussion of these structures, the radiative elements will be taken as omnidirectional point sources. This considerably reduces the complexity of the mathematics to aid with the comprehension of the structural relationships. The discussion of array structures will also start with linear arrays, as they are the simplest of all antenna array structures.

2.4.1 Linear Arrays

Consider a two element linear array where each of the elements is excited by the same amplitude E_o and phase θ, with ideal omnidirectional point source antenna elements and inter-element spacing of d [26], as shown in figure 2-1. By presenting a mathematical representation of an array in this form, with the idealised antenna elements with omnidirectional radiative fields, the array factor is calculated, as it will describe the structure of the array, and the effects of the different structural effects of that array on the radiation pattern for the simplest antenna model. Pattern multiplication is then used to create the complete radiation pattern, by multiplying the array factor by the isolated radiation pattern of an antenna element [27]. Thus various radiation patterns are generated from different structures and antenna elements. From this point on, the radiation pattern that is discussed will be the radiation pattern of an omnidirectional point source array. This is the simplest element radiation pattern. It is equivalent to the array factor, as the ideal omnidirectional point source's radiation pattern is equivalent to a sphere of equal power radiance, and thus equal to one in the pattern multiplication approach.

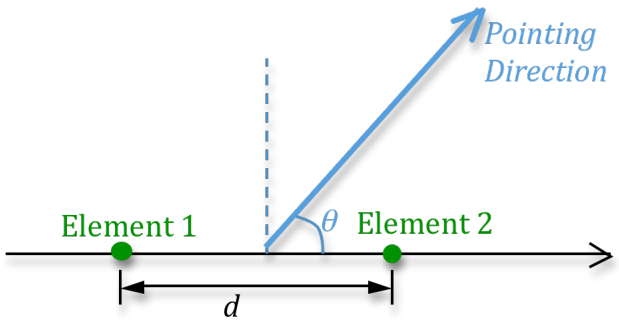

figure 2-1: A two element linear array with inter-element spacing of *d* and progressive phase shift to create a radiative pattern which will point in *θ* direction.

The array factor or group pattern is independent of antenna element types, and is dependent only on the array geometry, inter-element spacing and the phase difference of the elements of the array [25, 27]. The array factor of the afore-mentioned two element linear array with equally excited elements can be represented as

$$AF = E_o e^{-j\psi/2} + E_o e^{j\psi/2} \tag{2.1}$$

where $\psi = \frac{2\pi d}{\lambda}\cos\theta$

E_o is the electric field of each element of the array, assumes uniform elements,

d is the inter-element spacing,

λ is the wavelength,

θ is the pointing direction.

For the equally phased elements the pointing direction will be normal to the plane of the array, and from this it is easy to see that the pointing direction of the array can be altered by changing the phase relations between the elements, as previously mentioned in chapter 1. By adding progressive phase shifts between elements, the pointing of the direction of the array can be altered to any angle within the 180° azimuth of the array axis, as shown in figure 2-1 and figure 2-2. The progressive phase shift between elements that creates the steered radiation pattern can be calculated from the following equation (1.2), sourced from [8].

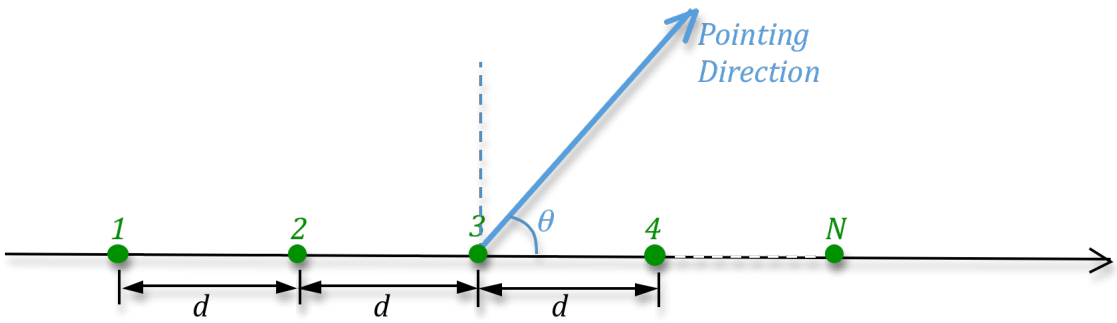

Figure 2-2: An N element linear array with inter-element spacing of *d* and a progressive phase shift that steers the radiation pattern in the *θ* direction.

$$\psi = \frac{2\pi d}{\lambda}\cos\theta + \delta \tag{2.2}$$

where δ is the progressive phase shift of each element.

The array factor of the radiation pattern with this progressive phase shift becomes

$$AF = E_o e^{-j\psi/2} + E_o e^{j\psi/2} \tag{2.3}$$

where $\psi = \frac{2\pi d}{\lambda}\cos\theta + \delta$

These equations can be extended to an N element linear array, where the first element is at the origin. As the array of elements are assumed to be omnidirectional antenna whose normalised radiation patterns are $E_o = 1$.

$$AF = 1 + e^{j\psi} + e^{j2\psi} + e^{j3\psi} + \quad \ldots \quad + e^{j(N-1)\psi} \tag{2.4}$$

This equation can be converted into a more useable format, by normalising it.

$$AF = \frac{1}{N}\left\{\frac{\sin\left(\frac{N\psi}{2}\right)}{\sin\left(\frac{\psi}{2}\right)}\right\} \tag{2.5}$$

where N is the total number of elements in the array, $N = n \times n$.

As has previously been mentioned, every antenna array creates a radiation pattern and these vary due to the array's geometry, the inputs and implementation errors. Therefore the easiest method of comparison of each array is to compare their radiation patterns.

This is done through a set of figures of merit upon which the radiation pattern is described and evaluated. These figures of merits are as follows, and are shown in figure 2-3.

1. Directivity
2. Main Beam's Pointing Direction
3. Main Beamwidth
4. Nulls - Location and Depth
5. Sidelobes – Location and Height

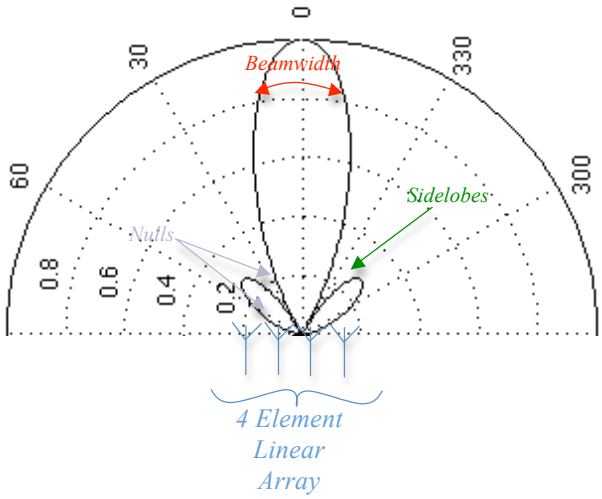

Figure 2-3: An ideal radiation pattern of a four element linear array, showing the normal pointing direction of the main beam, the beamwidth, the nulls and the sidelobes on either side of the main beam of the radiation pattern.

Directivity is a measure of the increased gain in a particular direction of that radiation pattern compared to that of a single omnidirectional antenna element's radiation pattern. As it is based on the radiation pattern, it is subject to the same contributing factors as the radiation pattern, and therefore will be different for each array structure. It can be theoretically predicted for a linear array by eqn. (2.6). The equation is courtesy of Balanis [25]. This text was a significant source of equations and expertise for the section.

$$D_o = 2N\left(\frac{d}{\lambda}\right) = 2\left(1+\frac{L}{d}\right)\frac{d}{\lambda} \tag{2.6}$$

where $L >> d$

L is the overall length of the array.

The main beam pointing direction, which is also know as the pointing direction of the array, is of course the direction in which the main beam is pointing, and therefore the direction of the maximum power in the radiation pattern. For an ideal linear array it can be estimated by:

$$\theta_m = \cos^{-1}\left(\pm\frac{m\lambda}{d}\right) \tag{2.7}$$

where m =0,1,2,... which are the number of maxima in the radiation pattern, i.e. the main and aft lobes.

The number of lobes, main and sidelobes, generated by an antenna array is proportional to the number of elements in the array, the array structure, the type of antennas used and the element spacing of the array.

The main beamwidth of the radiation pattern is the range of angles between the half power points either side of the main beam. They dictate the width of the main beam and therefore the coverage. This *3 dB* beamwidth depends primarily on the length of the array. The bandwidth and steer ability can be increased by the use of a non-equispaced array [28]. The beamwidth of a linear array can be estimated by:

$$\theta_h \approx 2\left(\frac{\pi}{2} - \cos^{-1}\left(\frac{1.391\lambda}{\pi N d}\right)\right) \tag{2.8}$$

where $\frac{\pi d}{\lambda} << 1$

The nulls of the radiation pattern are the zeros in the pattern, where the radiation pattern exerts no power. However this is just the theoretical idea of nulls: in practice the nulls are never quite zeros and a measure of their depths is essential to estimate their effectiveness. For an ideal linear array, their locations can be estimated by equation (2.9) and their depth is the amount of power in the radiation pattern in that direction.

$$\theta_n = \cos^{-1}\left(\pm \frac{n_{null}}{N}\frac{\lambda}{d}\right) \tag{2.9}$$

where $n_{null} = 1, 2, 3, \ldots,$ which is the nulls or minima of the radiation pattern.

The sidelobes of the radiation patterns, like each of its other features, are present in both transmit and receive operations of the array. However they are much easier to consider in terms of the gain of the radiation pattern. They can be considered as the other maxima of the radiation pattern. They are located in the area surrounding the main beam. The significance is that they point power in directions other then the desired pointing direction. Sidelobes are not always considered detrimental to the operation of the system, as they allow for the spatial filtering and frequency reuse that has previously been mentioned. However, since this is often not the case, most of the implementations want to completely eliminate sidelobes. Where this is not possible, then the sidelobe levels are made as low as possible [25, 29]. Sidelobe levels are primarily dependent upon the number of elements in the array and have less to do with the inter-element

spacing unless it exceeds 2λ [28]. The location of the sidelobes, again for an ideal linear array, can be estimated by equation (2.10) and the height of the sidelobes is the height of that radiation pattern in that location.

$$\theta_s \approx \cos^{-1}\left(\pm\frac{\lambda}{2d}\left(\frac{2s+1}{N}\right)\right) \tag{2.10}$$

where *s = 1, 2, 3, ...,* which are the sidelobes or minor lobe maxima of the radiation pattern.

From this analysis and prediction of their figures of merit, it is clear to see that the advantages of linear arrays are their simplicity and scalability. However these advantages are balanced by their disadvantages: the array is only able to steer in the azimuth plane; its performance is scan dependent; and the practical implementation issues. Scan dependence is where the radiation pattern features alter depending upon the steering angle of the array.

2.4.2 Planar Arrays

Planar arrays are the extension of linear arrays to create a two dimensional structure, by using linear arrays to create the rows and columns, this can be seen in Figure 2-4. The array factor of planar arrays is simply a sum of the linear arrays that create the rows and columns, and can be written as an *N x M* planar array.

$$AF = E_{nm}\sum_{n=1}^{N}\left[\sum_{m=1}^{M} e^{j(m-1)\left(kd_x \sin\theta\cos\phi+\delta_x\right)}\right]\cdot e^{j(n-1)\left(kd_y \sin\theta\sin\phi+\delta_y\right)} \tag{2.11}$$

where $k = \frac{2\pi}{\lambda}$

E_{nm} is the excitation coefficient of each element in the planar array

d_x is the inter-element spacing along each of the rows, parallel to the *x*-axis

d_y is the inter-element spacing along each of the columns, parallel to the *y*-axis

δ_x is the progressive phase shift along the rows of the planar array

δ_y is the progressive phase shift along the columns of the planar array.

This equation can be converted as before to a more usable format, by normalising it.

$$AF_N(\theta,\phi) = \left\{ \frac{1}{M} \frac{\sin\left(\frac{M\psi_x}{2}\right)}{\sin\left(\frac{\psi_x}{2}\right)} \right\} \left\{ \frac{1}{N} \frac{\sin\left(\frac{N\psi_y}{2}\right)}{\sin\left(\frac{\psi_y}{2}\right)} \right\} \tag{2.12}$$

where $\psi_x = kd_x \sin\theta\cos\phi + \delta_x$

$\psi_y = kd_y \sin\theta\sin\phi + \delta_y$

The same radiation pattern figure of merits applies to the radiation pattern of a planar array. The main difference between these parameters is the method of their theoretical estimation. There are two dimensions in which the pattern can be steered. As the planar arrays are an extension of the linear array, so they are the extension of their theoretical predictions of the figures of merits of the array. So starting with the directivity of a planar array which can be predicted for an ideal omnidirectional one by:

$$D_o = \frac{4\pi\left[AF(\theta_o,\phi_o)\right]\left[AF(\theta_o,\phi_o)^*\right]_{\max}}{\int_0^{2\pi}\int_0^{\pi}\left[AF(\theta,\phi)\right]\left[AF(\theta,\phi)\right]^* \sin\theta \quad d\theta \quad d\phi} \tag{2.13}$$

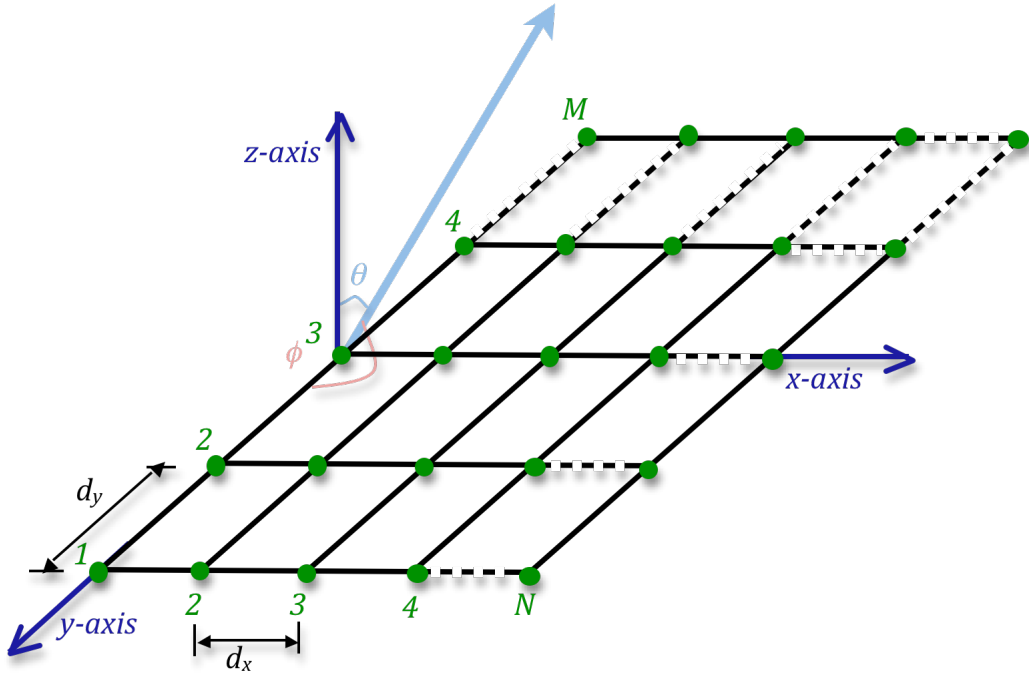

Figure 2-4: A planar array of N by M array, with inter-element spacing parallel to the *x* - axis is d_x and the inter-element spacing parallel to the *y*-axis is d_y a progressive phase shift in the rows of $\Delta\theta$ and the progressive phase shift of $\Delta\Phi$ in the columns to point the radiation pattern in the *(θ, Φ)* direction.

The next figure of merit is the main beam pointing direction, which can be predicted for the linear array by equation (2.7) for both the azimuth and elevation angles of the planar array. This use of linear array equations works for other planar array radiation pattern figures of merit. These are the nulls by equation (2.9) and the sidelobes from equation (2.10). The beamwidth of the planar array is an extension to the linear array equation (2.8) to create the following equation.

$$\theta_h = \sqrt{\frac{1}{\cos^2\theta_0\left[\Theta_{hx}^{-2}\cos\phi_0 + \Theta_{hy}^{-2}\sin^2\phi_0\right]}} \tag{2.14}$$

where Θ_{hx} is the half-power beamwidth of a broadside linear array along x – axis

Θ_{hy} is the half-power beamwidth of a broadside linear array along y – axis.

As the planar array is the extension of the linear array, it increases their complexity. Planar arrays do not have the linear array's advantages of simplicity. They are easy to scale as the elements can be added along either axis. This advantage is joined by the ability to scan the array in both the azimuth and elevation planes. These advantages are balanced by the scan dependent performance and the susceptibility of the array to practical implementation issues.

2.4.3 Circular Arrays

Circular arrays are different from the other two previously described array structures. The difference is that the array is based around a circle of antenna elements, with a radius of *a,* where each element is equidistant from the centre of the circle and each other, as shown in figure 2-5. The difference in this structure equates to very different radiation properties. This is more clearly seen from the array factor, and a discussion of the effects of the elements of the array. The array's radiation pattern predicted for an ideal array can be calculated by:

$$AF(\theta,\phi) = \sum_{n=1}^{N} E_n e^{j(ka\sin\theta\cos(\phi-\phi_m)+\delta_n)} \tag{2.15}$$

where $k = \dfrac{2\pi}{\lambda}$

δ_n is the phase excitation of the n^{th} element of the array

E_n is the amplitude excitation of the n^{th} element of the array.

Again the same radiation pattern figures of merit apply to the circular array, however due to the difference in the array structure the theoretical estimation is different. As before the directivity of a circular array is simply a comparison of the directivity of the circular array's radiation pattern compared to that of an omnidirectional antenna's one. For the other figure of merits they are estimated by the next series of equations.

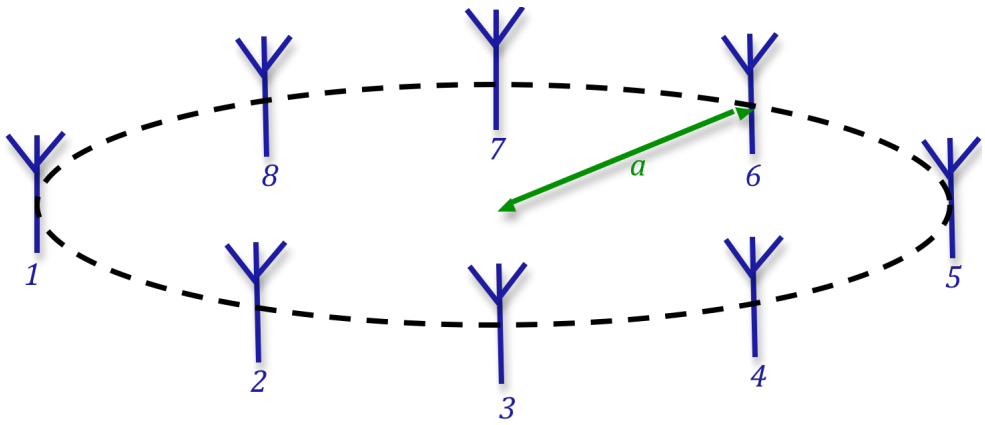

Figure 2-5: An eight element circular array of radius *a.*

Due to the symmetry of the circular array the maxima of the radiation pattern that they create can be predicted by the following equation. That is to say that the main beam's pointing direction and the sidelobe locations can be estimated by a single equation [30].

$$\phi_m = \frac{1}{M}(p\pi + \omega_o t) \tag{2.16}$$

where *2M* is the number of peaks in the radiation pattern,

ω_o is the desired angular frequency,

$p = 0, 1, 2, \ldots, 2M - 1$.

On the other hand, due to the symmetry of circular arrays, the nulls can be predicted by the following equation. as it estimates the minima of the radiation pattern [30].

$$\phi_n = \frac{1}{M}\left[\frac{(p+1)\pi}{2} + \omega_o t\right] \tag{2.17}$$

The advantages of circular arrays are different from these of linear and planar arrays as the structure of the array has different properties. Due to the symmetry of the array and their structure, its radiation pattern can be steered over 360^o [31]. As the radiation pattern of linear and planar arrays are scan dependent, the difference with circular arrays is that it is scan independent, *i.e.* the beamwidths, pointing direction and sidelobe levels shape and size are all unaffected by the steer angle of the array [32, 33]. The disadvantages are the lack of scalability of circular arrays and the effects of implementation issues. The scalability issue is more pronounced in circular arrays as the number of connections to a central point and the increase in the radius of the circle to accommodate the increased number of elements limits them.

2.5 Capabilities of Antenna Arrays

As previously discussed there are three main capabilities of antenna arrays, which are beamforming, DOA estimation and MIMO operation, though the capabilities are not limited to these. These capabilities are dependent upon the principles of antenna arrays and now that they have been presented, these can be considered. The explanations will be brief, as they are individually significant areas of research. These presentations are to give a flavour and appreciation of the possibilities of antenna arrays to more fully explain the importance of calibrating the array.

2.5.1 Beamforming

Beamforming is the capability to adapt the radiation pattern of the array to a particular scenario. It depends upon the weighting of the elements of the array. The beamforming depends upon the intelligence of the array, so for example for a dumb implementation of an antenna array, the switched beam implementation sets up fixed radiation patterns that are switched between. This is done using fixed feeder paths setup in matrices so that that can create multiple radiation patterns [34, 35]. These fixed feeder paths will be presented in more detail in the next chapter. However there are other forms of beamforming and they require higher intelligence implementation, such as direction finding and adaptive array. These more intelligent beamforming approaches are polynomial, algorithmic and evolutionary optimisations approaches. Each of these types of beamforming requires control of the weights of the array, and then they apply their particular methodology to the alteration of the radiation pattern to a specific scenario. This intelligence ranges from altering the radiation pattern so that the sidelobes close to the main beam are reduced and their power is redistributed to the sidelobes further away so that the signals close to the desired pointing directions are reduced further, such as in the Taylor beamformer [36-38], to the evolutionary optimization techniques which use optimization techniques to optimize the antenna weights for the particular scenario, such as the particle swarm algorithm or simulated annealing approach [39-50]. So for all of these beamforming approaches it is clear that the control and accuracy of the weights of the array are important. Therefore they are still susceptable to the implementation issues of antenna arrays.

2.5.2 Direction of Arrival

The direction of arrival capability uses the spatial filtering of the antenna array to calculate the DOA. Locating sources in the radio environment requires the ability to adaptively change the weights of the array and therefore the radiation pattern. This requires some intelligence in the antenna array implementation, so the antenna array needs to either be a direction finding or an adaptive array. DOA capability enables the array to know the steering direction of users and interferers. This provides the intelligence of the implementation. The calculation of this DOA for all the desired users is a challenge in a rich radio environment, with all of the other operators and users in an urban environment. This provides the need for adaptive nulling, which is where the

weights are adjusted with the look direction of the radiation pattern constant in order to null out jammers [51, 52].

As with beamformers, the DOA capabilities have many approaches with various levels of intelligence and approaches. There are two main DOA approaches, spectral estimation and parametric estimation techniques and the DOA performance varies based on the choice.

The spectral estimation techniques use the spectral environment to determine the local maxima, and these maxima are taken as the DOA of the signals for both the desired users and interferers [53]. These types of techniques vary significantly based on the approach, ranging from maximum likelihood method (MLM) [53] to eigenstructure based superresolution approaches such as multiple signal classification (MUSIC) [54] and estimation of signal parameters via rotational invariance techniques (ESPRIT) [18].

Parametric DOA methods are based on data models and multidimensional searches to find the DOA of the desired signals. These approaches are sometimes preferable to spectral DOA methods, particularly in the case of coherent signals. The intelligence of the parametric approaches will also dictate the performance of the DOA, as it will be based upon the method of data models, the assumptions associated with them and the multidimensional searches used. These searches are chosen based on the model detail and the intelligence of the system. This can be shown in the examples of deterministic maximum likelihood or the stochastic maximum likelihood search techniques [55].

2.5.3 Multiple Input Multiple Output

The MIMO capabilities of antenna arrays require the most intelligent implementations. Thus they require an active array implementation to turn the multipath environment into a benefit. It can increase the theoretical capacity of the system by the number of controllable channels [56, 57]. The MIMO techniques allow the DOA and the direction of departure (DOD) to be measured. This makes them comparable to the adaptive antenna array as these are the same difference as the AOI and AOA [58]. However the motivation for the use of MIMO capabilities is the increased capacity, increased diversity and interference suppression [59]. These capabilities are dependent upon the knowledge of the spatial-temporal characteristics of the propagation channel and are dependent upon the propagation parameter estimations by high resolution algorithms

such as space altering generalised expectations (SAGE) [58]. This is all possible because of the use of active antenna array that achieves very high spectral efficiency in high scattering environment. The electromagnetic environment is decorrelated to create many parallel subchannels, which is based on the degree of decorrelation and the number of antennas [60]. This combined with the orthogonal frequency division multiplexing (OFDM) system allows wideband transmission achieve a several-fold increase in data rates and spectral efficiencies [61]. Each of these requires a significant knowledge of the propagation channels created by the multipath environment and active antenna array. This information dictates the performance of the MIMO capabilities.

The propagation channel can be described by the channel state information (CSI). When the full CSI is known, eigenvector steering can be used to utilise the fill capacity potential of each MIMO channel. The throughput can be further maximised by the optimal power allocation by water filling techniques [62]. However when only partial CSI is available, a maximum likelihood is used at the transmitter to optimise the performance. This leads to a computationally expensive approach, with suboptimum performance due to the lack of information [62], whereas in the presence of interferers the capacity of the system is decreased due to the traditional additive Gaussian noise of the channels. Approaches have been developed to achieve the capacity of the system as if the system was without interference, such as an approach called Dirty Paper Coding Technique [59].

2.5.4 Other Capabilities

Though the above are the main capabilities of antenna arrays, these are not their only ones. Others include such capabilities as super directivity; array thinning and signal separation to name but a few.

Super directivity is a capability that is solely dependent on the number of elements in the array. It increases the directivity of the array by adding elements to the array, while not increasing its length. This is done by reducing the inter-element spacing [63]. The advantage of superdirectivity is to create a radiation pattern with more gain pointing in one direction, thus increasing the size of the main lobe and decreasing the size of the sidelobes.

Array thinning is the opposite of super directivity. It takes a large array and removes elements from the array to make non-uniform inter-element spacing. This can create radiation patterns with low sidelobes or desired directivity. However, this capability can require a considerable amount of design to achieve the desired radiation pattern [44, 64].

Finally, signal separation is a capability of antenna arrays that enable them to separate super imposed signals, though this requires knowledge of the signal sources, and requires the use of an estimation maximization (EM) algorithm that uses a ML search technique [51, 65, 66]. This is a useful capability, though it requires significant knowledge of the system to utilise it.

2.6 Summary

This chapter has presented antenna arrays in the context of their history from the origins in Maxwell's equations and their development in military applications, to their development to scanning arrays. This description shows the progress of their development, providing context for antenna arrays. This is followed by a discussion of antenna array implementations. Passive arrays are much simpler and easier to implement than active arrays. They offer fixed solutions to the matching of the amplitude and phase relationships of the array. The active arrays allow much greater control over the radiation pattern as they offer dynamic control over the amplitude and phase relationships of the array. The various implementations are discussed in terms of the capabilities. This description shows that passive arrays are the least intelligent or dumb approach as it uses a switched beam approach to adaptation, whereas active arrays provide much more intelligent implementations as they offer the greater performance capabilities, such as the ability to implement a MIMO system.

The next chapter will build on this understanding of antenna arrays and their capabilities to present the effects of manufacturing imperfections and non-ideal effects on antenna array performance. These effects are a significant impediment to achieving high performance antenna arrays and particularly active antenna arrays. Array calibration can be used to correct for these imperfections and thus is of critical interest. The next chapter will present the various approaches taken to this challenging task and discusses their capabilities and drawbacks.

Chapter 3

Errors, The Calibration Problem and Possible Solutions

3.1 Introduction

Different aspects dictate antenna array performance. The array's dependence upon its implementation and structure were covered in the previous chapter. This chapter will extend to consider the effect of error sources. This creates a calibration problem for the array, which needs to be solved. This chapter follows this by comparing the solutions previously taken to this problem.

3.2 Sources of Errors

The counterpoint to the advantages of antenna arrays is their difficulty of implementation and the resulting deviations from the ideal system. These imperfections severely degrade the performance of the array as they directly affect the radiation pattern. These imperfections stem from many sources, and are significantly worse in active antenna arrays as active arrays are more complex and have more sources of possible errors. The sources of these errors are diffuse, and arise from hardware, software and environmental effects - as shown in Table 3-1 [67-81]:

Table 3-1: The Sources of Errors for Antenna Arrays

Structural effects	Path lengths
	Mutual coupling
	Element Failures
	Element position errors
Environmental effects	Temperature
	Humidity
	Wind effects
Component effects	Finite manufacturing tolerances
	Component Aging
	Quantisation
	Finite linear operating region
Channel effects	Interference
	Target position
	Spectral overlap
	Atmospheric effects

Each of these sources of error will affect different aspects of the arrays: some will affect the amplitude and phase relationships and others the communication channel. The distinction is important as the antenna array can deal with communication channel errors, such as ones highlighted in the channel effects section of the table. This is particularly true when the array is being used within a MIMO application. For the remainder of this dissertation the sources of errors that focus on are the ones that have an effect on the radiation pattern and arise from mismatches in the amplitude and phase relationships between elements of the array.

Before considering the individual error mechanisms, the impact of mismatch amplitude and phase errors will be presented in terms of the impact on the radiation pattern of an ideal array. This will be illustrated by taking a single example of a series of simulated radiation patterns for an omnidirectional 4 by 4 planar array for differing degrees of mismatch error. A Gaussian distribution of errors were created based on a stated standard deviation , where the errors are ideal plus the individual elements errors and the maximum, minimum and mean errors of each array are also presented in table 3-2. The next set of figures, figure 3-1, show a series of cross sections of these radiation patterns, ranging from an ideal array in figure 3-1(a) to the radiation pattern of an array with a standard deviation of errors in the amplitude and phase relationships of ± 5dB and ± 20^o, figure 3-1(e). These radiation patterns show the degradation of the performance as the size of the errors increases. This is more clearly seen from the range of errors in the figures of merit of the radiation pattern presented in table 3-2. This table shows that for small errors, ± 0.5dB and ± 3^o, the radiation pattern is affected, as shown in figure 3-1(b). The sidelobe are no longer symmetrical. The beam pointing is off by ± 0.36^o. The beam widths have been altered. The nulls are no longer as deep as they are suppose to be. The location of the nulls and sidelobes are altered. As these amplitude

Table 3-2: The Ranges of Errors in the Radiation Pattern Figures of Merit for the Increasing Standard Deviation Errors in the Amplitude and Phase Relationships.

Error Ranges	±0.5dB and ±3°	±1dB and ±5°	±1.5dB and ±7°	±5dB and ± 20°
Max Element Errors	1.2dB and 10.3°	1.3dB and 10.7°	2.3dB and 20.4°	17.9dB and 60.7°
Mean Element Errors	0.6dB and 2.4°	0.5dB and 5.4°	0.9dB and 6.8°	4.8dB and 24.3°
Min Element Errors	0.04dB and 0.14°	0.07dB and 0.23°	0.12dB and 0.44°	0.62dB and 1.3°
Beampoint	±0.36°	±0.72°	±0.72°	±44.64°
Beamwidth	2.16°	1.08°	1.08°	9.72°
Null Depth	0.353 -> 0.0741	0.0157 -> 0.0945	0.01812 -> 0.21413	0.05129 -> 0.596
Null Location	4.68° -> -9.72°	4.68°-> -9.72°	3.24° -> -9.72°	120.36° -> -180°
Sidelobe Height	0.0279 -> 0.1218	0.0428 -> 0.09079	0.0247 ->-0.0263	0.3278 -> 0.6778
Sidelobe Location	±3.96°	±2.16°	±6.12°	±77.52°

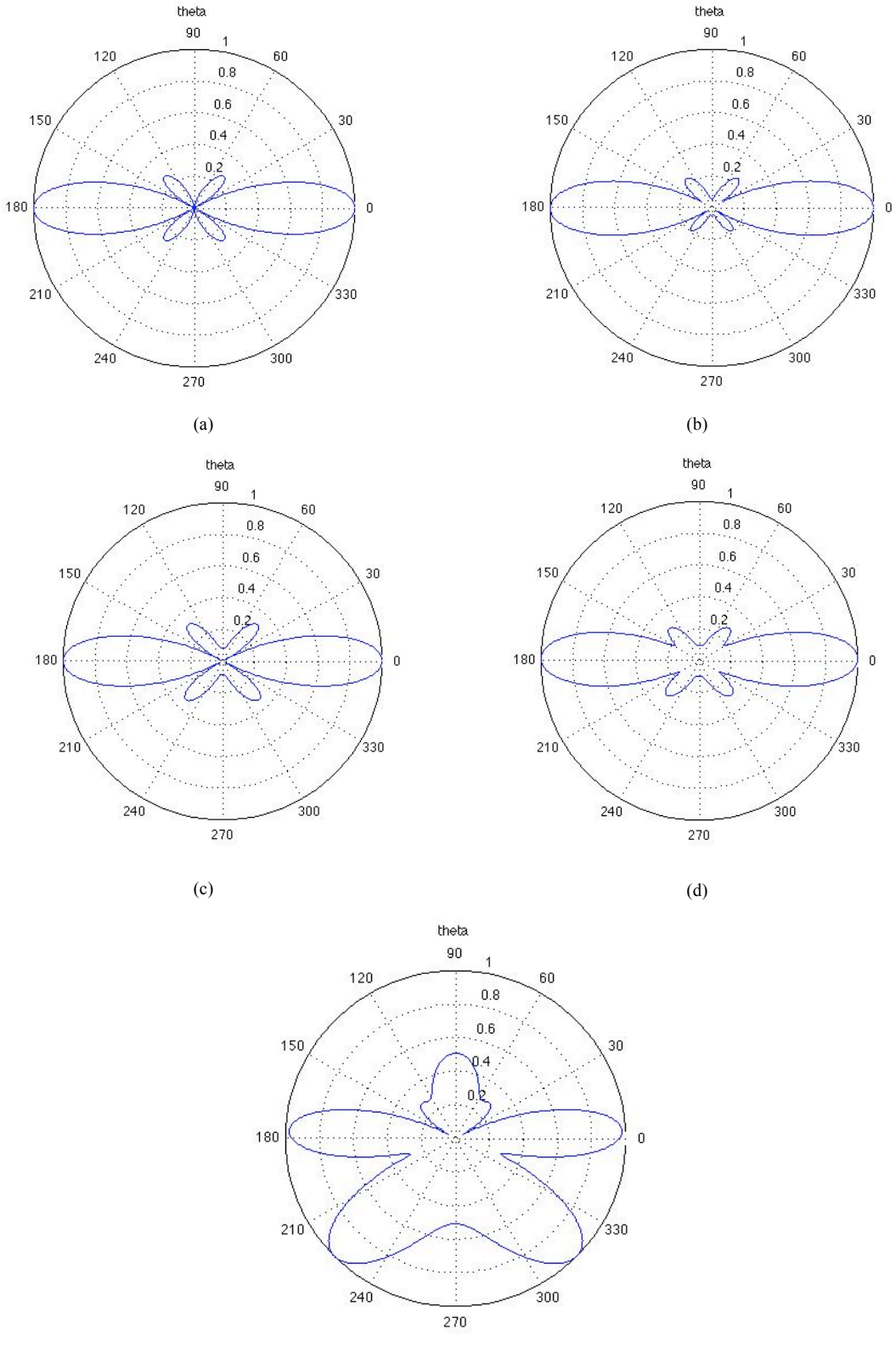

figure 3-1: Cross section of the radiation pattern produced by a 4 by 4 planar array with various imbalances in the amplitude and phase relationships, (a) ideal array, (b) an array with amplitude imbalances with a standard deviation of ± 0.5dB and phase of ± 3^{o}, (c) an array with amplitude imbalances with a standard deviation of ± 1dB and phase of ± 5^{o}, (d) an array with amplitude imbalances with a standard deviation of ± 1.5dB and phase of ± 7^{o}, and (e) an array with amplitude imbalances with a standard deviation of ± 5dB and phase of ± 20^{0}

and phase imbalances increase so do the effects upon the figures of merit. Some error ranges remain the same and some marginally improve for these single incidences of each case. However there is an overall decline in the radiation patterns as the amplitude and phase imbalances increase, through ± 1dB and 5^o as shown in figure 3-1(c) and ± 1.5dB and 7^o as shown in figure 3-1(d). This is culminated in the final cross section figure, figure 3-1(e), which shows a nearly unrecognisable radiation pattern with large errors in all of the figures of merit in the radiation pattern.

It is clear from the comparison of the radiation patterns figures of merits, that as the amplitude and phase relationship imbalances increase so does the distortion of the radiation pattern. This is however a comparison of single examples of these scenarios and show the effect of the imbalances. These effects upon the radiation pattern led to the consideration of the effect on the performance. The issue was considered in the EU ACTS program and the Technology in Smart Antennas for Universal Advance Mobile Infrastructure (TSUMAMI I and II) projects, where a variety of calibration approaches were explored. The TSUNAMI projects investigated the impact varying degrees of radiation pattern distortion would have on the system's performance. It highlighted that a change in the maximum null depth from *-60dB* to *-30dB* would result in approximately a *40%* reduction in the capacity. While with beam pointing errors that range between $\pm 3^o$, there is a corresponding *12%* reduction in capacity. When this error was increased to $\pm 6^o$ range, the percentage capacity reduction would increase to *28%* [82-84]. These figures are however another example to give a clearer impact of the amplitude and phase errors and an idea of their consequences. They are highlighted here as an indicator as opposed to an in depth analysis for each application. The sensitivity will be dictated by the application. So for example, a switched beam application as discussed in the previous chapter will be significantly less sensitive to errors than for a full MIMO application also discussed in the previous chapter.

These amplitude and phase relationship imbalances affect the radiation pattern and consequently the capacity and capabilities of the array. Therefore the effects need to be reduced or known in order to remove the detrimental effects. The calibration problem of the array is how the errors and imbalances can be removed. The implementation issues can be grouped into smaller groups of calibration issues, which are:

- Errors in Amplitude and Phase Relationships

- Position Errors
- Grating Lobes
- Mutual Coupling
- Array Blindness
- Printed Antenna Materials Effects

3.2.1 Errors in Amplitude and Phase Relationships

Errors in the amplitude and phase relationships of the array are one of the most detrimental implementation issues. The sources of amplitude and phase errors are various:

- Feeder Path Length Variations
- Manufacturing Tolerances
- Component Aging
- Thermal Effects
- Quantisation Errors
- Scattering
- Mutual Coupling

These error sources may appear diffuse. However, the problem is that they are cumulative and in some cases such as quantization errors, also interdependent, further complicating their impact on array behaviour. These errors will effect the system in both time and frequency [85]. From the description of the calibration problem, the degradation of the radiation problem starts with relatively small amplitude and phase errors. As the errors increase, so do the alterations of the radiation pattern. As these sources of these errors are cumulative, they can mount up rapidly.

Feeder path length variations are primarily a construction problem and can be perceived to have an easy solution. However this leads to a precision machined solution. This is an adequate solution for a passive array implementation. It is much less attractive for a MIMO approach. The significance of the feeder path variations comes from the construction of large arrays and the frequency. All arrays need to have feeder paths that are the same for each element. As the array size increases the feeder paths become more complex to achieve this goal. This can led to longer cables then necessary due to the structure of the array. As the elements further away will have longer cables then those

closer. To maintain the same length criteria, the nearer elements have the same length cables as the ones further away. Therefore they need to be looped or complexly routed to achieve this. This requires an added level of design. The matching of this cabling will also suffer from the manufacturing tolerance, thermal effects and element matching error sources due to the cumulative effects of the system. As the frequency increases, the wavelength of the signal decreases, which has the effect of shortening the length of cable that will result in a given phase error, which demands that the cable length be a fractions of millimetre accurate.

The manufacturing tolerances effect on the implementation of antenna arrays, it will impact the feeder path lengths. This is due to the nature of this error source. It comes from the realisation that no two manufactured components have identical properties. This leads to variations between any two components, due to the manufacturing process, the materials or even the precision of the assembly. Their significance comes from the cumulative effect. Consider a MIMO implementation, where each element has its own independent transceiver connected by its individual feeder cable connected to each element. Each transceiver is made up of components. Each component will have its own finite manufacturing tolerance. The combined error will be the some function of each component in the transceiver, and each will have its own manufacturing tolerance. Each feeder path and the antenna element will also have its own manufacturing tolerance. Therefore each baseband to radiation power path will have its own manufacturing tolerance. As the system increases in complexity, so does the contribution of the manufacturing tolerance effect on it. These manufacturing tolerance error sources do not only have a self-cumulative effect. They also experience a cumulative effect from the feeder path length variations, as previously mentioned, and also from component aging, thermal effects and element matching that will have contributing effects on the manufacturing tolerance errors.

Component aging can be considered as a sub-source of errors or a contributing source when considering manufacturing tolerances. It will have the same characterisation as the manufacturing tolerances, namely that they will be different for each component of the array. They will also be self-cumulative like the manufacturing tolerance errors. The difference is that the error is due to the degradation of a component due to the aging and

workload of that part. Component aging can thus be exacerbated by such error sources as thermal effects.

The effect of temperature can be as significant as each component will have a reaction to temperature changes. These can be severe depending upon the application and location. The principle motivational application outlined in the first chapter is a mobile telephony basestation, which have been used in all sorts of climates. Temperature ranges can be high or low and change significantly from day to night These sorts of extremes need to be considered when considering temperature effects on the amplitude and phase relationships between the elements of the arrays. The other consideration is complexity and implementation, as the more complex the setup the more sensitive it is to temperature differences. Again consider the active array implementation with the individual transceiver elements. Each of these transceiver elements will have a power amplifier (PA) and each of these PAs will dissipate heat. Depending upon the structure, the location and cooling of the array could cause temperature variations between sections of the array. As previously stated, temperature variations have significant impact on other error sources.

Quantization is another source of errors. It will affect systems that utilise a digital infrastructure. It will have a significant impact upon the antenna array, as it will affect several aspects of the system. For an antenna array that is fed by a digital baseband signal, there will be a quantization error associated with the input signal. This error will feed into the transceiver elements and feeder paths. Each of these components will affect this signal with their own individual errors due to the other error sources. For an antenna array that has a feedback structure that is provided digitally, this adds more quantization errors as the feedback signal will be affected by quantization. The feedback structure will create a loop. Where the input signal is affected by a quantization error, this signal is then fed into the transceiver element and feeder path. These each add errors to the signal. This signal is sent back through a feedback path. This will also add it own errors. This feedback signal is then quantized to convert it into the digital domain. Thus it is affected by the quantization error on the input and output of the system. The quantization is effected by all of the cumulative errors along each of the paths, i.e. the through path and the feedback one.

3.2.2 Position Errors

Position errors can come from manufacturing tolerances in the antenna array or an application such as sonar where the structure of the array is altered by external forces such as being towed in water. However the result is the same; the inter-element spacing of the array is changed. Though so far only uniform arrays have been considered, that does not mean the non-uniform arrays do not have benefits, as by altering the inter-element spacing of an array the radiation pattern can be altered. Non-uniform arrays need to be carefully designed to achieve the desired performance. However when a non-uniform array is created from position errors, the radiation pattern alterations are not always advantageous. They are generally considered to have detrimental effects on the directivity, main lobe, sidelobes and nulls of the array. This alteration of the radiation pattern will therefore have an impact on the capabilities of the array and the amplitude and phase relationships required for the array's operation.

3.2.3 Grating Lobes

Grating lobes are additional lobes as large as the main lobe in an undesired direction. They are created by large element spacing or subarray spacing. Grating lobes can be theoretically predicted for linear array using the following equation.

$$\sin\theta_p - \sin(\theta_o) + \frac{\rho\lambda}{d_x} \tag{3.1}$$

where $\rho = \pm 1, \quad 2, \quad ...$

d_x is the element spacing,

ρ is the grating lobe number,

λ is the wavelength of the array and

θ_ρ is the angle of the grating lobe.

As the generation of grating lobes is solely dependent upon the inter-element spacing of the array, it can be overcome by having smaller inter-element spacing [86]. Therefore it is helpful to determine the maximum spacing allowed before grating lobes become an issue of concern. This maximum spacing is defined as the spacing where the grating lobe is on the horizon of the radiation pattern, for the desired frequency of operation. This maximum spacing can be defined for linear array in the following equation [25, 87].

$$\frac{d_x}{\lambda_o} \leq \frac{1}{1+\sin\theta_o} \tag{3.2}$$

3.2.4 Mutual Coupling

Due to the close proximity of the radiative elements in the antenna array, there are electromagnetic interactions between the elements. This alters the radiative properties of the array. These interactions are called mutual coupling and are generally limited to an element's nearest neighbour and second nearest neighbour [86, 88-96], as shown in figure 3-2. This coupled energy alters the radiation pattern generated by the antenna array in transmit operation, by altering the individual antenna element patterns in such a way that it degrades the radiation pattern [85, 86, 92, 94, 97-132]. As the mutual coupling alters the radiation pattern, this will have an impact on the efficiency of the antenna array [104, 133-135] and a corresponding impact on the capacity [116, 122, 124, 136-138]. These distortions in the element patterns can also be attributed to the alteration in the resonant frequency and resonant impedance of the elements of the array [139].

Due to the dependence on the proximity of radiative elements, it can be shown that mutual coupling is inversely proportional to the inter-element spacing. Mutual coupling is not solely based upon this, it has other contributing factors such as the antenna type, antenna matching, array geometry, the surrounding environment, polarization and scan angle. While on the other hand, it is insensitive to other implementation parameters such as height from the ground plane [86, 88, 92, 99, 112, 113, 124, 127, 130, 136, 140-147].

Mutual coupling is a severe problem in antenna arrays and has a considerable number of contributing factors. Its contributing factors include the proximity problem. The elements of the antenna arrays interact, creating the directional patterns, but backward interactions between the elements degrade this performance. The inter-element spacing of an array is therefore significant as it dictates the quantity of mutual coupling. As the spacing is increased, the mutual coupling will decrease. There is a certain point beyond

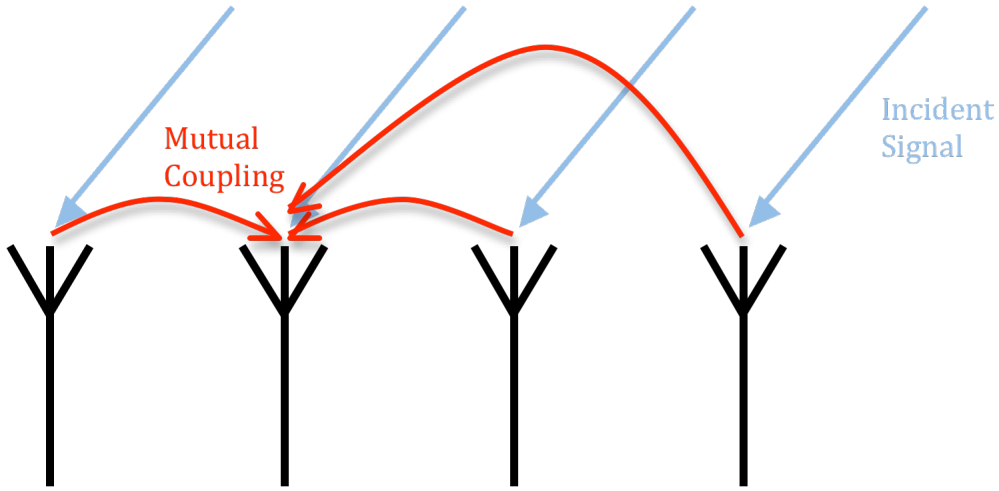

figure 3-2: Mutual Coupling Interactions.

which mutual coupling can be discounted completely. This point is when the inter-element spacing is 1.2 λ or above [148]. There is however a corresponding lower bound to mutual coupling, which is where mutual coupling cannot be eliminated without a compensation approach. This lower bound is generally taken to be 0.5 λ [149], though this does not mean that mutual coupling is not present. This dependence on inter-element spacing for the generation or elimination of mutual coupling is more severe in planar arrays as the central elements of the array are surrounded on all sides [92].

The next determining condition for mutual coupling is the distortion of the impedance and therefore the gain of each element of the array, which is determined by the source fed to an array element. The realisable gain of an antenna element is determined from its directionality and the return loss incurred due to the impedance matching [149]. Considering the general interaction between the elements, low gain antennas have their gain increased by their mutual coupling interactions, whereas high gain ones iare decreased by it. The significance of this is that the elements' radiation patterns are no longer proportional to their input sources [150]. This can in some cases remove the advantages of antenna arrays altogether [127, 149].

The gain and impedance are further altered by mutual coupling at different scan angles. There are differing opinions on the extent of this variation. The gain variation due to scan angle can be put down to the gain variation in the radiation pattern at different angles. The impedance varies due to the impedance matching, which is identical at broadside but becomes mismatched off broadside scan angles. Impedance variation has an impact on gain variations and hence the discord [99, 100, 112, 113, 151, 152].

Another aspect, is that mutual coupling interactions are reduced by increasing the inter-element spacing, whose maximum spacing is dictated by the generation of grating lobes. This has the effect of decreasing the achievable scan range and thus the performance of the array [99, 113, 149, 152-157].

Thus far considering the contributing factors of mutual coupling and their impact, it is easy to say that it has a significant effect on the arrays performance. The next contributing factor that needs to be considered is the array size. Contrary to intuition, as the size of the array increases the impact of mutual coupling decreases. This is because the elements at the centre see the same or similar electromagnetic environment. The reason for this similarity is the symmetry of the elements at the centre of the array. Therefore the patterns generated by the elements at the centre of the array are all the same or extremely similar, and can be called the embedded element pattern of the array [86, 89, 149]. The elements at the edge of the array are however not encompassed by this embedded element pattern, as they do not see the symmetry of the centre elements. So each element sees a different electromagnetic environment. This implies that the impact of mutual coupling is significantly more detrimental in a small array then in a large array due to the relative number of edge elements compared to the total number of elements [91, 92, 95, 116, 118, 121, 158-161]. So when a large array is combined with large inter-element spacing, i.e. between $\lambda/2$ and λ, mutual coupling is sometimes omitted due to the relatively small number of edge elements and the overall effect of the mutual coupling being uniform [162, 163]. It is however important to consider that the reasoning behind using large arrays is to achieve low sidelobes and or high gain. These two characteristics of an antennas radiation pattern are very sensitive to errors and mutual coupling is another error source. Therefore for most cases, mutual coupling cannot be discounted, even in large arrays [120].

The mutual coupling effects considered so far are backward mutual coupling where the effects are concentrated in the array [93, 116, 140]. Another mutual coupling effect is the forward coupling or platform effects. This is where the interactions between the elements cause a scattering effect caused by antenna elements, antenna mounting and nearby structures. This effect can be removed or mitigated by the choice of antenna elements and array mounting such as in conical minimum scattering antennas [85, 93, 116, 122, 135, 140, 164-168]. This separation of mutual coupling effects can also be

considered by their location, such as the area in which the array radiates as the scattering or forward mutual coupling region and the area which contains the elements and the feed network as the backward mutual coupling region [169].

After considering the effect of scattering and its mitigation by a choice of antenna, another characteristic should be considered and that is polarization. As mutual coupling alters the polarisation between elements when the array is uniformly polarised. This non-uniform polarisation increases the mutual coupling distortion on the array. So it creates a self-perpetuating problem. On the other hand, mutual coupling can be reduced between elements that are orthogonally polarized [112, 133].

As mutual coupling affects the radiation pattern of the array, it has effects on the capabilities of the array. It will of course have a detrimental effect on most of the capabilities, particularly beamforming. However in the case of MIMO there has been research done that mutual coupling will increase the capacity of a MIMO system because of its effect on the correlation of the communication channels. However there are inter-element space criteria for this enhancement due to mutual coupling [124, 138, 170, 171]. Although mutual coupling is a significant source of errors when considering antenna arrays, in some cases its presence may be used to enhance the system.

3.2.5 Array Blindness

Array blindness is actually a mutual coupling affect, but is considered separately as it is present in printed antenna arrays and has different effects and preventative measures. Array blindness is where a zero or null is created in the radiation pattern in a certain direction or angle. Though this is a mutual coupling effect, it has been tied to surface waves or leaky waves, which is where the surface waves are bound into the dielectric slab so that no real power enters or leaves the array structure, and the energy is stored in the surface waves [102, 133, 172-178]. This surface wave will resonate so as to cancel out the radiative energy of the array in a particular direction [179]. This effect is generally associated with printed antenna arrays as all of the elements are connected via the dielectric slab and ground plane used in such structures. This provides a medium for the surface waves to propagate [180]. This can be considered as a non-radiative or inductive coupling between printed antenna with inter-element spacing of less the λ [139]. As it is a dielectric of the printed array effect, the substrate parameters such as

length, width, separation, substrate thickness, dielectric constant and permittivity are factors that affect the array blindness angle. These are much more significant factors in the creating of a blind spot compared to the particular antenna types [181-183]. The array blindness can be linked to the impedance of each element and therefore the angle of blindness can be predicted by the reflection coefficient: it is unity or close to it at the blind spot [184]. The mutual coupling that causes the blind spot created in the array, effects the resonant frequency and the resonant input impedance of the patch antenna [139].

3.2.6 Printed Antenna Materials Effects

This is the final structural source of errors to be considered, as it is clear from the potential sources of errors, that careful design of the array is essential and an understanding of all of the possible error sources and the cumulative effects. Besides the contribution that permittivity and substrate thickness have in creating array blindness, they also have an effect upon the radiation pattern of the array. The permittivity of the substrate has the effect of reducing the efficiency of the antenna elements as it increases. Both permittivity and substrate thickness have a distorting effect upon the radiation pattern, as they effect the number of lobes and the null positions of the array [183]. Though it should be noted that by reducing the permittivity of the dielectric and increasing the substrate height the radiative power will be increased [185].

3.2.7 Summary of Sources of Errors

The sources of errors are diffuse. They have significant impact upon the operation of antenna arrays. This is because they alter the radiation pattern. The sources of error are so significantly varied that there is no single intuitive approach to solve them. The errors come from feeder path length variations, manufacturing tolerances, component aging, thermal effects, quantisation errors, element matching, scattering, mutual coupling, position errors, array blindness, grating lobes and printed antenna errors. Some of these errors can be removed using design techniques. Others require a single compensation, while dynamic error sources require constant monitoring and compensation.

3.3 The Calibration Problem

The sources of errors that effect the antenna array were presented in the last section. These errors are what require a calibration solution. This is because each of the error sources affects the radiation pattern and therefore the performance and capabilities of the array. Small changes in the radiation pattern, such as beam pointing direction has a large impact upon the capacity of the array. The error sources range from amplitude and phase matching, mutual coupling, position errors, array blindness, grating lobes and printed circuit effects. These errors come from the many sources and some have contradictory solutions.

The calibration problem is the problem of calibrating an antenna array. The errors need to be removed or their effects neutralised but the calibration problem is how this can be done. The calibration problem presents a series of questions that need to be tackled. Does the problem need to be tackled by a measurement approach or by a model based approach? What are the advantages of these and what are their disadvantages? How does the implementation and functionality affect the approaches taken to the problem? How do the type of errors impact upon the calibration problem?

As has been mentioned there are design techniques that can remove some of the errors, though some of these may be contradictory. These design techniques are considered alternative solutions that need to be balanced. A calibration solutions uses some aspect or property of the antenna arrays to correct the performance of the array, whether it's a once off measurement approach or a continual external reference signal comparison.

3.4 Solutions to the Problem

It is clear that calibration is an important step in the realisation of adaptive array systems that achieve their full potential. As with the sources of calibration errors, the approaches taken to solving this problem have taken many forms. They can be divided into calibration solutions and alternative solutions. Calibration solutions range from measurement based approaches to where reference signals are used for tackling the calibration problem. Alternative solutions take a design route using structural approaches to minimise errors or calibration-at-manufacture. Finally, targeted calibration is where a specific calibration error source is taken and calibrated out. Though these calibration groupings seem to have distinct differences, there is

considerable overlap. The grouping is done simply to present the alternative approaches taken to calibration in a meaningful and structured manner.

3.4.1 Calibration Solutions

These approaches are designated as such because they offer an ability to measure or compare an aspect of the array. This means that they can tackle both static and dynamic sources of errors. The first such calibration solution is the measurement based approachs.

3.4.1.1 Measurement based Calibration Approaches

The measurement approach to calibration is a structural based approach to calibration, which relies on the creation of measurement paths. These measurement paths are implemented based upon a measurement point and feedback structure they provide. The method of utilising these structures will be dictated by the effectiveness of the calibration. There are many different methods of calibration that utilise measurement structure approaches. The next set of techniques is presented to show the range of approaches and their advantages and disadvantages.

3.4.1.1.1 Auto Calibration Measurement Approach

The auto-calibration measurement structure is designed specifically for circular arrays and CDMA signals. It utilises directional couplers to create feedback paths. It places two directional couplers, one for receive calibration and another for transmit, as shown in figure 3-3. The directional couplers are placed between the antenna and the duplex that connects transmit and receive circuitry. The feedback structure is provided by transmit and receive circuitry. This is utilised in two steps. The first of these is the receive calibration, where the transmitter is used, then the signal is converted to the receiver's carrier frequency and fed back to the receiver circuitry. By these means the receiver's errors are measured. Then the transmitter is used again to transmit and again converted to the receiver's carrier frequency after the receiver's errors are taken into account, and the signal is then converted back to the transmitters' carrier frequency. Thus the transmitter errors are measured [186, 187].

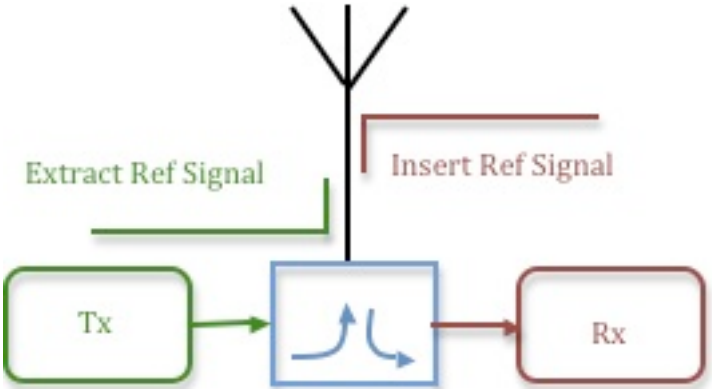

figure 3-3: Auto Calibration Measurement Approach.

This approach to calibration works for both transmit and receive operation of the array however, it does not consider the errors inherent in their measurement structure. As this is designed for a circular array, it makes it hard to scale. This approach could of course be adapted to any array structure but the infrastructure would be very complex. This is because the array structures that are easiest to scale, such as the linear array and planar arrays have closely packed elements. These elements need to be fed by paths of the same length. As more elements are added to the array, the more complex this matching becomes. This does not overcome the consideration of the measurement path errors.

3.4.1.1.2 Blind Calibration Measurement Approach

The blind calibration measurement structure is another measurement structure that can calibrate both transmit and receive paths and also take the measurement point directly behind that of the antenna. The difference in the two structures is that instead of each element at its measurement point using a directional coupler, the calibration is achieved simultaneously for all elements of the array in two steps, the receive calibration and transmit calibration. Both receive and transmit calibration use the calibration element, which consists of a combiner and a calibration receiver as shown in figure 3-4. Firstly to the receive calibration, the signal received at each of the antennas are fed to both the receiver elements of the array and to the calibration element. In the calibration element they are combined to create a reference signal. This reference signal is then compared to the output of the receiver elements at each element of the array. Then these weights are tuned by this comparison to achieve receive calibration. The transmit calibration is achieved by taking the outputs of the transmitter elements and feeding then into the calibration element where they are combined, this combined signal

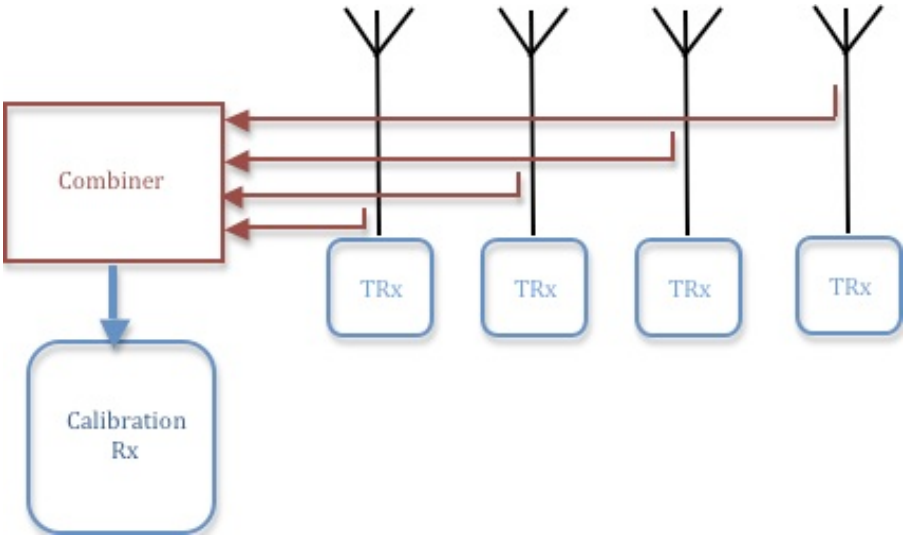

figure 3-4: Blind Calibration Measurement Approach.

is then compared to the desired output of the array with the measured one, to achieve transmit calibration [188].

This calibration structure cuts down on the hardware when compared to the auto-calibration measurement structure, by cutting down on the number of directional couplers connected to each element, thus reducing the effect of the measurement structure on the systems operation. The structure however does not consider the measurement errors contributed by the measurement structure and also does not consider scalability. The measurement element is considered to be ideal and will of course be subject to all of the same sources of errors as the rest of the elements of the array. The scalability of the array is limited by the number of connections that can be provided by the combiner in the calibration element and also by the assumption that the feeder paths between the directional coupler on each element are exactly the same length. This may require a fixed feeder path solution to keep them the same. However this approach has been extended to calculate the channel delays as its receive calibration is based upon external sources [189]. This is of particular significance in MIMO applications.

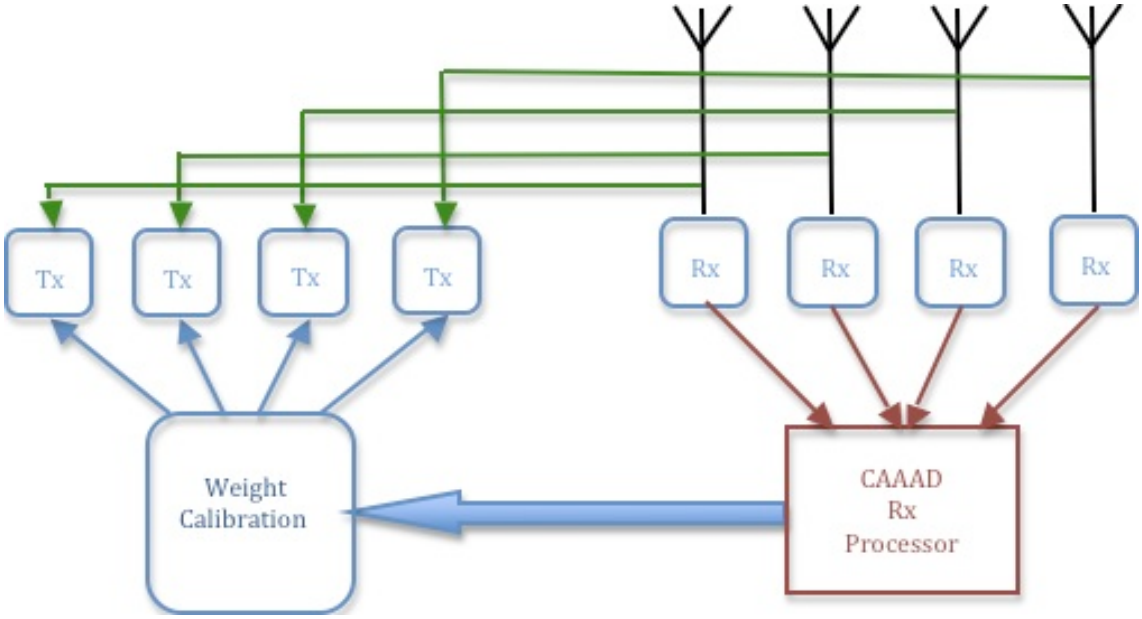

figure 3-5: Coherent Adaptive Antenna Array Diversity Measurement Approach.

3.4.1.1.3 Coherent Adaptive Antenna Array Diversity

The coherent adaptive antenna array diversity (CAAAD) system is a receive only calibration approach. It implements a measurement structure similar to that of the auto-calibration approach, that is to say that each element is measured individually. However it also has similarities with the blind calibration approach, as each of these individual measurements is controlled by a single adaptive weight controller, as shown in figure 3-5. This measurement structure is utilised for DOA estimation, by comparing the whole array's RAKE receiver outputs to calibrate the receiver. This however again does not consider the errors contributed by the measurement devices and the scalability of the array. It in fact highlights the differences of the two previous approaches as it adds individual measurement devices which have their own individual errors and these are controlled by a single adaptive weight controller and led to a single RAKE receiver which mean that path lengths need to be considered in the measurement structure [190].

3.4.1.1.4 Multiple Channel Calibration Measurement Structure

The measurement point is behind the antenna element, and is created by two directional couplers similar to the auto calibration measurement approach, as shown in figure 3-3. The significance of this measurement point is that the closer to the antenna element it can get, the more that is included in the calibration. As the further the antenna is away from the antenna, the more error sources that won't be measured and therefore will not be calibrated out. This approach uses two directional couplers. The calibration is done in two steps similar to the previous approaches. Connecting a RF probe at the receiver carrier frequency does the receiver calibration, and this is simultaneously injected into the receivers of the array via a power splitter. These signals are then measured by the receiver paths of the transceiver elements, thus the errors are measured in the baseband I and Q. The transmitter calibration is then simultaneously achieved by connecting all of the measurement points combined using a power combiner and measured via a calibration receiver element. This approach achieves both transmit and receive calibration, but it again suffers from the problem of not accounting for the receiver calibration element being a source of error or the RF probe being one. This does not account for the scalability issue of the connections of the receiver and transmitter calibration hardware, which will limit the number of possible array sizes and structures that can be achieved [191].

3.4.1.1.5 Vector Based Measurement Structure

In this section, two different vector based measurement structures are considered. They are both however capable of receive calibration only. The first structure uses a single receive calibration data signal that feeds to the element of the array via a power divider or switch setup and directional couplers. The two setups presented here use either a power divider or a switch to feed the receiver elements of the array. This leads to two types of calibration [192]. The significance of this choice lies in its ability to calibrate the array during operation or whether it requires a separate time slot. The systems so far have required a time slot for calibration as all the elements are calibrated simultaneously. This calibration approach is a vector based approach as for the array a vector response is taken in snapshots and these are used to calculate the calibration coefficients of the array in conjunction with the array correlations [192], as shown in figure 3-6.

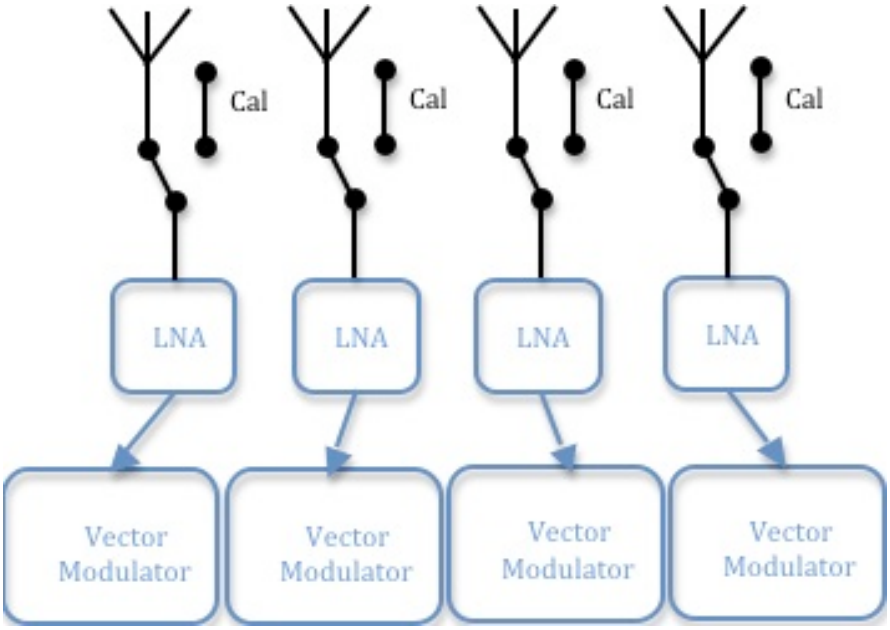

figure 3-6: Vector Based Measurement Approach.

The second vector based measurement structure uses a vector modulator that calibrates the array by calculating the control voltage versus amplitude and phases for each element of the array. This is done using a measurement structure that has a switch behind the antenna element, which switches between the element and a calibration signal point [193-195].

These approaches do not consider the contribution of the feed structure of the array and also the scalability. The second approach does not present an applicable structure for inserting calibration signals into the elements of the array whether they are separate sources or a single source, this will present a problem.

3.4.1.1.6 Automatic Calibration Method using a Transmitting Signal

All the measurement structures so far have been based on directional couplers. The automatic calibration method using a transmitting signal (ACTS) is a measurement structure that uses switches. Instead of a duplexer that generally connects the transmitter and receiver circuitry to the antenna, a switch is used. This creates a connection between the transmitter of a reference element to the receiver circuitry of the other elements as shown in figure 3-7. The receiver circuitry of the reference element can be connected to the transmitter circuitry of the other elements of the array. This provides a measurement structure using the internal circuitry of the array [196-198].

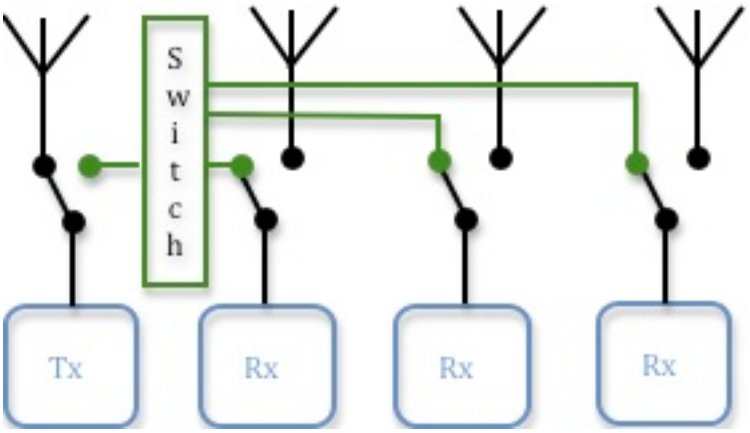

figure 3-7: ACTS Recieve Calibration Measurement Approach.

This structure requires a feed structure for the connections between the elements of the array. This calibration approach does not take this into account in the calibration structure as a source of error and scalability problem.

3.4.1.1.7 Technology in Smart Antennas for Universal Advance Mobile Infrastructure

The technology in smart antennas for universal advance mobile infrastructure (TSUNAMI) is a smart antenna system that can perform ray-tracing operations. Its development was split into two projects. TSUNAMI (I) was developed to investigate the space-division multiple access (SDMA) technique for a wireless communication system, in order to exploit the capacity enhancement, coverage extension, the ability to support higher data rates and to support hierarchical cell structure [199]. TSUNAMI (II) was an extension of this investigation to the application to future generations of mobile communication systems. This project aims to utilise the advantages of antenna arrays for mobile communications, such as the enhanced capacity to support user traffic, to provide low hardware costs, to provide flexibility to offer the variety of services required - all this while providing a good quality of service (QoS).

It has a measurement structure which connects a central calibration control unit via directional couplers and multiplexer, as shown in figure 3-8. The structure is used for both transmit and receiver calibration. Receive calibration is achieved by using a vacant timeslot to insert a carrier wave (CW) tone injection, as a reference signal. The correction factors of the array can be calculated by taking samples of the base band signal and RF signals, to achieve calibration [82, 200-208].

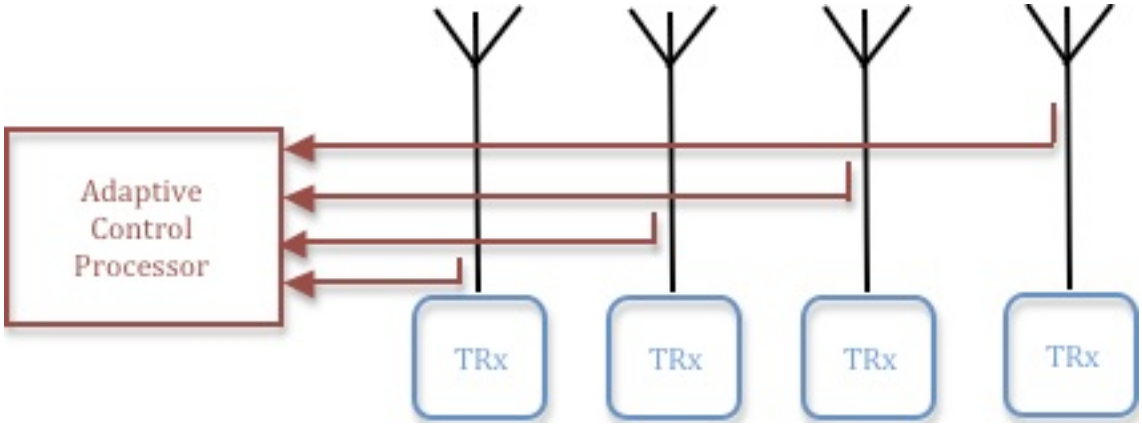

figure 3-8: TSUNAMI (II) Measurement Approach.

This approach does not account for the measurement device or reference signal as a source of errors. It also does not consider the impact of scalability on the central calibration unit.

3.4.1.2 Reference Signal Based Calibration

The use of reference sources has been previously mentioned in this dissertation. They were used to calibrate out position errors in antenna arrays. However this is not the only area of calibration that reference signals can be used in; they are used in significant areas of research into the calibration problem. Their use can generally be considered in two main categories, the use of internal array elements as the reference sources and the use of external ones. These groups are not rigid and there are combinations of the two groups.

3.4.1.2.1 Internal Elements as Reference Sources for Calibration

The use of internal elements of the array as calibration elements is a complete calibration approach, as it includes the antenna elements in the calibration. The calibration elements in the array are considered to be passive elements of the array, as they are not connected to a transceiver element. They are interspersed throughout the array. The elements of the array are grouped based on their nearest calibration element. The calibration elements are relatively few, approximately 1% of the total number of elements [209]. This type of calibration was designed for large arrays, such as 10,000 elements. There are several different approaches taken to utilising these internal

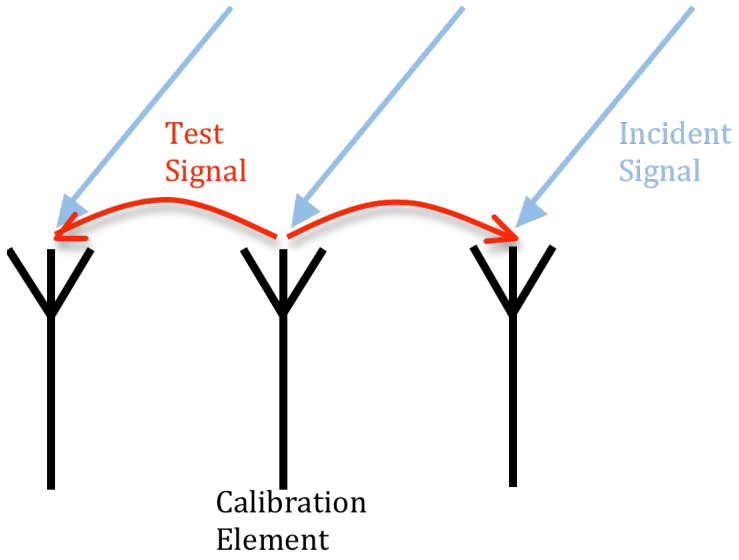

figure 3-9: Simultaneous Transmit and Receive Calibration of Phase Toggling Calibration.

calibration elements such as the Square Kilometre Array (SKA), which uses a multi-element phase toggling (MEP) method. The multi-element phase toggling approach to calibration requires the array to be able to simultaneously transmit and receive within the array, which is to say that the calibration element transmits a signal that is received by the elements to the calibration and vice versa. This is shown in **figure 3-9**.

The calibration is split into two sections, off line calibration and online calibration. The off line calibration consists of calculation of the difference between the transmitted test signal and the output of each element of the array to the test signal and the incident plane wave as shown in **figure 3-9**. The second section of calibration is the online calibration, and for this implementation it consists of calculating the amplitude and phase variations due to the test signal. This calibration is achieved by using the phase toggling approach. The phase toggling approach uses a training pulse with a selected pulse repetition frequency (PRF) to enable the elements to be calibrated from the reference source, as the elements of the SKA implementation are not separate transceiver elements and are fed by a coupled transmitter line [210]. Due to the communal feed, there is a need to isolate the element under test, and toggling the pulse-to-pulse signal by 180^{o} does this. This technique is extended to calibrate multiple elements simultaneous by exploiting the Fourier properties of the beamformer. This is that each element has a different phase setting so that the calibrated elements can be separated in the frequency domain, based on the phase properties of the time delay unit (TDU) of the implementation. The advantages of this technique are that the interference

signals are all collected in the bin 0 of the Fast Fourier spectrum and that the average amplitude and phase estimated can be calculated using the properties of the TDUs of the array. The phase shifters of the array can then be calibrated to an accuracy of half a degree [211-215].

This calibration approach requires a significant infrastructure to achieve the calibration of the array and the technique requires the elements of the array to be simultaneously fed. This leads to a less adaptable system and limits the operation of any potential implementation. This structure is inherently complex and costly and this will limit the scalability of the array.

3.4.1.2.2 External Reference Sources for Calibration

External reference sources are used extensively in array calibration. They have been presented in conjunction with array shape calibration and DOA calibration. The use of external sources is not limited to these incidences. To more fully present their use in calibration they have been grouped into three main categories. There is significant overlap between the groups, but they are used to add some structure to the variety of approaches. These groups are:

- Antenna Measurement Techniques
- Near Field Reference Sources
- Far Field Reference Sources

3.4.1.2.2.1 Antenna Measurement Techniques

Antenna measurement techniques characterise the radiation pattern of the array under test. Therefore the array can be calibrated to optimise the radiation pattern. These measurement processes are once off calibration approaches and are generally performed after construction or manufacture of the array. The reason behind this is that the measurement setups use specialised systems and locations. For instance for antennas or antenna arrays, a common practice is to use test ranges to characterise the radiation pattern. There are three types of test ranges, which are:

- Far Field Test Ranges
- Near Field Test Ranges
- Compact Test Ranges

Each of these ranges has its advantages and disadvantages, but in term of array calibration, each of them represent a once off calibration. Therefore they present an incomplete solution to the calibration problem.

Other measurement techniques include the use of field aperture probes (FAP) to measure the individual amplitude and phase of each element of the array. These measurements are usually taken in the reactive near field region of the array elements, so therefore right in front of each element. Then these near field measurements are converted to far field measurements using a Fast Fourier transform method [216, 217].

This near field measurement in once off calibration is attractive as it requires less space to implement. However as antenna arrays are steerable, it is important to consider the array at different azimuth and elevation angles. Therefore specialised measurement structures have been developed where the FAP is placed on a Perspex rotational arm, so that the radiation pattern can be more fully measured [217]. Other approaches taken to this 3D measurement of the radiation pattern employ multiple FAPs within an anechoic chamber [218]. Each of these approaches can be either near or far field depending upon the frequency of operation.

The significance of these measurement techniques is their ability to measure the radiation pattern and therefore fully characterise the performance of the array. Due to the required measurement equipment and locations used, dynamic calibration would be impractical. However, it is also important to note the limitations of any practical measurement technique, as with any practical system it has its own sources of errors. Although due to the stationary nature of the measurement equipment, they can be measured themselves, it is important to be aware of them. Here are some of the main sources of errors [219]:

- Mechanical Setup
    - Device Under Test Position
    - Measurement Devices
    - Measurement Device Positions
    - Cable Variations
- Stray Signals
- Electrical Inaccuracies
- Thermal Effects
- Leakage and Cross Talk

3.4.1.2.2.2 Near Field External Reference Source

The use of near field sources or probes that are either attached to or located near to the array have largely been associated with auto-calibration algorithms. These have been widely used as measurements can be transformed into far field measurements, though this does require a complete near field scan [220-222]. However these approaches are angularly dependent, so that the probe does not interfere with the array operation. Typically, they are placed at angles greater then 80^{o} off broadside [71, 223]. These errors offer the problem of angular dependence, which offers a reference signal with a particular angular property. This can have an effect on calibration if it is not known. When such probes are used to calibrate the array, they can be located in the far field of the antenna elements but it is within the near field of the antenna array. There is also sometimes more then one probe to overcome the angular dependence of the calibration results [224, 225].

An example of the use of calibration probes is the beamforming systems presented by Lier et al [81] which utilises the beamformer structure to implement calibration of the array. This is done by using a near field source or probe which allows the ability for both receiver and transmitter calibration, by the use of orthogonal codes to control the amplitude and phase of the array elements. This calibration cannot be performed during operation, as the communication signal distorts the measurement. This calibration approach does not depend upon the size of the array.

3.4.1.2.2.3 Far Field External Reference Source

Far field external reference sources are particularly prevalent in deep space and satellite applications as then can be operated from the ground [226, 227]. There are several methods for utilising these far field calibration sources for applications, such as splitting the array into subarrays so that the phase can be interpolated based on the subarray separation. Separate subarrays are used to continuously observe the phase of the reference [227] or to use the UMIST chirp sounder DOA estimator [228] for receive calibration. However for transmit calibration, the probes can be attached to the array in the elements far field for millimetre wave frequency of operations [225].

As has been mentioned, those external approaches to calibration are complete calibration ones, which just means that all aspects of the system are included, but this means that the external signal sources are required, and leads to expensive test equipment. This generally does not consider the signal source as an error source.

3.4.2 Alternative Solutions

These approaches utilise a structural or design approach to remove the errors, instead of having to compensate for them. The calibration approaches that have been presented so far have used a combination of the structural and compensation techniques to achieve calibration. So there is some overlap between the two types of approaches to the problem.

3.4.2.1 Structural Approaches

These approaches use structural design to remove the errors from the antenna arrays. It can be perceived to mean additional and complex hardware. This need not be the case; it strictly refers to those approaches that considered error sources when designing the system and exploit some property of the hardware, such as fixed feeder paths, phase lock loops and measurement structures.

3.4.2.1.1 Fixed Feeder Paths

Fixed feeder path are a structural approach whose main focus in to create fixed radiation patterns or a collection of fixed radiation patterns, which creates a switched beam implementation. These structures have particular implementations as the amplitude and phase relationships need to be exact to generate the switched beam radiation patterns. This however is of limited adaptability and needs to be designed specifically for a given scenario. There are two widely used feed structures: the Butler matrix and the Blass matrix. The principle difference between these two approaches is their method of creating the fixed feeder paths. The Butler matrix uses a combination of fixed phase shifters and directional couplers to feed the array [34, 35, 229-231]. The Blass matrix, on the other hand, is a time delay feeder approach, which utilises only directional couplers to achieve the switching between radiation patterns [35, 232].

3.4.2.1.2 Phase Lock Loop Approaches

The phase progression of antenna arrays for beam steering can be achieved by implementing phase shifters [233, 234]. This can also be a means of correction. This is done by the locking phenomena of oscillators in the phase shifters. This is implemented by applying an external signal to the oscillator at the same frequency. The oscillator will match it's phase to that of the inserted external reference signal, this is know as the 'pull-in' effect. This 'pull-in' effect can be modelled by Adler's equations [235]. This locking technique is also utilised by phase lock loops (PLL), which consist of phase detector (PD), voltage control oscillator (VCO) and loop filter (LP). The phase locking property of the oscillators does not mean that the phase errors are completely removed, as steady state phase errors and fluctuation errors are both present. When the phase errors are too large, the phase shifters will not lock to the inserted signal [236]. This property gives a focusing or calibration method to the array. This approach can be used on both receive and transmit array operations [237, 238]. There are a significant number of approaches taken to implementation and the differences depend upon the injection of the reference signals such as:

- Unilateral Injection Locking [234], which is where a single reference signal is used: such setups include:
    - Conventional Feed [234],
    - Cascade-Coupled Scanning Array [234],
    - Phase Reversal Switch Setup [239],
- Bilateral Injection Locking or Mutual Synchronization Methods [234], which is where two reference signals are used, and such setups include:
    - Inter-Injection Locking [234, 240-242],
    - Edge Detuning [234, 242, 243].

However the accuracy of these approaches is dependent upon the reference signal and feed structure of the system, not to mention the individual phase shifters. As these are active components, they will suffer from manufacturing tolerances, component aging and thermal effects to mention a few. Another consideration of this approach is that the amplitude relationships are ignored, and this is ill considered as the amplitude relationships have an impact on the radiation pattern of the array.

3.4.2.2 Approaches utilizing the Capabilities and Properties of the Array

As the removal of the error effects from the array is a prerequisite for its operation, it is intuitive to use the capabilities of the array to tackle the errors. This can be achieved by either removing the effect of the errors or by making the capability insensitive to them.

3.4.2.2.1 Beamforming Approaches

Beamforming approaches range from fixed paths to algorithms. The fixed path approaches to beamforming, matches the path lengths. These are used to match the amplitude and phase relation between the elements of the array. However this limits the operation of the system, as it would be a switched beam operation.

Beamforming approaches that have recognized the impact of array errors have taken both approaches to the matter. They try to make the beamformer insensitive to the errors such as using algorithms with constraints. This can be done by an iterative beamforming approach that compensates for the errors over time [244]. Alternatively limitations are put on the array itself, the adaptability of the hardware or by the beamformer approach

to conserve some desirable property. The constrained beamformers do not always provide the optimum solution; but they do optimise the scenario. Constraints placed on the beamformer to maintain a desired property of the radiation pattern are added to the beamformer so that it will be robust in the presence of array errors, signal errors and inaccurate estimates. The importance of this is that the degradation of the beamformers' performance is significant in the presence of any one of these errors, not to mention in the presence of all three [245]. These constraints can be created by using a single or multiple point. Single point ones are added to control a particular property of the radiation pattern, *i.e.* that the main beam is not reduced regardless of interferers locations. Multi-point ones are used to optimize the whole radiation pattern to a particular desirable pattern, i.e. such as broadening the main beam [48, 246, 247].

Some examples of the use of constraints in beamformer approaches are linearly constrained minimum variance (LCMV) beamformer, generalised sidelobe canceller (GSC) and constrained LMS. The linearly constrained minimum variance (LCMV) beamformer uses constraints to direct the radiation pattern in a particular direction and minimise the pattern everywhere else. The generalised sidelobe canceller (GSC) has constraints that are adapted into the formulation of the radiation pattern, so that the radiation pattern is optimized to reduce the sidelobes. Finally constrained LMS is a constrained from of the LMS algorithm, whose constraints are chosen depending on the criteria of the radiation pattern in particular scenarios [244, 246, 248-250].

3.4.2.2.2 Direction of Arrival Calibration Approaches

The DOA approaches are sensitive to small amplitude and phase imbalances in the antenna array elements [55, 251]. The errors have the effect of merging two spectral peaks which makes them indistinguishable [251]. The compensation of these errors can be done by a manipulation of the DOA approaches, for example the use of the covariance matrix of a linear array to estimate the DOA and the amplitude and phase errors [252]. Eigenvalue decomposition of the covariance matrix of the array can be used to estimate the amplitude and phase errors as well as the DOA of sources, which is not limited to linear arrays [253]. Predistortion can be used such as that used in the Capon beamformer to make it more robust to the element errors as the beamformer optimization is being corrupted by such errors [254].

Another approach to calibration using a DOA estimation approach is to calibrate out an implementation issue such as mutual coupling by using the extended noise subspace fitting (NSF) method, which is a DOA estimator that is extended to compensate for mutual coupling by creating a coupling matrix [255].

3.4.2.2.3 Multiple Input and Multiple Output Calibration Approaches

This seems to be a very limited area of research as the MIMO capabilities are very demanding. They are extremely sensitive to errors in the amplitude and phase relationships. To achieve the operation the array needs to be calibrated. That has generally been achieved by anechoic chamber and channel sounding [58, 61, 256, 257].

3.4.2.3 Targeted Approaches to Specific Error Sources

Discussion of the separate sources of potential errors for antenna arrays was the approach taken to present the scale of the problem. It is a logical approach to take specific source of errors. As previously mentioned some of the sources of errors are structural, so in most cases these are discounted with the assumption of careful consideration of their properties in the design stage. One such source of errors is the grating lobes of the array; by the correct choice of inter-element spacing it can be considered eliminated. Others may not need to be calibrated out, such as mutual coupling, for MIMO applications. However as the most significant contribution to the calibration problem is matching the amplitude and phase relationships of the array, it is touched on by most calibration approaches, it will not be discussed as a single targeted calibration approach, but will be discussed throughout the other targeted techniques. So considering this the first calibration method that targets a particular errors source will start with mutual coupling.

3.4.2.3.1 Mutual Coupling Approach

As mutual coupling is a significant challenge that affects the operation of antenna arrays, and therefore it has a large area of research associated with it. There are two major techniques taken to compensate for mutual coupling effects: one is to measure or model the effect of mutual coupling and the other is to use structural design approaches to eliminate the interactions that cause it.

3.4.2.3.1.1 Measurement and Modelling Approaches to Mutual Coupling Errors

These approaches are used to measure or anticipate the mutual coupling effects in the antenna array. As these effects stem from the interactions of the radiation patterns of the array, these approaches require specialised hardware or highly detailed models that fully encompass all the interaction properties of the array.

3.4.2.3.1.1.1 Measurement Approaches

Starting with the measurement approaches, there are many techniques to accomplish this measurement. There are approaches that use anechoic chambers or measurement test fields that can accomplish the measurement. The aim of this measurement is to identify the discontinuities that cause mutual coupling effects [258]. The other measurement approaches also include the calculation methods such as:

- Numerical Electromagnetics Code (NEC) [259-261]
- Transmission Line Matrix (TLM) [262-267]
- Aperture Modelling [268]
- The Reactive Theorem [269].
- Reflection Coefficient (Γ) [105]

These approaches can be considered exorbitantly expensive computationally or due to the complexity of the radiative field close to the elements and the close proximity of the antenna elements [23]. This is not even considering that these measurements are once offs and do not take into account any changes in the radiation pattern.

3.4.2.3.1.1.2 Modelling Approaches

Pattern Synthesis can be used to compensate for mutual coupling by coming up with a model for the radiation pattern, and therefore to predict the interaction between the elements [270]. Most pattern synthesis methods do not consider mutual coupling, such as the standard Chebyshev and Taylor methods. Therefore ways of adapting the pattern synthesis methods to account for mutual coupling are needed. Such include the use of characteristic modes, array modes, point matching or Madsen Technique [141, 271].

Pattern synthesis techniques can be altered to account for mutual coupling by using them in conjunction with active element patterns, which can predict the gain of the array

at a particular scan angle. An active element pattern requires that the radiation pattern of each element needs to be calculated. As a way to reduce this computational expense a hybrid active element pattern approach can be used. This means that instead of using an active element pattern for each element of the array, just two active element patterns are used for an array of any size. One of the active element patterns is to represent the inner elements and the other is to represent the edge elements of the array [89, 97, 121, 123, 152, 272, 273].

3.4.2.3.1.1.3 Matrix Compensation

The matrix compensation uses information about the mutual coupling interactions to create a coupling matrix, which is then applied inversely to the weighting vector of the array to mitigate the effect of mutual coupling on the array operation. The effectiveness of the mitigation depends upon the method of calculation of the mutual coupling interactions, i.e. from the measurement of the radiation pattern or pattern synthesis approach.

Matrix compensation can be extended to compensate for amplitude and phase errors in the antenna elements of the array, using several different approaches to calculating them, which include simulated annealing, iterative techniques and Woodward based technique for blind calibration, and MOM matrix compensation [85, 274-281]. The coupling matrix has been used to remove the effect of mutual coupling in DOA estimations, however it has been shown that in some cases of mutual coupling the coupling matrix is not always completely effective [116, 282, 283].

3.4.2.3.1.2 Structural Alteration Approach to Mutual Coupling Errors

As mutual coupling is caused by the interaction between the radiative elements of the array, therefore the intuitive approach to mitigating the mutual coupling effects is to alter the structure of the array to reduce or remove these effects. Such structural alterations used to compensate for mutual coupling effects are:

- Array structures,
- Radiative elements,
- Feed networks,
- Dummy columns or elements,

- Non-uniform sized antenna elements,
- Non-uniformly spaced arrays.

The choice of array structure of the array is an important choice as highlighted by the previous chapter. When considering the choice of structure and the impact mutual coupling will have on it, circular arrays are the best choice, as circular arrays use phase modes and spherical modes that exploit the symmetry of the array to reduce mutual coupling effects [116, 132, 166, 284, 285]. However if these properties are not utilised the effect of mutual coupling will be more severe than in linear arrays [93].

Whereas the choices of radiative element is a key deciding factor in the interactions between the elements because it dictates the quantity of mutual coupling in the array. It is possible to choose array elements that will reduce the mutual coupling such as minimum scattering (MS) antennas [24, 145, 160, 168, 286-292], electronically small resonant antennas [165] and active impedance elements [293].

Another structural approach taken to tackle the mutual coupling in an antenna array is that of feed networks, such as those taken to beamforming. The feed networks used for mutual coupling are lossless ones, where the feed network that is based upon power orthogonality used to compensate for mutual coupling [91, 111, 119, 127, 142, 155, 164, 294]. Another is the compensation coupling feed networks, which reduce reflection coefficients, such as a π type network, which will reduce the nearest neighbours effects but not the effect of elements further away [128, 129, 155, 295].

The next structural approach that can be taken to reduce the mutual coupling is to add dummy elements into the array. This creates a uniform radiative environment for each element of the array. Therefore the each element sees the same mutual coupling. This increases the number of elements in the array, but it raises the cost of the array and therefore makes this approach less attractive [111, 296].

Another structural approach taken to mitigate mutual coupling effects is that of non-uniform sized antenna elements. The effect of non-uniform sized array can reduce the amount of signal coupled between the two elements, if there is a large size ratio between the elements [150].

Finally, non-uniformly spaced arrays are used to mitigate the effects of mutual coupling by altering the inter-element spacing. The significance of this is that increasing the inter-element spacing will reduce mutual coupling, whereas reducing it will increase mutual coupling effects. So to utilise non-uniform element spacing, a complex design process needs to be undertaken to achieve the reduction in mutual coupling while maintaining the radiation pattern [28, 162].

3.4.2.3.2 Approaches to Remove the Position Errors

The removal of position errors in an array is of importance as these errors led to degradation in the radiation pattern and the capabilities of the array. The calibration of these position errors is known as array shape calibration, which in turn is the general name give to three classifications of array element position error calibration capabilities. These classifications are array shape calibration, array orientation calibration and the array position calibration. Array shape calibration is defined as the locating of the element positions of the array relative to a reference element position. Array orientation calibration is the ability to define the rotation of the array relative to the x-axis of the coordinate system. Finally the array position calibration is the ability to define the exact coordinates of the array elements [297-301].

External calibration techniques have a variety of different approaches that are distinguished by the type of calibration sources. The two ways of specifying the type of calibration sources by the location of the source, *i.e.* in the near field or the far field of the array, or the type of signals used by the sources, *i.e.* switched signals, spectrally or temporally disjointed signals or non-disjointed signals. Near field sources are used under the assumption that they are far from the array. First, consider the location of the source whether they are in the near field or far field of the array or whether they are in a known or unknown location. Near and far field sources have varying effects on the performance of the array shape calibration. Far field sources can effectively calibrate the array shape and orientation of the array, but not the array position. These calibrations can be achieved only if at least one of the far field sources' location is known. Linear arrays cannot however have their array shape calibrated using far field sources, as the intersection of lines are used for this calibration and in the presence of small measurement errors the parallel nature of the array will experience large calibration errors [302].

For near field sources one can calibrate the array shape, array orientation and the array positions using two near field sources in known locations along with a sufficient number of sources that can be made up of sources in unknown locations. The required number of sources when using near-field sources can be specified: for a four element array a minimum of five sources is needed, for a five element array a minimum of four sources is needed and finally for an array with six or more elements needs a minimum of three sources to calibrate the array shape. The reduction in the number of sources as the array size increases is a general rule and will depend upon the type of sources and their location. The significance of this criterion is that it makes it capable of calibrating a linear array. The benefits of both types of location of sources can be taken advantage of by having both far field and near field sources [302-305].

Next consider the types of signals used for calibration. These signals are switched, spectrally or temporally disjointed and non-disjointed. There are several approaches, which use these sources to overcome signal recognition issues. The use of switched signals is so that they can easily be recognised due to their timing sequence of these signals. This recognition can be used with an eigenstructure method to calculate out the position errors and the phase errors of the array [304].

The use of disjointed sources is so that the different calibration sources can be recognised by their difference in frequency or timing and so used to calibrate out the position errors. For example, this can be done by using the disjointed sources with unknown locations along with carry-on or internal reference elements to act as a coordinate system. This has the ability to calibrate out the position errors and the amplitude and phase errors of the array using an eigenstructure approach [306].

Finally the use of non-disjointed sources has the advantage of not having the stringent requirements of the two previous cases. It is therefore easier to implement an example of an approach using these types of sources such as the previously mentioned ML approach [297-300, 303].

Other calibration approaches take an array design approach to the calibration. Firstly there is the use of internal references that generate the calibration signals [307, 308], the use of a rigid frame to mount the sources so that they are precisely known and synchronised [309] and finally mechanical scanning of the array is used for calibration

of the array shape [310]. Another method is inspired by the constant modulus algorithm, which uses the external sources outlined above [311].

These external sources can be used to calibrate the amplitude and phase imbalances in the elements of the array. This can be done using all of the above array shape calibration along with the correct processing which will allow the measurement and identification of the errors.

3.4.2.4 Approaches to Remove Array Blindness

Array blindness, though a mutual coupling effect, was considered as a separate implementation issue as it has different compensation approaches from mutual coupling. These approaches vary significantly in their attempts to eliminate or mitigate these effects. The first of them is to use subarrays, though this will limit scan range [312]. Another approach is to extend the bandwidth of printed antennas by the loading of varactor diodes to mitigate the effect of array blindness [313]. By using non-uniform arrays the surface waves which cause array blindness are disrupted; randomising techniques are used to generate the non-uniformity that will disrupt the coherent and incoherent culmination that cause the blind spots [314-318]. Finally, parasitic elements can be used in conjunction with the subarrays to eliminate the scan blindness in the printed antenna arrays, though it reduces beam efficiency due to the increased cell size [319].

This shows that the array blindness elimination techniques have different drawbacks. The effect of array blindness is of reduced concern in arrays with a small finite numbers of elements. So, it is important to note that even though the significance of the mutual coupling effect reduces as the size of the array increases, array blindness becomes more significant [320].

3.5 Discussion

The approaches taken to calibrate out these effects are as numerous as the sources of errors as is shown in the comparison presented in Table 3-3 and Table 3-4. Measurement structures can be used to calibrate the antenna array; two of the distinguishing features are the measurement point and measurement structure. There are multiple measurement structure approaches, generally based upon a measurement point

directly behind the antenna elements. The significance of this measurement point is that it is the point closest to the antenna so that all of the hardware up to this point is included in the calibration. These measurement points are fed back to a central measurement device. These structures provide a means of measuring all of the elements of the array. It is important to note that these structural approaches are limited in scalability due to the central measurement structure. This means that there is a need for a well-designed feed structure to provide this, such as the fixed feeder paths. The measurement structure is also a source of errors, particularly as it requires active components. They are therefore as vulnerable as the normal signal paths thus introducing a similar set of errors with similar effects. This increases the complexity and cost of any practical solution.

Reference signals are also used to calibrate the imbalances in the amplitude and phase relationships. These require a known source to generate a reference signal that can be used to calibrate the array. These approaches range from internal reference elements to external reference signals. The uses of these sources require the system to be able to transmit and receive simultaneously and a time slot in which to calibrate the array. These techniques are used to calibrate not only the amplitude and phase errors but also the element position errors. This approach provides a full calibration technique, which is to say it covers the whole antenna array, including the antenna elements. The drawback of such an approach is the requirement of external hardware, known reference signals and calibration time slots. There is another set of reference source calibrations that occur at manufacture. These measure the antenna performance in some way, such as with an anechoic change or an antenna measurement test range. These are again complete calibration techniques; however, they are subject to the same limitations of other reference source techniques, and cannot provide in-situ calibration.

Modelling based calibration has been used for amplitude and phase imbalances, mutual coupling and grating lobes, while providing a scalable approach to the calibration problem. This modelling approach to calibration only offers a once off calibration and requires considerable computational power and its performance depends upon the assumptions made by the model.

Each of these four approaches were compared with the concept of an ideal calibration approach in table 3-3. This ideal approach has the ability to calibrate out amplitude and

phase imbalances, position errors, mutual coupling and grating lobes. This is done while providing dynamic and accurate calibration using a scalable and low cost system. When the other approaches are compared with this concept, it is clear that their capabilities are balanced by performance. For example the measurement structure approaches are capable of calibrating out amplitude and phase imbalances while providing dynamic calibration, however using a structure that is not scalable. Whereas measurement approaches are capable of calibrating out amplitude and phase imbalances, mutual coupling, position errors and grating lobes, while providing accurate and scalable calibration. However these approaches do not offer dynamic calibration.

Table 3-3: Strengths and Weaknesses of the Different Calibration Approaches and the Error Sources they Calibrate.

Approaches	Uses	Advantages	Disadvantages
Measurement	Amplitude and Phase Imbalances	Accurate Calibration	Extra Hardware
	Mutual Coupling		
	Position Errors	Scalable	Once Off Calibration
	Grating Lobes		
Measurement Structure	Amplitude and Phase Imbalances	Dynamic Calibration	Not Scalable
			Additional Hardware
			Does not Consider the Measurement Device as a Source of Errors
Modelling	Amplitude and Phase Imbalances	Scalable	Once Off Calibration
	Mutual Coupling		Significant Computational Power
	Grating Lobes		Performance Depends Upon Assumptions
Reference Signal	Amplitude and Phase Imbalances	Dynamic Calibration	Additional Hardware
			Does not Consider the Reference Source as a Source of Errors
	Position Errors		Effected by Multipath Environment
			Can Have Limited Scalability
Ideal Calibration	Amplitude and Phase Imbalances	Dynamic Calibration	None
	Position Errors	Accurate Calibration	
	Mutual Coupling	Scalable	
	Grating Lobes	Low Cost	

Table 3-4 presents the structural approaches. These start with the simplest, the active elements and dummy elements which both are used to mitigate the impact of mutual coupling by effecting that inter-element interactions. They both do not provide dynamic calibration. However, adding dummy elements into the array can limit the scan range and also increases the array size. The next of the calibration approaches is that of the phase lock loop. It provides dynamic calibration, though it is limited to phase shifter implementations. These have limited operational abilities and a non-scalable approach to calibration.

The beamforming approaches can be split into two types of approaches, structural and algorithmic ones. The distinction between these approaches is a fundamental one: the correction achieved by a structural approach is a static approach where the feed network of the array is designed to create predefined radiation patterns. This tackles the amplitude and phase imbalances by designing the feed network to create fixed amplitude and phase interactions. On the other hand, the algorithmic approaches taken to this is based upon a search criteria to generate the weights for the array. These search

Table 3-4: Strengths and Weaknesses of the Different Structural Approaches and the Error Sources they Calibrate.

Active Elements	Mutual Coupling	Simple	Does Not Offer Dynamic Calibration
Dummy Elements	Mutual Coupling	Simple	Does Not Offer Dynamic Calibration
			Limits Scan Range
			Increases the Size of the Array
Fixed Feeder Paths	Amplitude and Phase Imbalances	Accuracy Calibration	Limits Operation
		Simplicity	Not Scalable
			Does Not Offer Dynamic Calibration
Phase Lock Loop	Amplitude and Phase Imbalances	Dynamic Calibration	Limits Operation
			Not Scalable
			Additional Hardware
Measurement Structure	Amplitude and Phase Imbalances	Dynamic Calibration	Not Scalable
			Additional Hardware
			Does not Consider the Measurement Device as a Source of Errors

algorithms utilise constraints upon the searches in an effort to make the system less sensitive to errors.

3.6 Summary

The calibration problem is an impediment to the implementation of antenna arrays for practical wireless communication systems. There are numerous sources of errors that cause the calibration problem ranging from structural effects to channel effects, as clearly laid out in table 1. The most significant of these are the amplitude and phase imbalances as these relationships are affected by most of the other sources of errors, such as path lengths variations, manufacturing tolerances, component aging and thermal effects to name but a few. These errors have a significant effect on the performance of the antenna array as they affect the interactions of the elements' radiation patterns. This was clearly shown by the comparison of the radiation patterns with progressively larger standard deviation of the amplitude and phase errors associated with the array. The approaches taken to the calibration of these errors are numerous. They range from structural based solutions to calibration of the array. The discussion of the advantages and disadvantages of the solutions taken to removing the effect of these errors highlighted that measurement structure approaches provide a means to measure the array and calibrate the array dynamically, though they do not provide ideal calibration solution. Thus combining structural and algorithmic approaches, which is the most effective. They are however not without their limitations, which are scalability and accuracy issues due to not considering the measurement structure as a potential source of errors.

The next chapter will present the calibration approach taken by this dissertation, which is a measurement structure approach that proposes to overcome the scalability and accuracy issues identified in this chapter. It will cover the motivation for the approach, the principles of the concept and the methodology it will employ.

Chapter 4

The Crux of the Matter

4.1 Introduction

Mismatch of elements and feeder paths within an antenna array is a problem that severely affects the radiation pattern. Even small variations in the location and shape of the radiation pattern can have a significant impact upon performance. These distortions in the radiation pattern are directly related to the amplitude and phase relationships between the elements of the array. Therefore to have an array that provides efficient performance, these relationships need to be known, as has been highlighted by the previous chapters.

In practical systems, this is a challenging criterion as antenna arrays can operate at high frequencies so that small distortions in path lengths, mutual coupling, finite manufacturing tolerances, component aging, and thermal effects will have significant effects. These errors are both static and dynamic. Active antenna arrays are significantly more vulnerable to these errors than passive networks. However if we can develop a calibration methodology that allows for correction of these effects in an active array, then we will be rewarded with enhanced and adaptive performance when compared to passive systems. This chapter will present a technique which achieves the necessary performance yet does so in a manner that is low-cost, flexible is its application to different antenna array implementations, i.e. array size, operating frequency and modulation scheme, and robust to manufacturing imperfections.

4.2 Principles of the Calibration Approach

The aim of this thesis is to develop an approach to calibrate antenna arrays. An active array was chosen because it gives the most potential reward and also gives rise to the greatest engineering challenges. The aim is not unique but its approach and implementation are. To present it to it full advantage, it will be put in context of other solutions presented in the previous chapter.

The variety of approaches taken to the problem range from structural to algorithmic ones. These can be classified as either internal or external techniques. The significance of this choice affects the internal system architecture, the required system equipment, the cost of the system, and the inclusion of possible error sources and thus the effectiveness of the approach. This means that considerable care needs to be taken when considering the implications of this choice. From the discussion of the calibration approaches in Chapter 3, the most effective approaches employed a combination of structural and algorithmic means of calibration. However, these approaches are still classed as external and internal types of calibration.

For the external source based calibration approach, which can be considered a radiative calibration system, there is a need for external hardware to calibrate the antenna array. This radiative calibration method permits the inclusion of error sources, such as environmental effect and propagation effects. With, internal calibration approaches or non-radiative calibration systems, internal hardware is used to create a feedback path. The advantages of each of these approaches are balanced by their limitations and challenges.

This leads to a further choice of implementation styles. Due to the previously stated criteria, the requirement is for a practical solution. This favours the internal calibration approach as it will limit the hardware profile by not utilising external calibration equipment and also makes it self contained. This also has the effect of removing the possible error sources from calibration path such as propagation effects, *i.e.* scattering and multipath propagation. However this does not imply that the internal approach is ideal. These systems suffer from scalability and accuracy issues associated with measurement errors.

Measurement approaches, presented in the previous chapter, are dependent upon the point at which the measurement is taken, the sensor used and the structure which feeds it back. Due to the single sensor used and the need for machined paths to create the structure, these approaches are therefore limited by their scalability and vulnerability to manufacturing errors. This limits the accuracy that can be achieved in realisable systems.

These limitations are interdependent. These systems are not scalable as the measurement path to each signal need to be exactly the same length or they will introduce significant measurement errors, similar to the feeder paths in antenna arrays. Active arrays create a more challenging calibration problem as previously stated and therefore the impact of measurement errors only exaggerates this problem. It makes it harder to scale: as the number of elements increases so does the number of paths. The complexity of the measurement paths can become prohibitively complex and the paths need to be individually designed for each array size.

This challenge in scalability is due to the need to limit measurement errors, as increases in these errors led to a reduction in the calibration accuracy, unless they are accounted for. Unknown errors in calibration will be returned as errors in the correction, thus inducing additional errors in the signal paths. Thus, an unexpected measurement error can cause a significant detrimental impact. Therefore, as the measurement errors increase, the calibration accuracy decreases and the viable size of the array is reduced. Thus, the measurement errors are of high significance in these calibration approaches and they need to be accounted for. It is important to consider their sources, some of which are:

- Feeder Path Length Variations
- Measurement Point Errors
    - Passive Devices
        - Directional Couplers
        - Passive Switches
    - Active Devices
        - LNA Switches
- Feedback Mechanism
    - Digital Feedback
        - Quantization
    - Analogue Feedback
        - Mixer Errors

4.3 Concept

The rich background in antenna array calibration has led to a broad understanding of the system and the capabilities of the possible solutions. Measurement based methods, which provide a mix of structural and algorithmic approaches to the calibration problem, have been the most effective. They provide dynamic calibration that can be implemented with limited additional equipment. However, they do not meet all the criteria. A new measurement approach was created to solve this.

The concept behind the thesis is to create a scalable approach that is practical; the concept of this solution is to use multiple measurement devices or sensors to calibrate the array. The sensors are connected to a small number of elements, and then the elements are connected to multiple sensors. The group of elements being covered by each sensor deliberately overlaps with the groups belonging to other sensors. This overlapping or redundancy in the system offers a means of calibrating the array without the need for precision sensors or communication between these sensors. For the purposes of this discussion, a precision sensor is one with an accuracy of 14 to 16 bit or capable of receiving signals as low as -130dB. The types of sensors that this thesis considered were of the order of 10 to 12 bit accuracy and received signal levels of -80dB. This is by virtue of the unique redundancy incorporated into the measurement structure. The concept also allows the utilisation of practical transceiver elements and does not require precision reference elements for calibration. This is unique and immensely valuable. This approach will allow the use of off-the-shelf components and techniques for designing the measurement and feedback network without impacting on calibration performance. This will significantly reduce the difficulty and cost of producing a calibrated antenna array.

4.4 Measurement Structure

The calibration approach taken by this dissertation is a measurement-based approach, as it provides an internal method that can be used for dynamic calibration. The approach taken adds novel aspects in its measurement structure. The approach uses multiple measurement devices and elements connected to multiple measurement devices as mentioned in the previous sections overcome the limitations of other measurement-based approaches. This measurement concept allows for a scalable dynamic calibration approach to be implemented in practice.

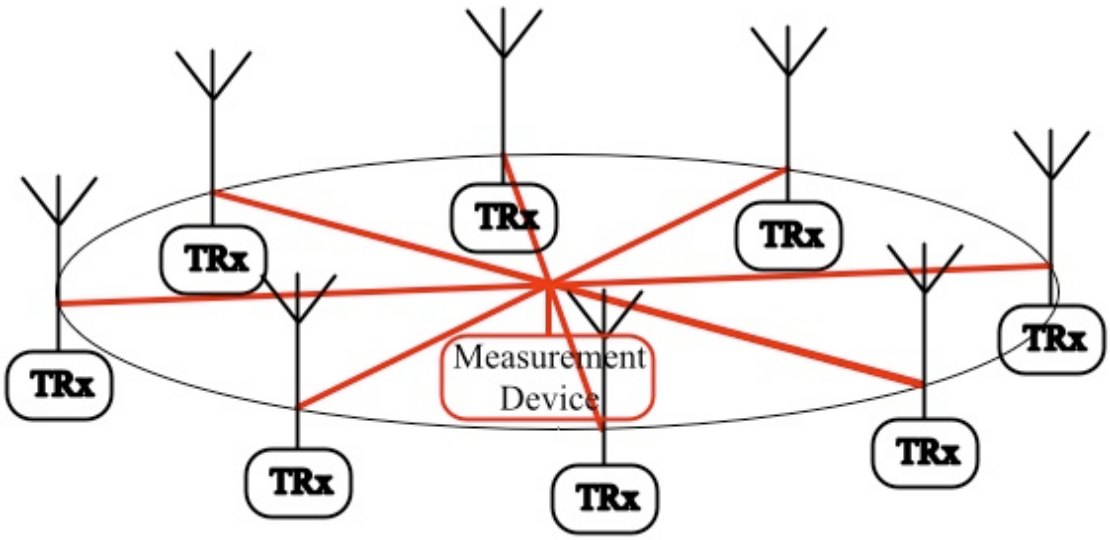

Figure 4-1: Eight Element Circular Array with Distributed Transceiver Elements and a Central Measurement Device.

The architecture employed to actualise the concept is based upon the array structures presented in chapter 2. The most scalable antenna array structure is the planar array. It offers the greatest control of the radiation pattern, as the larger the array the thinner the beamwidth of the main lobe and the smaller the sidelobes, making the array more directional, while the increased number of elements creates a greater number of control parameters which can manipulate the radiation pattern. Planar arrays use this ability to steer the array in both the azimuth and elevation angles. This is a significant advantage over linear arrays, which only provide radiation pattern control in the azimuth angles, and increases the directionality of the radiation pattern by increasing the size of the array in the azimuth. Circular arrays have the directional control comparable to the planar array, but to increase the number of elements led to impractically large arrays.

These array structures highlight the balance between complexity and capabilities. They are used to create the new measurement structure by combining the advantages of planar arrays, namely their scalability and directionality, with the advantages of circular arrays such as the equidistance from central measurement structures. By blending these two structures, the advantages are combined and the limitations are overcome, providing a scalable measurement structure.

The advantages of planar arrays are balanced by the challenge of implementing a measurement path structure, as the number of elements in the array can be large and the elements are closely spaced. This leads to a complex measurement path structure to

create matched path lengths. Linear arrays are simpler to implement, as can be seen from the measurement structure approaches presented in Chapter 3. However, for measurement structure implementation, circular arrays are the simplest and most elegant, as they are based around a central point, where each element is equidistant from this point, as can be seen in figure 4-1. However, as previously mentioned, circular arrays are the hardest to scale because as the number of elements increases, the size of the array needs to increase to maintain element separation. Also, the number of elements increases the connections to the central measurement element become impractical, as shown in figure 4-2.

To realise the concept proposed by this dissertation, the advantages of planar and circular arrays are combined to create a measurement structure that is easily scalable for a planar antenna array upon which calibration can be implemented. This was achieved by considering a small circular array, as shown in Figure 4-3*(a)*. This circular array consists of four elements equidistant from each other and from the centre of the array, at which is the central measurement sensor. This circular array can be equated to a *2 by 2* planar as each of the elements is equidistant, if the planar array included a sensor at its centre, as shown in Figure 4-3*(b)*. This equivalence is the key to the scalability of the array and measurement structure.

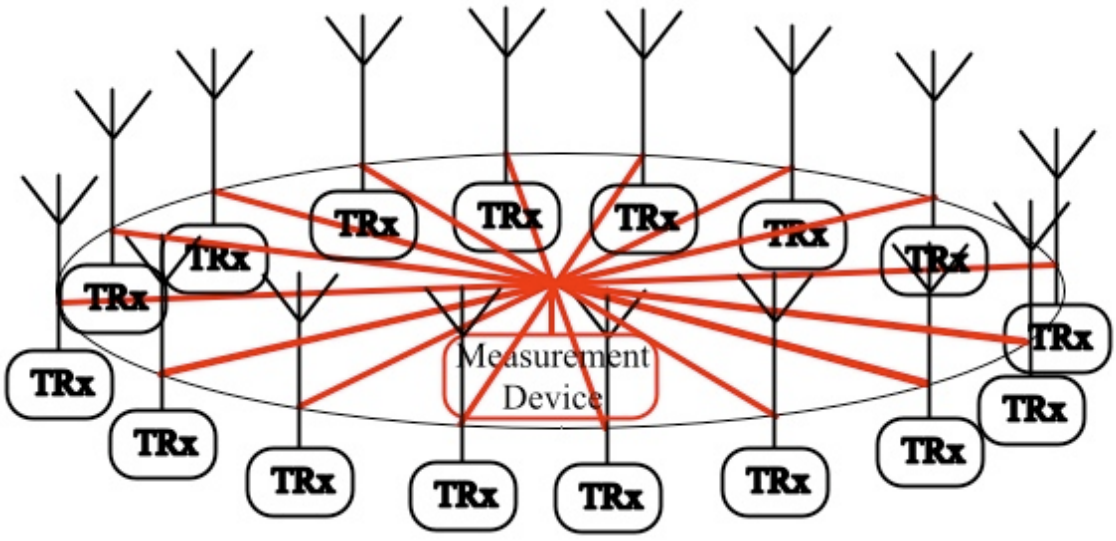

Figure 4-2: Sixteen Element Circular Array with Distributed Transceiver Elements and a Central Measurement Device.

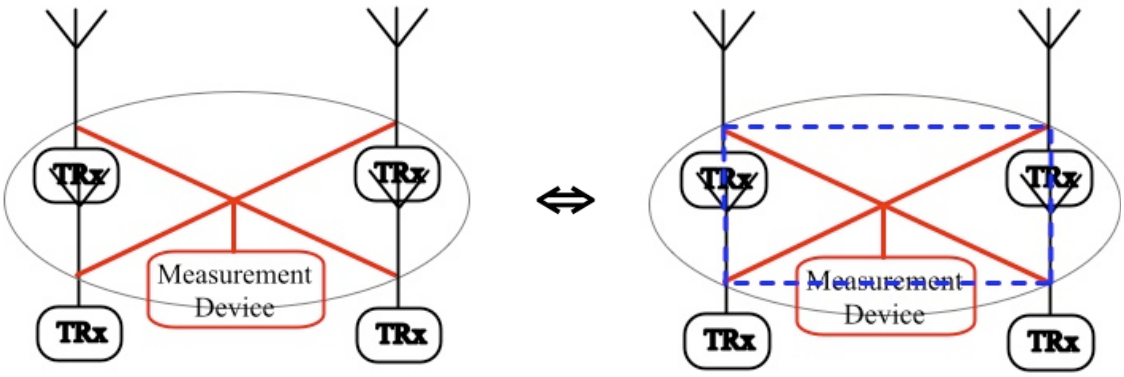

(a) *(b)*

Figure 4-3: The Equivalent of *(a)* a Four Element Distributed Transceiver Element Circular Array with a Central Measurement Device and *(b)* a 2 by 2 Distributed Transceiver Element Planar Array with a Central Measurement Device.

This *2 by 2* array is used as a single tile for the creation of the multiple measurement sensors for the structure. When multiple tiles are connected together it creates an array with multiple measurement sensors in a structure where every element is equidistant from a sensor and in most cases multiple ones. Two tiles are overlaid to create a 2 by 3 array; the tiles use two common elements per overlapping tile, thereby using two common elements in total. This overlapping can be seen in Figure 4-4. This creates an array of measurement devices within the antenna array. For a *n x n* antenna array, there is a *(n-1) x (n-1)* array of measurement sensors. This creates a scalable measurement structure.

A distinguishing feature of this measurement structure is that of a scalable structure which provides multiple measurement paths for array elements, with equi-spaced sensor elements between equi-spaced array elements. The use of such a fixed measurement structure provides the ability to implement dynamic calibration, while not requiring any external hardware. The next important feature is that each of the sensors is that they do not need to communicate with each other. They are not required to be precision sensors. This is possible because of the overlapping sensor groups. Each sensor needs only be accurate in terms of its own group of array elements (similar to circular array calibration). The overlapping allows for correction of sensor mismatch as the multiple sensing of common elements allows us to move to a relative-measurement framework rather than an objective measurement. This additional sensing, and the redundant information, can also be utilised by the calibration algorithms and methodology to

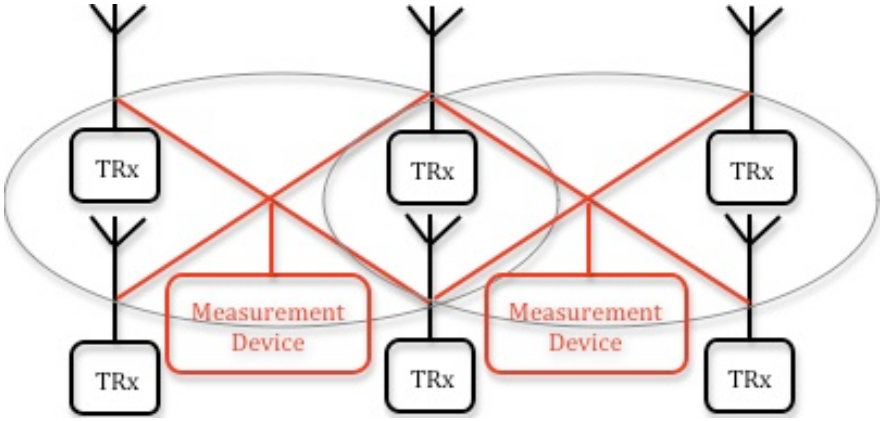

Figure 4-4: Four Element Circular Arrays Tiled to create a 2 by 3 Planar Array.

minimise the impact of mismatch errors in the feedback network. This greatly relaxes our design constraints. The overall impact is that this unique structure provides scalable dynamic calibration for planar arrays that does not require precision sensors as reference elements.

The calibration method has been described in the context of transmit-calibration where signals are being transmitted by the array. Transmit calibration is easiest to understand. However the architecture is symmetrical and can also be used for receive calibration. This requires the sensed elements to transmit a reference signal (modulated or not). Then the normal receiver systems are used to measure amplitude and phase. This is a normal feature of any modern receiver system. The remainder of this thesis will continue to focus on transmit calibration for clarity. Receive calibration is possible with this measurement structure by replacing the measurement sensor with a reference signal source.

4.5 Benefits of Overlapping Sensing

The measurement structure presented in this thesis provides additional measurements beyond the required minimum, yielding redundant information. This occurs due to the overlapping tiles where each antenna is connected to multiple sensors. This structure provides nearly four times as many measurements then is absolutely necessary.

This redundant information can be used by the calibration algorithms to remove array element errors, sensor element errors and to mitigate for other measurement structure errors. The immediate benefits are three-fold. The most significant benefit is that the array measurement network and the sensor elements do not need to be precise or

matched to the other sensing elements. The redundant information benefits the network in different ways, which will be explained in detail later in the thesis. The second benefit is that each of the *2 by 2* tiles is locally calibrated to a common point. Thus the sensor feeds back measurement information based on relative errors within the tile. However as the tiles are overlaid, it is possible to generate a composite understanding of how each relative error corresponds to the aggregate error of the array. This relaxes the sensor performance requirements from an absolute measurement specification to just requiring a local relative measurement. This greatly simplifies the sensing challenge.

The third benefit of the overlapping tiles is that it is possible to get multiple perspectives on the error in each antenna element from the perspective of different sensors – both close to the element and those not directly connected to it. In that context it is possible to select some of these perspectives to allow us to combine them in such a way that the coupler errors are combined in parallel. As these errors are Gaussian in nature, combining multiple such errors together can be averaged to reduce the aggregate error.

The benefits and capabilities offered by the additional information will be explained in more detail as each of the key elements of the calibration system is presented in the following sections.

4.6 Coupler

The measurement feedback structure is a key section of the calibration approach; there are implementation aspects that need to be considered in order for the concept to work as it is intended. The measurement structure presents the idea of multiple measurement sensors interlaced between the elements of the array that connect to multiple elements. To achieve such a structure, the connections need to have limited interference with the through paths from the transceiver element to the antenna elements. They need to provide four paths with equal signal levels. Therefore, they need to be symmetrical around the array elements. A similar set of criteria are placed upon the connections to the measurement sensors. These connections need to be symmetrical across the whole array so that each element of the array is equidistant from each of the sensors it is connected to.

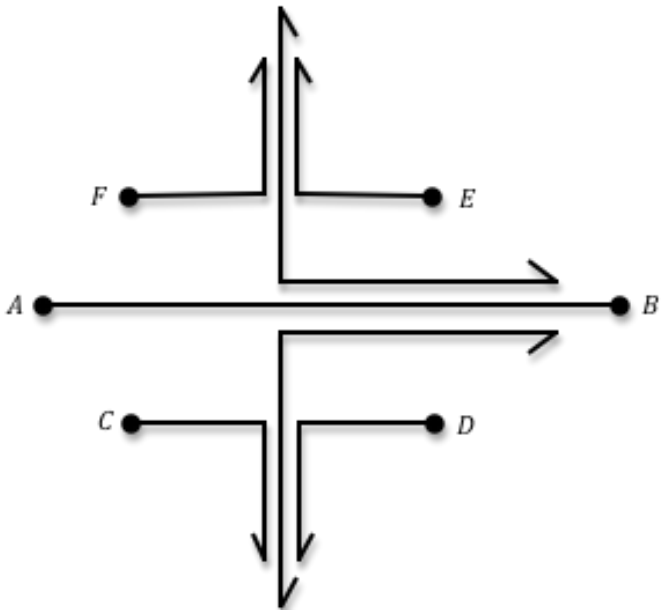

figure 4-5: Schematic Representation of the Six-Port Directional Coupler.

These points were touched upon in the description of the measurement structure, but the proposed solution was not. The requirements for the structure are very constraining and required the design of a novel directional coupler as the measurement infrastructure as there is a need of four connections to each element of the array and four connections for each sensor element.

The directional coupler was chosen as it provides the means of siphoning of a portion of the signal while not affecting the integrity of the through path. Due to the symmetry that needs to be achieved, three line couplers in a six-port edge coupled structure were used to create the four required symmetrical connections to the array or sensor elements.

This design approach was taken as the quantity and quality of the signals that flow along these paths are important, as well as the paths lengths. The design of the six port directional coupler consists of three-line edge couplers arranged in such a way as to create four connections to the sensors of array elements that carry symmetrical signal loads. The first of these edge couplers is located along the through path between the transceiver (Port A) and the antenna element (Port B) upon the array element, which can be seen in figure 4-5. This creates two paths that carry equal portions of the signals; these paths feed the other two edge couplers to create the four connections (Port C – Port F) to the array elements.

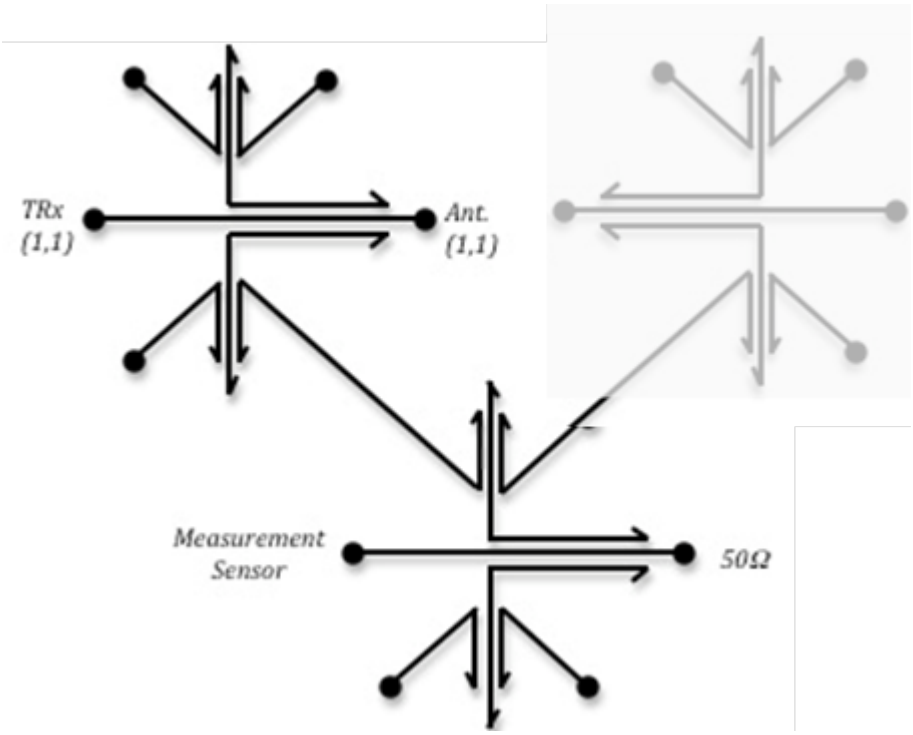

figure 4-6: Two Six-Port Couplers used in Series to Create the Connectivity Between the Antenna Array Elements and Sensor Elements.

The six-port coupler structure provides one half of the required connectivity. The couplers are used in series to create the connectivity between the antenna elements and sensors, as shown in figure 4-6. The connection to the sensor element is shown to be terminated in a 50Ω load. This is not always the case, this load will depend upon the antennas used and the directional couplers matching to those antennas. The advantage of these symmetrical couplers provides the fixed match path length required for the construction of the measurement structure while ensuring the limited interference with the through path signal which means that the performance of the antenna array will be affected as little as possible. Finally, the three line edge couplers provide the four required connections while maintaining symmetrical signal levels, which will be required to perform the calibration. The flow of the signals is facilitated by the combination of two coupler networks. This is shown in the measurement structure shown schematically in figure 4-6, where the interconnections between the array and sensor elements and the interconnectivity between the tiles can be seen (second antenna element and coupler network shown in gray).

The combination of these six port couplers creates the measurement structure while establishing the ability to interconnect the tiles that gave rise to the scalable

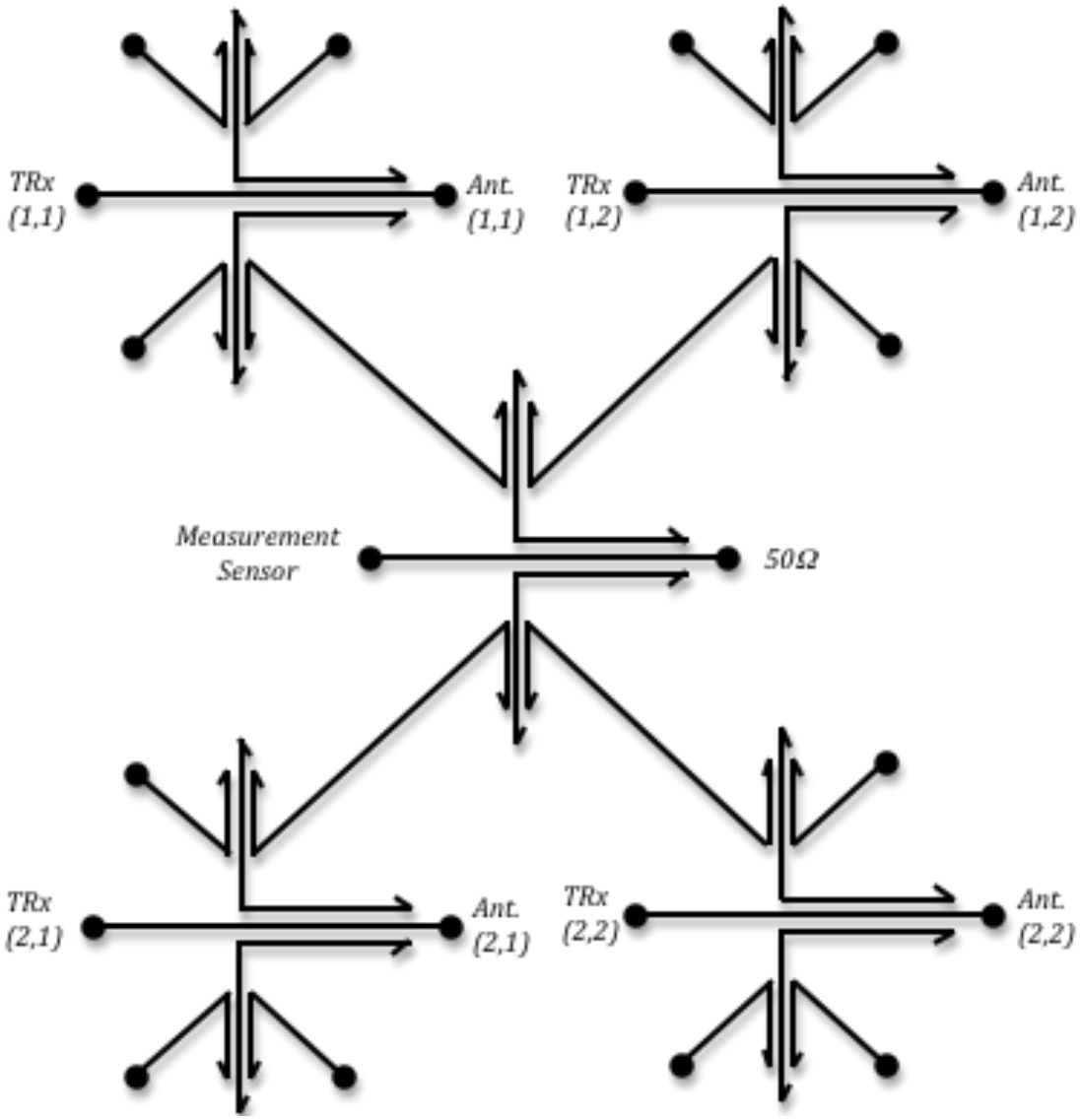

figure 4-7: Schematic of the Directional Coupler Measurement Structure for a 2 by 2 Antenna Array.

measurement structure. This can be more clearly seen in the linking of the six port structures to provide the interconnectivity for the multiple sensors connected to multiple elements and the ability to scale the structure in a tiled manor by the measurement structure. This can be seen from the two by two array directional coupler schematic shown in figure 4-7. This novel directional coupler implementation creates the means of creating the measurement structure that is a unique scalable calibration solution presented in this thesis and is described in more detail in section 6.2.

4.7 Measurement Device

The next major component is the measurement device or sensor, as it will dictate the capabilities of the calibration approach, since it will control what the calibration algorithm sees. For a calibration system that requires detection of complex modulated signals, an appropriate measurement device is required such as a full receiver. For the calibration of RF sinusoidal signals a much less complex measurement device is required to measure the amplitude and phase of the sinusoid. For a CDMA or WCDMA system, to be able to perform calibration requires a CDMA or WCDMA receiver, as appropriate. The application of the antenna array will dictate the choice of measurement device. The advantage of this measurement structure is that by simply replacing the sensors in the measurement structure, this calibration structure can be applied to a variety of communication systems. This means that the overall structure of the calibration will remain the same; the appropriate measurement device will just be slotted in.

The measurement device will also dictate the severity of array errors that the system will be capable of tackling. To clarify what is meant by this, consider a system that is capable of providing phase errors of greater then one wavelength, *i.e.* very high frequency applications where small variations in feeder path length led to large phase errors. The measurement device then requires the ability to measure the phase variations over multiple wavelengths. This might require two stages of measurement of the phase. So let us say the first stage gives a rough approximation of phase, *i.e.* that the signal is greater then 360^o out of phase and less then 720^o out of phase. Then the second stage pinpoints the actual phase error between 360^o and 720^o. This is not a concern in sinusoidal signals, however for modulated signals this could be an issue. The capability of the measurement sensor will dictate what range of phase errors can be measured.

The other aspects of the measurement structure reduce the demand upon the sensor elements, such as to achieve calibration the sensors do not need to be precision ones and they do not need to communicate with each other. The advantages arise from the redundancy created in the array by the multiple measurement sensors. The structure of the measurement approach allows this, as it creates multiple connections between the sensors and the elements. This redundancy in the structure offers the additional information, which means that the errors associated with each of the sensors due to

feeder length variations, manufacturing tolerances and component variations can be removed. The redundancy in this measurement structure offers the ability to remove these errors and this means that there is no need for precision sensors. This is based upon the assumption that all of these errors will effect the measurements of each element in the same way. However if the errors are vary between measurements of two different elements, they will still effect the calibration of the array. This simplifies the hardware requirements. This ability to use redundancy in the structure to remove the measurement device errors from the calibration also means that there is no need to communicate between the sensors. This comes from the multiple connections to the elements of the array. By removing the need for communication between the sensors of the measurement structure means that the structure does not need to be complicated by an additional inter sensor communication network. The sensors do however connect back to a control unit, which manages the calibration and utilised the measurements, this control unit does not need to synchronise or calibrate then sensors to each other.

These advantages are significant for the practical implementation of the measurement structure that will create a scalable, dynamic calibration approach that does not require precision sensors or communication between the sensors. This offers significant practical and implementation advantages.

4.8 Calibration Algorithms

The last major component in this novel measurement based approach is the set of calibration algorithms developed specifically for this structure. They use the feedback created by the multiple measurement devices or sensors connected to the directional coupler measurement structure. The calibration algorithms manipulate the measurements offered by the structure in such a way that the calibration can be accurate while utilising all of the advantages and novel approaches that have been presented in previous sections. The approach takes imperfect measurements and constructs a high quality composite result.

The algorithms utilise the non-radiative calibration paths to calibrate the array. A single such calibration path is on figure 4-8. This path shows the components included in the measurement path and each of these components is an error source. From the transceiver element, the through path, the directional coupler, which connects the sensor

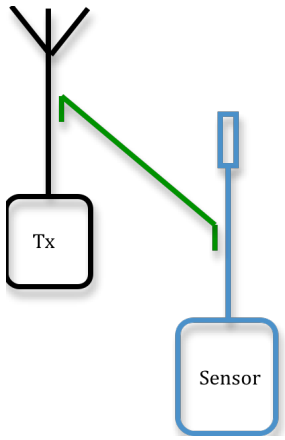

Figure 4-8: A Single Calibration or Measurement Path.

to the array element, and finally the measurement sensor are all sources of errors. The errors come from the effects that also have an impact upon antenna arrays, namely manufacturing tolerances, path length variations, component aging and thermal effects. These error sources will affect each of the components along the measurement paths. The components along each calibration path effect the measurements and therefore the calibration. This redundancy provides the means for the calibration algorithms to remove the errors due to the transceiver and sensor components and to mitigate the impact of the directional coupler errors.

The consideration of these measurement errors is a significant advantage of this approach, it facilitates the use of independent transceiver elements throughout the array as their errors can be removed. This allows these transceivers elements to be used as reference elements for calibration by virtue of this redundancy. The consideration of the measurement errors means that these advantages are possible, making the approach practical to implement.

The variety of calibration algorithms that have been developed for the measurement structure show the properties of the calibration approach, which will be discussed in more detail in the next chapter. The properties that they portray are the ability to remove the measurement errors from the sensors and to reduce the impact of the errors associated with the directional couplers from the manipulation of the multiple measurements. This is possible while maintaining the ability to use independent sensors and transceiver elements. Another advantage to this is that there is not a requirement for

communication or precision elements. Whereas other approaches use a single sensor element, so therefore communication was not required.

4.9 Effectiveness of the Calibration Approach

The principles of this calibration approach have been discussed in terms of their practical implementation, and their motivation and calibration errors. So for a more visual understanding of this calibration approach its effectiveness is considered through a set of simulations of *4 by 4* planar array radiation patterns. The simulation presented will be a single incidence of an ideal, an uncalibrated and a predicted radiation pattern of a calibrated *4 by 4* array based upon results from the system. This gives a graphical representation of the effectiveness of calibration and an understanding of the significance of the calibration problem. A more detailed analysis of the performance of the calibration approach will be shown in Chapter 6, which follows an analysis of the various calibration algorithms developed for this calibration structure, presented in Chapter 5.

4.9.1 Ideal 4 by 4 Radiation Pattern

The radiation pattern of a 4 by 4 ideal array is shown in figure 4-9 from the 3D graph and a set of θ and Φ planes. This shows that the main and aft beams are symmetrical and the two sets of sidelobes for each are clearly visible and separated by deep nulls. This is presented in several formats to show the symmetrical lobe nature of the ideal pattern.

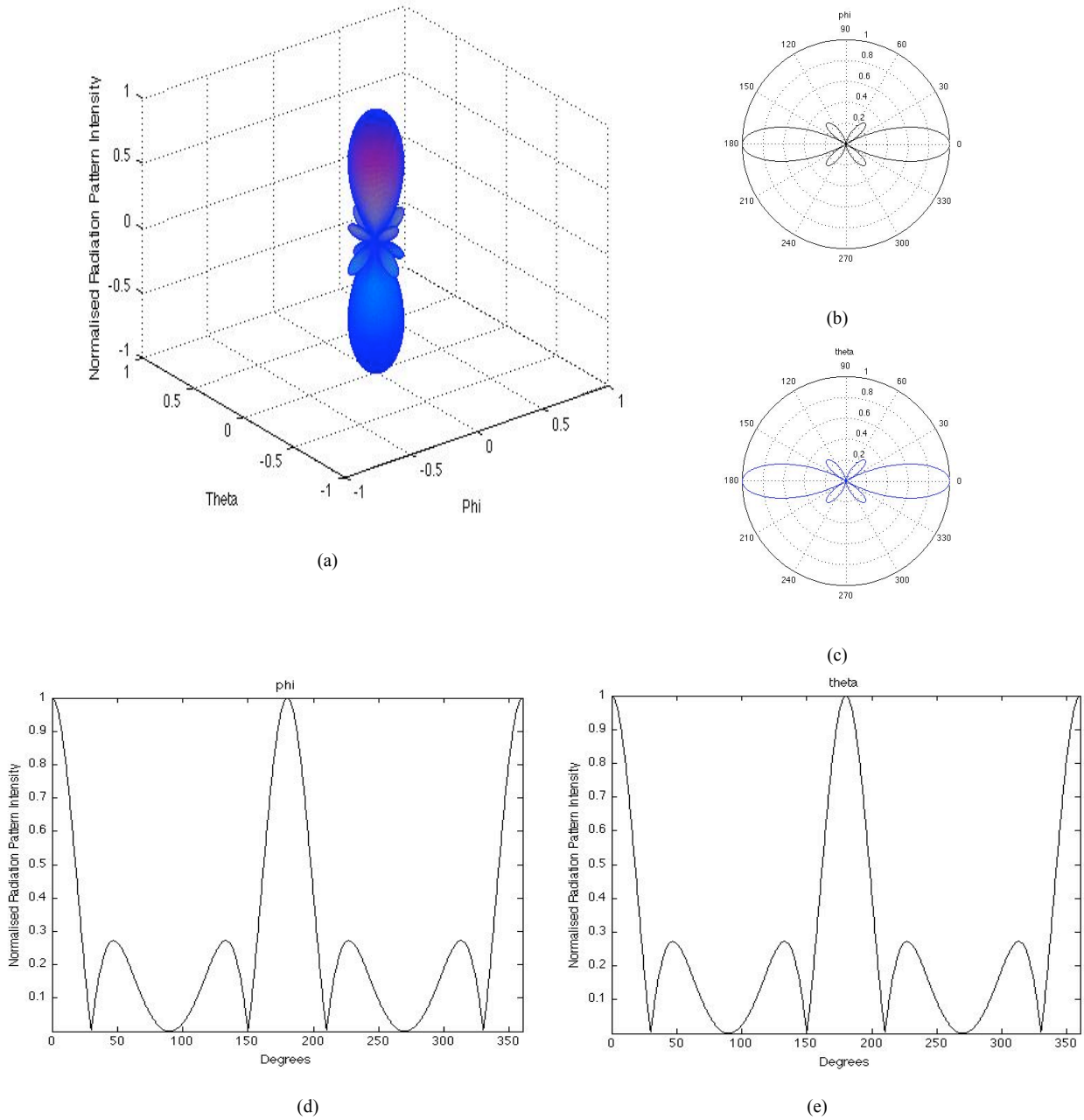

figure 4-9: Simulated Radiation Pattern of an Ideal 4 by 4 Planar Array, a) 3D plot of the Radiation Pattern, b) Polar plot of the Phi Cross-Section of the Radiation Pattern, c) Polar Plot of the Theta Cross-Section of the Radiation Pattern, d) Phi Cross-Section of the Radiation Pattern and e) Theta Cross-Section of the Radiation Pattern.

4.9.2 Uncalibrated 4 by 4 Radiation Pattern

The ideal pattern shows a symmetrical lobe nature of the radiation pattern. An uncalibrated array will distort this symmetry by the imbalances between its amplitude and phase relationships in the array. This is seen in figure 4-10 where the radiation pattern of an array was generated from randomly picked phase mismatch between 0 and 360 degrees and a 3 dB amplitude mismatch, the maximum, minimum and mean errors on an array elements are shown in table 4-10. The figure clearly shows the distortion of

the main and aft lobes in their shape and location. The sidelobes are also distorted, where they merge together and their shape and location has also been altered. The nulls of the pattern are also degraded. All of this combines to make an unrecognisable radiation pattern.

Table 4-1: Uncalibrated Array Element Errors which Generate the Radiation Pattern in figure 4-10.

Uncalibrated Array Element Errors	Amplitude	Phase
Maximum	5.4dB	163.2^{o}
Minimum	0.2dB	1.3^{o}
Mean	2.2dB	70.7^{o}

4.9.3 Calibrated 4 by 4 Radiation Pattern

Figure 4-11 displays the radiation pattern for a calibrated *4 by 4* array. This array is calibrated by the Dual Path calibration algorithm, which will be covered in much more detail in the next chapter, where the algorithm is used to calibrate a model of a practical antenna array. The radiation pattern that it produces is much easier to equate with the ideal radiation pattern, where the main and aft lobe are symmetrical. The sidelobes are clearly visible though a little larger or smaller then the ideal as the sidelobes of the radiation pattern is very sensitive to any array errors. The null depths that separate the sidelobes are shallower then the ideal but still clearly separate the sidelobes from the main and aft beams. When compared to the uncalibrated version, it is clear that the calibration algorithm shows vast improvement over an uncalibrated system. It will be shown in the next chapter that this approach achieves sufficiently good performance for use in a commercial system.

These results represent a single simulated example of the impact of this calibration approach to give an idea of the effectiveness of this approach. The next chapter will present a much more in-depth representation of the calibration algorithms that were designed for this measurement structure, presenting the manipulation of the algorithms of the structure to calibrate the array.

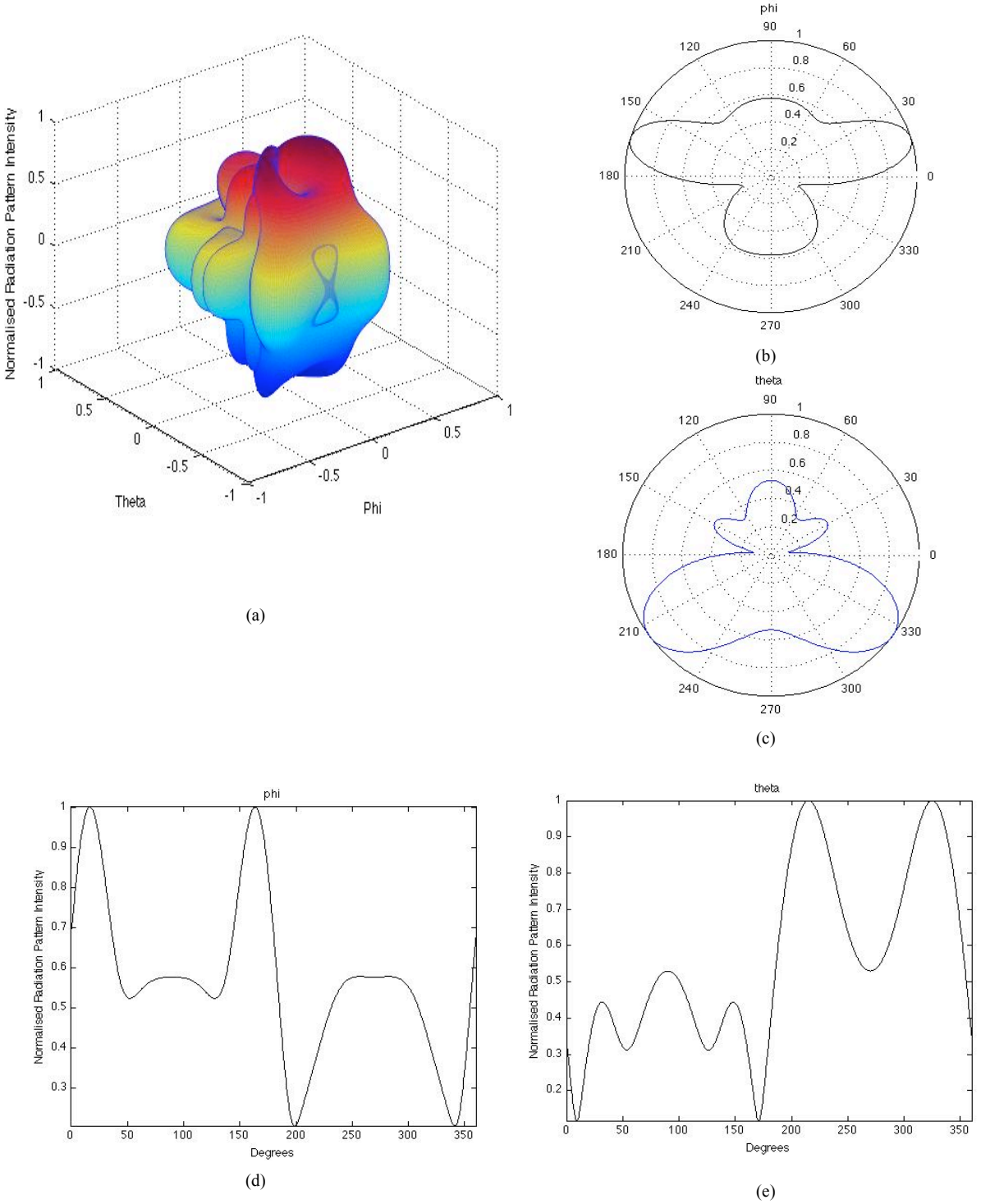

figure 4-10: Simulated Radiation Pattern of an Uncalibrated 4 by 4 Planar Array, a) 3D plot of the Radiation Pattern, b) Polar plot of the Phi Cross-Section of the Radiation Pattern, c) Polar Plot of the Theta Cross-Section of the Radiation Pattern, d) Phi Cross-Section of the Radiation Pattern and e) Theta Cross-Section of the Radiation Pattern.

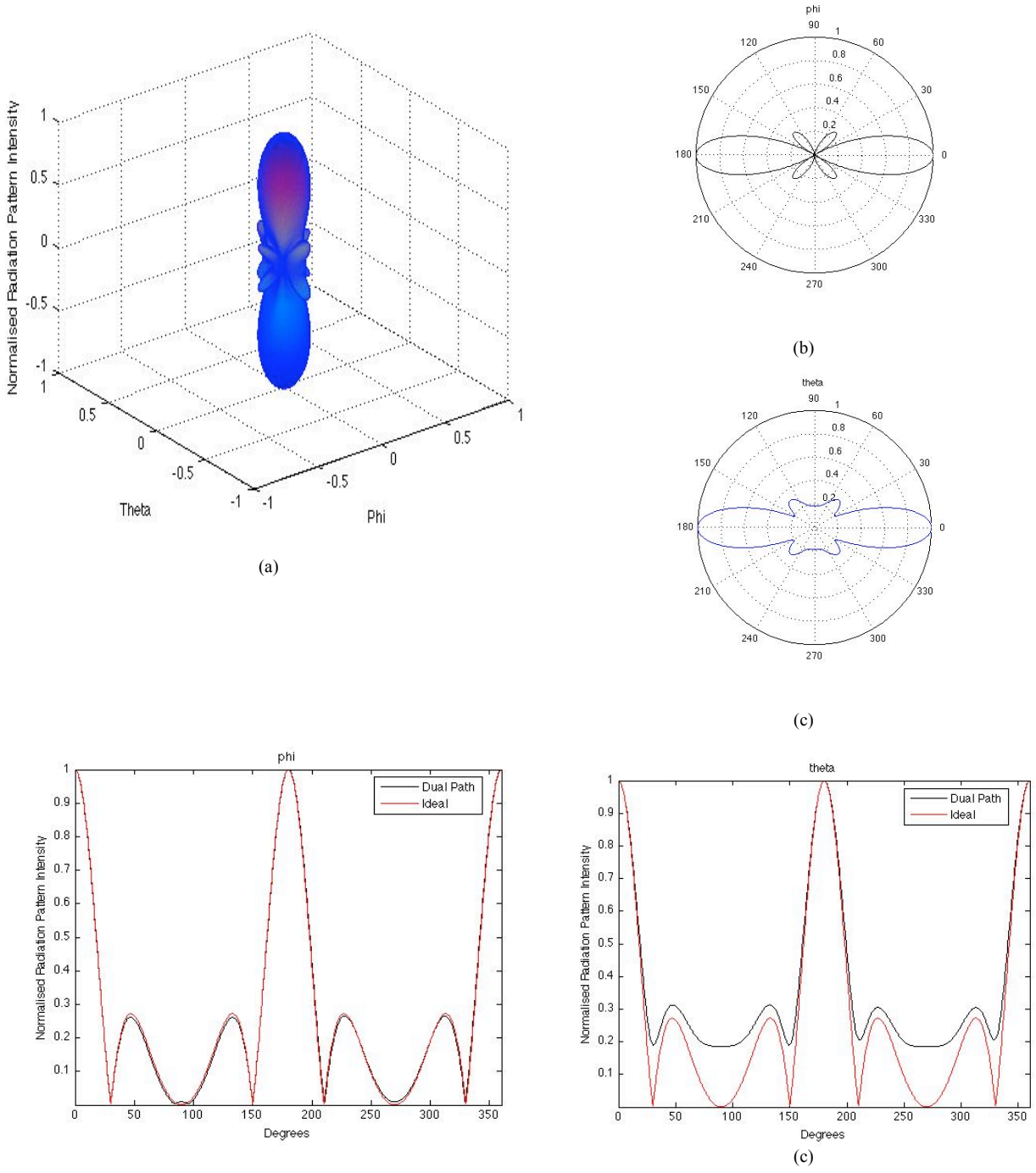

figure 4-11: Simulated Radiation Pattern of an Dual Path Calibrated 4 by 4 Planar Array, a) 3D plot of the Radiation Pattern, b) Polar plot of the Phi Cross-Section of the Radiation Pattern, c) Polar Plot of the Theta Cross-Section of the Radiation Pattern, d) Phi Cross-Section of the Radiation Pattern which is compared with the Ideal Radiation Pattern and e) Theta Cross-Section of the Radiation Pattern which is compared with the Ideal Radiation Pattern.

4.10 Summary

This calibration approach is based upon a measurement structure, which has been developed to be scalable and allow a dynamic calibration system that does not require any external hardware. This approach utilises a novel measurement structure based upon overlapping tiles of four element circular arrays to create a scalable planar array. The

structure uses a unique six-port coupler to provide the required symmetrical connectivity for the calibration and to scalably link the measurement tiles.

This structure has the ability to provide calibration for any communication system by the appropriate choice of measurement sensor. By utilising the built-in redundancy of this structure, the sensors do not need to communicate with each other or need to have matched performance. Algorithms can take advantage of this multiple sensing so that enhanced performance and robustness to errors can be achieved.

The next chapter will present in detail a number of calibration algorithms that have been developed specifically for this measurement structure to show the capabilities of the system, the properties of the structure and the significance of the choice of calibration algorithms.

Chapter 5

The Algorithmic Investigation

5.1 Introduction

The measurement based calibration approach taken by this dissertation has been outlined in the previous chapter. As was pointed out the measurement structure needs to be utilised by an algorithmic-based calibration approach to fully realise the potential of the system. The measurement structure provides a means of scalable and non-radiative calibration. However, due to the multiple measurement devices, the algorithmic-based calibration approach needs to be designed specifically for the structure and to minimise the potential of the structure and the measurement devices as possible sources of calibration errors. This chapter will present a range of such calibration algorithms to show various effective approaches applied to this measurement structure. The calibration algorithms range from simple measure and correct principles through to inter-element comparison calibration and onto more complex optimization approaches. These algorithms are compared based upon simulated predictions of their performance to identify the viable candidates for experimental testing.

5.2 Calibration Algorithms

The calibration algorithms utilise the non-radiative measurement structure that provides multiple measurement paths. This provides a scalable structure, but with multiple measurement paths and measurement devices or sensors. There are multiple sources of measurement errors contributing to the inaccuracy of the calibration. Therefore, the algorithms are important in mitigating these effects upon the calibration. To illustrate the significance of the calibration algorithms, a series of algorithms are presented and developed specifically to utilise the structure to its full extent. These calibration approaches are designed to utilise the measurement structure in different ways and are grouped into four categories, which are:

- Error Comparison Algorithm
- Reference Element Algorithms
- Optimization Algorithms

- Multipath Algorithms

5.2.1 Error Comparison Algorithm

The error comparison algorithm is a calibration approach that measures the elements of the array and then compares the measurements. This is the simplest calibration algorithm, and is also called the measure and correct algorithm. It is the simplest algorithm because it does not consider the measurement structure as a source of errors. The reason it is included in this discussion of the development of calibration algorithms is that it provides insight into the measurement structure and the significance of including it as a source of errors for the calibration accuracy.

5.2.1.1 Procedure

The measure and correct procedure is simple, as has previously been mentioned. It measures each element of the array by only one of their measurement sensors. As the elements of the array are connected to multiple measurement sensors, as shown in Figure 5-1, the selection of which sensor to use is purely arbitrary. For discussion, it was decided to measure the elements using the sensor below and to the left, when there is a choice. These measurements are taken and averaged over the whole array. This average is then used as the reference measurement for the array and the each individual element's measurement is compared to it and that comparison is then used to calibrate the element. This calibrates all of the elements of the array to a single value.

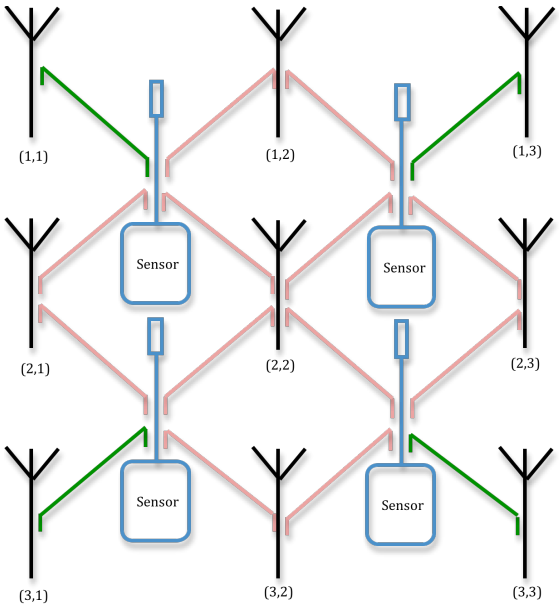

Figure 5-1: Multiple Measurement Paths (in pink) Provided by the Measurement Structure.

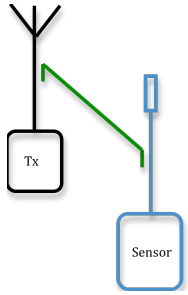

Figure 5-2: A Single Calibration or Measurement Path.

5.2.1.2 Simulation Results

Before a discussion of the simulation results can take place the simulation methodology must be presented. The simulations of the algorithmic performance are based upon a model of the antenna array upon which the calibration algorithms are implemented. The antenna array is modelled using component blocks, which are randomly generated based upon a mean value and normal distribution of errors with a standard deviation; these are presented in Table 5-1, which was derived from experimental measurements described in chapter 6 in section 6.2.3. For simplicity, the antenna array is modelled by a transmitter array, so each measurement path contains an input signal, a transmitter block, a coupler path and a sensor element, which is more clearly seen in Figure 5-2. These component blocks are varied randomly based upon the mean value (μ) and standard deviation (σ) from Table 5-1 to give each array a unique value. Once the non-ideal array is defined the algorithm is applied to this model to calibrate the array. Each set of present simulation results is a result formed from 10,000 of these calibrated arrays.

Now that the principles of the simulations have been presented, the simulation results for the measure and correct calibration algorithm will be discussed. As is clear from the description of the algorithm, it does not consider the structure of the array and therefore is does not consider the measurement structure as a source of errors. Therefore when considering the performance of the measure and correct algorithm, the distribution of

Table 5-1: Component Block Imbalances.

Component$_{(i,j)}$	$\mu_{(i,j)}$ Amp	$\sigma_{(i,j)}$ Amp	$\mu_{(i,j)\,\phi}$	$\sigma_{(i,j)\,\phi}$
Tx S_{21}	50dB	3dB	10^o	5^o
Sensor S_{21}	60dB	6dB	85^o	5^o
Coupler S_{21}	20.3295dB	0.3295dB	90.197^o	1.1175^o

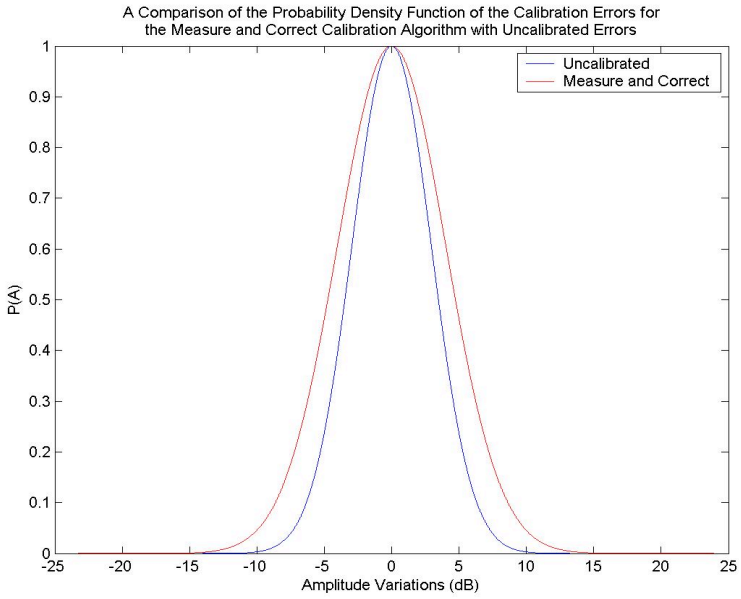

(a)

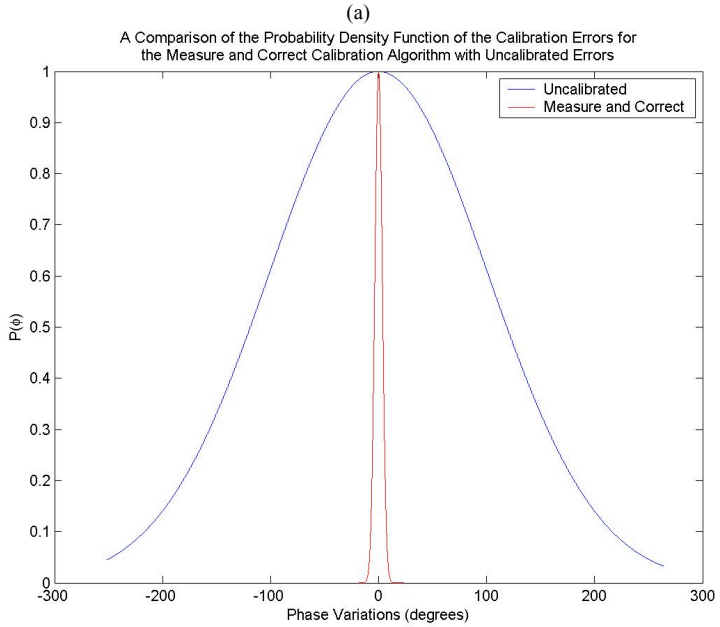

(b)

figure 5-3: The Probability Density Function of the Calibration Errors for the Measure and Correct Calibration Algorithm compared with Uncalibrated Errors for 10,000 Omnidirectional 4 by 4 Planar Arrays, (a) Amplitude and (b) Phase.

calibration errors for a single array size is considered. This is shown in figure 5-3, and it is the distribution of an omnidirectional 4 by 4 planar array.

This distribution shows a large standard deviation of errors. This is made up of the contributing factors of the multiple measurement device errors, the transceiver element and the measurement structure errors in the averaged signal of the reference signal that are included into the calibration of each element of the array. This can more clearly be seen from the theoretical prediction of the accuracy of the calibration algorithm, which

is derived in Appendix A, and presented by the next equation, which theoretically predicts the errors that impact upon the calibration of each element of the array.

$$\sigma_A = (N-2)\sigma_S + (N-2)\sigma_{TRx} + (N-1)\sigma_{Coupler} + (N-1)\sigma_{Sensor}\left(\sigma_S + \sigma_{TRx} + \sigma_{Coupler}\right) \quad (5.1)$$

where σ_A is the standard deviation of the array,

σ_S is the standard deviation of the input signal,

σ_{TRx} is the standard deviation of the transceiver component block,

σ_{Senor} is the standard deviation of the measurement sensor component block,

$\sigma_{Coupler}$ is the standard deviation of the directional coupler path that makes the measurement paths,

and N is the number of elements in the array, $N = n \times n$.

As can be seen from the theoretical prediction, the element errors are not reduced by the size of the array, as they are the same for each element of the array regardless of size. Therefore the standard deviation error of the whole array will decrease as the size of the array increases as there is more cancellation of the random errors. This can be seen from the predicted simulated performance of the measure and correct algorithm as the size of the array increases as shown in figure 5-4, the bounding effect in these graphs is an averaging effect. Omnidirectional antennas are used they have uniform radiation patterns and is an ideal antenna.

5.2.1.3 Summary

The measure and correct calibration algorithm is very ineffectual as it does not consider the structure of the antenna array and the possible sources of errors it can introduce. So that the calibration errors incorporate the errors introduced from the measurement structure. These errors show that the measurement structure is not considered as a source of errors, which can be seen here is a significant impediment to the calibration accuracy of the algorithm. This approach does not utilise the additional information that arises from the overlapping tiles and multiple measurements. This highlights some of the issues that the other algorithms will endeavour to overcome by using the features of our measurement network.

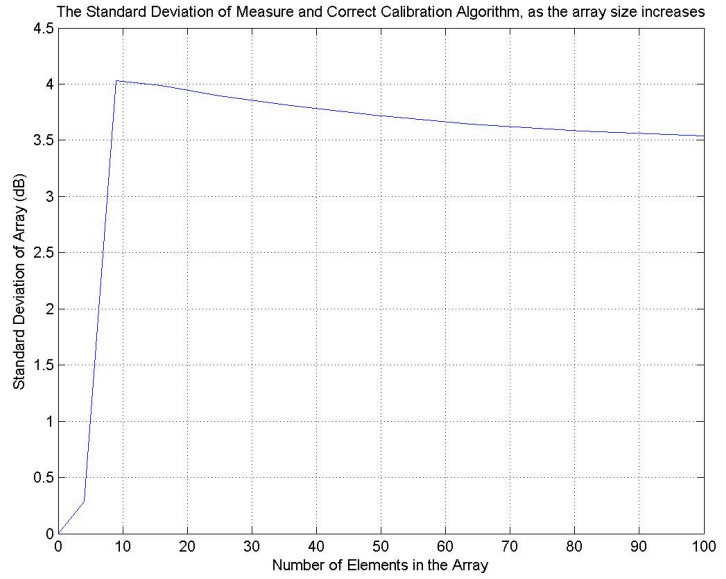

(a)

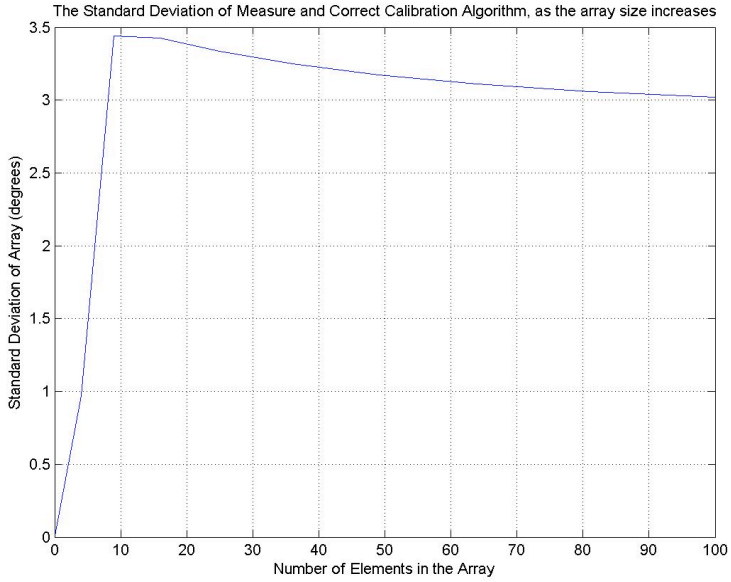

(a) (b)

figure 5-4: Comparison of the standard deviation of square omnidirectional planar arras as the size of the array increases, (a) amplitude and (b) phase.

5.2.2 Reference Element Algorithms

The reference element calibration algorithms take a different approach to the calibration of the array, as they select an element in the array to use as a reference and then each of the remaining elements of the array are calibrated to this reference element. This approach has the benefit of considering the measurement structure, taking multiple measurements and using them to calibrate the array. The choice of the reference element is significant in these approaches as it will dictate the quantity of calibration errors that

are included in the elements on the array. To show this effect, two different reference element comparison based algorithms are considered here; these are:

- Top Left Reference Element Calibration Algorithm,
- Shortest Path Calibration Algorithm.

5.2.2.1 Top Left Reference Element Calibration Algorithm

As previously mentioned, these reference element based calibration techniques are comparison based approaches, that is to say that a reference element is chosen and its measurements are then compared to the measurements of its nearest neighbours. Then these nearest neighbours are assigned as intermediate reference elements and the calibration is extended to the whole array.

5.2.2.1.1 Procedure

The top left reference algorithm chooses the reference element in the top left corner of the array. The reference element is then measured only by the measurement sensor connected to it. The same sensor is then used to measure the other elements connected to it, as shown in figure 5-5. These measurements are then compared to the measurement of the reference element. Correction factors are calculated in order to match all the array elements to that of the reference element, where each elements amplitude and phase are modified to calibrate them using this corrections factor, which is an amplitude and phase values used to correct the input signals of the transceivers.

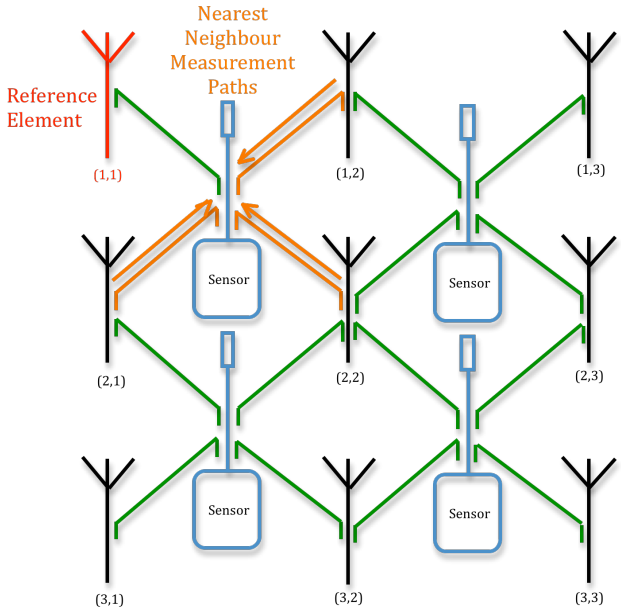

figure 5-5: The first step in the comparison based approach used to calibrate the reference element based algorithm.

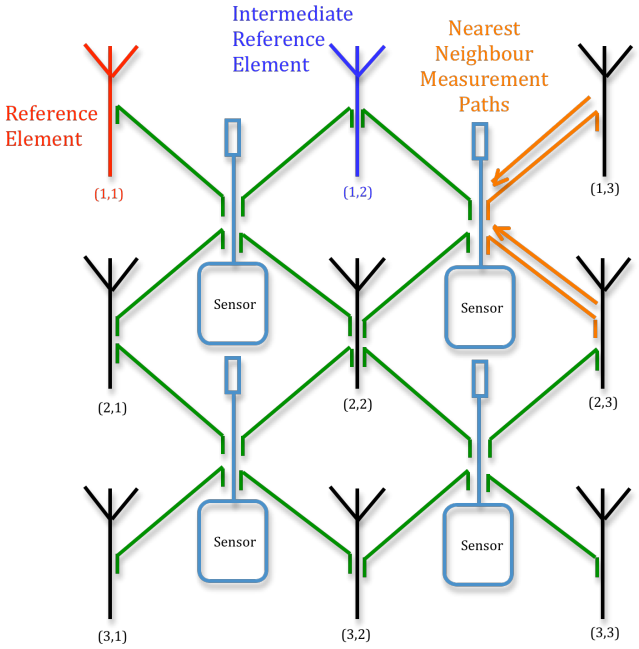

figure 5-6: The second step in the comparison based approach used to calibrate the reference element based algorithm.

These intermediate reference elements are then used to calibrate the next set of elements. This is achieved by measuring the intermediate reference element from another measurement sensor and then measuring the elements connected to that sensor and comparing those measurements, as shown in figure 5-6. The intermediate reference element is defined as the top-left element for the new tile. This element has been calibrated in the previous iteration.

These local comparisons of the measurements are the key to the propagation of the calibration through the elements of the array. Each new intermediate reference point has been previously calibrated and thus enables the local calibration of the new tile. The local comparisons allow any error contributed by the sensor to each measurement is not included in the correction factor.

This approach is superior to the "measure and correct" approach as it avoids the errors arising from mismatch between the measurement sensors, by using comparisons. At each stage the correction is calculated relative the top-left element of the tile. When the top-left element is an intermediate reference, then the newly correct elements will be matched not only to the top-left element but also to the elements calibrated in all previous tiles. In this manner, the relative measurement means that measurement sensor errors are avoided.

A detailed analysis of the error mechanisms is presented in Appendix B and the expected error is shown below. From this, it can be seen that measurement device error is no longer contributing but coupler errors still persist. Thus showing that the accuracy is dependent upon the coupler performance.

$$\sigma_A = \frac{\sigma_{Coup}}{N-1}\left(\frac{n\left(4n^2-3n-1\right)}{6}\right) \tag{5.2}$$

where σ_A is the standard deviation of the calibration error of the whole array,

N is the total number of element in the array, $N = n \; x \; n$,

and $n \; x \; n$ is the total number of element in the square array.

5.2.2.1.2 Simulation Results

To demonstrate performance, the top left reference calibration algorithm's performance is compared to that of the "measure and correct" approach to show the improvement in performance. The difference will be due to the avoidance of sensor errors. The superior performance can be seen by comparing the distribution of the errors of the measure and correct algorithm with that of the top left reference one, for simulation of the 10,000 omnidirectional 4 by 4 planar arrays, as seen in **(b)**

figure 5-7.

The difference in the spread of the distribution shows the significance of including the measurement sensor in the consideration of the calibration techniques effectiveness. The top left reference algorithm removes the measurement sensors as a source of errors but the other source of errors from the measurement structure is that of coupler path errors, and it is clear from the theoretical prediction of the accuracy of the algorithm that as the size of the array increases so does the number of coupler paths used to calibrate the array. Therefore as the array size increases, the standard deviation of the errors also increases, as shown in figure 5-8, unlike the measure and correct algorithm.

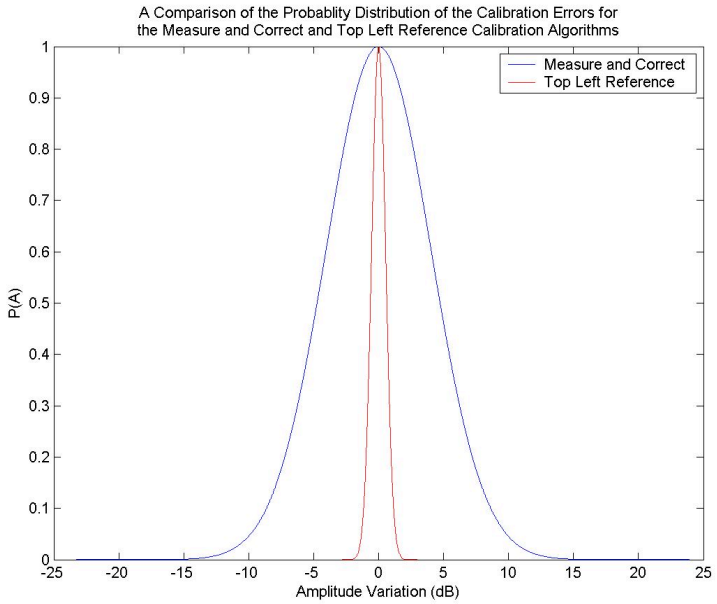

(a)

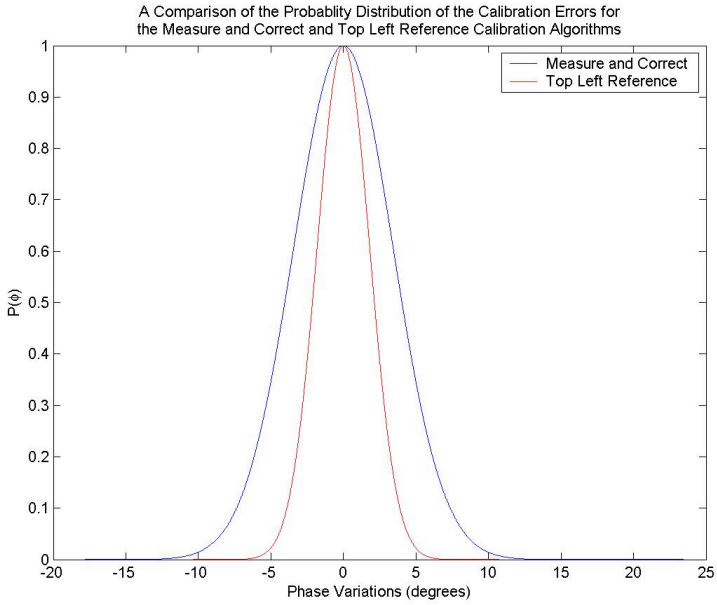

(b)

figure 5-7: The Comparison between the Probability Density Function of the Calibration Performance of the Top Left Reference and the Measure and Correct Calibration Algorithms for 10,000 omnidirectional 4 by 4 Planar Arrays, (a) Amplitude and (b) Phase.

5.2.2.1.3 Summary

This top left reference calibration algorithm takes into account the measurement structure, but due to the location of the reference element, there are a considerable number of coupler paths included in the calibration. The array can have significant calibration error due to the number of coupler paths included in the calibration, as predicted by equation (1.2).

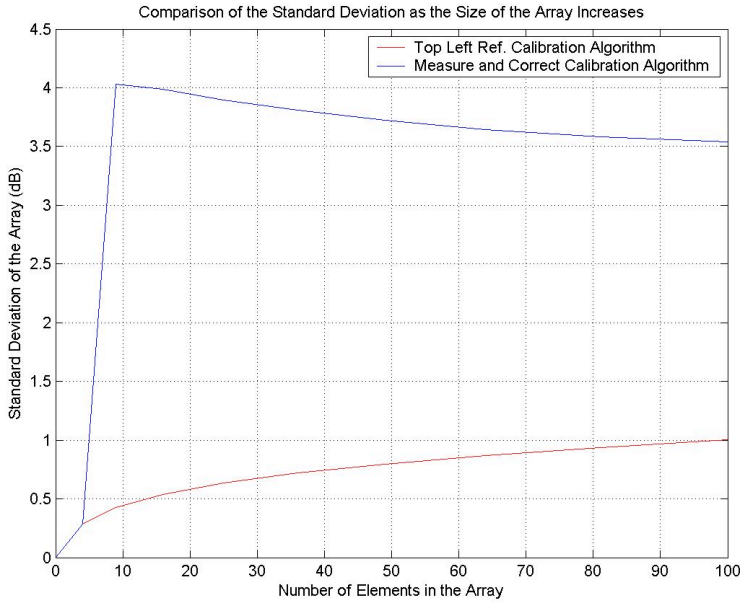

(a)

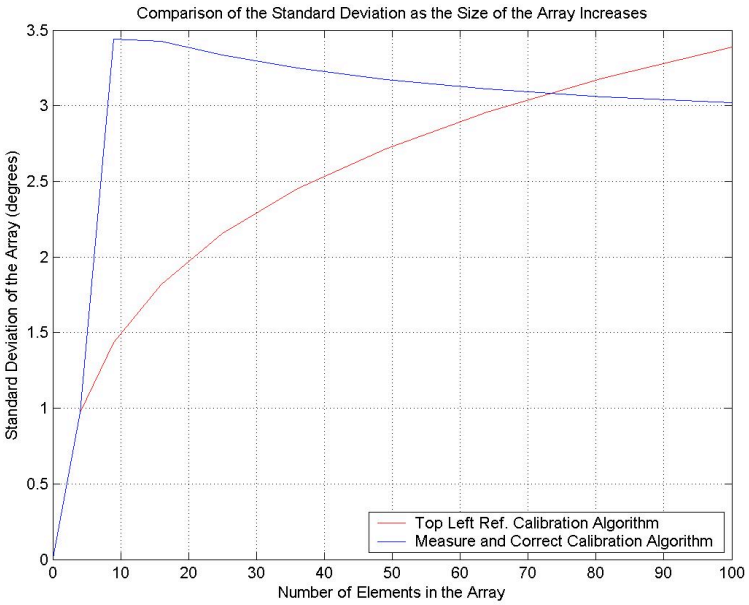

(b)

figure 5-8: Comparison of the Standard Deviation of the Calibration Errors for the Measure and Correct and Top Left Reference Calibration Algorithms of Square Omnidirectional Planar Arrays as the Size of the Array Increases, (a) Amplitude and (b) Phase.

5.2.2.2 Shortest Path Calibration Algorithm

The choice of the reference element's location is important, as shown by the top left reference calibration algorithm, as the comparison based algorithm's accuracy is apparent by the number of coupler paths taken to the elements of the array from the reference element. The optimum reference element location would therefore be the centre of the array. The choice of paths through the array is also significant as it will dictate the number of coupler paths contributing to the calibration accuracy.

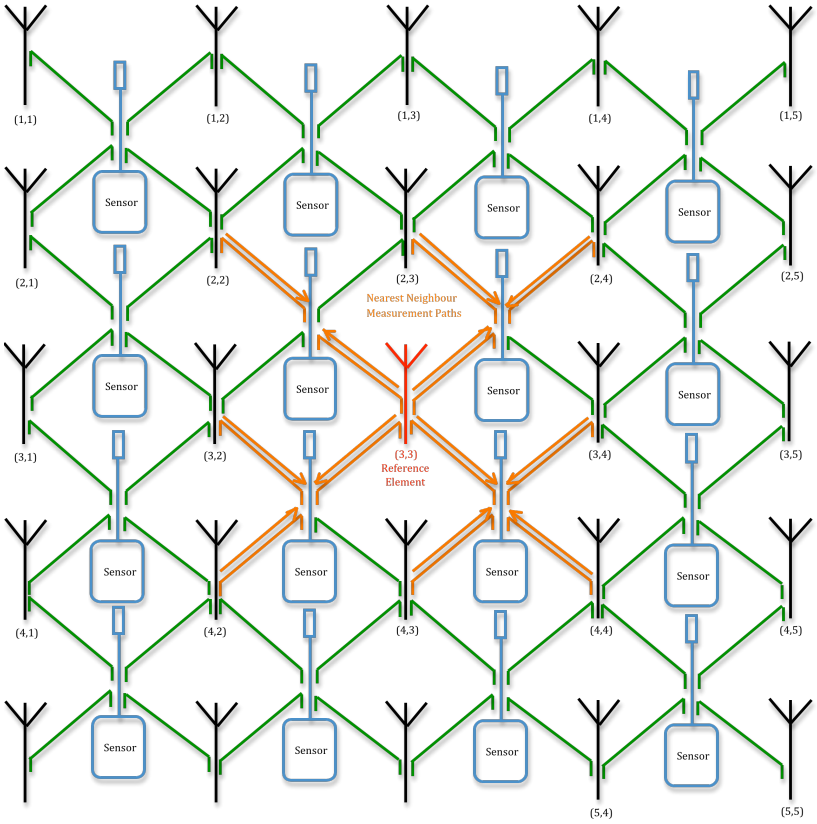

figure 5-9: The First Step in the Comparison based Approach used to Calibrate the Shortest Path Reference Based Algorithm.

5.2.2.2.1 Procedure

As mentioned, the shortest path calibration algorithm selects a reference element located at the centre of the array. When the array does not have a single central element, the element is chosen to be the top left element of the central quartet. This is an arbitrary selection but chosen thus to be consistent. From this the reference element is measured by the sensors connected to it. Then this sensor measures the nearest neighbours and the comparisons are done using the same measurement sensors, this is more clearly seen in figure 5-9.

These elements are then calibrated based upon these comparisons. The elements are then selected to be intermediate reference elements. These intermediate references are then used to calibrate the elements further out, by the shortest path to each element. This is shown in more clearly in figure 5-10, where the next circle of elements is shown (in blue).

These comparisons are, as before, the basis of the propagation of the calibration. From the location of the reference element, the number of couplers between the starting

element and the element being calibrated is reduced. Therefore the accuracy of the calibration is improved. This is predicted by the following equations, which are derived in Appendix C, which again highlight that the accuracy of this calibration approach is solely limited by the coupler performance.

When *n* is even:

$$\sigma_A = \frac{\sigma_{coupler}}{N-1}\sum_{i=1}^{\frac{n}{2}-1}(8i)(i) + \frac{2n-1}{N-1}\frac{n}{2}\sigma_{coupler} \tag{5.3}$$

When *n* is odd:

$$\sigma_A = \frac{\sigma_{coupler}}{N-1}\sum_{i=1}^{\frac{n-1}{2}}(8i)(i) \tag{5.4}$$

5.2.2.2.2 Simulation Results

As these reference algorithms are dependent upon the number of coupler paths included in the calibration of each element of the array, the choice of reference element location is very significant in the accuracy of the resulting calibration. To more fully see this, the distribution of calibration errors of the shortest path algorithm is compared with that of the top left reference element's distribution for a 4 by 4 omnidirectional planar array, in figure 5-11; this shows the improvement offered by the relocation of the reference element and the choice of calibration path taken to each element. These figures show the improvement in both the amplitude and phase calibration errors. Therefore, the reduction in the number of coupler paths taken through the array has an impact upon the calibration accuracy in these comparison based calibration approaches. This is also reinforced when the standard deviation of the calibration errors is considered for both algorithms as the size of the array increases, as shown in figure 5-12.

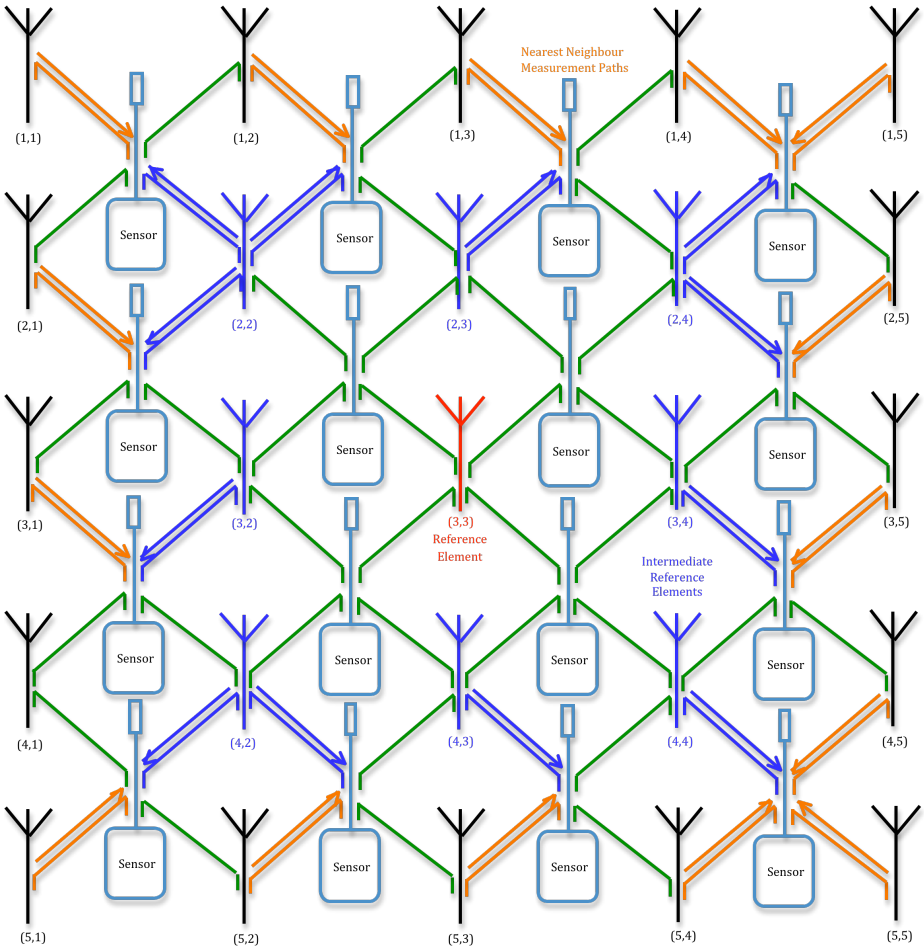

figure 5-10: The Second (Blue) and Third (Red) Steps in the Calibration based Approach used to Calibrate the Shortest Path Reference Based Algorithm.

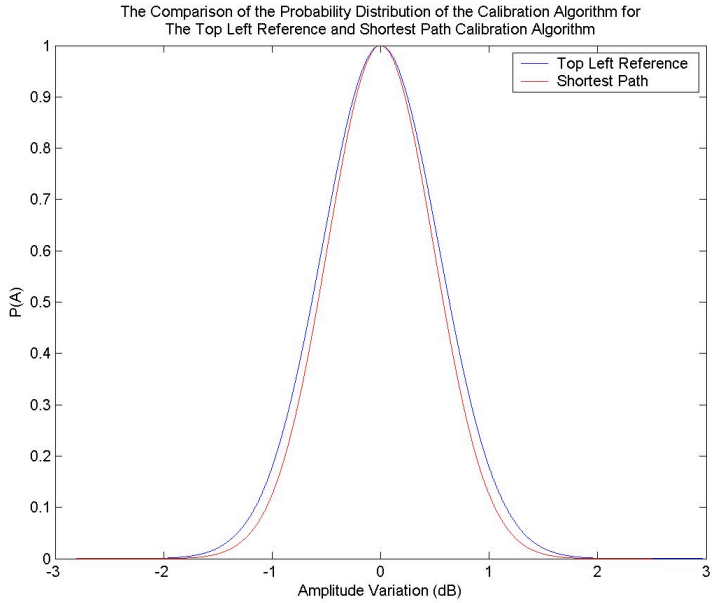

(a)

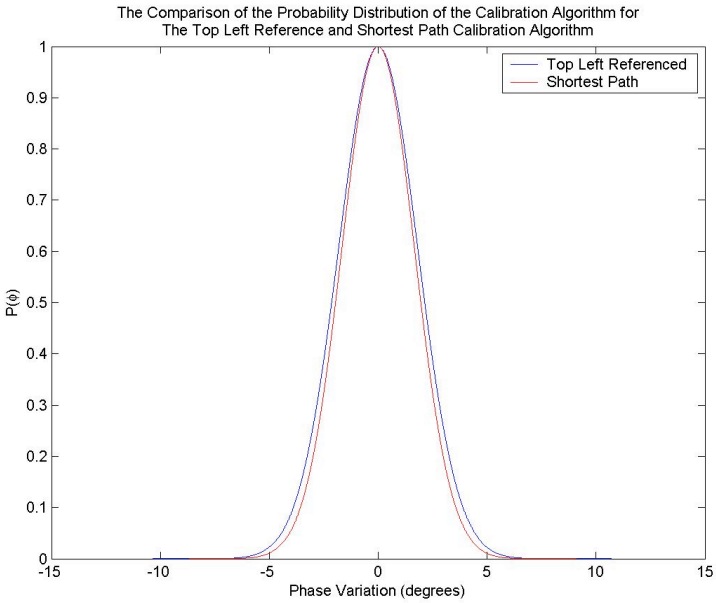

(b)

figure 5-11: The Comparison between the Probability Density Function of the Calibration Errors for the Top Left Reference and the Shortest Path Calibration Algorithms for 10,000 omnidirectional 4 by 4 Planar Arrays, (a) Amplitude and (b) Phase.

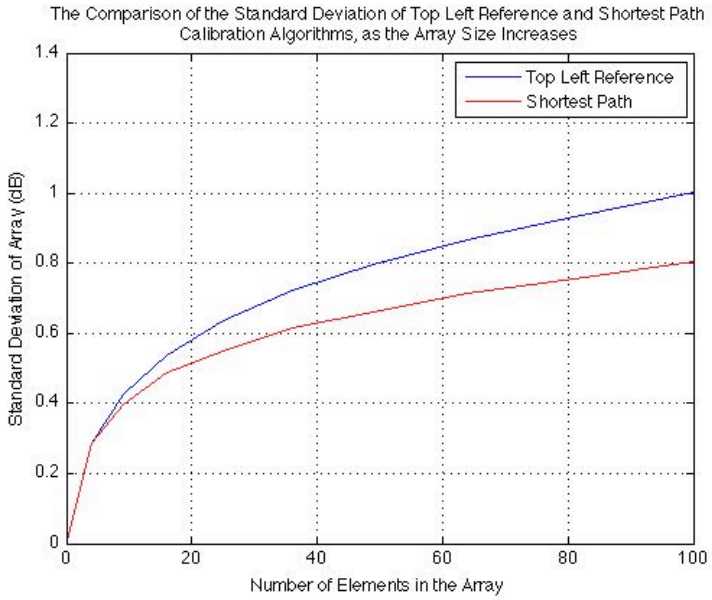

(a)

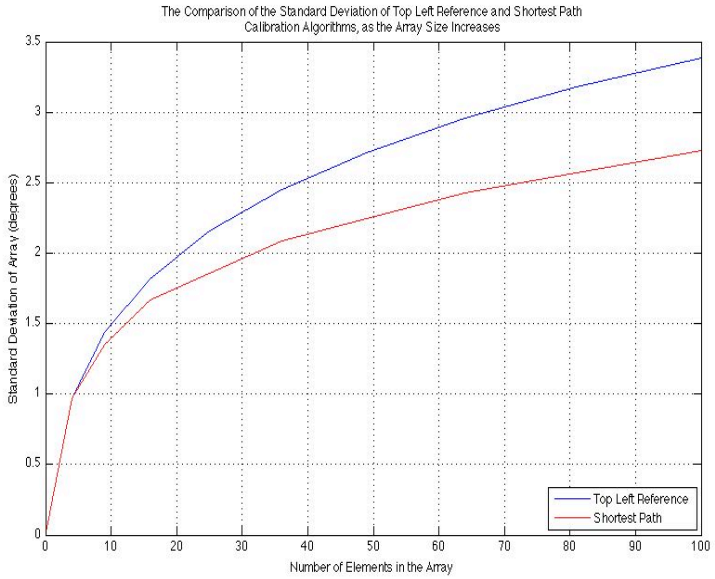

(b)

figure 5-12: Comparison of the Standard Deviation of the Calibration Errors for the Top Left Reference and Shortest Path Calibration Algorithms of Square Omnidirectional Planar Arrays as the Size of the Array Increases, (a) Amplitude and (b) Phase.

5.2.2.2.3 Summary

The shortest path algorithm was designed to utilise the comparison based approach to calibration that was presented with the top left reference algorithm using a reference element was the subsequent intermediate reference elements to calibrate the whole array by utilising the multiple measurement paths provided by the measurement structure. It however attempts to overcome the top left reference algorithms dependence upon the number of directional coupler paths included in the calibration of the elements of the

array by moving the reference element to the centre of the array, and then taking the path with the least number of couplers to each element of the array. This does not eliminate the dependency of these algorithms upon the coupler structure but it does reduce its impact upon the individual elements of the array – particularly for larger arrays. This can be seen from the improved calibration accuracy achieved by these alterations to the top left reference algorithm.

5.2.3 Optimization Algorithms

The previous calibration algorithms, "measure and correct", top left reference and shortest path reference, only use a subset of the available measurement paths that exist within the measurement network. These unused paths are most visible for the shortest paths, in figure 5-13. The objective was to utilise optimisation algorithms, developed in other areas, to give a heuristic method of utilising these redundant, un-used paths. The optimisation approach that was adopted for this calibration technique was that of simulated annealing, due to its global optimisation approach. There was a concern that this simulated annealing approach could get caught in a local maximum that would be disastrous for overall array performance. Simulated annealing was found to be ineffectual as it had no knowledge of the measurement structure and therefore was as susceptible to the measurement structure errors as the "measure and correct" calibration algorithm. Due to the approach taken to implement the simulated annealing algorithm, the elements at the edge of the array are much more affected by these errors, so a reduced simulated annealing approach was used to try and combat this, though this was of limited success. The following sections detail the implementation of these two approaches and discuss the challenges faced by an unguided optimisation approach.

5.2.3.1 Simulated Annealing Calibration Algorithm

A tolerance-based approach was taken to implement the simulated annealing, thus making the evaluation criteria of the algorithm hard to implement as the measurement structure will distort any criteria based upon it. The measurement structure does not allow access to the antenna feed point, as this point is connected to the measurement structure and is highlighted in the discussion of an alternative measurement structure. It is therefore a source of errors as the measurements will be distorted by the contribution of the measurement structure. For the purposes of exploring this approach, the criterion for success was selected as the variation in the transmitter block estimation. Where the

transmitter block estimation is the algorithm's estimation of the contribution of the transmitter upon the output signal. This was chosen as the criteria for success as the optimum measurement of success would have been the signal at the connection between the transceiver and the antenna. This is however not possible as the measurement device adds its own errors to this signal.

5.2.3.1.1 Procedure

The simulated annealing approach is based upon the idea that if the component values are known then the input signal could be corrected for the variations that affect the output and not the rest of the variations along the calibration path. This is done by using the multiple measurements for each antenna element provided by the structure of the array. This process will be described for the transmit calibration for greater ease of

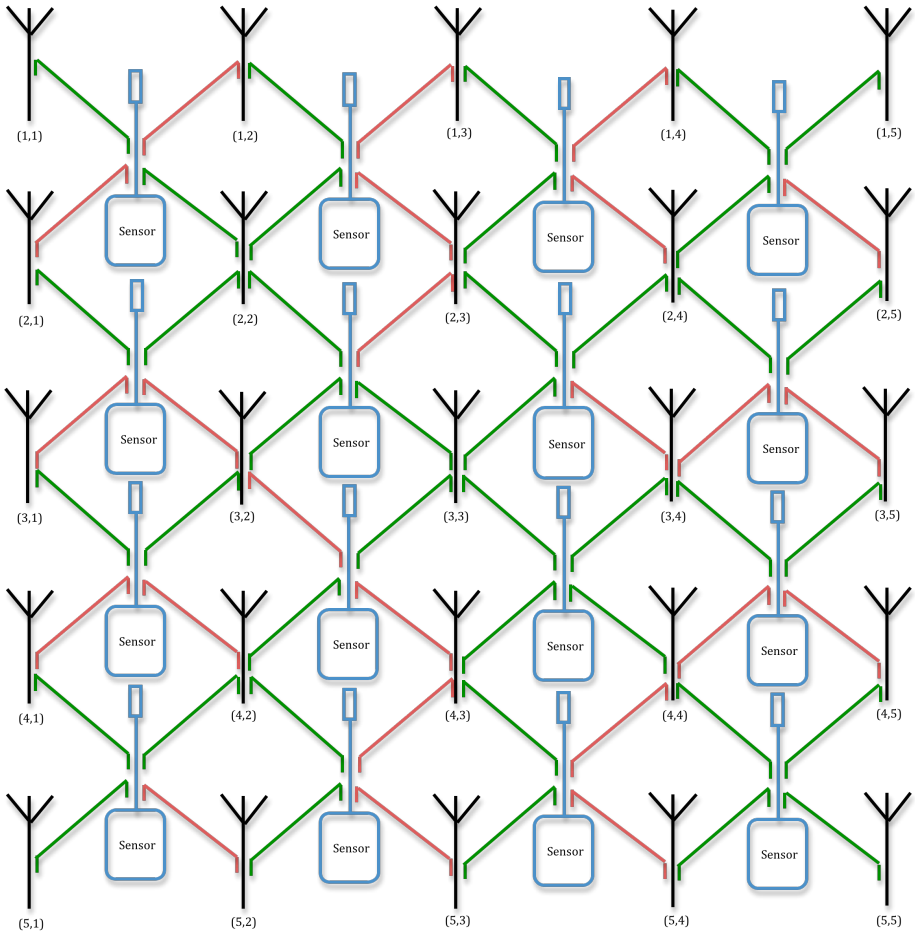

figure 5-13: The Redundant Paths, which are highlighted in red, in the Measurement Structure in the Shortest Path Implementation.

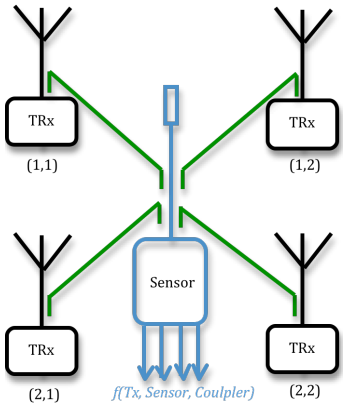

figure 5-14: The Four Measurements taken by a Single Measurement Sensor.

understanding. These measurements correspond to the component blocks of the calibration paths whose value vary around the mean value with a normal distribution with a known standard deviation. The calibration begins by measuring the whole array, which can clearly be seen by the four measurements represented in the 2 by 2 array in figure 5-14. The measurements taken for the array are split into groups of four, these groups based upon the measurement sensor that took the measurements. These measurements are a function of the proximate coupler, sensor and transmitter contributions to the input signals. These measurements are then compared to the mean transmitter block, input signal, sensor block and coupler block contribution, with one standard deviation variation from their means. Any values that lie outside this distribution is classed as an outlier and removed from the comparison as it would throw off the prediction. The remaining error measurements, without the outliers, are averaged and are used to estimate the reference blocks variations from its mean.

The second phase is to estimate the transmitter block. This is possible due to the multiple measurements taken by the multiple sensors connected to the transceiver elements of the array. These are more clearly seen in figure 5-15. Therefore the function equivalent of the first step is to measure each transmitter by the four neighbouring sensor elements. These measurements are corrected for the sensor block values of each individual sensor element made in the first stage. These vary due to the different coupler paths taken away with again the sensor error's inferred value taken as a known quantity. Based on this assumption, the resultant error signals are a function of the coupler variation due to the different coupler paths and the common transceiver element alone.

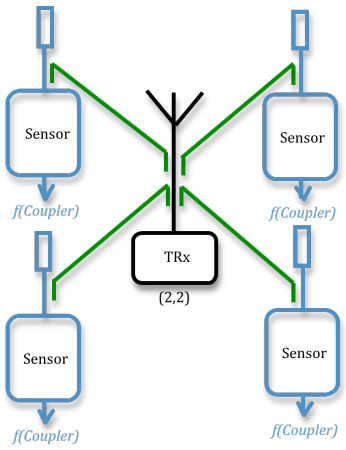

figure 5-15: The Four Measurements taken of a Single Transceiver Element, by Four Measurement Sensors.

By extrapolating the transmitter error by using the same process of discarding outliers and averaging the coupler variations may be calculated. These coupler variations are then removed from the measurements by averaging. This average is taken to be the common elements transmitter and signal variation values. Thus the variation due to only the contributing error factors to the array output are used to calibrate the array. This iterative process is repeated until the transmitter block estimation is ± 5% of the last estimation. This was chosen as the cut off criteria as the output of the array is accessible to the calibration approach.

5.2.3.1.2 Simulation Results

This optimization approach was not successful. It made faulty assumptions about the impact of the measurement structure upon the measurement signals. These compounded assumptions led to an ineffectual calibration approach since the iterative process spread the errors through the array rather than eliminating them. At each successive iteration, the dependency of the weighting error signal spread in successive concentric circle of array elements surrounding the reference. Consider element *(2, 3)* in figure 5-16, where after each iteration, a circle of elements represent the errors associated with element *(2,,3)*. As the figure shows, the contributing errors increase as the iterations increase, but in reduced amounts, thus improving calibration as well as sources of errors. This is more clearly seen in figure 5-18, which show the standard deviation of the calibration error for the *4 by 4* array for each iteration. As it is a heuristic algorithm, it shows the improvement as the number of iterations increases. This shows that the algorithm starts

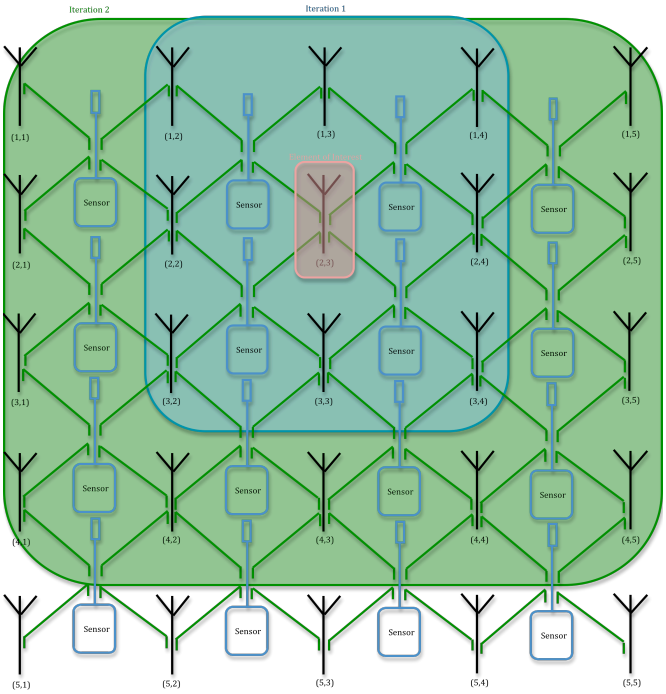

figure 5-16: The Concentric Circles of Errors Distributions of Element (2, 3) as the Simulated Annealing Progresses Through its Iterations.

off well, but due to an inability to access the output of the array the cut off criteria does not terminate the calibration algorithm at its optimum performance.

As each of the previous calibration algorithms have firstly been considered in terms of their distribution of errors for an omnidirectional 4 by 4 planar array, this algorithm will be no different. For perspective, however, it will be compared to the shortest path algorithm to show its ineffectiveness and also with the measure and correct approach to show its improvement by considering the measurement structure as a source of errors, as shown in figure 5-17.

As it is clear to see from figure 5-17, the simulated annealing approach is not the most effective calibration approach but it does have the interesting property of improving its calibration accuracy as the size of the array increases. This is due to the consecutive errors being spread further through the array. Therefore for larger arrays this means the errors can be spread further. This can be seen by the comparison of the simulated annealing simulation of the standard deviation of the calibration errors as the size of the array increases. This is again compared to the shortest path to show that even though the calibration accuracy improves it is still not a good calibration algorithm.

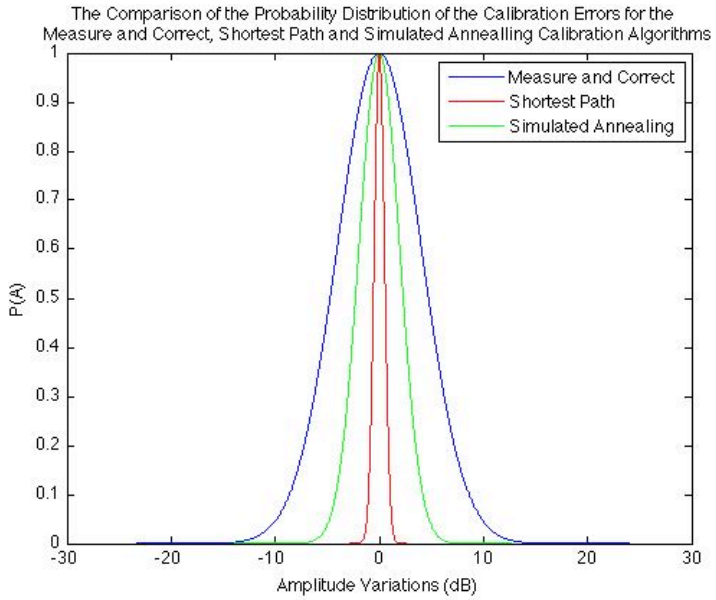

(a)

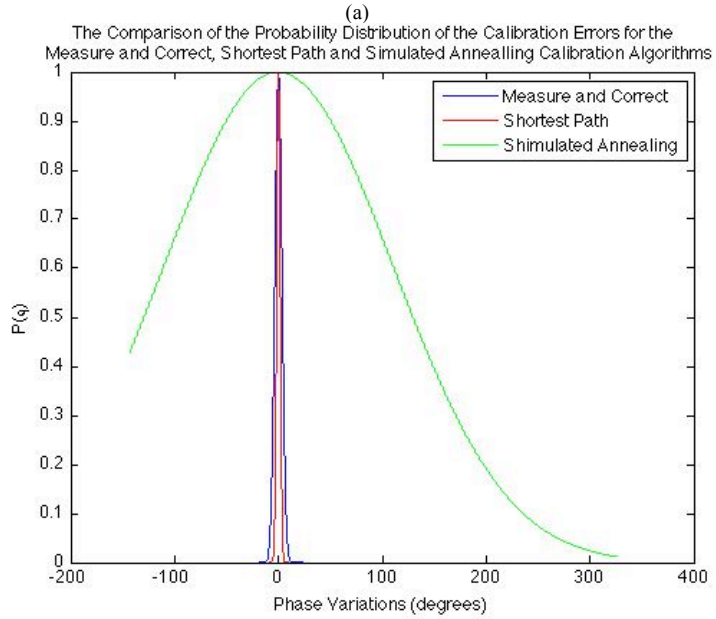

(b)

figure 5-17: The Comparison between the Probability Density Function of the Calibration Errors for the Measure and Correct, Shortest Path and Simulated Annealing Calibration Algorithms for 10,000 Omnidirectional 4 by 4 Planar Arrays, (a) Amplitude and (b) Phase.

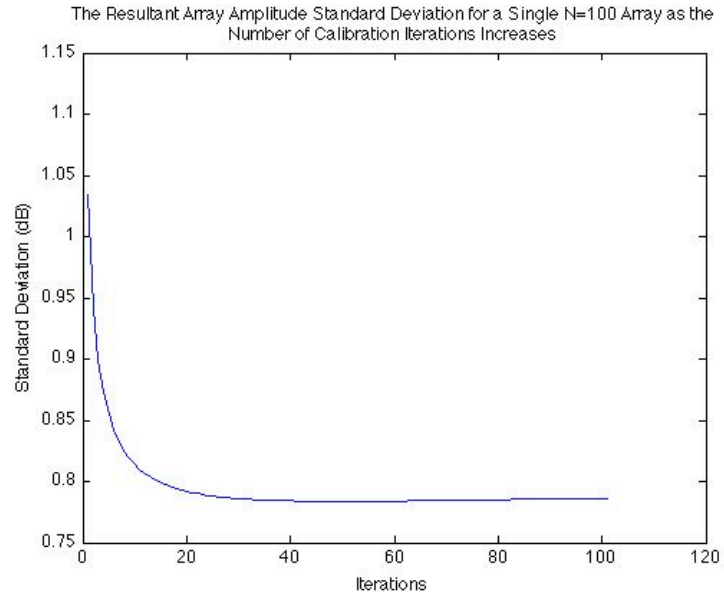

(a)

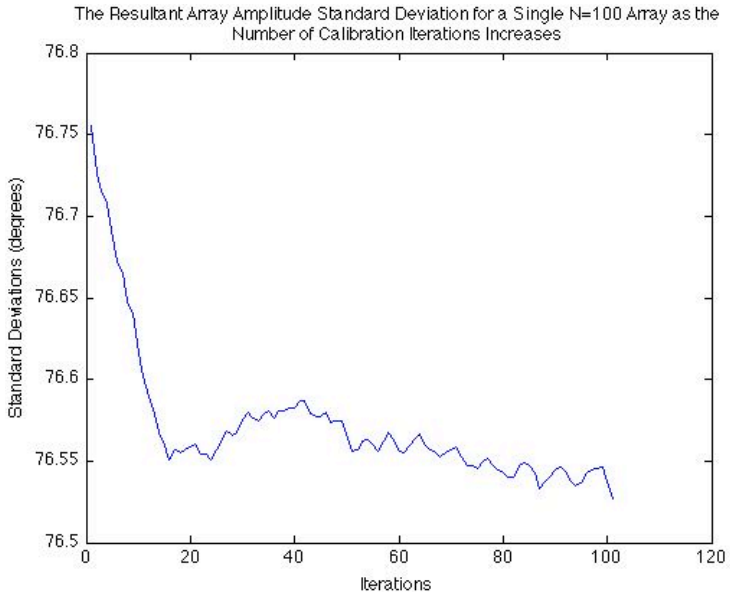

(b)

figure 5-18: The Standard Deviation of the Simulated Annealing Calibration Errors as the number of Iterations increases, (a) Amplitude and (b) Phase.

As this heuristic approach to calibration is iterative it is important to consider its effectiveness over the iterations of the algorithm; these are shown in figure 5-18. This shows the standard deviation for the amplitude and phase errors of the array as the number of iterations increases. This shows that the algorithm starts off well, but due to an inability to access the output of the array the cut-off criteria does not exit the calibration algorithm at its optimum performance.

5.2.3.1.3 Summary

As can clearly be seen from the comparison of the implementation of the simulated annealing approach, this is not an effective calibration algorithm. Though it considers the measurement structure, it requires significant number of assumptions about the nature of these errors. This is compounded by the inability of the algorithm to exit at its optimum performance.

There are some interesting behaviours revealed that are related to the array shape: one that is that as the size of the array increases, the calibration errors decrease. This is due to the nature of calibration errors; they are spread through the array at each iteration of the algorithm. A detrimental property of the algorithm is that it bases its calibration on the assumption of four measurement paths per element. However, this is not the case for the edge elements of the array, which only have one or two sensors connected to them, which is more clearly seen in figure 5-20, in the next section. This means that the calibration of those elements is significantly worse than the other elements of the array.

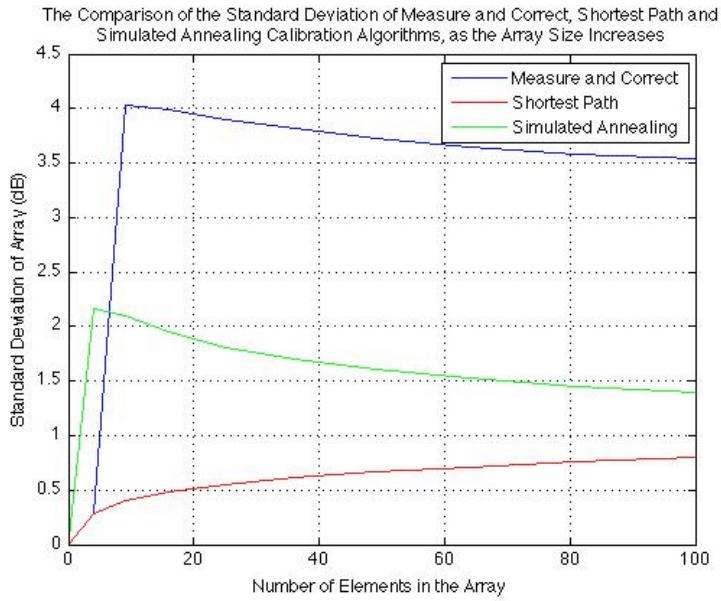

(a)

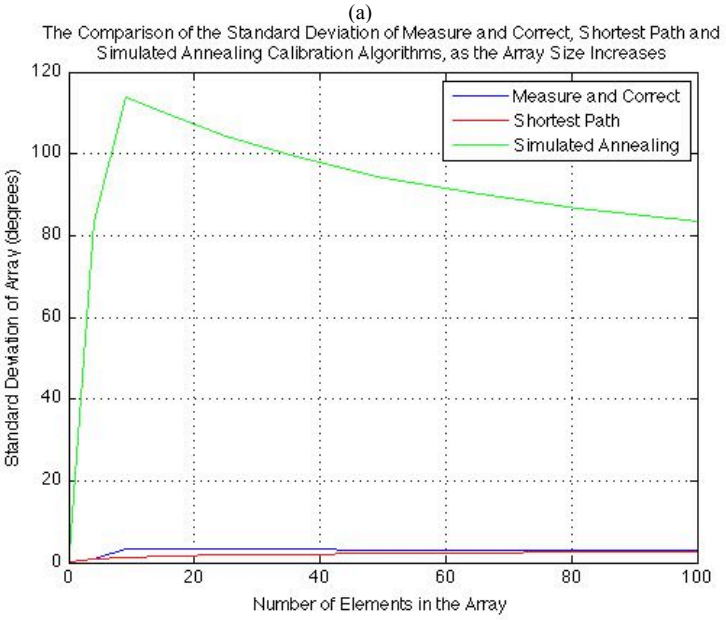

(b)

figure 5-19: Comparison of the Standard Deviation of the Calibration Errors for the Measure and Correct, Shortest Path and Simulated Annealing Calibration Algorithms of Square Omnidirectional Planar Arrays as the Size of the Array Increases, (a) Amplitude and (b) Phase.

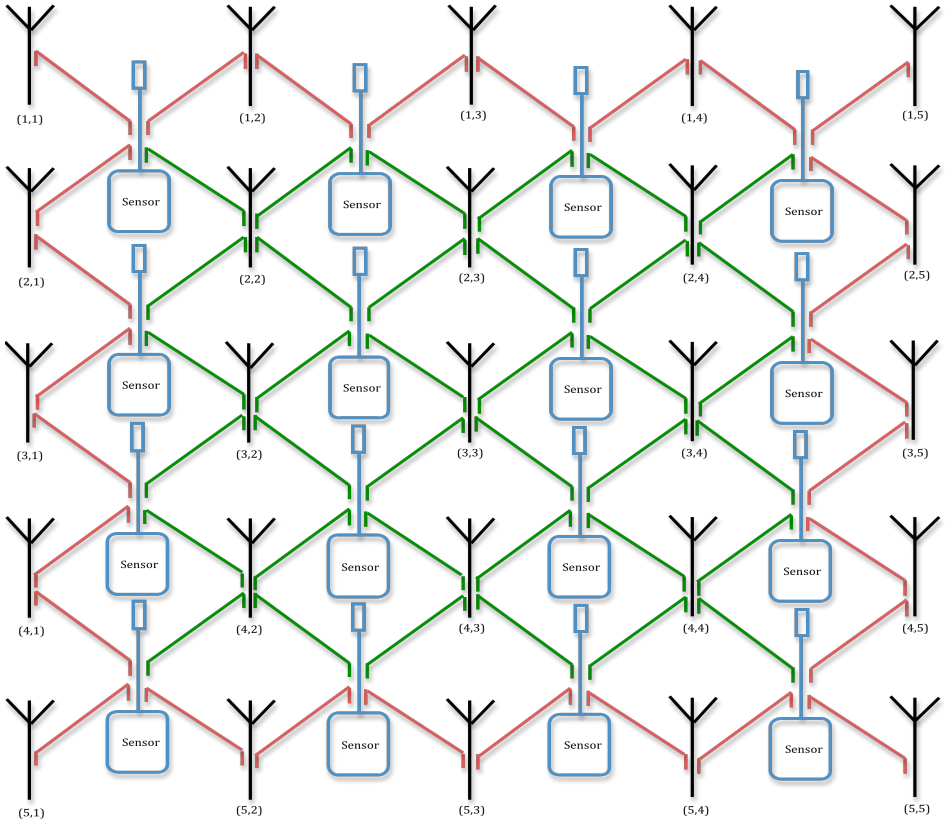

figure 5-20: The Reduced Number of Measurement Paths Available to the Edge and Corner Elements of the Array.

5.2.3.2 Reduced Simulated Annealing Calibration Algorithm

As was mentioned above the simulated annealing approach taken to calibration is based upon the assumption that each element of the array has four measurement paths. This is however not the case for the edge elements of the array which have two on the sides and only one at the corners. This is shown more clearly in figure 5-20.

This has led to the reduced simulated annealing algorithm whose premise is very simply to remove these edge elements from the final array. This is an expensive way of improving the calibration algorithm as it requires a *5 by 5* array to implement a *4 by 4* array. This could, however, be used in conjunction with dummy elements to reduce mutual coupling effects. However, the reduced simulated annealing calibration approach does not improve the performance significantly to make it a viable option for calibration.

5.2.3.2.1 Procedure

The procedure for implementing calibration of the reduced simulated annealing is simple; for a particular size array, the next larger sized array needs to be chosen so for a 7 by 7 planar array, an 8 by 8 planar array is needed. When the calibration is performed the edge elements of the array are switched off, making them dummy elements. This completes the calibration.

5.2.3.2.2 Simulation Results

As this algorithm is essentially the simulated annealing algorithm merely edited after calibration, it will be compared to the simulated annealing algorithm to show its significant improvement over it and with the shortest path algorithm to show how this approach's performance is comparable to that of the comparison based reference element approach. As has been shown for the simulated annealing algorithms, the contributing errors increase as the iteration increase, but in reduced amounts, thus improving calibration as well as sources of errors. This is more clearly seen in figure 5-21, which shows the standard deviation of the calibration error for *4 by 4* array for each iteration. As it is a heuristic algorithm, it shows the improvement as the number of iterations increases. Just like in the simulated annealing case, this shows that the algorithm starts off well, but due to an inability to access the output of the array the cut off criteria does not terminate the calibration algorithm at its optimum performance. However what is clear to see is that the performance per iteration is significantly better in the reduced simulated annealing algorithm.

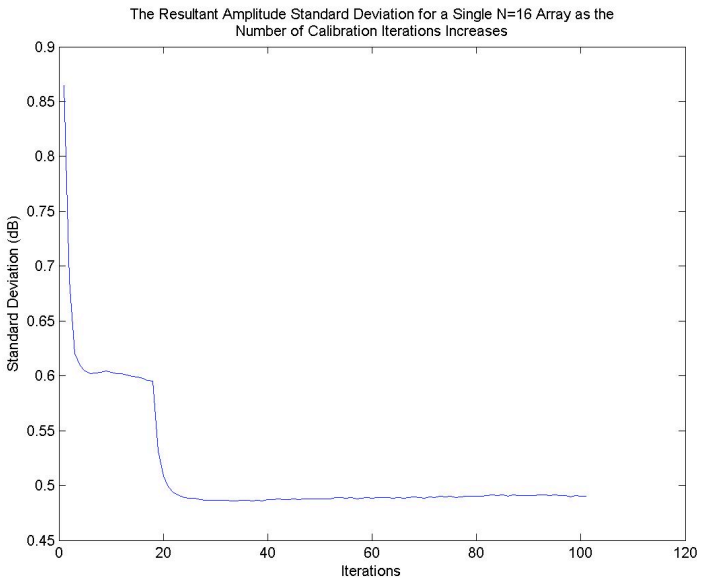

(a)

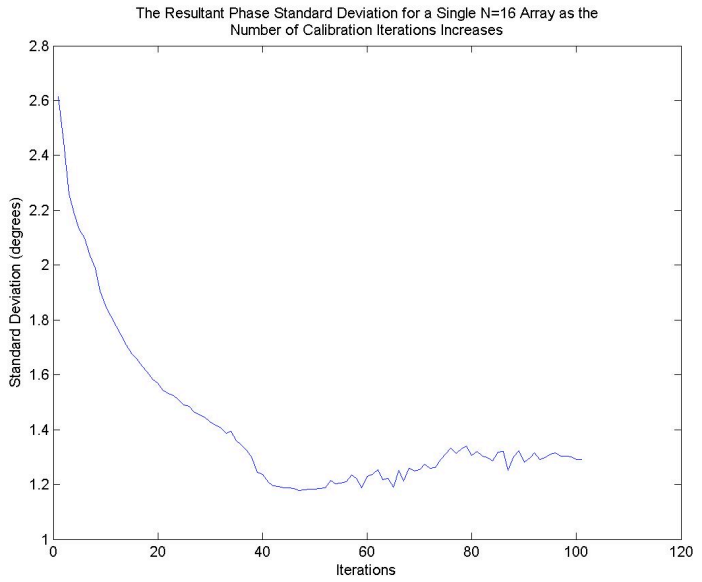

(b)

figure 5-21: The Standard Deviation of the Reduced Simulated Annealing Calibration Errors as the number of Iterations increases, (a) Amplitude and (b) Phase.

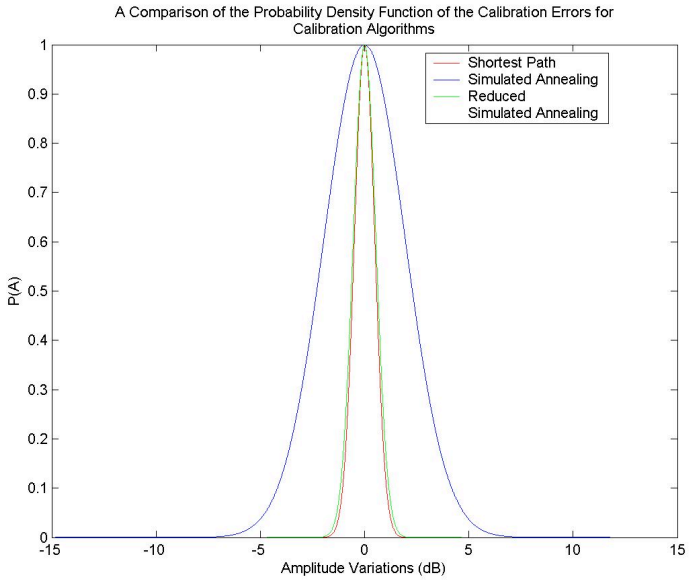

(a)

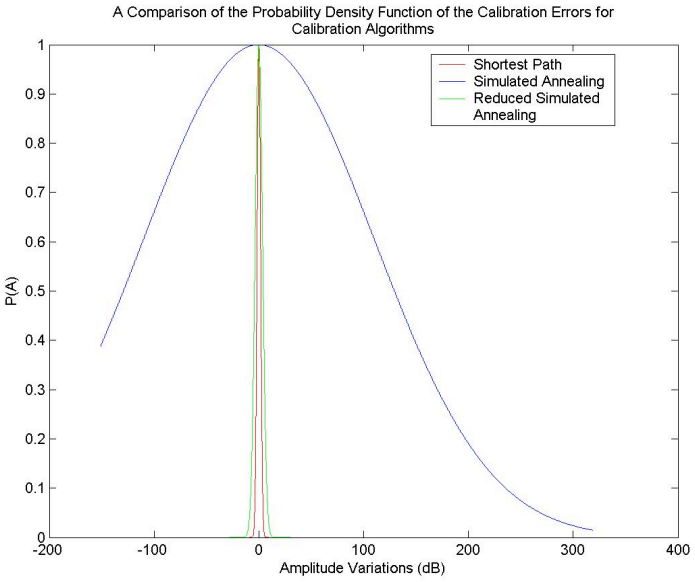

(b)

figure 5-22: The Comparison between the Probability Density Function of the Calibration Errors for the Simulated Annealing, Reduced Simulated Annealing and Shortest Path Calibration Algorithms for 10,000 Omnidirectional 4 by 4 Planar Arrays, (a) Amplitude and (b) Phase.

This performance improvement is clearly shown in the comparison of the distributions of the omnidirectional 4 by 4 planar array calibration errors shown in figure 5-22. The performance of the simulated annealing algorithm is so poor that this distorts the comparison between the reduced simulated annealing and shortest path calibration algorithms. This comparison is more clearly seen in figure 5-23. This shows that the reduced simulated annealing algorithm has marginally worse performance for the amplitude calibration errors, and in phase calibration errors. However the tails of the

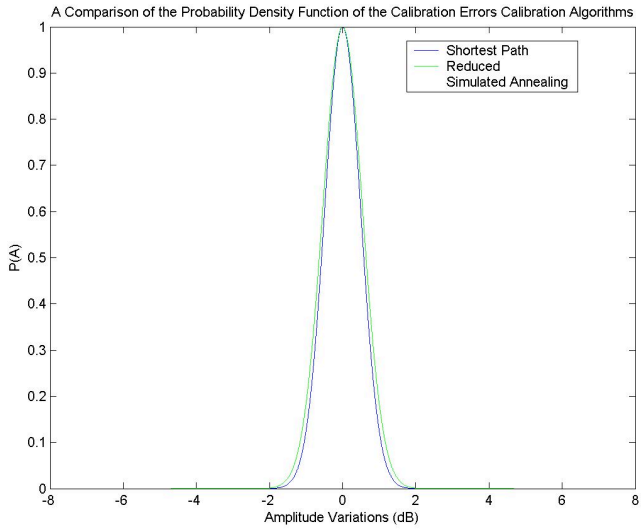

(a)

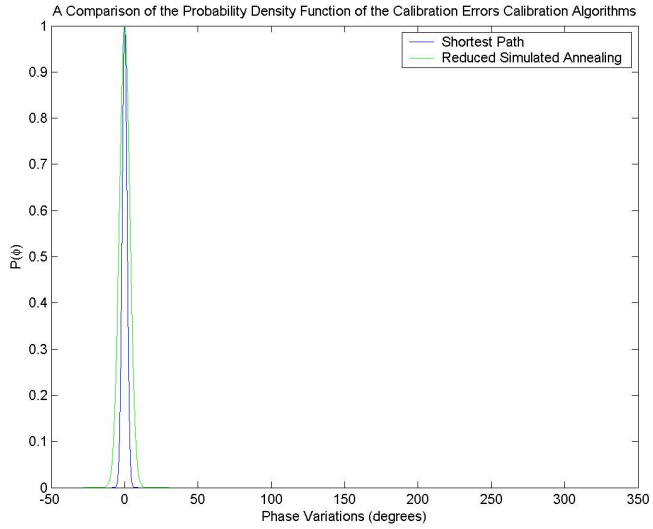

(b)

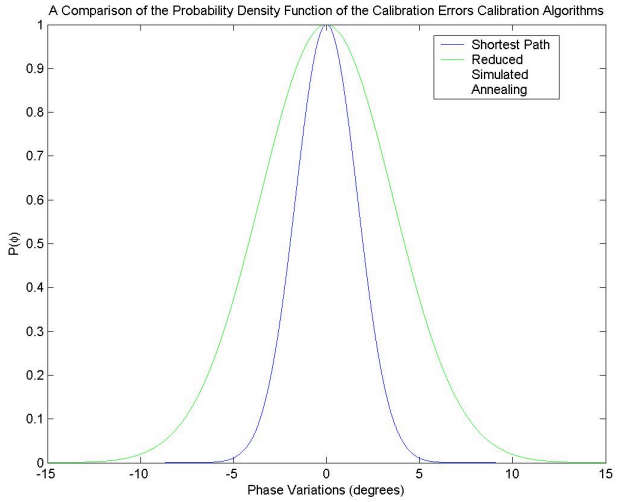

(c)

figure 5-23: The Comparison between the Probability Density Function of the Calibration Errors for the Reduced Simulated Annealing and Shortest Path Calibration Algorithms for 10,000 Omnidirectional 4 by 4 Planar Arrays, (a) Amplitude, (b) Phase and (c) Phase Close Up.

phase distribution are extremely large. This makes it harder to see the comparable performance, so a close up on the curve was plotted to show this more clearly in figure 5-23(c). This improvement over the simulated annealing approach is due to the spreading of the calibration errors throughout the array, and the removal of the ill estimated outer ring of elements.

The understanding of the reduced simulated annealing algorithms performance is reinforced by the comparison of the standard deviation of the calibration errors as the size of the array increases. The same reduction was seen as the size of the array increases as in the case of the simulated annealing algorithm, and the comparable performance with the shortest path algorithm's performance as shown in figure 5-24. It is interesting to note that for larger array sizes, the reduced simulated annealing approach becomes competitive to that of the shortest-path technique.

Though again it is hard to see this clearly due to the poor performance of the simulated annealing, it is much more clearly seen in the comparison of the shortest path performance and the reduced simulated annealing algorithms. The reason for the sharp spike in the graph at the beginning of the graph is due to the array's size, meaning that there are fewer elements for the errors to be spread to as in figure 5-25.

5.2.3.2.3 Summary

From this presentation of the reduced simulated annealing algorithm it is clear to see that the assumption that each element of the array has four measurement paths has a significant impact upon the performance. When the elements with one or two measurements paths are removed, the performance improves. However, when compared to the best performing algorithm so far the performance is not as good. For large arrays, the standard deviation of the error is superior to that of the shortest-path approach; however, it has wider tails for the phase error. The phase performance has a greater effect upon the radiation pattern than the amplitude errors. Therefore, overall performance may not be improved. Though removal of the outer ring of elements yields improved performance, the explored optimisation techniques are not recommended for use in array calibration.

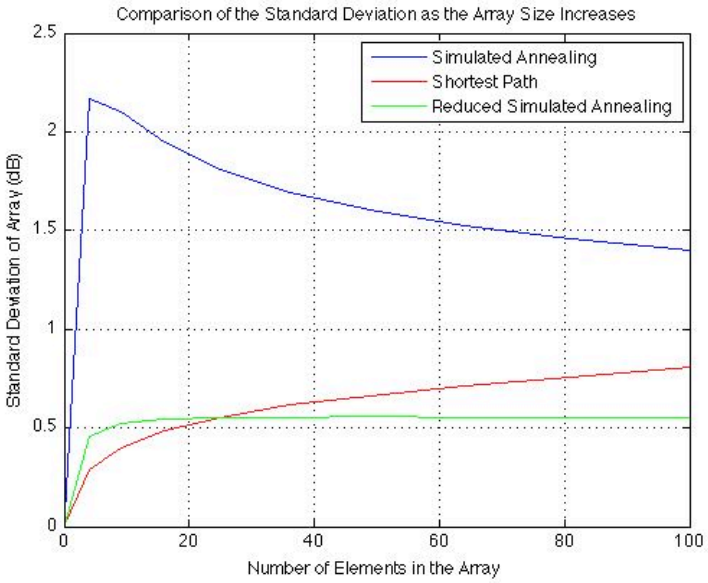

(a)

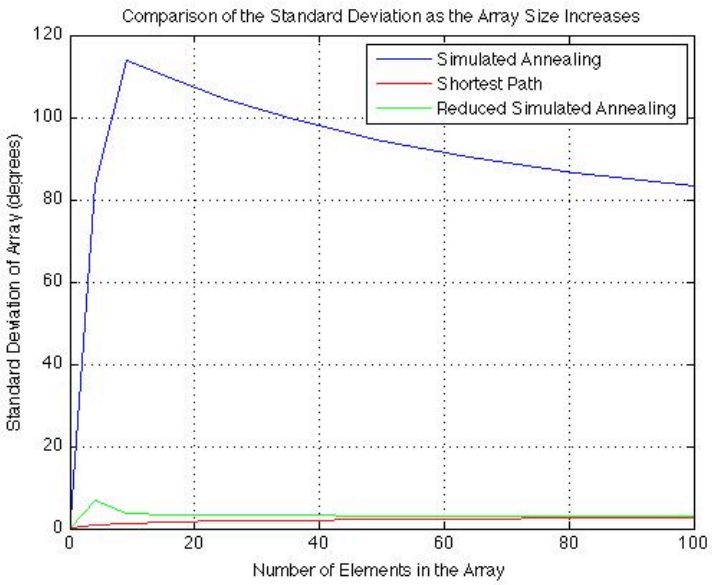

(b)

figure 5-24: Comparison of the Standard Deviation of the Calibration Errors for the Shortest Path, Simulated Annealing and Reduced Simulated Annealing Calibration Algorithms of Square Omnidirectional Planar Arrays as the Size of the Array Increases, (a) Amplitude and (b) Phase.

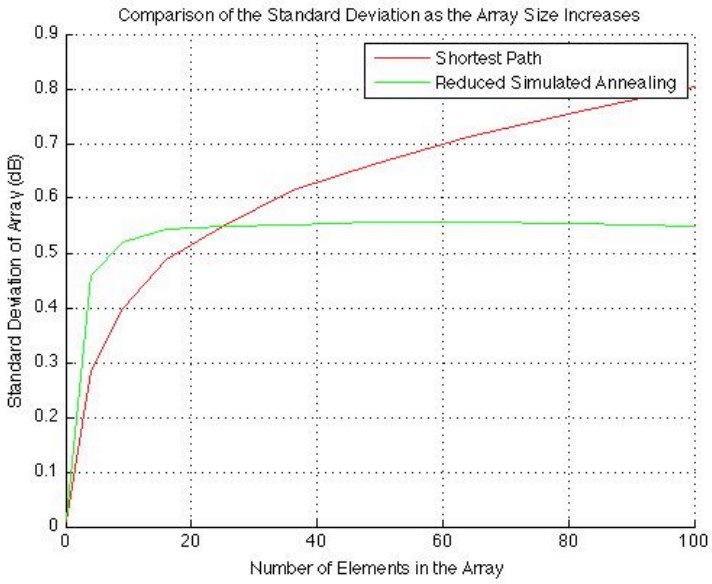

(a)

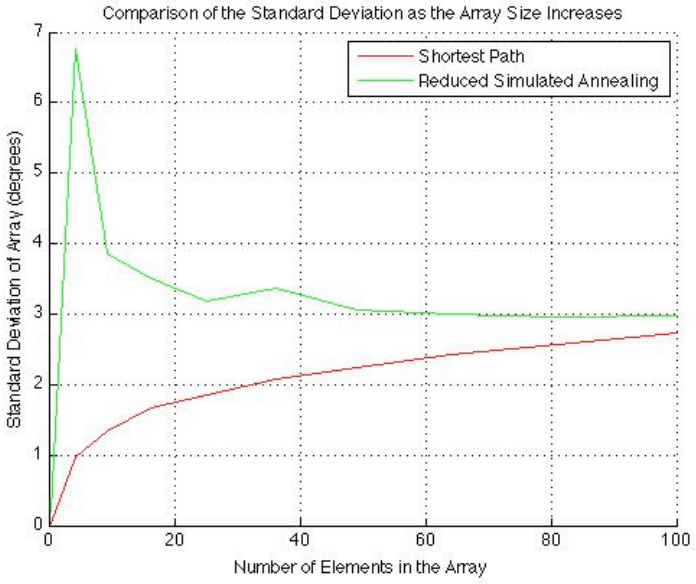

(b)

figure 5-25: Comparison of the Standard Deviation of the Calibration Errors for the Shortest Path , Simulated Annealing and Reduced Simulated Annealing Calibration Algorithms of Square Omnidirectional Planar Arrays as the Size of the Array Increases, (a) Amplitude and (b) Phase.

5.2.4 Multipath Algorithms

The relative success of optimization algorithms, at a great cost, led to the investigation of other calibration algorithms that would utilise the redundant paths provided by the measurement structure to improve the performance of the comparison based reference element calibration algorithms. This led to the use of directed selection of multiple paths to calibrate each element of the array. These are the multipath calibration and the dual path approaches. The latter was seen in the previous chapter. The reasoning behind

presenting them in this way was first to use all of the redundant paths to calibrate the array. This had limited success in the multipath algorithm as it was comparing calibration paths of different lengths to calibrate the array. As the reference element calibration algorithms comparison has clearly shown, the number of coupler paths taken to calibrate an element is of significance. By comparing multiple paths of different lengths the calibration was less then optimum. This led to the creation of the dual path calibration algorithm, which takes two paths of exactly the same length to calibrate the elements of the array where possible. By comparing two paths of the same length the problem encountered by the multipath approach is avoided.

5.2.4.1 Multipath Calibration Algorithm

As mentioned above the calibration algorithm was presented as a solution to the problem of utilising the array measurement structure while still building upon the success of the comparison based upon reference element approaches. The multipath algorithm proposed to do this by taking all the multiple paths from a reference element to each element of the array. These calibration paths used the comparison-based calibration to achieve this, thus building upon the success of the reference element calibration approaches.

5.2.4.1.1 Procedure

This multipath algorithm selects a reference element in the top left corner of the array. This seems counter intuitive as the comparison of the reference element calibration algorithms showed that the optimum reference element location is in the centre of the array. To overcome this the results will be compared with that of the top left reference algorithm to shown that the choice of reference element is comparable. The reason behind choosing the top left corner is simply to fully investigate the possibilities of this approach as there are more possible paths to the elements further away. After choosing a reference element, the first element to be calibrated is chosen and a list of possible paths are made and from these paths calibration factors are created for these paths. When these are calculated for each element of the array, the generated list of correction factors is averaged for each element of the array and the array is thus calibrated.

5.2.4.1.2 Simulation Results

As the reference element was chosen in the top left corner of the array to increase the number of possible paths, so the calibration algorithms will be compared to that of the top left reference to remove the performance comparison of the reference element location. As was previously mentioned, the multipath is less successful then the top left reference algorithm, as can be seen from the comparison of the omnidirectional *4 by 4* planar array calibration distributions, as shown in figure 5-26.

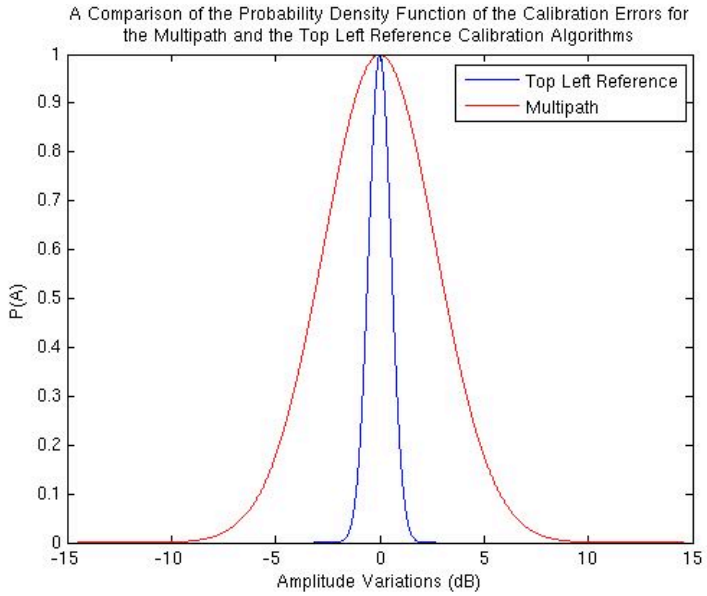

(a)

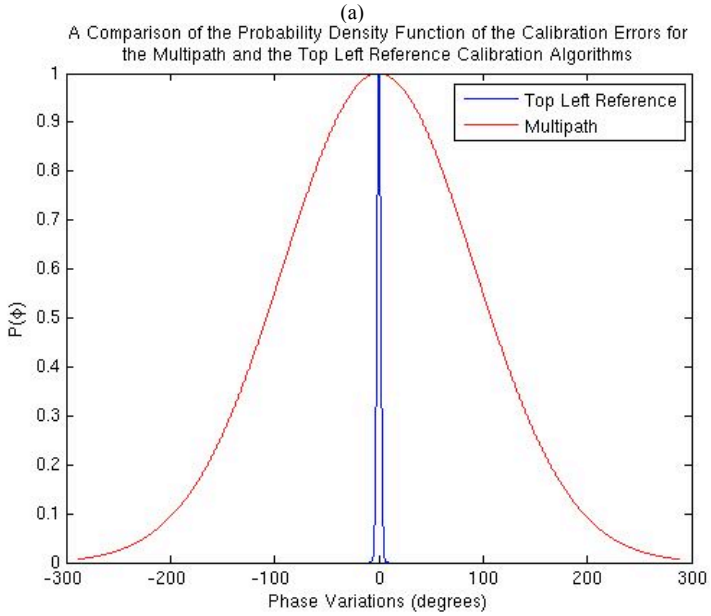

(b)

figure 5-26: The Comparison between the Probability Density Function of the Calibration Errors for the Top Left Reference and the Multipath Calibration Algorithms for 10,000 Omnidirectional 4 by 4 Planar Arrays, (a) Amplitude and (b) Phase.

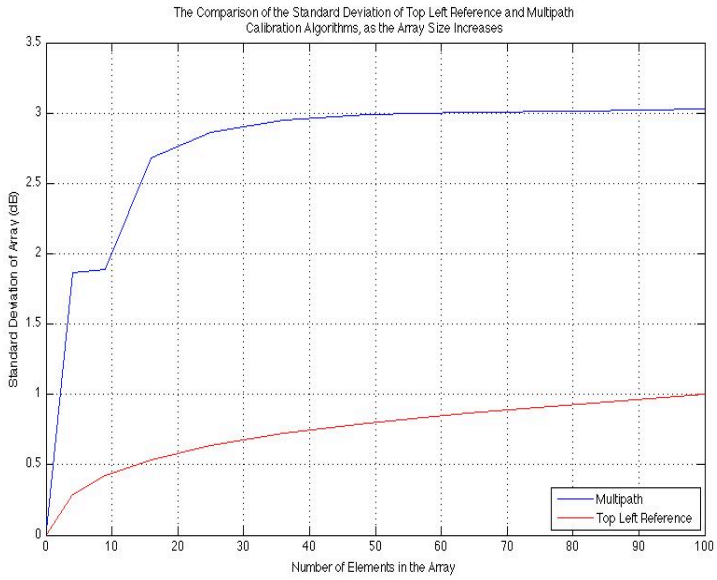

(a)

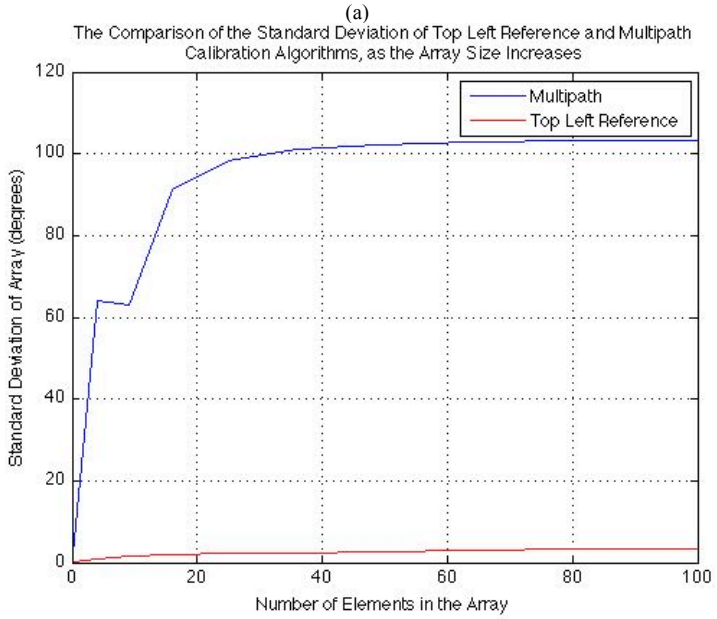

(b)

figure 5-27: Comparison of the Standard Deviation of the Calibration Errors for the Multipath and Top Left Reference Calibration Algorithms of Square Omnidirectional Planar Arrays as the Size of the Array Increases, (a) Amplitude and (b) Phase.

The reason behind the degradation in this performance is the averaging of multiple calibration paths of different lengths and therefore more coupler path variations are included in the calibration of the individual elements. This is more clearly seen from the comparison of the standard deviation of the calibration errors as the size of the array increases, which clearly shows the more dramatic increase of the multipath calibration algorithms of the standard deviation in comparison to that of the top left reference algorithm as shown in figure 5-27.

5.2.4.1.3 Summary

The motivation of the multipath calibration algorithm was to more fully utilise the measurement structure in the calibration, while building upon the success of the comparison based reference element calibration algorithms. The algorithm had limited success at this as it took all of the paths from the reference element to the element to be calibrated. This meant averaging calibration path of different lengths, and therefore including more coupler errors into the calibration. This has a detrimental effect upon the calibration accuracy.

5.2.4.2 Dual Path Calibration Algorithms

The lesson learned from the multipath calibration algorithm led to the dual path algorithm that was that the comparison of the calibration paths must be of the same length in order to mitigate the impact of the coupler errors on the calibration algorithm, as shown in figure 5-28. This was presented in the previous chapter. However, for a better understanding of the advantages of the dual path calibration algorithm, for completeness it needs to be compared with the shortest path, the reduced simulated annealing and multipath calibration algorithm's accuracy.

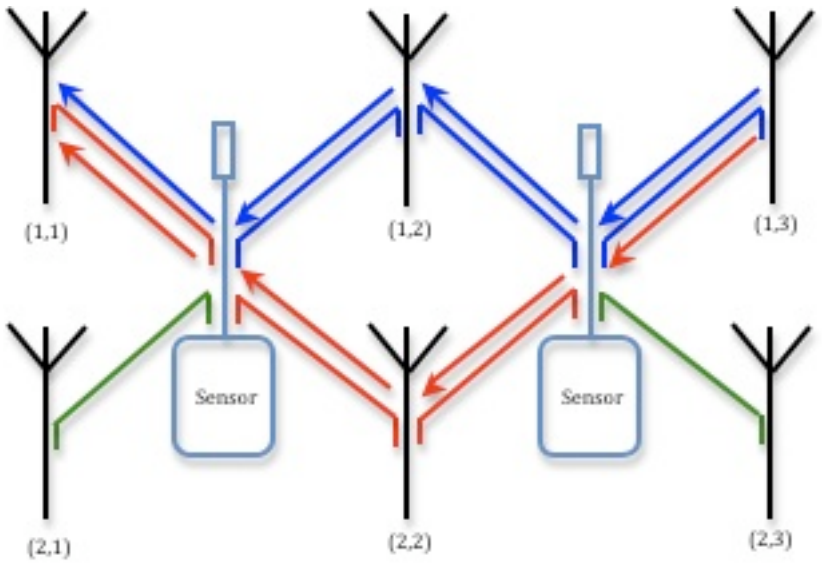

figure 5-28: Diagram of the Dual Path Algorithm Paths where two paths are via which element (1,3) is calibrated.

5.2.4.2.1 Simulation Results

The dual path algorithm utilises the measurement structure to mitigate the impact of coupler errors. It achieves what the multipath algorithm set out to do by taking calibration paths of the same length instead of all possible paths. This is more clearly seen by comparing the distribution of calibration errors for the omnidirectional 4 by 4 planar array with the result of the multipath algorithm, as shown in figure 5-29.

This comparison shows the effectiveness of the dual path algorithm at achieving what the multipath algorithm tried to do. However for a better comparison of the calibration algorithm's effectiveness, it was compared with the shortest paths predicted performance, which is shown in figure 5-30. Due to the large tails of the reduced simulated annealing phase distributions, the comparison is much easier to see in the close up on the curve of the phase distribution as shown in figure 5-30 (c).

These comparisons conclude with the comparison of the standard deviation of the calibration errors of these algorithms as the size of the array increases. The first comparison shows that again the performance of the multipath algorithm, due to the multiple paths of different lengths, does not provide an effective approach, which is shown in figure 5-31. The performance of the dual path algorithm is much easier to see

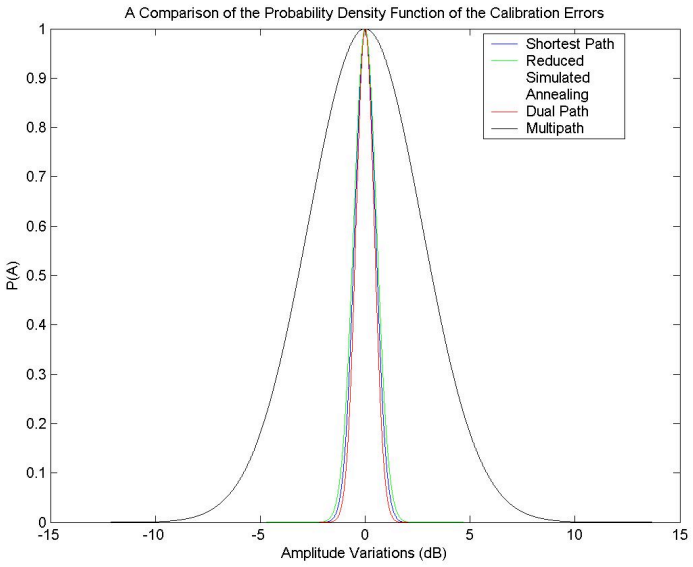

(a)

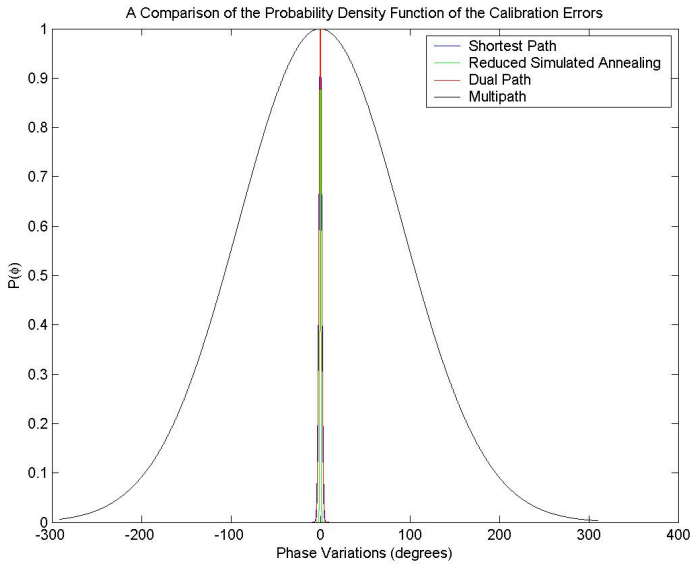

(b)

figure 5-29: The Comparison between the Probability Density Function of the Calibration Errors for the Multipath, Reduced Simulated Annealing, Shortest Path and Dual Path Calibration Algorithms for 10,000 Omnidirectional 4 by 4 Planar Arrays, (a) Amplitude and (b) Phase.

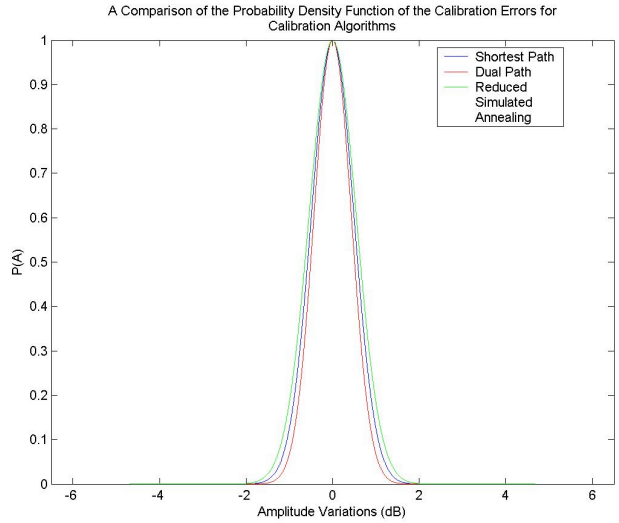

(a)

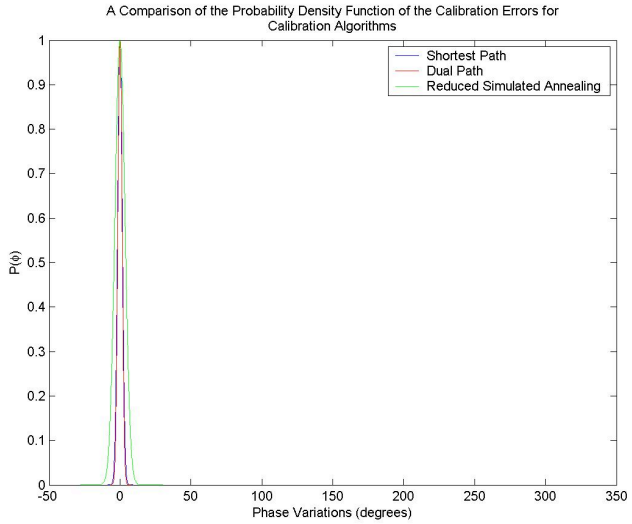

(b)

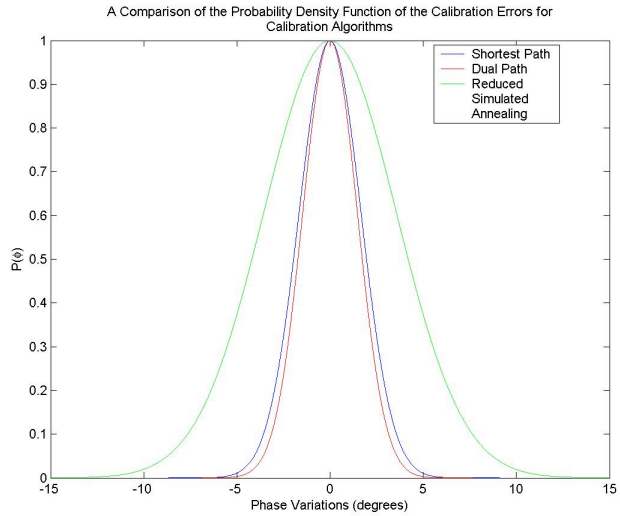

(c)

figure 5-30: The Comparison between the Probability Density Function of the Calibration Errors for the Reduced Simulated Annealing, Shortest Path and Dual Path Calibration Algorithms for 10,000 Omnidirectional 4 by 4 Planar Arrays, (a) Amplitude, (b) Phase and (c) Close Up on Phase.

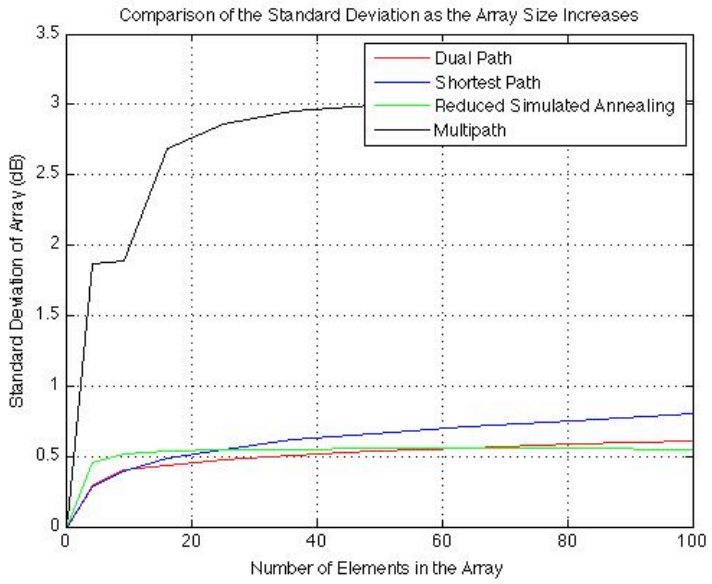

(a)

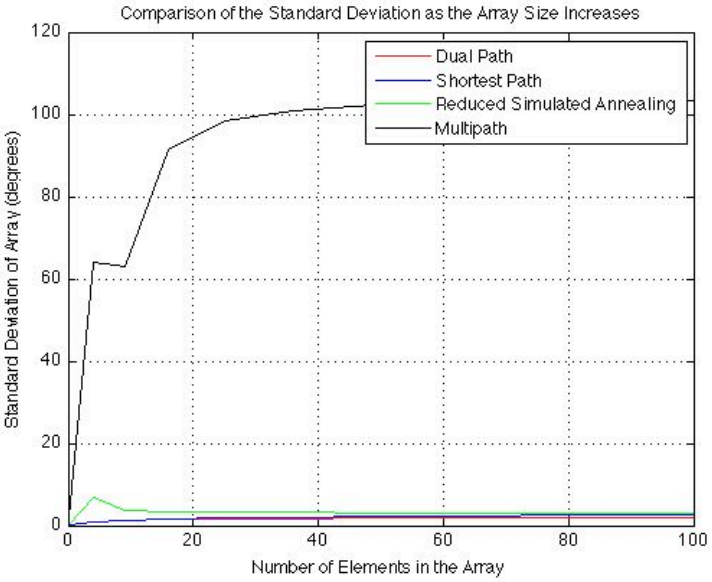

(b)

figure 5-31: Comparison of the Standard Deviation of the Calibration Errors for the Multipath, Shortest Path, Reduced Simulated Annealing and Dual Path Calibration Algorithms of Square Omnidirectional Planar Arrays as the Size of the Array Increases, (a) Amplitude and (b) Phase.

when it is compared to shortest path and reduced simulated annealing comparison which shows that over the same number of coupler paths to calibrate each element of the array the dual path algorithm is effective in mitigating the coupler error's impact upon the accuracy of the calibration. This is even more clearly seen in the comparison between the shortest path and the dual path algorithms standard deviation as the size of the array increases, as shown in figure 5-32 where there is approximately a 25% improvement for a *10 by 10* array.

5.2.4.2.2 Summary

The aim of the dual path calibration algorithm was to mitigate the impact of the coupler errors upon the accuracy of the calibration, by taking two paths to calibrate the elements of the array and averaging them. This has been successful; though it will reduce large errors it will in turn increase small errors due to the averaging, but will still have an overall positive impact upon the calibration accuracy. The improvement in performance of the dual path algorithms by its mitigation of the coupler errors highlights that they limit the accuracy of the calibration algorithm.

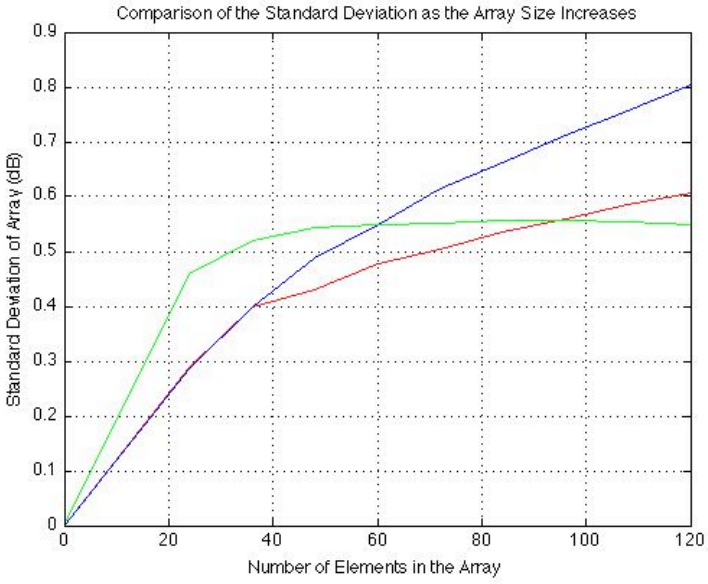

(a)

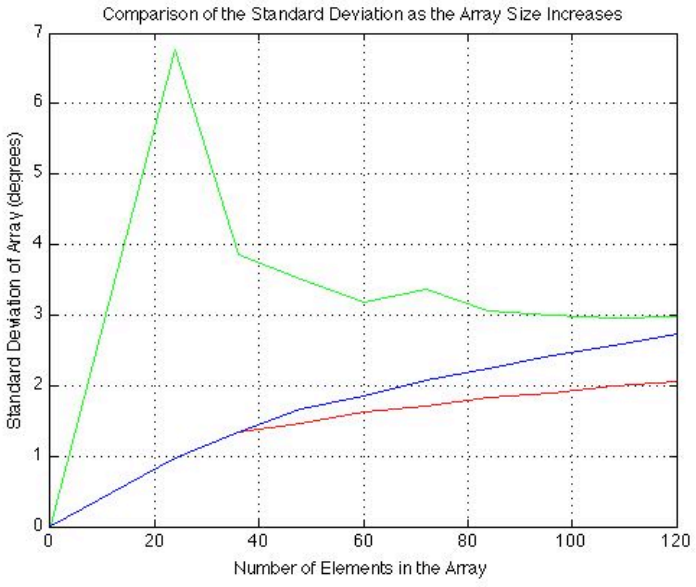

(b)

figure 5-32: Comparison of the Standard Deviation of the Calibration Errors for the Reduced Simulated Annealing, Shortest Path and Dual Path Calibration Algorithms of Square Omnidirectional Planar Arrays as the Size of the Array Increases, (a) Amplitude and (b) Phase The Legend for this figure is the same as that for figure 5-31.

5.3 Comparison of Radiation Pattern Figures of Merits

As was mentioned in chapter 2, the measure of the performance of the antenna array is in its radiation pattern. This was also highlighted in chapter 3 when discussing the calibration problem of antenna arrays. The radiation pattern is very sensitive to imbalances in the amplitude and phase relationships within the antenna array. So far the performances of the calibration algorithms have been measured by the distribution of their errors and comparison of their standard deviations as the size of the array increases. From these comparisons, it has been clear that the comparison based algorithms have been the most effective approach taken and with the use of dual path averaging the dependence of the calibration accuracy on the coupler paths is reduced and the performance is therefore improved, as shown in figure 5-32.

This section will present these calibration algorithms in terms of their predicted radiation pattern performance to show the effectiveness of the calibration algorithms. For this comparison the dual path algorithm is compared with the shortest path one. The radiation patterns are generated by Matlab using the beamforming equations of an ideal planar array, which is the ideal beamforming equations of two linear arrays oriented along different axis and multiplied together [25]. The beamforming equation assumes omnidirectional antenna elements.

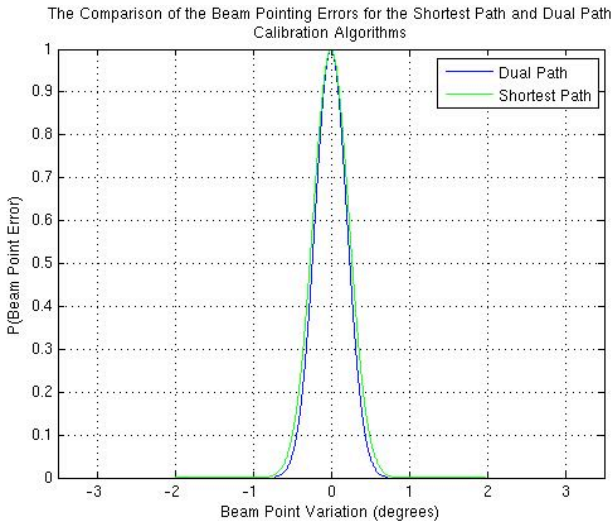

figure 5-33; The Comparison between the Dual Path and Shortest Path Calibration Algorithms in terms of the Probability Density Function of the Distribution of their Beam Pointing Errors.

$$AF = \sum_{n=1}^{N}\sum_{m=1}^{M} e^{j(n-1)kd_x \sin\theta\cos\phi+\beta_x} e^{j(m-1)kd_y \sin\theta\cos\phi+\beta_y} \tag{5.5}$$

where $sin\theta\, cos\phi$ are the 3D radiation pattern of the linear array along the x-axis,

$sin\theta\, sin\phi$ is the 3D radiation pattern of the linear array along the y-axis,

d_x and d_y are the element spacing of the linear arrays along the x and y-axis,

β_x and β_y are the steering angles of the linear arrays along the x and y-axis.

This equation can be simplified for our purposes by assuming that each linear array can only steer in one direction [321], and therefore the equation reduces to:

$$AF = \sum_{n=1}^{N}\sum_{m=1}^{M} e^{j(n-1)kd_x \sin\theta+\beta_x} e^{j(m-1)kd_y \sin\theta+\beta_y} \tag{5.6}$$

The next step is to include the element variations, which can be done by multiplication as shown in [322].

$$AF = \sum_{n=1}^{N}\sum_{m=1}^{M} A_{nm} e^{j(n-1)kd_x \sin\theta\cos\phi+\beta_x} e^{j(m-1)kd_y \sin\theta\cos\phi+\beta_y} e^{j\Delta\phi_{nm}} \tag{5.7}$$

where A_{nm} is each element's amplitude variation,

$\Delta\phi_{nm}$ is each element's phase variation.

The beamforming equations (5.6 and 5.7) were used in Matlab to simulate the effect of calibration on the radiation patterns of 4 by 4 antenna array. The simulations were set up by defining non-ideal arrays and calibrating them, as before. These simulations were taken for 10,000 arrays calibrated by dual path and shortest path algorithms. These results were analysed based upon the radiation pattern figures of merits and the error ranges are presented in Table 5-2. This table shows that the dual path calibration algorithm outperforms the shortest path one, though there is not a significant improvement in all areas, and some figures of merit are more sensitive to calibration errors then others. Starting with the beam pointing error ranges it is clear to see that this is the one figure of merit in which the dual path algorithm is significantly superior with an error range of 0^o to 0.72^o when compared to the shortest path's error range of 0^o to 3.24^o, which can also be seen in figure 5-33. The error ranges for other figures of merit,

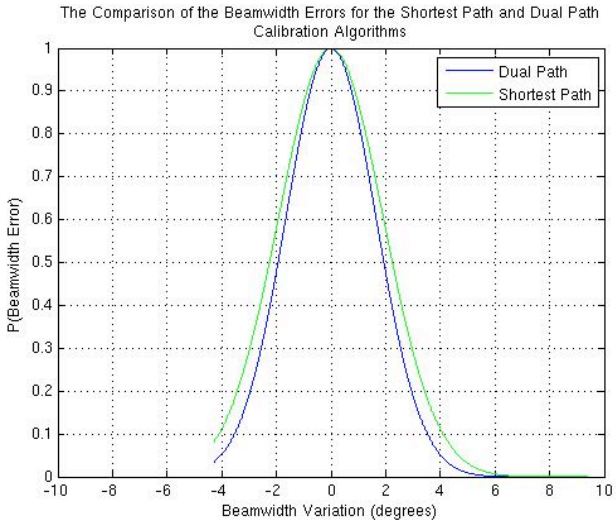

figure 5-34: The Comparison between the Dual Path and Shortest Path Calibration Algorithms in terms of the Probability Density Function of the Distribution of their Beamwidth Errors.

such as beamwidth, null and sidelobe locations, are the same. The improvement is seen in the average value of the error, which in each case shows the improvement offered by the dual path algorithm. This can more clearly be seen by comparing the distribution of the errors, as in figure 5-34, figure 5-35 and **figure 5-37** respectively.

Finally the sidelobe height and null depth error ranges show the superiority of the dual path algorithm in the error ranges, when their maximum errors and average errors are considered, which is also more clearly seen by comparing their distributions in figure 5-38 and **figure 5-39** respectively.

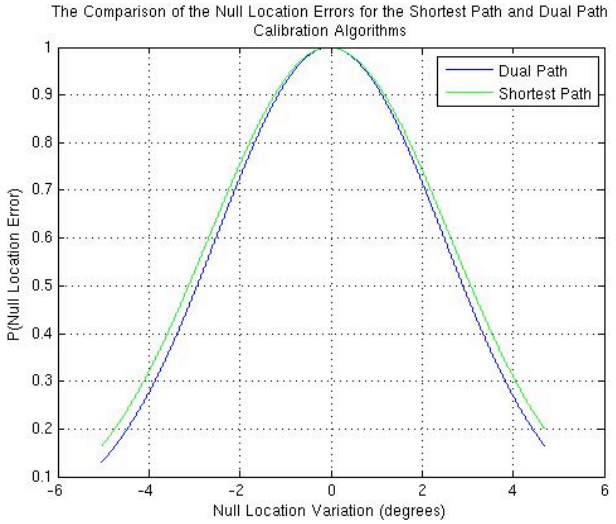

figure 5-35: The Comparison between the Dual Path and Shortest Path Calibration Algorithms in terms of the Probability Density Function of the Distribution of their Null Location Errors.

Table 5-2: Radiation Pattern Figures of Merit Error Ranges for the Dual Path and Shortest Path Calibration Algorithms.

		Error		
		Max	Min	Average
Beam Point	Shortest Path	3.24^{o}	0^{o}	0.138546^{o}
	Dual Path	0.72^{o}	0^{o}	0.11314625^{o}
Beamwidth	Shortest Path	9.36^{o}	$7.11x10^{-15\ o}$	1.431429^{o}
	Dual Path	9.36^{o}	$7.11x10^{-15\ o}$	1.239966^{o}
Null Depth	Shortest Path	0.479444	$3.40x10^{-22}$	0.09771545
	Dual Path	0.45102	$3.40x10^{-22}$	0.08372433
Null Location	Shortest Path	9.72^{o}	0^{o}	2.19218^{o}
	Dual Path	9.72^{o}	0^{o}	2.044172^{o}
Sidelobe Height	Shortest Path	0.588401	$2.74x10^{-6}$	0.07662003
	Dual Path	0.359956	$4.5x10^{-8}$	0.05724433
Sidelobe Location	Shortest Path	49.68^{o}	0^{o}	3.2299692^{o}
	Dual Path	49.68^{o}	0^{o}	2.320236^{o}

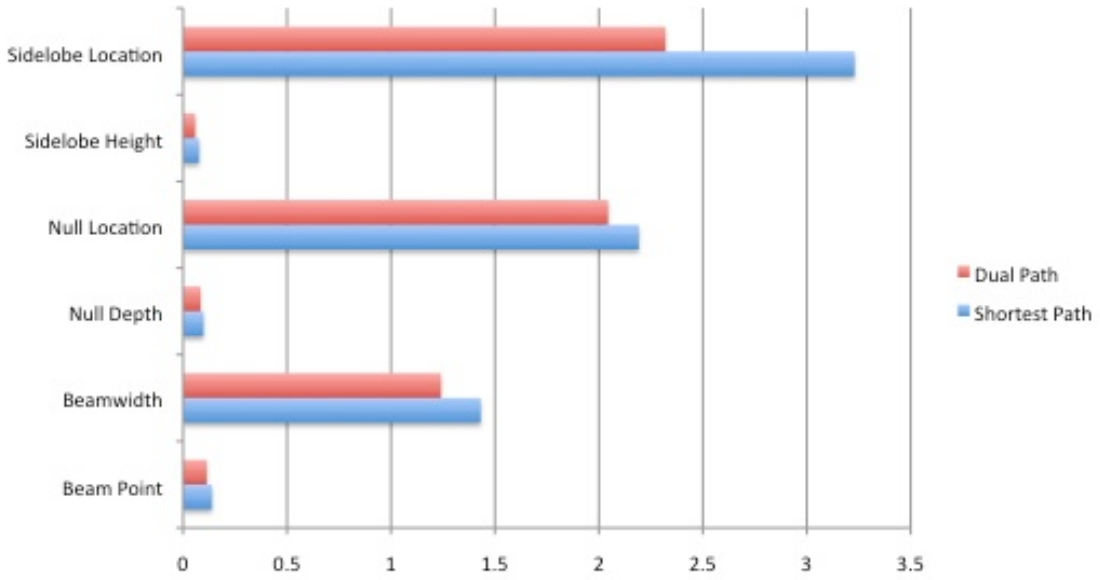

figure 5-36: Comparison of the average values of the each of the figure of merits for shortest path and dual path algorithm.

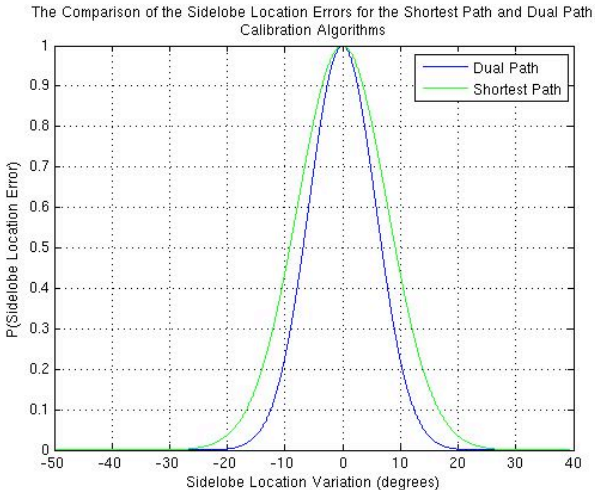

figure 5-37: The Comparison between the Dual Path and Shortest Path Calibration Algorithms in terms of the Probability Density Function of the Distribution of their Sidelobe Location Errors.

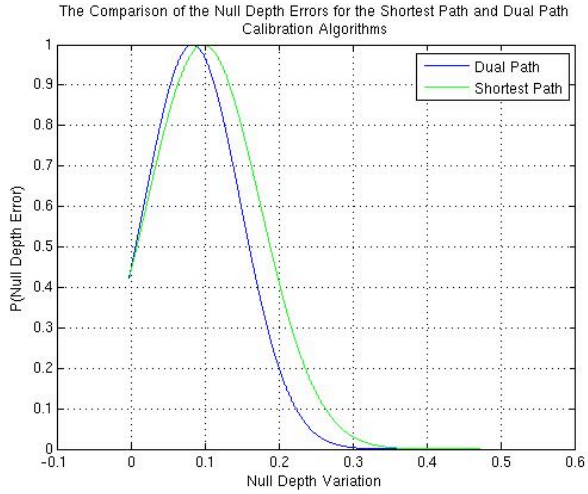

figure 5-38: The Comparison between the Dual Path and Shortest Path Calibration Algorithms in terms of the Probability Density Function of the Distribution of their Null Depth Errors.

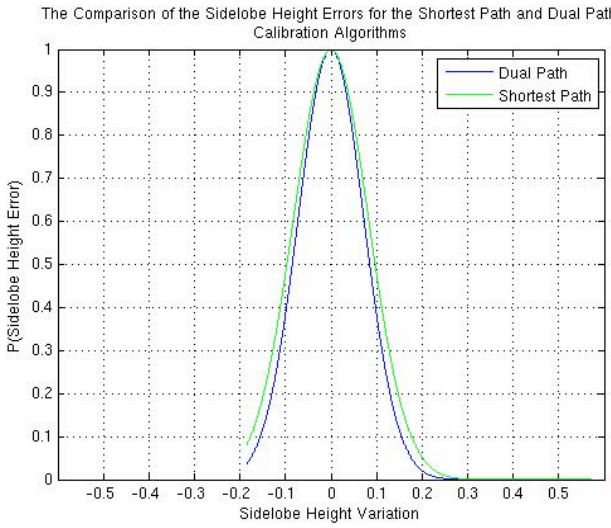

figure 5-39: The Comparison between the Dual Path and Shortest Path Calibration Algorithms in terms of the Probability Density Function of the Distribution of their Sidelobe Height Errors.

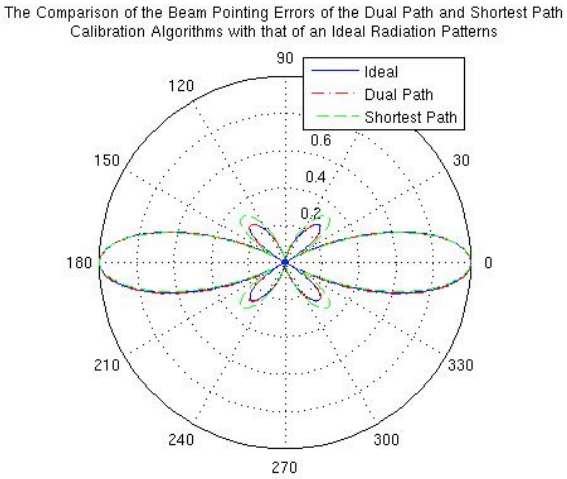

figure 5-40: The Comparison of the Dual Path and Shortest Path Calibration Algorithms in terms of the Cross Section of the Radiation Pattern for the Maximum Beam pointing Errors.

These results show the improvement of the dual path algorithm over the shortest path in terms of the figures of merit. However it does not show the interdependence of these figures of merit, which can be seen by comparing the cross section of the radiation, plots of the maximum errors versus the ideal radiation pattern. Starting again with the beam pointing errors, as shown in figure 5-40, it is hard to see the alteration of the radiation pattern due to the beam pointing direction errors for either the shortest path or the dual path algorithms. However, what is clear to see from this figure is the alteration in the sidelobe levels for the shortest path calibration algorithm. The next figure of merit to be considered is the beamwidth, which is shown in figure 5-41. The figure shows the

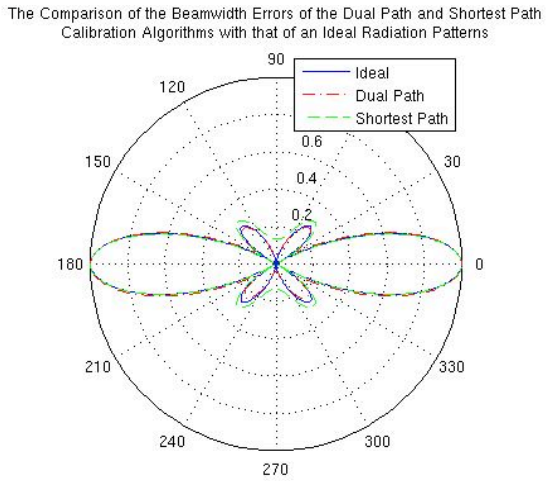

figure 5-41: The Comparison of the Dual Path and Shortest Path Calibration Algorithms in terms of the Cross Section of the Radiation Pattern of the Maximum Beamwidth Errors.

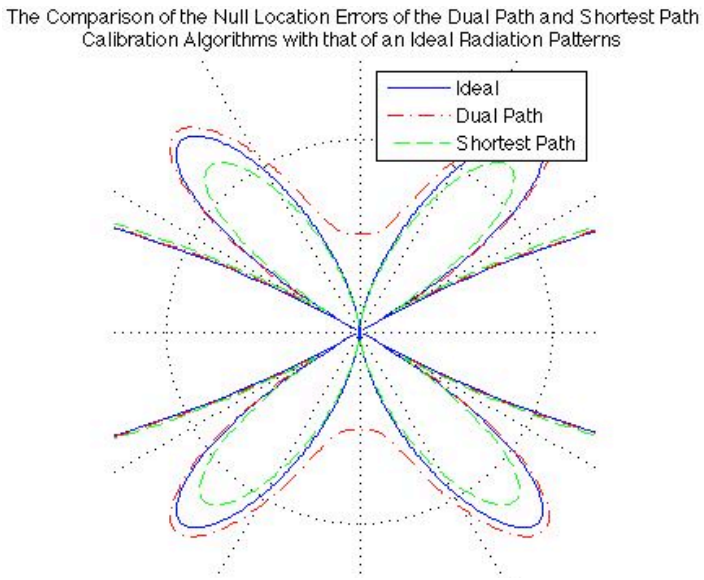

figure 5-42: The Comparison of the Dual Path and Shortest Path Calibration Algorithms in terms of the Cross Section of the Radiation Pattern of the Maximum Null Location Errors.

maximum beamwidth error for both calibration algorithms. The difference is hard to distinguish, but what is clear is the alteration in the sidelobe levels and null depths for the shortest path algorithm. The interdependency of the figures of merits does not always back up the performance improvement of the dual path algorithm, as is more clearly seen in the comparison of the null locations in figure 5-42. This shows the alteration in the null locations due to the calibration accuracy of the two algorithms.

Though again these errors are hard to see, the null depths for the central null in the dual path's radiation pattern are much shallower then either the shortest path or the ideal ones. This shows that though the null location errors are lower for the dual path algorithm the null depths associated with this radiation pattern are higher. This phenomenon is less clearly seen but still present when the sidelobe locations are considered.

The null depths need to be considered first. They are very sensitive to calibration errors, which is very clear from figure 5-43. The shallow null depths have distorted the radiation pattern immensely as it has removed the separation between the sidelobes and the main beams, which gives them the appearance that they have merged together. The distinguishing features of the radiation pattern has been muted and the beamwidth has also spread. The one consoling factor is that for the worst-case scenario of the null

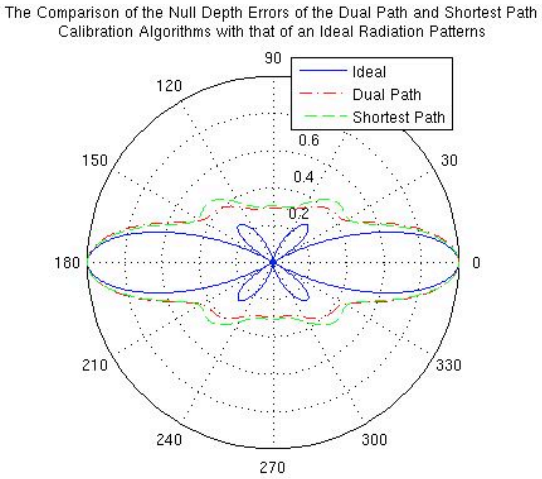

figure 5-43: The Comparison of the Dual Path and Shortest Path Calibration Algorithms in terms of the Cross Section of the Radiation Pattern for the Maximum Null Depth Errors.

depths, the dual path calibration algorithm is slightly less distorted then the shortest path. When considering the sidelobe location errors in the radiation pattern as in figure 5-44, the phenomena where even though the dual path is less distorted in the sidelobe location errors, this worst case sidelobe error is associated with a detrimental effect upon another figure of merit in the radiation pattern.

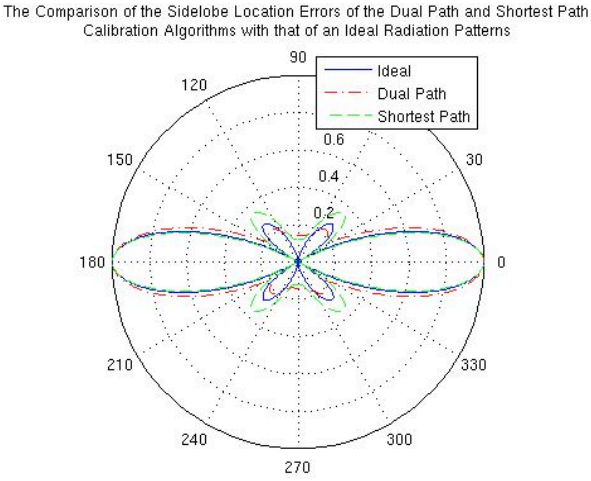

figure 5-44: The Comparison of the Dual Path and Shortest Path Calibration Algorithms in terms of the Cross Section of the Radiation Pattern for the Maximum Sidelobe Location Errors.

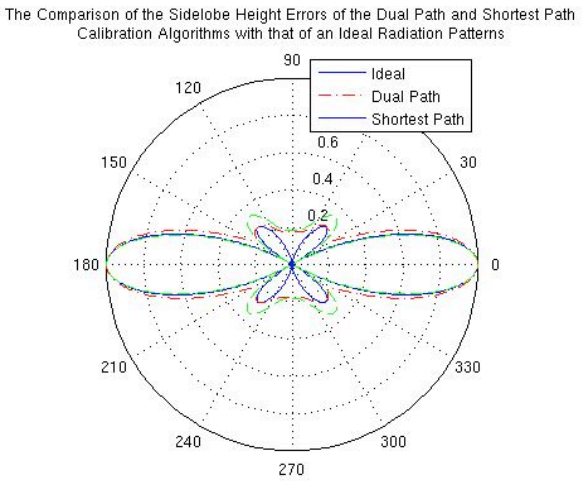

figure 5-45: The Comparison of the Dual Path and Shortest Path Calibration Algorithms in terms of the Cross Section of the Radiation Pattern for the Maximum Sidelobe Height Errors.

In this case it is both the null depth and the sidelobe level. This affects both of the calibration algorithms; however, the dual path calibration algorithm has a slightly shallower null depth than that of the shortest path, and lower sidelobe levels, though this is sometimes considered to be an advantage. The shortest path calibration algorithm has much higher sidelobe levels associated with the sidelobe location errors. Finally, the last figure of merit to be considered is the sidelobe height comparison, which can be seen in figure 5-45. This shows the interrelation between the sidelobe levels, the null depths and the beamwidths, where neither calibration algorithm is unaffected, and each by a different figure of merit interaction. These interactions between the figures of merit is unsurprising considering they are affected by the same source - the amplitude and phase imbalances that are also key parameters dependent on the calibration accuracy of the array.

5.4 Summary

The consideration of the measurement structure as a source of errors has a significant impact upon the achievable calibration accuracy, which was demonstrated in the comparison between the top left reference algorithms and the measure and correct error comparison approach. The subsequent calibration algorithms took various different approaches to this consideration with various degrees of success. The comparison based algorithms show that comparing the measurements taken by individual measurement sensors removes the impact of the sensors on the calibration. Therefore the accuracy of

these algorithms is dependent upon the number of coupler paths taken to calibrate each element of the array and making the calibration errors scale with the size. This is overcome to a degree by using dual paths and averaging then to reduce the impact of the coupler errors and this is successful as the calibration errors do not scale up as quickly.

The other styles of approaches that were taken were optimization approaches, which spread the calibration errors throughout the array with the heuristic approach, which meant that the calibration errors reduce as the size of the array increases. However, the simulated annealing approach was not successful at any level of calibration due to some faulty assumptions it made about the structure of the array. However, the prospect of optimisation algorithm, which calibrate an array with the simulated annealing algorithm but simply remove the outside ring of elements vastly improved the performance compared to the simulated annealing algorithm, but at a significant hardware cost.

Each of these algorithms were designed specifically for this measurement structure. They are unique incidences of this type of algorithms. In other areas, there maybe algorithms with similar naming conventions, however, there is not a similar measurement structure and therefore there are not similar algorithms.

Chapter 6

The Experimental Investigation

6.1 Introduction

The principles and algorithmic manipulation of the measurement structure has been presented in the previous two chapters. These chapters have made assertions about the possibilities and abilities of the calibration approach taken by this dissertation. This chapter will test these assertions by presenting the experimental prototypes created to prove the concept and feasibility of this system.

6.2 Measurement Structure

The calibration approach is based around a scalable measurement structure that utilises multiple measurement points as shown in figure 6-1. The uniqueness of the structure is the multiple sensor elements connected to multiple common elements to create a scalable measurement structure as presented in chapter 4. This is one of the key concepts, which facilitates the calibration in this approach. The six port directional coupler was developed to create the required connections to create this measurement structure. It is created based upon the four element circular array tiles, which are overlapped to create a scalable structure. This scalability requires four connections at each element and at each sensor device. This required a specially designed feeder structure to achieve these connections while providing as little interference to the antenna array's performance as possible, while providing symmetrical signals to each of the connections from the array elements. These considerations led to the development of the six port directional coupler, which has been described in chapter 4 and shown in figure 6-2. The six-port coupler was designed to fill the need for symmetrical measurement points and that each of the measurement sensors is equidistant from each of the elements that they are connected to. The structure provides the means of implementing calibration, as discussed in chapter 4, and it provides a novel directional coupler implementation to provide a solution to the connectivity requirements of the structure.

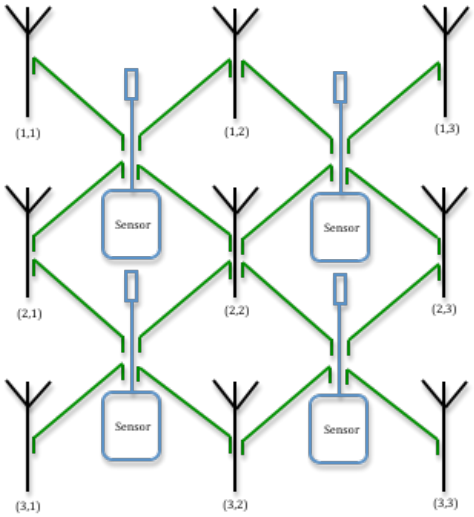

figure 6-1: The Multiple Measurement Structure for a 3 by 3 Array.

The six-port coupler was designed to fill the connectivity requirements created by the novel measurement structure. It had to be designed specifically to have four connections that provided symmetrical signals and interfered with the through path of the array element as little as possible. These criteria led to the development of this unique directional coupler structure. It provides a passive structure where each element is equidistant from the sensor element it is connected to. Based upon these requirements, a directional coupler approach was taken to the problem. This was because the coupler can siphon off a portion of the through path signal without interrupting its' flow. The connectivity requirements led to the choice of the three line edge couplers as they provide two connections with equal proportions of the signals. These connections are then feed into a second set of three line couplers to create the four symmetrical connections required for each element of the array. The initial prototype structure was designed in the Institute of Microelectronics and Wireless Systems by Dr. Tim Cooper, Dr. Ronan Farrell and Ger Baldwin [323]. The author designed subsequent enhancements, adding switching, covered in section 6.2.6.

This structure was developed to have highly coupled ports. The coupling factors between the ports of the measurement board are high. There is -40dB coupling between transceiver elements and the sensor ones. This creates > -80dB isolation between adjacent elements. These high coupling factors have the advantage of isolating adjacent elements from each other, and also reducing the signals so that transmit or receive calibration can be achieved. These highly coupled ports are designed to be amplitude and phase balanced. This is important as small coupler errors have an impact upon the

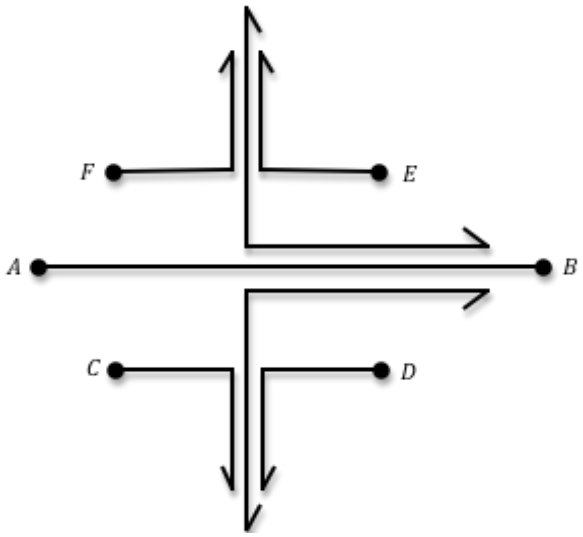

figure 6-2: Schematic Representation of the Six-Port Directional Coupler.

calibration accuracy of this approach. This has been analysed in the previous chapter and a mitigation technique was discussed there also.

The directional coupler structure was developed in stages where the design was perfected through implementation. The initial design was done using the technique outlined by Pozar [324] for individual edge couplers. The approach taken to designing the three coupled line directional coupler used Pozar's two-line directional coupler analysis in the design process, contrary to common practice. This approach has simplified the synthesis process, while providing adequate impedance matching over the band of interest, 2.4GHz to 2.5GHz. This impedance matching was achieved even while disregarding the other coupling modes of the structure. When considering the input impedance matching the six-port coupler achieved this with S_{11} (Port A) < -20dB. The output impedance matching of one of the four coupled ports, Port C, achieved this with S_{33} (Port C) < -13dB at 2.46 GHz. As was mentioned above, the six-port coupler was designed to be a high coupling port structure, each three line edge coupler was designed to have -10dB coupling factor. The six-port coupler therefore has -20dB coupling factor for each of the coupled connector ports, i.e. from port A to port C.

The operation of this six-port coupler is easier to consider in terms of its connections, as shown in figure 6-2. When port A is connected to the measurement sensor, then the through path is terminated in a 50Ω load at port B. This makes port C – F, the coupled paths to the connected transceiver elements. These coupled paths consist of two coupler

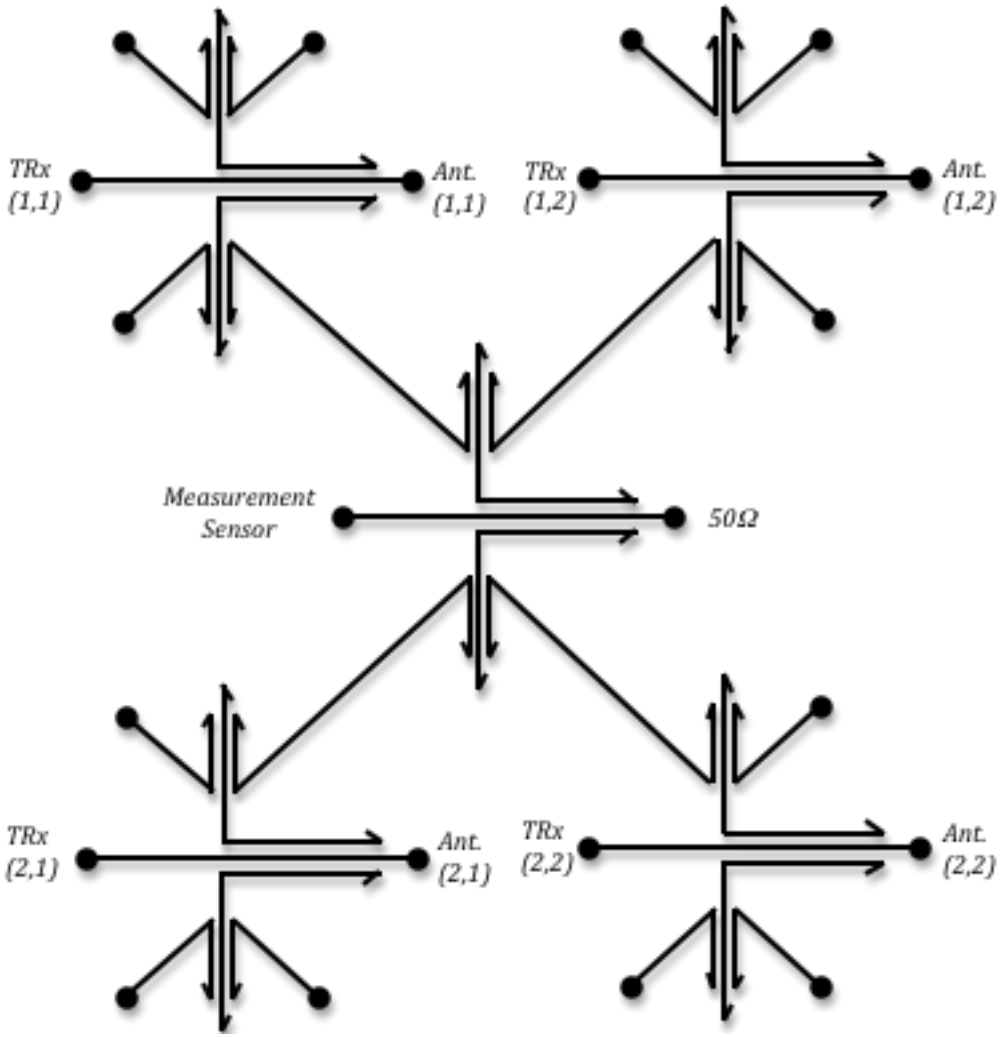

figure 6-3: Schematic of the Directional Coupler Measurement Structure for a 2 by 2 Antenna Array.

paths, which are symmetric around the central through path creating the four required connection ports. When the six port coupler is centred around the through path of the array element, then the transceiver is connected to port A and the antenna element is connected to port B. This makes the coupler paths to Port C through F the paths connecting the array element to the measurement sensors.

The six-port structure is used in series to create the complete connectivity used between the array elements and the sensors of the array. This is shown in figure 6-3. This figure shows a 2 by 2 array of directional coupler measurement board schematic, where a six-port coupler surrounds each element of the array. The central sensor element is surrounded by another six port coupler, which is connected to each of the four array elements. This schematic shows the symmetry of connections, which facilitate the addition of elements and additional sensor - in other words, the scalability of the

structure. Each of the of the six-port directional couplers provide four connections with -20dB coupling factor. Therefore there is a -40dB coupling factor between the elements of the array and the sensor elements. This provides theoretically > -80dB isolation between adjacent elements of the array, while scaling the signals from transmit to receive sensitivity levels. However in practice the isolation achieved ranged from -49.2dB to -82.6dB. Therefore receive and transmit calibration can be achieved by reusing components, so long as these components are frequency compatible.

6.2.1 Implementation

This is a passive structure. This means that the coupler paths are fixed. Therefore, the symmetrical coupling creates fixed paths of equal length between each element of the array and the connected sensors. Each element of the array is equidistant from its surrounding elements. This is by virtue of the structure. These paths should ideally be perfectly matched but the algorithms discussed in chapter 4 will help minimise the effect of any errors. For this experimental system, the couplers were prototyped upon FR-4 substrate. This medium-grade substrate was chosen for three reasons. The first of which is the cost of the substrate, as its lower cost made it much more attractive for the repeated manufacturing iterations that were taken to perfect the performance of the six port directional coupler. The second reason was the practicality of choosing a lower grade substrate. This will demonstrate that the directional coupler measurement structure and partner algorithms can yield excellent performance using FR-4 substrates. Performance would be enhanced with higher quality, more controlled substrates. The final reason is the ridged structure that the FR-4 provides. The is provided by the FR-4 thickness; the directional coupler was designed upon a stripline material with substrate thickness of 1.6 mm between the stripline copper layers, which are each 35μm thick.

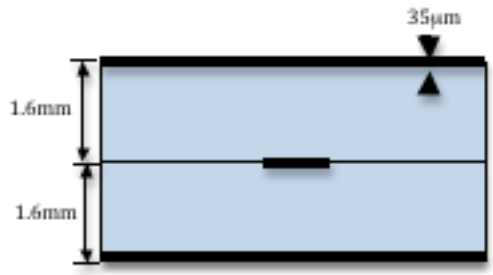

figure 6-4: Cross Section of Directional Coupler Measurement Boards, Stripline Layout.

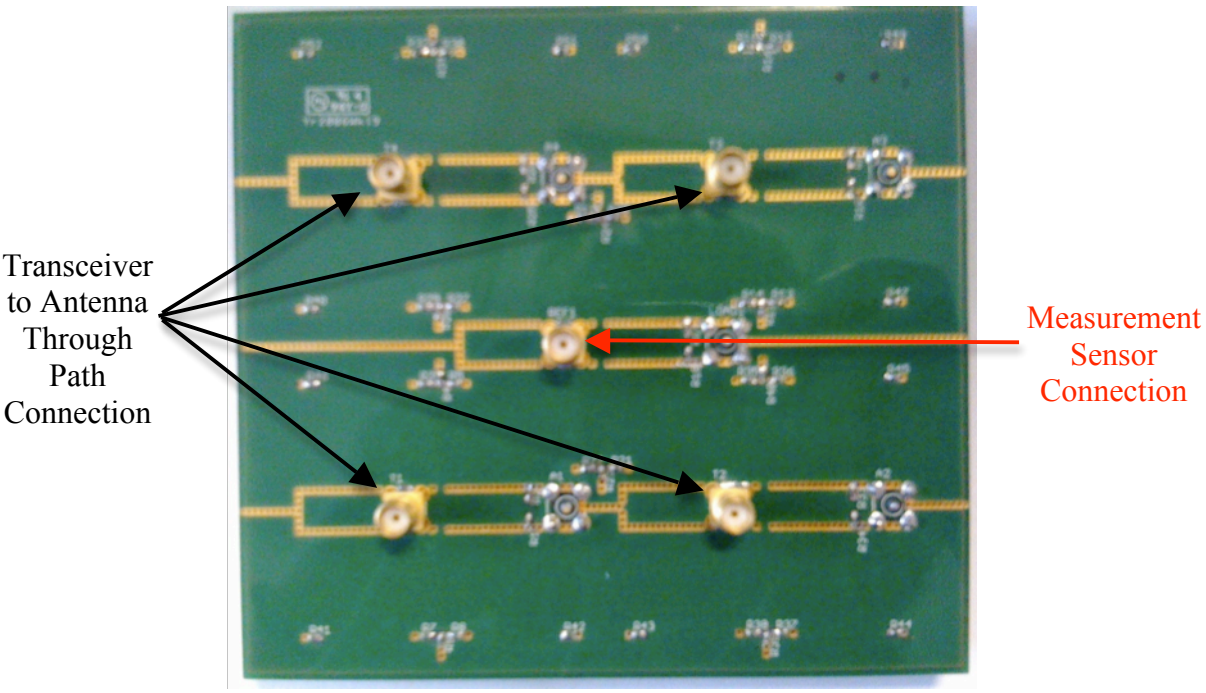

figure 6-5: 2 by 2 Prototype Directional Coupler Measurement Board.

The cross-section of this is shown in figure 6-4. This results in a ridged board, which can be seen in figure 6-5. The advantage of creating a ridged board is that it will be robust to wear and tear in the laboratory environment. It will maintain signal path integrity throughout the experimental process. It is also capable of providing structural support for the prototype, so there will be a fixed, unmoving piece of equipment during testing.

6.2.2 Simulations

The performance of the directional coupler measurement structure was simulated using Agilent's Advanced Design System (ADS). This was used in conjunction with prototyping to create the six port directional coupler and the scalable directional coupler board. ADS was used to simulate the performance in stages, such as a single coupled path from transceiver to sensor path, which is shown in figure 6-7. This schematic was used to predict the coupling factor of this path and thus the performance of the measurement paths of the whole array. The performance of this schematic was predicted to have the following S parameters for the ports of interest, which are shown in Table 6-1. These S-parameter shows 0.51dB drop in the through path signal from transceiver to antenna, which is a result of the -10dB three line edge coupler along this path. While the coupled measurement path has close to the estimated -40dB coupling factor, and achieving -38dB.

Table 6-1: S-Parameters of Interest for a Single Coupled Path for the Directional Coupler Measurement Structure.

Path	S-Parameters	Values
Transceiver to Antenna Through Path	S_{78}	-0.5137dB
Input (Transceiver) Impedance Matching	S_{88}	-41.27dB
Output (Antenna) Impedance Matching	S_{77}	-42.2945dB
Output (Measurement) Impedance Matching	$S_{10\,10}$	-41.272dB
Coupled Path (Transceiver to Measurement Device)	$S_{10\,8}$	-38.11dB

The simulations presented in Table 6-1 are taken at 2.46GHz, the operating frequency at which the board was designed for. The ADS simulations were also used to predict the performance over a range of frequencies. This is shown in figure 6-6 and figure 6-8. These simulations predict the performance of the single coupled paths from transceiver to sensor element, shown in figure 6-7, over 1 GHz range from 2GHz to 3GHz, and from 2.4GHz to 2.5GHz respectively. The first figure, figure 6-6, shows a change in the coupling factor that ranges from -39.7dB to -38.15dB. This alteration is minor over this range, peaking at 2.48GHz, which is slightly off the 2.46GHz designed operational frequency.

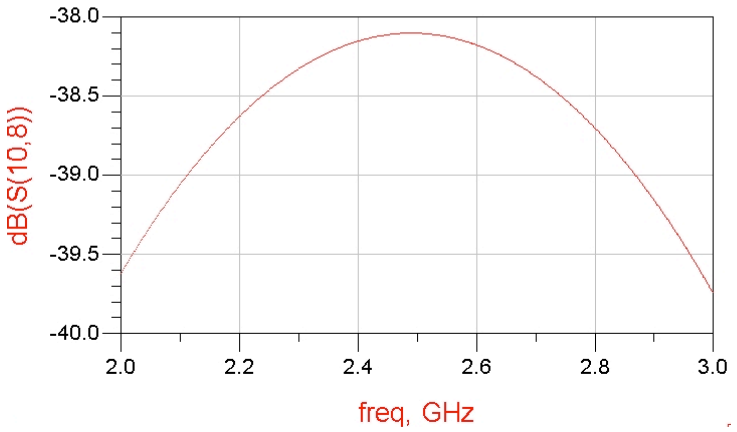

figure 6-6: Coupled Path S-Parameter for the ADS Simulation of the schematic shown in figure 6-7, over the frequency range 2GHz to 3GHz.

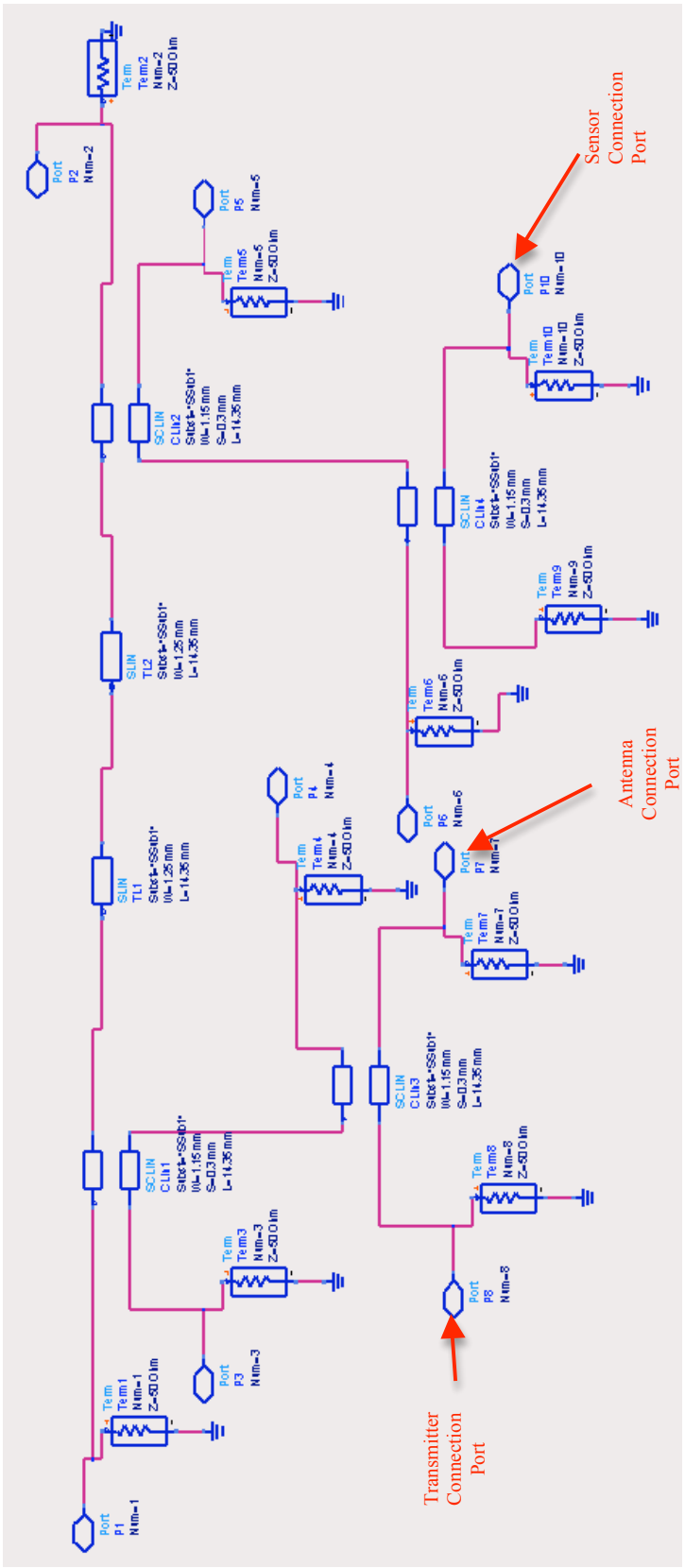

figure 6-7: ADS Schematic of a Single Coupled Path in the Measurement Structure.

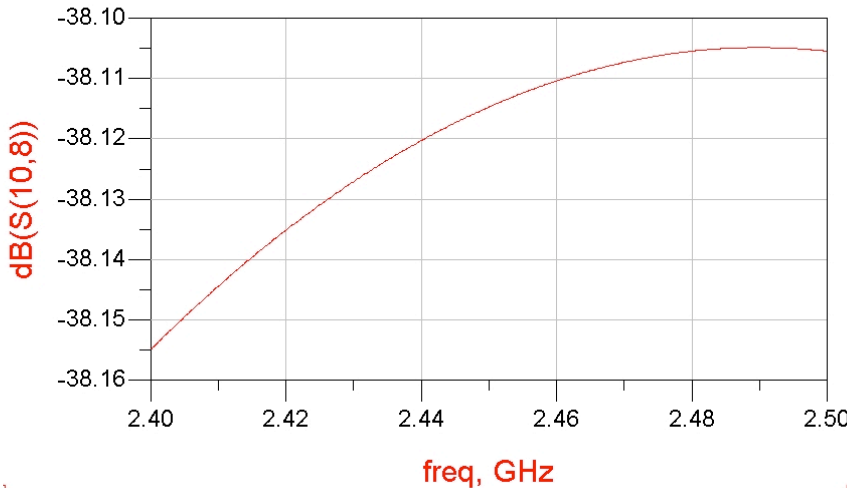

figure 6-8: Coupled Path S-Parameter for the ADS Simulation of the schematic shown in figure 6-7, over the frequency range 2.4GHz to 2.5GHz.

The second figure, figure 6-8, shows the same slow progression in the coupling factor over a smaller frequency range. This shows a -38.11dB coupling factor at 2.46GHz compared to a peak coupling factor of -38.15dB at 2.48GHz. This shows the small alterations in the coupling factors over a range of frequencies. Due to the passive nature of the structure, the performance of the couplers will change uniformly over the whole array when the operational frequency is altered. This is the advantage of this approach even with the narrowband nature of the stripline design. This consistent coupling factor achieved by the coupler at different frequencies is possible while preserving the essential operational abilities of the measurement structure.

6.2.3 Prototype

The directional coupler board was prototyped on an FR-4 substrate. The measurement board was developed in stages. The first complete board that was made was a *2 by 2* array. The principles and techniques for the layout of these boards were used for the larger arrays.

The stripline structure was laid out for PCB (printed circuit board) fabrication in CadSoft Eagle Layout Editor, the stripline layer of this layout is shown in figure 6-9. Shielding was added during layout because the prototype is to work at high frequencies. Therefore the interactions between the couplers became a concern, this is due to the close proximity of the couplers. The transmission line length and half wavelength a criterion for the antenna array element spacing are small as they are dictated by the high

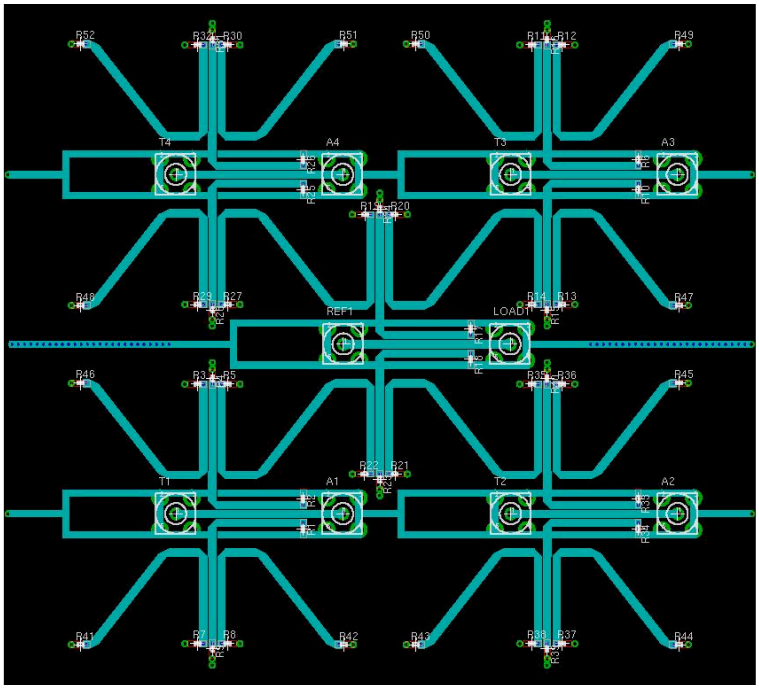

figure 6-9: PCB Layout of 2 by 2 Prototype Directional Coupler Measurement Board.

frequency of operation. There is little coupling from the end of the coupler lines; the shielding was put in place to remove any surface waves.

The shielding that was used between the couplers were a set of vias arranged in a rectangle around the through path couplers for the array elements and the sensor ones. These through-hole vias connect the grounded plates above and below the stripline couplers creating a shielding box. These shielding vias can be seen in both figure 6-5 and figure 6-9.

The *2 by 2* boards were fabricated off site by a PCB fabrication company called ECSCircuits. A photo of the finished board is shown in figure 6-5. Two of the *2 by 2* coupler boards were manufactured. They were tested using a Rohde & Schwarz ZVB20 Vector Network Analyser (VNA). This performance is presented in the series of tables, Table 6-2 to Table 6-5. These contain the amplitude and phase S-parameter measurements of all of the ports of the boards. These measurements led to the calculation of the relative errors between each of the measurement paths of the two 2 by 2 coupler boards. These errors come from the manufacturing tolerances, path length variations, coupling factors, connectors and component tolerances. These predictions are graphed to show the measured distribution of errors in figure 6-10. These distributions show that the manufacturing errors of ±0.4dB amplitude and -2.3^{o} and +1.2^{o}. These measured distributions of errors have a standard deviation of 0.4dB and

1.12°. These standard deviations were used in the simulation models used to develop the algorithms.

Table 6-2: The Amplitude Measurements for the First 2 by 2 Directional Coupler Measurement Board.

Coupled Paths		S_{11}	S_{22}	S_{12}	S_{21}
		dB	dB	dB	dB
TRx 1	Sensor	-30.4	-29.3	-39.4	-39.4
TRx 2	Sensor	-30.3	-26.7	-39.4	-39.4
TRx 3	Sensor	-30.1	-23.8	-39.1	-39
TRx 4	Sensor	-30.4	-27.8	-38.7	-38.6

Table 6-3: The Phase Measurements for the First 2 by 2 Directional Coupler Measurement Board.

Coupled Paths		S_{11}	S_{22}	S_{12}	S_{21}
		degrees	degrees	degrees	degrees
TRx 1	Sensor	-62.6	-30.4	-31	-31.3
TRx 2	Sensor	-61.7	-17.4	-31.5	-31.8
TRx 3	Sensor	-63.4	-17.9	-31.6	-31.7
TRx 4	Sensor	-61	-6.3	-33.8	-34.2

Table 6-4: The Amplitude Measurements for the Second 2 by 2 Directional Coupler Measurement Board.

Coupled Paths		S_{11}	S_{22}	S_{12}	S_{21}
		dB	dB	dB	dB
TRx 1	Sensor	24.1	-29.7	-38.7	-38.7
TRx 2	Sensor	-26.4	-30.1	-38.5	-38.5
TRx 3	Sensor	-30.9	-30.1	-38	-38
TRx 4	Sensor	-34.1	-30.1	-37.9	-37.9

Table 6-5: The Phase Measurements for the Second 2 by 2 Directional Coupler Measurement Board.

Coupled Paths		S_{11}	S_{22}	S_{12}	S_{21}
		degrees	degrees	degrees	degrees
TRx 1	Sensor	-113.9	-54.7	-2.1	-2.2
TRx 2	Sensor	-148.9	-54.6	-2	-1.9
TRx 3	Sensor	-141.2	-54.4	-3.6	-3.5
TRx 4	Sensor	-3.5	-54.4	-3.6	-3.5

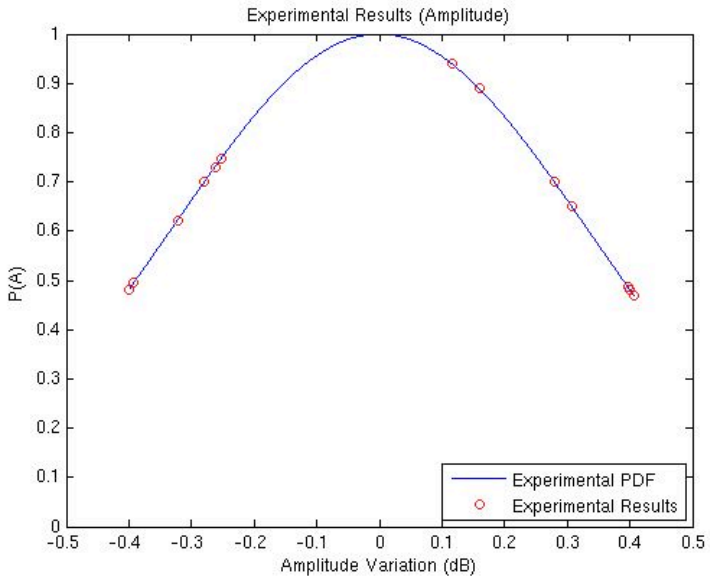

(a)

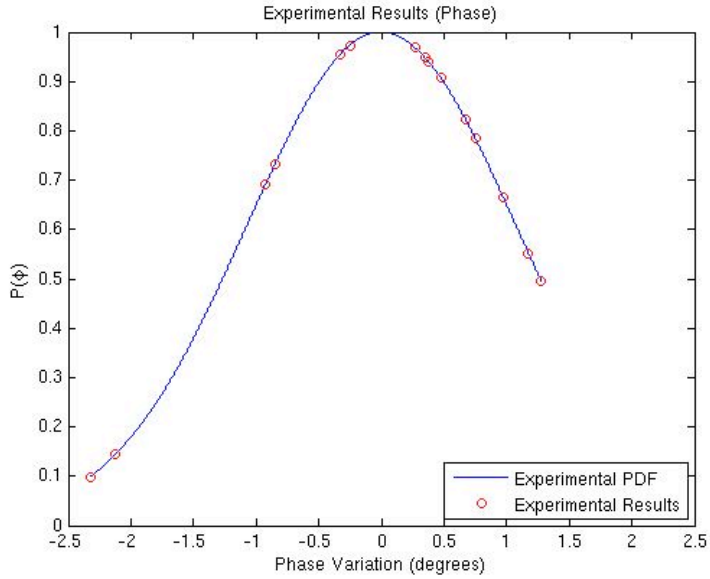

(b)

figure 6-10: The Probability Density Function of the Coupler Errors for the 2 by 2 Directional Coupler Measurement Boards.

6.2.4 Implementation Issue

The approach used to fabricate larger arrays was to use the scalable connectivity provided by the six port coupler and to replicate the required number of tiles. The larger arrays that were prototyped were a *2 by 4* and a *4 by 4* boards, which are shown in figure 6-11 and figure 6-12. With the prototyping of the larger boards an implementation issue was identified - the larger boards warped. This warping affected the boards by bowing the whole board. For the *2 by 4* board, it is only apparent along the longest axis of the board, which is to be expected. The *2 by 2* boards did not exhibit

this effect. The *4 by 4* board was effected along both its' axis. This warping can be seen in figure 6-13, which shows the warping of the *2 by 4* board. This shows a side view o the board sitting upon a counter top. Each of the connectors should be flat with the surface. They are not; the space between the connectors and the counter top is clearly visible.

The warping comes from the construction of the directional coupler boards from FR-4 substrate. These boards are fabricated by sandwiching two layers of FR-4 together to create the stripline structure. These two layers react differently to environmental effects. As the array size gets larger the differences become more apparent. The warping presented in these boards are due to the manufacturing process and laboratory environmental conditions and could be corrected through the use of different materials.

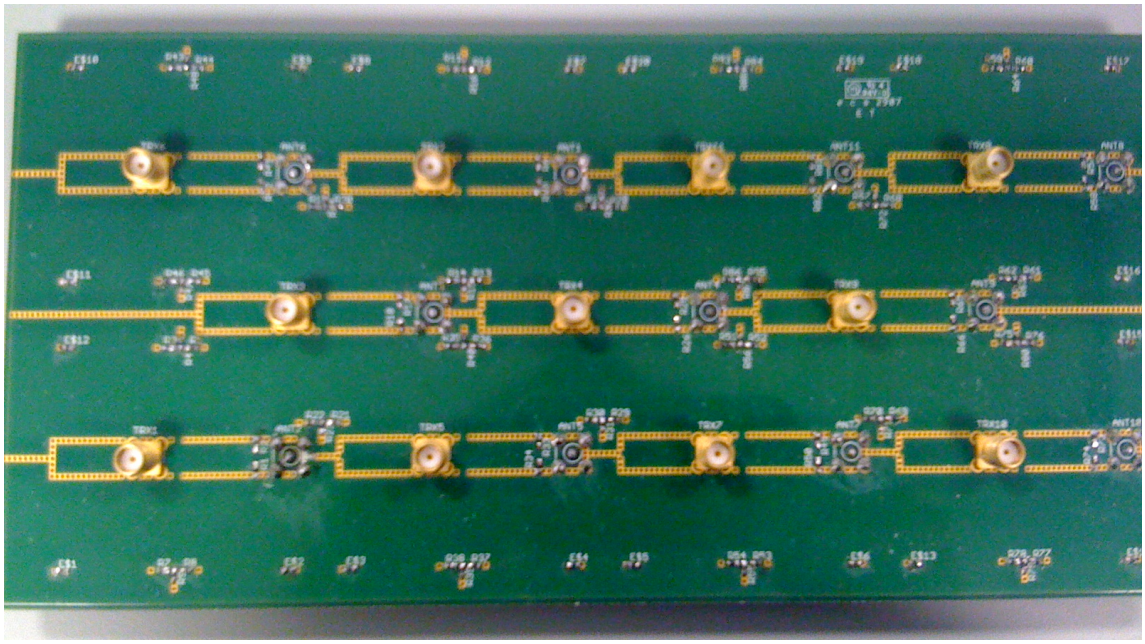

figure 6-11: 2 by 4 Prototype Directional Coupler Measurement Board.

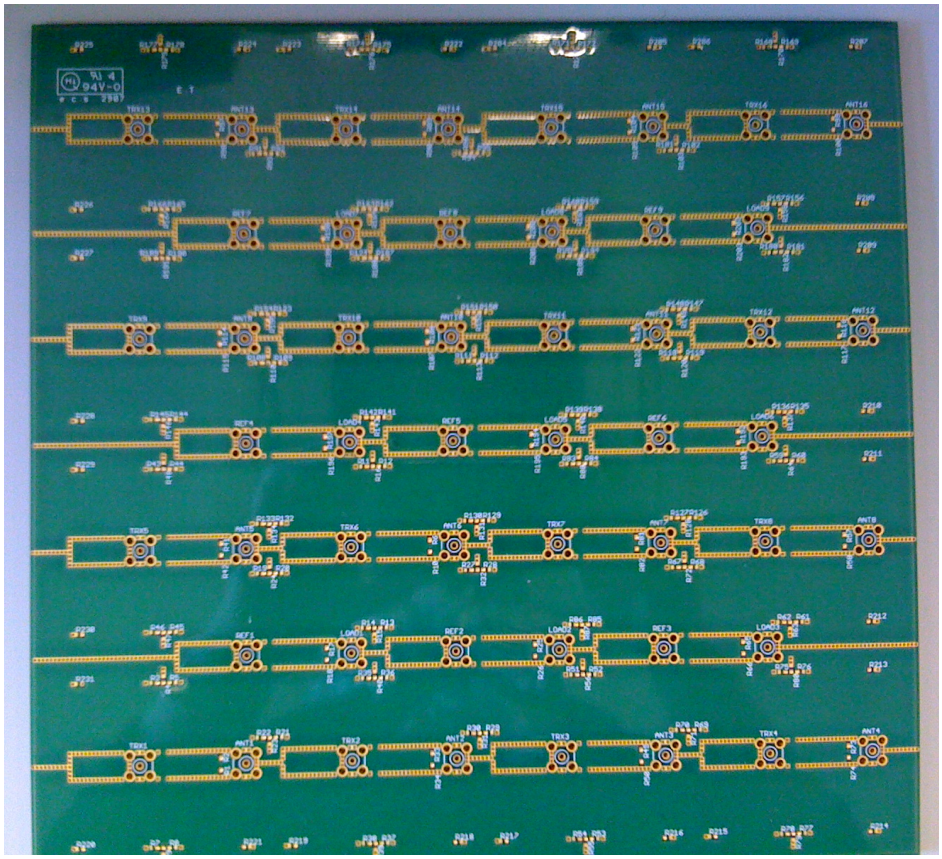

figure 6-12: 4 by 4 Prototype Directional Coupler Measurement Board, Unpopulated.

6.2.4.1 The Effect of the Warping Implementation Issue

The directional coupler measurement board is a source of measurement errors for the calibration approach, such as the errors from the manufacturing tolerances, path length variations, coupling factors, connectors and component tolerances, as seen from the distribution of errors in the 2 by 2 boards. These errors are understood and have been taken into consideration in the calibration of the system by the dual path calibration algorithms.

The warping of the board will alter these errors, as it will alter the symmetry created by the coupler by the distortion of the substrate. This means that the stripline tracks will also be altered. This has the effect of altering the coupler errors in quantity and size. These effects depend upon the degree of warping experienced by a particular board.

The effect of warping upon the measurement paths will be compared looking at the distribution of errors for each of the manufactured prototypes. The first is that of the *2 by 2* board results plotted against the *2 by 4* board ones where the distribution is generated based upon the measurements in tables 6-2 to 6-7, in figure 6-14. These

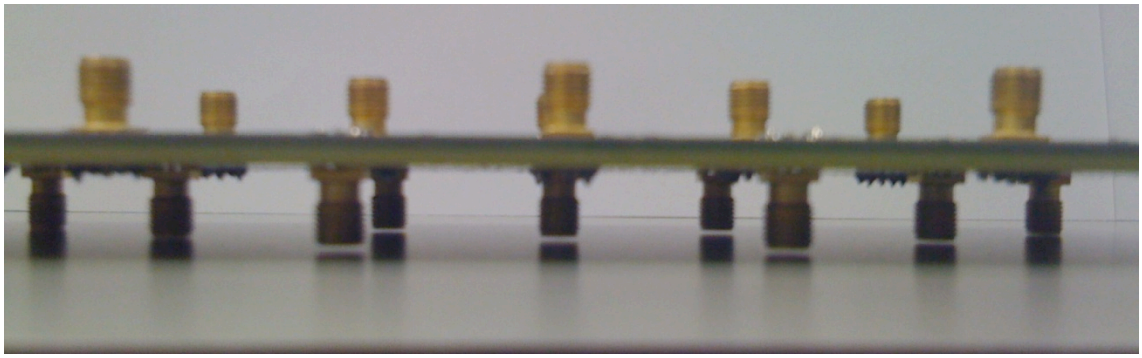

figure 6-13: Side View of the 2 by 4 Prototype Directional Coupler Measurement Board to show the Warping.

figures show the wider distribution for both the amplitude and phase errors. The errors show the impact of warping along a single axis on the measurement path errors. From the distribution of errors, it is clear to see that a majority of the phase errors are centred along the distribution except a few outliers on the tails. The same property can be seen in the amplitude distribution to a limited extent. The next comparison is of the *2 by 2*, *2 by 4* and the *4 by 4* boards measurement path errors, which are shown in figure 6-15. This comparison shows an improvement in the amplitude errors and a large improvement in the phase errors of the *4 by 4* board compared to the *2 by 4* one. These results show a wider distribution for the amplitude errors when compared to the *2 by 2* board results. There is a marginal widening of the distribution of the phase errors when they are compared to the *2 by 2* boards. This improvement in performance of the *4 by 4* measurement errors over the *2 by 4* ones is from the symmetry of warping, as the *4 by 4* board is warped on both axes. This has led to consistently high path mismatch errors rather than large outliers as seen in the 2 by 4 board. This assertion is easier to see by looking at the measurements taken from the *2 by 4* and *4 by 4* prototype boards, which are presented in Table 6-6, Table 6-7, Table 6-8 and Table 6-9. These tables also contain the amplitude and phase measurements of the two *2 by 2* prototypes boards for perspective. The results are the errors from the ideal value of -40dB and the measured value.

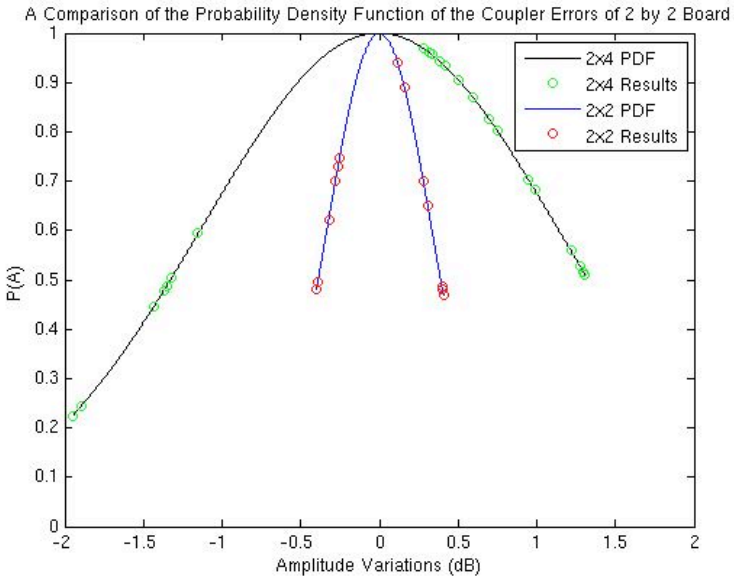

(a)

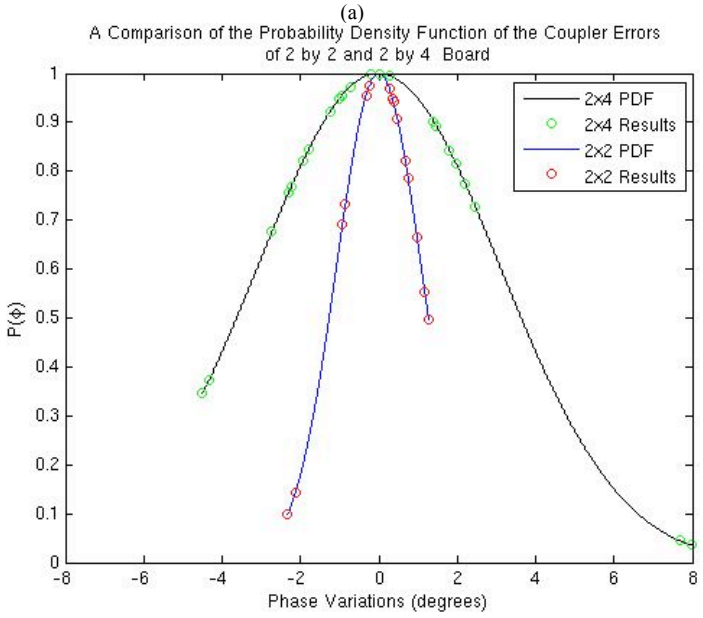

(b)

figure 6-14: The Comparison of the Probability Density Function of Coupler Errors for the 2 by 2 and 2 by 4 Directional Coupler Measurement Boards.

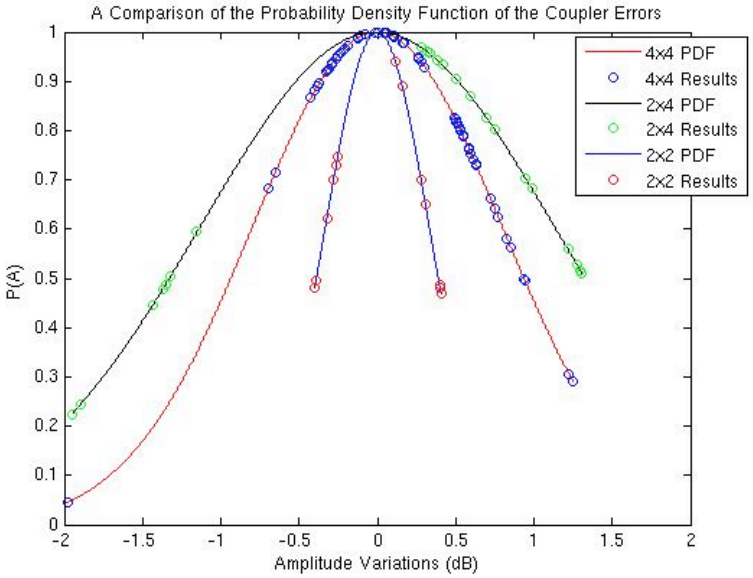

(a)

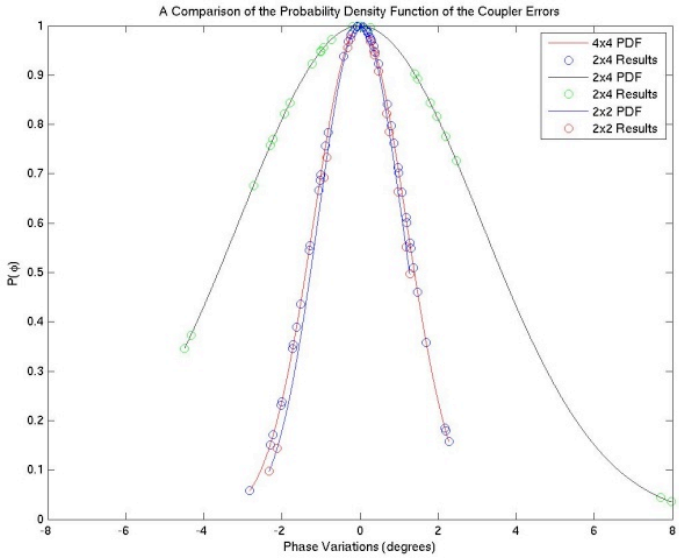

(b)

figure 6-15: The Comparison of the Probability Density Function of Coupler Errors for the 2 by 2, 2 by 4 and the 4 by 4 Directional Coupler Measurement Boards.

Table 6-6: The Amplitude Measurements for the 2 by 4 Directional Coupler Measurement Board.

Coupled Paths		S_{11}	S_{22}	S_{12}	S_{21}
		dB	dB	dB	dB
(1,1)	Sensor 1	-29.3	-25.4	-39.2	-39.2
(2,1)	Sensor 1	-29.3	-25.5	-39.7	-39.7
(2,2)	Sensor 1	-29.3	-39.5	-39.7	-39.7
(1,2)	Sensor 1	-29.2	-18.2	-39	-39.1
(1,2)	Sensor 2	-25.6	-35.6	-41.2	-41.3
(2,2)	Sensor 2	-25.6	-39.2	-41.4	-41.5
(2,3)	Sensor 2	-25.5	-22.1	-41.3	-41.3
(1,3)	Sensor 2	-25.8	-43	-41.4	-41.4
(1,3)	Sensor 3	-29.1	-29.1	-39	-38.9
(2,3)	Sensor 3	-28.8	-21.9	-39.9	-39.8
(1,4)	Sensor 3	-29.5	-20.8	-38.9	-38.8
(2,4)	Sensor 3	-29.4	-25.6	-39	-39.7

Table 6-7: The Phase Measurements for the 2 by 4 Directional Coupler Measurement Board.

Coupled Paths		S_{11}	S_{22}	S_{12}	S_{21}
		degrees	degrees	degrees	degrees
(1,1)	Sensor 1	-98.6	4.2	-39.7	-39.5
(2,1)	Sensor 1	-97.6	-17.5	-39.7	-39.7
(2,2)	Sensor 1	-98	-72.3	-40.9	-41.3
(1,2)	Sensor 1	-98.8	-51.5	-44.4	-44.3
(1,2)	Sensor 2	-49.5	-25.4	-38.4	-38.3
(2,2)	Sensor 2	-47.8	-78.9	-40.2	-40.3
(2,3)	Sensor 2	-47.5	-18.1	-40	-39.9
(1,3)	Sensor 2	-47	-43.1	-43	-43.1
(1,3)	Sensor 3	-61.4	-26.6	-45.1	-45.4
(2,3)	Sensor 3	-63.2	-17.3	-43.3	-43.4
(1,4)	Sensor 3	-57.8	-4.1	-43.6	-43.5
(2,4)	Sensor 3	-58.1	-14.8	-41.6	-41.8

Table 6-8: The Amplitude Measurements for the 4 by 4 Directional Coupler Measurement Board.

Coupled Paths		S_{11}	S_{22}	S_{12}	S_{21}
		dB	dB	dB	dB
(4,1)	Sensor 3	-18.07	-29.59	-39.62	-39.64
(3,1)	Sensor 3	-18.85	-29.59	-38.84	-38.83
(3,2)	Sensor 3	-17.89	-29.81	-39.15	-39.15
(4,2)	Sensor 3	-18.85	-29.89	-39.66	-39.68
(4,2)	Sensor 6	-18.84	-21.97	-39.12	-39.14
(3,2)	Sensor 6	-17.9	-21.97	-39.93	-39.87
(3,3)	Sensor 6	-18.33	-22	-39.96	-39.97
(4,3)	Sensor 6	-17.56	-22	-41.95	-41.98
(4,3)	Sensor 9	-17.57	-30.04	-39.92	-39.9
(3,3)	Sensor 9	-18.35	-30.09	-39.04	-39.05
(3,4)	Sensor 9	-19.09	-30.02	-38.92	-38.96
(4,4)	Sensor 9	-18.15	-30.04	-39.61	-39.58
(3,4)	Sensor 8	-19.06	-25.08	-39.39	-39.38
(2,4)	Sensor 8	-18.45	-25.16	-39.14	-39.18
(2,3)	Sensor 8	-10.56	-25.12	-38.84	-38.91
(3,3)	Sensor 8	-18.36	-25.13	-39.41	-39.42
(3,3)	Sensor 5	-18.37	-21.84	-41.69	-41.66
(2,3)	Sensor 5	-10.56	-21.88	-40.32	-40.38
(2,2)	Sensor 5	-17.98	-21.89	-39.98	-39.95
(3,2)	Sensor 5	-17.99	-21.79	-39.08	-39.1
(3,2)	Sensor 2	-17.89	-33.85	-40.07	-40.11
(3,1)	Sensor 2	-18.76	-33.94	-39.99	-40.01
(2,1)	Sensor 2	-19.27	-33.84	-38.42	-38.46
(2,2)	Sensor 2	-17.98	-33.82	-38.73	-38.74
(2,2)	Sensor 1	-17.85	-28.64	-39.77	-39.76
(2,1)	Sensor 1	-19.32	-28.71	-39.77	-39.81
(1,1)	Sensor 1	-17.28	-28.69	-39.56	-39.59
(1,2)	Sensor 1	-18.29	-28.71	-39.66	-39.7
(1,2)	Sensor 4	-18.3	-21.27	-40.04	-40.07
(2,2)	Sensor 4	-17.88	-21.29	-39.17	-39.14
(2,3)	Sensor 4	-10.52	-21.31	-41.89	-41.94
(1,3)	Sensor 4	-18	-21.27	-39.9	-39.89
(1,3)	Sensor 7	-18.02	-33.27	-39.16	-39.19
(2,3)	Sensor 7	-10.54	-33.22	-39.79	-39.89
(2,4)	Sensor 7	-18.82	-33.24	-39.5	-39.52
(1,4)	Sensor 7	-18.05	-33.99	-39.07	-39.07

Table 6-9: The Phase Measurements for the 4 by 4 Directional Coupler Measurement Board.

Coupled Paths		S_{11}	S_{22}	S_{12}	S_{21}
		degrees	Degrees	degrees	degrees
(4,1)	Sensor 3	-161.78	-105.14	-59.9	-60.7
(3,1)	Sensor 3	-163.41	-104.86	-62.3	-63.2
(3,2)	Sensor 3	-163.14	-107.59	-61.88	-62.5
(4,2)	Sensor 3	-164.75	-107.21	-60.6	-61.5
(4,2)	Sensor 6	-164.72	-163.92	-59.6	-60.4
(3,2)	Sensor 6	-163.38	-163.86	-58.4	-59.5
(3,3)	Sensor 6	-163.34	-164.02	-60.9	-61.8
(4,3)	Sensor 6	-165.8	-164.07	-58.4	-59.4
(4,3)	Sensor 9	-165.7	-100.92	-59.9	-60.3
(3,3)	Sensor 9	-163.47	-101.43	-60.5	-61.2
(3,4)	Sensor 9	-163.07	-101.43	-61.6	-61.9
(4,4)	Sensor 9	-166.37	-101.93	-60.3	-60.5
(3,4)	Sensor 8	-162.68	-118.13	-60.8	-61.9
(2,4)	Sensor 8	-170.4	-118.3	-60.9	-61.9
(2,3)	Sensor 8	-164.65	-118.12	-59.8	-61.5
(3,3)	Sensor 8	-163.11	-118.06	-61.6	-62.7
(3,3)	Sensor 5	-162.97	-153.16	-59.9	-60.8
(2,3)	Sensor 5	167.21	-153.29	-62.9	-64.5
(2,2)	Sensor 5	-151.77	-153.49	-62.6	-63.9
(3,2)	Sensor 5	-163.06	-153.51	-59.4	-60.6
(3,2)	Sensor 2	-162.93	-141.27	-58.9	-60.2
(3,1)	Sensor 2	177.71	-140.32	-62.6	-63.7
(2,1)	Sensor 2	-174.43	-140.83	-59.3	-60.5
(2,2)	Sensor 2	-151.89	-141.2	-60.3	-61.4
(2,2)	Sensor 1	-151.91	-107.15	-60.4	-61.6
(2,1)	Sensor 1	-174.85	-107.56	-60.5	-61.6
(1,1)	Sensor 1	-167.58	-107.85	-59.4	-60.5
(1,2)	Sensor 1	-172.74	-107.43	-61.9	-63.3
(1,2)	Sensor 4	-172.9	-147.32	-60.9	-62.1
(2,2)	Sensor 4	-151.54	-147.29	-59.8	-61.9
(2,3)	Sensor 4	167.22	-147.33	-60.2	-61.6
(1,3)	Sensor 4	-161.38	-147.33	-62.32	-63.7
(1,3)	Sensor 7	-161.33	-94.78	-60.34	-61.47
(2,3)	Sensor 7	167.1	-95.66	-60.25	-61.53
(2,4)	Sensor 7	-167.73	-95.58	-60.67	-61.73
(1,4)	Sensor 7	-156.93	-96.63	-61.48	-62.74

6.2.5 Summary

This section has presented the unique six-port directional coupler that was designed to meet the requirements of the novel multi-sensor measurement structure that is at the centre of this dissertations calibration approach. The six-port coupler provides symmetrical connectivity. When they are used in series, a scalable measurement structure is created. This scalable measurement board was designed, simulated and prototyped. The prototypes were made on FR-4 substrate, which give rise to sources of measurement errors for the calibration approach. These errors come from manufacturing tolerances, path length variations, coupling factors, connectors and component tolerances. These will affect every practical implementation. The multiple sensors interleaved with the elements of the array allow for the mitigation of the impact of the errors upon calibration. Due to the choice of material used for the prototypes, a warping issue was introduced for larger array sizes. This warping has an effect upon the board errors and will in turn have an effect upon calibration.

The passive nature of the measurement structure has a disadvantage that will only affect systems without a dedicated calibration slot. As the structure is based upon a passive coupler, it provides coupler paths feeding into a single point, as shown in figure 6-3. This provides a symmetrical circuit. It, however, provides a measurement problem as this only allows sequential measurements of the four elements connected to a sensor – this requiring sequencing of the transmitters with the remaining transmitters turned off. This is due to the inability to selectivity access individual channels in our initial coupler design.

6.2.6 The Switched Directional Coupler Measurement Board

To resolve this issue, a switched directional coupler was developed. This is an alternative to the passive directional coupler measurement structure with added switches along the coupler paths so that the antenna array can be calibrated during operation. This is easiest to consider in terms of transmit operation. There were several different possible approaches considered for the implementation of this switching. The first switched implementation is that of switching along the coupler paths to the measurement sensor, as shown in schematic form in figure 6-16.

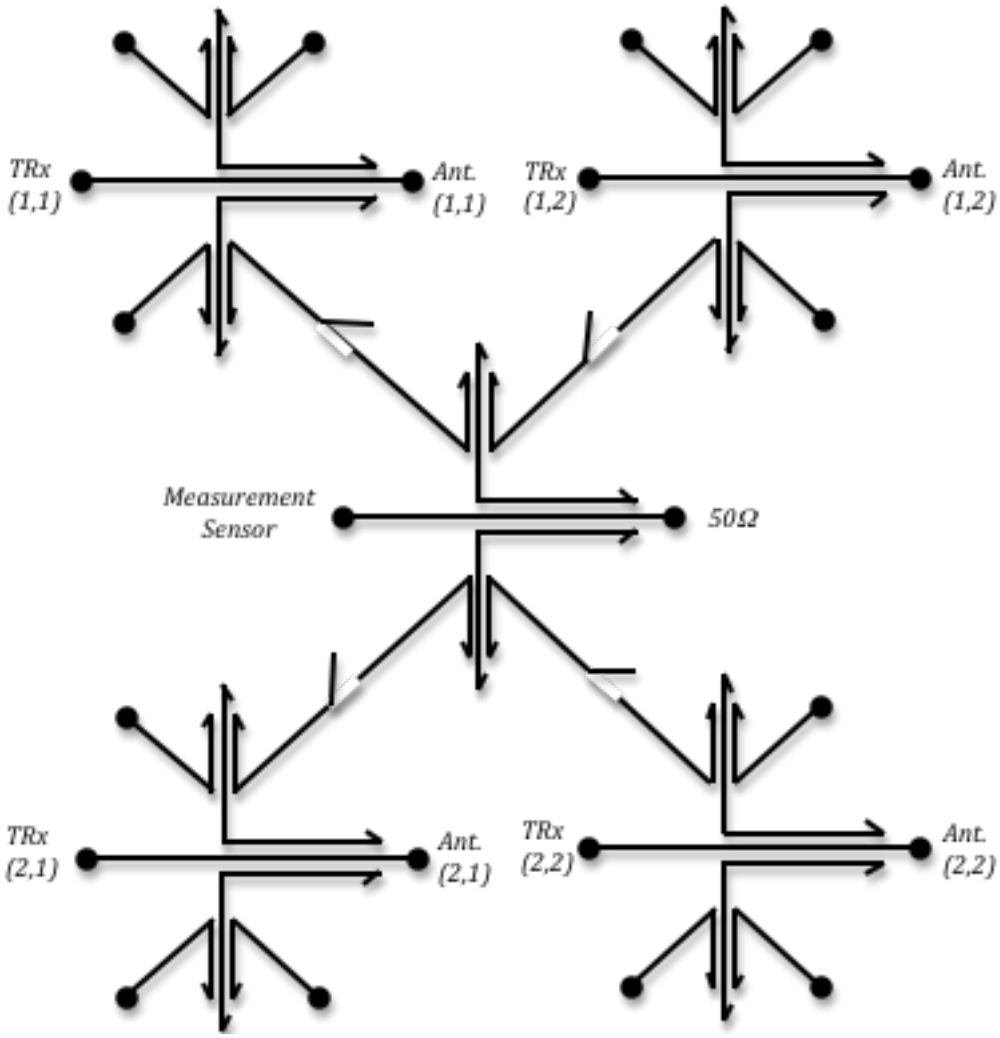

figure 6-16: Schematic of a Switched Directional Coupler Measurement Structure for a 2 by 2 Antenna Array.

Secondly there was the choice of using a four port switch (SP4T) instead of the six port coupler at the measurement port connection, such as shown in figure 6-17. The last alternative that was considered was to have the switch as a separate component. This would make the coupler paths feed into a separate switch, SP4T, via SMA connectors, such as shown in figure 6-18. Each of these approaches had its merits. The switched coupler paths are the least invasive approach, though it alters the passive structure of the coupled paths by adding switches. It does maintain the symmetry of the circuit but adds another source of measurement errors by adding active components to the structure.

The single central SP4T switch setup altars the measurement structure considerably by introduced an active element and removing the six-port coupler surrounding the sensor element. This switching approach maintains the symmetry of the layout. The approach uses a surface mounted switch. This will alter the stripline structure and therefore the

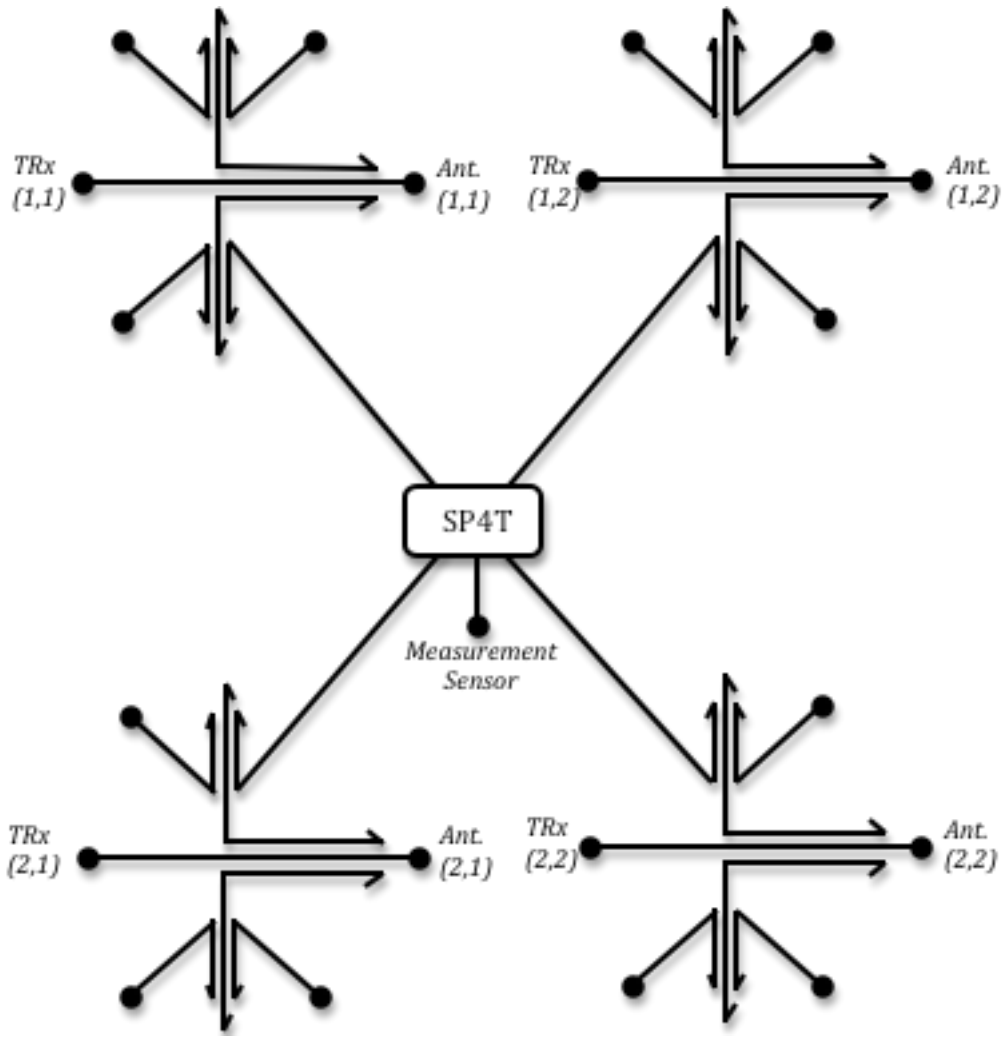

figure 6-17: Schematic of a Surface Mounted Switched Directional Coupler Measurement Structure for a 2 by 2 Antenna Array.

performance of the board will be excessively changed, particularly for the FR4 substrate chosen. This made it unsuitable for our prototype.

The choice of removing the switches from the measurement board altogether would alter the structure considerably in a similar manner to the surface mount switch approach, as it will remove the six-port coupler surrounding the sensor element. It uses SMA connectors to transfer the stripling structure to the external switch. The external switches that were considered included RF MEMs. The splitting of the measurement structure was however considered an unattractive option as the space was small and the connectivity required proved problematic. Therefore this approach was discounted.

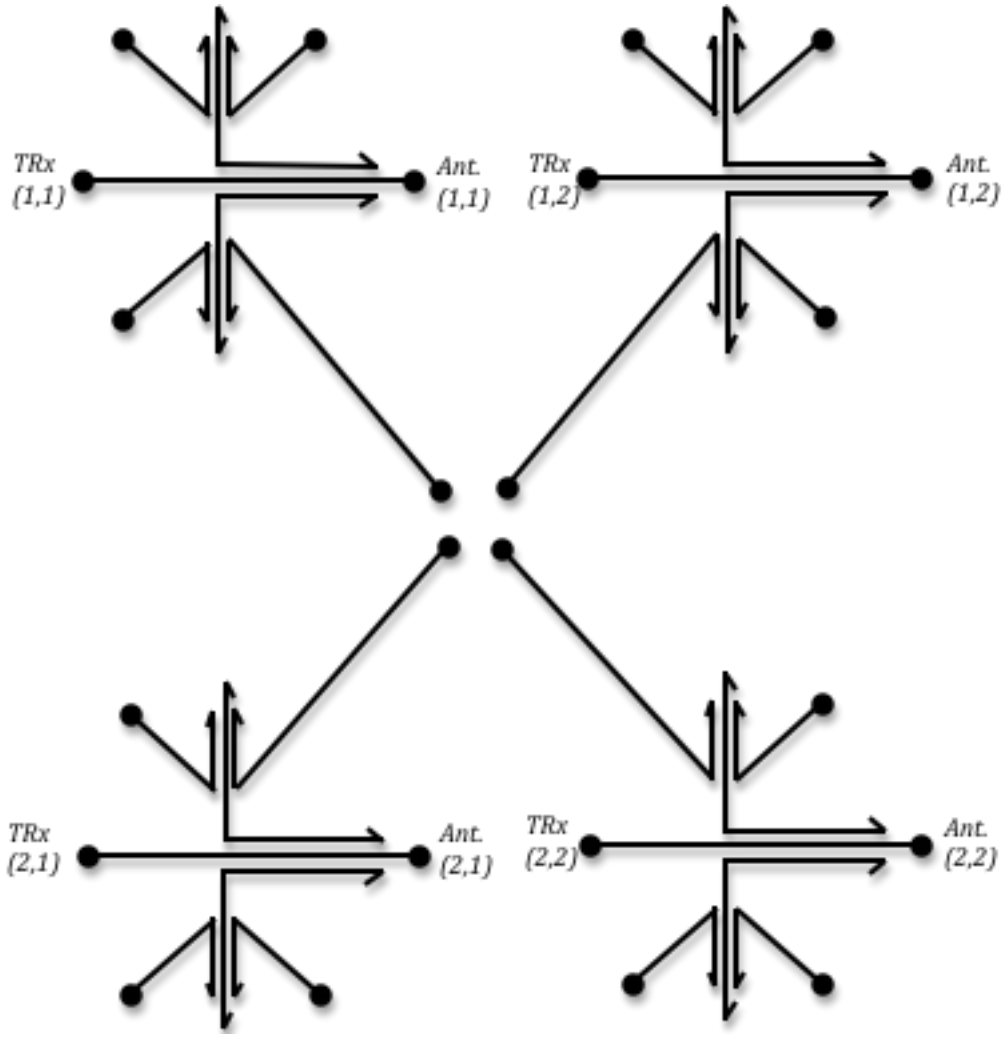

figure 6-18: Schematic of a Switched Directional Coupler Measurement Structure with External Switching for a 2 by 2 Antenna Array.

The last two switching implementations were discounted due to voltage requirements and disruption to the stripline structure for the surface mounted switch approach and for the space and cost of splitting the measurement structure for the separate switching implementation. This leaves the switched coupler paths technique. There were two different switching techniques considered for this, the first was surface mounted switches and the second was a pin diode approach. The surface mounted switch approach was discounted for the same reasons as it was when it was considered for the replacement of the measurement port's six-port coupler. The reason was the surface mounted distortion of the signals and coupled paths.

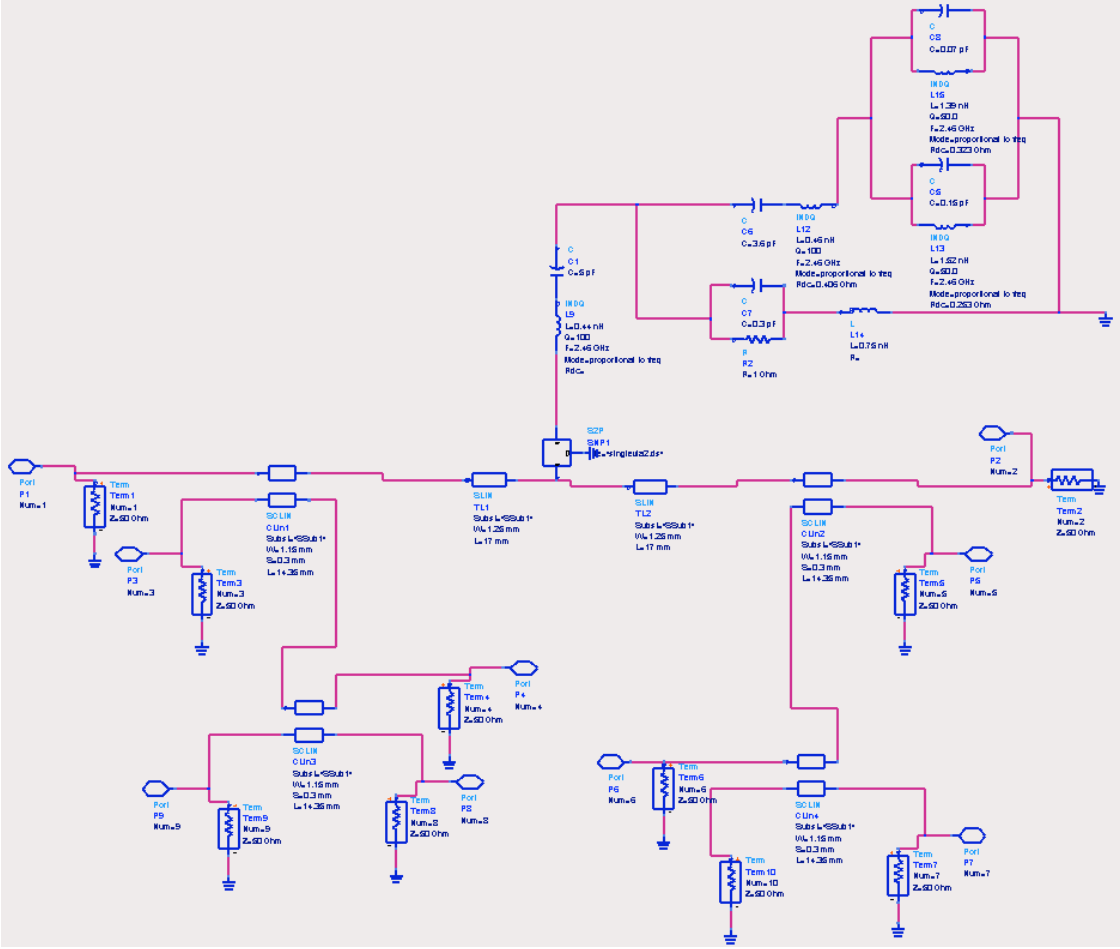

figure 6-19: ADS Schematic of a Single Switched Coupled Path in the Measurement Structure.

This left the pin diode approach, which was to connect a pin diode to the coupler path using a via. When the diode is switched on, the signal upon the coupled path is shorted to ground. The coupled paths signal would flow unencumbered, when the diode is switched off.

This circuit was designed in Agilent's ADS to give the greatest isolation when the switch was turned on and the least interference in the signal when it was turned off. The ADS schematic of the circuit can be seen in figure 6-19. This shows the pin diode connected mid way along the diagonal connecting path between the two sets of six port couplers, in a single transceiver to measurement port coupler path. The diode is modelled as a resistor, in parallel with a capacitor. These are in series with an inductor. The rest of the matching circuitry is to model real component values to give the simulation much more accuracy, these were provided by Murata's online database.

Table 6-10: S-Parameter of Interest for a Single Switched Coupled Path for the Directional Coupler Measurement Structure.

Path	S-Parameters	Values
Transceiver to Antenna Through Path	S_{89}	-0.5129dB
Input (Transceiver) Impedance Matching	S_{99}	-44.5dB
Output (Antenna) Impedance Matching	S_{88}	-42.2925dB
Output (Measurement) Impedance Matching	S_{77}	-44.5dB
Coupled Path (Transceiver to Measurement Device) When PIN Diode is switched on	S_{79}	-76dB
Coupled Path (Transceiver to Mesurement Device) When PIN Diode is switched off	S_{79}	-38.11dB

The performance of this circuit is shown in the table of its S-parameters of interest in Table 6-10. The coupler path's parameter $S_{7\,9}$ is presented graphically to give a better understanding of the performance of the switched coupled path, in figure 6-20 and figure 6-21. These show the narrow band nature of the switching circuit due to the vias and matching circuitry. The performance shown over 1 GHz range shows this nature, as it presents a deep null of isolation at the frequency of interest, 2.46GHz. The isolation ranges from -44dB to -76.5dB over this range. The operation of the switch gives an isolation greater then -70dB over a range of 50MHz, from 2.43GHz to 2.48GHz. This range has a variation in isolation that ranges from -70dB to -76.5dB, centred at 2.4553GHz, and is -76dB at 2.46GHz.

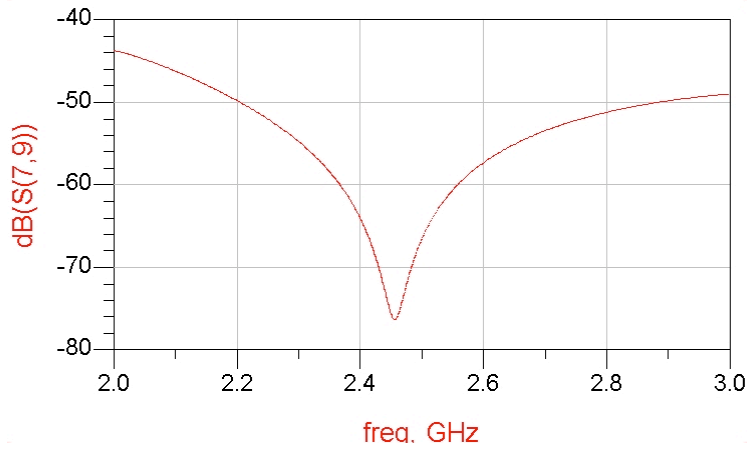

figure 6-20: Switched Coupled Path S-Parameter for the ADS Simulation of the schematic shown in figure 6-19, over the frequency range 2GHz to 3GHz.

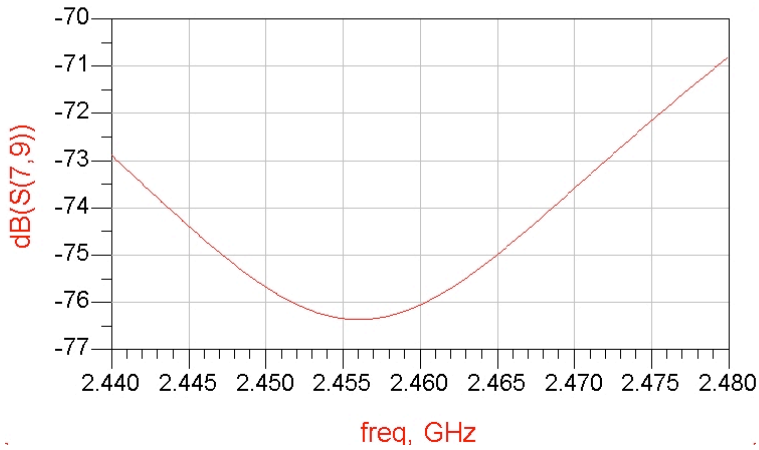

figure 6-21: Switched Coupled Path S-Parameter for the ADS Simulation of the schematic shown in figure 6-19, over the frequency range 2.4GHz to 2.5GHz.

Though the predicted performance does not have a wide range of practical implementations, the board was laid out to check whether it would be implementable in the small confines of the directional coupler measurement board structure. The circuitry fit neatly in to the allotted space as can be seen from the PCB layout of the circuit, in figure 6-22.

6.2.6.1 Summary of the Switched Directional Coupler Measurement Board

The analysis of the switched coupler board shows the feasibility of the switching in both performance and layout. The ADS simulation showed that the developed switch had a narrow band of operation, approximately 50MHz range. This fractional bandwidth is useful for many applications, including GSM and UMTS but would need to be widened for some schemes, such as IEEE 802.11b. For these schemes, a wider bandwidth may be possible with superior design experience or perhaps a different method of switching may be needed. If the distortion due to the disruption of the stripline structure caused by a surface mounted switch could be overcome, the surface mounted SP4T approach would provide the required switching performance.

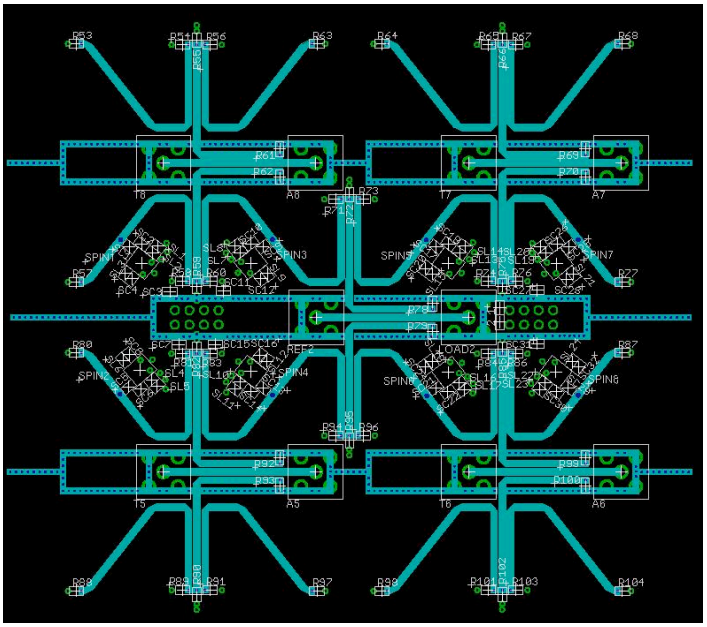

figure 6-22: PCB Layout of 2 by 2 Prototype Switched Directional Coupler Measurement Board.

6.3 Experimental Test-bed

The experimental setup to verify the operation of this measurement based calibration of antenna arrays was undertaken in two sections, the first was using a 2 by 4 array to verify the operation of the representative experimental setup and the second stage was using a 4 by 4 array. The reason for the two stages was for the verification of the representative experimental setup. The reason why a representative experimental setup was chosen was to have the ability to adjust and increase the errors in the system.

6.3.1 2 by 4 Experimental Test-Bed

The experimental setup was split into two sections, the first of which is *2 by 4* array. The system was implemented using a representative system. The system replaces the transceiver elements of the array with components that have the ability to alter the amplitude and phase relationships. This approach was taken as it creates the ability to increase the amplitude and phase errors on the array. This would be more complex to implement upon a full transceiver system. The amplitude and phase control components are implemented using voltage controlled attenuators and phase shifters. An additional alteration to the experimental setup is to replace the antenna elements with connections to a high speed oscilloscope, Agilent Infiniium 54853A DSO, whose maximum frequency is 2.5GHz. This allows ease of measurement and accuracy during testing.

6.3.1.1 Implementation of 2 by 4 Test-Bed

The 2 by 4 test-bed implementation was constructed of voltage controlled units, which alter the amplitude and phase relationships between the elements. These components contain a voltage controlled attenuator (Mini Circuits RVA-3000) and two voltage controlled phase shifters (Mini Circuits JSPHS-2484) to emulate the variations between each of the array elements. These components are essential for the operation of the experiments as they dictate the level of imbalances between the elements and the accuracy with which the calibration can be done. This is because when the calibration is done the appropriate voltage will be applied to these components to create a calibrated output.

The experimental system is shown in block diagram format in figure 6-23, which shows the transmit operations for calibration. This was chosen as it is the simplest calibration to implement, and also it gives more control to the representative system to fully test the capabilities of the measurement structure methodology. Receive calibration can also be achieved using this structure, if the measurement ports of the directional coupler board are connected to transmitters, or representative components, and the transceiver ports of the directional coupler board are connected to measurement devices.

The operation of the 2 by 4 experimental setup that is shown starts with the signal generator, (Hewlett Packard Synthesized CW Generator 83712B (10MHz to 20GHz)). This feeds the system with an RF sinusoid at 2.46GHz. This sinusoidal signal output is then sent to the directional coupler (Mini-Circuits ZABDC20-252H-S+ 800 – 2500MHz). The through path of this directional coupler feeds the power splitter, whereas the coupled path is fed as a reference signal to the measurement device, the Vector Volt Meter.

Following the through path of this experimental setup, the signal flows to the power splitter. This signal is then split into eight signals using power splitter (Mini-Circuits Power Splitter ZB8PD-4.5+ 2600 – 4200MHz). Each of these signals flow into each element's voltage controlled attenuator and phase shifters, two phase shifters are used for each element to achieve 360^{o} of phase control for each element. Each element has its own attenuator and phase shifter circuit, which have their own individually controlled voltages that are set via the breakout boxes (National Instruments BNC – 2110)

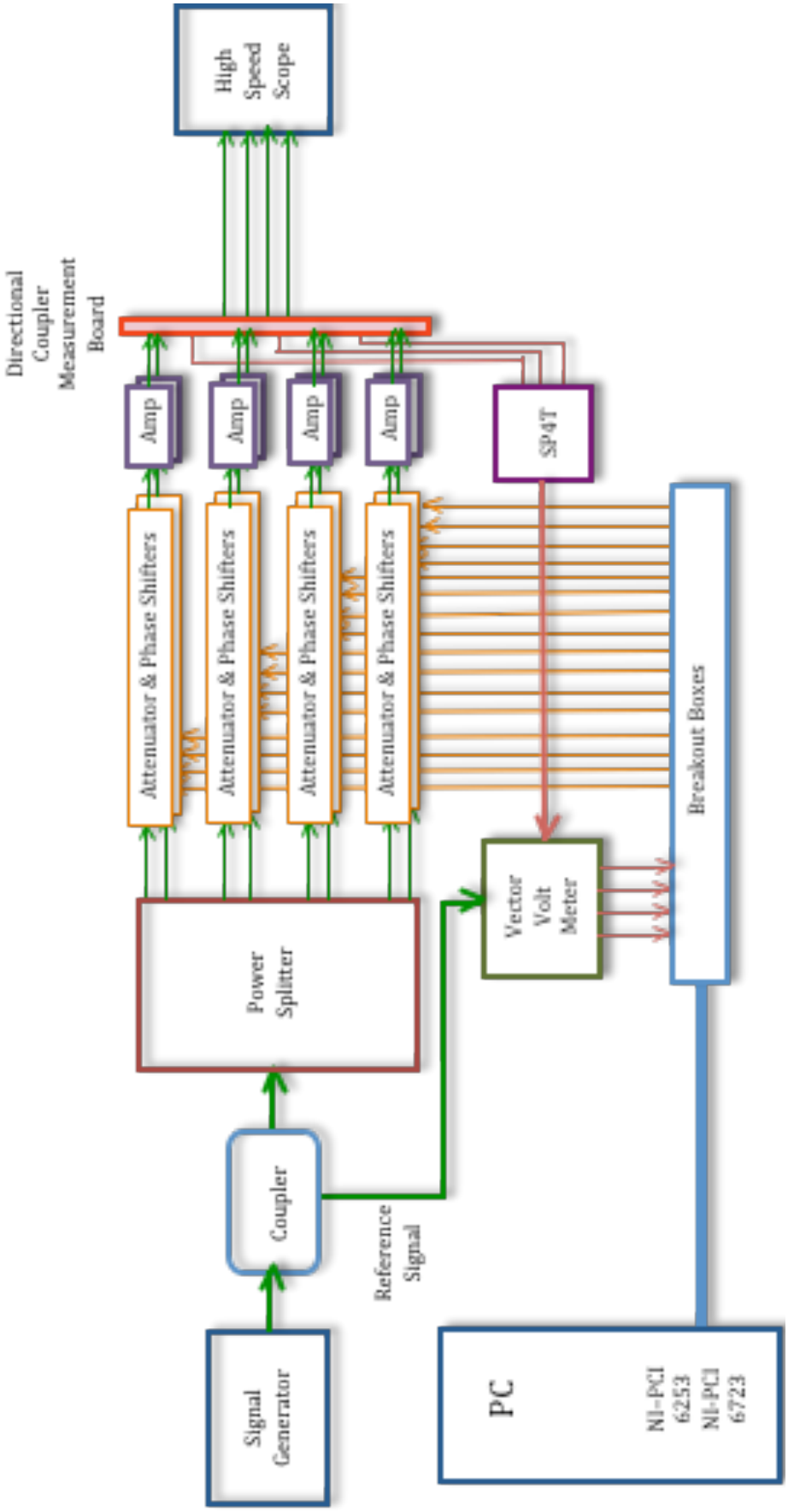

figure 6-23: Block Diagram of the 2 by 4 Experimental Setup.

by the LabVIEW Graphical Programming Environment. LabVIEW provides the means to digitally setup the experimental test-bed to have individual amplitude and phase errors for each element of the array and then to implement the calibration algorithms. The control provided by LabVIEW via the breakout boxes is shown by the orange inputs to each of the attenuator and phase shifter circuits.

Once the attenuation and phase shifts have been set for each element of the array, these signals are then sent to the element amplifier (Mini-Circuits VNA-25), which are included to ensure the signal levels are within the range of the measurement device. Finally, the signals are fed to the directional coupler board where the through path is fed to the high-speed oscilloscope (Agilent Infiniium 54853A DSO 2.3GHz) for measurement. The coupled paths are fed back to LabVIEW to implement calibration, via a SP4T switch (Mini-Circuits Switch SP4T ZSWA-4-30DR DC – 3GHz), which chooses the measurement port to measure, through to the measurement device.

For the purposes of measurement, the antenna elements were replaced by connecting the outputs of the directional coupler measurement board to a high-speed oscilloscope. This 2 by 4 representative system is more clearly seen in the block diagram of its setup as shown in figure 6-23. The elements not connected to the oscilloscope are terminated in 50Ω loads.

The measurement device that was chosen for this representative system was a Vector Volt Meter (VVM) circuit. The reason for this choice is that it represents the operation of the receiver by measuring the amplitude and phase of the RF sinusoidal signal. It does this by using a pair of logarithmic amplifiers to transfer the RF signals large dynamic range to that of a DC voltage small dynamic range. This is provided by Analog Devices LF – 2.7GHZ RF/IF Gain and Phase Detector AD8302 that outputs two voltages. These are a DC voltage representation of the Amplitude and Phase of the RF signal. That is calculated by comparing the measurement signal to the reference signal provided by the directional coupler at the start of the experimental setup block diagram, figure 6-23.

The process by which the calibration is achieved by applying voltages to the attenuators and phase shifters of each element of the array, in order to create an array with amplitude and phase imbalances in the array. The calibration algorithm is then started in

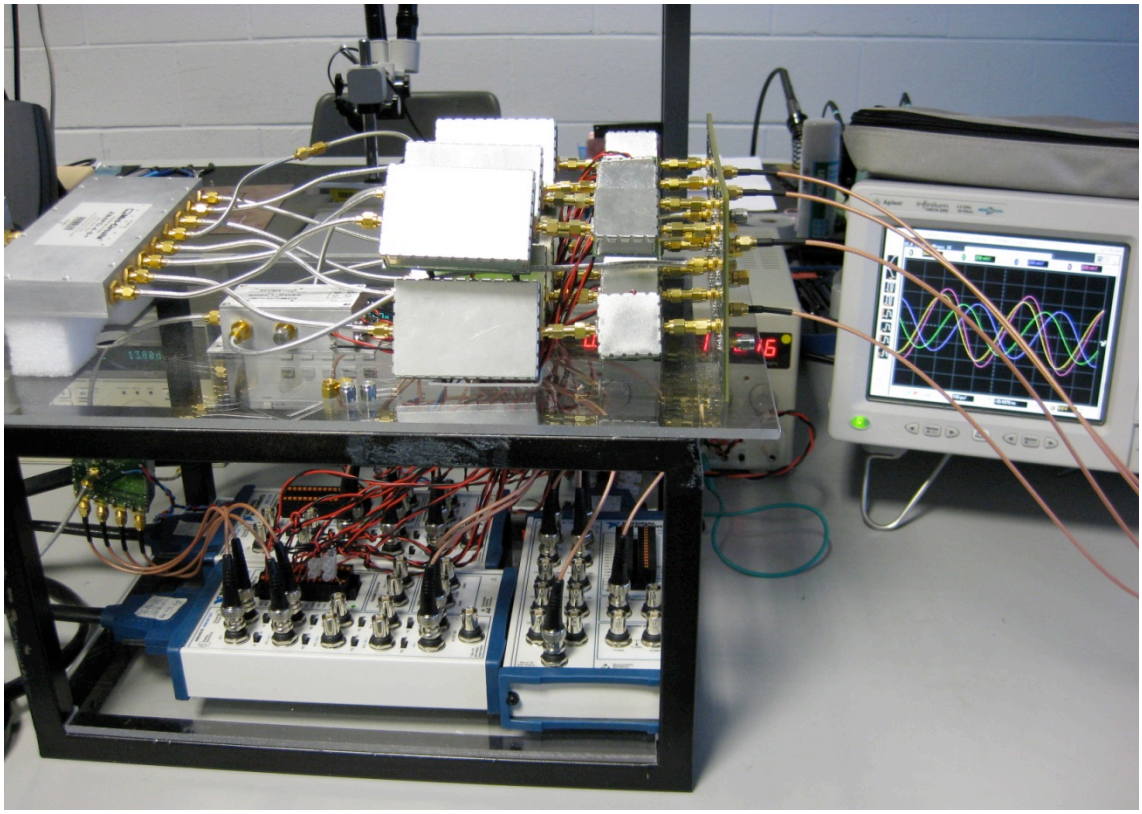

figure 6-24: Photograph of the 2 by 4 Experimental Setup.

LabVIEW, Where each element is measured using the VVM and this measurement is used to correct the input voltages for the element being calibrated. At the end of the calibration of the whole array, the individual attenuator and phase shifters have different voltages which reflect the differences in the calibration paths and components that are considered in order to calibrate the array.

A single AD8302 chip outputs one voltage corresponding to phase. The phase measurement voltage is symmetrical around 0^{o}, which means that -90^{o} and $+90^{o}$ have the same output voltages. To overcome this impediment, two AD8302 chips were used, where the RF signal was shifted by 90^{o}, so that the second phase voltage would indicate in which quadrant the phase is located. Therefore there are four voltage measurements outputted by the VVM to LabVIEW, which represent two amplitude and phase measurements respectively. The actual 2 by 4 experimental setup is shown in figure 6-24.

6.3.1.2 Calibration Methodology Implemented By NI LabVIEW

The calibration algorithms were implemented using National Instruments (NI) LabVIEW. This was achieved through the feedback structure that starts with the directional coupler measurement board which fed back a portion of the transmit signals to the VVM, where the RF signal is converted to four DC voltages. These voltages are fed back to the PC using the breakout boxes, which are connected to the two NI cards needed for this system. The first of these is NI PCI 6253 that provides 2 analog outputs, 16 analog inputs and 24 digital inputs or outputs. The second card is NI PCI 6723 that provides 32 analog outputs. These cards are used to provide output voltages to control the attenuator and phase shifter circuits. They also measure the VVM amplitude and phase voltages. These boards are utilised by LabVIEW to achieve calibration.

Each of the algorithms starts off by setting amplitude and phase errors for each element of the array. This is achieved using the cluster and subvi (virtual instruments) functionality of LabVIEW for the collection and grouping of the parameters. Then each of the calibration algorithms are implemented in LabVIEW based upon the methodology that was described in Chapter 5. The algorithms are implemented sequentially as the prototype directional coupler boards used are the passive ones. There is no switching between the coupler paths, they are all measured at once. To achieve calibration the algorithms are implemented by sequentially measuring and calibrating each element.

Another aspect to the LabVIEW implementation of the calibration algorithms has to do with the actual calibration of each element. The attenuator and phase shifter circuits are controlled by two separate voltages, one for the attenuator and the other for the two phase shifters. However the voltage to attenuation relationship is not fully linear, and this also applies to the voltage to phase shifts relationships. Therefore to find the correct calibration voltage a search needs to be implemented. This was done using proportional control loop, where depending upon the comparison between the current measurement and the measurement of the reference element, the input voltage to the attenuator and phase shifter circuit is stepped up or down; this is more clearly seen from the block diagram of the calibration control in figure 6-25. Other types of control structures could be implemented for this control process, such as PI or PID controllers.

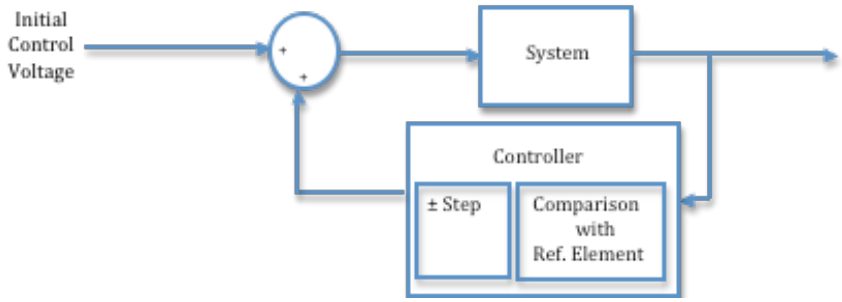

figure 6-25: Control Loop Block Diagram.

Once the appropriate control voltage is found for the attenuator, the process is repeated for the phase shifter's control voltage. This is repeated for both the attenuator and phase shifter's control voltages three more times. The reason for this repetition is that the attenuator and phase shifters are interdependent. An alteration to the control voltage of the attenuator will cause an alteration in the phase shifter's output, and vice versa. These alterations in the attenuation and phase of the element become less as the alterations are smaller, therefore the need to repeat the process several times. This is a particular implementation issue of this experimental test-bed and not a property of the calibration approach. A digital beamformer would not suffer from this issue.

6.3.1.3 Experimental Test-Bed Results

The *2 by 4* experimental test-bed was designed to test the calibration capabilities of this calibration approach. That is to say that the principle of calibration is under test, as well as the measurement structure and the algorithms. The algorithms that were implemented in the 2 by 4 implementation were the top left reference, shortest path and dual path algorithms. The algorithm's performance was then compared to performance targets of ±0.5dB and 5^{o} amplitude and phase errors, which are the required performance of passive or fixed antenna array implementation for commercial systems [325]. Active arrays are required to hit these targets as well. If these targets are exceeded, then this will result in better performance of the array.

The calibration of the experimental test bed for each algorithm starts with applying amplitude and phase errors to the array. This is done by applying a voltage to the attenuator and another to the two phase shifters. The calibration errors that were applied to the 2 by 4 array are shown in Table 6-11. Errors were not applied to element (1,1) as for the top left reference case this is the element to which the rest of the array is calibrated to. As the elements are centred at the operating phase centre of the device the

Table 6-11: Uncalibrated Amplitude and Phase Errors for the 2 by 4 Experimental Test-bed.

Element	Amplitude Errors (dB)	Phase Errors (degrees)
(1,2)	-2.2	104.5
(2,1)	2.3	-15.5
(2,2)	-1.0	-88.6
(1,3)	-6.0	70.8
(2,3)	1.1	26.1
(1,4)	-1.6	107.6
(2,4)	-2.9	-90.3

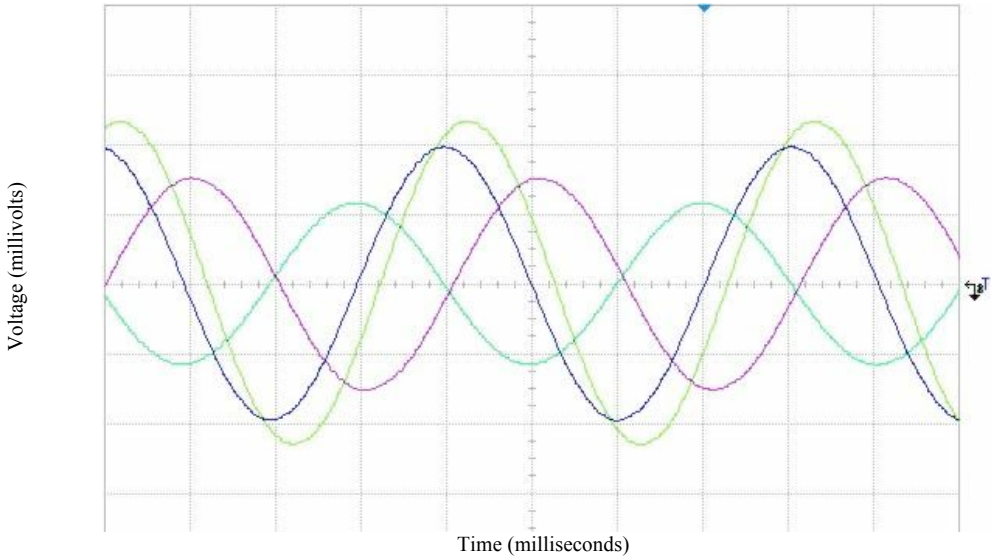

figure 6-26: Screen Shot of four Uncalibrated Signals from the 2 by 4 Experimental Test-bed.

reference element is set to have zero amplitude and phase errors. This allows more range for the errors in the other elements. The other elements errors were chosen to show the capabilities of this calibration approach, as we are not limited to small errors. These errors are shown graphically in figure 6-26, which shows 4 of the eight channels in a screen shot taken by the high speed oscilloscope. From this point the calibration algorithms can be applied to the uncalibrated array.

6.3.1.3.1 Top Left Reference Algorithm

The top left reference calibration algorithm was chosen to be applied to the experimental test bed as it is simple to implement and has good performance, being a comparison-based approach. This choice was made as it provided a quick verification of the performance of the experimental test bed. This algorithm was applied using LabVIEW and the algorithms methodology, which was presented in Chapter 5. This algorithm calibration performance is presented in figure 6-27, which shows four of the

eight elements of the array after calibration. This shows a significant change in the signals amplitude and phase relationships when compared to the uncalibrated signal. The results are presented in Table 6-12. These results show that the errors range from -0.55dB to 0dB and -5.7^{o} to 1.59^{o} for the amplitude and phase relationships. These results show that the performance has not hit the desired targets with two outliers in both amplitude and phase, where the amplitude outliers are -0.52dB and -0.558dB. The phase outliers are -5.14^{o} and -5.76^{o}. These results, though they have not achieved the desired targets, do compare favourably to the predicted performance, from Matlab presented in chapter 5. This comparison is shown in figure 6-28. This shows that the measured phase performance has a wider distribution, but that the points are within the

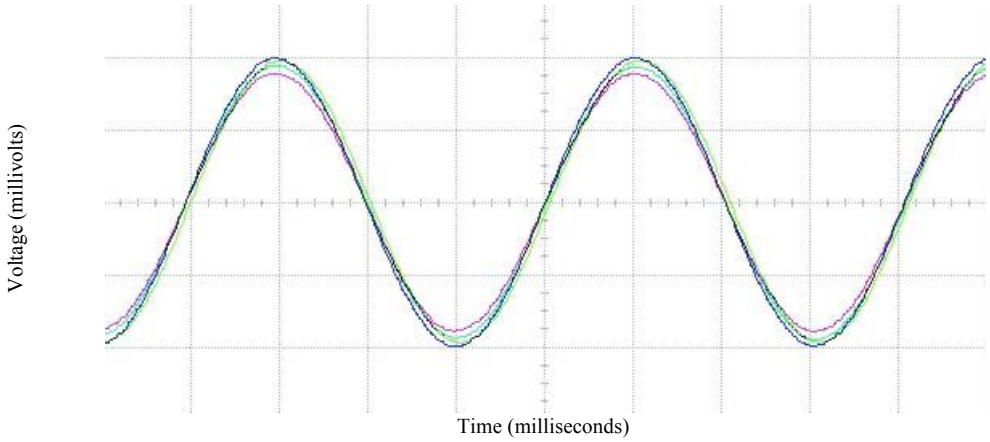

figure 6-27: Screen Shot of four of the Calibrated Signals from the 2 by 4 Experimental Test-bed Calibrated by the Top Left Reference Calibration Algorithm.

Table 6-12: Top Left Reference Algorithms Calibration Amplitude and Phase Errors for the 2 by 4 Experimental Test-bed.

Element	Amplitude Errors (dB)	Phase Errors (degrees)
(1,2)	0	0.44
(2,1)	-0.52	-2.66
(2,2)	-0.47	-1.59
(1,3)	-0.25	-3.10
(2,3)	-0.03	1.59
(1,4)	-0.33	-5.76
(2,4)	-0.55	-5.14

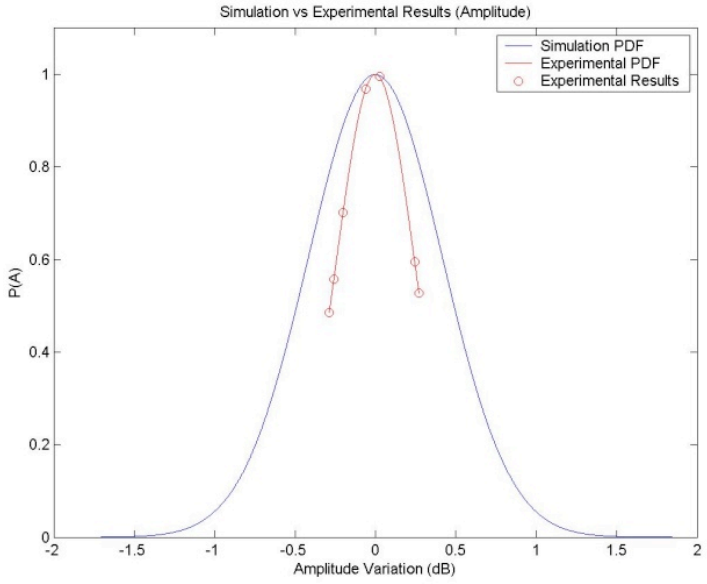

(a)

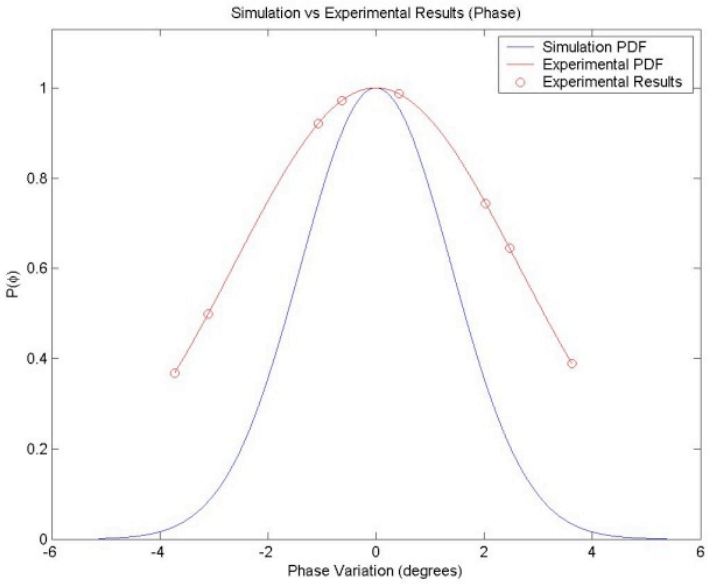

(b)

figure 6-28: The Simulation Results vs. the Experimental Results for the Top Left Reference Calibration Algorithm for a 2 by 4 Array, (a) Amplitude and (b) Phase.

predicted range of the errors. The amplitude performance shows a significantly narrower distribution of errors, thus showing that the actual performance is superior to the predicted one.

This experimental test-bed was implemented using the 2 by 4 directional coupler measurement board. This board experiences warping along its longest length. This affects the coupler errors experienced by the calibration. As the top left reference calibration algorithm does not employ any mitigation techniques these errors directly affect the calibration accuracy. These errors can be seen in Table 6-13. The coupler

errors are larger then the calibration errors experienced by the array. This is due to the sequential nature of the coupler errors, so that errors can cancel each other out. Consider the calibration path to element (1,4), this element is calibrated to element (1,3). Element (1,3) was calibrated to element (1,2), which was calibrated to the reference element (1,1). The chain of these calibration elements contain an absolute maximum amplitude error of -1.8925dB and phase error of 7.9667^{o}, this creates a calculated error of 1.1625dB and 6.562^{o} amplitude and phase error experienced by element (1,4). This is not the case, the calibration error for element (1,4) is -0.33dB and -5.756^{o}. This improvement over the predicted cancelation in the coupler errors comes from the cancelation of the measurement sensor errors, as it will see some of the coupler error as part of the sensor's error contribution.

6.3.1.3.2 Shortest Path Calibration Algorithm

The shortest path algorithm was the next to be implemented upon the experimental test-bed. After the top left reference algorithm, the shortest path is the simplest algorithm. It has the advantage of shorter calibration paths to the elements of the array over the top left algorithm. This was implemented to show the impact of this shortening. The shortest path algorithm presented better performance then the top left algorithm, as predicted. This is seen in Table 6-14. The calibration errors range from -0.139dB to 0.449dB and -5.7^{o} to 3.98^{o} amplitude and phase respectively. These error ranges meet the ±0.5dB amplitude error criteria, while having one outlier to the 5^{o} phase error criteria at -5.756^{o}. The experimental results compare favourably to the theoretical predicted performance, as shown in figure 6-29. The amplitude distribution is narrower than the predicted results, similar to the top left reference algorithm's performance. The phase distribution comparison shows a wider distribution of errors for the experimental results, while showing that the errors remain within the predicted range of errors except the outlier at -5.7^{o}.

Table 6-13: The Amplitude and Phase Errors for Coupler Paths used by the Top Left Reference on the 2 by 4 Directional Coupler Measurement Board.

Coupled Paths		Top Left Reference Calibration Algorithm	
		dB	degrees
(1,1)	Sensor 1	0.94	-0.73
(2,1)	Sensor 1	0.28	-1.93
(2,2)	Sensor 1	0.34	0.27
(1,2)	Sensor 1	1.30	2.47
(1,2)	Sensor 2	-1.15	7.97
(2,2)	Sensor 2	-	-
(2,3)	Sensor 2	-1.37	-1.23
(1,3)	Sensor 2	-1.89	1.97
(1,3)	Sensor 3	0.75	-2.23
(2,3)	Sensor 3	-	-
(1,4)	Sensor 3	1.22	-4.33

The shortest path algorithm also experiences the increased coupler errors due to the warping of the board, the same as the top left algorithm. The shortest path does not implement any mitigation techniques either. The improvement achieved over the top left algorithm is due to the shorter paths between the reference element and the rest of the elements of the array. This improvement can be seen from the comparisons of the calibration results in table 6-15 and table 6-16 for amplitude and phase comparisons respectively. This comparison is shown graphically in figure 6-30. This representation shows that the amplitude calibration errors for both algorithms have the same distributions; however, the top left algorithm has more elements at the tail. The phase error distribution shows that that the top left algorithm has a narrower distribution then that of the shortest path, even with it having more elements as outliers for the performance criteria. This increased distribution is due to warping error along the paths as the shortest path is centred at element (1,2) and for it to calibrate the elements of the array, it uses paths with consistently higher error, producing fewer elements with tiny calibration errors. The coupler path errors used by the shortest path algorithm are shown in table 6-17.

Table 6-14: Shortest Path Algorithms Calibration Amplitude and Phase Errors for the 2 by 4 Experimental Test-bed.

Element	Amplitude Errors (dB)	Phase Errors (degrees)
(1,1)	0.027	3.99
(2,1)	0.37	3.1
(2,2)	0.43	0.18
(1,3)	0.19	3.99
(2,3)	0.14	-2.66
(1,4)	-0.14	-5.76
(2,4)	0.45	-3.09

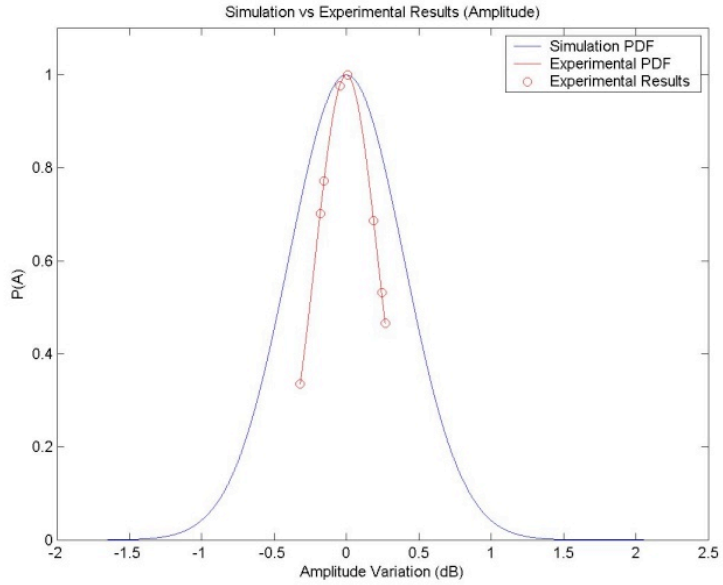

(a)

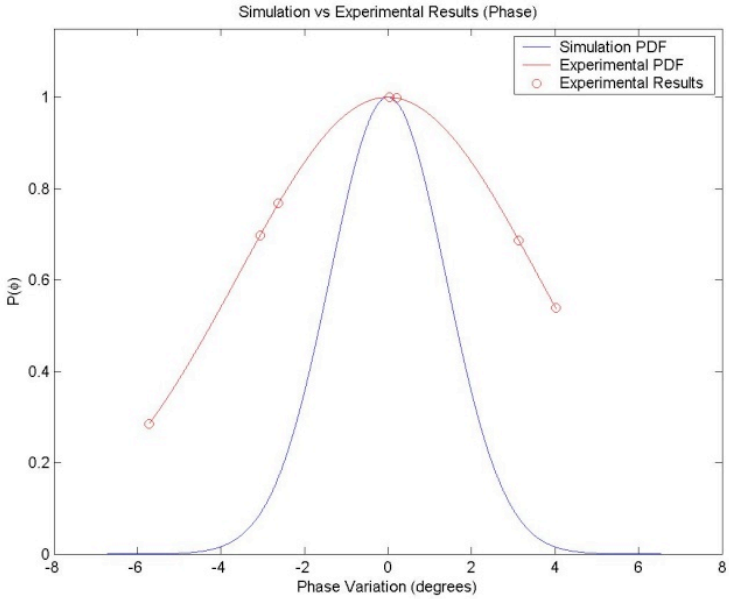

(b)

figure 6-29: The Simulation Results vs. the Experimental Results for the Shortest Path Calibration Algorithm for a 2 by 4 Array, (a) Amplitude and (b) Phase.

Table 6-15: Comparison of Amplitude Calibration Errors of the Top Left Reference Algorithm and the Shortest Path Algorithm for the 2 by 4 Experimental Test-bed.

Element	Top Left (dB)	Shortest Path (dB)
(1,1)	0	0.03
(1,2)	0	0
(2,1)	-0.53	0.37
(2,2)	-0.47	0.43
(1,3)	-0.25	0.19
(2,3)	-0.03	0.14
(1,4)	-0.33	-0.14
(2,4)	-0.56	0.45

Table 6-16: Comparison of Phase Calibration Errors of the Top Left Reference Algorithm and the Shortest Path Algorithm for the 2 by 4 Experimental Test-bed.

Element	Top Left (degrees)	Shortest Path (degrees)
(1,1)	0	3.99
(1,2)	0.44	0
(2,1)	-2.66	3.1
(2,2)	-1.59	0.18
(1,3)	-3.1	3.99
(2,3)	1.59	-2.66
(1,4)	-5.76	-5.76
(2,4)	-5.14	-3.1

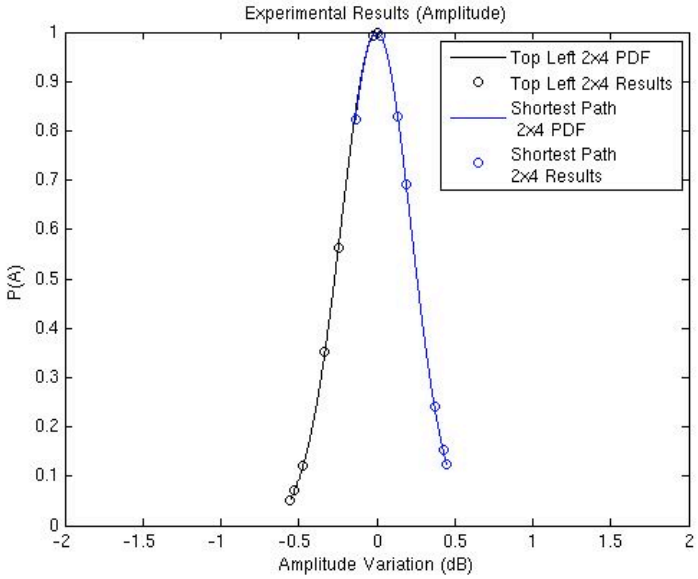

(a)

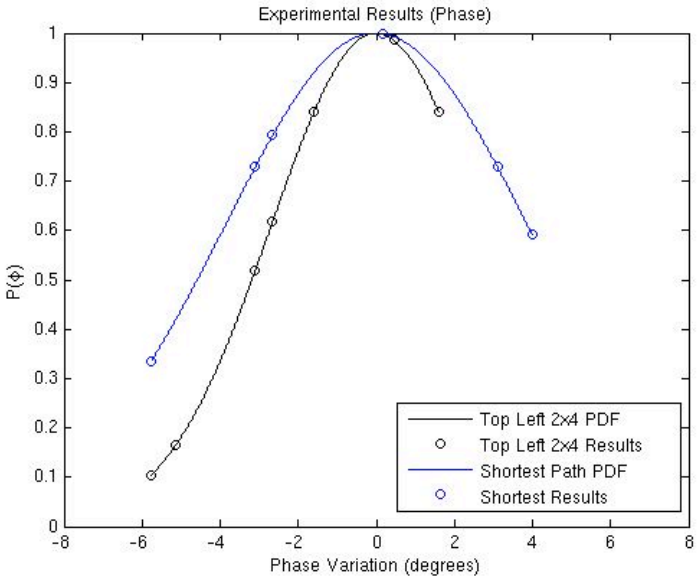

(b)

figure 6-30: The Comparison of the Probability Density Functions of the Calibration Errors for the Top Left Reference and Shortest Path Algorithms on the 2 by 4 Directional Coupler Measurement Boards, (a) Amplitude and (b) Phase.

Table 6-17: The Amplitude and Phase Errors for Coupler Paths used by the Shortest Path Calibration Algorithms on the 2 by 4 Directional Coupler Measurement Board.

Coupled Paths		Shortest Path Calibration Algorithm	
		dB	degrees
(1,1)	Sensor 1	0.94	-0.73
(2,1)	Sensor 1	0.27	-1.93
(2,2)	Sensor 1	0.33	0.27
(1,2)	Sensor 1	1.31	2.47
(1,2)	Sensor 2	-1.15	7.97
(2,2)	Sensor 2	-	-
(2,3)	Sensor 2	-1.37	-1.23
(1,3)	Sensor 2	-1.89	1.97
(1,3)	Sensor 3	0.75	-2.23
(2,3)	Sensor 3	-	-
(1,4)	Sensor 3	1.22	-4.33
(2,4)	Sensor 3	0.42	-2.73

6.3.1.3.3 Dual Path Calibration Algorithm

The final calibration algorithm that was implemented upon the 2 by 4 experimental testbed was the dual path approach. This dual path algorithm that was implemented was where the reference element was at element (1,1). The reason behind this choice was due to the performance of the shortest path. The dual path algorithm utilises a mitigation technique for the coupler errors. However, by implementing it using the reference element at (1,2), the calibration would be comparing calibration paths with large errors. This would not display the performance of the algorithm to its best advantage.

The choice of reference location was advantageous as the performance of this implementation shows how successful the dual path algorithm is compared to both the top left and shortest path algorithms at calibrating the array. This improvement comes from the averaging of the two calibration paths to mitigate the coupler errors. This performance is shown in Table 6-18. It presents error ranges of -0.55dB to 0.0268dB and -2.3^{o} to 0.7^{o} amplitude and phase relationships respectively. These error ranges show significant improvement over the top left and shortest path algorithms when using

Table 6-18: Dual Path Algorithm Calibration Amplitude and Phase Errors for the 2 by 4 Experimental Test-bed.

Element	Amplitude Errors (dB)	Phase Errors (degrees)
(1,2)	0.03	0.44
(2,1)	-0.47	-1.59
(2,2)	-0.56	-1.95
(1,3)	-0.25	-1.33
(2,3)	-0.16	0.70
(1,4)	0	-2.30
(2,4)	-0.27	-1.95

Table 6-19: Comparison of Amplitude Calibration Errors of the Top Left Reference, Shortest Path and Dual Path Algorithms for the 2 by 4 Experimental Test-bed.

Element	Top Left (dB)	Shortest Path (dB)	Dual Path (dB)
(1,1)	0	0.03	0
(1,2)	0	0	0.03
(2,1)	-0.53	0.37	-0.47
(2,2)	-0.47	0.43	-0.56
(1,3)	-0.25	0.19	-0.25
(2,3)	-0.03	0.14	-0.16
(1,4)	-0.33	-0.14	0
(2,4)	-0.558	0.449	-0.27

paths of the same length as the top left algorithm. The improvement is solely based upon the coupler error mitigation technique utilised by the algorithm. The improvement over the other algorithms is shown in table 6-19 and table 6-20, and this is shown graphically in figure 6-31. These tables show the amplitude and phase errors respectively for each of the algorithms. These show improvements from -5.7^{o} phase error for element (1,4) for both the top left and shortest path algorithms to -2.3^{o} for the dual path algorithm. However, this improvement is not always the case. The amplitude errors were increased for one element where the error was -0.47dB and 0.42dB for the top left and shortest path algorithms respectively. This error was increased to -0.55dB for the dual path algorithm.

Table 6-20: Comparison of Phase Calibration Errors of the Top Left Reference, Shortest Path and Dual Path Algorithms for the 2 by 4 Experimental Test-bed.

Element	Top Left (degrees)	Shortest Path (degrees)	Dual Path (degrees)
(1,1)	0	3.99	0
(1,2)	0.44	0	0.44
(2,1)	-2.66	3.1	-1.59
(2,2)	-1.59	0.18	-1.95
(1,3)	-3.1	3.99	-1.33
(2,3)	1.59	-2.66	0.71
(1,4)	-5.76	-5.76	-2.30
(2,4)	-5.14	-3.1	-1.95

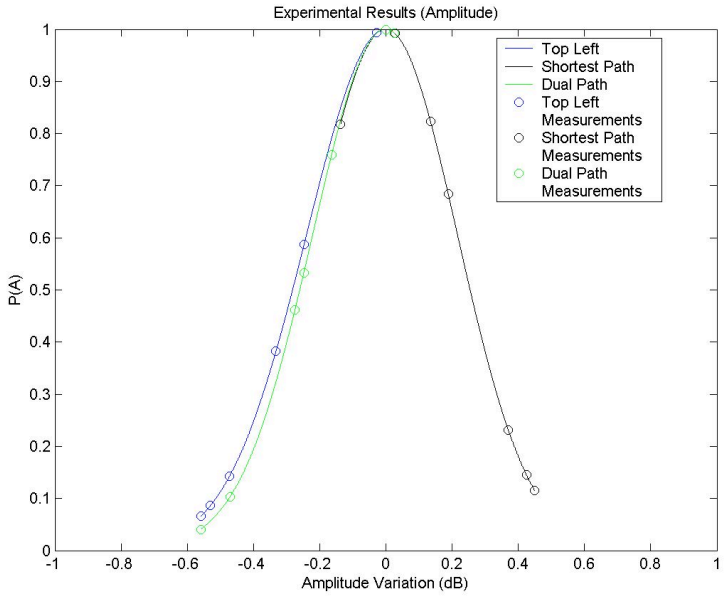

(a)

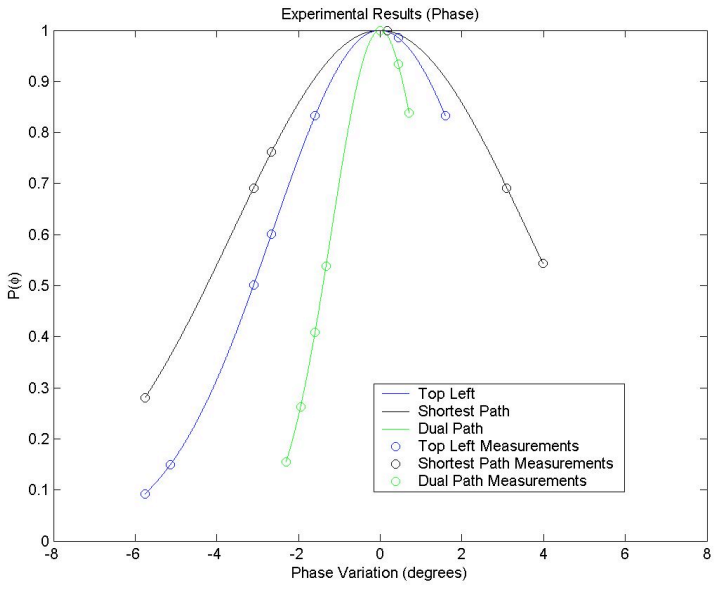

(b)

figure 6-31: The Comparison of the Probability Density Functions of the Calibration Errors for the Top Left Reference, Shortest Path and Dual Path Algorithms on the 2 by 4 Directional Coupler Measurement Boards, (a) Amplitude and (b) Phase.

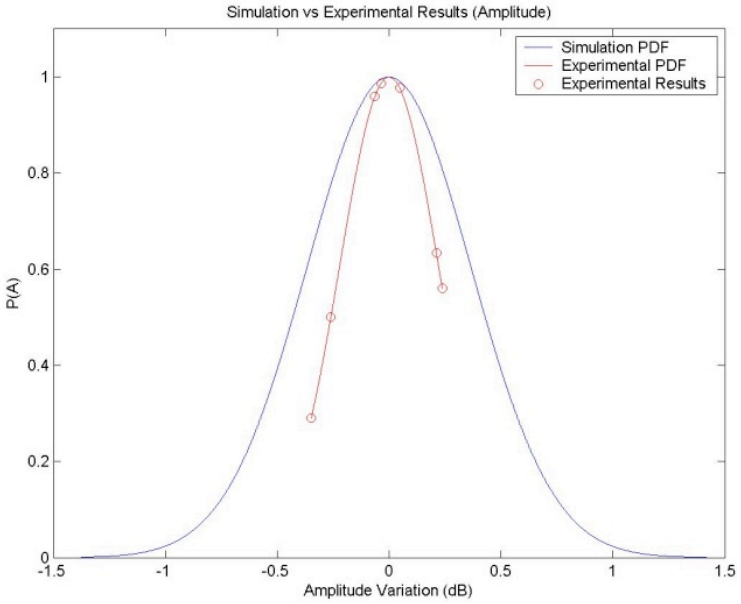

(a)

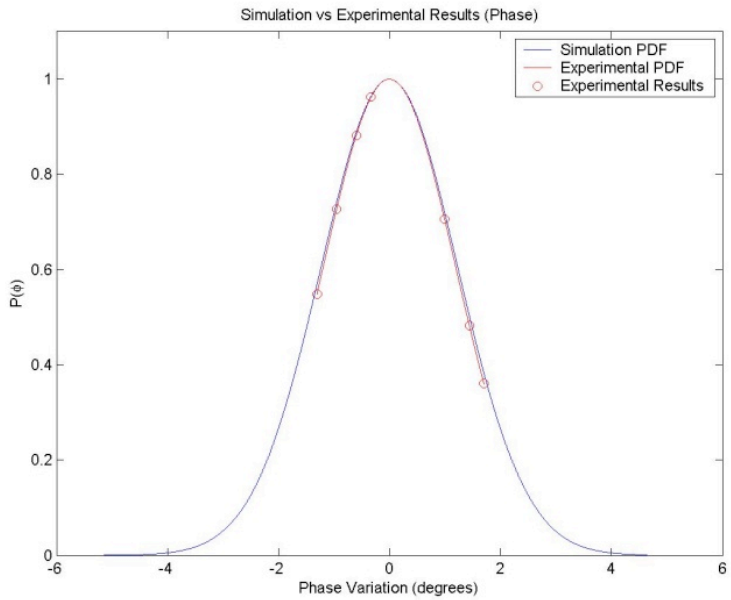

(b)

figure 6-32: The Simulation Results vs. the Experimental Results for the Dual Path Calibration Algorithm for a 2 by 4 Array, (a) Amplitude and (b) Phase.

The reason why the error was increased was due to the combination of two paths, one with a larger error then the one used for the other two algorithms. This increased the error due to the averaging process used to mitigate the coupler errors. This error is the one outlier to the desired performance error ranges of ±0.5dB and 5^{o}, as there are no phase outliers. This algorithms experimental performance is finally compared to its predicted performance in figure 6-32. This shows that the experimental results have a narrower distribution of amplitude errors, similar to the previous two algorithms, which indicates the model used to estimate the amplitude errors is too conservative. The phase errors have the same distribution as the predicted one.

6.3.2 Summary of 2 by 4 Experimental Test-bed

The aim of the 2 by 4 experimental test-bed was to test the feasibility of the representative system. This section showed that the representative system could provide successful calibration of the array, that it provides enough control and accuracy to show the differences between the algorithms and show the effectiveness of this calibration approach.

This test-bed verified the performance of the top left reference, shortest path and dual path algorithms. The performance of each of these algorithms is shown, by comparing their predicted results, to give a consistently better amplitude distribution than expected from the theoretical results given the measured coupler parameters. However, for the top left and shortest path algorithms, their phase distributions were wider compared to the simulations, although the errors did not exceed the predicted spread. The dual path algorithm, on the other hand, showed a distribution extremely close to the predicted one. The experimental results show that the performance of the calibration algorithms was generally as predicted from the previous chapter and that the dual path algorithm is the best performing one. This is shown with only a single amplitude outlier to the ±0.5dB criteria.

The only noteworthy difference from the predicted performance was the shortest path distribution of errors, which was wider, then that of the top left reference algorithms'. This was due to the warping experienced by the directional coupler measurement board. The performance of this algorithm was still better then the top left one, with only a single phase outlier to the 5^{o} criteria. This could be overcome by decreasing the coupler path errors seen by this element, by reducing the error in the directional coupler or choosing a different set of paths to that particular element. This outlier will distort the radiation pattern of the array, this may not be a problem though it would depend upon the application.

Another point to observe about the test bed was that there was very little change in a calibrated array over time, and the efficiency of the calibration over time. This is however an observation in the confines of the laboratory. The second consideration was that when the channels that were connected to the oscilloscope or when there was no

channels connected to the oscilloscope during calibration, there was no observed difference in the calibration accuracy results.

6.3.3 4 by 4 Experimental Test-bed

The second test-bed was the 4 by 4 array size. After the success of the 2 by 4 test-bed, the array size was extended to the 4 by 4 to more fully look at the calibration approach. This extension was chosen as it creates a square array that will be of sufficient size that will test the calibration algorithms more fully. Some of the calibration algorithms work better over square arrays then rectangular ones, highlighted in the 2 by 4 testbed by the significance of path choice through the array during calibration. This is due to the symmetry of the square arrays; the calibration algorithms can take advantage of this by the choice of reference elements, such as in the shortest path calibration algorithm. This led to the choice of the 4 by 4 array.

6.3.3.1 Implementation of the 4 by 4 Experimental Test-Bed

The same repeating system was used to create the 4 by 4 test-bed. The same voltage controlled units were used for the additional 8 elements. This is shown in the block diagram of the 4 by 4 test-bed, in figure 6-33. The system adds 8 additional elements and this requires some additional components. This block diagram shows the transmit setup for calibration. The reason for this choice is that it was the simplest to implement. The receive calibration can be done by swopping the voltage controlled attenuators and phase shifter units with the measurement devices and visa versa.

The representative system is fed by a sinusoidal signal at 2.46GHz. This signal is then passed through an amplifier circuit (Mini-Circuits VNA-25). This feeds the directional coupler that provides the reference signal for the measurement device. The directional coupler through path provides a signal to the power splitters. To accommodate the additional signals, a two-tier splitter architecture was employed. It consists of a three-way splitter (Mini-Circuits Power Splitter 2B3PD- 2400W - S 700 – 2400MHz), which splits the signal into two. Each of these signals is passed to an eight-way splitter. These provide the required 16 equal signals. The through path of the experimental setup is completed with each channel having its own voltage controlled attenuator and phase shifter circuit followed by an amplifier. These signals are fed into the transceiver ports

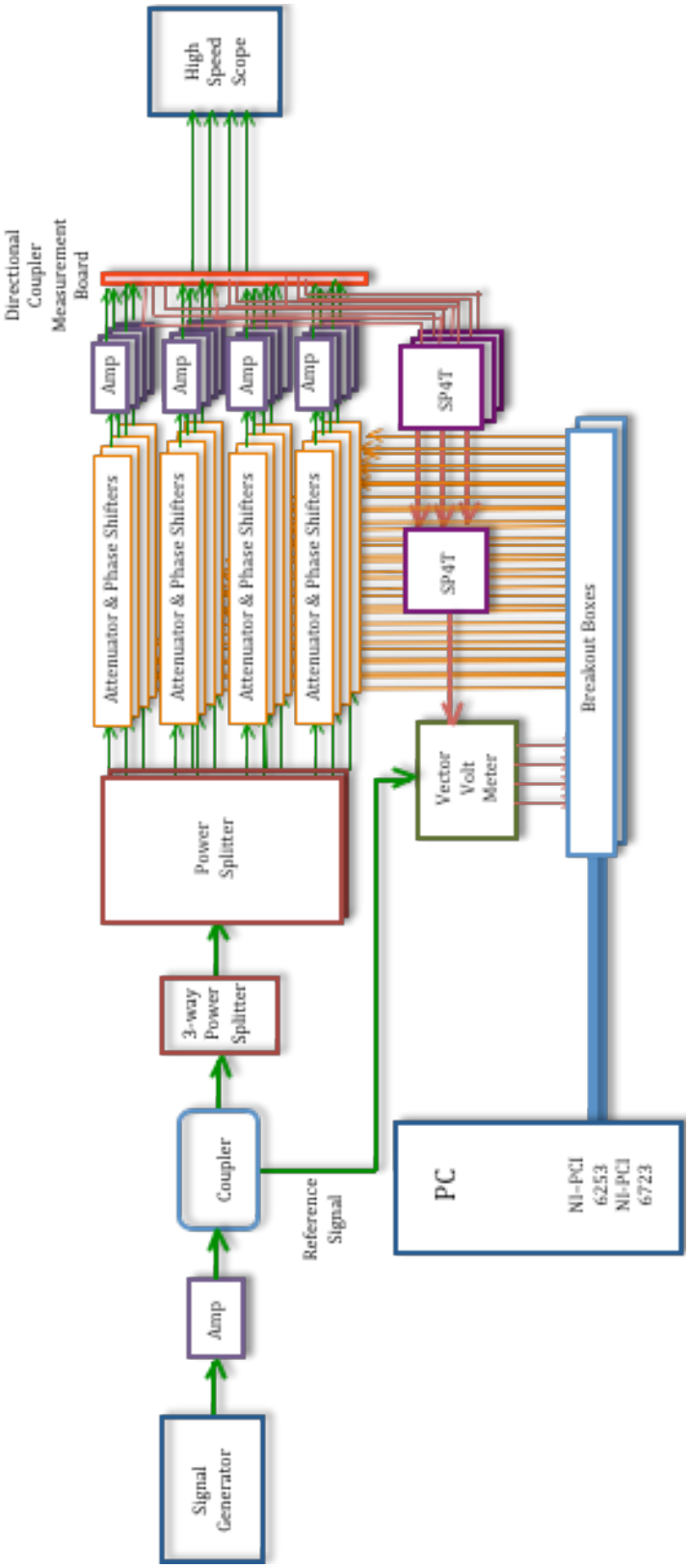

figure 6-33: Block Diagram of the 4 by 4 Experimental Setup.

of the 4 by 4 directional coupler measurement board. The output of this board is measured by the high-speed oscilloscope.

The feedback path for the 4 by 4 test-bed was created by taking the signals from the sensor ports of the directional coupler measurement board and feeding them into a two tier switching setup. Each row of measurement signals is fed into a single SP4T switch, which chooses between them. Then the output of these three switches is fed into a second level SP4T switch, which chooses the row of interest. This is connected to the measurement device, VVM. LabVIEW uses the output of this to calibrate the array. The actual 4 by 4 test-bed can be seen in the series of photos, in figure 6-34, figure 6-35 and figure 6-36.

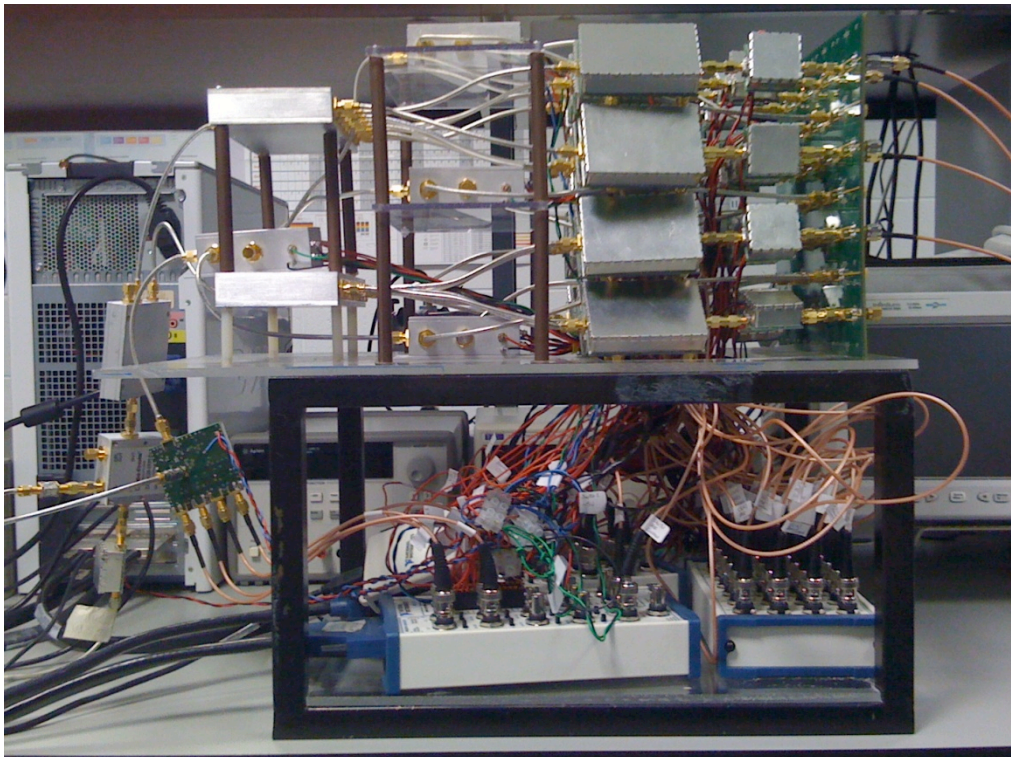

figure 6-34: Side View of 4 by 4 Experimental Test-bed.

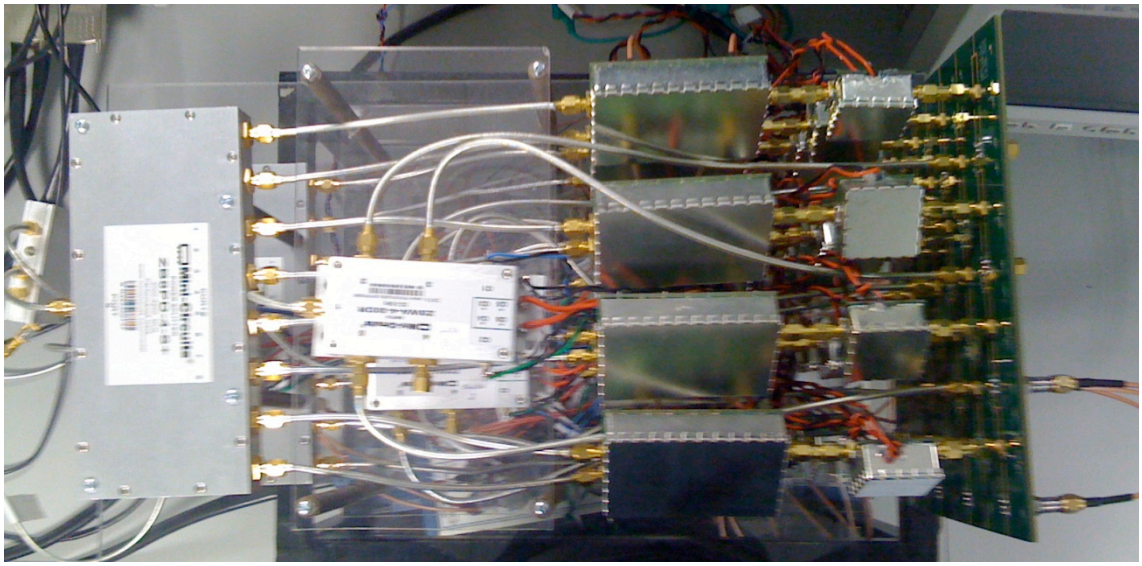

figure 6-35: Top View of 4 by 4 Experimental Test-bed.

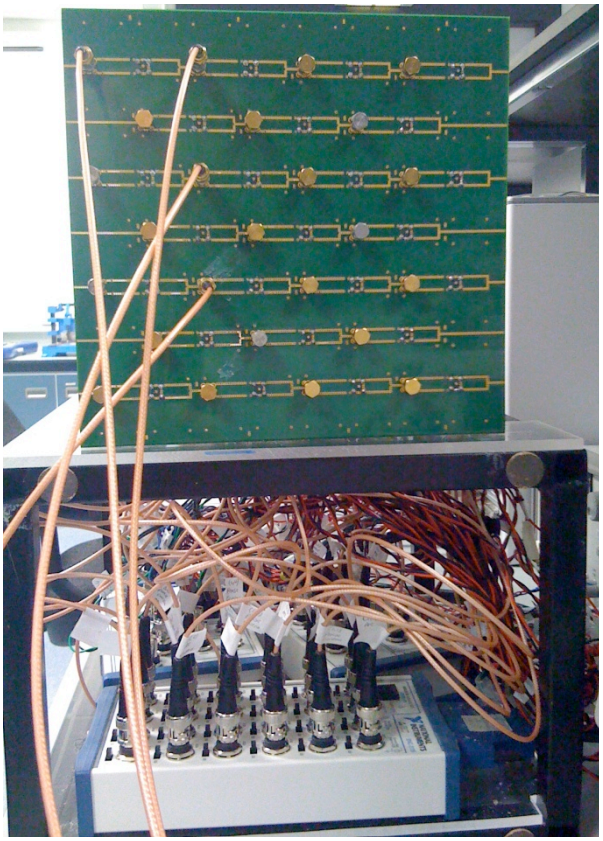

figure 6-36: End View of the 4 by 4 Experimental Test-bed.

6.3.3.2 Experimental Results of 4 by 4 Experimental Test-Bed

The results of the 2 by 4 test-bed hinted at the significance of the choice of calibration paths. This was a motivating factor for the extension of the experimental test-bed. This also explains why some of the algorithms perform better upon a square array rather then on a rectangular one. The significance of the calibration paths came to light due to the effect of warping upon the shortest path calibration algorithm's performance. This highlighted that even though the performance of the shortest path was predicted to be superior to that of the top left reference one, the distribution of the calibration errors was wider for the shortest path.

This effect of warping will also severely impact upon the 4 by 4 experimental test-bed. This is due to the 4 by 4 directional coupler board experiencing more severe warping than presented in the 2 by 4 one. The warping, a discussed in section 6.2.4, affects the 4 by 4 board to a greater degree and along both axes. This has an effect upon the coupler errors, though in a different way then those in the 2 by 4. Due to the symmetry of the warping, the amplitude and phase errors are more consistent, with higher errors in general, but fewer outliers. This is particularly true for the amplitude errors. There was a mechanical method taken to attempt to correct the warping, which was to apply weight to the board over a couple of weeks. This had no noticeable effect upon the warping.

Due to the impact of these errors, and how they show the significance of the choice of calibration path, an investigation of different reference element locations for each of the algorithms of interest was necessary. The top left algorithm was implemented using four different reference element locations, using the four corners of the array. Whereas the shortest path algorithm utilised the four central elements, i.e. (2,2), (2,3), (3,2) and (3,3) as reference elements in separate tests. Due to the significance of the calibration algorithms' choice of paths, the dual path algorithm was implemented using eight different reference element locations, the top left reference's reference locations and the shortest path's ones. For completeness, each of these algorithms were implemented upon 3 by 3 and 4 by 4 array sizes to show the difference in the size and shape of the calibration.

The extensive and systematic approach taken to the calibration is presented in detail in Appendix A with the key results presented here. The results will be presented as a

discussion rather then an exhaustive presentation of numerical results. The aim is to highlight the significance of the choice of calibration path, and the performance of each algorithm in the presence of significant coupler errors.

6.3.3.2.1 Top Left Reference Algorithm

The first algorithm implemented upon the 4 by 4 test-bed was the top left reference algorithm. This was implemented using four different reference element locations, corresponding to the corners of the array, i.e. (1,1), (1,4), (4,1) and (4,4). The results of these calibrations varied significantly for both the 3 by 3 and 4 by 4 implementations; the 3 by 3 one had different paths for optimum amplitude and phase performance. These were the reference elements at (1,1) and (1,4) for the amplitude and phase performance of the calibration. This alone shows the significance of the choice of the calibration paths. The calibration of the 3 by 3 array when the reference element is located at (1,1) achieved calibration errors of -0.22dB to 1.16dB and -8.86^{o} to 6.64^{o} for the amplitude and phase respectively; these results are presented in Table 6-21. Theses errors do not meet the calibration criteria of ±0.5dB and 5^{o}. When compared with the predicted performance of the algorithm, as shown in figure 6-37, they do not perform well. This is the best performing configuration of the amplitude calibration of the 3 by 3 array. The best phase results were achieved by the calibration when the reference element was located at (1,4).

Table 6-21: Top Left Reference Algorithm's Calibration Amplitude and Phase Errors for a 3 by 3 array on the 4 by 4 Experimental Test-bed, when the Reference Element is Located at Element (1,1).

Element	Amplitude Errors (dB)	Phase Errors (degrees)
(1,2)	-0.22	-2.66
(1,3)	-0.14	-8.86
(2,1)	0.14	-2.21
(2,2)	-0.04	-5.31
(2,3)	1.07	2.21
(3,1)	1.16	1.77
(3,2)	1.13	3.1
(3,3)	1.16	6.64

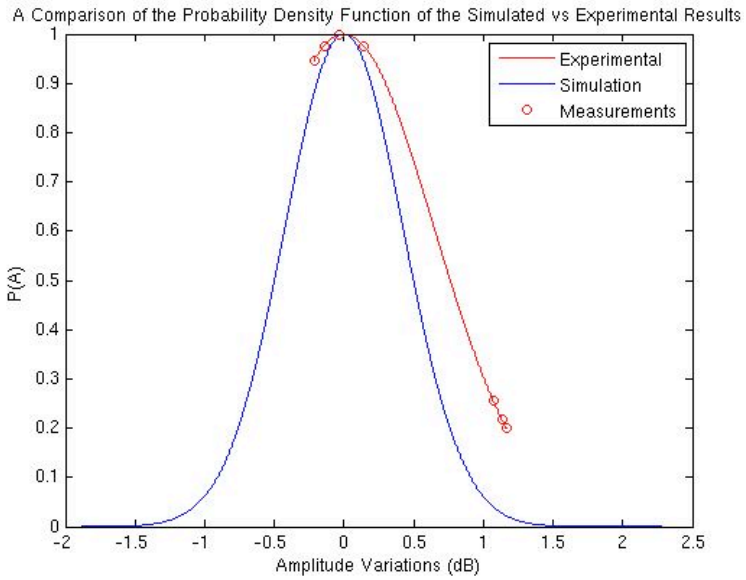

(a)

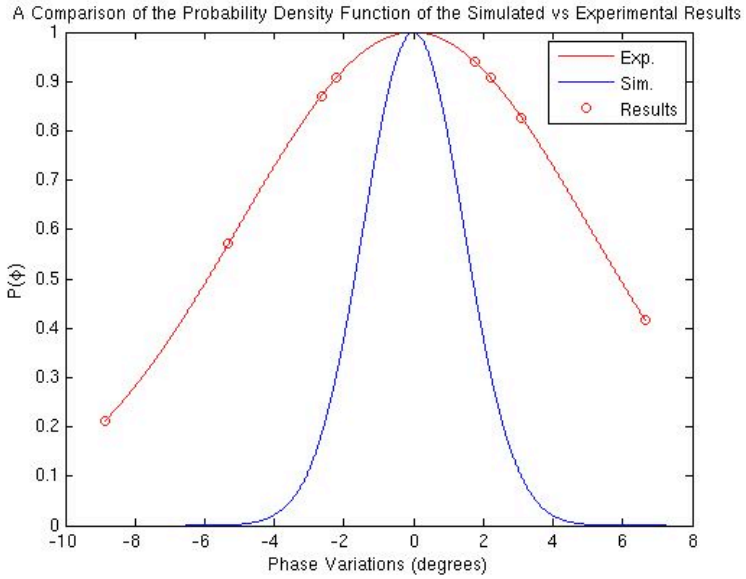

(b)

figure 6-37: The Comparison of the Probability Density Function of the Calibration Errors of the Top Left Reference Algorithm for a 3 by 3 array, where the Reference Element is (1,1), upon the 4 by 4 Directional Coupler Measurement Board: (a) Amplitude and (b) Phase.

This achieved calibration error ranges of -0.39dB to 1dB and -6.6^{o} to 6.6^{o} for the amplitude and phase respectively. These errors are presented in Table 6-22. These results do not meet the criteria of the ±0.5dB and 5^{o} errors. When compared with the predicted results they show larger error ranges and distributions, as shown in figure 6-38. These errors are much higher then the predictions. This continues with the 4 by 4 array results, which also have two different path choices for amplitude and phase performance; a (1,1) reference location for the amplitude performance and (4,4) for the phase. The viability of the use of two different references will only depend upon the

Table 6-22: Top Left Reference Algorithm's Calibration Amplitude and Phase Errors for a 3 by 3 array on the 4 by 4 Experimental Test-bed, when the Reference Element is Located at Element (1,4).

Element	Amplitude Errors (dB)	Phase Errors (degrees)
(1,2)	-0.10	5.76
(1,3)	-0.10	1.33
(2,2)	-0.80	6.64
(2,3)	0.39	6.2
(2,4)	0.16	2.66
(3,2)	-0.44	6.2
(3,3)	0.13	2.21
(3,4)	-1.02	-6.64

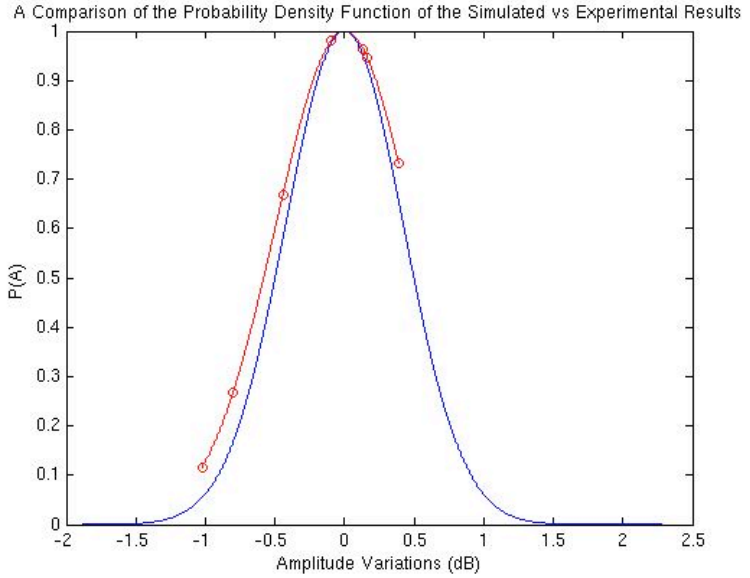

(a)

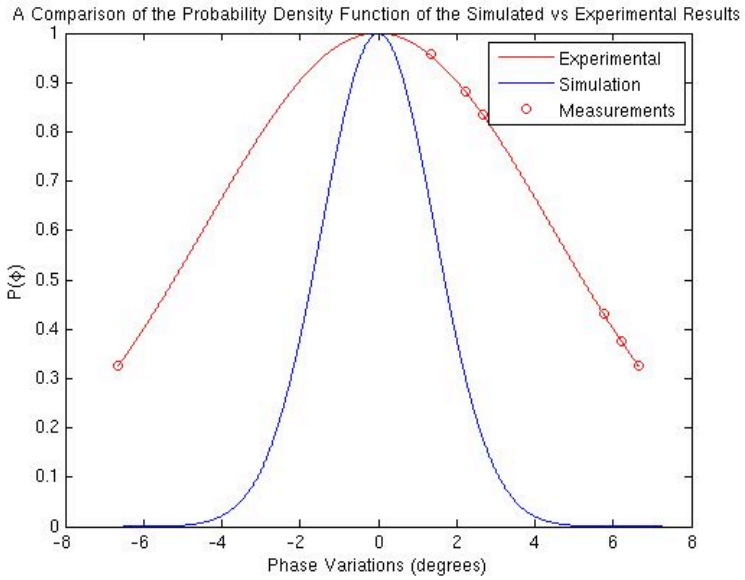

(b)

figure 6-38: The Comparison of the Probability Density Function of the Calibration Errors of the Top Left Reference Algorithm for a 3 by 3 array, where the Reference Element is (1,4), upon the 4 by 4 Directional Coupler Measurement Board: (a) Amplitude and (b) Phase.

intelligence of the control unit programme. The amplitude performance achieved by the 4 by 4 implementation was -0.22dB to 2.57dB. This is significantly worse then that of the 3 by 3 array.

The phase calibration error range achieved by this was -11.07^{o} to 16.3^{o}. These results are presented in Table 6-23. When compared to the predicted performance of the algorithm these results have larger errors and wider distributions for the phase results. The amplitude results show a better comparison, where the distribution is narrower then the predicted performance as shown in figure 6-39. The best phase performance of the top left reference algorithm implementations on the 4 by 4 array size achieved calibration error ranges of -3dB to -1.1dB and -19.48^{o} to 3.98^{o}. These results are shown in Table 6-24 and compared to their predicted performance in figure 6-40. These results show wider distributions and errors then the predictions. These error ranges exceed the criteria of ±0.5dB and 5^{o}.

Table 6-23: Top Left Reference Algorithm's Calibration Amplitude and Phase Errors for the 4 by 4 Experimental Test-bed, when the Reference Element is Located at Element (1, 1).

Element	Amplitude Errors (dB)	Phase Errors (degrees)
(1,2)	-0.22	-2.66
(1,3)	-0.14	-8.86
(1,4)	-0.07	-11.07
(2,1)	0.14	-2.21
(2,2)	-0.04	-5.31
(2,3)	1.07	2.21
(2,4)	-0.04	-9.3
(3,1)	1.16	1.77
(3,2)	1.13	3.1
(3,3)	1.16	6.64
(3,4)	1.65	13.73
(4,1)	1.68	11.07
(4,2)	1.65	9.74
(4,3)	2.49	13.73
(4,4)	2.57	16.38

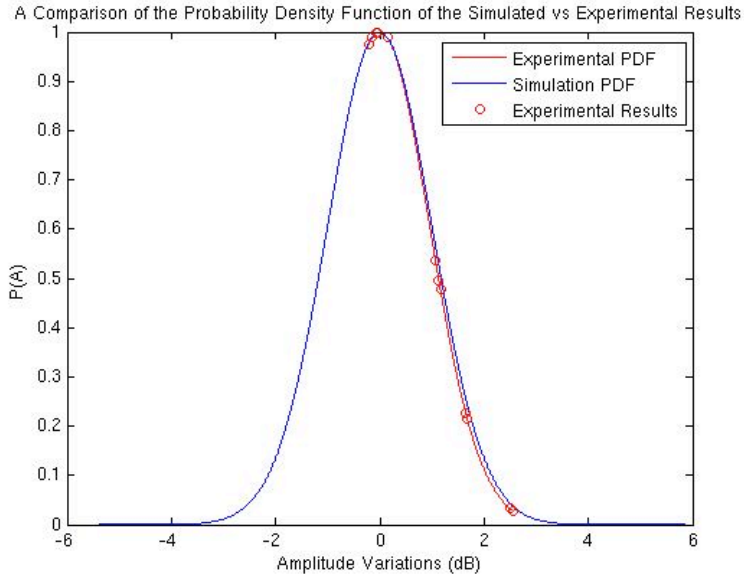

(a)

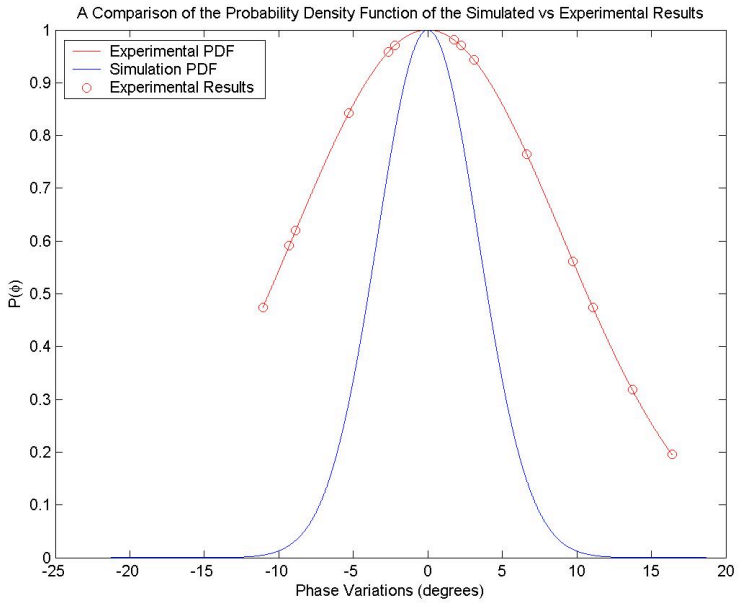

(b)

figure 6-39: The Comparison of the Probability Density Function of the Calibration Errors of the Top Left Reference Algorithm for a 4 by 4 array, where the Reference Element is (1,1), upon the 4 by 4 Directional Coupler Measurement Board: (a) Amplitude and (b) Phase.

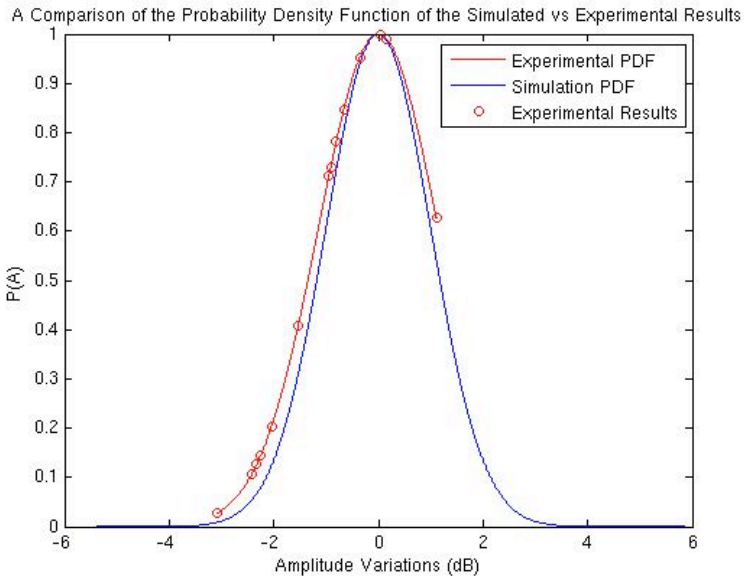

(a)

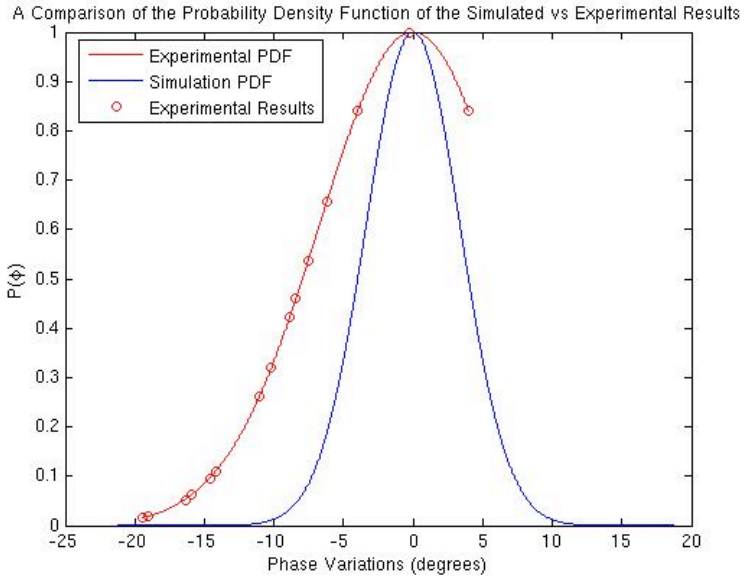

(b)

figure 6-40: The Comparison of the Probability Density Function of the Calibration Errors of the Top Left Reference Algorithm for a 4 by 4 array, where the Reference Element is (4,4), upon the 4 by 4 Directional Coupler Measurement Board: (a) Amplitude and (b) Phase.

Each of the top left reference algorithm implementation presented thus far has been presented in terms of their error ranges, comparison with their predicted performance and finally with the criteria of ±0.5dB and 5^{o} error ranges. These results did not perform well when compared in this way, bar a few exceptions such as the amplitude performance of the 4 by 4 implementation. These results do show the top left algorithm's tendency to increase the calibration errors as the size of the array increases. This also shows the significance of the calibration path choice in this calibration,

Table 6-24: Top Left Reference Algorithm's Calibration Amplitude and Phase Errors for the 4 by 4 Experimental Test-bed, when the Reference Element is Located at Element (4, 4).

Element	Amplitude Errors (dB)	Phase Errors (degrees)
(1,1)	-2.04	-8.41
(1,2)	-2.41	-15.94
(1,3)	-0.36	-19.48
(1,4)	-0.91	-7.53
(2,1)	-3.07	-14.17
(2,2)	-2.25	-19.04
(2,3)	-0.80	-11.07
(2,4)	-0.94	-10.18
(3,1)	-0.66	-0.27
(3,2)	-1.53	-14.61
(3,3)	0.16	-6.2
(3,4)	-0.66	-8.86
(4,1)	0.03	3.99
(4,2)	-2.33	-16.38
(4,3)	1.11	-3.99

particularly as this calibration algorithm does not employ any mitigation technique to deal with the coupler errors.

The causes of the high errors presented by this 4 by 4 test-bed implementation have several sources, the most significant of which are the coupler errors. They have a larger effect on amplitude than phase. However, the coupler errors are consistently high over the whole array, with few outliers. These errors are presented in Table 6-25. These errors, though increased due to warping, are not large enough to solely explain the performance of the 4 by 4 test-bed.

This experimental test-bed is based upon the use of the voltage controlled attenuator and phase shifter circuits. These circuits offer valuable control over the amplitude and phase errors that can be introduced to the system for calibration. They are, however, interdependent. Therefore, a voltage applied to the attenuator will affect the phase shifter's output. This has the effect of altering the response of the system based upon amplitude and phase errors. This property was highlighted in the implementation of the LabVIEW calibration, as it requires multiple iterations to calibrate a single element. However it also has the impact of altering the calibration of the elements due to higher amplitude and phase errors.

Table 6-25: The Errors for the 4 by 4 Directional Coupler Measurement Board.

Coupled Paths		S_{12}		S_{21}	
		dB	degrees	dB	degrees
(4,1)	Sensor 3	0.048	0.696	0.044	0.974
(3,1)	Sensor 3	0.828	-1.704	0.853	-1.526
(3,2)	Sensor 3	0.518	-1.284	0.534	-0.826
(4,2)	Sensor 3	0.008	-0.004	0.004	0.174
(4,2)	Sensor 6	0.548	0.996	0.544	1.274
(3,2)	Sensor 6	-0.262	2.196	-0.186	2.174
(3,3)	Sensor 6	-0.292	-0.304	-0.286	-0.126
(4,3)	Sensor 6	-2.282	2.196	-2.296	2.274
(4,3)	Sensor 9	-0.252	0.696	-0.216	1.374
(3,3)	Sensor 9	0.628	0.096	0.634	0.474
(3,4)	Sensor 9	0.748	-1.004	0.724	-0.226
(4,4)	Sensor 9	0.058	0.296	0.104	1.174
(3,4)	Sensor 8	0.278	-0.204	0.304	-0.226
(2,4)	Sensor 8	0.528	-0.304	0.504	-0.226
(2,3)	Sensor 8	0.828	0.796	0.774	0.174
(3,3)	Sensor 8	0.258	-1.004	0.264	-1.026
(3,3)	Sensor 5	-2.022	0.696	-1.976	0.874
(2,3)	Sensor 5	-0.652	-2.304	-0.696	-2.826
(2,2)	Sensor 5	-0.312	-2.004	-0.266	-2.226
(3,2)	Sensor 5	0.588	1.196	0.584	1.074
(3,2)	Sensor 2	-0.402	1.696	-0.426	1.474
(3,1)	Sensor 2	-0.322	-2.004	-0.326	-2.026
(2,1)	Sensor 2	1.248	1.296	1.224	1.174
(2,2)	Sensor 2	0.938	0.296	0.944	0.274
(2,2)	Sensor 1	-0.102	0.196	-0.076	0.074
(2,1)	Sensor 1	-0.102	0.096	-0.126	0.074
(1,1)	Sensor 1	0.108	1.196	0.094	1.174
(1,2)	Sensor 1	0.008	-1.304	-0.016	-1.626
(1,2)	Sensor 4	-0.372	-0.304	-0.386	-0.426
(2,2)	Sensor 4	0.498	0.796	0.544	-0.226
(2,3)	Sensor 4	-2.222	0.396	-2.26	0.074
(1,3)	Sensor 4	-0.232	-1.724	-0.206	-2.026
(1,3)	Sensor 7	0.508	0.256	0.494	0.204
(2,3)	Sensor 7	-0.122	0.346	-0.206	0.144
(2,4)	Sensor 7	0.168	-0.074	0.164	-0.056
(1,4)	Sensor 7	0.598	-0.884	0.614	-1.066

The final source of errors is due to the signal levels in the system. Due to the addition of two tier power splitters and the two tier switching, the levels of the signals feedback to the measurement device where significantly lower, even with the addition of the extra amplification stage added in right after the signal generator, the signal levels that reached the measurement sensor were reduced by nearly 10dB. This, in conjunction with a mismatch between the reference signal and the feedback signal levels led to less accurate measurements. This signal level difference is an issue of this implementation and a measurement sensor issue. It can be over come by an alternative implementation but is not an source of errors that can easily be considered in the algorithms calibration. Though with sufficient intelligence this could possibly be done.

Each of these sources of errors, when combined, explain the high errors achieved by the top left calibration algorithms. However, they will also affect the other algorithms. Therefore the relative performance will be compared, and the significance of the choice of the calibration paths taken by the algorithms will be explored. It should be noted that these errors are implementation artefacts from the prototype and are not inherent in the methodology or architecture. This does not mean that an alternative implementation would not suffer from implementation artefacts, but they will different depending upon the particular implementation.

6.3.3.2.2 Shortest Path Calibration Algorithm

The shortest path calibration algorithm was implemented upon the 4 by 4 experimental test bed utilising it to create 3 by 3 arrays and 4 by 4 ones. These were implemented using four difference reference element locations in the centre of the array, i.e. (2,2), (2,3), (3,2) and (3,3). These results were then compared, and it was shown that the best performing 3 by 3 arrays were different for amplitude and phase. It was the same situation for the 4 by 4 array.

Table 6-26: Shortest Path Algorithm's Calibration Amplitude and Phase Errors for a 3 by 3 array on the 4 by 4 Experimental Test-bed, when the Reference Element is Located at Element (3,3).

Element	Amplitude Errors (dB)	Phase Errors (degrees)
(2,2)	-0.84	-10.18
(2,3)	-0.45	2.66
(2,4)	-0.52	-3.54
(3,2)	0.07	4.43
(3,4)	-0.17	-1.33
(4,2)	-0.38	-2.21
(4,3)	0.39	8.41
(4,4)	0.23	5.76

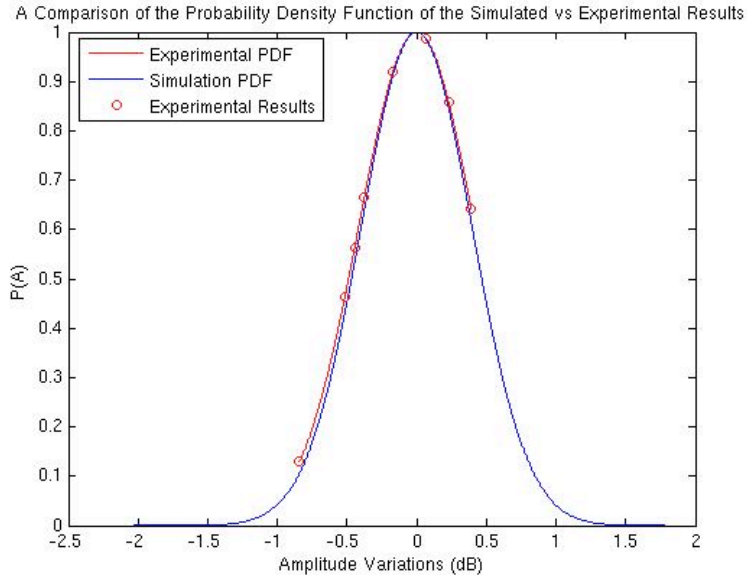

(a)

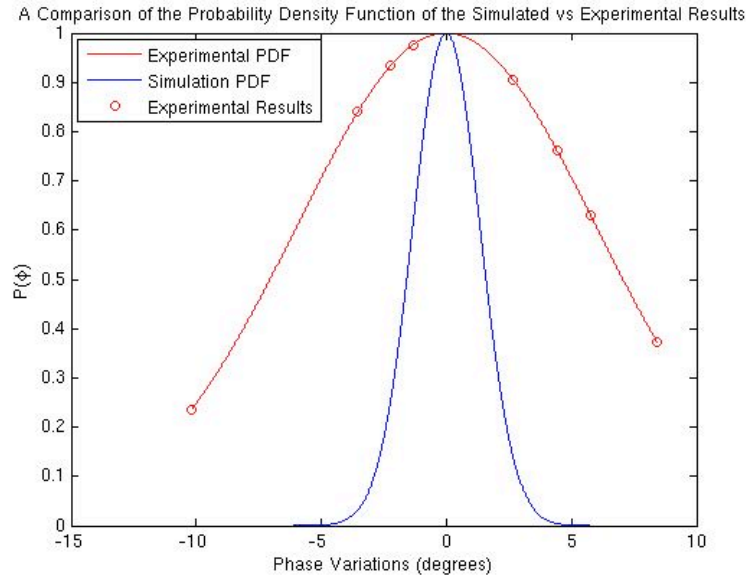

(b)

figure 6-41: The Comparison of the Probability Density Function of the Calibration Errors of the Shortest Path Algorithm for a 3 by 3 array, where the Reference Element is (3,3), upon the 4 by 4 Directional Coupler Measurement Board: (a) Amplitude and (b) Phase.

The presentation of these results starts with the 3 by 3 array that gave the best amplitude performance. These results are presented in Table 6-26. These calibration errors range from -0.39dB to 1.23dB and -10.2^{o} to 8.4^{o} for amplitude and phase respectively. These errors exceed the criteria of ±0.5dB and 5^{o}. When compared to the predicted performance they show good amplitude matching, as the distribution of the measured errors is close to that of the predicted performance. The phase errors show a much wider distribution, however, this shows the significance of path choice, and that it does not necessarily mean that it will perform in the same way for both amplitude and phase.

The array with the best phase results are presented in Table 6-27. This table presents results that range from -2dB to 2.2dB and -5.7^{o} to 6.2^{o} for amplitude and phase respectively. These error ranges exceed the desired criteria. This shows a wide distribution for both amplitude and phase. The phase results are much closer to the distributions error range then the previous set.

These performances are affected by the same set of error contributions as the top left. By moving the reference location and its choice of calibration paths through the array the amplitude error range has been reduced by 0.15dB, from 1.38dB to 1.23dB. The phase error ranges have improved by 1.3^{o}, from 13.2^{o} to 11.9^{o}. These error ranges are still high, but they show the improvement in the performance of the best performing amplitude and phase results of the 3 by 3 array results between the top left reference and shortest path algorithm implementations.

The same situation can be seen for the 4 by 4 array implementation, whose best-case amplitude results are presented in Table 6-28. This shows calibration error ranges for the amplitude of -1.1dB to 0.39dB and for the phase of -10.2^{o} to 8.4^{o}. These results are compared with the predicted performance, as shown in figure 6-43, which show that the amplitude performance is much narrower then the predicted performance. The phase error comparison is not as favourable. The distribution is wider, but the errors are within the error range of the distribution.

Table 6-27: Shortest Path Algorithm's Calibration Amplitude and Phase Errors for a 3 by 3 array on the 4 by 4 Experimental Test-bed, when the Reference Element is Located at Element (2, 3).

Element	Amplitude Errors (dB)	Phase Errors (degrees)
(1,2)	-1.68	-4.87
(1,3)	-0.63	-0.27
(1,4)	-0.80	-5.76
(2,2)	-2.06	-5.76
(2,4)	2.22	6.2
(3,2)	-1.5	-0.27
(3,3)	0.56	1.33
(3,4)	0.23	6.2

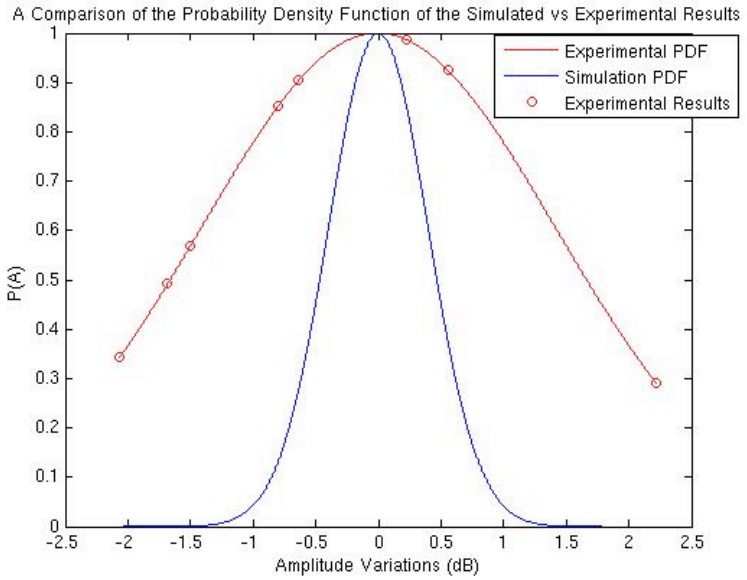

(a)

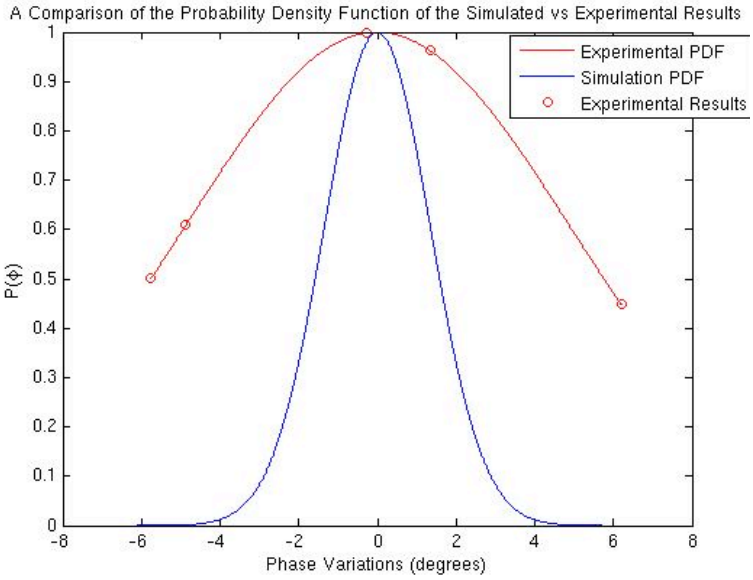

(b)

figure 6-42: The Comparison of the Probability Density Function of the Calibration Errors of the Shortest Path Algorithm for a 3 by 3 array, where the Reference Element is (2,3), upon the 4 by 4 Directional Coupler Measurement Board: (a) Amplitude and (b) Phase.

Table 6-28: Shortest Path Algorithm's Calibration Amplitude and Phase Errors for the 4 by 4 Experimental Test-bed, when the Reference Element is Located at Element (3, 3).

Element	Amplitude Errors (dB)	Phase Errors (degrees)
(1,1)	-1.10	-5.31
(1,2)	-0.10	-3.1
(1,3)	-0.62	-5.76
(1,4)	-0.59	-3.1
(2,1)	-0.7	-4.43
(2,2)	-0.84	-10.18
(2,3)	-0.45	2.66
(2,4)	-0.52	-3.54
(3,1)	-0.24	3.1
(3,2)	0.07	4.43
(3,4)	-0.17	-1.33
(4,1)	-0.38	-0.44
(4,2)	-0.38	-2.21
(4,3)	0.39	8.41
(4,4)	0.23	5.76

The best-case phase performance of the 4 by 4 array results is presented in Table 6-29. These results range from -2dB to 2.2dB and -5.7^{o} to 9.29^{o} for the amplitude and phase errors respectively. These measured errors are compared to the predicted results in figure 6-44. This comparison of distributions show that the measured results has wider curves. The phase results remain within the error range of the predictions, as do the amplitude results.

These performances of the 4 by 4 array implementation of the shortest path algorithm provide larger benefits when compared to that of the top left one. They are effected by the same set of error contributions as the top left. The amplitude error range width is improved by 1.3dB, from 2.79dB to 1.49dB. The phase one is improved by 8.47^{o}, from 23.46^{o} to 14.99^{o}. These improvements are larger then the improvements seen by the 3 by 3 implementation. They are from the same sources. Shortening the calibration paths taken through the array and the choice of the shortest paths between elements have created these improvements in performance. These improvements show the choice of the calibration paths is important. The different paths chosen for the amplitude and phase also highlight the significance of this choice.

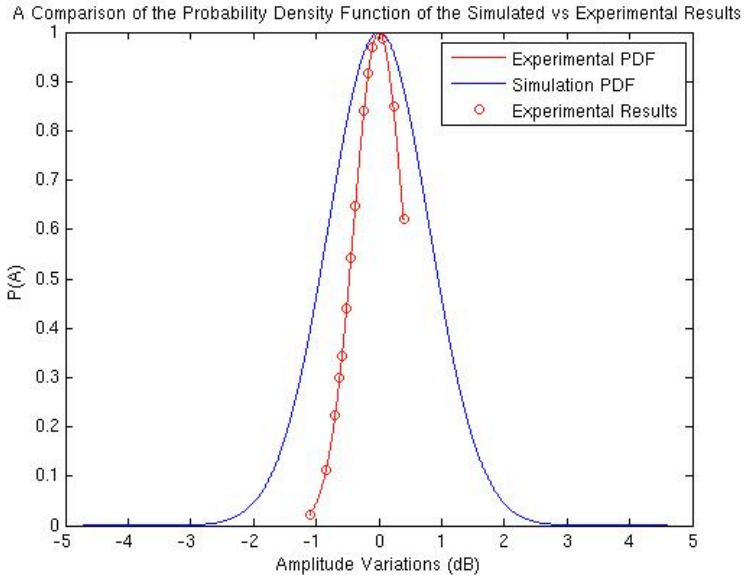

(a)

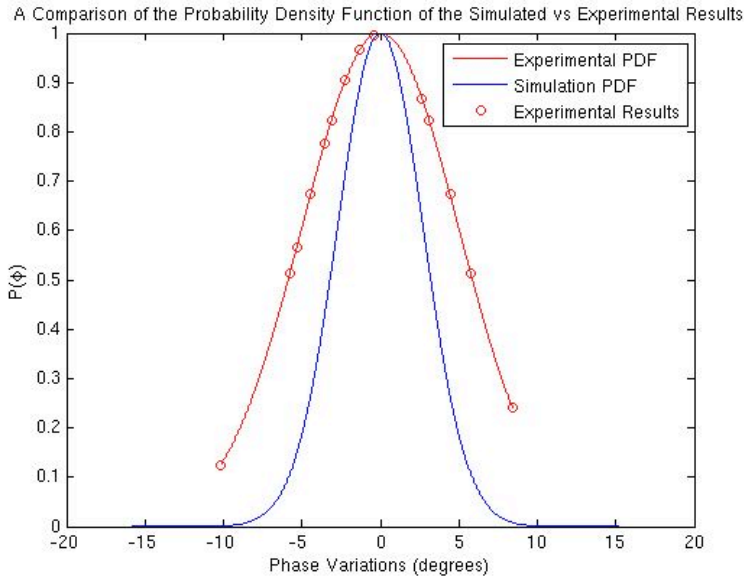

(b)

figure 6-43: The Comparison of the Probability Density Function of the Calibration Errors of the Shortest Path Algorithm for a 4 by 4 array, where the Reference Element is (3,3), upon the 4 by 4 Directional Coupler Measurement Board: (a) Amplitude and (b) Phase.

Table 6-29: Shortest Path Algorithm's Calibration Amplitude and Phase Errors for the 4 by 4 Experimental Test-bed, when the Reference Element is Located at Element (2, 3).

Element	Amplitude Errors (dB)	Phase Errors (degrees)
(1,1)	-1.59	-0.44
(1,2)	-1.68	-4.87
(1,3)	-0.63	-0.27
(1,4)	-0.80	-5.76
(2,1)	-1.87	-3.99
(2,2)	-2.06	-5.76
(2,4)	2.22	6.2
(3,1)	-1.41	2.66
(3,2)	-1.5	-0.27
(3,3)	0.56	1.33
(3,4)	0.23	6.2
(4,1)	-0.97	9.3
(4,2)	-1.97	-3.99
(4,3)	0.91	5.76
(4,4)	1.04	7.08

6.3.3.2.3 Dual Path Calibration Algorithm

Due to the importance of choosing the calibration path, this algorithm was implemented using eight different reference element locations. These were the four used by the top left reference algorithms, i.e. (1,1), (1,4), (4,1) and (4,4), and the shortest path reference locations, i.e. (2,2), (2,3), (3,2) and (3,3). The results from the calibration implementation presented some interesting results. The best performing 3 by 3 implementation for amplitude results are by using the shortest path reference location of (3,3). The best phase performance is achieved using the top left reference location of (4,4). This shows how the choice of calibration paths varies from parameter to parameter and from path to path. The dual path calibration algorithm uses two paths for the calibration of the elements of the array, therefore the choice of path will have a greater impact upon the results.

The best-case amplitude results of the 3 by 3 array, using reference element (3,3) is presented in Table 6-30. The results presented in this table show amplitude error ranging from -1.04dB to 0.44dB and phase errors ranging from -10.62^o to 7.5^o. When these results were compared to the predicted performance of the algorithm, as shown in figure 6-45, it shows a good matching with the amplitude distribution, though slightly wider. The phase distribution for this reference element location is significantly wider with outlier values.

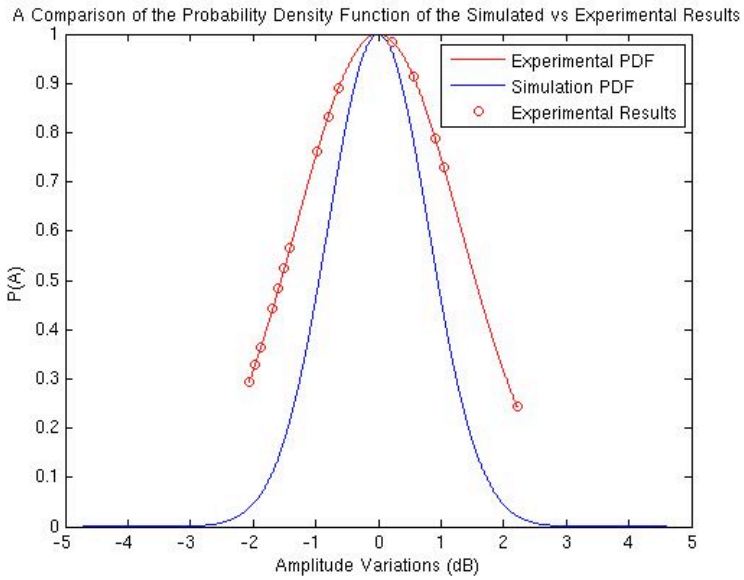

(a)

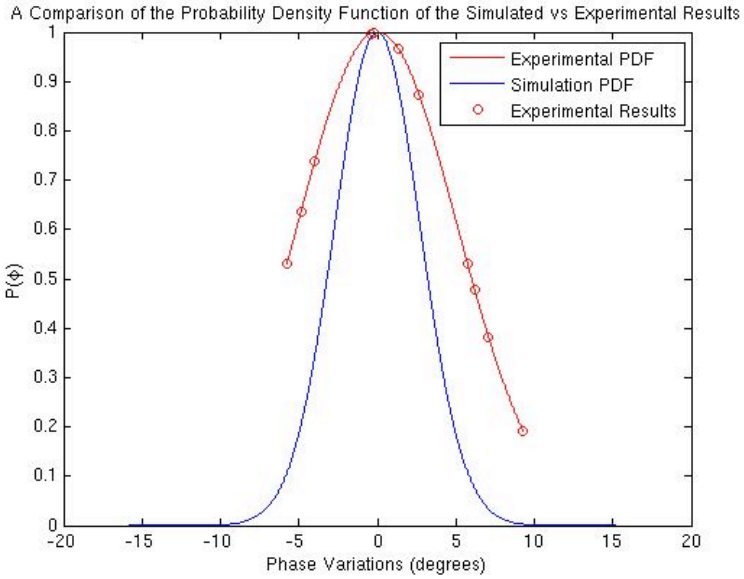

(b)

figure 6-44: The Comparison of the Probability Density Function of the Calibration Errors of the Shortest Path Algorithm for a 4 by 4 array, where the Reference Element is (2,3), upon the 4 by 4 Directional Coupler Measurement Board: (a) Amplitude and (b) Phase.

Table 6-30: Dual Path Algorithm's Calibration Amplitude and Phase Errors for a 3 by 3 array on the 4 by 4 Experimental Test-bed, when the Reference Element is Located at Element (3,3).

Element	Amplitude Errors (dB)	Phase Errors (degrees)
(2,2)	-1.05	3.99
(2,3)	-0.47	-8.41
(2,4)	-0.47	-6.64
(3,2)	-0.17	2.66
(3,4)	-0.65	4.87
(4,2)	-0.37	-4.43
(4,3)	0.45	2.21
(4,4)	0.26	7.53

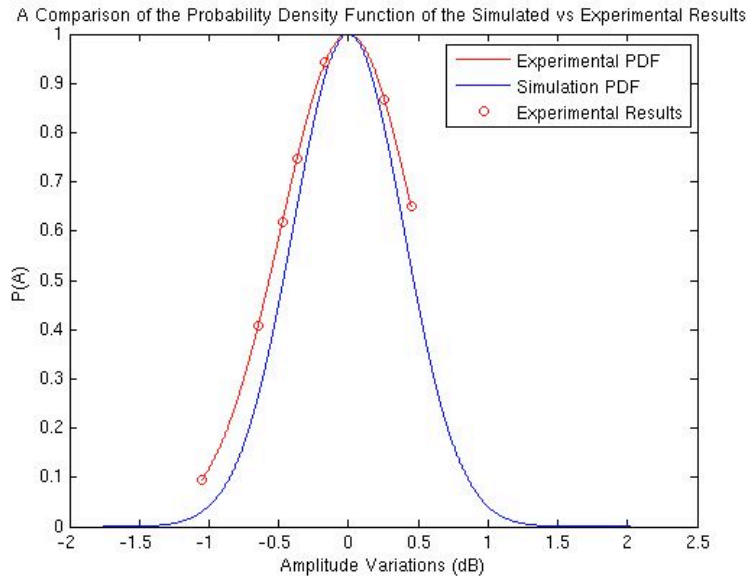

(a)

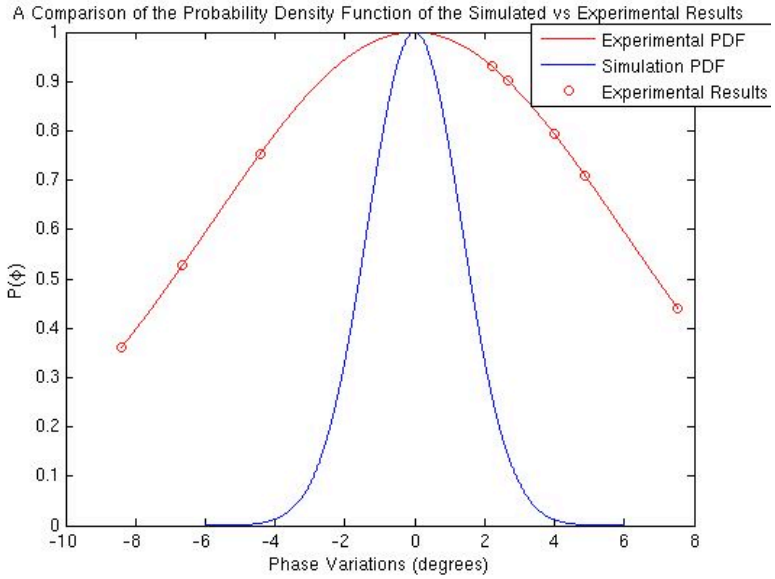

(b)

figure 6-45: The Comparison of the Probability Density Function of the Calibration Errors of the Dual Path Algorithm for a 3 by 3 array, where the Reference Element is (3,3), upon the 4 by 4 Directional Coupler Measurement Board: (a) Amplitude and (b) Phase.

Table 6-31: Dual Path Algorithm's Calibration Amplitude and Phase Errors for a 3 by 3 array on the 4 by 4 Experimental Test-bed, when the Reference Element is Located at Element (2,3).

Element	Amplitude Errors (dB)	Phase Errors (degrees)
(1,1)	-2.25	-0.89
(1,2)	-1.86	-3.99
(1,3)	-0.76	-2.21
(2,1)	-1.86	-0.27
(2,2)	-2.01	-6.64
(3,1)	-0.88	3.99
(3,2)	-1.54	1.33
(3,3)	0	-0.44

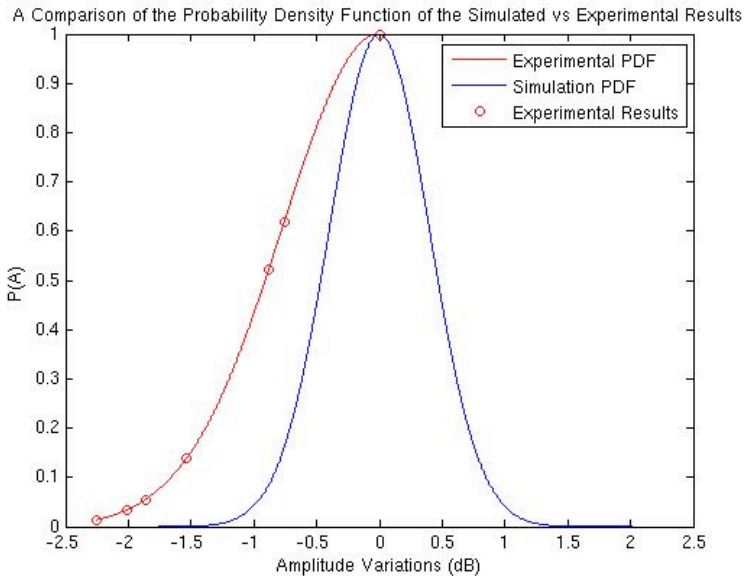

(a)

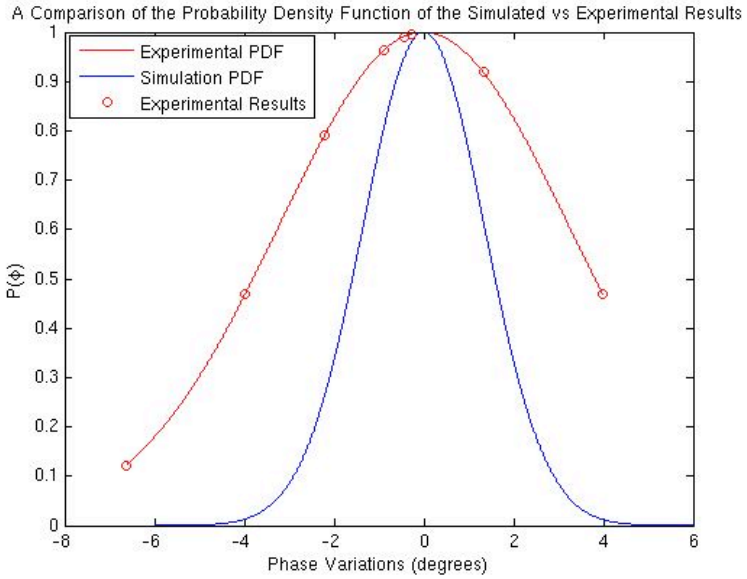

(b)

figure 6-46: The Comparison of the Probability Density Function of the Calibration Errors of the Dual Path Algorithm for a 3 by 3 array, where the Reference Element is (2,3), upon the 4 by 4 Directional Coupler Measurement Boards, (a) Amplitude and (b) Phase.

The best-case phase performance was achieved using the shortest path reference location of (2,3), which is presented in table 6-31. The results achieved an amplitude calibration range of -2.24dB to 0dB and a phase one of -6.64^o to 3.98^o. Though there were smaller ranges of errors the overall errors were larger. These errors were compared to the predicted results, as shown in figure 6-46. This comparison shows a distribution of errors which is larger for both amplitude and phase. The phase errors distribution is larger, with one outlier to the predicted error range of the algorithm.

The 3 by 3 array implementation of the dual path calibration showed that similar to the previous two algorithms, the best-case amplitude and phase performance do not take the same reference locations. This algorithm's performance when compared to that of the top left reference algorithm and the shortest path one, does not perform as favourably as predicted. The amplitude performance is worse then that of the shortest path one, with a error range of 1.48dB compared to the shortest path error range of 1.23dB. The phase performance shows that the dual path calibration has superior performance with an improvement in the error range from 11.9^{o} for the shortest path to 10.62^{o}.

The 4 by 4 array size results show a slightly different trend. The 3 by 3 array performances were for the most part better for the reference elements in one of central locations. The 4 by 4 array performance for both amplitude and phase where better for a single shortest path location. However, the next best performing reference location for both was a top left reference location.

The best performing dual path calibration algorithm implementation has its reference element at (3,2). The results of this calibration are shown in Table 6-32. This shows that the calibration error ranges are -1.04dB to 0.44dB and -8.41^{o} to 7.5^{o} for the amplitude and phase errors respectively. These measurements were then compared to the predicted performance of the dual path calibration algorithm over an array of the same size and the comparison is shown in figure 6-47. This comparison shows that the distribution of errors for both the amplitude and phase are wider then the predictions. The phase distribution has several outliers to the error range predicted by the simulations. The amplitude has only one.

Table 6-32: Dual Path Algorithm's Calibration Amplitude and Phase Errors for the 4 by 4 Experimental Test-bed, when the Reference Element is Located at Element (3, 2).

Element	Amplitude Errors (dB)	Phase Errors (degrees)
(1,1)	-0.91	-7.53
(1,2)	-0.95	-4.43
(1,3)	-0.13	-8.86
(1,4)	0.73	-0.886
(2,1)	-1.25	-10.63
(2,2)	-0.80	-8.41
(2,3)	0.70	1.33
(2,4)	0.67	4.43
(3,1)	-0.59	-0.44
(3,3)	0	-4.43
(3,4)	1.98	1.33
(4,1)	0.29	2.21
(4,2)	0.26	-0.89
(4,3)	1.09	8.86
(4,4)	0.86	3.99

When these results are compared to the other two algorithms, its performance shows an improvement in the amplitude performance, from 1.49dB amplitude error range of the shortest path algorithms to 1.48dB. The phase performance did not show an improvement. it presented an error range of 15.91^{o}, whereas the shortest path algorithm achieved a phase error range of 14.99^{o}. The difference between the algorithms is that the dual path algorithm includes a mitigation technique for the coupler errors. Due to the warping of the coupler board, all the errors have been increased and are very similar to each other. This makes the mitigation technique unable to combat the coupler errors effectively. This highlights the limitations of the mitigation technique, however its improvement in the performance it achieved in the 2 by 4 array shows the importance of the mitigation technique and that they can operate on a system with large error. However its failure on the 4 by 4 array test bed show that there is a limit to its operation due to the size and type of errors.

This is in conjunction with the other preciously mentioned implementation issues of the 4 by 4 experimental test-bed, the signal levels and reference signal matching for the measurement device and the attenuator and phase shifter interdependence.

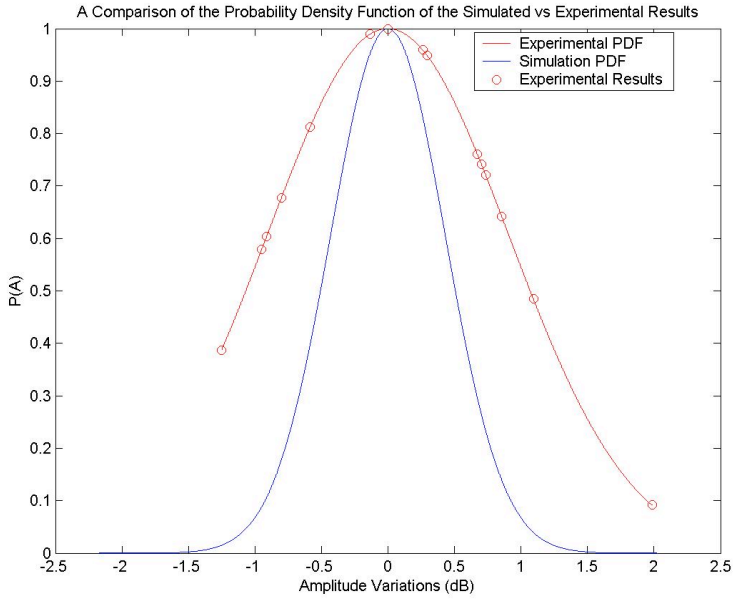

(a)

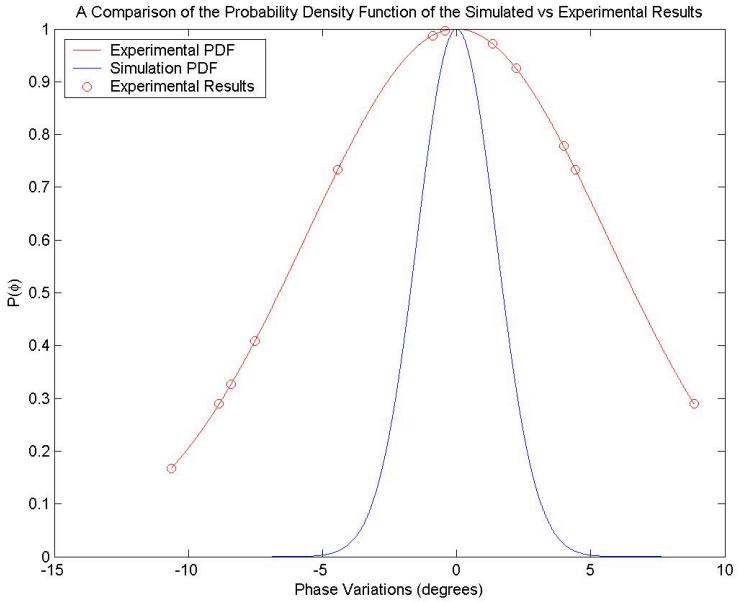

(b)

figure 6-47: The Comparison of the Probability Density Function of the Calibration Errors of the Dual Path Algorithm for a 4 by 4 array, where the Reference Element is (3,2), upon the 4 by 4 Directional Coupler Measurement Board: (a) Amplitude and (b) Phase.

6.3.3.2.4 Path Choice in the Calibration of the 4 by 4 Experimental Test-Bed

The significance of path choices has been highlighted in the discussion of the calibration of the 4 by 4 experimental test-bed. To show the impact of this, the standard deviation of each of the 16 set of calibration results were plotted against the standard deviation of the coupler path errors that those algorithms would experience. These were plotted in four separate groups, the top left reference, the shortest path, and the dual

path which uses the top left reference element locations and the dual path that uses the shortest path reference elements. These are all plotted with a corresponding line fit to show the trends in the calibration accuracy as the coupler errors increase. These results are shown in figure 6-48 and figure 6-49.

The amplitude results, figure 6-48, shows an interesting trend for the top left reference and the dual path algorithms that uses its reference element locations, that is as the coupler errors increase the calibration accuracy increases. This could be due to the longer path lengths offered by this reference element choice. It offers more cancellation of the coupler errors. Another aspect of this comparison of these two algorithms is lower, the dual path performs worse then that of the top left algorithm, this could be due to mitigation of the coupler errors are in fact increasing the calibration errors.

The shortest path and the dual path algorithm that uses the same reference element locations shows that as the coupler errors increase, so does the calibration errors. The dual path algorithm presents a similar worse performance at low coupler errors as its top left counterpart. However, as the coupler errors increase, the increase in the dual path calibration errors are much slower then that of the shortest path one.

For the phase results, the performance of all of the algorithms worsens as the coupler errors increase, as to be expected. When comparing the top left reference algorithm with its dual path counterpart, the dual path algorithm calibration errors increase at a faster

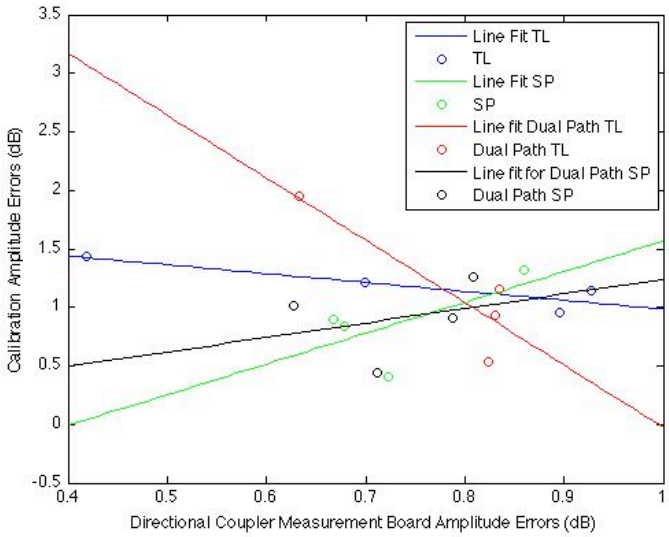

figure 6-48: Comparison of the Calibration Amplitude Accuracy of the Top Left, Shortest Path, Dual Path with Top Left Reference Locations and Dual Path with Shortest Path Reference Locations Algorithms as the Directional Coupler Measurement Board Error Increase.

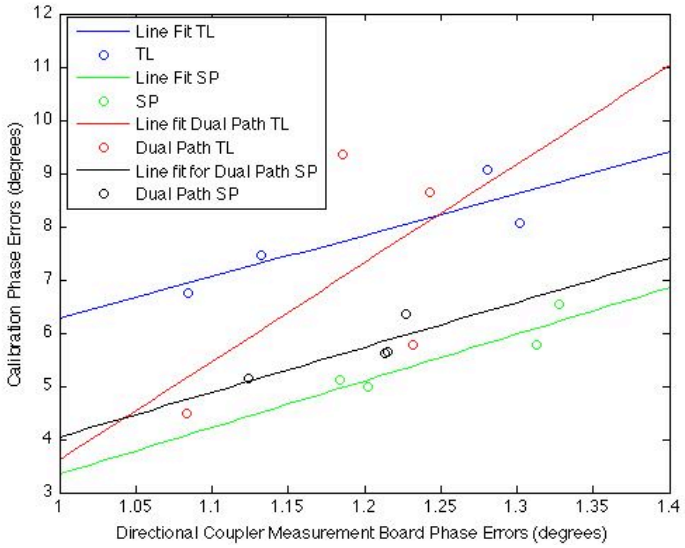

figure 6-49: Comparison of the Calibration Phase Accuracy of the Top Left, Shortest Path, Dual Path with Top Left Reference Locations and Dual Path with Shortest Path Reference Locations Algorithms as the Directional Coupler Measurement Board Error Increase.

rate then the top left reference ones as the coupler errors increase. This backs up the assertion that the dual path needs differences in the errors to offer an advantage. Errors that are correlated will not be mitigated to the same degree. When the shortest path algorithm and its dual part equivalent are compared, the dual path algorithm shows consistently higher calibration errors as the coupler error increases. This shows the dependence of the differences in the coupler path errors in mitigation performance when dealing with large coupler errors.

These graphs are based upon a single 4 by 4 coupler board and experimental setup. This means that four measurements are used for each of the predictions. With more information these predictions would be much more accurate. As they are, they are useful in highlighting trends in the data.

6.3.4 Summary of 4 by 4 Experimental Test-bed

The 4 by 4 experimental test-bed suffered from multiple implementation issues, such as warping of the directional coupler measurement board, signal levels and reference signal mismatch for the measurement device and the interdependency of the attenuator and phase shifters. These are all implementation issues specific to this test-bed and do not represent problems in the calibration concept. These issues led to high calibration errors.

This test-bed did show trends in the calibration approach, that might not have come to light had it not suffered from these implementation issues. As predicted the shortest path calibration algorithm outperformed the top left reference one, because of its use of shorter calibration paths. The dual path algorithm does not always outperform the shortest path algorithm. This will depend upon the error environment. An effect of this is that the top left reference element locations can perform as well as a shortest path one. Therefore the dual path algorithm's advantage over other algorithms depends upon the coupler errors being different between the paths. The trends in the results are summerized in Table 6-33 and Table 6-34. These tables show the amplitude and phase

Table 6-33: Comparison Table of the Amplitude and Phase Error Ranges of the Calibration Algorithm Implementations for a 3 by 3 array.

Algorithm	Reference Element	Amplitude Range (dB)	Amplitude Range Width (dB)	Phase Range (degrees)	Phase Range Width (degrees)
Top Left Reference	(1,1)	-0.22dB→1.16dB	1.38	$-8.86^o \rightarrow 6.64^o$	15.5
	(1,4)	-0.39dB → 1dB	1.39	$-6.6^o \rightarrow 6.6^o$	13.2
Shortest Path	(2,3)	-2dB → 2.2dB	4.2	$-5.7^o \rightarrow 6.2^o$	11.9
	(3,3)	-0.84dB → 0.39dB	1.23	$-10.2^o \rightarrow 8.4^o$	18.6
Dual Path	(2,3)	-2.24dB → 0dB	2.24	$-6.64^o \rightarrow 3.98^o$	10.62
	(3,3)	-1.04dB→0.44dB	1.48	$-8.41^o \rightarrow 7.5^o$	15.91

Table 6-34: Comparison Table of the Amplitude and Phase Error Ranges of the Calibration Algorithm Implementations for a 4 by 4 array.

Algorithm	Reference Element	Amplitude Range (dB)	Amplitude Range Width (dB)	Phase Range (degrees)	Phase Range Width (degrees)
Top Left Reference	(1,1)	-0.22dB→2.57dB	2.79	$-11.07^o \rightarrow 16.3^o$	27.38
	(4,4)	-3dB → 1.1dB	4.1	$-19.48^o \rightarrow 3.98^o$	23.46
Shortest Path	(2,3)	-2dB → 2.2dB	4.2	$-5.7^o \rightarrow 9.29^o$	14.99
	(3,3)	-1.1dB → 0.39dB	1.49	$-10.2^o \rightarrow 8.4^o$	18.6
Dual Path	(4,4)	-2.09dB→0.12dB	2.217	$-15.94^o \rightarrow 1.32^o$	17.26
	(3,3)	-1.04dB→0.44dB	1.48	$-8.41^o \rightarrow 7.5^o$	15.91

ranges of calibration errors for the 3 by 3 and 4 by 4 array implementations. The 4 by 4 array implementation shows the dual path's first and second best performance to show the varying reference locations.

These trends were analysed when considering the path lengths and coupler errors. This showed that the top left algorithm offers the best possiblity of coupler error cancellation. The shortest path offers the greatest advantage for avoiding errors by choosing the shortest path between the reference element and the rest of the array. The dual path algorithm has similar properties in how it chooses the reference element locations. When the dual path algorithm chooses reference element locations from the top left aglorithm, it offers the greatest possibility of coupler error cancellation. It does increase the errors that will be included and the possibilities of increasing the cumulative errors with the longer paths. The dual path that employs the shortest path algorithms reference element locations has the possibility of avoiding errors by choosing the shortest path. It limits its ability to remove more of the coupler errors by having more elements directly connected to the reference element and therefore reducing the number of possible dual paths.

6.4 Investigation of Possible Wideband Operation

The calibration experiments presented so far are narrowband in nature using a single sinusoidal signal. There is significant interest in wideband array calibration. This is more difficult and requires complex digital beamformers. However preliminary exploration using the testbed verify that the methodology being proposed is highly suitable to wideband characterisation of antenna arrays.

The directional coupler has a 50 MHz bandwidth which is relatively narrow. The RF circuitry that was purchased is similarly narrowband. Together, the experiments possible were limited to a relatively narrow range of frequencies, but successful array characterisation over 50 MHz would still be a significant achievement.

The methodology and architecture proposed in the earlier chapters is based on the idea of relative measurement. The performance of the coupler and sensing electronics will degrade as they move out of their band of operation. However if they degrade

consistently within the 2 by 2 tile, the characterisation of the phase and gain mismatch will remain viable and perform to a high degree.

This was tested by calibrating the 2 by 4 test-bed over a range of frequencies. This is an acceptable approach allowing for an interpolated spectral response to be generated. This will allow for a digital filter to be designed with the inverse response in the digital beamformer or the baseband.

The 2 by 4 array size was chosen as it does not experience the high errors experienced but the 4 by 4 array. The frequency range of interest was chosen based upon the frequency of operation of the components of the test-bed and the test-bed ability to perform calibration over the range. This resulted in frequency range of 2.42GHz to 2.48GHz creating a 50MHz frequency range for this test-bed. This experiment sets out to test the theory of calibration in the presence of graceful degradation of performance as we move to a wider band of operation.

The results of the preliminary experiments were excellent. The standard deviations of amplitude and phase performance of the test-bed are graphed over the frequency range, 2.42GHz to 2.48GHz, as shown in figure 6-50 and figure 6-51 respectively. This data is

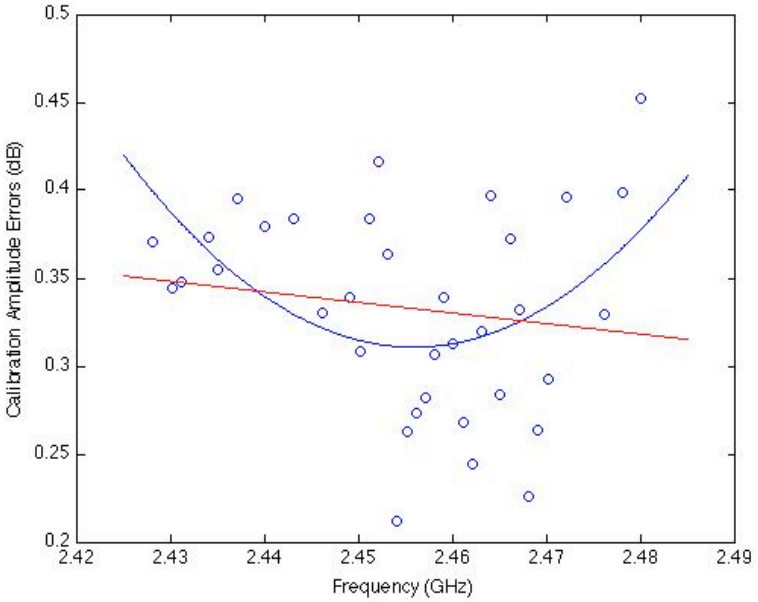

figure 6-50: The Calibration Amplitude Accuracy over the Frequency Range 2.42GHz to 2.48GHz on the 2 by 4 Experimental Test-Bed.

Table 6-35: Comparison of the effectiveness of the least squares fit line and curve.

Fit Errors	Curve	Line
Maximum	0.104	0.1336
Minimum	1.8769×10^{-4}	9.892×10^{-4}
Mean	0.0414	0.0442

presented as points, and then used to create a least squares fit curve to show a trend in this data. For the amplitude results, two least squares approximation were used. The comparison of these approximations are presented in table 6-35, which show that the curve is the better fit. It shows for both amplitude and phase that the calibration performs best at the centre frequency of operation, 2.46GHz. They then start to increase as the frequency increase from this centre frequency. The errors slowly curve up as the frequency lowers from the centre frequency. The performance accuracy of the calibration algorithm degrades from 0.31 dB to 0.35 dB and from 2.5^{o} to 3.5^{o} standard deviation errors for gain and phase respectively. This is a significant achievement over a 50 MHz bandwidth, considering the quality of components and the known issues in the 2 by 4 testbed coupler network.

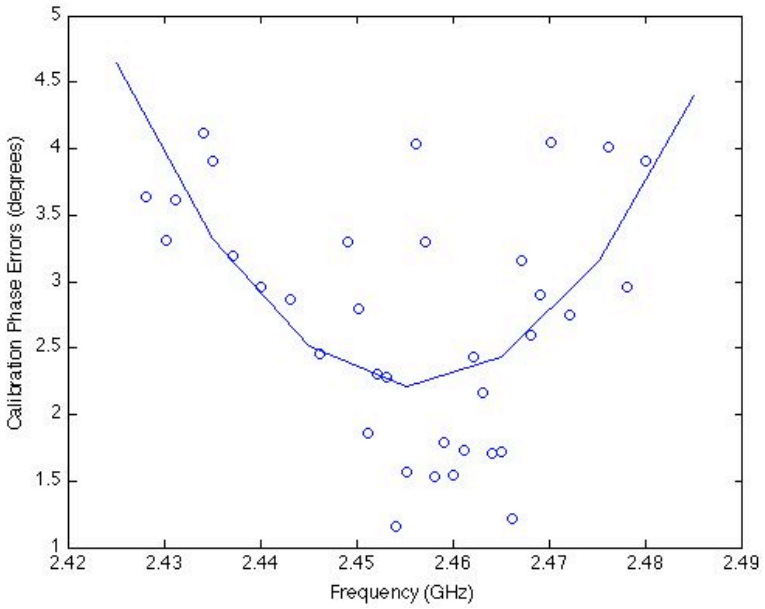

figure 6-51: The Calibration Phase Accuracy over the Frequency Range 2.42GHz to 2.48GHz on the 2 by 4 Experimental Test-Bed.

6.5 Comparison with other Published Techniques

Thus far the results of this calibration approach have been discussed in terms of the performance compared to itself and the industry-provided ±0.5dB and 5^{o} amplitude and phase mismatch criteria. This section will discuss the results in terms of the published results from some of the other techniques that have been used. Two well-recognised techniques from Chapter 3 were discussed - the Automatic Calibration Method using a Transmit Signal (ACTS) [197, 198], and the results from the TSUNAMI (II) [207] project. These two examples are representative of the other approaches to calibration and give good benchmarks for what is possible.

The ACTS method of calibration published two sets of calibration results for different array structures: the first was for a three element circular array; and the second for a 3 element linear array. The circular array results reported ±0.05dB and 0.83^{o} for the range of remaining amplitude and phase mismatch error. The linear array results increase the phase error range to ±3^{o}. Circular arrays are always optimal as they have uniform path lengths to each element with their inherent measurement structure and a high quality measurement sensor may be used. The results for the linear array are substantially worse as the path lengths to the elements need to be matched using a feed network, which would induce new errors. From the 3 element array comparison it is clear to see the errors increase significantly. This would only worsen for increased array size. In comparison with the results from our new approach, the circular array is, as to be expected, superior to our results. For the linear array however, the experimental results presented from our approach yield significantly better results (even with the warping).

The TSUNAMI (II) project published a set of results for a linear array that achieved ±0.04dB and ±0.4^{o} for amplitude and phase calibration accuracy. These results are extremely accurate and offer the best published performance. They are achieved by using a single precision sensor element and basestation grade circuitry with an external transmit signal for calibration. Fewer feedback errors than other published work are yielded from this project's use of expensive basestation-grade components and precision components for the path routing. For receive calibration, the TSUNAMI project utilised an additional antenna for external signal generation. In comparison with the results presented in this thesis, the TSUNAMI results are superior. With additional attention to detail and expertise in designing the coupler network, it would be

possible to improve the accuracy of this thesis' approach. However a distinguishing feature is the scalability of our new approach. The TSUNAMI project still suffers from the challenge in routing large numbers of feedback paths to a single reference point. Beyond a certain size this is unfeasible. The TSUNAMI project offers no solutions past eight elements.

In conclusion, the methodology presented in this thesis is comparable with the published techniques, where the calibration accuracy is traded off for scalability. The other published approaches get superior performance but this is at the cost of scalability. Our approach delivers scalability and could improve its accuracy with some attention paid to the directional coupler design. There is no architectural impediment to achieving this performance. It is primarily limited by the coupler design. With a better coupler design and substrate, performance would improve its accuracy and deliver the scalability.

6.6 Summary

This chapter has presented an experimental test-bed which was used to test the calibration approach proffered by this thesis. The calibration approach showed effective calibration and interesting trends in results. This chapter shows the ability of the mitigation techniques to reduce the impact of the coupler errors on the calibration accuracy.

The chapter started with a presentation of the measurement structure implementation and how the six pirt directional coupler was designed specifically for this project to create the unique overlaping measurement structure with the multiple measurement sensors. This was implemented upon FR-4 substrate, which achieved approximately -39dB coupled paths. The implementation of the directional coupler measurement board suffers from warping as the array size increased. This was due to the thickness of the substrate used. They were sandwiched together and react differently to the environmental effects. These boards are passive in nature and are capable of graceful degradation of performance outside of their frequency of operation, while requiring a sequential approach to calibration. A switched version of the boards where designed to overcome this. It had narrowband performance over 50MHz range, while providing good isolation.

The experimental investigation of this calibration approach uses the passive directional coupler measurement boards in 2 by 4 and 4 by 4 test-beds which prove the calibration capabilities of the approach. The 2 by 4 array test-bed showed that the amplitude performance of the calibration is better then predicted. The phase performance was not as good, but the dual path calibration algorithm performs as well as predicted. It also meet the ±0.5dB and 5^{o} criteria for all but one amplitude error for one element.

The experimental test-bed was extended to create a 4 by 4 array. This array showed more clearly the effects of the warping, the impact of the reference signal mismatch and signal levels on the measurement device. It also showed the impact of the interdependence of the voltage controlled attenuator and phase shifters. All of these error sources are implementation issues and will not effect other implementations. These errors did not prevent the calibration of the test-bed though they led to high calibration errors. This implementation highlights trends in the results, that might not have come to light had it not suffered from these implementation issues. The shortest path calibration algorithm outperformed the top left reference one as was expected from its use of shorter calibration paths. The dual path algorithm does not always outperform the shortest path algorithm. This showed a dependence upon the error environment. The dual path algorithm's advantage over other algorithms depends upon the coupler errors being different between the paths in order for it to mitigate for them.

These trends of the results were considered in terms of the path choice and the coupler errors of the algorithms. This showed that the top left algorithm overs the most possiblity of cancelation. The shortest path offers the greatest advantage for avoiding errors by choosing the shortest path between the reference element and the rest of the array. The dual path algorithm has similar properties to the other algorithms, when it chooses similar reference element locations.

The investigation of the calibration approach and the experimental test-bed was finally used to look at the impact of frequency upon the calibration. This showed that the calibration errors increase as the frequency of operation moves away from 2.46GHz. These errors were shown over a frequency range of 50MHz; the errors are all within the range of 0.2dB to 0.5dB and for the phase results the range is 1^{o} to 4.5^{o}. This showed that degraded performance in the implementation is not an impediment to high quality

calibration. With this understanding, it was demonstrated that wideband calibration should be possible, only limited by the components used in our testbed.

The presentation of experimental results finished with a comparison of experimental results with those presented by other published techniques, Auto Calibration Technique, ACTS and TSUNAMI (II). The calibration techniques presented by this dissertation showed comparable performance to the ACTS approach when compared to the 3 element linear array. When the relative sizes of the array were considered the ACTS approach was limited. Finally the comparison of the TSUNAMI (II) project was considered. The results it reported were extremely accurate. This technique uses basestation grade circuitry and an external calibration source. While our approach's results were not as accurate, they were achieved on a system that it easily scalable, created using low cost components and in the presence of warping effects. With a better experimental system, our results would substantially improve. The coupler solely limits the accuracy of this system.

Chapter 7

The Conclusion

7.1 Summary

This thesis presented a novel approach to the calibration of antenna arrays, with its focus being scalability and dynamic calibration. The approach utilises multiple measurement sensors to achieve this. Each sensor is connected to multiple array elements to create a circular array or tile. These tiles are overlapped, so that most elements of the array are connected to multiple sensors. This created redundancy in the system, and this is employed by calibration algorithms to remove element and sensor errors and mitigate for other sources of errors. The accuracy of this novel approach is limited solely by the performance of the measurement structure, as the architecture offers no impediment to the accuracy.

Key points of this thesis are:

- The calibration approach presented by this research is novel. It utilises a network of circular arrays to create a scalable array structure that provides a measurement structure. By creating a measurement structure, dynamic calibration can be achieved without the need for additional external hardware.
- Algorithms were specifically developed to exploit the nature of the network of circular arrays to calibrate the array. These algorithms remove the element and sensor errors from the array and have the capability to mitigate the other sources of errors.
- The network of circular arrays requires symmetrical connectivity for the calibration to be effective. A unique directional coupler was developed to create this. This provides all the sensors that are connected to an array element with equal signals.
- The experimental test bed was built for purpose for this unique calibration approach. It provides the means to fully test the capabilities of the calibration

principle, and the means to test further developments in the area of scalable measurement structure algorithms.

- The calibration approach was demonstrated and measured upon a representative experimental test-bed. This achieved calibration that met the industrial requirement that it provide ±0.5dB and 5^{o} amplitude and phase mismatch criterion for all but a single amplitude outlier, 0.55dB. This accuracy is solely dependent upon the coupler's performance.

Each of these points contributes to the creation of a new paradigm for array characterisation and calibration.

7.2 Conclusions

This thesis presented a method to calibrate antenna arrays using a scalable approach that does not need additional external hardware to provide dynamic calibration. This approach is based upon a novel measurement structure with multiple measurement sensors that utilised a specially designed six port directional coupler to provide connectivity. This provides redundancy of measurement based upon the concept of tiling circular arrays to produce large planar array structures. This redundancy was exploited by calibration algorithms, which were specifically designed for this calibration approach and have the ability to remove the sensor and array element errors and mitigated the other measurement structure errors. The calibration methodology provides an efficient calibration of antenna arrays in which every aspect of them is susceptible to errors, in other words non-ideal implementations, and does not require any precision hardware to implement. The accuracy of this approach is solely dependent upon the coupler. This was shown on the experimental testbed, which was built for purpose but can be further utilised for the development of alternative approaches to the calibration problem. The architecture integrates the strengths of circular arrays into other array shapes without loss of performance. This provides a general solution to the calibration of any array shape, frequency or modulation scheme.

7.3 Future Work

An idea for the further development of this research could include a second iteration of the test bed design where special attention is paid to the directional coupler boards and component operation. This would be used to verify that improved performance can be achieved by this calibration approach using improved equipment. This could then be compared to the other published techniques.

The future avenues of investigation would be wideband applications and switching networks. The performance of this calibration approach showed promising results in wideband signal calibration. An investigation in to this would led to a significantly wider variety of applications for which antenna arrays could be used. The switching networks touched upon here showed the possibility to provide calibration during operation. This would be beneficial in time sensitive applications. The switching network creates the interesting problem of providing wideband switching while obtaining high isolation.

Appendix A

Measure and Correct Calculation of Calibration Errors

This appendix is concerned with the effectiveness of the measure and correct calibration algorithm. This means that the sources of errors of the measurement path are considered and the effectiveness of the measure and correct algorithm in removing these errors is analysed. The mechanism of calibration employed is described in Chapter 5. Therefore the description will start here with the objective to present the calculation of the effectiveness. The measurement path is shown in figure 8-1, showing the transmit operation of the measurement path. This shows the source of errors; these are represented as contributions to the signal.

The signal is inputted into the transmitter block, this signal is at a specific frequency and level and will vary around this level in both amplitude and phase. This is then added to by the transmitters effect on the signal with its own variation in amplitude and phase. Then the signal flows through the directional coupler, which adds its own contribution in amplitude and phase. Then finally this measurement device measures this signal. It is also a source of amplitude and

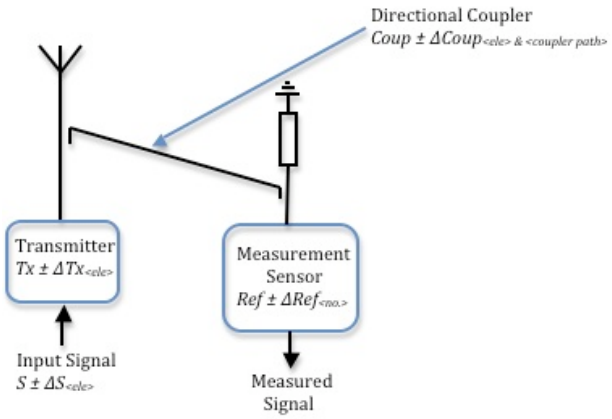

figure 8-1: Single Transmit Measurement Path showing the Component Blocks and Their Contribution as an Error Source.

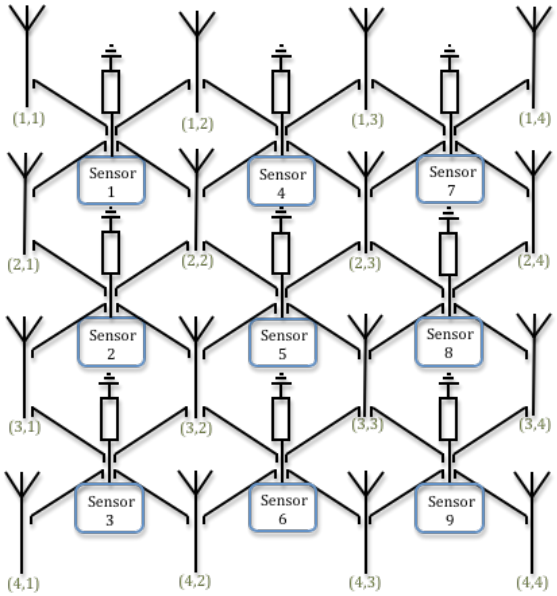

figure 8-2: a 4 by 4 Antenna Array including Element and Measurement Sensor Numbering.

phase errors. Each of these sources of errors will affect the accuracy of the calibration algorithms. It is important to consider how the calibration is performed and in this way decipher which errors sources are tackled by the calibration algorithm.

The measurement and correct calibration algorithm, as mentioned in chapter 5, measures each of the elements and then creates an average measurement. This average measurement is then used to create the correction factor for each element of the array. Then, the array is calibrated using these correction factors.

The calculation of the effectiveness of the measurement and correct calibration algorithm is presented in a series of tables and the equation is created for each element of the array to show the trends in the sources of errors. This is then used to create an overall equation that estimates the effectiveness of the calibration. The equations to describe the sources of errors that will effect the calibration algorithms are created in terms of the individual elements; the numbering convention for the elements of the array and the measurement sensors are shown in figure 8-2 and the method of indentifying the coupler paths connected to an element are shown in figure 8-3.

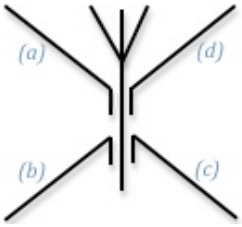

figure 8-3: Coupler Path Identification.

The first table, Table 8-1, contains the output signal in terms of its contributing factors and then the measured signal in those terms for each element. These equations were generated manually and used to create equation 5.1. The notation used in the following tables are:

S_{RC} – is the input signal to element located at row, R, and column, C,

Tx – is the transmitter block's modelled value,

$\Delta Tx_{R,C}$ – is the element located at row, R, and column, C, transmitter block's variation from the transmitter block modelled value,

$Coup$ – is the coupler paths' modelled value,

$\Delta Coup_{R,C,I}$ – this is the element located at row, R, and column, C, and using the coupler path identified by I, coupler path's variation from the coupler paths' modelled value,

Ref – is the measurement sensor's modelled value,

ΔRef_{SN} – this is the measurement sensor identified by its identification number SN, which are shown in figure 8-2, measurement sensor's variation from the measurement sensor's modelled value,

$Output$ – is the signal seen at the antenna point of the element,

$Measurement$ – is the signal measured by the measurement sensor for the element.

Table 8-1: Output and Measured Signal for Each Element of the Array in terms of the Sources of Errors.

Type	Element	Equation	
Output	(1,1)	$S_{11} + Tx + \Delta Tx_{11}$	(8.1)
Measurement	(1,1)	$S_{11} + Tx + \Delta Tx_{11} + Coup + \Delta Coup_{11c} + Ref + \Delta Ref_1(S_{11} + Tx + \Delta Tx_{11} + Coup + \Delta Coup_{11c})$	(8.2)
Output	(1,2)	$S_{12} + Tx + \Delta Tx_{12}$	(8.3)
Measurement	(1,2)	$S_{12} + Tx + \Delta Tx_{12} + Coup + \Delta Coup_{12c} + Ref + \Delta Ref_4(S_{12} + Tx + \Delta Tx_{12} + Coup + \Delta Coup_{12c})$	(8.4)
Output	(1,3)	$S_{13} + Tx + \Delta Tx_{13}$	(8.5)
Measurement	(1,3)	$S_{13} + Tx + \Delta Tx_{13} + Coup + \Delta Coup_{13c} + Ref + \Delta Ref_7(S_{13} +$	(8.6)

		$Tx + \Delta Tx_{13} + Coup + \Delta Coup_{13c}$)	
Output	(1,4)	$S_{14} + Tx + \Delta Tx_{14}$	(8.7)
Measurement	(1,4)	$S_{14} + Tx + \Delta Tx_{14} + Coup + \Delta Coup_{14b} + Ref + \Delta Ref_7(S_{14} +$ $Tx + \Delta Tx_{14} + Coup + \Delta Coup_{14b})$	(8.8)
Output	(2,1)	$S_{21} + Tx + \Delta Tx_{21}$	(8.9)
Measurement	(2,1)	$S_{21} + Tx + \Delta Tx_{21} + Coup + \Delta Coup_{21c} + Ref + \Delta Ref_2(S_{21} +$ $Tx + \Delta Tx_{21} + Coup + \Delta Coup_{21c})$	(8.10)
Output	(2,2)	$S_{22} + Tx + \Delta Tx_{22}$	(8.11)
Measurement	(2,2)	$S_{22} + Tx + \Delta Tx_{22} + Coup + \Delta Coup_{22c} + Ref + \Delta Ref_5(S_{22} +$ $Tx + \Delta Tx_{22} + Coup + \Delta Coup_{22c})$	(8.12)
Output	(2,3)	$S_{23} + Tx + \Delta Tx_{23}$	(8.13)
Measurement	(2,3)	$S_{23} + Tx + \Delta Tx_{23} + Coup + \Delta Coup_{23c} + Ref + \Delta Ref_8(S_{23} +$ $Tx + \Delta Tx_{23} + Coup + \Delta Coup_{23c})$	(8.14)
Output	(2,4)	$S_{24} + Tx + \Delta Tx_{24}$	(8.15)
Measurement	(2,4)	$S_{24} + Tx + \Delta Tx_{24} + Coup + \Delta Coup_{24c} + Ref + \Delta Ref_8(S_{24} +$ $Tx + \Delta Tx_{24} + Coup + \Delta Coup_{24c})$	(8.16)
Output	(3,1)	$S_{31} + Tx + \Delta Tx_{31}$	(8.17)
Measurement	(3,1)	$S_{31} + Tx + \Delta Tx_{31} + Coup + \Delta Coup_{31c} + Ref + \Delta Ref_3(S_{31} +$ $Tx + \Delta Tx_{31} + Coup + \Delta Coup_{31c})$	(8.18)
Output	(3,2)	$S_{32} + Tx + \Delta Tx_{32}$	(8.19)
Measurement	(3,2)	$S_{32} + Tx + \Delta Tx_{32} + Coup + \Delta Coup_{32c} + Ref + \Delta Ref_6(S_{32} +$ $Tx + \Delta Tx_{32} + Coup + \Delta Coup_{32c})$	(8.20)
Output	(3,3)	$S_{33} + Tx + \Delta Tx_{33}$	(8.21)
Measurement	(3,3)	$S_{33} + Tx + \Delta Tx_{33} + Coup + \Delta Coup_{33c} + Ref + \Delta Ref_9(S_{33} +$ $Tx + \Delta Tx_{33} + Coup + \Delta Coup_{33c})$	(8.22)
Output	(3,4)	$S_{34} + Tx + \Delta Tx_{34}$	(8.23)
Measurement	(3,4)	$S_{34} + Tx + \Delta Tx_{34} + Coup + \Delta Coup_{34b} + Ref + \Delta Ref_9(S_{34} +$ $Tx + \Delta Tx_{34} + Coup + \Delta Coup_{34b})$	(8.24)
Output	(4,1)	$S_{41} + Tx + \Delta Tx_{41}$	(8.25)
Measurement	(4,1)	$S_{41} + Tx + \Delta Tx_{41} + Coup + \Delta Coup_{41d} + Ref + \Delta Ref_3(S_{41} +$ $Tx + \Delta Tx_{41} + Coup + \Delta Coup_{41d})$	(8.26)
Output	(4,2)	$S_{42} + Tx + \Delta Tx_{42}$	(8.27)
Measurement	(4,2)	$S_{42} + Tx + \Delta Tx_{42} + Coup + \Delta Coup_{42d} + Ref + \Delta Ref_6(S_{42} +$ $Tx + \Delta Tx_{42} + Coup + \Delta Coup_{42d})$	(8.28)
Output	(4,3)	$S_{43} + Tx + \Delta Tx_{43}$	(8.29)
Measurement	(4,3)	$S_{43} + Tx + \Delta Tx_{43} + Coup + \Delta Coup_{43d} + Ref + \Delta Ref_9(S_{43} +$ $Tx + \Delta Tx_{43} + Coup + \Delta Coup_{43d})$	(8.30)
Output	(4,4)	$S_{44} + Tx + \Delta Tx_{44}$	(8.31)
Measurement	(4,4)	$S_{44} + Tx + \Delta Tx_{44} + Coup + \Delta Coup_{44a} + Ref + \Delta Ref_9(S_{44} +$ $Tx + \Delta Tx_{44} + Coup + \Delta Coup_{44a})$	(8.32)

The next table, Table 8-2, consists of the total measurement signals, this followed by the average of the measurement signal in Table 8-3. This average measurement signal is used to compare to each element's measurement signal, and this comparison is used to create the correction factor for each element of the array.

Table 8-2: The Sum of all Measured Signals.

Type	Element	Equation	
Total Measurement	All	$S_{11} + S_{12} + S_{13} + S_{14} + S_{21} + S_{22} + S_{23} + S_{24} + S_{31} + S_{32} + S_{33} + S_{34} + S_{41} + S_{42} + S_{43} + S_{44} + 16Tx + \Delta Tx_{11} + \Delta Tx_{12} + \Delta Tx_{13} + \Delta Tx_{14} + \Delta Tx_{21} + \Delta Tx_{22} + \Delta Tx_{23} + \Delta Tx_{24} + \Delta Tx_{31} + \Delta Tx_{32} + \Delta Tx_{33} + \Delta Tx_{34} + \Delta Tx_{41} + \Delta Tx_{42} + \Delta Tx_{43} + \Delta Tx_{44} + 16Coup + \Delta Coup_{11c} + \Delta Coup_{12c} + \Delta Coup_{13c} + \Delta Coup_{14b} + \Delta Coup_{21c} + \Delta Coup_{22c} + \Delta Coup_{23c} + \Delta Coup_{24c} + \Delta Coup_{31c} + \Delta Coup_{32c} + \Delta Coup_{33c} + \Delta Coup_{34b} + \Delta Coup_{41d} + \Delta Coup_{42d} + \Delta Coup_{43d} + \Delta Coup_{44a} + 16Ref + \Delta Ref_1(S_{11} + Tx + \Delta Tx_{11} + Coup + \Delta Coup_{11c}) + \Delta Ref_4(S_{12} + Tx + \Delta Tx_{12} + Coup + \Delta Coup_{12c}) + \Delta Ref_7(S_{13} + Tx + \Delta Tx_{13} + Coup + \Delta Coup_{13c}) + \Delta Ref_7(S_{14} + Tx + \Delta Tx_{14} + Coup + \Delta Coup_{14b}) + \Delta Ref_2(S_{21} + Tx + \Delta Tx_{21} + Coup + \Delta Coup_{21c}) + \Delta Ref_5(S_{22} + Tx + \Delta Tx_{22} + Coup + \Delta Coup_{22c}) + \Delta Ref_8(S_{23} + Tx + \Delta Tx_{23} + Coup + \Delta Coup_{23c}) + \Delta Ref_8(S_{24} + Tx + \Delta Tx_{24} + Coup + \Delta Coup_{24c}) + \Delta Ref_3(S_{31} + Tx + \Delta Tx_{31} + Coup + \Delta Coup_{31c}) + \Delta Ref_6(S_{32} + Tx + \Delta Tx_{32} + Coup + \Delta Coup_{32c}) + \Delta Ref_9(S_{33} + Tx + \Delta Tx_{33} + Coup + \Delta Coup_{33c}) + \Delta Ref_9(S_{34} + Tx + \Delta Tx_{34} + Coup + \Delta Coup_{34b}) + \Delta Ref_3(S_{41} + Tx + \Delta Tx_{41} + Coup + \Delta Coup_{41d}) + \Delta Ref_6(S_{42} + Tx + \Delta Tx_{42} + Coup + \Delta Coup_{42d}) + \Delta Ref_9(S_{43} + Tx + \Delta Tx_{43} + Coup + \Delta Coup_{43d}) + \Delta Ref_9(S_{44} + Tx + \Delta Tx_{44} + Coup + \Delta Coup_{44a})$	(8.33)

Table 8-3: The Average Measured Signal.

Type	Element	Equation	
Average	All	$(S_{11} + S_{12} + S_{13} + S_{14} + S_{21} + S_{22} + S_{23} + S_{24} + S_{31} + S_{32} + S_{33} + S_{34} + S_{41} + S_{42} + S_{43} + S_{44})/16 + Tx + (\Delta Tx_{11} + \Delta Tx_{12} + \Delta Tx_{13} + \Delta Tx_{14} + \Delta Tx_{21} + \Delta Tx_{22} + \Delta Tx_{23} + \Delta Tx_{24} + \Delta Tx_{31} + \Delta Tx_{32} + \Delta Tx_{33} + \Delta Tx_{34} + \Delta Tx_{41} + \Delta Tx_{42} + \Delta Tx_{43} + \Delta Tx_{44})/16 + Coup + (\Delta Coup_{11c} + \Delta Coup_{12c} + \Delta Coup_{13c} + \Delta Coup_{14b} + \Delta Coup_{21c} + \Delta Coup_{22c} + \Delta Coup_{23c} + \Delta Coup_{24c} + \Delta Coup_{31c} + \Delta Coup_{32c} + \Delta Coup_{33c} + \Delta Coup_{34b} + \Delta Coup_{41d} + \Delta Coup_{42d} + \Delta Coup_{43d} + \Delta Coup_{44a})/16 + Ref + [\Delta Ref_1(S_{11} + Tx + \Delta Tx_{11} + Coup + \Delta Coup_{11c}) + \Delta Ref_4(S_{12} + Tx + \Delta Tx_{12} + Coup + \Delta Coup_{12c}) + \Delta Ref_7(S_{13} + Tx + \Delta Tx_{13} + Coup + \Delta Coup_{13c}) + \Delta Ref_7(S_{14} + Tx + \Delta Tx_{14} + Coup + \Delta Coup_{14b}) + \Delta Ref_2(S_{21} + Tx + \Delta Tx_{21} + Coup + \Delta Coup_{21c}) + \Delta Ref_5(S_{22} + Tx + \Delta Tx_{22} + Coup + \Delta Coup_{22c}) + \Delta Ref_8(S_{23} + Tx + \Delta Tx_{23} + Coup + \Delta Coup_{23c}) + \Delta Ref_8(S_{24} + Tx + \Delta Tx_{24} + Coup + \Delta Coup_{24c}) + \Delta Ref_3(S_{31} + Tx + \Delta Tx_{31} + Coup + \Delta Coup_{31c}) + \Delta Ref_6(S_{32} + Tx + \Delta Tx_{32} + Coup + \Delta Coup_{32c}) + \Delta Ref_9(S_{33} + Tx + \Delta Tx_{33} + Coup + \Delta Coup_{33c}) + \Delta Ref_9(S_{34} + Tx + \Delta Tx_{34} + Coup + \Delta Coup_{34b}) + \Delta Ref_3(S_{41} + Tx + \Delta Tx_{41} + Coup + \Delta Coup_{41d}) + \Delta Ref_6(S_{42} + Tx + \Delta Tx_{42} + Coup + \Delta Coup_{42d}) + \Delta Ref_9(S_{43} + Tx + \Delta Tx_{43} + Coup + \Delta Coup_{43d}) + \Delta Ref_9(S_{44} + Tx + \Delta Tx_{44} + Coup + \Delta Coup_{44a})]/16$	(8.34)

The calculation of each element's correction factor is shown in Table 8-4. As can be seen from these correction factors they have a contribution from each of the error sources in the array.

Table 8-4: Correction Factor for Each Element of the Array in terms of the Sources of Errors.

Type	Element	Equation	
Correction Factor	(1,1)	$-[(S_{12}+S_{13}+S_{14}+S_{21}+S_{22}+S_{23}+S_{24}+S_{31}+S_{32}+S_{33}+S_{34}+S_{41}+S_{42}+S_{43}+S_{44})/16+(\Delta Tx_{12}+\Delta Tx_{13}+\Delta Tx_{14}+\Delta Tx_{21}+\Delta Tx_{22}+\Delta Tx_{23}+\Delta Tx_{24}+\Delta Tx_{31}+\Delta Tx_{32}+\Delta Tx_{33}+\Delta Tx_{34}+\Delta Tx_{41}+\Delta Tx_{42}+\Delta Tx_{43}+\Delta Tx_{44})/16+(\Delta Coup_{12c}+\Delta Coup_{13c}+\Delta Coup_{14b}+\Delta Coup_{21c}+\Delta Coup_{22c}+\Delta Coup_{23c}+\Delta Coup_{24c}+\Delta Coup_{31c}+\Delta Coup_{32c}+\Delta Coup_{33c}+\Delta Coup_{34b}+\Delta Coup_{41d}+\Delta Coup_{42d}+\Delta Coup_{43d}+\Delta Coup_{44a})/16+[\Delta Ref_4(S_{12}+Tx+\Delta Tx_{12}+Coup+\Delta Coup_{12c})+\Delta Ref_7(S_{13}+Tx+\Delta Tx_{13}+Coup+\Delta Coup_{13c})+\Delta Ref_7(S_{14}+Tx+\Delta Tx_{14}+Coup+\Delta Coup_{14b})+\Delta Ref_2(S_{21}+Tx+\Delta Tx_{21}+Coup+\Delta Coup_{21c})+\Delta Ref_5(S_{22}+Tx+\Delta Tx_{22}+Coup+\Delta Coup_{22c})+\Delta Ref_8(S_{23}+Tx+\Delta Tx_{23}+Coup+\Delta Coup_{23c})+\Delta Ref_8(S_{24}+Tx+\Delta Tx_{24}+Coup+\Delta Coup_{24c})+\Delta Ref_3(S_{31}+Tx+\Delta Tx_{31}+Coup+\Delta Coup_{31c})+\Delta Ref_6(S_{32}+Tx+\Delta Tx_{32}+Coup+\Delta Coup_{32c})+\Delta Ref_9(S_{33}+Tx+\Delta Tx_{33}+Coup+\Delta Coup_{33c})+\Delta Ref_9(S_{34}+Tx+\Delta Tx_{34}+Coup+\Delta Coup_{34b})+\Delta Ref_3(S_{41}+Tx+\Delta Tx_{41}+Coup+\Delta Coup_{41d})+\Delta Ref_6(S_{42}+Tx+\Delta Tx_{42}+Coup+\Delta Coup_{42d})+\Delta Ref_9(S_{43}+Tx+\Delta Tx_{43}+Coup+\Delta Coup_{43d})+\Delta Ref_9(S_{44}+Tx+\Delta Tx_{44}+Coup+\Delta Coup_{44a})]/16]$	(8.35)
Correction Factor	(1,2)	$-[(S_{11}+S_{13}+S_{14}+S_{21}+S_{22}+S_{23}+S_{24}+S_{31}+S_{32}+S_{33}+S_{34}+S_{41}+S_{42}+S_{43}+S_{44})/16+(\Delta Tx_{11}+\Delta Tx_{12}+\Delta Tx_{13}+\Delta Tx_{14}+\Delta Tx_{21}+\Delta Tx_{22}+\Delta Tx_{23}+\Delta Tx_{24}+\Delta Tx_{31}+\Delta Tx_{32}+\Delta Tx_{33}+\Delta Tx_{34}+\Delta Tx_{41}+\Delta Tx_{42}+\Delta Tx_{43}+\Delta Tx_{44})/16+(\Delta Coup_{11c}+\Delta Coup_{13c}+\Delta Coup_{14b}+\Delta Coup_{21c}+\Delta Coup_{22c}+\Delta Coup_{23c}+\Delta Coup_{24c}+\Delta Coup_{31c}+\Delta Coup_{32c}+\Delta Coup_{33c}+\Delta Coup_{34b}+\Delta Coup_{41d}+\Delta Coup_{42d}+\Delta Coup_{43d}+\Delta Coup_{44a})/16+[\Delta Ref_1(S_{11}+Tx+\Delta Tx_{11}+Coup+\Delta Coup_{11c})+\Delta Ref_7(S_{13}+Tx+\Delta Tx_{13}+Coup+\Delta Coup_{13c})+\Delta Ref_7(S_{14}+Tx+\Delta Tx_{14}+Coup+\Delta Coup_{14b})+\Delta Ref_2(S_{21}+Tx+\Delta Tx_{21}+Coup+\Delta Coup_{21c})+\Delta Ref_5(S_{22}+Tx+\Delta Tx_{22}+Coup+\Delta Coup_{22c})+\Delta Ref_8(S_{23}+Tx+\Delta Tx_{23}+Coup+\Delta Coup_{23c})+\Delta Ref_8(S_{24}+Tx+\Delta Tx_{24}+Coup+\Delta Coup_{24c})+\Delta Ref_3(S_{31}+Tx+\Delta Tx_{31}+Coup+\Delta Coup_{31c})+\Delta Ref_6(S_{32}+Tx+\Delta Tx_{32}+Coup+\Delta Coup_{32c})+\Delta Ref_9(S_{33}+Tx+\Delta Tx_{33}+Coup+\Delta Coup_{33c})+\Delta Ref_9(S_{34}+Tx+\Delta Tx_{34}+Coup+\Delta Coup_{34b})+\Delta Ref_3(S_{41}+Tx+\Delta Tx_{41}+Coup+\Delta Coup_{41d})+\Delta Ref_6(S_{42}+Tx+\Delta Tx_{42}+Coup+\Delta Coup_{42d})+\Delta Ref_9(S_{43}+Tx+\Delta Tx_{43}+Coup+\Delta Coup_{43d})+\Delta Ref_9(S_{44}+Tx+\Delta Tx_{44}+Coup+\Delta Coup_{44a})]/16]$	(8.36)
Correction Factor	(1,3)	$-[(S_{11}+S_{12}+S_{14}+S_{21}+S_{22}+S_{23}+S_{24}+S_{31}+S_{32}+S_{33}+S_{34}+S_{41}+S_{42}+S_{43}+S_{44})/16+(\Delta Tx_{11}+\Delta Tx_{12}+\Delta Tx_{14}+\Delta Tx_{21}+\Delta Tx_{22}+\Delta Tx_{23}+\Delta Tx_{24}+\Delta Tx_{31}+\Delta Tx_{32}+\Delta Tx_{33}+\Delta Tx_{34}+\Delta Tx_{41}+\Delta Tx_{42}+\Delta Tx_{43}+\Delta Tx_{44})/16+(\Delta Coup_{11c}+\Delta Coup_{12c}+\Delta Coup_{14b}+\Delta Coup_{21c}+\Delta Coup_{22c}+\Delta Coup_{23c}+\Delta Coup_{24c}+\Delta Coup_{31c}+\Delta Coup_{32c}+\Delta Coup_{33c}+\Delta Coup_{34b}+\Delta Coup_{41d}+\Delta Coup_{42d}+\Delta Coup_{43d}+\Delta Coup_{44a}$	(8.37)

		$)/16 + [\Delta Ref_1(S_{11} + Tx + \Delta Tx_{11} + Coup + \Delta Coup_{11c}) + \Delta Ref_4(S_{12} + Tx + \Delta Tx_{12} + Coup + \Delta Coup_{12c}) + \Delta Ref_7(S_{14} + Tx + \Delta Tx_{14} + Coup + \Delta Coup_{14b}) + \Delta Ref_2(S_{21} + Tx + \Delta Tx_{21} + Coup + \Delta Coup_{21c}) + \Delta Ref_5(S_{22} + Tx + \Delta Tx_{22} + Coup + \Delta Coup_{22c}) + \Delta Ref_8(S_{23} + Tx + \Delta Tx_{23} + Coup + \Delta Coup_{23c}) + \Delta Ref_8(S_{24} + Tx + \Delta Tx_{24} + Coup + \Delta Coup_{24c}) + \Delta Ref_3(S_{31} + Tx + \Delta Tx_{31} + Coup + \Delta Coup_{31c}) + \Delta Ref_6(S_{32} + Tx + \Delta Tx_{32} + Coup + \Delta Coup_{32c}) + \Delta Ref_9(S_{33} + Tx + \Delta Tx_{33} + Coup + \Delta Coup_{33c}) + \Delta Ref_9(S_{34} + Tx + \Delta Tx_{34} + Coup + \Delta Coup_{34b}) + \Delta Ref_3(S_{41} + Tx + \Delta Tx_{41} + Coup + \Delta Coup_{41d}) + \Delta Ref_6(S_{42} + Tx + \Delta Tx_{42} + Coup + \Delta Coup_{42d}) + \Delta Ref_9(S_{43} + Tx + \Delta Tx_{43} + Coup + \Delta Coup_{43d}) + \Delta Ref_9(S_{44} + Tx + \Delta Tx_{44} + Coup + \Delta Coup_{44a})]/16]$	
Correction Factor	(1,4)	$- [(S_{11} + S_{12} + S_{13} + S_{21} + S_{22} + S_{23} + S_{24} + S_{31} + S_{32} + S_{33} + S_{34} + S_{41} + S_{42} + S_{43} + S_{44})/16 + (\Delta Tx_{11} + \Delta Tx_{12} + \Delta Tx_{13} + \Delta Tx_{21} + \Delta Tx_{22} + \Delta Tx_{23} + \Delta Tx_{24} + \Delta Tx_{31} + \Delta Tx_{32} + \Delta Tx_{33} + \Delta Tx_{34} + \Delta Tx_{41} + \Delta Tx_{42} + \Delta Tx_{43} + \Delta Tx_{44})/16 + (\Delta Coup_{11c} + \Delta Coup_{12c} + \Delta Coup_{13c} + \Delta Coup_{21c} + \Delta Coup_{22c} + \Delta Coup_{23c} + \Delta Coup_{24c} + \Delta Coup_{31c} + \Delta Coup_{32c} + \Delta Coup_{33c} + \Delta Coup_{34b} + \Delta Coup_{41d} + \Delta Coup_{42d} + \Delta Coup_{43d} + \Delta Coup_{44a})/16 + [\Delta Ref_1(S_{11} + Tx + \Delta Tx_{11} + Coup + \Delta Coup_{11c}) + \Delta Ref_4(S_{12} + Tx + \Delta Tx_{12} + Coup + \Delta Coup_{12c}) + \Delta Ref_7(S_{13} + Tx + \Delta Tx_{13} + Coup + \Delta Coup_{13c}) + \Delta Ref_2(S_{21} + Tx + \Delta Tx_{21} + Coup + \Delta Coup_{21c}) + \Delta Ref_5(S_{22} + Tx + \Delta Tx_{22} + Coup + \Delta Coup_{22c}) + \Delta Ref_8(S_{23} + Tx + \Delta Tx_{23} + Coup + \Delta Coup_{23c}) + \Delta Ref_8(S_{24} + Tx + \Delta Tx_{24} + Coup + \Delta Coup_{24c}) + \Delta Ref_3(S_{31} + Tx + \Delta Tx_{31} + Coup + \Delta Coup_{31c}) + \Delta Ref_6(S_{32} + Tx + \Delta Tx_{32} + Coup + \Delta Coup_{32c}) + \Delta Ref_9(S_{33} + Tx + \Delta Tx_{33} + Coup + \Delta Coup_{33c}) + \Delta Ref_9(S_{34} + Tx + \Delta Tx_{34} + Coup + \Delta Coup_{34b}) + \Delta Ref_3(S_{41} + Tx + \Delta Tx_{41} + Coup + \Delta Coup_{41d}) + \Delta Ref_6(S_{42} + Tx + \Delta Tx_{42} + Coup + \Delta Coup_{42d}) + \Delta Ref_9(S_{43} + Tx + \Delta Tx_{43} + Coup + \Delta Coup_{43d}) + \Delta Ref_9(S_{44} + Tx + \Delta Tx_{44} + Coup + \Delta Coup_{44a})]/16]$	(8.38)
Correction Factor	(2,1)	$- (S_{11} + S_{12} + S_{13} + S_{14} + S_{22} + S_{23} + S_{24} + S_{31} + S_{32} + S_{33} + S_{34} + S_{41} + S_{42} + S_{43} + S_{44})/16 + (\Delta Tx_{11} + \Delta Tx_{12} + \Delta Tx_{13} + \Delta Tx_{14} + \Delta Tx_{22} + \Delta Tx_{23} + \Delta Tx_{24} + \Delta Tx_{31} + \Delta Tx_{32} + \Delta Tx_{33} + \Delta Tx_{34} + \Delta Tx_{41} + \Delta Tx_{42} + \Delta Tx_{43} + \Delta Tx_{44})/16 + (\Delta Coup_{11c} + \Delta Coup_{12c} + \Delta Coup_{13c} + \Delta Coup_{14b} + \Delta Coup_{22c} + \Delta Coup_{23c} + \Delta Coup_{24c} + \Delta Coup_{31c} + \Delta Coup_{32c} + \Delta Coup_{33c} + \Delta Coup_{34b} + \Delta Coup_{41d} + \Delta Coup_{42d} + \Delta Coup_{43d} + \Delta Coup_{44a})/16 + [\Delta Ref_1(S_{11} + Tx + \Delta Tx_{11} + Coup + \Delta Coup_{11c}) + \Delta Ref_4(S_{12} + Tx + \Delta Tx_{12} + Coup + \Delta Coup_{12c}) + \Delta Ref_7(S_{13} + Tx + \Delta Tx_{13} + Coup + \Delta Coup_{13c}) + \Delta Ref_7(S_{14} + Tx + \Delta Tx_{14} + Coup + \Delta Coup_{14b}) + \Delta Ref_5(S_{22} + Tx + \Delta Tx_{22} + Coup + \Delta Coup_{22c}) + \Delta Ref_8(S_{23} + Tx + \Delta Tx_{23} + Coup + \Delta Coup_{23c}) + \Delta Ref_8(S_{24} + Tx + \Delta Tx_{24} + Coup + \Delta Coup_{24c}) + \Delta Ref_3(S_{31} + Tx + \Delta Tx_{31} + Coup + \Delta Coup_{31c}) + \Delta Ref_6(S_{32} + Tx + \Delta Tx_{32} + Coup + \Delta Coup_{32c}) + \Delta Ref_9(S_{33} + Tx + \Delta Tx_{33} + Coup + \Delta Coup_{33c}) + \Delta Ref_9(S_{34} + Tx + \Delta Tx_{34} + Coup + \Delta Coup_{34b}) + \Delta Ref_3(S_{41} + Tx + \Delta Tx_{41} + Coup + \Delta Coup_{41d}) + \Delta Ref_6(S_{42} + Tx + \Delta Tx_{42} + Coup + \Delta Coup_{42d}) + \Delta Ref_9(S_{43} + Tx + \Delta Tx_{43} + Coup + \Delta Coup_{43d}) + \Delta Ref_9(S_{44} + Tx + \Delta Tx_{44} + Coup + \Delta Coup_{44a})]/16]$	(8.39)
Correction Factor	(2,2)	$- [(S_{11} + S_{12} + S_{13} + S_{14} + S_{21} + S_{23} + S_{24} + S_{31} + S_{32} + S_{33} + S_{34} + S_{41} + S_{42} + S_{43} + S_{44})/16 + (\Delta Tx_{11} + \Delta Tx_{12} + \Delta Tx_{13} + \Delta Tx_{14} + \Delta Tx_{21} + \Delta Tx_{23} + \Delta Tx_{24} + \Delta Tx_{31} + \Delta Tx_{32} +$	(8.40)

		$\Delta Tx_{33} + \Delta Tx_{34} + \Delta Tx_{41} + \Delta Tx_{42} + \Delta Tx_{43} + \Delta Tx_{44})/16 + (\Delta Coup_{11c} + \Delta Coup_{12c} + \Delta Coup_{13c} + \Delta Coup_{14b} + \Delta Coup_{21c} + \Delta Coup_{23c} + \Delta Coup_{24c} + \Delta Coup_{31c} + \Delta Coup_{32c} + \Delta Coup_{33c} + \Delta Coup_{34b} + \Delta Coup_{41d} + \Delta Coup_{42d} + \Delta Coup_{43d} + \Delta Coup_{44a})/16 + [\Delta Ref_1(S_{11} + Tx + \Delta Tx_{11} + Coup + \Delta Coup_{11c}) + \Delta Ref_4(S_{12} + Tx + \Delta Tx_{12} + Coup + \Delta Coup_{12c}) + \Delta Ref_7(S_{13} + Tx + \Delta Tx_{13} + Coup + \Delta Coup_{13c}) + \Delta Ref_7(S_{14} + Tx + \Delta Tx_{14} + Coup + \Delta Coup_{14b}) + \Delta Ref_2(S_{21} + Tx + \Delta Tx_{21} + Coup + \Delta Coup_{21c}) + \Delta Ref_8(S_{23} + Tx + \Delta Tx_{23} + Coup + \Delta Coup_{23c}) + \Delta Ref_8(S_{24} + Tx + \Delta Tx_{24} + Coup + \Delta Coup_{24c}) + \Delta Ref_3(S_{31} + Tx + \Delta Tx_{31} + Coup + \Delta Coup_{31c}) + \Delta Ref_6(S_{32} + Tx + \Delta Tx_{32} + Coup + \Delta Coup_{32c}) + \Delta Ref_9(S_{33} + Tx + \Delta Tx_{33} + Coup + \Delta Coup_{33c}) + \Delta Ref_9(S_{34} + Tx + \Delta Tx_{34} + Coup + \Delta Coup_{34b}) + \Delta Ref_3(S_{41} + Tx + \Delta Tx_{41} + Coup + \Delta Coup_{41d}) + \Delta Ref_6(S_{42} + Tx + \Delta Tx_{42} + Coup + \Delta Coup_{42d}) + \Delta Ref_9(S_{43} + Tx + \Delta Tx_{43} + Coup + \Delta Coup_{43d}) + \Delta Ref_9(S_{44} + Tx + \Delta Tx_{44} + Coup + \Delta Coup_{44a})]/16]$	
Correction Factor	(2,3)	$- [(S_{11} + S_{12} + S_{13} + S_{14} + S_{21} + S_{22} + S_{24} + S_{31} + S_{32} + S_{33} + S_{34} + S_{41} + S_{42} + S_{43} + S_{44})/16 + (\Delta Tx_{11} + \Delta Tx_{12} + \Delta Tx_{13} + \Delta Tx_{14} + \Delta Tx_{21} + \Delta Tx_{22} + \Delta Tx_{24} + \Delta Tx_{31} + \Delta Tx_{32} + \Delta Tx_{33} + \Delta Tx_{34} + \Delta Tx_{41} + \Delta Tx_{42} + \Delta Tx_{43} + \Delta Tx_{44})/16 + (\Delta Coup_{11c} + \Delta Coup_{12c} + \Delta Coup_{13c} + \Delta Coup_{14b} + \Delta Coup_{21c} + \Delta Coup_{22c} + \Delta Coup_{24c} + \Delta Coup_{31c} + \Delta Coup_{32c} + \Delta Coup_{33c} + \Delta Coup_{34b} + \Delta Coup_{41d} + \Delta Coup_{42d} + \Delta Coup_{43d} + \Delta Coup_{44a})/16 + [\Delta Ref_1(S_{11} + Tx + \Delta Tx_{11} + Coup + \Delta Coup_{11c}) + \Delta Ref_4(S_{12} + Tx + \Delta Tx_{12} + Coup + \Delta Coup_{12c}) + \Delta Ref_7(S_{13} + Tx + \Delta Tx_{13} + Coup + \Delta Coup_{13c}) + \Delta Ref_7(S_{14} + Tx + \Delta Tx_{14} + Coup + \Delta Coup_{14b}) + \Delta Ref_2(S_{21} + Tx + \Delta Tx_{21} + Coup + \Delta Coup_{21c}) + \Delta Ref_5(S_{22} + Tx + \Delta Tx_{22} + Coup + \Delta Coup_{22c}) + \Delta Ref_8(S_{24} + Tx + \Delta Tx_{24} + Coup + \Delta Coup_{24c}) + \Delta Ref_3(S_{31} + Tx + \Delta Tx_{31} + Coup + \Delta Coup_{31c}) + \Delta Ref_6(S_{32} + Tx + \Delta Tx_{32} + Coup + \Delta Coup_{32c}) + \Delta Ref_9(S_{33} + Tx + \Delta Tx_{33} + Coup + \Delta Coup_{33c}) + \Delta Ref_9(S_{34} + Tx + \Delta Tx_{34} + Coup + \Delta Coup_{34b}) + \Delta Ref_3(S_{41} + Tx + \Delta Tx_{41} + Coup + \Delta Coup_{41d}) + \Delta Ref_6(S_{42} + Tx + \Delta Tx_{42} + Coup + \Delta Coup_{42d}) + \Delta Ref_9(S_{43} + Tx + \Delta Tx_{43} + Coup + \Delta Coup_{43d}) + \Delta Ref_9(S_{44} + Tx + \Delta Tx_{44} + Coup + \Delta Coup_{44a})]/16]$	(8.41)
Correction Factor	(2,4)	$- [(S_{11} + S_{12} + S_{13} + S_{14} + S_{21} + S_{22} + S_{23} + S_{31} + S_{32} + S_{33} + S_{34} + S_{41} + S_{42} + S_{43} + S_{44})/16 + (\Delta Tx_{11} + \Delta Tx_{12} + \Delta Tx_{13} + \Delta Tx_{14} + \Delta Tx_{21} + \Delta Tx_{22} + \Delta Tx_{23} + \Delta Tx_{31} + \Delta Tx_{32} + \Delta Tx_{33} + \Delta Tx_{34} + \Delta Tx_{41} + \Delta Tx_{42} + \Delta Tx_{43} + \Delta Tx_{44})/16 + (\Delta Coup_{11c} + \Delta Coup_{12c} + \Delta Coup_{13c} + \Delta Coup_{14b} + \Delta Coup_{21c} + \Delta Coup_{22c} + \Delta Coup_{23c} + \Delta Coup_{31c} + \Delta Coup_{32c} + \Delta Coup_{33c} + \Delta Coup_{34b} + \Delta Coup_{41d} + \Delta Coup_{42d} + \Delta Coup_{43d} + \Delta Coup_{44a})/16 + [\Delta Ref_1(S_{11} + Tx + \Delta Tx_{11} + Coup + \Delta Coup_{11c}) + \Delta Ref_4(S_{12} + Tx + \Delta Tx_{12} + Coup + \Delta Coup_{12c}) + \Delta Ref_7(S_{13} + Tx + \Delta Tx_{13} + Coup + \Delta Coup_{13c}) + \Delta Ref_7(S_{14} + Tx + \Delta Tx_{14} + Coup + \Delta Coup_{14b}) + \Delta Ref_2(S_{21} + Tx + \Delta Tx_{21} + Coup + \Delta Coup_{21c}) + \Delta Ref_5(S_{22} + Tx + \Delta Tx_{22} + Coup + \Delta Coup_{22c}) + \Delta Ref_8(S_{23} + Tx + \Delta Tx_{23} + Coup + \Delta Coup_{23c}) + \Delta Ref_3(S_{31} + Tx + \Delta Tx_{31} + Coup + \Delta Coup_{31c}) + \Delta Ref_6(S_{32} + Tx + \Delta Tx_{32} + Coup + \Delta Coup_{32c}) + \Delta Ref_9(S_{33} + Tx + \Delta Tx_{33} + Coup + \Delta Coup_{33c}) + \Delta Ref_9(S_{34} + Tx + \Delta Tx_{34} + Coup + \Delta Coup_{34b}) + \Delta Ref_3(S_{41} + Tx + \Delta Tx_{41} + Coup + \Delta Coup_{41d}) + \Delta Ref_6(S_{42} + Tx + \Delta Tx_{42} + Coup + \Delta Coup_{42d}) + \Delta Ref_9(S_{43} + Tx + \Delta Tx_{43} + Coup + \Delta Coup_{43d}) + \Delta Ref_9(S_{44} + Tx + \Delta Tx_{44} + Coup + \Delta Coup_{44a})]/16]$	(8.42)

Correction Factor	(3,1)	$-[(S_{11} + S_{12} + S_{13} + S_{14} + S_{21} + S_{22} + S_{23} + S_{24} + S_{31} + S_{32} + S_{33} + S_{34} + S_{41} + S_{42} + S_{43} + S_{44})/16 + (\Delta Tx_{11} + \Delta Tx_{12} + \Delta Tx_{13} + \Delta Tx_{14} + \Delta Tx_{21} + \Delta Tx_{22} + \Delta Tx_{23} + \Delta Tx_{24} + \Delta Tx_{32} + \Delta Tx_{33} + \Delta Tx_{34} + \Delta Tx_{41} + \Delta Tx_{42} + \Delta Tx_{43} + \Delta Tx_{44})/16 + (\Delta Coup_{11c} + \Delta Coup_{12c} + \Delta Coup_{13c} + \Delta Coup_{14b} + \Delta Coup_{21c} + \Delta Coup_{22c} + \Delta Coup_{23c} + \Delta Coup_{24c} + \Delta Coup_{32c} + \Delta Coup_{33c} + \Delta Coup_{34b} + \Delta Coup_{41d} + \Delta Coup_{42d} + \Delta Coup_{43d} + \Delta Coup_{44a})/16 + [\Delta Ref_1(S_{11} + Tx + \Delta Tx_{11} + Coup + \Delta Coup_{11c}) + \Delta Ref_4(S_{12} + Tx + \Delta Tx_{12} + Coup + \Delta Coup_{12c}) + \Delta Ref_7(S_{13} + Tx + \Delta Tx_{13} + Coup + \Delta Coup_{13c}) + \Delta Ref_7(S_{14} + Tx + \Delta Tx_{14} + Coup + \Delta Coup_{14b}) + \Delta Ref_2(S_{21} + Tx + \Delta Tx_{21} + Coup + \Delta Coup_{21c}) + \Delta Ref_5(S_{22} + Tx + \Delta Tx_{22} + Coup + \Delta Coup_{22c}) + \Delta Ref_8(S_{23} + Tx + \Delta Tx_{23} + Coup + \Delta Coup_{23c}) + \Delta Ref_8(S_{24} + Tx + \Delta Tx_{24} + Coup + \Delta Coup_{24c}) + \Delta Ref_6(S_{32} + Tx + \Delta Tx_{32} + Coup + \Delta Coup_{32c}) + \Delta Ref_9(S_{33} + Tx + \Delta Tx_{33} + Coup + \Delta Coup_{33c}) + \Delta Ref_9(S_{34} + Tx + \Delta Tx_{34} + Coup + \Delta Coup_{34b}) + \Delta Ref_3(S_{41} + Tx + \Delta Tx_{41} + Coup + \Delta Coup_{41d}) + \Delta Ref_6(S_{42} + Tx + \Delta Tx_{42} + Coup + \Delta Coup_{42d}) + \Delta Ref_9(S_{43} + Tx + \Delta Tx_{43} + Coup + \Delta Coup_{43d}) + \Delta Ref_9(S_{44} + Tx + \Delta Tx_{44} + Coup + \Delta Coup_{44a})]/16]$	(8.43)
Correction Factor	(3,2)	$-[(S_{11} + S_{12} + S_{13} + S_{14} + S_{21} + S_{22} + S_{23} + S_{24} + S_{31} + S_{33} + S_{34} + S_{41} + S_{42} + S_{43} + S_{44})/16 + (\Delta Tx_{11} + \Delta Tx_{12} + \Delta Tx_{13} + \Delta Tx_{14} + \Delta Tx_{21} + \Delta Tx_{22} + \Delta Tx_{23} + \Delta Tx_{24} + \Delta Tx_{31} + \Delta Tx_{33} + \Delta Tx_{34} + \Delta Tx_{41} + \Delta Tx_{42} + \Delta Tx_{43} + \Delta Tx_{44})/16 + (\Delta Coup_{11c} + \Delta Coup_{12c} + \Delta Coup_{13c} + \Delta Coup_{14b} + \Delta Coup_{21c} + \Delta Coup_{22c} + \Delta Coup_{23c} + \Delta Coup_{24c} + \Delta Coup_{31c} + \Delta Coup_{33c} + \Delta Coup_{34b} + \Delta Coup_{41d} + \Delta Coup_{42d} + \Delta Coup_{43d} + \Delta Coup_{44a})/16 + [\Delta Ref_1(S_{11} + Tx + \Delta Tx_{11} + Coup + \Delta Coup_{11c}) + \Delta Ref_4(S_{12} + Tx + \Delta Tx_{12} + Coup + \Delta Coup_{12c}) + \Delta Ref_7(S_{13} + Tx + \Delta Tx_{13} + Coup + \Delta Coup_{13c}) + \Delta Ref_7(S_{14} + Tx + \Delta Tx_{14} + Coup + \Delta Coup_{14b}) + \Delta Ref_2(S_{21} + Tx + \Delta Tx_{21} + Coup + \Delta Coup_{21c}) + \Delta Ref_5(S_{22} + Tx + \Delta Tx_{22} + Coup + \Delta Coup_{22c}) + \Delta Ref_8(S_{23} + Tx + \Delta Tx_{23} + Coup + \Delta Coup_{23c}) + \Delta Ref_8(S_{24} + Tx + \Delta Tx_{24} + Coup + \Delta Coup_{24c}) + \Delta Ref_3(S_{31} + Tx + \Delta Tx_{31} + Coup + \Delta Coup_{31c}) + \Delta Ref_9(S_{33} + Tx + \Delta Tx_{33} + Coup + \Delta Coup_{33c}) + \Delta Ref_9(S_{34} + Tx + \Delta Tx_{34} + Coup + \Delta Coup_{34b}) + \Delta Ref_3(S_{41} + Tx + \Delta Tx_{41} + Coup + \Delta Coup_{41d}) + \Delta Ref_6(S_{42} + Tx + \Delta Tx_{42} + Coup + \Delta Coup_{42d}) + \Delta Ref_9(S_{43} + Tx + \Delta Tx_{43} + Coup + \Delta Coup_{43d}) + \Delta Ref_9(S_{44} + Tx + \Delta Tx_{44} + Coup + \Delta Coup_{44a})]/16]$	(8.44)
Correction Factor	(3,3)	$-[(S_{11} + S_{12} + S_{13} + S_{14} + S_{21} + S_{22} + S_{23} + S_{24} + S_{31} + S_{32} + S_{34} + S_{41} + S_{42} + S_{43} + S_{44})/16 + (\Delta Tx_{11} + \Delta Tx_{12} + \Delta Tx_{13} + \Delta Tx_{14} + \Delta Tx_{21} + \Delta Tx_{22} + \Delta Tx_{23} + \Delta Tx_{24} + \Delta Tx_{31} + \Delta Tx_{32} + \Delta Tx_{34} + \Delta Tx_{41} + \Delta Tx_{42} + \Delta Tx_{43} + \Delta Tx_{44})/16 + (\Delta Coup_{11c} + \Delta Coup_{12c} + \Delta Coup_{13c} + \Delta Coup_{14b} + \Delta Coup_{21c} + \Delta Coup_{22c} + \Delta Coup_{23c} + \Delta Coup_{24c} + \Delta Coup_{31c} + \Delta Coup_{32c} + \Delta Coup_{34b} + \Delta Coup_{41d} + \Delta Coup_{42d} + \Delta Coup_{43d} + \Delta Coup_{44a})/16 + [\Delta Ref_1(S_{11} + Tx + \Delta Tx_{11} + Coup + \Delta Coup_{11c}) + \Delta Ref_4(S_{12} + Tx + \Delta Tx_{12} + Coup + \Delta Coup_{12c}) + \Delta Ref_7(S_{13} + Tx + \Delta Tx_{13} + Coup + \Delta Coup_{13c}) + \Delta Ref_7(S_{14} + Tx + \Delta Tx_{14} + Coup + \Delta Coup_{14b}) + \Delta Ref_2(S_{21} + Tx + \Delta Tx_{21} + Coup + \Delta Coup_{21c}) + \Delta Ref_5(S_{22} + Tx + \Delta Tx_{22} + Coup + \Delta Coup_{22c}) + \Delta Ref_8(S_{23} + Tx + \Delta Tx_{23} + Coup + \Delta Coup_{23c}) + \Delta Ref_8(S_{24} + Tx + \Delta Tx_{24} + Coup + \Delta Coup_{24c}) + \Delta Ref_3(S_{31} + Tx + \Delta Tx_{31} + Coup + \Delta Coup_{31c}) + \Delta Ref_6(S_{32} + Tx + \Delta Tx_{32} + Coup + \Delta Coup_{32c}) + \Delta Ref_9(S_{34} + Tx + \Delta Tx_{34} + Coup + \Delta Coup_{34b}) +$	(8.45)

		$\Delta Ref_3(S_{41} + Tx + \Delta Tx_{41} + Coup + \Delta Coup_{41d}) + \Delta Ref_6(S_{42} + Tx + \Delta Tx_{42} + Coup + \Delta Coup_{42d}) + \Delta Ref_9(S_{43} + Tx + \Delta Tx_{43} + Coup + \Delta Coup_{43d}) + \Delta Ref_9(S_{44} + Tx + \Delta Tx_{44} + Coup + \Delta Coup_{44a})]/16]$	
Correction Factor	(3,4)	$- [(S_{11} + S_{12} + S_{13} + S_{14} + S_{21} + S_{22} + S_{23} + S_{24} + S_{31} + S_{32} + S_{33} + S_{41} + S_{42} + S_{43} + S_{44})/16 + (\Delta Tx_{11} + \Delta Tx_{12} + \Delta Tx_{13} + \Delta Tx_{14} + \Delta Tx_{21} + \Delta Tx_{22} + \Delta Tx_{23} + \Delta Tx_{24} + \Delta Tx_{31} + \Delta Tx_{32} + \Delta Tx_{33} + \Delta Tx_{41} + \Delta Tx_{42} + \Delta Tx_{43} + \Delta Tx_{44})/16 + (\Delta Coup_{11c} + \Delta Coup_{12c} + \Delta Coup_{13c} + \Delta Coup_{14b} + \Delta Coup_{21c} + \Delta Coup_{22c} + \Delta Coup_{23c} + \Delta Coup_{24c} + \Delta Coup_{31c} + \Delta Coup_{32c} + \Delta Coup_{33c} + \Delta Coup_{41d} + \Delta Coup_{42d} + \Delta Coup_{43d} + \Delta Coup_{44a})/16 + [\Delta Ref_1(S_{11} + Tx + \Delta Tx_{11} + Coup + \Delta Coup_{11c}) + \Delta Ref_4(S_{12} + Tx + \Delta Tx_{12} + Coup + \Delta Coup_{12c}) + \Delta Ref_7(S_{13} + Tx + \Delta Tx_{13} + Coup + \Delta Coup_{13c}) + \Delta Ref_7(S_{14} + Tx + \Delta Tx_{14} + Coup + \Delta Coup_{14b}) + \Delta Ref_2(S_{21} + Tx + \Delta Tx_{21} + Coup + \Delta Coup_{21c}) + \Delta Ref_5(S_{22} + Tx + \Delta Tx_{22} + Coup + \Delta Coup_{22c}) + \Delta Ref_8(S_{23} + Tx + \Delta Tx_{23} + Coup + \Delta Coup_{23c}) + \Delta Ref_8(S_{24} + Tx + \Delta Tx_{24} + Coup + \Delta Coup_{24c}) + \Delta Ref_3(S_{31} + Tx + \Delta Tx_{31} + Coup + \Delta Coup_{31c}) + \Delta Ref_6(S_{32} + Tx + \Delta Tx_{32} + Coup + \Delta Coup_{32c}) + \Delta Ref_9(S_{33} + Tx + \Delta Tx_{33} + Coup + \Delta Coup_{33c}) + \Delta Ref_3(S_{41} + Tx + \Delta Tx_{41} + Coup + \Delta Coup_{41d}) + \Delta Ref_6(S_{42} + Tx + \Delta Tx_{42} + Coup + \Delta Coup_{42d}) + \Delta Ref_9(S_{43} + Tx + \Delta Tx_{43} + Coup + \Delta Coup_{43d}) + \Delta Ref_9(S_{44} + Tx + \Delta Tx_{44} + Coup + \Delta Coup_{44a})]/16]$	(8.46)
Correction Factor	(4,1)	$- [(S_{11} + S_{12} + S_{13} + S_{14} + S_{21} + S_{22} + S_{23} + S_{24} + S_{31} + S_{32} + S_{33} + S_{34} + S_{42} + S_{43} + S_{44})/16 + (\Delta Tx_{11} + \Delta Tx_{12} + \Delta Tx_{13} + \Delta Tx_{14} + \Delta Tx_{21} + \Delta Tx_{22} + \Delta Tx_{23} + \Delta Tx_{24} + \Delta Tx_{31} + \Delta Tx_{32} + \Delta Tx_{33} + \Delta Tx_{34} + \Delta Tx_{42} + \Delta Tx_{43} + \Delta Tx_{44})/16 + (\Delta Coup_{11c} + \Delta Coup_{12c} + \Delta Coup_{13c} + \Delta Coup_{14b} + \Delta Coup_{21c} + \Delta Coup_{22c} + \Delta Coup_{23c} + \Delta Coup_{24c} + \Delta Coup_{31c} + \Delta Coup_{32c} + \Delta Coup_{33c} + \Delta Coup_{34b} + \Delta Coup_{42d} + \Delta Coup_{43d} + \Delta Coup_{44a})/16 + [\Delta Ref_1(S_{11} + Tx + \Delta Tx_{11} + Coup + \Delta Coup_{11c}) + \Delta Ref_4(S_{12} + Tx + \Delta Tx_{12} + Coup + \Delta Coup_{12c}) + \Delta Ref_7(S_{13} + Tx + \Delta Tx_{13} + Coup + \Delta Coup_{13c}) + \Delta Ref_7(S_{14} + Tx + \Delta Tx_{14} + Coup + \Delta Coup_{14b}) + \Delta Ref_2(S_{21} + Tx + \Delta Tx_{21} + Coup + \Delta Coup_{21c}) + \Delta Ref_5(S_{22} + Tx + \Delta Tx_{22} + Coup + \Delta Coup_{22c}) + \Delta Ref_8(S_{23} + Tx + \Delta Tx_{23} + Coup + \Delta Coup_{23c}) + \Delta Ref_8(S_{24} + Tx + \Delta Tx_{24} + Coup + \Delta Coup_{24c}) + \Delta Ref_3(S_{31} + Tx + \Delta Tx_{31} + Coup + \Delta Coup_{31c}) + \Delta Ref_6(S_{32} + Tx + \Delta Tx_{32} + Coup + \Delta Coup_{32c}) + \Delta Ref_9(S_{33} + Tx + \Delta Tx_{33} + Coup + \Delta Coup_{33c}) + \Delta Ref_9(S_{34} + Tx + \Delta Tx_{34} + Coup + \Delta Coup_{34b}) + \Delta Ref_6(S_{42} + Tx + \Delta Tx_{42} + Coup + \Delta Coup_{42d}) + \Delta Ref_9(S_{43} + Tx + \Delta Tx_{43} + Coup + \Delta Coup_{43d}) + \Delta Ref_9(S_{44} + Tx + \Delta Tx_{44} + Coup + \Delta Coup_{44a})]/16]$	(8.47)
Correction Factor	(4,2)	$- [(S_{11} + S_{12} + S_{13} + S_{14} + S_{21} + S_{22} + S_{23} + S_{24} + S_{31} + S_{32} + S_{33} + S_{34} + S_{41} + S_{43} + S_{44})/16 + (\Delta Tx_{11} + \Delta Tx_{12} + \Delta Tx_{13} + \Delta Tx_{14} + \Delta Tx_{21} + \Delta Tx_{22} + \Delta Tx_{23} + \Delta Tx_{24} + \Delta Tx_{31} + \Delta Tx_{32} + \Delta Tx_{33} + \Delta Tx_{34} + \Delta Tx_{41} + \Delta Tx_{43} + \Delta Tx_{44})/16 + (\Delta Coup_{11c} + \Delta Coup_{12c} + \Delta Coup_{13c} + \Delta Coup_{14b} + \Delta Coup_{21c} + \Delta Coup_{22c} + \Delta Coup_{23c} + \Delta Coup_{24c} + \Delta Coup_{31c} + \Delta Coup_{32c} + \Delta Coup_{33c} + \Delta Coup_{34b} + \Delta Coup_{41d} + \Delta Coup_{43d} + \Delta Coup_{44a})/16 + [\Delta Ref_1(S_{11} + Tx + \Delta Tx_{11} + Coup + \Delta Coup_{11c}) + \Delta Ref_4(S_{12} + Tx + \Delta Tx_{12} + Coup + \Delta Coup_{12c}) + \Delta Ref_7(S_{13} + Tx + \Delta Tx_{13} + Coup + \Delta Coup_{13c}) + \Delta Ref_7(S_{14} + Tx + \Delta Tx_{14} + Coup + \Delta Coup_{14b}) + \Delta Ref_2(S_{21} + Tx + \Delta Tx_{21} + Coup + \Delta Coup_{21c}) + \Delta Ref_5(S_{22} + Tx + \Delta Tx_{22} + Coup + \Delta Coup_{22c}) +$	(8.48)

		$\Delta Ref_8(S_{23} + Tx + \Delta Tx_{23} + Coup + \Delta Coup_{23c}) + \Delta Ref_8(S_{24} + Tx + \Delta Tx_{24} + Coup + \Delta Coup_{24c}) + \Delta Ref_3(S_{31} + Tx + \Delta Tx_{31} + Coup + \Delta Coup_{31c}) + \Delta Ref_6(S_{32} + Tx + \Delta Tx_{32} + Coup + \Delta Coup_{32c}) + \Delta Ref_9(S_{33} + Tx + \Delta Tx_{33} + Coup + \Delta Coup_{33c}) + \Delta Ref_9(S_{34} + Tx + \Delta Tx_{34} + Coup + \Delta Coup_{34b}) + \Delta Ref_3(S_{41} + Tx + \Delta Tx_{41} + Coup + \Delta Coup_{41d}) + \Delta Ref_9(S_{43} + Tx + \Delta Tx_{43} + Coup + \Delta Coup_{43d}) + \Delta Ref_9(S_{44} + Tx + \Delta Tx_{44} + Coup + \Delta Coup_{44a})]/16]$	
Correction Factor	(4,3)	$- [(S_{11} + S_{12} + S_{13} + S_{14} + S_{21} + S_{22} + S_{23} + S_{24} + S_{31} + S_{32} + S_{33} + S_{34} + S_{41} + S_{42} + S_{44})/16 + (\Delta Tx_{11} + \Delta Tx_{12} + \Delta Tx_{13} + \Delta Tx_{14} + \Delta Tx_{21} + \Delta Tx_{22} + \Delta Tx_{23} + \Delta Tx_{24} + \Delta Tx_{31} + \Delta Tx_{32} + \Delta Tx_{33} + \Delta Tx_{34} + \Delta Tx_{41} + \Delta Tx_{42} + \Delta Tx_{44})/16 + (\Delta Coup_{11c} + \Delta Coup_{12c} + \Delta Coup_{13c} + \Delta Coup_{14b} + \Delta Coup_{21c} + \Delta Coup_{22c} + \Delta Coup_{23c} + \Delta Coup_{24c} + \Delta Coup_{31c} + \Delta Coup_{32c} + \Delta Coup_{33c} + \Delta Coup_{34b} + \Delta Coup_{41d} + \Delta Coup_{42d} + \Delta Coup_{44a})/16 + [\Delta Ref_1(S_{11} + Tx + \Delta Tx_{11} + Coup + \Delta Coup_{11c}) + \Delta Ref_4(S_{12} + Tx + \Delta Tx_{12} + Coup + \Delta Coup_{12c}) + \Delta Ref_7(S_{13} + Tx + \Delta Tx_{13} + Coup + \Delta Coup_{13c}) + \Delta Ref_7(S_{14} + Tx + \Delta Tx_{14} + Coup + \Delta Coup_{14b}) + \Delta Ref_2(S_{21} + Tx + \Delta Tx_{21} + Coup + \Delta Coup_{21c}) + \Delta Ref_5(S_{22} + Tx + \Delta Tx_{22} + Coup + \Delta Coup_{22c}) + \Delta Ref_8(S_{23} + Tx + \Delta Tx_{23} + Coup + \Delta Coup_{23c}) + \Delta Ref_8(S_{24} + Tx + \Delta Tx_{24} + Coup + \Delta Coup_{24c}) + \Delta Ref_3(S_{31} + Tx + \Delta Tx_{31} + Coup + \Delta Coup_{31c}) + \Delta Ref_6(S_{32} + Tx + \Delta Tx_{32} + Coup + \Delta Coup_{32c}) + \Delta Ref_9(S_{33} + Tx + \Delta Tx_{33} + Coup + \Delta Coup_{33c}) + \Delta Ref_9(S_{34} + Tx + \Delta Tx_{34} + Coup + \Delta Coup_{34b}) + \Delta Ref_3(S_{41} + Tx + \Delta Tx_{41} + Coup + \Delta Coup_{41d}) + \Delta Ref_6(S_{42} + Tx + \Delta Tx_{42} + Coup + \Delta Coup_{42d}) + \Delta Ref_9(S_{44} + Tx + \Delta Tx_{44} + Coup + \Delta Coup_{44a})]/16]$	(8.49)
Correction Factor	(4,4)	$[S_{44} + Tx + \Delta Tx_{44} + Coup + \Delta Coup_{44a} + Ref + \Delta Ref_9(S_{44} + Tx + \Delta Tx_{44} + Coup + \Delta Coup_{44a})] - [(S_{11} + S_{12} + S_{13} + S_{14} + S_{21} + S_{22} + S_{23} + S_{24} + S_{31} + S_{32} + S_{33} + S_{34} + S_{41} + S_{42} + S_{43})/16 + (\Delta Tx_{11} + \Delta Tx_{12} + \Delta Tx_{13} + \Delta Tx_{14} + \Delta Tx_{21} + \Delta Tx_{22} + \Delta Tx_{23} + \Delta Tx_{24} + \Delta Tx_{31} + \Delta Tx_{32} + \Delta Tx_{33} + \Delta Tx_{34} + \Delta Tx_{41} + \Delta Tx_{42} + \Delta Tx_{43})/16 + (\Delta Coup_{11c} + \Delta Coup_{12c} + \Delta Coup_{13c} + \Delta Coup_{14b} + \Delta Coup_{21c} + \Delta Coup_{22c} + \Delta Coup_{23c} + \Delta Coup_{24c} + \Delta Coup_{31c} + \Delta Coup_{32c} + \Delta Coup_{33c} + \Delta Coup_{34b} + \Delta Coup_{41d} + \Delta Coup_{42d} + \Delta Coup_{43d})/16 + [\Delta Ref_1(S_{11} + Tx + \Delta Tx_{11} + Coup + \Delta Coup_{11c}) + \Delta Ref_4(S_{12} + Tx + \Delta Tx_{12} + Coup + \Delta Coup_{12c}) + \Delta Ref_7(S_{13} + Tx + \Delta Tx_{13} + Coup + \Delta Coup_{13c}) + \Delta Ref_7(S_{14} + Tx + \Delta Tx_{14} + Coup + \Delta Coup_{14b}) + \Delta Ref_2(S_{21} + Tx + \Delta Tx_{21} + Coup + \Delta Coup_{21c}) + \Delta Ref_5(S_{22} + Tx + \Delta Tx_{22} + Coup + \Delta Coup_{22c}) + \Delta Ref_8(S_{23} + Tx + \Delta Tx_{23} + Coup + \Delta Coup_{23c}) + \Delta Ref_8(S_{24} + Tx + \Delta Tx_{24} + Coup + \Delta Coup_{24c}) + \Delta Ref_3(S_{31} + Tx + \Delta Tx_{31} + Coup + \Delta Coup_{31c}) + \Delta Ref_6(S_{32} + Tx + \Delta Tx_{32} + Coup + \Delta Coup_{32c}) + \Delta Ref_9(S_{33} + Tx + \Delta Tx_{33} + Coup + \Delta Coup_{33c}) + \Delta Ref_9(S_{34} + Tx + \Delta Tx_{34} + Coup + \Delta Coup_{34b}) + \Delta Ref_3(S_{41} + Tx + \Delta Tx_{41} + Coup + \Delta Coup_{41d}) + \Delta Ref_6(S_{42} + Tx + \Delta Tx_{42} + Coup + \Delta Coup_{42d}) + \Delta Ref_9(S_{43} + Tx + \Delta Tx_{43} + Coup + \Delta Coup_{43d})]/16]$	(8.50)

From the above tables, it is clear that the effect of calibration is to spread the contributing error sources' effects throughout the array, producing more of a blanket effect. When these equations are considered in more general terms, as in considering the variation of each component block as its standard deviation, then the equations become much simpler; the calibrated signal for each element when the correction factor is taken from the output signal. Then the calibration errors for each element is:

$$\sigma_{ele} = \frac{(N-2)\sigma_s}{N} + \frac{(N-2)\sigma_{TRx}}{N} + \frac{(N-1)\sigma_{Coupler}}{N} + \frac{(N-1)\sigma_{Sensor}\left(\sigma_S + \sigma_{TRx} + \sigma_{Coupler}\right)}{N} \quad (8.51)$$

Where σ_{ele} - the standard deviation of elements of the array

σ_S- the standard deviation of the input signals

σ_{TRx}- the standard deviation of the transmitter component blocks

$\sigma_{Coupler}$- the standard deviation of the directional coupler

σ_{Sensor}- the standard deviation of the measurement sensor

It is clear from this equation that not only are the individual elements not calibrated as they still contain an input signal with variation, a transmitter component contribution with variation and it includes a directional coupler variation dependent on the number of the elements in the array. This is extended to the array errors in equation 8.52.

$$\sigma_A = (N-2)\sigma_s + (N-2)\sigma_{TRx} + (N-1)\sigma_{Coupler} + (N-1)\sigma_{Sensor}\left(\sigma_S + \sigma_{TRx} + \sigma_{Coupler}\right) \quad (8.52)$$

Where σ_A- the standard deviation of the array

Appendix B

Top Left Reference Calculation of Calibration Errors

This appendix is concerned with the calculation of the top left reference calibration algorithm's accuracy. The mechanism of this algorithm is described in Chapter 5, based upon the errors associated with each of the calibration paths of the array, as shown in figure 8-1. This notation will be used to calculate the calibration accuracy of the top left reference algorithm for a 4 by 4 array, as shown in figure 8-2, with the coupler path identification as shown in figure 8-3. The calculation of this algorithm's effectiveness starts with the measurement of the elements, and their comparisons and correction factors, as shown in Table 9-1.

Table 9-1: Calculation of the Correction Factors for Each Element of the 4 by 4 Array.

Type	Element	Equation	
Output	(1,1)	$S_{11} + Tx + \Delta Tx_{11}$	(9.1)
Measurement	(1,1)	$S_{11} + Tx + \Delta Tx_{11} + Coup + \Delta Coup_{11c} + Ref + \Delta Ref_1$	(9.2)
Output	(1,2)	$S_{12} + Tx + \Delta Tx_{12}$	(9.3)
Measurement	(1,2)	$S_{12} + Tx + \Delta Tx_{12} + Coup + \Delta Coup_{12b} + Ref + \Delta Ref_1$	(9.4)
Comparison	(1,2)	$S_{12} + Tx + \Delta Tx_{12} + Coup + \Delta Coup_{12b} + Ref + \Delta Ref_1 - [S_{11} + Tx + \Delta Tx_{11} + Coup + \Delta Coup_{11c} + Ref + \Delta Ref_1]$	(9.5)
Correction Factor	(1,2)	$S_{12} + \Delta Tx_{12} + \Delta Coup_{12b} - S_{11} - \Delta Tx_{11} - \Delta Coup_{11c}$	(9.6)
Calibrated Signal	(1,2)	$Tx - \Delta Coup_{12b} - S_{11} - \Delta Tx_{11} - \Delta Coup_{11c}$	(9.7)
Output	(1,3)	$S_{13} + Tx + \Delta Tx_{13}$	(9.8)
Measurement	(1,3)	$S_{13} + Tx + \Delta Tx_{13} + Coup + \Delta Coup_{13b} + Ref + \Delta Ref_4$	(9.9)
Comparison	(1,3)	$S_{13} + Tx + \Delta Tx_{13} + Coup + \Delta Coup_{13b} + Ref + \Delta Ref_4 - [Tx - S_{11} - \Delta Tx_{11} - \Delta Coup_{11c} + Coup + Ref + \Delta Ref_4]$	(9.10)
Correction Factor	(1,3)	$S_{13} + \Delta Tx_{13} + \Delta Coup_{13b} + S_{11} + \Delta Tx_{11} + \Delta Coup_{11c} - \Delta Coup_{12b} + \Delta Coup_{12c}$	(9.11)
Calibrated Signal	(1,3)	$+ Tx - \Delta Coup_{13b} - S_{11} - \Delta Tx_{11} - \Delta Coup_{11c} + \Delta Coup_{12b} - \Delta Coup_{12c}$	(9.12)
Output	(1,4)	$S_{14} + Tx + \Delta Tx_{14}$	(9.13)
Measurement	(1,4)	$S_{14} + Tx + \Delta Tx_{14} + Coup + \Delta Coup_{14b} + Ref + \Delta Ref_7$	(9.14)
Comparison	(1,4)	$S_{14} + Tx + \Delta Tx_{14} + Coup + \Delta Coup_{14b} + Ref + \Delta Ref_7 - [+ Tx - \Delta Coup_{13b} - S_{11} - \Delta Tx_{11} - \Delta Coup_{11c} + \Delta Coup_{12b} - \Delta Coup_{12c} + S_{13} + \Delta Tx_{13} + Coup + \Delta Coup_{13c} + Ref + \Delta Ref_7]$	(9.15)
Correction	(1,4)	$S_{14} + \Delta Tx_{14} + \Delta Coup_{14b} + \Delta Coup_{13b} + S_{11} + \Delta Tx_{11}$	(9.16)

Factor		$+\Delta Coup_{11c} - \Delta Coup_{12b} + \Delta Coup_{12c} + \Delta Coup_{13c}$	
Calibration Signal	(1,4)	$+ Tx - \Delta Coup_{14b} - \Delta Coup_{13b} - S_{11} - \Delta Tx_{11} - \Delta Coup_{11c} + \Delta Coup_{12b} - \Delta Coup_{12c} - \Delta Coup_{13c}$	(9.17)
Output	(2,1)	$S_{21} + Tx + \Delta Tx_{21}$	(9.18)
Measurement	(2,1)	$S_{21} + Tx + \Delta Tx_{21} + Coup + \Delta Coup_{21c} + Ref + \Delta Ref_2$	(9.19)
Comparison	(2,1)	$S_{21} + Tx + \Delta Tx_{21} + Coup + \Delta Coup_{21d} + Ref + \Delta Ref_1 - [S_{11} + Tx + \Delta Tx_{11} + Coup + \Delta Coup_{11c} + Ref + \Delta Ref_1]$	(9.20)
Correction Factor	(2,1)	$S_{21} + \Delta Tx_{21} + \Delta Coup_{21d} - S_{11} - \Delta Tx_{11} - \Delta Coup_{11c}$	(9.21)
Calibrated Signal	(2,1)	$Tx - \Delta Coup_{21d} + S_{11} + \Delta Tx_{11} + \Delta Coup_{11c}$	(9.22)
Output	(2,2)	$S_{22} + Tx + \Delta Tx_{22}$	(9.23)
Measurement	(2,2)	$S_{22} + Tx + \Delta Tx_{22} + Coup + \Delta Coup_{22a} + Ref + \Delta Ref_1$	(9.24)
Comparison	(2,2)	$S_{22} + Tx + \Delta Tx_{22} + Coup + \Delta Coup_{22a} + Ref + \Delta Ref_1 - [S_{11} + Tx + \Delta Tx_{11} + Coup + \Delta Coup_{11c} + Ref + \Delta Ref_1]$	(9.25)
Correction Factor	(2,2)	$S_{22} + \Delta Tx_{22} + \Delta Coup_{22a} - S_{11} - \Delta Tx_{11} - \Delta Coup_{11c}$	(9.26)
Calibrated Signal	(2,2)	$Tx - \Delta Coup_{22a} - S_{11} - \Delta Tx_{11} - \Delta Coup_{11c}$	(9.27)
Output	(2,3)	$S_{23} + Tx + \Delta Tx_{23}$	(9.28)
Measurement	(2,3)	$S_{23} + Tx + \Delta Tx_{23} + Coup + \Delta Coup_{23a} + Ref + \Delta Ref_4$	(9.29)
Comparison	(2,3)	$S_{23} + Tx + \Delta Tx_{23} + Coup + \Delta Coup_{23a} + Ref + \Delta Ref_4 - [Tx - S_{11} - \Delta Tx_{11} - \Delta Coup_{11c} + Coup + Ref + \Delta Ref_4]$	(9.30)
Correction Factor	(2,3)	$S_{23} + \Delta Tx_{23} + \Delta Coup_{23a} + S_{11} + \Delta Tx_{11} + \Delta Coup_{11c}$	(9.31)
Calibrated Signal	(2,3)	$+ Tx - \Delta Coup_{23a} - S_{11} - \Delta Tx_{11} - \Delta Coup_{11c}$	(9.32)
Output	(2,4)	$S_{24} + Tx + \Delta Tx_{24}$	(9.33)
Measurement	(2,4)	$S_{24} + Tx + \Delta Tx_{24} + Coup + \Delta Coup_{24c} + Ref + \Delta Ref_7$	(9.34)
Comparison	(2,4)	$S_{24} + Tx + \Delta Tx_{24} + Coup + \Delta Coup_{24c} + Ref + \Delta Ref_7 - [+ Tx - \Delta Coup_{13b} - S_{11} - \Delta Tx_{11} - \Delta Coup_{11c} + \Delta Coup_{12b} - \Delta Coup_{12c} + S_{13} + \Delta Tx_{13} + Coup + \Delta Coup_{13c} + Ref + \Delta Ref_7]$	(9.35)
Correction Factor	(2,4)	$S_{24} + \Delta Tx_{24} + \Delta Coup_{24c} + \Delta Coup_{13b} + S_{11} + \Delta Tx_{11} + \Delta Coup_{11c} - \Delta Coup_{12b} + \Delta Coup_{12c} - S_{13} + -\Delta Tx_{13} - \Delta Coup_{13c}$	(9.36)
Calibrated Signal	(2,4)	$Tx - \Delta Coup_{24c} - \Delta Coup_{13b} - S_{11} - \Delta Tx_{11} - \Delta Coup_{11c} + \Delta Coup_{12b} - \Delta Coup_{12c} + \Delta Coup_{13c}$	(9.37)
Output	(3,1)	$S_{31} + Tx + \Delta Tx_{31}$	(9.38)
Measurement	(3,1)	$S_{31} + Tx + \Delta Tx_{31} + Coup + \Delta Coup_{31d} + Ref + \Delta Ref_2$	(9.39)
Comparison	(3,1)	$S_{31} + Tx + \Delta Tx_{31} + Coup + \Delta Coup_{31d} + Ref + \Delta Ref_2 - [Tx - \Delta Coup_{21d} + S_{11} + \Delta Tx_{11} + \Delta Coup_{11c} + Coup + \Delta Coup_{21c} + Ref + \Delta Ref_2]$	(9.40)
Correction Factor	(3,1)	$S_{31} + \Delta Tx_{31} + \Delta Coup_{31d} + \Delta Coup_{21d} - S_{11} - \Delta Tx_{11} - \Delta Coup_{11c} - \Delta Coup_{21c}$	(9.41)
Calibrated Signal	(3,1)	$Tx - \Delta Coup_{31d} - \Delta Coup_{21d} + S_{11} + \Delta Tx_{11} + \Delta Coup_{11c} + \Delta Coup_{21c}$	(9.42)
Output	(3,2)	$S_{32} + Tx + \Delta Tx_{32}$	(9.43)
Measurement	(3,2)	$S_{32} + Tx + \Delta Tx_{32} + Coup + \Delta Coup_{32a} + Ref + \Delta Ref_2$	(9.44)

Comparison	(3,2)	$S_{32} + Tx + \Delta Tx_{32} + Coup + \Delta Coup_{32a} + Ref + \Delta Ref_2 – [Tx – \Delta Coup_{21d} + S_{11} + \Delta Tx_{11} + \Delta Coup_{11c} + Coup + \Delta Coup_{21c} + Ref + \Delta Ref_2]$	(9.45)
Correction Factor	(3,2)	$S_{32} + \Delta Tx_{32} + \Delta Coup_{32a} + \Delta Coup_{21d} - S_{11} - \Delta Tx_{11} - \Delta Coup_{11c} - \Delta Coup_{21c}$	(9.46)
Calibrated Signal	(3,2)	$Tx – \Delta Coup_{32a} - \Delta Coup_{21d} + S_{11} + \Delta Tx_{11} + \Delta Coup_{11c} + \Delta Coup_{21c}$	(9.47)
Output	(3,3)	$S_{33} + Tx + \Delta Tx_{33}$	(9.48)
Measurement	(3,3)	$S_{33} + Tx + \Delta Tx_{33} + Coup + \Delta Coup_{33a} + Ref + \Delta Ref_5$	(9.49)
Comparison	(3,3)	$S_{33} + Tx + \Delta Tx_{33} + Coup + \Delta Coup_{33a} + Ref + \Delta Ref_5 – [Tx – \Delta Coup_{22a} - S_{11} - \Delta Tx_{11} - \Delta Coup_{11c} + Coup + \Delta Coup_{22c} + Ref + \Delta Ref_5]$	(9.50)
Correction Factor	(3,3)	$S_{33} + \Delta Tx_{33} + \Delta Coup_{33a} + \Delta Coup_{22a} + S_{11} + \Delta Tx_{11} + \Delta Coup_{11c} - \Delta Coup_{22c}$	(9.51)
Calibrated Signal	(3,3)	$Tx - \Delta Coup_{33a} - \Delta Coup_{22a} - S_{11} + \Delta Tx_{11} - \Delta Coup_{11c} + \Delta Coup_{22c}$	(9.52)
Output	(3,4)	$S_{34} + Tx + \Delta Tx_{34}$	(9.53)
Measurement	(3,4)	$S_{34} + Tx + \Delta Tx_{34} + Coup + \Delta Coup_{34a} + Ref + \Delta Ref_8$	(9.54)
Comparison	(3,4)	$S_{34} + Tx + \Delta Tx_{34} + Coup + \Delta Coup_{34a} + Ref + \Delta Ref_8 – [+ Tx – \Delta Coup_{23a} - S_{11} - \Delta Tx_{11} - \Delta Coup_{11c} + Coup + \Delta Coup_{23c} + Ref + \Delta Ref_8]$	(9.55)
Correction Factor	(3,4)	$S_{34} + \Delta Tx_{34} + \Delta Coup_{34a} + \Delta Coup_{23a} + S_{11} + \Delta Tx_{11} + \Delta Coup_{11c} - \Delta Coup_{23c}$	(9.56)
Calibrated Signal	(3,4)	$Tx – \Delta Coup_{34a} - \Delta Coup_{23a} - S_{11} - \Delta Tx_{11} - \Delta Coup_{11c} + \Delta Coup_{23c}$	(9.57)
Output	(4,1)	$S_{41} + Tx + \Delta Tx_{41}$	(9.58)
Measurement	(4,1)	$S_{41} + Tx + \Delta Tx_{41} + Coup + \Delta Coup_{41d} + Ref + \Delta Ref_3$	(9.59)
Comparison	(4,1)	$S_{41} + Tx + \Delta Tx_{41} + Coup + \Delta Coup_{41d} + Ref + \Delta Ref_3 – [Tx – \Delta Coup_{31d} - \Delta Coup_{21d} + S_{11} + \Delta Tx_{11} + \Delta Coup_{11c} + \Delta Coup_{21c} + Coup + \Delta Coup_{31c} + Ref + \Delta Ref_3]$	(9.60)
Correction Factor	(4,1)	$S_{41} + \Delta Tx_{41} + \Delta Coup_{41d} + \Delta Coup_{31d} + \Delta Coup_{21d} - S_{11} - \Delta Tx_{11} - \Delta Coup_{11c} - \Delta Coup_{21c} - \Delta Coup_{31c}$	(9.61)
Calibrated Signal	(4,1)	$Tx – \Delta Coup_{41d} - \Delta Coup_{31d} - \Delta Coup_{21d} + S_{11} + \Delta Tx_{11} + \Delta Coup_{11c} + \Delta Coup_{21c} + \Delta Coup_{31c}$	(9.62)
Output	(4,2)	$S_{42} + Tx + \Delta Tx_{42}$	(9.63)
Measurement	(4,2)	$S_{42} + Tx + \Delta Tx_{42} + Coup + \Delta Coup_{42a} + Ref + \Delta Ref_3$	(9.64)
Comparison	(4,2)	$S_{42} + Tx + \Delta Tx_{42} + Coup + \Delta Coup_{42a} + Ref + \Delta Ref_3 – [Tx – \Delta Coup_{31d} - \Delta Coup_{21d} + S_{11} + \Delta Tx_{11} + \Delta Coup_{11c} + \Delta Coup_{21c} + Coup + \Delta Coup_{31c} + Ref + \Delta Ref_3]$	(9.65)
Correction Factor	(4,2)	$S_{42} + \Delta Tx_{42} + \Delta Coup_{42a} + \Delta Coup_{31d} + \Delta Coup_{21d} - S_{11} - \Delta Tx_{11} - \Delta Coup_{11c} - \Delta Coup_{21c} - \Delta Coup_{31c}$	(9.66)
Calibrated Signal	(4,2)	$Tx – \Delta Coup_{42a} - \Delta Coup_{31d} - \Delta Coup_{21d} + S_{11} + \Delta Tx_{11} + \Delta Coup_{11c} + \Delta Coup_{21c} + \Delta Coup_{31c}$	(9.67)
Output	(4,3)	$S_{43} + Tx + \Delta Tx_{43}$	(9.68)
Measurement	(4,3)	$S_{43} + Tx + \Delta Tx_{43} + Coup + \Delta Coup_{43a} + Ref + \Delta Ref_6$	(9.69)
Comparison	(4,3)	$S_{43} + Tx + \Delta Tx_{43} + Coup + \Delta Coup_{43a} + Ref + \Delta Ref_6 – [Tx– \Delta Coup_{32a} - \Delta Coup_{21d} + S_{11} + \Delta Tx_{11} + \Delta Coup_{11c} + \Delta Coup_{21c} + Coup + \Delta Coup_{32c} + Ref + \Delta Ref_6]$	(9.70)
Correction Factor	(4,3)	$S_{43} + \Delta Tx_{43} + \Delta Coup_{43a} + \Delta Coup_{32a} + \Delta Coup_{21d} - S_{11} - \Delta Tx_{11} - \Delta Coup_{11c} - \Delta Coup_{21c} - \Delta Coup_{32c}$	(9.71)
Calibrated	(4,3)	$Tx – \Delta Coup_{43a} - \Delta Coup_{32a} - \Delta Coup_{21d} + S_{11} + \Delta Tx_{11}$	(9.72)

Signal		$+\Delta Coup_{11c} + \Delta Coup_{21c} + \Delta Coup_{32c}$	
Output	(4,4)	$S_{44} + Tx + \Delta Tx_{44}$	(9.73)
Measurement	(4,4)	$S_{44} + Tx + \Delta Tx_{44} + Coup + \Delta Coup_{44a} + Ref + \Delta Ref_9$	(9.74)
Comparison	(4,4)	$S_{44} + Tx + \Delta Tx_{44} + Coup + \Delta Coup_{44a} + Ref + \Delta Ref_9 - [Tx - \Delta Coup_{33a} - \Delta Coup_{22a} - S_{11} + \Delta Tx_{11} - \Delta Coup_{11c} + \Delta Coup_{22c} + Coup + \Delta Coup_{33c} + Ref + \Delta Ref_9]$	(9.75)
Correction Factor	(4,4)	$S_{44} + \Delta Tx_{44} + \Delta Coup_{44a} + \Delta Coup_{33a} + \Delta Coup_{22a} + S_{11} + \Delta Tx_{11} + \Delta Coup_{11c} - \Delta Coup_{22c} - \Delta Coup_{33c}$	(9.76)
Calibrated Signal	(4,4)	$Tx - \Delta Coup_{44a} - \Delta Coup_{33a} - \Delta Coup_{22a} - S_{11} - \Delta Tx_{11} - \Delta Coup_{11c} + \Delta Coup_{22c} + \Delta Coup_{33c}$	(9.77)

From the above table, it is clear that the effect of calibration is to spread the contributing error source's effects throughout the array, producing scaling of calibration errors as the size of the array increases. When these equations are considered in more general terms, i.e. considering the variation of each component block as its standard deviation, then the equations become much simpler for the calibrated signal for each element. This results in an equation that shows the dependence of the top left reference algorithm on the couplers for the calibration accuracy.

$$\sigma_A = \frac{\sigma_{Coupler}}{N-1}\sum_{i=1}^{n}(2i-1)(i-1) \tag{9.78}$$

Where σ_A - the standard deviation of the array

σ_{Coup} - the standard deviation of the directional coupler

N – total number of elements in the array, $N = n \times n$,

$n \times n$ - the total number of elements in the square array

Which can be reduced to:

$$\sigma_A = \frac{\sigma_{Coup}}{N-1}\left(\frac{n\left(4n^2-3n-1\right)}{6}\right) \tag{9.79}$$

Where σ_A - the standard deviation of the array

σ_{Coup} - the standard deviation of the directional coupler

N – total number of elements in the array, $N = n \times n$,

$n \times n$ - the total number of elements in the square array

Appendix C

Shortest Path Calculation of Calibration Errors

As with the top left reference calibration algorithm, the shortest path one uses a series of comparisons throughout the array to calibrate the elements. It does not employ a mitigation tactic to perform this calibration. Therefore the calibration accuracy will depend upon the number of coupler paths taken to calibrate each element of the array. The top left reference algorithms accuracy scaled out from the top left corner, as shown in Table 10-1. The scaling of the shortest path is different due to its choice of reference element and calibration paths, and this is shown in Table 10-2. This makes the predicted calibration accuracy equations for the shortest path:

When n is even: (10.1)

$$\sigma_A = \frac{\sigma_{Coupler}}{N-1}\sum_{i=1}^{\frac{n}{2}-1}(8i)(i) + \frac{2n-1}{N-1}\frac{n}{2}\sigma_{Coupler} \tag{10.2}$$

When n is odd:

$$\sigma_A = \frac{\sigma_{Coupler}}{N-1}\sum_{i=1}^{\frac{n-1}{2}}(8i)(i) \tag{10.3}$$

Where σ_A - the standard deviation of the array

σ_{Coup} - the standard deviation of the directional coupler

N – total number of elements in the array

n x n - the total number of elements in the square array

0	2	4	6
2	2	4	6
4	4	4	6
6	6	6	6

Table 10-1: Scaling of Coupler Errors for the Top Left Reference Calibration Algorithm

2	2	2	4
2	0	2	4
2	2	2	4
4	4	4	4

Table 10-2: Scaling of Coupler Errors for the Shortest Path Calibration Algorithm.

Appendix D

Extensive Investigation of the 4 by 4 Test-Bed Performance

The calibration of the 4 by 4 test-bed was extensive as it presented larger calibration errors then the 2 by 4 array. The impact of these errors was investigated by calibrating the array for the top left reference and the shortest path algorithms, each using 4 different reference element locations. Then the calibration performed by the dual path calibration algorithm was done using all eight of the reference element locations. This was to show the impact of the choice of calibration paths taken through the array and the trends in the calibration. These results were discussed in Chapter 6. The following set of tables contain the calibration results for each of these experiments for both the 3 by 3 and 4 by 4 array sizes upon which the discussion was based.

Table 11-1: Top Left Reference Algorithm's Calibration Amplitude and Phase Errors for a 3 by 3 array on the 4 by 4 Experimental Test-bed, when the Reference Element is Located at Element (1,1).

Element	Amplitude Errors (dB)	Phase Errors (degrees)
(1,2)	-0.22	-2.66
(1,3)	-0.14	-8.86
(2,1)	0.14	-2.21
(2,2)	-0.04	-5.31
(2,3)	1.07	2.21
(3,1)	1.16	1.77
(3,2)	1.13	3.1
(3,3)	1.16	6.64

Table 11-2: Top Left Reference Algorithm's Calibration Amplitude and Phase Errors for the 4 by 4 Experimental Test-bed, when the Reference Element is Located at Element (1, 1).

Element	Amplitude Errors (dB)	Phase Errors (degrees)
(1,2)	-0.22	-2.66
(1,3)	-0.14	-8.86
(1,4)	-0.07	-11.07
(2,1)	0.14	-2.21
(2,2)	-0.04	-5.31
(2,3)	1.07	2.21
(2,4)	-0.04	-9.3
(3,1)	1.16	1.77
(3,2)	1.13	3.1
(3,3)	1.16	6.64
(3,4)	1.65	13.73
(4,1)	1.68	11.07
(4,2)	1.65	9.74
(4,3)	2.49	13.73
(4,4)	2.57	16.38

Table 11-3: Top Left Reference Algorithm's Calibration Amplitude and Phase Errors for a 3 by 3 array on the 4 by 4 Experimental Test-bed, when the Reference Element is Located at Element (1,4).

Element	Amplitude Errors (dB)	Phase Errors (degrees)
(1,2)	-0.10	5.76
(1,3)	-0.10	1.33
(2,2)	-0.80	6.64
(2,3)	0.39	6.2
(2,4)	0.16	2.66
(3,2)	-0.44	6.2
(3,3)	0.13	2.21
(3,4)	-1.02	-6.64

Table 11-4: Top Left Reference Algorithm's Calibration Amplitude and Phase Errors for the 4 by 4 Experimental Test-bed, when the Reference Element is Located at Element (1, 4).

Element	Amplitude Errors (dB)	Phase Errors (degrees)
(1,1)	0.16	5.31
(1,2)	-0.10	5.76
(1,3)	-0.10	1.33
(2,1)	0.197	3.099
(2,2)	-0.80	6.64
(2,3)	0.39	6.199
(2,4)	0.16	2.66
(3,1)	-5.23	-20.81
(3,2)	-0.44	6.199
(3,3)	0.13	2.21
(3,4)	-1.02	-6.64
(4,1)	0.13	7.97
(4,2)	-0.07	7.08
(4,3)	0.76	7.08
(4,4)	0.70	6.64

Table 11-5: Top Left Reference Algorithm's Calibration Amplitude and Phase Errors for a 3 by 3 array on the 4 by 4 Experimental Test-bed, when the Reference Element is Located at Element (4, 1).

Element	Amplitude Errors (dB)	Phase Errors (degrees)
(2,1)	-1.69	-10.18
(2,2)	-1.58	-12.399
(2,3)	0.59	5.31
(3,1)	-0.597	-7.53
(3,2)	-0.43	-3.99
(3,3)	0.589	-0.44
(4,2)	0	3.099
(4,3)	1.82	-13.73

Table 11-6: Top Left Reference Algorithm's Calibration Amplitude and Phase Errors for the 4 by 4 Experimental Test-bed, when the Reference Element is Located at Element (4, 1).

Element	Amplitude Errors (dB)	Phase Errors (degrees)
(1,1)	-10.18	-1.62
(1,2)	-10.18	-1.58
(1,3)	-4.87	-0.70
(1,4)	-5.76	0.35
(2,1)	-10.18	-1.69
(2,2)	-12.399	-1.58
(2,3)	5.31	0.589
(2,4)	1.33	0.28
(3,1)	-7.53	-0.597
(3,2)	-3.99	-0.43
(3,3)	-0.44	0.589
(3,4)	13.73	1.196
(4,2)	3.099	0
(4,3)	-13.73	1.82
(4,4)	-15.498	1.87

Table 11-7: Top Left Reference Algorithm's Calibration Amplitude and Phase Errors for a 3 by 3 array on the 4 by 4 Experimental Test-bed, when the Reference Element is Located at Element (4, 4).

Element	Amplitude Errors (dB)	Phase Errors (degrees)
(2,2)	-2.25	-19.04
(2,3)	-0.80	-11.07
(2,4)	-0.94	-10.18
(3,2)	-1.53	-14.61
(3,3)	0.16	-6.199
(3,4)	-0.66	-8.86
(4,2)	-2.33	-16.38
(4,3)	1.11	-3.99

Table 11-8: Top Left Reference Algorithm's Calibration Amplitude and Phase Errors for the 4 by 4 Experimental Test-bed, when the Reference Element is Located at Element (4, 4).

Element	Amplitude Errors (dB)	Phase Errors (degrees)
(1,1)	-2.04	-8.41
(1,2)	-2.41	-15.94
(1,3)	-0.36	-19.48
(1,4)	-0.91	-7.53
(2,1)	-3.07	-14.17
(2,2)	-2.25	-19.04
(2,3)	-0.80	-11.07
(2,4)	-0.94	-10.18
(3,1)	-0.66	-0.266
(3,2)	-1.53	-14.61
(3,3)	0.16	-6.199
(3,4)	-0.66	-8.86
(4,1)	0.03	3.99
(4,2)	-2.33	-16.38
(4,3)	1.11	-3.99

Table 11-9: Shortest Path Algorithm's Calibration Amplitude and Phase Errors for a 3 by 3 array on the 4 by 4 Experimental Test-bed, when the Reference Element is Located at Element (2, 2).

Element	Amplitude Errors (dB)	Phase Errors (degrees)
(1,1)	-0.68	-0.27
(1,2)	-0.37	-3.1
(1,3)	0.73	-1.33
(2,1)	-0.33	0.886
(2,3)	1.75	12.84
(3,1)	1.03	2.21
(3,2)	0.999	6.64
(3,3)	1.22	5.76

Table 11-10: Shortest Path Algorithm's Calibration Amplitude and Phase Errors for the 4 by 4 Experimental Test-bed, when the Reference Element is Located at Element (2, 2).

Element	Amplitude Errors (dB)	Phase Errors (degrees)
(1,1)	-0.68	-0.27
(1,2)	-0.37	-3.1
(1,3)	0.73	-1.33
(1,4)	0.90	-3.1
(2,1)	-0.33	0.886
(2,3)	1.75	12.84
(2,4)	1.71	8.86
(3,1)	1.03	2.21
(3,2)	0.999	6.64
(3,3)	1.22	5.76
(3,4)	1.596	7.97
(4,1)	1.53	6.199
(4,2)	1.38	9.74
(4,3)	2.38	20.37
(4,4)	1.92	10.63

Table 11-11: Shortest Path Algorithm's Calibration Amplitude and Phase Errors for a 3 by 3 array on the 4 by 4 Experimental Test-bed, when the Reference Element is Located at Element (2, 3).

Element	Amplitude Errors (dB)	Phase Errors (degrees)
(1,2)	-1.68	-4.87
(1,3)	-0.63	-0.27
(1,4)	-0.80	-5.76
(2,2)	-2.06	-5.76
(2,4)	2.22	6.199
(3,2)	-1.499	-0.27
(3,3)	0.56	1.33
(3,4)	0.23	6.199

Table 11-12: Shortest Path Algorithm's Calibration Amplitude and Phase Errors for the 4 by 4 Experimental Test-bed, when the Reference Element is Located at Element (2, 3).

Element	Amplitude Errors (dB)	Phase Errors (degrees)
(1,1)	-1.59	-0.44
(1,2)	-1.68	-4.87
(1,3)	-0.63	-0.27
(1,4)	-0.80	-5.76
(2,1)	-1.87	-3.99
(2,2)	-2.06	-5.76
(2,4)	2.22	6.199
(3,1)	-1.41	2.66
(3,2)	-1.5	-0.27
(3,3)	0.56	1.33
(3,4)	0.23	6.2
(4,1)	-0.97	9.299
(4,2)	-1.97	-3.99
(4,3)	0.91	5.76
(4,4)	1.04	7.08

Table 11-13: Shortest Path Algorithm's Calibration Amplitude and Phase Errors for a 3 by 3 array on the 4 by 4 Experimental Test-bed, when the Reference Element is Located at Element (3,2).

Element	Amplitude Errors (dB)	Phase Errors (degrees)
(2,1)	-1.21	-7.97
(2,2)	-0.69	-10.63
(2,3)	0.82	1.33
(3,1)	-0.73	-3.99
(3,3)	-0.27	-3.1
(4,1)	-0.03	4.43
(4,2)	0	2.66
(4,3)	0.76	6.64

Table 11-14: Shortest Path Algorithm's Calibration Amplitude and Phase Errors for the 4 by 4 Experimental Test-bed, when the Reference Element is Located at Element (3, 2).

Element	Amplitude Errors (dB)	Phase Errors (degrees)
(1,1)	-1.36	-4.87
(1,2)	-0.62	-5.31
(1,3)	0	-9.74
(1,4)	0.94	-3.1
(2,1)	-1.21	-7.97
(2,2)	-0.69	-10.63
(2,3)	0.82	1.33
(2,4)	1.12	2.21
(3,1)	-0.73	-3.99
(3,3)	-0.27	-3.1
(3,4)	-0.20	-3.99
(4,1)	-0.03	4.43
(4,2)	0	2.66
(4,3)	0.76	6.64
(4,4)	1.32	7.97

Table 11-15: Shortest Path Algorithm's Calibration Amplitude and Phase Errors for a 3 by 3 array on the 4 by 4 Experimental Test-bed, when the Reference Element is Located at Element (3,3).

Element	Amplitude Errors (dB)	Phase Errors (degrees)
(2,2)	-0.84	-10.18
(2,3)	-0.45	2.66
(2,4)	-0.52	-3.54
(3,2)	0.07	4.43
(3,4)	-0.17	-1.33
(4,2)	-0.38	-2.21
(4,3)	0.39	8.41
(4,4)	0.23	5.76

Table 11-16: Shortest Path Algorithm's Calibration Amplitude and Phase Errors for the 4 by 4 Experimental Test-bed, when the Reference Element is Located at Element (3, 3).

Element	Amplitude Errors (dB)	Phase Errors (degrees)
(1,1)	-1.10	-5.31
(1,2)	-0.10	-3.1
(1,3)	-0.62	-5.76
(1,4)	-0.59	-3.1
(2,1)	-0.695	-4.43
(2,2)	-0.84	-10.18
(2,3)	-0.45	2.66
(2,4)	-0.52	-3.54
(3,1)	-0.24	3.1
(3,2)	0.07	4.43
(3,4)	-0.17	-1.33
(4,1)	-0.38	-0.44
(4,2)	-0.38	-2.21
(4,3)	0.39	8.41
(4,4)	0.23	5.76

Table 11-17: Dual Path Algorithm's Calibration Amplitude and Phase Errors for a 3 by 3 array on the 4 by 4 Experimental Test-bed, when the Reference Element is Located at Element (1,1).

Element	Amplitude Errors (dB)	Phase Errors (degrees)
(1,2)	0.11	-1.77
(1,3)	0.38	1.33
(2,1)	-0.22	-1.33
(2,2)	0.14	-0.27
(2,3)	1.71	13.73
(3,1)	3.53	5.31
(3,2)	1.14	5.76
(3,3)	1.92	18.598

Table 11-18: Dual Path Algorithm's Calibration Amplitude and Phase Errors for the 4 by 4 Experimental Test-bed, when the Reference Element is Located at Element (1, 1).

Element	Amplitude Errors (dB)	Phase Errors (degrees)
(1,2)	0.11	-1.77
(1,3)	0.38	1.33
(1,4)	0.79	0.27
(2,1)	-0.22	-1.33
(2,2)	0.14	-0.27
(2,3)	1.71	13.73
(2,4)	0.95	2.21
(3,1)	3.53	5.31
(3,2)	1.14	5.76
(3,3)	1.92	18.598
(3,4)	2.06	11.96
(4,1)	1.74	9.74
(4,2)	1.71	9.74
(4,3)	2.92	23.03
(4,4)	3.19	23.91

Table 11-19: Dual Path Algorithm's Calibration Amplitude and Phase Errors for a 3 by 3 array on the 4 by 4 Experimental Test-bed, when the Reference Element is Located at Element (1,4).

Element	Amplitude Errors (dB)	Phase Errors (degrees)
(1,2)	-0.13	1.77
(1,3)	-0.03	4.87
(2,2)	-0.69	-3.1
(2,3)	0.45	-9.74
(2,4)	0.26	2.66
(3,2)	-0.69	0.89
(3,3)	0.51	7.53
(3,4)	2.03	11.07

Table 11-20: Dual Path Algorithm's Calibration Amplitude and Phase Errors for the 4 by 4 Experimental Test-bed, when the Reference Element is Located at Element (1, 4).

Element	Amplitude Errors (dB)	Phase Errors (degrees)
(1,1)	-0.798	-1.33
(1,2)	-0.13	1.77
(1,3)	-0.03	4.87
(2,1)	-0.58	-2.21
(2,2)	-0.69	-3.1
(2,3)	0.45	-9.74
(2,4)	0.26	2.66
(3,1)	-6.36	-23.91
(3,2)	-0.69	0.89
(3,3)	0.51	7.53
(3,4)	2.03	11.07
(4,1)	-2.39	-6.64
(4,2)	-0.24	-1.33
(4,3)	1.21	13.28
(4,4)	1.21	10.18

Table 11-21: Dual Path Algorithm's Calibration Amplitude and Phase Errors for a 3 by 3 array on the 4 by 4 Experimental Test-bed, when the Reference Element is Located at Element (4,1).

Element	Amplitude Errors (dB)	Phase Errors (degrees)
(2,1)	-1.75	-11.96
(2,2)	-1.66	-5.76
(2,3)	0	-8.41
(3,1)	-0.89	-4.87
(3,2)	-0.60	-0.27
(3,3)	-0.098	-6.2
(4,2)	-0.16	0.89
(4,3)	1.32	8.86

Table 11-22: Dual Path Algorithm's Calibration Amplitude and Phase Errors for the 4 by 4 Experimental Test-bed, when the Reference Element is Located at Element (4, 1).

Element	Amplitude Errors (dB)	Phase Errors (degrees)
(1,1)	-1.25	-8.41
(1,2)	-1.33	-4.87
(1,3)	-0.89	-12.84
(1,4)	0.06	-7.97
(2,1)	-1.75	-11.96
(2,2)	-1.64	-5.76
(2,3)	0	-8.41
(2,4)	0.26	-3.1
(3,1)	-0.89	-4.87
(3,2)	-0.60	-0.27
(3,3)	-0.098	-6.2
(3,4)	0.54	-2.66
(4,2)	-0.16	0.89
(4,3)	1.32	8.86
(4,4)	1.04	3.54

Table 11-23: Dual Path Algorithm's Calibration Amplitude and Phase Errors for a 3 by 3 on the 4 by 4 Experimental Test-bed, when the Reference Element is Located at Element (4,4).

Element	Amplitude Errors (dB)	Phase Errors (degrees)
(2,2)	-0.91	-11.96
(2,3)	-0.67	-6.64
(2,4)	-0.95	-7.53
(3,2)	-0.91	-7.53
(3,3)	-0.53	-5.76
(3,4)	-0.63	-7.53
(4,2)	-1.62	-11.96
(4,3)	0.13	-3.1

Table 11-24: Dual Path Algorithm's Calibration Amplitude and Phase Errors for the 4 by 4 Experimental Test-bed, when the Reference Element is Located at Element (4, 4).

Element	Amplitude Errors (dB)	Phase Errors (degrees)
(1,1)	-1.24	-2.21
(1,2)	-0.98	-7.97
(1,3)	-0.43	-15.94
(1,4)	-1.02	-5.31
(2,1)	-2.09	-3.1
(2,2)	-0.91	-11.96
(2,3)	-0.67	-6.64
(2,4)	-0.95	-7.53
(3,1)	-0.88	-1.77
(3,2)	-0.91	-7.53
(3,3)	-0.53	-5.76
(3,4)	-0.63	-7.53
(4,1)	-0.23	1.33
(4,2)	-1.62	-11.96
(4,3)	0.13	-3.1

Table 11-25: Dual Path Algorithm's Calibration Amplitude and Phase Errors for a 3 by 3 array on the 4 by 4 Experimental Test-bed, when the Reference Element is Located at Element (2,2).

Element	Amplitude Errors (dB)	Phase Errors (degrees)
(1,1)	-0.53	-3.99
(1,2)	-0.36	0.27
(1,3)	0.97	-1.33
(2,1)	-0.04	-2.66
(2,3)	2.26	12.398
(3,1)	1.05	4.87
(3,2)	1.39	3.1
(3,3)	1.36	6.64

Table 11-26: Dual Path Algorithm's Calibration Amplitude and Phase Errors for the 4 by 4 Experimental Test-bed, when the Reference Element is Located at Element (2, 2).

Element	Amplitude Errors (dB)	Phase Errors (degrees)
(1,1)	-0.53	-3.99
(1,2)	-0.36	0.27
(1,3)	0.97	-1.33
(1,4)	1.49	1.33
(2,1)	-0.04	-2.66
(2,3)	2.26	12.398
(2,4)	1.82	5.76
(3,1)	1.05	4.87
(3,2)	1.39	3.1
(3,3)	1.36	6.64
(3,4)	2.38	13.28
(4,1)	1.69	9.74
(4,2)	1.95	6.64
(4,3)	2.79	15.06
(4,4)	2.47	15.06

Table 11-27: Dual Path Algorithm's Calibration Amplitude and Phase Errors for a 3 by 3 array on the 4 by 4 Experimental Test-bed, when the Reference Element is Located at Element (2,3).

Element	Amplitude Errors (dB)	Phase Errors (degrees)
(1,1)	-2.25	-0.89
(1,2)	-1.86	-3.99
(1,3)	-0.76	-2.21
(2,1)	-1.86	-0.27
(2,2)	-2.01	-6.64
(3,1)	-0.88	3.99
(3,2)	-1.54	1.33
(3,3)	0	-0.44

Table 11-28: Dual Path Algorithm's Calibration Amplitude and Phase Errors for the 4 by 4 Experimental Test-bed, when the Reference Element is Located at Element (2, 3).

Element	Amplitude Errors (dB)	Phase Errors (degrees)
(1,1)	-2.25	-0.89
(1,2)	-1.86	-3.99
(1,3)	-0.76	-2.21
(1,4)	-1.14	-3.1
(2,1)	-1.86	-0.27
(2,2)	-2.01	-6.64
(2,4)	2.21	12.84
(3,1)	-0.88	3.99
(3,2)	-1.54	1.33
(3,3)	0	-0.44
(3,4)	-0.63	-1.33
(4,1)	0.15	7.53
(4,2)	-0.88	-3.1
(4,3)	0.90	5.76
(4,4)	0.83	10.63

Table 11-29: Dual Path Algorithm's Calibration Amplitude and Phase Errors for a 3 by 3 array on the 4 by 4 Experimental Test-bed, when the Reference Element is Located at Element (3,2).

Element	Amplitude Errors (dB)	Phase Errors (degrees)
(2,1)	-1.25	-10.63
(2,2)	-0.80	-8.41
(2,3)	0.70	1.33
(3,1)	-0.59	-0.44
(3,3)	0	-4.43
(4,1)	0.29	2.21
(4,2)	0.26	-0.89
(4,3)	1.09	8.86

Table 11-30: Dual Path Algorithm's Calibration Amplitude and Phase Errors for the 4 by 4 Experimental Test-bed, when the Reference Element is Located at Element (3, 2).

Element	Amplitude Errors (dB)	Phase Errors (degrees)
(1,1)	-0.91	-7.53
(1,2)	-0.95	-4.43
(1,3)	-0.13	-8.86
(1,4)	0.73	-0.89
(2,1)	-1.25	-10.63
(2,2)	-0.80	-8.41
(2,3)	0.70	1.33
(2,4)	0.67	4.43
(3,1)	-0.59	-0.44
(3,3)	0	-4.43
(3,4)	1.98	1.33
(4,1)	0.29	2.21
(4,2)	0.26	-0.89
(4,3)	1.09	8.86
(4,4)	0.86	3.99

Table 11-31: Dual Path Algorithm's Calibration Amplitude and Phase Errors for a 3 by 3 array on the 4 by 4 Experimental Test-bed, when the Reference Element is Located at Element (3,3).

Element	Amplitude Errors (dB)	Phase Errors (degrees)
(2,2)	-1.05	3.99
(2,3)	-0.47	-8.41
(2,4)	-0.47	-6.64
(3,2)	-0.17	2.66
(3,4)	-0.65	4.87
(4,2)	-0.37	-4.43
(4,3)	0.45	2.21
(4,4)	0.26	7.53

Table 11-32: Dual Path Algorithm's Calibration Amplitude and Phase Errors for the 4 by 4 Experimental Test-bed, when the Reference Element is Located at Element (3, 3).

Element	Amplitude Errors (dB)	Phase Errors (degrees)
(1,1)	-0.90	-0.89
(1,2)	-0.61	-7.97
(1,3)	-0.65	-6.64
(1,4)	-0.76	-6.2
(2,1)	-0.86	-3.99
(2,2)	-1.05	3.99
(2,3)	-0.47	-8.41
(2,4)	-0.47	-6.64
(3,1)	-0.47	-2.21
(3,2)	-0.17	2.66
(3,4)	-0.65	4.87
(4,1)	0.25	1.33
(4,2)	-0.37	-4.43
(4,3)	0.45	2.21
(4,4)	0.26	7.53

Appendix E

This appendices contains the following papers:

- T. Cooper, J. M. Cormack, R. Farrell, and G. Baldwin, "Towards Scalable Automated Tower Top Phased Array Calibration," in *IEEE 65th Vehicular Technology Conference VTC-2007* Dublin, Ireland, 2007, pp. 1-5.
- J. McCormack, T. Cooper, and R. Farrell, "A Multi-Path Algorithmic Approach to Phased Array Calibration," in *Antennas and Propagation, 2007. EuCAP 2007. The Second European Conference on*, 2007, pp. 1-6.
- J. McCormack, T. Cooper, and R. Farrell, "Tower-Top Antenna Array Calibration Scheme for Next Generation Networks," *EURASIP Journal on Wireless Communications and Networking,* vol. 2007, pp. 1-13, Jan 1 2007.
- L. Barrandon, J. McCormack, T. S. Cooper, and R. Farrell, "On the Accuracy and Hardware Requirements of Cordic-Based Phased Array Calibration," in *Antennas and Propagation, 2007. EuCAP 2007. The Second European Conference on*, 2007, pp. 1-5.
- J. McCormack, L. Lengier, J. Dooley, and R. Farrell, "The Effectiveness of Non-Radiative Calibration Approaches of a Tower Top Distributed Transceiver System " in *URSI Colloquium on Wireless Communications* Dublin, 2008.
- J. McCormack, G. Corley, and R. Farrell, "Experimental results of non-radiative calibration of a tower top adaptive array," in *Antennas and Propagation, 2009. EuCAP 2009. 3rd European Conference on*, 2009, pp. 3389-3393.
- G. P. Corley, J. M. McCormack, and R. J. Farrell, "Demonstrator Platform for Antenna Array Calibration " in *China - Ireland International Conference on Information and Communications Technologies (CIICT)* Maynooth, 2009.

Toward Scalable, Automated Tower-Top Phased Array Calibration

Tim Cooper, Justine McCormack, Ronan Farrell and Gerard Baldwin
Centre for Telecommunications Value-Chain Research (CTVR)
Institute of Microelectronics and Wireless Systems
National University of Ireland, Maynooth
Co. Kildare, Ireland
Email: tcooper@eeng.nuim.ie

***Abstract*— The tower-top deployment of base station electronics could prove of utility in future cellular communication applications. We present a scalable, non-radiative, automated calibration scheme for such a system, which employs an array of independently phased transceivers. By coupling an interlinear row of reference transceivers to the array, feedpoint calibration of the array is possible. The theoretical justification for the scheme is presented together with assessment of the accuracy of calibration possible using commercial off the shelf components.**

I. Introduction

The principle motivation behind relocation of the base station electronics to the tower top are the versatility, performance and space saving benefits such a system would yield. The use of a tower-top base station may also reduce capital costs because the need for both feeder cables and large resonant cavity duplexer filters is obviated. There are, however, many significant engineering challenges to the implementation of such a scheme. One of the most significant is obtaining the same RF output power as that of a conventional, tower-bottom, system. We conject that the RF system specifications will be easier to meet in the distributed tower-top system of figure 1, wherein, the RF transceiver electronics are distributed amongst the individual array elements. Appropriate summation and weighting is performed within a tower-top controller unit. The remaining demodulation functions are then performed by a tower-bottom baseband radio.

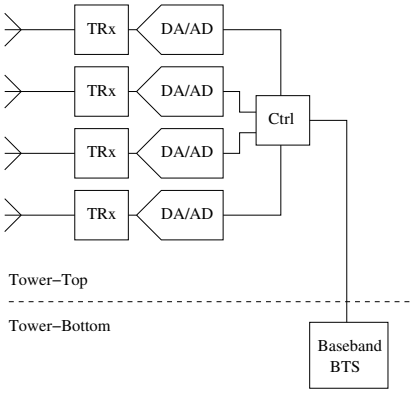

Fig. 1. A single sector of the tower-top system sees the transceiver electronics distributed between each element (here four are shown) within the array.

This distribution between array elements will allow the transition to lower cost ceramic duplexers [1] because, given an element gain of 5 dBi, a directional 30 element array would require feed-point power of 3.2 W to meet the current GSM specification. It is anticipated that this will also assist meeting the stringent reliability requirements and heat dissipation performance needed of a tower-top radio. Whether such a transceiver can be implemented, and produced affordably, remains the subject of continued interest.

The aforementioned benefits are offset by several disadvantages. The two most pertinent are reliability and accurate phasing of the array, also known as 'the calibration problem'. It is the latter of these two problems which this paper addresses in the context of a tower-top cellular system. Aspects of this calibration scheme are protected by patent pending (S2006/0482).

II. Array Calibration

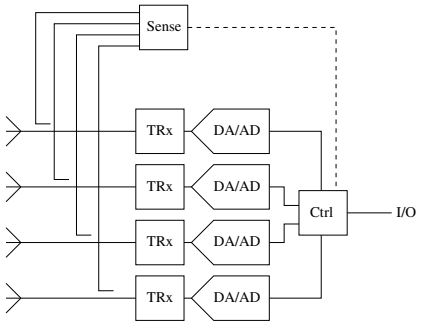

Fig. 2. Conventional array calibration wherein a coupled feedback path allows measurement of the transmitted signal and injection of calibration signals.

Where calibration is non-radiative, i.e. does not employ remote or local signals radiated in free space as the main calibration medium then array calibration, typically, is based on a closed feedback loop between a single sensing device and the outputs of the array, as shown in figure 2. It is well known that calibration relative to a single reference element, by means of weighting the input to the array, can yield accurate amplitude and phasing at the antenna feedpoint. This is usually

conditional upon the paths between the antenna feed point and reference element being equal and that the transceiver local oscillators are frequency coherent. Potential difficulties with this type of calibration scheme are that, in scaling it to arrays of significant dimensions, such as those which could be required to make a tower-top cellular transceiver, can give rise to complex calibration coupler arrangements which must be carefully designed to avoid unwanted coupling and electrical path length imbalance.

III. Interlinear Reference Calibration

To accommodate larger numbers of array elements, each with a separate transceiver, the calibration scheme shown in figure 3 is proposed. Here each group of four transceivers is coupled to a central sensing device capable of generating or receiving calibration signals for both transmit or receive band calibration. This coupling is achieved here by a hypothetical six port directional coupler structure. The output of the sensing electronics is therefore terminated in a matched impedance Z.

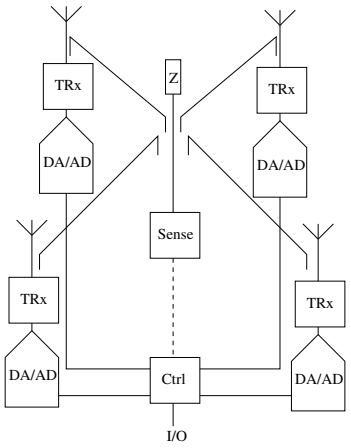

Fig. 3. Calibration relative to a single central sensing element equidistant from the neighboring radiative transceivers. Calibration is applied through the conventional feedback mechanisms.

For the purpose of this paper we will describe only transmit calibration although, by reciprocity, receive calibration is also possible. For transmitter calibration, the role of the central sensing element is to perform feed-point measurements of the transmitter phase and amplitude via the coupler structure. Thus allowing direct comparison of the feedpoint signals of each of the array's transmitters. To effect calibration, one of the radiative transmitter elements is selected to calibrate the rest of the array relative to, say, the bottom left. Our reference sensor then records the phase and amplitude of the coupled signal from that transmitter. Each of the other three elements then have their output sampled in turn, by the same reference sensor. It is then a simple matter to apply a corrective digital baseband weighting to each of the three transmitter inputs, such that their outputs - as measured by our reference, are all equal to that of the bottom left hand element. Thus enabling accurate phasing of the array.

By repeating this tessellating coupler structure (see figure 4 a) the calibration scheme may, in principal, be scaled to arrays of any proportions - each group of four transceivers being calibrated relative to a central 'reference' element (which contains the control and sensing functionality of previous figures). This process is repeated across the whole array with each transceiver being calibrated relative to a previously calibrated array element until the whole array is accurately phased.

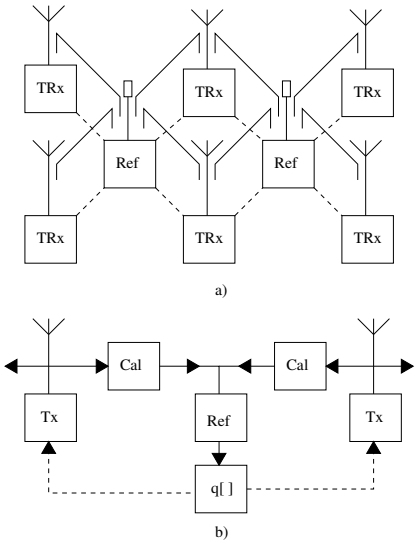

Fig. 4. a) Arrangement of coupler and sensing elements to calibrate a rectilinear array. b) Block schematic representation of the linear array calibration simulation.

A system level schematic representation of the calibration process, simplified to a linear array, is shown in figure 4 b). Here a uniform linear array is calibrated by a row of reference elements (Ref) placed between the adjacent radiative transmitters (Tx) which form the array. The transmitted signal from the first transceiver is coupled via the calibration coupler network (Cal) to a reference element[1]. This measurement is subsequently compared with measurements from neighboring elements and the transmitters output adjusted accordingly, effecting calibration. This process is repeated for all elements of the array sequentially, starting from the centre of the array. In this paper we consider the reference receiver input signal's accuracy to be limited, in a process which mimics quantisation without adding the attendant noise, denoted q[ ]. We assume that the effects of quantisation noise will be negligible. Although the system is designed explicitly to correct for them, for now we will also ignore the influence of time dependent phenomenon such as component aging and thermal effects and focus on static error correction.

IV. Predicting Calibration Performance

In practical systems hardware can only be produced to finite accuracy and tolerance. Our goal was to derive a closed form

[1]It is important to note that the calibration block shown here (error = σ_c) subsumes both of the individual couplers of the preceding figure.

expression which would give us a statistical prediction of the accuracy of calibration of the array. This prediction is based only upon *a priori* knowledge of the errors of the constituent components of our array system.

A. The Linear Array

In the case of static, single frequency operation, with perfect impedance matching, we define each block of our array radio system to have some predefined average performance, gain A (dB) and phase ϕ°. The actual value of this will vary by some error $\Delta(A,\phi)$ from this ideal. Recalling that the calibration process relies on baseband feedback weighting we also define an error signal $\epsilon(A,\phi)$. Where the input signal to the nth transmitter is a pure sinusoid, $x_n(A,\phi)$, measured by the mth reference with error Δ_{R_m}. It is simple to see from the error signal that perfect array calibration is possible:

$$\epsilon(A,\phi) = (x_1 + \Delta_{R_m}) - (x_n + \Delta_{R_m}) \tag{1}$$

If we now introduce coupler errors $\Delta_c(a,\phi)$ we can see that the accuracy of the calibration of the nth transmitter is degraded by the sum of all of the errors between it and the first transmitter.

$$\epsilon_n(A,\phi) = (x_1 + \Delta_{R_m}) - \left(x_n + \Delta_{R_m} + \sum_{i=1}^{N} \Delta c_i\right) \tag{2}$$

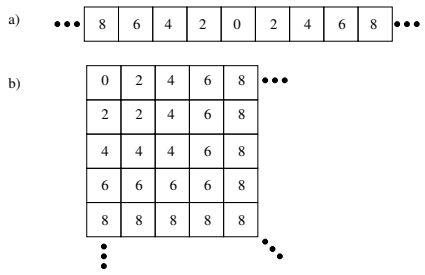

Fig. 5. a) Diagram illustrating graphically the minimum number of calibration paths incurred in calibrating the linear array. b) A similar diagram for a rectilinear array calibrated from the array top-left corner.

Figure 5 a) represents a linear array - each box corresponds to an array element. Using the convention of figure 4 b), the numbers within the boxes represent the sequence and number of coupler calibration path errors accrued during the calibration process. Here calibration starts with the centre-most element. Assuming these coupled paths each have a Gaussian error associated with them and that calibration starts with the centre-most element: An expression for the resultant output error distribution for a N element linear array σ_a, in terms of the coupled calibration path errors σ_c may be derived:

$$\sigma_a^2 = \frac{2}{N-1} 2\sigma_c^2 + \frac{2}{N-1} 4\sigma_c^2 + ... + \frac{\alpha}{N-1} M\sigma_c^2 \tag{3}$$

Where, in the last term, $\alpha = 1$ if $N - 1 = \text{odd}$ elsewhere $\alpha = 2$ and M is N/2 rounded to the nearest integer value. And the reference sensor measurement resolution error contribution is insignificant.

B. The Rectilinear Array

To develop an expression for the rectilinear array we extend this principle to that illustrated in figure 5 b) for an N element square array. Here calibration begins at the top-left hand corner of the array. The numbers therefore denote, not only the sequence that the calibration is performed in, but the number of couplers incurred between the start element (0) and the transceiver being calibrated. As with the linear array, given Gaussian error distribution in coupled path error, by summing and weighting these variances according to the frequency with which they occur, it is possible to calculate the resultant distribution. For the calibration process shown in figure 5 b) the resultant error distribution's phase variance for the array ($\sigma_{\phi_a}^2$) due to this coupled path error is given by:

$$\sigma_{\phi_a}^2 = \sum_{i=2}^{N} \left(\frac{i^2 - [i-1]^2}{N-1}\right) 2(i-1)\sigma_{\phi_c}^2 \tag{4}$$

with coupled path phase error variance $\sigma_{\phi_c}^2$ centered around a mean value equal to the phase of the first element. Similarly for the array amplitude error variance:

$$\sigma_{A_a}^2 = \sum_{i=2}^{N} \left(\frac{i^2 - [i-1]^2}{N-1}\right) 2(i-1)\sigma_{A_c}^2 \tag{5}$$

with coupler amplitude error variance $\sigma_{A_c}^2$ with the distribution centred around the amplitude of the first element.

V. Simulation

A. Theoretical Comparison

To test the accuracy of these predictions, the calibration scheme representation of figure 5 b) was extended to a rectilinear array as shown in figure 6. In the regime $\Delta_c < \Delta_{Tx}$ and q=14 bits, expressions 4 and 5 were found, to good approximation, to describe array calibration accuracy.

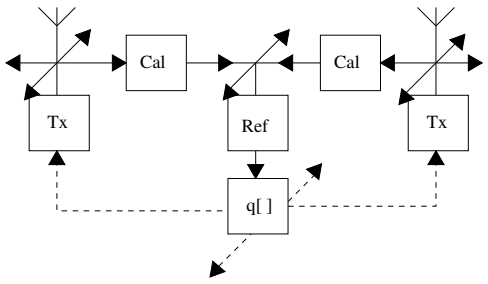

Fig. 6. A block schematic diagram representing the simulation of figure 4 b) modified for the rectilinear case.

This is illustrated in figure 7, which shows how the standard deviation of the array calibration error increases with array size, on this scale the theoretical and simulated results are coincident. Figure 8 shows the mean array error as a function of array size - this again illustrates the accuracy with which our statistical method can predict the array calibration accuracy. The simulation results were obtained by combining the output of 10 000 simulations to obtain statistically significant results.

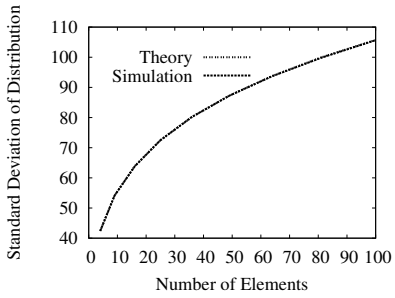

Fig. 7. Comparison of theoretical and simulation predictions for the resultant error distribution given a coupled path with σ_c = 30.

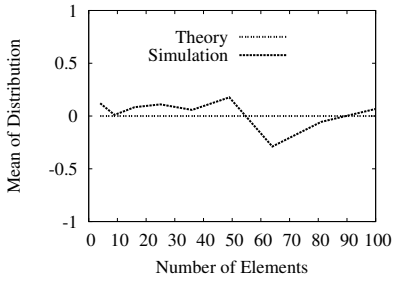

Fig. 8. Comparison of theoretical and simulation predictions for the resultant error distribution given a coupled path with σ_c = 30.

B. Practical Array System Calibration

To generate useful predictions of the performance of a physical array which uses our calibration scheme, values based on available manufacturer's data were attributed to each of the blocks of the simulation scheme of figures 4 b) and 6 . Associated with the phase (ϕ) and amplitude (A) of each S-Parameter (average μ) is a Gaussian error standard deviation, σ, with values as shown in the table below. The initial condition of the input signal to the transmitter block was selected as -20 dBm with a standard deviation of 0.5 dB and uniformly distributed arbitrary phase.

Component	μ_A	σ_A	μ_ϕ	σ_ϕ
Tx S_{21}	50 dB	3 dB	10°	20°
Ref S_{21}	60 dB	3 dB	85°	20°
Cal S_{21}	-40 dB	0.2 dB	95°	2°

These values were selected to reflect low-cost, low quality, commercially available hardware. The specification for the calibration coupler, however, had to be inferred due to the lack of commercially available high balance coupler structures. The coupler phase error is based upon the series connection of a pair of power dividers, each with 3° of peak phase error and an RMS phase error of 1° [2]. Based on the combination of two independent identically distributed random variables this gives a resultant RMS phase error of 1.4°, this was rounded up to 2° to conservatively represent low cost hardware. Similarly an RMS amplitude error of 0.2 dB RMS was calculated for the amplitude imbalance. Work on our own high phase and amplitude balance coupler is on-going and we hope to improve significantly on these figures.

1) Practical Linear Array: To assess the feasibility of our calibration scheme the radiation polar plot feedpoint accuracy of the 30 element linear array of section I, fed by the simulated output of our calibration scheme, was examined. Equation 3 predicts phase and amplitude imbalance of the order of $\sigma = 7.9°$ and 0.69 dB this compares with the values of 8.07 ° and 0.61 dB obtained from 1000 runs of the calibration simulation above. The radiation polar plot of a representative linear array

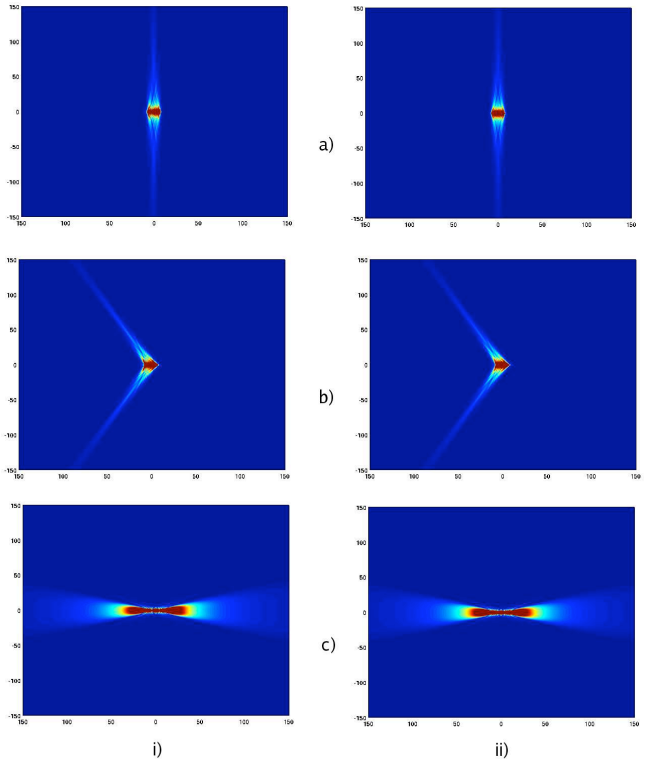

Fig. 9. i) Beamforming performance of the calibration scheme for a 30 element $\frac{\lambda}{2}$ spaced dipole array relative to ii) perfect beamformed output for the same array. a) Broadside, b) 45° and c) endfire radiation patterns shown.

result, in the absence of antenna mutual coupling, is shown in figure 9. Figure 9 i) a) shows broadside, figure 9 i) b) 45° and figure 9 i) c) endfire beamformed radiation. The equivalent ideal beamformed radiation are shown in figures 9 ii) a–c). From these results we can see that the directional beamforming error incurred is unmeasurable and a slight increase in sidelobe level observed in the case of the broadside radiation pattern.

The reason for the lack of beamforming error in figure 9 may be that the larger errors are relegated to the periphery of the array. Anecdotal evidence for this can be seen in Kraus [3], however, the effect of the magnitude of element error distribution on beamforming requires further examination. We will not consider this single array's performance further as our predictions and results are principally concerned with statistical ensembles of arrays. Future work will focus on a method for extracting peak and mean sidelobe levels, as well as directivity error from groups of such plots.

2) Practical Rectilinear Array: To gauge the size of array which can be practically employed using this calibration scheme, the simulated rectilinear array results are plotted as a function of array size in figure 10.

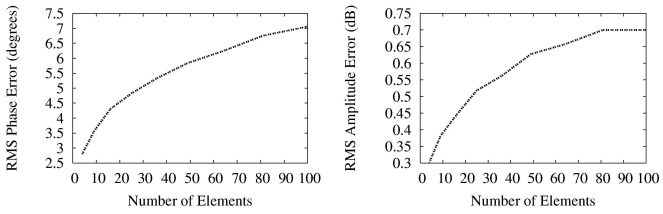

Fig. 10. Phase and amplitude calibration accuracy predicted by the rectilinear array simulation.

To put these figures into context we define two specifications. The first is a stringent phase and amplitude specification based on that of the TSUNAMI (II) array [4], whose amplitude and phasing specifications are maximum 3° peak phase error and 0.5 dB peak amplitude imbalance between any two elements. This is necessary to provide the -30 dB null depth specified for their project. Their hardware embodiment only ever met approximately 10° and 1 dB of imbalance at DCS 1800 frequencies. For a conventional (non-SDMA) tower-top replacement BTS, we define a looser specification of 5° RMS phase error and 1 dB amplitude.

Based on these specifications a provisional coupler accuracy can be generated for a given level of accuracy. Returning to our 30 element rectilinear array requires a coupler balance of 0.42 dB and 2° RMS. This results in a feedpoint calibration accuracy of 1 dB and 5° RMS. Similarly, to satisfy the more stringent SDMA calibration requirement, coupler balance of 0.4° RMS and 0.27 dB is needed, resulting in 0.5 dB and 3° calibration accuracy. Ways of relaxing this coupler balance specification by employing alternative calibration algorithms, are currently under study and will be the subject of future publication.

VI. The Effect of Calibration on Side-Lobe Level

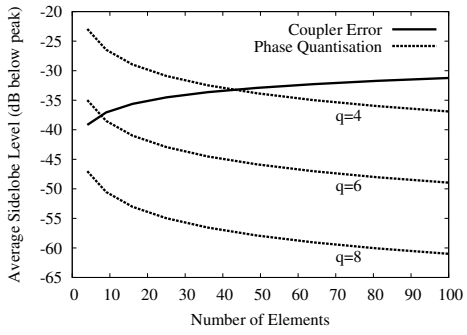

Fig. 11. Sidelobe level contributions due to the calibration scheme (predicted by equations 4 and 5) compared with that due to phase quantisation, note that 14 bit phase quantisation error $\leq$ -80 dB and is not visible on this scale.

To give some indication of the performance and further insight into the behaviour of our calibration scheme in a practical setting, we have taken the predictions of equations 4 and 5 and combined them with the method given by Mailloux [5], to predict the resultant mean sidelobe level due to calibration error. This was undertaken understanding that peak sidelobe level is the key sidelobe parameter for a static cellular systems. Typical cellular BTS antennas require a peak sidelobe level $\leq$ -20 dB, unfortunately we cannot reliably predict the peak sidelobe level from the statistically derived RMS sidelobe level.

Because sidelobe level is a function of array size we can see in figure 11 that the RMS sidelobe level tends towards -30dB below the main lobe radiation for our hypothetical 30 element rectilinear array. This, coincidentally, is the sidelobe level predicted (using the the same method) as for our 30 element linear array. For comparison the RMS sidelobe level due to phase quantisation is also shown in figure 11. This may also serve as some explanation for the limited effect of quantisation rounding, and justification for the exclusion of quantisation noise from our simulation, the average sidelobe level for 14 bit quantisation in the case of the 30 element array is -91.8 dB. The precise influence of quantisation on the accuracy of calibration will be the subject of future study.

VII. Conclusion

In this paper we have introduced a scalable array calibration scheme whose performance is limited by the phase and amplitude imbalance of the passive coupler network employed to couple transmitted power to a reference receiver. Furthermore, we have presented a theoretical basis for the limits of the performance of this system and have confirmed it by simulation in the regime, quantisation greater than 14 bits. This allowed us to derive calibration coupler requirements for both static (2° RMS and 0.42 dB) and SDMA (0.4° RMS and 0.27 dB) beamforming applications. Initial simulation, using the parameters of commercially available components, showed that arrays of up to 100 elements may be produced with a mean sidelobe level over 30 dB below the main lobe of radiation.

Acknowledgment

The authors would like to thank SFI for their generous funding of this project through the CTVR.

References

[1] UBE *Dielectric Ceramic Duplexer, Bandpass Filter Catalog*, Tokyo, Japan, 2006.

[2] Minicircuits, *RF/IC Designers Catalog*, SCN-2-11. New Jersey, USA, 2006.

[3] J.D. Kraus, *Antennas*, 2nd ed. New York, USA: Mc Graw Hill, 1988.

[4] Simmonds, C.M.; Beach, M.A., *"Downlink calibration requirements for the TSUNAMI (II) adaptive antenna testbed,"* Pers., Ind. and Mob. Rad. Comms., 1998. The Ninth IEEE Intl. Symp., vol.3, pp.1260-1264, Sep. 1998

[5] R.J. Mailloux, *Phased Array Antenna Handbook*, 2nd ed. London, England: Artech House, 1999.

A MULTI-PATH ALGORITHMIC APPROACH TO PHASED ARRAY CALIBRATION

Justine Mc Cormack, Tim Cooper and Ronan Farrell

Centre of Telecommunications Value Chain Research,
Institute of Microelectronics and Wireless Systems,
National University of Ireland Maynooth,
Co. Kildare, Ireland.
jmccormack@eeng.nuim.ie, tcooper@eeng.nuim.ie, rfarrell@eeng.nuim.ie

Keywords: Phase Array Antennas, Calibration, Tower-Top, Distributed Source Array, Autocalibration.

Abstract

The performance of phased arrays is dependent upon the amplitude and phase relationships between the elements of the array. In the presence of finite manufacturing tolerances and environmental effects these relationships cannot always be guaranteed, therefore synchronisation of these relationships is necessary. This paper presents an algorithmic approach to the calibration of these relationships, backed up with simulation results and comparisons.

1. Introduction

Adaptive antenna systems have been used for several years [10 – 11, 17]. Their performance is dependent upon the amplitude and phase relationships between elements [27], which are affected by multiple environmental effects and by manufacturing variations in system components. These effects cause imbalances in the amplitude and phase relationships from such potential causes as: thermal effects, antenna mutual coupling, component aging and finite manufacturing tolerances [1, 9, 21 - 23]. There are several different approaches taken to solving this synchronisation problem, which range from fixed feeder paths [2, 8, 14 – 15, 18, 25] to calibration algorithms [4 - 5, 19 – 22, 24, 26,]. Calibration algorithms are generally used in conjunction with fixed feeder paths, as the transceiver electronics located at the tower bottom also requires synchronisation. In situations where the transceiver electronics are connected directly to the antenna elements, synchronisation may only be achieved through the use of calibration algorithms. An example of such a setup is the tower top deployment of basestation electronics presented in [4 - 5].

This paper presents a calibration algorithm for a tower top system. The basestation electronics are deployed to the tower top, where each element of the array is connected to a transceiver element. The calibration algorithm uses additional distributed measurement elements and takes advantage of the structure of the array to minimise the complexity of the calibration challenge.

The paper is laid out as followed: section 2 presents an introduction to the tower top system. Which is followed by a description of the calibration algorithm in section 3. Finally an evaluation of the performance of the calibration algorithm is presented in section 4.

2. The Tower Top Antenna Array

A tower top system has the basestation electronics redeployed to the tower top, where each element of the array has its own transceiver element. These arrays are generally planar arrays from 16 to 64 elements, as planar arrays are more compact than circular arrays [6, 12]. Tower top array synchronisation is generally done by either radiative or non-radiative calibration.

The system presented here uses non-radiative calibration to remove the need for external calibration equipment. The calibration algorithm uses the structure of the array to simplify the calibration of large arrays. The array is a planar array interlaced with reference elements, as shown in figure 1. Each reference element is connected to four transceiver elements via directional couplers [3]. This interconnection structure provides at least one calibration path for each of the transceiver elements of the array. These calibration paths, as shown in figure 2, are completed by digital feedback from the reference element to each of the transceiver elements.

The planar array structure of the system can be considered in terms of building blocks. The array consists of reference elements; each reference element is surrounded by four transceiver elements. If you consider one reference element surrounded by the four transceiver elements as a single tile, then the whole array can be considered just a construct of overlapping tiles. The reason for considering the array in this way is that a single reference element surrounded by four elements is basically a circular array. The layout looks square but each of the antennas is equidistant from the reference element, thus describing a circle. The advantage of using small circular arrays and tiling them to produce a larger array is that the scaling problem of circular arrays is overcome. Circular arrays are difficult to scale for a number of reasons [6, 12] for example, the larger the array the more area the array requires [16], fixed feeder paths are required to connect each element to the central reference element which can require long looped cables, and there is also a physical limitation to the number of connections a single reference element can handle. Thereby tiling small circular arrays together a scalable array can be constructed with a scalable calibration mechanism.

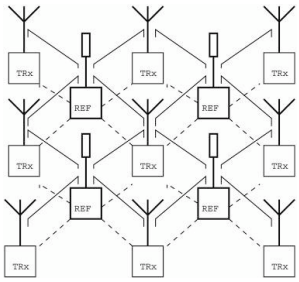

Figure 1: Tower-Top, Cellular, Phased Array Antenna System.

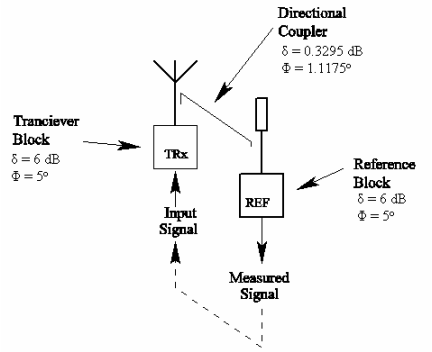

Figure 2: The Calibration Path of an Antenna Element.

3. Algorithmic Approaches

The algorithmic approach presented in this paper is compared with the shortest path algorithm, the best performing algorithm presented to date for this structure [4]. Both algorithms are based upon comparisons between elements, so a brief description of the shortest path algorithm is presented first, followed by a description of the new algorithm and a comparison of the simulation results of both algorithms.

3.1 Shortest Path Calibration Algorithmic Approach

The shortest path algorithm is based upon comparisons between elements. These comparisons start out from a reference transceiver element in the array; this element is measured by a reference element connected to it. Then another element connected directly to the same reference element is measured. The measured signals are then compared; the correction factor from this comparison is feed back into the second element to calibrate it to the reference transceiver element. These comparisons are continued throughout the array, by using intermediate reference transceiver elements and by calibrating around the reference elements in a similar way. This has the effect of removing the imbalances in the amplitude and phase relationships of the array due to the reference blocks, as each of the comparisons use measurements taken from the same reference elements. The reference element variations for the two compared measurements are the same so the reference element variations do not affect the correction factors. The comparisons also have the effect of removing individual transceiver block variations, as the comparisons of the transceiver elements are corrected to the reference transceiver' specific imbalance.

The elimination of the component block variations is only possible if the measurement taken by the reference blocks is accurate. This accuracy is affected by not only the measurement but also by the resolution of the analog to digital converters (ADC), because of the digital feedback of the system. These challenges can be over come by using high resolution ADCs in conjunction with a measurement technique such as cordic [19], or by themselves. However these issues will not be discussed in detail as they are beyond the scope of this paper.

Due to the elimination of the component block variations, the overall array variation is dependent on the number of coupler variations that affect each element of the array, due to its correction factor. The correction factor generated from each comparison includes a coupler variation. This coupler variation is a composite of the coupler variations included in each of the measured signals in the comparison. As the number of comparisons required to calibrate the whole array increases, so does the number of coupler variations included in the correction factors, therefore the longer the calibration trail is to an element, the more coupler errors included in its correction factor. So each element's accuracy is dependent on its correction factor, the further away it is from the reference transceiver element, the greater the number of coupler variations that affect it, and the less accurate it is.

The accuracy of the array is dependent upon the number of couplers along the calibration trials from the reference transceiver elements to rest of the array. The accuracy can be improved by shortening the length of these paths, so by moving the reference transceiver element to the center of the array, the maximum distance from the reference transceiver element is shortened. By only calibrating previously uncalibrated elements the accuracy of the calibration is also improved, as calibrated elements are not recalibrated with less accurate correction factors due to longer paths.

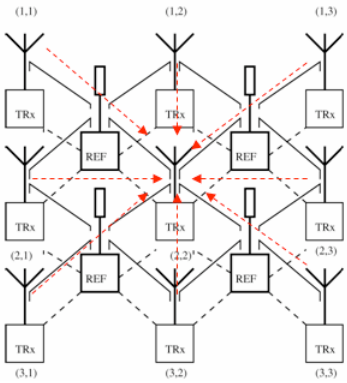

Figure 3: Comparison of the shortest path algorithm on a 3x3 array.

The shortest path algorithm calibrates the shortest path to each element, as shown in figure 3, for a three by three array. The shortest path algorithm calibrates in rings around the reference transceiver element, calibrating the elements directly connected to the reference transceiver element to it. Then as it moves further out, the next ring of elements are calibrated to the ring of previously calibrated elements directly connected to them, and so forth until the entire array is calibrated. This has the advantage of calibrating each

element along the shortest route from the reference transceiver element to it, and only calibrating each element once. This type of comparison algorithm maximises the performance of a single step comparison approach.
The accuracy of this algorithm can be predicted by calculating the number of couplers which affect each element of the array. The following expressions present in terms of odd and even *n*, $n^2 = N$, *N* is the number of elements in the array.
Even *n*:

$$\sigma_{ak}^2 = \left(\frac{\sigma_{ck}^2}{N-1}\sum_{i=1}^{\frac{n}{2}-1} 8i^2\right) + \left(\frac{2n-1}{N-1}\right)\left(\frac{n}{2}\right)\sigma_{ck}^2 \quad (1)$$

Odd *n*:

$$\sigma_{ak}^2 = \left(\frac{\sigma_{ck}^2}{N-1}\sum_{i=1}^{\frac{n-1}{2}} 8i^2\right) \quad (2)$$

Where, σ_{ak}^2 and σ_{ck}^2 are the RMS array variance and the RMS coupler variance respectively.

3.2 Dual Path Calibration Algorithmic Approach

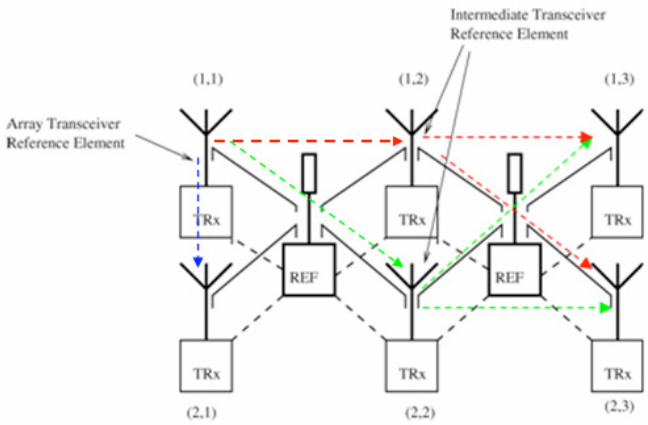

Figure 4: Dual Path Calibration Comparisons for a 2x3 Array.

This proposed algorithm differs from other comparison based algorithms as it takes two routes to elements, where available, in order to reduce the effect of the coupler variation. This is achieved by taking two routes of the same length to any element, as shown in figure 4. The elements directly connected to the reference transceiver element are calibrated directly to the reference transceiver element, the same way as the shortest path algorithm. The elements further away are calibrated using two paths of the same length, each of these paths generate a correction factor for the element they are calibrating. These correction factors are averaged; thus statistically reducing the effect of couplers along the routes. This averaging reduces the effect of outlier coupler elements, but can also increase the variation of couplers with very small variations.
As the accuracy of the algorithm is affected by the coupler variations, the algorithm's accuracy can be predicted by calculating the number of coupler variations that affect each element of the array. The following expressions calculate the accuracy of the array relative to the reference transceiver element, which is not affected by coupler variations. The representation of the array in this way is conveniently expressed in terms of odd and even *n*, where $n^2 = N$, *N* is the number of elements in the array.
Even *n*:

$$\sigma_{ak}^2 = \left(\frac{8\sigma_{ck}^2}{N-1}\right) + \left(\frac{\bar{\sigma}_{ck}^2}{N-1}\sum_{i=2}^{\frac{n}{2}-1} 8i^2\right) + \left(\frac{2n-1}{N-1}\right)\left(\frac{n}{2}\right)\bar{\sigma}_{ck}^2 \quad (3)$$

Odd *n:*

$$\sigma_{ak}^2 = \left(\frac{8\sigma_{ck}^2}{N-1}\right) + \left(\frac{\bar{\sigma}_{ck}^2}{N-1}\sum_{i=2}^{\frac{n-1}{2}} 8i^2\right) \quad (4)$$

Where σ_{ak}^2 and σ_{ck}^2 are the RMS array variance and the RMS coupler variance respectively and $\bar{\sigma}_{ck}^2$ is the averaged RMS coupler variance. The first term in each expression represent the eight elements directly connected to the reference transceiver element, and are calibrated by only one path each. For small array sizes less than a 4x4 array, the performance of the single-path algorithm (1,2) and that of the dual-path approach (3,4) are the same, as all elements are directly connected to the reference transceiver and thus can only be calibrated along one path. As the size of the array increases then the number of coupler variations increase, this is a straight forward calculation for the shortest path algorithm prediction equations (1) and (2). However, for the dual path algorithm prediction equations (3) and (4) the calculation is slightly different. The first term in equation (3) and (4) is a calculation of the eight elements of the array directly surrounding the central reference transceiver element; which is calibrated by a single path. The remaining elements of the array are calibrated by dual paths. From (3) and (4) the second and third terms calculate the number of elements calibrated by averaged coupler variations.

4. Simulation Results

Both algorithms have been simulated using Matlab, and have been implemented on a Matlab model, where each of the antenna chains is composed of component blocks of the system, as shown in figure 2, which are given a random variation in line with the manufacturing tolerances of that particular component block, as shown in table 1. Each transceiver is feed with a 20 dB signal that varies with a 0.5 dB standard deviation, and a random phase. These are the base components of the models upon which simulations of the algorithms were performed.

Component (i,j)	$\mu_{(i,j)\,A}$	$\Sigma_{(i,j)\,A}$	$\mu_{(i,j)\Phi}$	$\Sigma_{(i,j)\Phi}$
Tx S21	50 dB	3 dB	10^o	5^o
Ref S21	60 dB	6 dB	85^o	5^o
Coupler S21	-20.3295 dB	0.3295 dB	90.197^o	1.1175^o

Table 1: Component Block Imbalances.

4.1 Comparison of Theory and Simulation

Ten thousand simulations of the dual path algorithm were run to give a statistically significant result for square arrays ranging in size from a 2x2 array to a 10x10 array. These simulations were compared to the predicted accuracy of the dual path algorithm as estimated by (3) and (4). This comparison is shown in figure 5. Due to the prediction equations being based upon standard deviations of the couplers, the averaged coupler terms are estimated by a percentage reduction in the coupler standard deviation. The percentage reduction is calculated based upon size of the array, and therefore scales up as the size of the array increases. As can be seen in figure 5, this is a good approximation of the accuracy of the algorithm. The RMS array error increases as the size of the array increases due to the dependency of the array accuracy on coupler variations.

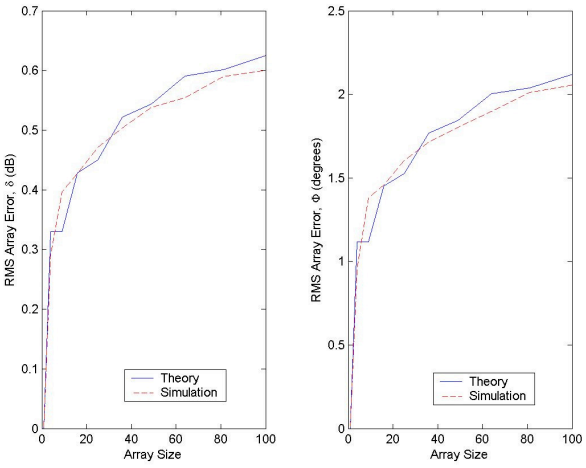

Figure 5: The overall array calibration accuracy predicted by equation 1 and 2 and calibration simulations.

4.2 Comparison of the Two Calibration Algorithms Simulation Results

A comparison between the two algorithms, shortest path algorithm and dual path algorithm, is presented in figure 6. Again 10,000 simulations of each size array are taken as a statistically significant measure. These results show that as the size of the array increases so does the RMS array error, as the calibration routes increase for each element, the more coupler variations that are included. Figure 6 clearly shows that as the size of the array increases so does the dual path algorithm performs improve in comparison to the shortest path algorithm performance. This is due to both algorithms performance being dependent upon the number of coupler variations included in each element's correction factors. The dual path algorithm however uses an averaging of two paths of identical lengths to reduce the effect of the coupler variations, which will have more of an effect on the output of larger arrays as dual path calibration will be performed on proportionally more elements.

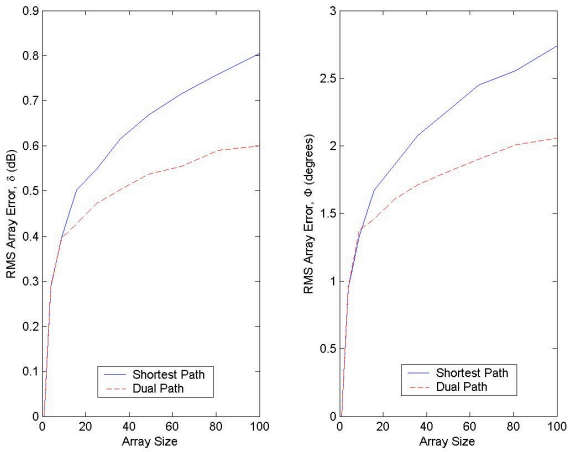

Figure 6: Comparison of RMS Array Error of Shortest Path and Dual Path Calibration Algorithms, as the Size of the Array increases.

A comparison of the number of elements that fall within the absolute array variations is shown in figures 7 and 8. This is based upon 10,000 simulations of a five by five array. The results are consistent with the previous set of comparison results, as the first 30% of elements (approximately 8 elements per array) are exactly the same as that of the shortest path. Which is consistent with the two algorithms, as they both share a ring of elements that surround the reference transceiver element that are calibrated in exactly the same way. The results diverge at this point, which is consistent with the dual path averaging of the correction paths to reduce the overall error.

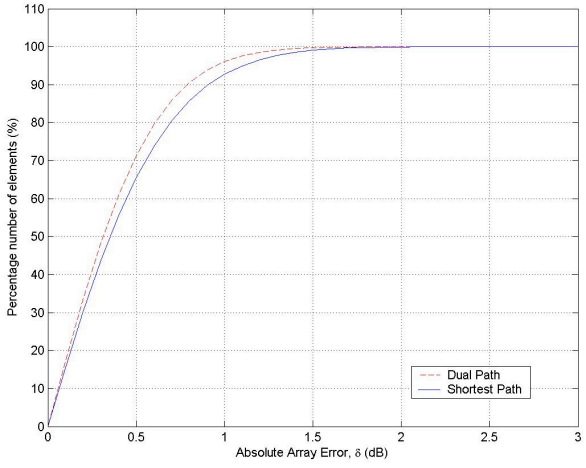

Figure 7: Percentage Number of Elements vs. the Absolute Amplitude Variation.

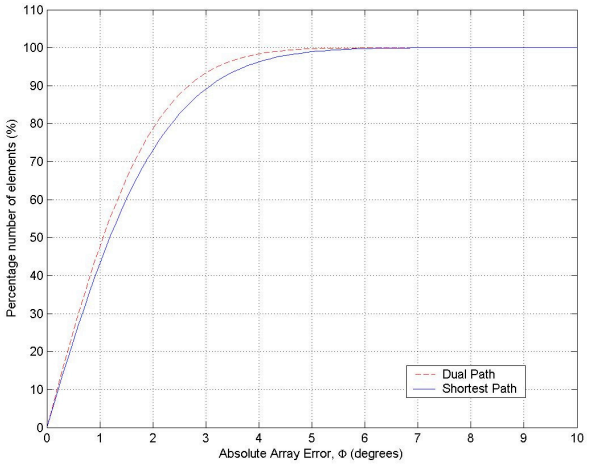

Figure 8: Percentage Number of Elements vs. the Absolute Phase Variation

5. Conclusions

Synchronisation of phased arrays is of vital importance to the performance of the array. This synchronisation can be achieved through a combination of, or solely by, fixed feeder networks and calibration algorithms. This paper focuses on novel calibration algorithms that utilises the tessellated structure of rectilinear arrays. A scalable method was presented for calibrating planar arrays using a built-in non-radiative calibration mechanism. The structure of the array provides multiple calibration paths for the elements of the array. The dual path algorithm utilises these multiple paths to improve the accuracy of the array. The dual path algorithm presented simulation results that show improvement over the previously presented shortest path calibration algorithm for this system. It shows a marked improvement as the array size increases, to an improvement of up to 0.2047 dB and 0.6833^{o}. This improvement is down to the reduction of the directional coupler variation effect on the RMS array error variation, by averaging two paths of the same length to achieve this reduction. Future work will focus on the implementation of a 4x4 array prototype.

Acknowledgements

Special thanks to Science Foundation Ireland (SFI) for their generous funding of this project through the Centre of Telecommunications Value Chain Research (CTVR).

References

[8] M. Adibi, K. Clements, R. Kafka and J. Stoval. "Remote Measurement Calibration", *IEEE Computer Applications in Power, Vol. 3, Iss. 4, Oct. 1994,* pp. 37 - 42.

[12] D. C. Chang, S. H. Jou, "The study of Butler Matrix BFN for 4 Beams Antennas System", *IEEE International Symposium on Antennas and Propagation, Vol. 4, June 2003,* pp. 176 - 179.

[23] T. S. Cooper, G. Baldwin and R. Farrell "Six – port Precession Directional Coupler", *Electronic Letters, Vol. 42, No. 21, 12 Oct. 2006,* pp. 1232 - 1234.

[17] T. S. Cooper, J. Mc Cormack, R. Farrell and G. Baldwin. "Towards Scalable, Automated Tower – Top Phased Array Calibration", *in Vehicular Technology Conference, Dublin Ireland April 23 – 25, 2007.*

[16] T. S. Cooper, J. Mc Cormack, and R. Farrell. "Tower – Top Antenna Array Calibration Scheme for Next Generation Networks", *Eurosip 2007,* accepted.

[25] E. D. Di Claudio, "Asymptotically Perfect Wideband Focusing of Multi-ring Circular Array", *IEEE Trans. On Signal Processing, Vol. 53, No. 10, Oct. 2005,* pp. 3661 - 3673.

[22] L.C. Godara "Smart Antennas", *CRC Press LLC, 2004,* pp. 325 - 348.

[11] H. Hayashi, D. A. Hitko, C. G. Sodini, "Four – Element Planar Butler Matrix using half – wavelength open stubs", *IEEE microwave and wireless components letters, Vol. 12, No. 3, March 2002.*

[7] I. Jonsdottir and A. Hanksdottir. "Integrity Monitoring and Estimation of Systematic Errors in Radar Data Systems", *IEEE Int. Radar Conference,* May 1995, pp. 310 - 316.

[2] T. Kaiser, et el. "When will smart antennas be ready for market? Part 1", *IEEE Signal Processing Magazine,* pp. 87 - 92, March (2005).

[3] T. Kaiser, et el. "When will smart antennas be ready for market? Part 2 - Results", *IEEE Signal Processing Magazine,* pp. 174 - 176, November (2005).

[24] M. Latman, "Circular Array STAP", *IEEE Trans. On Aerospace and Electronic Systems, Vol. 36, No. 2, April 2000,* pp. 510 - 517.

[21] R. J. Mailloux, "A Phased Array Error Correction Scheme", *International Symposium on Antennas and Propagation Society, Vol. 1, June 1993,* pp. 202 - 205.

[14] S. Mosca, F. Bilotti, A. Toscano and L. Vegni "A Novel Design Method for Blass Matrix Beamforming Networks", *IEEE Trans. On Antennas and Propagation, Vol. 50, No. 2, Feb 2002.*

[10] H. Nord, "Implementation of 8x8 – Butler Matrix in Microstrip", *Diploma Thesis, Royal Institute of Technology Stockholm, Germany 2000.*

[26] C. C. Phillips, "A New Approach to Antenna Beam-Shaping – The 'Coke - Bottle' Antennas", *WESCON/60 Conference Record, Vol. 4, Part 1, Aug. 1960,* pp. 74 - 82.

[1] F. Rayal. "Why have smart antennas not yet gained traction with wireless network operators?", IEEE *Antennas and Propagation Magazine*, **Vol 47**, No. 6, pp. 124 - 126, Dec (2005).

[13] K. Shetty, "A Novel Algorithm for Uplink Interference Suppression using Smart Antennas in Mobile Communications", *Masters of Science Thesis, Florida State University 2004.*

[27] C. Shipley and D. Woods, "Mutual Coupling – Based Calibration of Phased Array Antennas", *IEEE International Conference on Phased Array Systems and Technology, 21 – 25 May 2000,* pp. 529 - 532.

[20] K. Takao, M. Fujita and T. Nishi, "An Adaptive Antenna Array under Directional Constraint", *IEEE Trans. On*

Antennas and Propagation, Vol. AP - 24, No. 5, Sept. 1976.

[5] G. Tsoulos, J. McGeehan, M. Beach. "Space Division Multiple Access (SDMA) Field Trials. Part 2: Calibration and Linearity Issues", *IEE Proc. Radar, Sonar Navig. Vol. 145, No. 1,* pp., February (1998).

[6] N. Tyler, B. Allen and H. Aghvami. "Adaptive Antennas: The Calibration Problem", *IEEE Comms. Magazine, Vol. 42, Iss. 12, Dec. 2004,* pp. 114 - 122.

[9] N. Tyler, B. Allen, A. H. Aghvami. "Calibration of Smart Antenna Systems: Measurements and Results", *IET Microwaves, Antennas and Propagation, Vol. 7, Iss. 3, June 2007,* pp. 629 - 638.

[19] B. O. Van Veen and K. M. Buckley, "Beamforming: A Versatile Approach to Spatial Filtering", *IEEE ASSP Magazine, Vol. 5, Iss. 2, April 1988,* pp. 4 - 24.

[15] S. L. Vetterlein, P. S. Hall, "Multiple Beam Microstrip Patch Array with Integrated Beamformer", *IEE Proceedings, Vol. 138, No. 2, April 1991*.

[18] J. E. Volder, "The CORDIC Trigonometric Computing Technique", *IRE Trans. Comp., Vol. EC-8, No. 3, 1959,* pp. 330 - 334.

[4] H. S. C. Wang, "Performing of Phased Array Antennas under Error Conditions", *IEEE Aerospace applications Conference Digest.* 12 – 17 Feb. 1989*,* pp. 1 - 25.

Hindawi Publishing Corporation
EURASIP Journal on Wireless Communications and Networking
Volume 2007, Article ID 41941, 12 pages
doi:10.1155/2007/41941

Research Article

Tower-Top Antenna Array Calibration Scheme for Next Generation Networks

Justine McCormack, Tim Cooper, and Ronan Farrell

Centre for Telecommunications Value-Chain Research, Institute of Microelectronics and Wireless Systems, National University of Ireland, Kildare, Ireland

Received 1 November 2006; Accepted 31 July 2007

Recommended by A. Alexiou

Recently, there has been increased interest in moving the RF electronics in basestations from the bottom of the tower to the top, yielding improved power efficiencies and reductions in infrastructural costs. Tower-top systems have faced resistance in the past due to such issues as increased weight, size, and poor potential reliability. However, modern advances in reducing the size and complexity of RF subsystems have made the tower-top model more viable. Tower-top relocation, however, faces many significant engineering challenges. Two such challenges are the calibration of the tower-top array and ensuring adequate reliability. We present a tower-top smart antenna calibration scheme designed for high-reliability tower-top operation. Our calibration scheme is based upon an array of coupled reference elements which sense the array's output. We outline the theoretical limits of the accuracy of this calibration, using simple feedback-based calibration algorithms, and present their predicted performance based on initial prototyping of a precision coupler circuit for a 2×2 array. As the basis for future study a more sophisticated algorithm for array calibration is also presented whose performance improves with array size.

1. INTRODUCTION

Antennas arrays have been commercially deployed in recent years in a range of applications such as mobile telephony, in order to provide directivity of coverage and increase system capacity. To achieve this, the gain and phase relationship between the elements of the antenna array must be known. Imbalances in these relationships can arise from thermal effects, antenna mutual coupling, component aging, and finite manufacturing tolerance [1]. To overcome these issues, calibration is required [2, 3]. Traditionally, calibration would have been undertaken at the manufacturer, address static effects arising from the manufacturing tolerances. However, imbalances due to dynamic effects require continual or dynamic calibration.

Array calibration of cellular systems has been the subject of much interest over the last decade (e.g., [4–6]), and although many calibration processes already exist, the issue of array calibration has, until now, been studied in a "tower-bottom" smart antenna context (e.g., tsunami(II) [2]). Industry acceptance of smart antennas has been slow, principally due to their expense, complexity, and stringent reliability requirements. Therefore, alternative technologies have been used to increase network performance, such as cell splitting and tower-bottom hardware upgrades [7, 8].

To address the key impediments to industry acceptance of complexity and expense, we have been studying the feasibility of a self-contained, self-calibrating "tower-top" base transceiver station (BTS). This system sees the RF and mixed signal components of the base station relocated next to the antennas. This provides potential capital and operational savings from the perspective of the network operator due to the elimination of the feeder cables and machined duplexer filter. Furthermore, the self-contained calibration electronics simplify the issue of phasing the tower-top array from the perspective of the network provider.

Recent base station architectures have seen some departure from the conventional tower-bottom BTS and tower-top antenna model. First, amongst these was the deployment of tower-top duplexer low-noise amplifiers (TT-LNA), demonstrating a tacit willingness on the part of the network operator to relocate equipment to the tower-top if performance gains proved adequate and sufficient reliability could be achieved [9]. This willingness can be seen with the

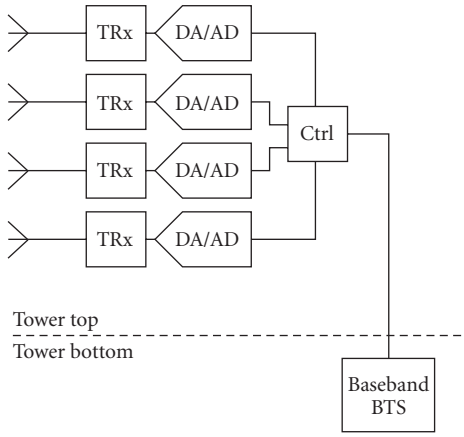

Figure 1: The hardware division between tower top and bottom for the tower-top BTS.

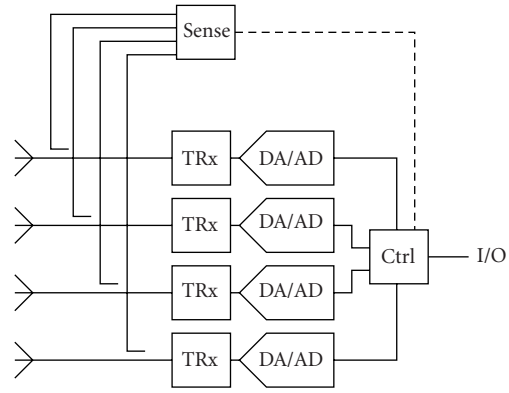

Figure 2: A simplified block schematic diagram of a typical array calibration system.

exploration of novel basestation architectures, with examples such as reduced RF feeder structures utilising novel switching methodologies [10, 11], and the development of basestation hotelling with remote RF heads [12]. Such approaches aim to reduce capital infrastructure costs, and also site rental or acquisition costs [13].

In this paper, we present our progress toward a reliable, self-contained, low-cost calibration system for a tower-top cellular BTS. The paper initially presents a novel scheme for the calibration of an arbitray-sized rectilinear array using a structure of interlaced reference elements. This is followed in Section 3 by a theoretical analysis of this scheme and predicted performance. Section 4 presents a description of a prototype implementation with a comparison between experimental and predicted performance. Section 5 presents some alternative calibration approaches utilising the same physical structure.

2. RECTILINEAR ARRAY CALIBRATION

2.1. Array calibration

To yield a cost-effective solution for the cellular BTS market, we have been studying the tower-top transceiver configuration shown in Figure 1. This configuration has numerous advantages over the tower-bottom system but, most notably, considerably lower hardware cost than a conventional tower-bottom BTS may be achieved [14].

We define two varieties of array calibration. The first, radiative calibration, employs free space as the calibration path between antennas. The second, where calibration is performed by means of a wired or transmission line path and any radiation from the array in the process of calibration is ancillary, is refered to as "nonradiative" calibration. The setup of Figure 2 is typically of a nonradiative calibration process [2]. This process is based upon a closed feedback loop between the radiative elements of the array and a sensor. This sensor provides error information on the array output and generates an error signal. This error signal is fed back to correctively weight the array element's input (transmit calibration) or output (receive calibration). It is important to observe that this method of calibration does not correct for errors induced by antenna mutual coupling. Note that in our calibration scheme, a twofold approach will be taken to compensate for mutual coupling. The first is to minimise mutual coupling by screening neighbouring antennas—and perhaps using electromagnetic (EM) bandgap materials to reduce surface wave propagation to distant antennas in large arrays. The second is the use of EM modelling-based mitigation such as that demonstrated by Dandekar et al. [6]. Further discussion of mutual coupling compensation is beyond the scope of this paper.

While wideband calibration is of increasing interest, it remains difficult to implement. On the other hand, narrowband calibration schemes are more likely to be practically implemented [1]. The calibration approach presented here is directed towards narrowband calibration. However, the methodology supports wideband calibration through sampling at different frequencies.

2.2. Calibration of a 2×2 array

Our calibration process employs the same nonradiative calibration principle as shown in Figure 2. The basic building block, however, upon which our calibration system is based is shown in Figure 3. This features four radiative array transceiver elements, each of which is coupled by transmission line to a central, nonradiative reference element.

In the case of transmit calibration (although by reciprocity receive calibration is also possible), the transmit signal is sent as a digital baseband signal to the tower-top and is split (individually addressed) to each transmitter for SISO (MIMO) operation. This functionality is subsumed into the control (Ctrl) unit of Figure 3.

Remaining with our transmit calibration example, the reference element sequentially receives the signals in turn from the feed point of each of the radiative array elements. This enables the measurement of their phase and amplitude relative to some reference signal. This information on the

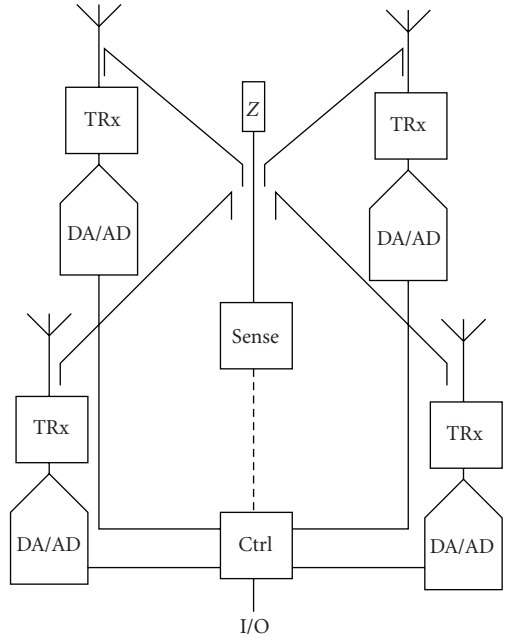

Figure 3: A central, nonradiative reference sensor element coupled to four radiative array transceiver elements.

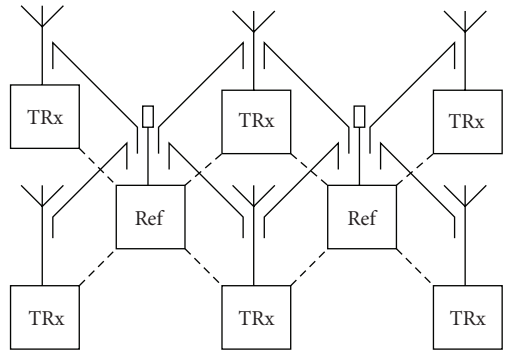

Figure 4: A pair of reference elements, used to calibrate a 2×3 array.

relative phase and amplitude imbalance between the feed points of each of the transceivers is used to create an error signal. This error signal is fed back and used to weight the input signal to the transceiver element—effecting calibration. Repeating this procedure for the two remaining elements calibrates our simple 2×2 array. This baseband feedback system is to be implemented in the digital domain, at the tower-top. The functionality of this system and the attendant computing power, energy, and cost requirements of this system are currently under investigation.

2.3. Calibration of an $n \times n$ array

By repeating this basic 2×2 pattern with a central reference element, it becomes possible to calibrate larger arrays [15]. Figure 4 shows the extension of this basic calibration principle to a 2×3 array.

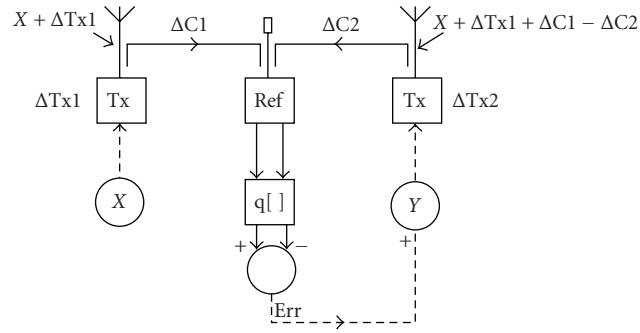

Figure 5: Propagation of error between calibrating elements.

To calibrate a large, $n \times n$, antenna array, it is easy to see how this tessellation of array transceivers and reference elements could be extended arbitrarily to make any rectilinear array geometry.

From the perspective of a conventional array, this has the effect of interleaving a second array of reference sensor elements between the lines of radiative transceiver elements, herein referred to as "interlinear" reference elements, to perform calibration. Each reference is coupled to four adjacent radiative antenna elements via the six-port transmission line structure as before. Importantly, because there are reference elements shared by multiple radiative transceiver elements, a sequence must be imposed on the calibration process. Thus, each transceiver must be calibrated relative to those already characterised.

Cursorily, this increase in hardware at the tower-top due to our interlinear reference elements has the deleterious effect of increasing the cost, weight, and power inefficiency of the radio system. The reference element hardware overhead, however, produces three important benefits in a tower-top system: (i) many shared reference elements will enhance the reliability of the calibration scheme—a critical parameter for a tower-top array; (ii) the array design is inherently scalable to large, arbitrary shape, planar array geometries; (iii) as we will show later in this paper, whilst these reference nodes are functional, the multiple calibration paths between them may potentially be used to improve the calibration accuracy of the array. For now, however, we consider basic calibration based on a closed loop feedback mechanism.

3. RECTILINEAR CALIBRATION—THEORY OF OPERATION

3.1. Basic calibration

Figure 5 shows a portion of an $n \times n$ array where two of the radiative elements of our array are coupled to a central reference transceiver. As detailed in Section 2.2, the calibration begins by comparing the output of transceiver 1 with transceiver 2, via the coupled interlinear reference element. Assuming phase only calibration of a SISO system, at a single frequency and with perfect impedance matching, each of the arbitrary phase errors incured on the signals, that are sent through the calibration system, may be considered additive

constants (Δi, where i is the system element in question). Where there is no variation between the coupled paths and the accuracy of the phase measurement process is arbitrarily high, then, as can be seen in Figure 5, the calibration process is essentially perfect.

However, due to finite measurement accuracy and coupler balance, errors propagate through the calibration scheme. Initial sensitivity analysis [16] showed that when the resolution of the measurement accuracy, q[ ], is greater than or equal to 14 bits (such as that attainable using modern DDS, e.g., AD9954 [17] for phase control), the dominant source of error is the coupler imbalance.

From Figure 5 it is clear that an error, equal in magnitude to the pair of coupler imbalances that the calibration signal encounters, is passed on to the feed point of each calibrated transceiver. If this second transceiver is then used in subsequent calibration operations, this error is passed on. Clearly, this cumulative calibration error is proportional to the number of the calibration couplers in a given calibration path. For simple calibration algorithms such as that shown in Figure 5, the array geometry and calibration path limit the accuracy with which the array may be calibrated.

3.2. Theoretical calibration accuracy

3.2.1. Linear array

Figure 6(a) shows the hypothetical calibration path taken in phasing a linear array of antennas. Each square represents a radiative array element. Each number denotes the number of coupled calibration paths accrued in the calibration of that element, relative to the first element numbered 0 (here the centremost). If we choose to model the phase and amplitude imbalance of the coupler (σ_{c_k}) as identically distributed Gaussian, independent random variables, then the accuracy of calibration for the linear array of N elements relative to the centre element, σ_{a_k}, will be given by the following:

even N:

$$\sigma_{a_k}^2 = \frac{2\sigma_{c_k^2}}{N-1}\sum_{i=1}^{N/2} 2i, \tag{1}$$

odd N:

$$\sigma_{a_k}^2 = \frac{2\sigma_{c_k^2}}{N-1}\left(\left[\sum_{i=1}^{N/2} 2i\right] + 1\right), \tag{2}$$

where the subscript $k = A$ or ϕ for amplitude or phase error. With this calibration topology, linear arrays are the hardest to accurately phase as they encounter the highest cumulative error. This can be mitigated in part (as shown here) by starting the calibration at the centre of the array.

3.2.2. Square array

Based on this observation, a superior array geometry for this calibration scheme is a square. Two example square arrays calibration methods are shown in Figures 6(b) and 6(c). The former initiates calibration relative to the top-left hand transceiver element. The calibration path then propagates down through to the rest of the array taking the shortest path possible. Based upon the preceding analysis, the predicted calibration accuracy due to coupler imbalance of an $n \times n$ array is given by

$$\sigma_{a_k}^2 = \frac{2\sigma_{c_k}^2}{N-1}\sum_{i=1}^{n}(2i-1)(i-1) \tag{3}$$

with coupler error variance $\sigma_{c_k}^2$, centred around a mean equal to the value of the first element.

Figure 6(c) shows the optimal calibration path for a square array, starting at the centre and then radiating to the periphery of the array by the shortest path possible. The closed form expressions for predicting the overall calibration accuracy of the array relative to element 0 are most conveniently expressed for the odd and even n, where $n^2 = N$:

even n:

$$\sigma_{a_k}^2 = \frac{2\sigma_{c_k}^2}{N-1}\left(\left[\sum_{i=1}^{n/2-1}(8i)(2i)\right]\right) + \frac{2n-1}{N-1}n\sigma_{c_k}^2, \tag{4}$$

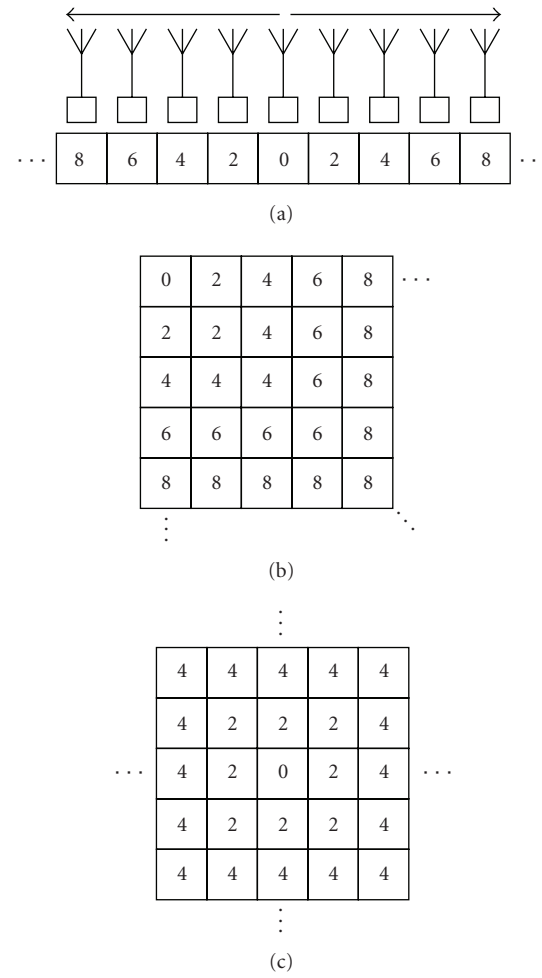

Figure 6: Calibration paths through (a) the linear array. Also the square array starting from (b) the top left and (c) the centre of the array.

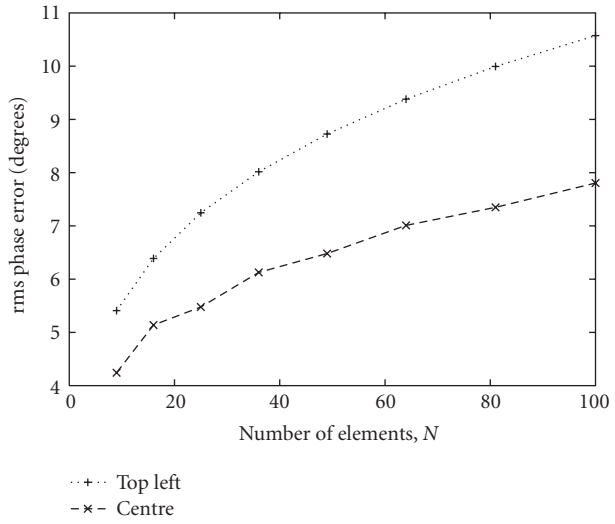

Figure 7: Comparison of the theoretical phase accuracy predicted by the closed form expressions for the square array calibration schemes, with $\sigma_{c_\phi} = 3^\circ$.

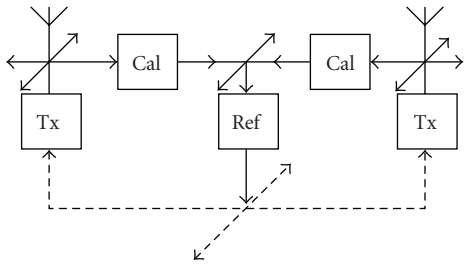

Figure 8: Block schematic diagram of the array calibration simulation used to test the accuracy of the theoretical predictions.

odd n:

$$\sigma_{a_k}^2 = \frac{2\sigma_{c_k}^2}{N-1} \sum_{i=1}^{n/2-1/2} (8i)(2i). \tag{5}$$

A graph of the relative performance of each of these two calibration paths as a function of array size (for square arrays only) is shown in Figure 7. This shows, as predicted, that the phasing error increases with array size. The effect of this error accumulation is reduced when the number of coupler errors accrued in that calibration is lower—that is, when the calibration path is shorter. Hence, the performance of the centre calibrated array is superior and does not degrade as severely as the top-left calibrated array for large array sizes.

As array sizes increase, the calibration path lengths will inherently increase. This will mean that the outer elements will tend to have a greater error compared to those near the reference element. While this will have impact on the array performance, for example, in beamforming, it is difficult to quantify. However, in a large array the impact of a small number of elements with relatively large errors is reduced.

Table 1

Component (i)	μ_{i_A}	σ_{i_A}	μ_{i_ϕ}	σ_{i_ϕ}
Tx S_{21}	50 dB	3 dB	10°	20°
Ref S_{21}	60 dB	3 dB	85°	20°
Cal S_{21}	−40 dB	0.1 dB	95°	3°

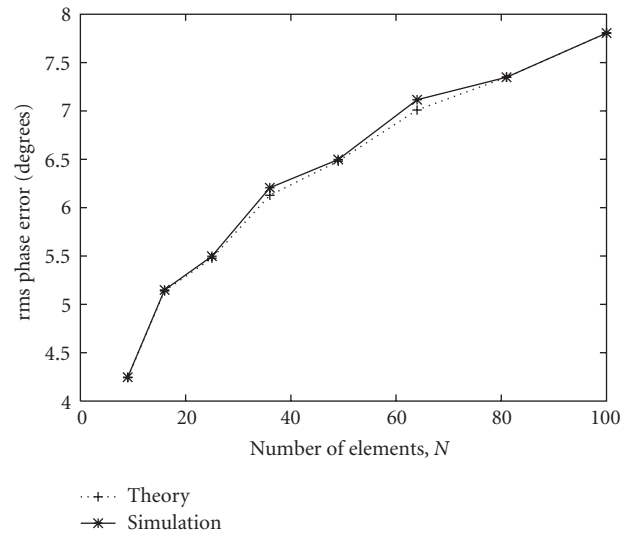

Figure 9: The overall array calibration accuracy predicted by (4) and the calibration simulation for $\sigma_{c_\phi} = 3^\circ$.

3.3. Simulation

3.3.1. Calibration simulation system

To determine the accuracy of our theoretical predictions on array calibration, a simulation comprising the system shown in Figure 8 was implemented. This simulation was based on the S-parameters of each block of the system, again assuming perfect impedance matching and infinite measurement resolution. Attributed to each block of this schematic was a mean performance (μ_{i_k}) and a normally distributed rms error (σ_{i_k}), which are shown in Table 1.

3.3.2. Results

For each of the square array sizes, the results of 10 000 simulations were complied to obtain a statistically significant sample of results. For brevity and clarity, only the phase results for the centre-referenced calibration are shown, although comparable accuracy was also attained for both the amplitude output and the "top-left" algorithm. Figure 9 shows the phase accuracy of the centre-referenced calibration algorithm. Here we can see good agreement between theory and simulation. The reason for the fluctuation in both the theoretical and simulated values is because of the difference between the even and odd n predictions for the array accuracy. This difference arises because even n arrays do not have a centre element, thus the periphery of the array farthest from the nominated centre element incurs slightly higher error.

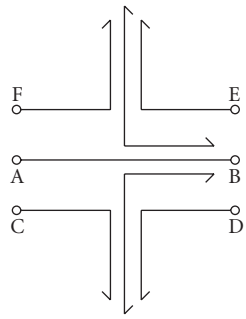

Figure 10: Schematic representation of the six-port, precision directional coupler.

3.3.3. Practical calibration accuracy

These calibration schemes are only useful if they can calibrate the array to within the limits useful for adaptive beamforming. The principle criterion on which this usefulness is based is on meeting the specifications of 1 dB peak amplitude error and 5° rms phase error [16]. The preceding analysis has shown that, in the absence of measurement error,

$$\lim_{\sigma_c \to 0} \sigma_a \longrightarrow 0, \tag{6}$$

where σ_a is the rms error of the overall array calibration error. Because of this, limiting the dominant source of phase and amplitude imbalance, that of the array feed-point coupler structure, will directly improve the accuracy of the array calibration.

4. THE CALIBRATION COUPLER

4.1. 2×2 array calibration coupler

The phase and amplitude balance of the six-port coupler structure at the feed point of every transceiver and reference element in Figure 4 is crucial to the performance of our calibration scheme. This six-port coupler structure is shown schematically in Figure 10. In the case of the reference element, the output (port B) is terminated in a matched load (antenna) and the input connected to the reference element hardware (port A). Ports C−F of the coupler feed adjacent transceiver or reference elements. Similarly, for the radiative transceiver element, port B is connected to the antenna element and port A the transceiver RF hardware. For the individual coupler shown in Figure 10 using conventional low-cost, stripline, board fabrication techniques, phase balance of 0.2 dB and 0.9° is possible [18]. By interconnecting five of these couplers, then the basic 2×2 array plus single reference sensor element building block of our scheme is formed. It is this pair of precision six-port directional couplers whose combined error will form the individual calibration paths between transceiver and reference element.

A schematic representation of the 2×2 array coupler is shown in Figure 11. This forms the feed-point coupler structure of Figure 4, with the central coupler (port 1) connected to the reference element and the load (port 2). Each peripheral couplers is connected to a radiative transceiver element (ports 3–6). By tiling identical couplers at half integer wavelength spacing, our objective was to produce a coupler network with very high phase and amplitude balance.

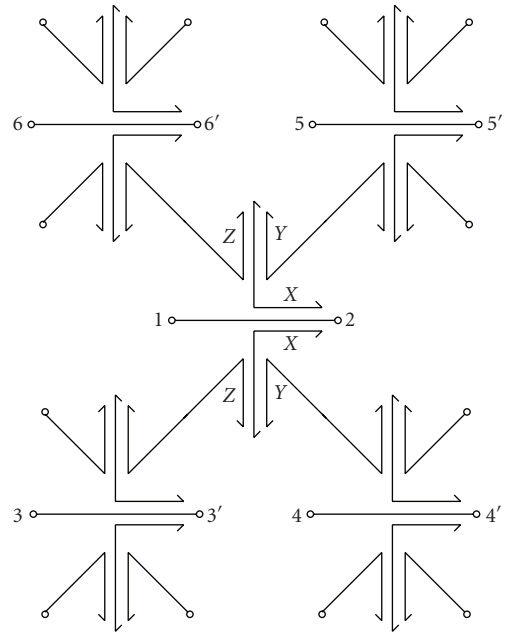

Figure 11: Five precision couplers configured for 2×2 array calibration.

4.2. Theoretical coupler performance

The simulation results for our coupler design, using ADS momentum, are shown in Figure 12 [19]. Insertion loss at the design frequency of 2.46 GHz is predicted as 0.7 dB. The intertransceiver isolation is high—a minimum of 70.4 dB between transceivers. In the design of the coupler structure, a tradeoff exists between insertion loss and transceiver isolation. By reducing the coupling factor between the antenna feeder transmission line and the coupled calibration path (marked X on Figure 11), higher efficiency may be attained. However, weaker calibration coupling than −40 dBm is undesirable from the perspective of calibration reference element efficiency and measurement reliability. This necessitates stronger coupling between the calibration couplers—this stronger coupling in the second coupler stage (marked Y or Z on Figure 11) will reduce transceiver isolation. It is for this reason that −20 dB couplers are employed in all instances (X, Y, and Z).

The ADS simulation predicts that the calibration path will exhibit a coupling factor of −44.4 dB, slightly higher than desired.

The phase and amplitude balance predicted by the simulation is shown in Figures 13 and 14. This is lower than reported for a single coupler. This is because the individual coupler exhibits a natural bias toward high phase balance between the symmetrical pairs of coupled lines—ports D,E and C,F of Figure 10. In placing the couplers as shown in Figure 11, the error in the coupled path sees the sum of an

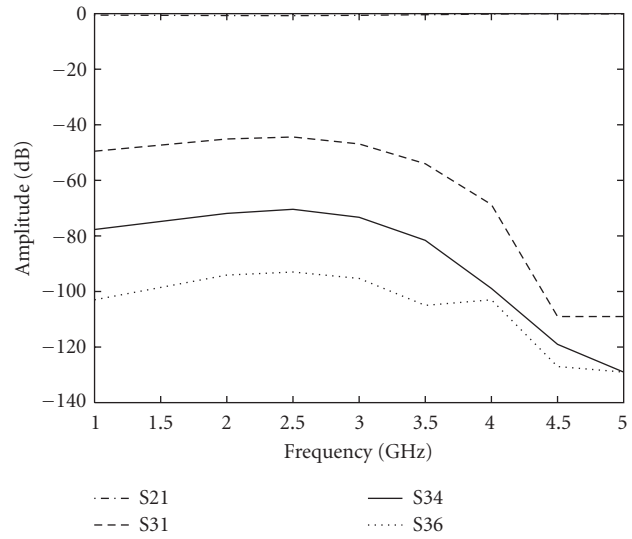

Figure 12: The theoretically predicted response of the ideal 2 × 2 coupler.

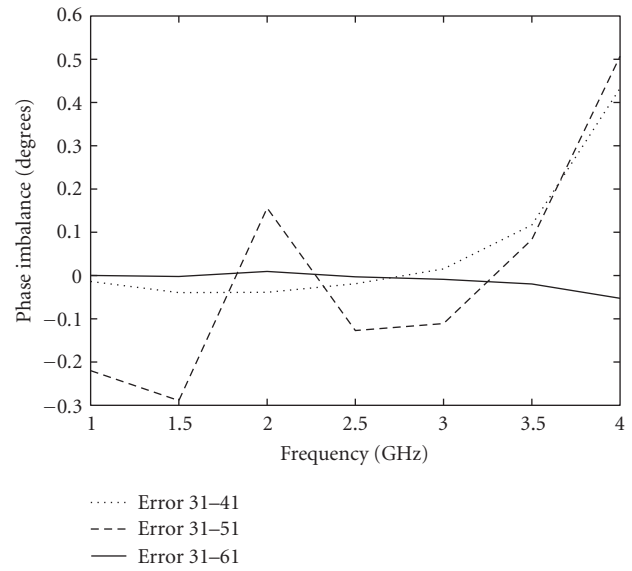

Figure 13: The predicted phase imbalance of an ideal 2 × 2 coupler.

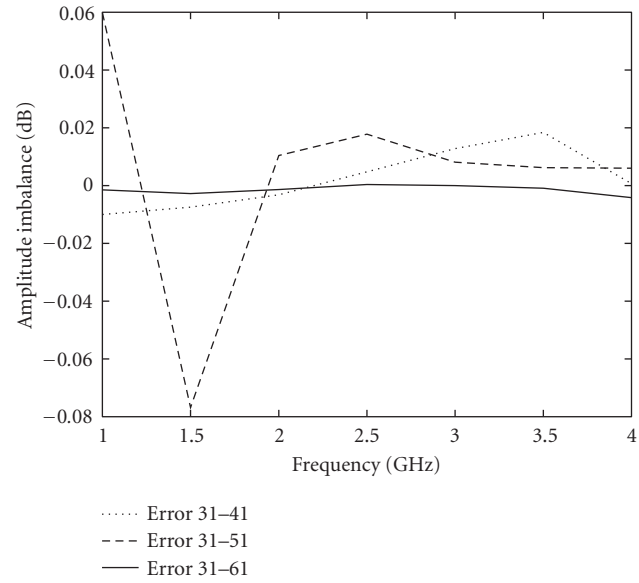

Figure 14: The predicted amplitude imbalance of an ideal 2 × 2 coupler.

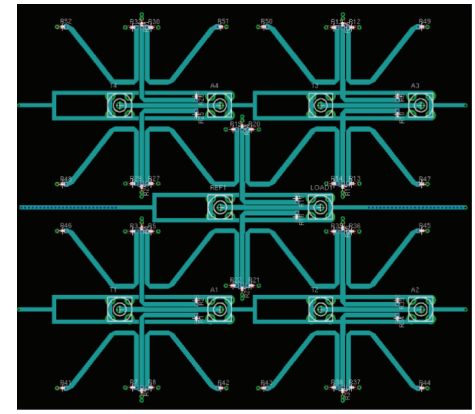

Figure 15: The PCB layout of the centre stripline controlled impedance conductor layer.

A,D (X,Z) type error and an A,C (X,Y) type error. This has the overall effect of reducing error. Were there to be a diagonal bias toward the distribution of error, then the error would accumulate.

Also visible in these results is a greater phase and amplitude balance between the symmetrically identical coupler pairs. For example, the phase and amplitude imbalance between ports 3 and 6 is very high. This leads to efforts to increase symmetry in the design, particularly the grounding via screens.

4.3. Measured coupler performance

Our design for Figure 11 was manufactured on a low-cost FR-4 substrate using a stripline design produced in Eagle [20]—see Figure 15. Additional grounding strips, connected by blind vias to the top and bottom ground layers, are visible which provide isolation between the individual couplers. A photograph of the finished 2 × 2 coupler manufactured by ECS circuits [21] is shown in Figure 16. Each of the coupler arms is terminated in low-quality surface mount 47 Ω resistors.

The 2 × 2 coupler was then tested using an R&S ZVB20 vector network analyser [22]. The results of this measurement with an input power of 0 dBm and 100 kHz of resolution bandwidth are shown in Figure 17. The coupler insertion loss is marginally higher than the theoretical prediction at 1.2 dB. This will affect the noise performance of the receiver and the transmit efficiency and hence must be budgeted for in our tower-top transceiver design. The

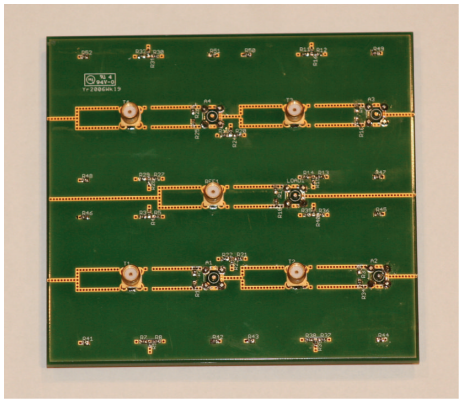

Figure 16: A photograph of the transceiver side of the calibration coupler board. The opposite side connects to the antenna array and acts as the ground plane.

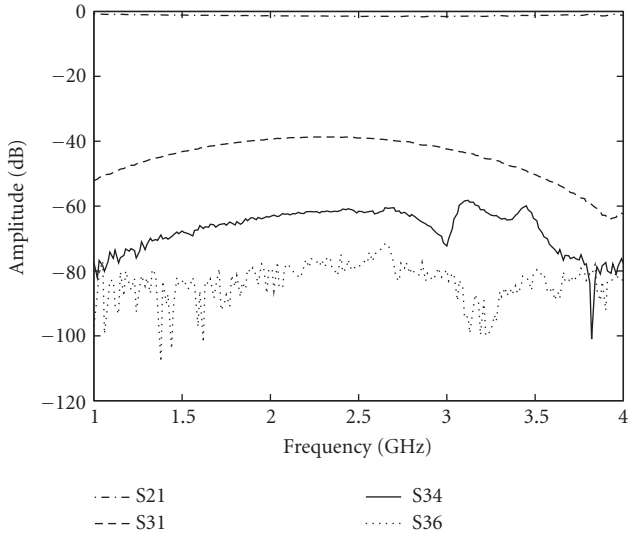

Figure 17: The measured performance of the prototype 2 × 2 coupler.

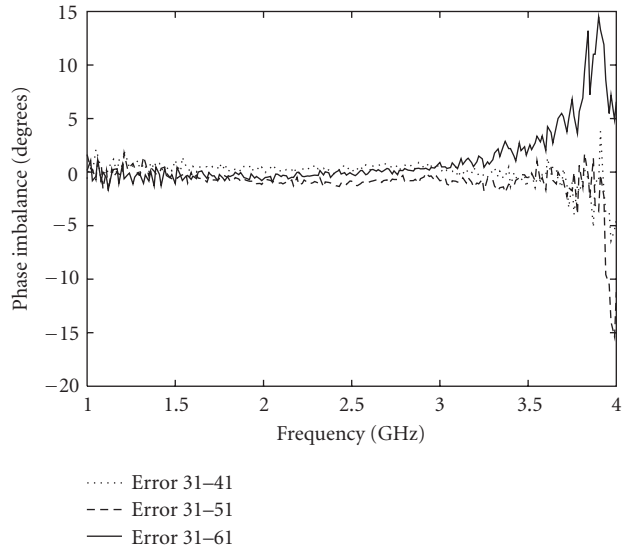

Figure 18: The measured phase imbalance of the 2 × 2 coupler.

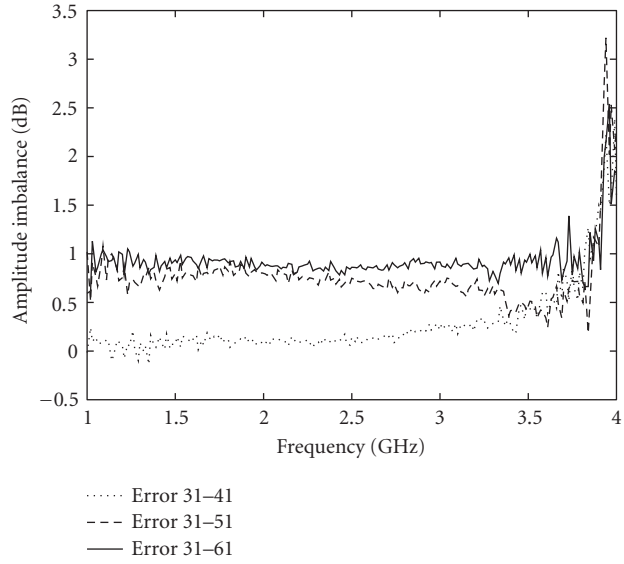

Figure 19: The measured amplitude imbalance of the 2 × 2 coupler.

coupled calibration path exhibits the desired coupling factor of −38.8 dB at our design frequency of 2.46 GHz. This stronger coupling, together with the finite loss tangent of our FR4 substrate, explain the increased insertion loss. The measured inter-transceiver isolation was measured at a minimum of −60.9 dB—thus the dominant source of (neighboring) inter-element coupling is likely to be antenna mutual coupling.

The other important characteristics of the coupler, its phase and amplitude balance, are shown in Figures 18 and 19 respectively. Phase balance is significantly poorer than indicated by the theoretical value. The maximum phase error recorded at our design frequency of 2.46 GHz for this coupler is 0.938°—almost an order of magnitude worse than the predicted imbalance shown in Figure 13.

The amplitude balance results, Figure 19, are similarly inferior to the ADS predictions (contrast with Figure 14). The greatest amplitude imbalance is between S31 and S61 of 0.78 dB—compared with 0.18 dB in simulation. However, clearly visible in the amplitude response, and hidden in the phase error response, is the grouping of error characteristics between the paths S31-S41 and S51-S61.

Because the coupler error did not cancel as predicted by the ADS simulation, but is closer in performance to the series connection of a pair of individual couplers, future simulation of the calibration coupler should include Monte Carlo analysis based upon fabrication tolerance to improve the accuracy of phase and amplitude balance predictions.

Clearly a single coupler board cannot be used to characterise all couplers. To improve the statistical relevance of our

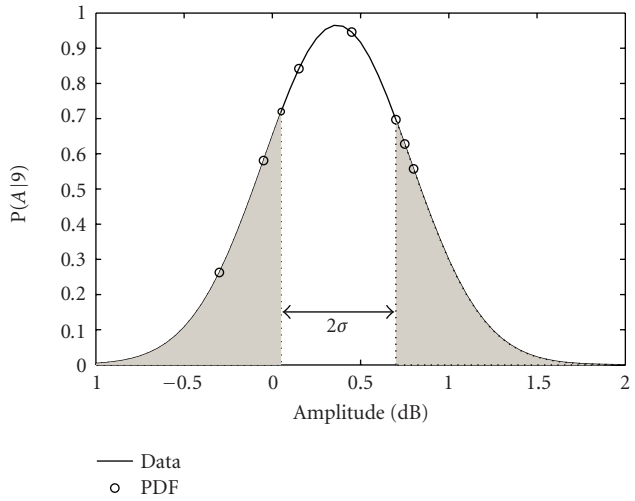

Figure 20: The measured coupler amplitude imbalance fitted a Gaussian probability density function, $\sigma_A = 0.4131$ dB, $\mu_A = 0.366$ dB.

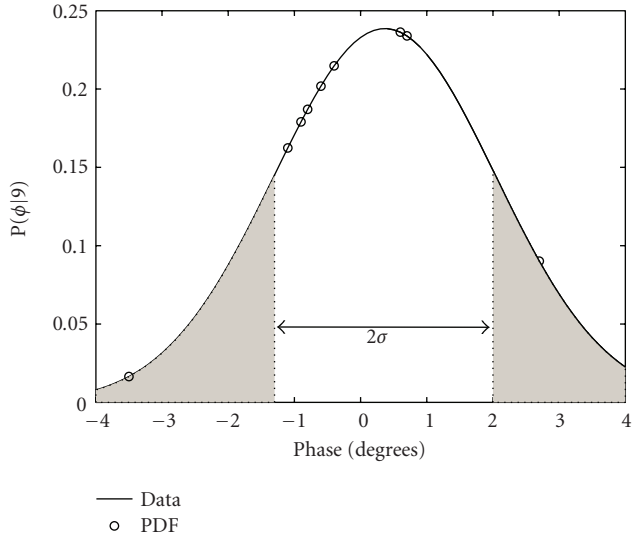

Figure 21: The measured coupler phase imbalance fitted to a Gaussian probability density function $\sigma_\phi = 1.672°$, $\mu_\phi = 0.371°$.

results, three 2×2 coupler boards were manufactured and the phase and amplitude balance of each of them recorded at our design frequency of 2.46 GHz. These results are plotted against the Gaussian distribution to which the results were fitted for the amplitude and phase (Figures 20 and 21 correspondingly). Whilst not formed from a statistically significant sample (only nine points were available for each distribution), these results are perhaps representative of the calibration path imbalance in a small array. The mean and standard deviation of the coupler amplitude imbalance distribution are $\mu_{c_A} = 0.366$ dB and $\sigma_{c_A} = 0.4131$ dB. This error is somewhat higher than predicted by our theoretical study. Work toward improved amplitude balance is ongoing. The phase balance, with an rms error of 1.672°, is of the order anticipated given the performance of the individual coupler.

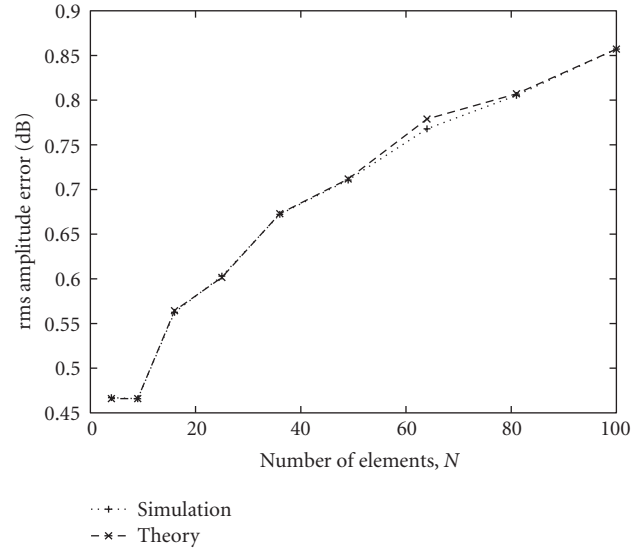

Figure 22: The theoretical prediction of overall array amplitude calibration accuracy based upon the use of the coupler hardware of Section 4.1.

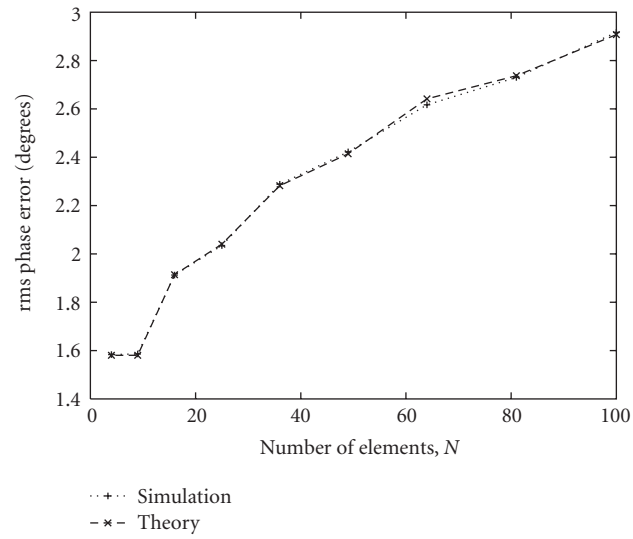

Figure 23: The theoretical prediction of overall array phase calibration accuracy based upon the use of the coupler hardware of Section 4.1.

With this additional insight into the statistical distribution of error for a single coupled calibration path, we may make inferences about the overall array calibration accuracy possible with such a system.

4.4. Predicted array calibration performance

To investigate the utility, or otherwise, of our practical array calibration system, the coupler statistics derived from our hardware measurements were fed into both the centre-referenced calibration algorithm simulation and the theoretical prediction of Section 3. The results of this simulation are shown in Figures 22 and 23.

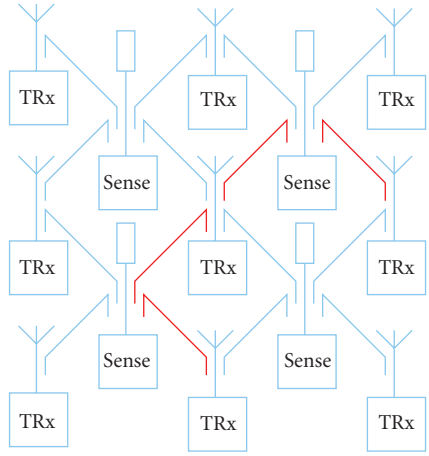

FIGURE 24: The redundant coupled calibration paths which may be useful in enhancing the quality of calibration.

The results from these figures show that the approach yields a highly accurate calibration, with rms phase errors for a typical 16-element array of less than 2° and a gain imbalance of less than 0.55 dB. As arrays increase in size, the errors do increase. For phase calibration, the increase is small even for very large arrays. Gain calibration is more sensitive to size and a 96-element array would have a 0.85 dB rms error. Ongoing work is focused upon improving the gain calibration performance for larger arrays. The following section is presenting some initial results for alternative calibration schemes which utilise the additional information from the redundant calibration paths.

5. FUTURE WORK

5.1. Redundant coupler paths

In each of the calibration algorithms discussed thus far, only a fraction of the available coupled calibration paths is employed. Figure 24 shows the coupled paths which are redundant in the "top-left" calibration scheme of Figure 6(b). The focus of future work will be to exploit the extra information which can be obtained from these redundant coupler paths.

5.2. Iterative technique

5.2.1. Operation

Given that we cannot measure the array output without incurring error due to the imbalance of each coupler, we have devised a heuristic method for enhancing the antenna array calibration accuracy. This method is designed to exploit the additional, unused coupler paths and information about the general distribution and component tolerance of the errors within the calibration system, to improve calibration accuracy. One candidate technique is based loosely on the iterative algorithmic processes outlined in [23]. Our method is a heuristic, threshold-based algorithm and attempts to infer the actual error in each component of the calibration system—allowing them to be compensated for.

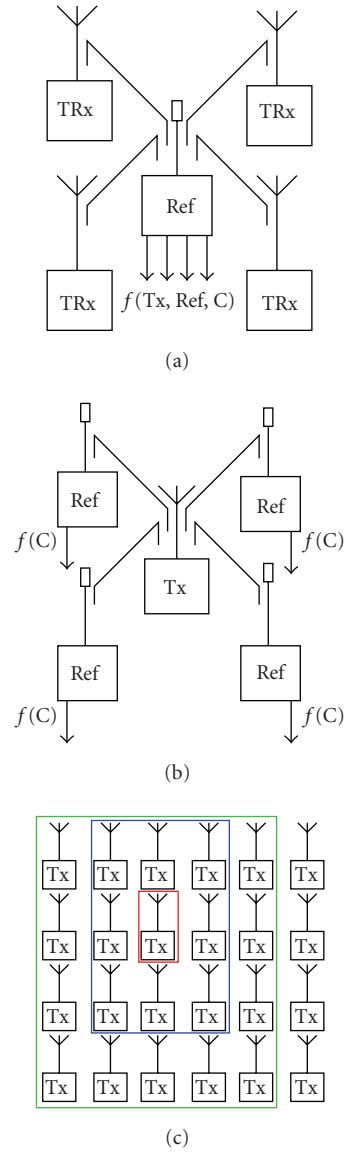

FIGURE 25: The two main processes of our heuristic method: (a) reference characterisation and (b) transmitter characterisation. (c) The error dependency spreads from the neighbouring elements with each iteration of the heuristic process.

Figure 25 illustrates the two main processes of our iterative heuristic algorithm. The first stage, Figure 25(a), is the measurement of each of the transmitters by the reference elements connected to them. The output of these measurements, for each reference, then have the mean performance of each neighbouring measured blocks subtracted. This results in four error measurements (per reference element) that are a function of the proximate coupler, reference and transmitter errors. Any error measurements which are greater than one standard deviation from the mean transmitter and coupler output are discarded. The remaining error measurements, without the outliers, are averaged and are used to estimate the reference element error.

The second phase, Figure 25(b), repeats the process described above, this time for each transmitter. Here the functionally equivalent step of measuring each transmitter by the four neighbouring references is performed. Again, the mean performance of each block in the signal path is calculated and subtracted. However, during this phase the reference error is treated as a *known* quantity—using the inferred value from the previous measurement. Based on this assumption, the resultant error signal is a function of the coupler error and the common transceiver element alone.

By extrapolating the transmitter error, using the same process as for the reference element, the coupler errors may be calculated and compensated for by weighting the transceiver input. This process is repeated. In each subsequent iteration, the dependency of the weighting error signal is dependent upon successive concentric array elements as illustrated in Figure 25(c).

The iterative process continues for much greater than n iterations, until either subsequent corrective weightings are within a predefined accuracy, or until a time limit is reached.

Cognisant of the negative effect that the peripheral elements of the array will have on the outcome of this calibration scheme, these results are discarded. For the results presented here, this corresponds to the connection of an additional ring of peripheral reference elements to the array. Future work will focus on the combining algorithmic and conventional calibration techniques to negate the need for this additional hardware.

5.2.2. Provisional results

To test the performance of this calibration procedure, the results are of 1000 simulations of a 10×10 array, each performed for 100 calibration iterations, was simulated using the system settings of Section 4.4. The centre calibration scheme gave an overall rms array calibration accuracy (σ_a) of 0.857 dB and 2.91°. The iterative calibration procedure gives a resultant phase accuracy of 1.32° and amplitude accuracy of 0.7148 dB. Figure 26 shows how the amplitude accuracy of the iterative calibration varies with each successive iteration. The horizontal line indicates the performance of the centre-referenced calibration. A characteristic of the algorithm is its periodic convergence. This trait, shared by simulated annealing algorithms, prevents convergence to (false) local minima early in the calibration process. This, unfortunately, also limits the ultimate accuracy of the array calibration. For instance, the phase accuracy of this array (Figure 27) degrades by 0.1° to 1.32° from its minimum value, reached on the 37th iteration. Future work will focus on tuning the algorithm's performance, perhaps to attenuate this oscillation in later iterations with a temperature parameter (T) and associated reduction function $f(T)$. Hybrid algorithms—targeting different calibration techniques at different sections of the array—are also currently under investigation.

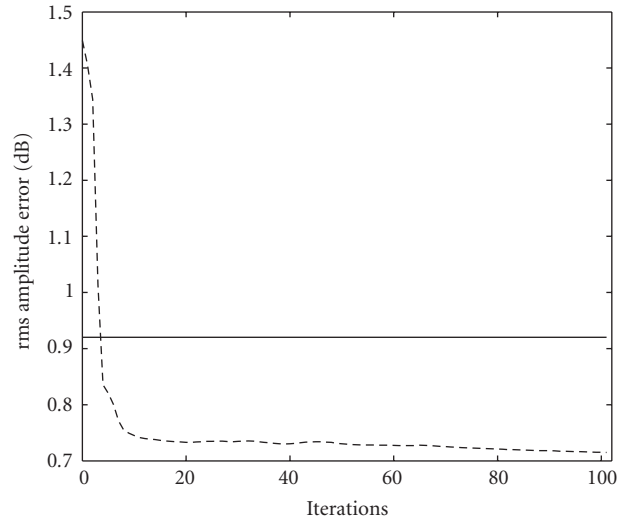

Figure 26: Resultant array amplitude feed-point calibration accuracy (σ_{a_A}) for a single $N = 100$ array, plotted versus the number of calibration iterations.

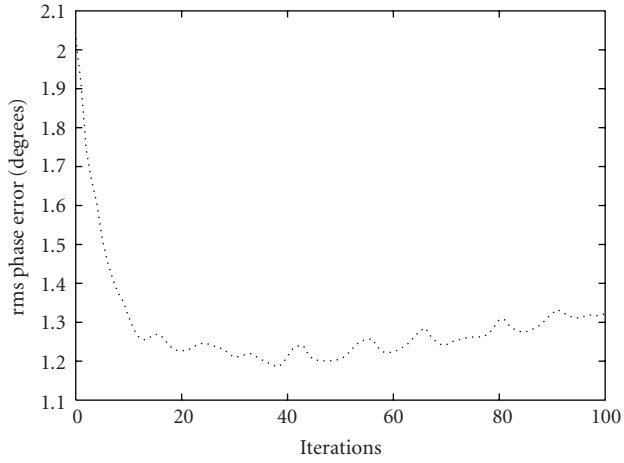

Figure 27: Resultant array phasing feed-point calibration accuracy (σ_{a_ϕ}) for a single $N = 100$ array, plotted versus the number of calibration iterations.

6. CONCLUSION

In this paper, we have presented a new scheme for tower-top array calibration, using a series of nonradiative, interlinear reference elements to sense the output of the array. The accuracy of this calibration scheme is a function of the array size, the calibration path taken in calibrating the array, and the coupler performance. Where the measurement accuracy is unlimited, then the accuracy of this calibration is dependent upon the number of couplers in a given calibration path.

The basic building block of this calibration scheme is the 2×2 array calibration coupler. We have shown that using low-cost fabrication techniques and low-quality FR-4 substrate, a broadband coupler network with rms phase balance of 1.1175° and amplitude balance of 0.3295 dB is realisable.

Based upon this coupler hardware, we have shown that phase calibration accurate enough for cellular smart antenna applications is possible. Although amplitude accuracy is still outside our initial target, work is ongoing on improving the

precision coupler network and on the development of calibration algorithms to further reduce this requirement.

Finally, we presented examples of one such algorithm—whose performance, unlike that of the conventional feedback algorithms, improves with array size. Moreover, this calibration algorithm, which is based upon exploiting randomness within the array, outperforms conventional calibration for large arrays. Future work will focus on use of simulated annealing and hybrid calibration algorithms to increase calibration accuracy.

ACKNOWLEDGMENT

The authors would like to thank Science Foundation Ireland for their generous funding of this project through the Centre for Telecommunications Value-Chain Research (CTVR).

REFERENCES

[1] N. Tyler, B. Allen, and H. Aghvami, "Adaptive antennas: the calibration problem," *IEEE Communications Magazine*, vol. 42, no. 12, pp. 114–122, 2004.

[2] C. M. Simmonds and M. A. Beach, "Downlink calibration requirements for the TSUNAMI (II) adaptive antenna testbed," in *Proceedings of the 9th IEEE International Symposium on Personal, Indoor and Mobile Radio Communications (PIMRC '98)*, vol. 3, pp. 1260–1264, Boston, Mass, USA, September 1998.

[3] K. Sakaguchi, K. Kuroda, J.-I. Takada, and K. Araki, "Comprehensive calibration for MIMO system," in *Proceedings of the 5th International Symposium on Wireless Personal Multimedia Communications (WPMC 3'02)*, vol. 2, pp. 440–443, Honolulu, Hawaii, USA, October 2002.

[4] C. M. S. See, "Sensor array calibration in the presence of mutual coupling and unknown sensor gains and phases," *Electronics Letters*, vol. 30, no. 5, pp. 373–374, 1994.

[5] R. Sorace, "Phased array calibration," *IEEE Transactions on Antennas and Propagation*, vol. 49, no. 4, pp. 517–525, 2001.

[6] K. R. Dandekar, L. Hao, and X. Guanghan, "Smart antenna array calibration procedure including amplitude and phase mismatch and mutual coupling effects," in *Proceedings of the IEEE International Conference on Personal Wireless Communications (ICPWC '00)*, pp. 293–297, Hyderabad, India, December 2000.

[7] T. Kaiser, "When will smart antennas be ready for the market? Part I," *IEEE Signal Processing Magazine*, vol. 22, no. 2, pp. 87–92, 2005.

[8] F. Rayal, "Why have smart antennas not yet gained traction with wireless network operators?" *IEEE Antennas and Propagation Magazine*, vol. 47, no. 6, pp. 124–126, 2005.

[9] G. Brown, "3G base station design and wireless network economics," *Unstrung Insider*, vol. 5, no. 10, pp. 1–30, 2006.

[10] J. D. Fredrick, Y. Wang, and T. Itoh, "A smart antenna receiver array using a single RF channel and digital beamforming," *IEEE Transactions on Microwave Theory and Techniques*, vol. 50, no. 12, pp. 3052–3058, 2002.

[11] S. Ishii, A. Hoshikuki, and R. Kohno, "Space hopping scheme under short range Rician multipath fading environment," in *Proceedings of the 52nd Vehicular Technology Conference (VTC '00)*, vol. 1, pp. 99–104, Boston, Mass, USA, September 2000.

[12] A. J. Cooper, "'Fibre/radio' for the provision of cordless/mobile telephony services in the access network," *Electronics Letters*, vol. 26, no. 24, pp. 2054–2056, 1990.

[13] G. Brown, "Open basestation bonanza," *Unstrung Insider*, vol. 4, no. 7, pp. 1–20, 2005.

[14] T. Cooper and R. Farrell, "Value-chain engineering of a tower-top cellular base station system," in *Proceedings of the IEEE 65th Vehicular Technology Conference (VTC '07)*, pp. 3184–3188, Dublin, Ireland, April 2007.

[15] T. S. Cooper, R. Farrell, and G. Baldwin, "Array Calibration," Patent Pending S2006/0482.

[16] T. Cooper, J. McCormack, R. Farrell, and G. Baldwin, "Toward scalable, automated tower-top phased array calibration," in *Proceedings of the IEEE 65th Vehicular Technology Conference (VTC '07)*, pp. 362–366, Dublin, Ireland, April 2007.

[17] Analog Devices Datasheet, "400 MSPS 14-Bit DAC 1.8V CMOS Direct Digital Synthesizer," January 2003.

[18] T. S. Cooper, G. Baldwin, and R. Farrell, "Six-port precision directional coupler," *Electronics Letters*, vol. 42, no. 21, pp. 1232–1234, 2006.

[19] Agilent EEsof, Palo Alto, Calif, USA. Advanced Design System, Momentum.

[20] CadSoft Computer, 801 South Federal Hwy., Suite 201, Delray Beach, FL 33483-5185. Eagle.

[21] ECS Circuits, Unit 2, Western Business Park, Oak Close, Dublin 12, Ireland.

[22] Rhode & Schwartz Vertiriebs-GmbH, Muehldorfstrasse 15, 81671 Muenchen, Germany.

[23] J. Hromkovic, *Algorithmics for Hard Problems*, Springer, Berlin, Germany, 2nd edition, 2004.

ON THE ACCURACY AND HARDWARE REQUIREMENTS OF CORDIC-BASED PHASED ARRAY CALIBRATION

L. Barrandon, J. McCormack, T.S. Cooper, R. Farrell

Centre for Telecommunications Value-Chain Research
Institute of Microelectronics and Wireless Systems
NUI Maynooth, Ireland
lbarrandon@eeng.nuim.ie

Keywords: phased array, calibration, CORDIC, measurement accuracy.

Abstract

The beamforming performance of a phased array is determined by the amplitude and phase relationships; however finite manufacturing tolerances and environmental effects cause imbalances in these relationships. These imbalances can be addressed by a calibration scheme. Normally such calibration schemes require either a known or unmodulated pilot signal, thereby interrupting service. In this paper we present a novel approach utilising the CORDIC algorithm to allow for collaboration with modulated data streams.

1. Introduction

Phased arrays use beamforming to utilise the spatial domain, however, the beamforming performance of an array is dependent upon the amplitude and phase relationships between the elements of the array [3]. The accuracy and reliability of these relationships is the calibration problem of the array [5], which can solved in several ways; by setting up known relationships between the elements, or using a calibration algorithm to autocalibrate the array. These relationships are subject to change from such causes as thermal effects, antenna mutual coupling, component aging and finite manufacturing tolerances [4 - 5]. Due to the dynamic nature of these relationships, all calibration solutions should include continual calibration approaches, thus making autocalibration approaches more attractive.

However most existing calibration schemes require a known signal using which some estimate of the gain and phase error can be calculated. This requires that the data signal to the antenna array be modified or interrupted. This is not desirable when frequent calibration is needed. In this paper we will present a mechanism whereby it is possible to extract from a modulated data stream the relevant phase and gain mismatch compared to a given reference element. This approach will use the CORDIC algorithm which is more commonly used to implement modulation schemes for wireless communications [6]. The choice of the CORDIC algorithm mainly relies on its flexibility as it can be widely customized which allows an exploration study aimed to optimize the accuracy.

This paper will focus on the necessary performance required for calibration given an example calibration scheme and the resolution and accuracy for the CORDIC algorithm in determining phase and gain mismatch.

2. The accuracy issue

For phased arrays with separate transceiver elements the demand for successful calibration is clearer, as the elements of the array have no relation to each other. Therefore, they require calibration to achieve any kind of coherent beamforming. This problem has previously been considered in terms of a tower-top, cellular, transmitter [1]. Due to the conflicting requirements of reliability, cost, scalability and performance - the solution shown in figure 1 was proposed [2].

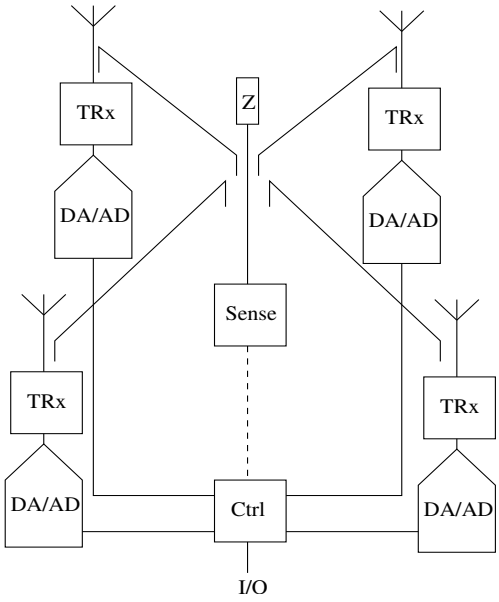

Figure 1. The tower-top calibration system.

Each transmitting element (TRx) is linked to a receiving element (*sense* on the previous figure) by a coupler. The

sense block is composed of a mixer to transpose the modulated signal in base-band and an ADC which provide this digitized data to the digital control block (*ctrl*). This last element contains the CORDIC-based calibration system.

This system may be scaled to an array of any size by repeating this tessellating structure, which provides a non-radiating mechanism for calibration. This mechanism has been utilised by different autocalibration approaches previously and the best performing presented for this system to date is the shortest path algorithm [2]. From the approach taken by the shortest path algorithm it can be shown that the calibration accuracy of this system is limited by i) the balance of the electromagnetic coupler structure and ii) sensor measurement accuracy [1].

Consider the accuracy of the calibration in terms of the balance of the electromagnetic coupler structure only first. In these terms, the accuracy of the shortest path algorithm can be predicted by calculating the number of couplers affecting each of the elements of the array, when the RMS error of an electromagnetic coupler is $\Phi_c = 1.117°$ ($19.5\ 10^{-3}$ rad) and $\delta_c = 0.3295$ dB [2]. The following expressions calculate this and are present in terms of odd and even n, $n^2 = N$, where N is the number of elements in the array.

Even n:

$$\sigma_{ak}^2 = \left(\frac{\sigma_{ck}^2}{N-1} \sum_{i=1}^{\frac{n}{2}-1} 8i^2 \right) + \left(\frac{2n-1}{N-1} \right) \left(\frac{n}{2} \right) \sigma_{ck}^2 \qquad (1)$$

Odd n:

$$\sigma_{ak}^2 = \left(\frac{\sigma_{ck}^2}{N-1} \sum_{i=1}^{\frac{n-1}{2}} 8i^2 \right) \qquad (2)$$

where, σ_{ak}^2 and σ_{ck}^2 are the RMS array variance and the RMS coupler variance respectively.

The performance of the calibration algorithm is not solely based upon the balance of the electromagnetic coupler structure: the measurement accuracy of the system, including the CORDIC algorithm itself, is also a factor in the accuracy of the array. The calibration algorithm can only compensate for errors it can measure; therefore the measurement accuracy of the array is important. Due to the structure of the array, each element of the array is connected to at least one reference element. These reference elements measure the transceiver elements connected to it. Depending upon the calibration algorithm, a correction factor can be fed back to each of the connecting transceiver elements. This digital feedback is subject to measurement errors and ADC resolution.

Imbalances in the relationships between the elements will affect the radiation pattern of the array. For cases where the amplitude and phase errors are small, there will not be any noticeable changes in the near-in sidelobe levels or the main lobe. Therefore the effect of small errors in the amplitude and phase relationships will affect only the far-out sidelobe levels in the radiation pattern [8].

Considering only small amplitude and phase errors, and working from the RMS array variance of arrays calibrated by the shortest path algorithm, it can be shown that the measurement accuracy can further degrade the far-out sidelobe levels. For example, a 5x5 array was considered. A series of achievable far-out sidelobe levels were plotted in relation to the amplitude and phase errors allowable, as shown in figure 2. The RMS array error (ε_c) of a 5x5 array was plotted also, represented by the line ε_c. A -35 dB sidelobe level specification was derived for the far-out sidelobe level for this array. The shaded area determines the allowable amplitude and phase measurement errors. This highlights that large amplitude and phase measurement errors can severely degrade the performance of the array. Therefore improving the accuracy of the measurements is important to the overall performance of the system.

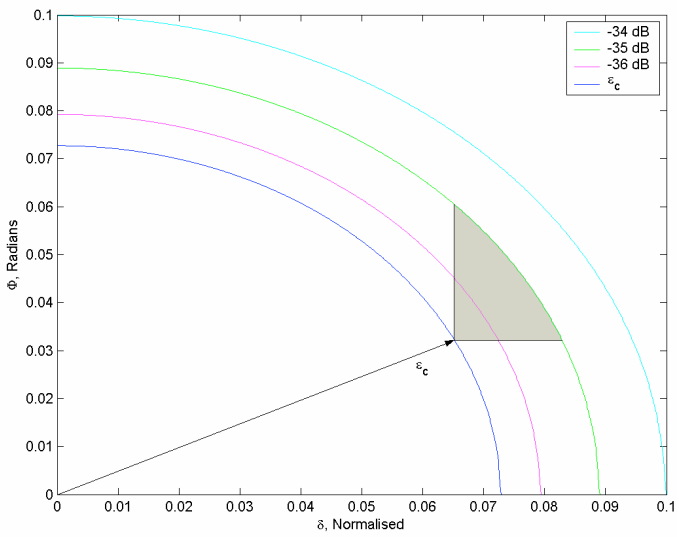

Figure 2. Array calibration error due to coupler imbalance and its effect on RMS sidelobe level, for a 25-element array.

3. Presentation of the calibration system

3.1. The CORDIC algorithm

CORDIC (COordinate Rotation DIgital Computer) is a simple and efficient algorithm to calculate hyperbolic and trigonometric functions [7]. It is commonly used to avoid the implementation of multipliers or to save logic resources (e.g., simple microcontrollers and FPGAs) as the only operations it requires are addition, subtraction, bitshift and table lookup. Based on this iterative algorithm, the following operations can be obtained: vector rotation, vector translation, trigonometric functions (sin, cos and atan), hyperbolic functions (sinh, cosh and atanh), square root, exponential function and amplitude computation and compensation.

The features we will be interested in deal with vector rotation (called *rotation mode*) and sine/cosine computation (*vector mode*).

3.2. The calibration system operation

In this paragraph, the calibration of a single Tx channel is introduced first, and the multichannel extension will then be discussed.

Calibration of a single Tx channel

Five main operations are to be done by the calibration system.

- First, it has to detect the phase of the received base-band I/Q signal of each channel. This phase includes the offsets due to the whole transmission/reception path (see 1.1). This is the "phase detection", made by a vector mode CORDIC block
- Then, these phases must be compared to a reference which, in that case, is the original base-band digital signal. To make such a comparison, the phase of the generated signal must be computed. This requires the use of the same kind of CORDIC block as previously mentioned.
- Transmitted and received signal phases are compared with a subtracter. A memory delays the input so as to synchronize both signals. Its size depends on the latency of the whole path followed by a transmitted signal (principally ADCs and DACs).
- A rotation mode CORDIC function is used to compensate the phase offset measured. Its inputs are the original base-band signal and the opposite of the phase offset.
- A "delayed integrator" filters the phase information so as not to consider the correction as part of the phase offset.

The block diagram of the simulation test bench shown on figure 3 uses the following notations:

- ϕ_{input} is the phase of the input signal;
- ϕ_{offset} is the phase error introduced by the measurement path.

It illustrates the basic calibration system; this corresponds to the *sense* and *control* blocks of figure 1.

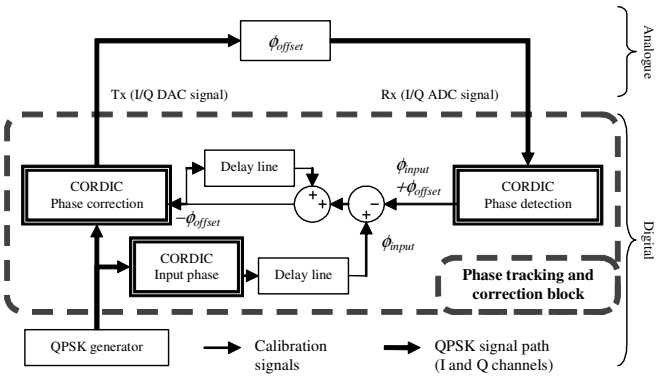

Figure 3. Calibration measurement and control scheme

To sum up, three CORDIC blocks are used to effect QPSK calibration: vector mode CORDIC measures the transmitter output, then rotation mode CORDIC (after additional processing) applies the calibration. The second vector mode CORDIC allows a phase offset to the input base-band transmit signal, permitting beamforming.

The correction of the amplitude error is also taken into account in the system and basically uses the same structure. While computing the phase, the Rx vector mode CORDIC also gives the information about the amplitude of the I/Q vector. As the amplitude of the input is supposed to be known and fixed, the amplitude of the received signal does not have to be compared to the transmitted version. The correction is obtained by using a multiplier: the first input is the output of each CORDIC block, the second one is fed by the amplitude correction data.

Calibration of a complete array

It is important to point out that the global system is completely scalable: this means that it is described so as to let the end user chose the resolution of the inputs and outputs (ADCs, DACs, generator), the resolution of the processing and the total number N of elements of the array.

The phase offset for each element is not supposed to vary quickly in time, compared to the speed at which the calibration process can be performed. Indeed, the phenomena like temperature drift affect the phase offset quite slowly. These statements lead to consider a hardware solution sharing as much resource as possible between each element.

The most straightforward way of calibrating an antenna array is to dedicate a vector mode CORDIC block to each transmitter so as to permit a permanent correction. As there is only one signal generated and one receiver for the system, the two other CORDIC blocks are shared. This means that a time-interleaving scheme is used, taking advantage of the fact that the phase error is a slow perturbation. The steps of the calibration are described on figure 4.

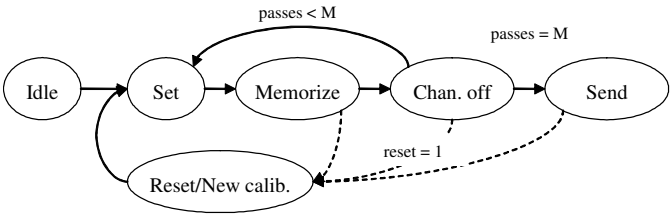

Figure 4. Finite state machine managing the calibration system.

The FSM works according to the following steps:

1 SET: The first Tx channel is activated.
2 MEMORIZE: The measurements results (phase and amplitude) are buffered
3 CHANNEL OFF: The channel is deactivated
4 The same chronology is followed for each one of the N channels from step 1 to 4

5 SEND: Once all the channels are characterized, the system is calibrated and operates normally.

6 RESET/NEW CALIB: After an activation of the reset input or after a preset constant delay, a new calibration can be initiated.

4. Accuracy

4.1. Accuracy of the CORDIC algorithm

The output quantization error can be split into two components: the output quantization error due to the input quantization and the output quantization error due to internal precision.

The input quantization error is due to the 1/2 least significant bit of quantization noise on I, Q and phase inputs. Thus for small inputs the effect of input quantization noise on input quantization error is greatly magnified. This phenomenon is depicted on figure 5.

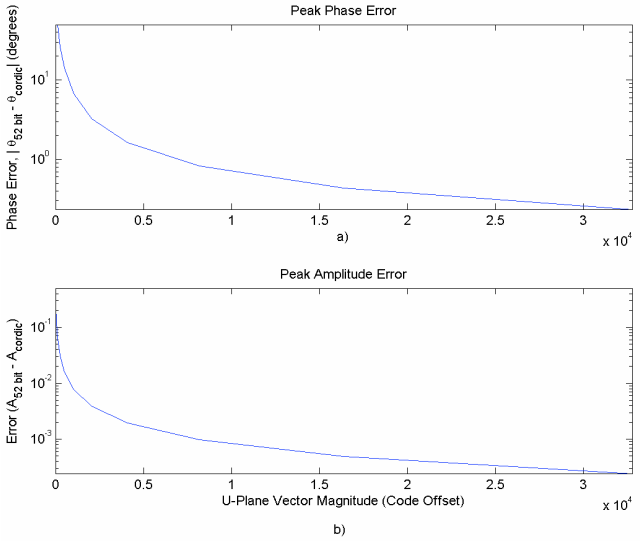

Figure 5. The impact of reduced input magnitude on vector mode CORDIC accuracy.

The Internal Precision error is due to the limited precision of internal calculations. In the CORDIC core, the default internal precision is set such that the accumulated Internal Precision error is less than 1/2 the Input Quantization error.

4.2. Resolution needed for the digital processing

The accuracy of the vector mode CORDIC block is shown as a function of ADC code offset (up to 15 bits) in figure 5. We derive formalism showing that after three calibration cycles, due to noise and overshoot, that 50% of the ADC resolution (M) is accessible. Moreover, that for a given sidelobe level (σ^2) the required ADC resolution is given by:

$$M - 1 = \log_2\left(\frac{1}{1.2\delta_m}\right) \tag{3}$$

$$\bar{\sigma}^2 = \frac{\Phi^2 + \delta^2}{N} \tag{4}$$

$$\bar{\sigma}^2 = \frac{(\Phi_C + c.\delta_M.\alpha)^2 + (\delta_C + \delta_M.\alpha)^2}{N} \tag{5}$$

$$\delta_M = \frac{1}{(c^2+1).\alpha}.\left[-(c.\Phi_C + \delta_C) \pm \sqrt{\Delta}\right]$$
$$\Delta = -\Phi_C{}^2 + 2.c.\Phi_C.\delta_C - c^2.\delta_C{}^2 + (c^2+1).N.\bar{\sigma}^2 \tag{6}$$

where N = the number of elements of the array, $c = 5.68$ for CORDIC and α is a constant, dependent upon both the calibration algorithm and array size employed.

5. Results

5.1. Simulations

The system depicted on figure 3 was simulated and characterized using a behavioural VHDL testbench. The input (generator) is a QPSK signal which can be either pre-programmed or random. The simulation uses a data rate of 100Msps. Φ_{offset} sweeps 360 values from -π to π to check the validity of the system for any phase error. The result we are interested in is the accuracy of the system. To observe it easily, the difference between the phase error detected and the phase error applied is plotted. The correction accuracy follows two steps: first, a rough calibration is made (within 2% of the ideal value) and the second loop in the system provides a result which is, as expected, within +/- 1bit of the ideal value.

The simulation results shown on figure 6 were obtained using a global data resolution of 12 bits.

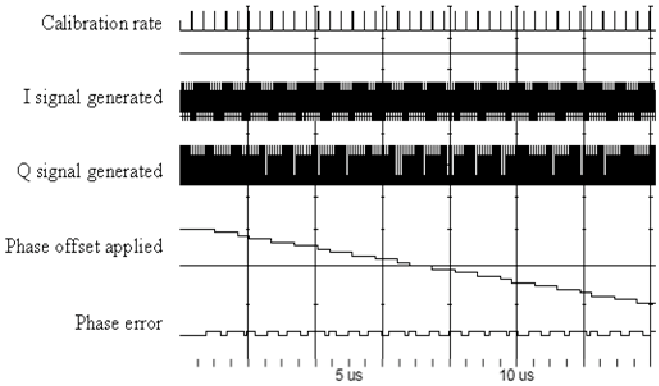

Figure 6. Simulation results with ModelSim.

This simulation is repeated for several data resolution, from 8 to 14 bits. The standard deviation of the measurements error on the phase are extracted and injected in equations (3) and (6). A graph plotting these equations (see figure 7) shows that our specification is met by M = 10 bits, however, increased calibration accuracy is accessible through higher ADC resolution. Results from these simulations, also shown in the same figure, validate our theoretical predictions.

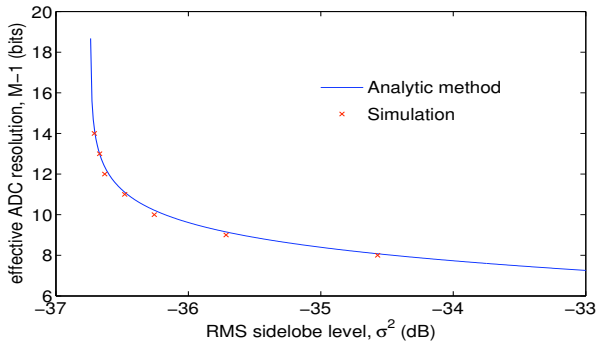

Figure 6. Predicted and simulated (α =1.66, c=5.68) ADC resolution results for N=25.

5.2. Synthesis

Synthesis for a VIRTEXII PRO-XC2VP30 target FPGA [9] demonstrates operation up to 130 MHz using only 2488 slices (18%) for the measurement on a single channel in a 12-bit version. Each extra channel uses almost 1000 slices, this figure varying according to the resolution M and the number of elements M. Improvements are currently led to increase the maximum number of channels which can be driven by a single FPGA.

6. Conclusions

In this paper we presented a methodology that utilises the CORDIC algorithm to extract the phase and gain mismatch of each of the individual modulated signals in the antenna array. The resolution of this process is limited by the hardware accuracy and the time available to the CORDIC block for processing. In this paper an analysis was presented for the required accuracy requirements for both the hardware and algorithmic components of the sensing system. The sensing algorithms have been implemented on an FPGA and the demonstrated for a QPSK modulated signal.

Future work will involve extending this analysis to other modulation schemes. In addition, a 16 element array is being designed to explore the capabilities of this approach to larger systems.

Acknowledgements

This research has been supported by Science Foundation Ireland and Enterprise Ireland within the Centre of Telecommunications Value Chain Research (CTVR).

References

[1] T. S. Cooper, J. Mc Cormack, R. Farrell and G. Baldwin. “Towards Scalable, Automated Tower – Top Phased Array Calibration”, in Vehicular Technology Conference, Dublin Ireland April 23 – 25, 2007

[2] T.S. Cooper, R. Farrell, G. Baldwin, “Six-Port Precision Directional Coupler” Elec. Lett., pp.1232-1234, Oct. 2006.

[3] K. R. Dandekar, H. Ling and G. Xu, “Smart Antenna Array Calibration Procedure Including Amplitude and Phase Mismatch and Mutual Coupling Effects” IEEE International Conference on Personal Wireless Communications. 17 – 20 Dec. 2000, pp. 293 - 297.

[4] G. Tsoulos, J. McGeehan, M. Beach. “Space Division Multiple Access (SDMA) Field Trials. Part 2: Calibration and Linearity Issues”, IEE Proc. Radar, Sonar Navig. Vol. 145, No. 1, pp., February (1998).

[5] N. Tyler, B. Allen and H. Aghvami. “Adaptive Antennas: The Calibration Problem”, IEEE Comms. Magazine, Vol. 42, Iss. 12, Dec. 2004, pp. 114 - 122.

[6] J. Valls, T. Sansaloni, A. Perez-Pascual, V. Torres, V. Almenar, “The use of CORDIC in software defined radios: a tutorial”, Communications Magazine, IEEE, Volume: 44, Issue: 9, pp. 46- 50, Sept. 2006.

[7] J.E. Volder, “The CORDIC Trigonometric Computing Technique” IRE. Trans. Comp. Vol. EC-8, No. 3, pp. 330-334, (1959).

[8] H. S. C. Wang, “Performance of Phased Array Antennas under Error Conditions”, IEEE Aerospace Applications Conference Digest., 12 – 17 Feb., 1989, pp 1 – 25.

[9] Xilinx VIRTEX II PRO-XC2VP30, www.xilinx.com.

The Effectiveness of Non-Radiative Calibration Approaches of a Tower Top Distributed Transceiver System

Justine Mc Cormack, Lukasz Lengier, John Dooley and Ronan Farrell
Centre of Telecommunication Value Chain Research,
Institute of Microelectronics and Wireless Systems,
National University of Ireland, Maynooth,
Co. Kildare, Ireland.
jmccormack@nuim.eeng.ie, llengier@nuim.eeng.ie, jdooley@nuim.eeng.ie, rfarrell@nuim.eeng.ie.

***Abstract*-Adaptive antenna arrays are dependent upon the amplitude and phase relationships between their elements. These relationships affect the radiation pattern of the array. Any imbalances in these amplitude and phase relationships are damaging to the performance of the system. The removal of the element imbalances of the array is important, and can be achieved by calibration of the array. The accuracy of calibration of an adaptive array is therefore of great importance to the overall performance of the array. This paper presents a comparison of two such calibration approaches based upon their radiation pattern, which highlights the effect of calibration accuracy on the radiation pattern of the array.**

I. INTRODUCTION

Wireless communication systems employ beamforming for a variety of reasons, such as enhanced channel capacity or to reduce the problems associated with multi-path propagation [1]. There are two types of beamforming, analog and digital. Digital beamforming is more prevalent due to its adaptability and ease of design.

Digital beamforming generally assumes that each element is identical or that each elements variance is known. However in a practical array this is not always the case, as there are imbalances in the amplitude and phase relationships between the elements. These element imbalances are affected by such things as, thermal effects, antenna mutual coupling, component aging, and finite manufacturing tolerances [2]. These amplitude and phase balances need to be known or synchronised. However depending upon the system, measurement of these variances may not possible. There are many techniques for synchronisation, from fixed feeder paths [3] to calibration algorithms [4, 5].

These variations affect the radiation pattern generated by the array, by altering their beam pointing direction, sidelobe level, half power beamwidth and null depth. These parameters are compared to show the effect of varying factors on the radiation pattern [6]. There is a roughly linear relationship between amplitude and phase errors and beam pointing direction [7], the beamwidth [8], sidelobe levels [9, 10] and null depths of the radiation pattern. However, the effect of the amplitude and phase errors on side lobe levels can be mitigated by increasing the number of elements. The sidelobe levels can also be reduced by increasing the size of the actual antenna elements. Planar arrays of N^2 of elements are more robust to the pattern deterioration then linear arrays of N elements [9].

This paper will compare a set of calibration algorithms with varying calibration accuracies. This is to show the effectiveness of calibration of an array on the beamforming performance of that array.

Some adaptive antenna structures are more susceptible to amplitude and phase imbalances [11]. Therefore it is important to note that the adaptive array is a tower top distributed transceiver array, which has a built in measurement structure to reduce the effect of amplitude and phase imbalance by calibration.

II. TOWER TOP SYSTEM

The tower top distributed transceiver array, consists of low power distributed transceiver elements, interwoven with reference elements, as can be seen in fig 1. This structure provides a calibration infrastructure for the array, which is non-radiative. The non-radiative calibration is achieved by means of a measurement path for each array elements. These measurement or calibration paths consist of the transceiver element, a directional coupler [12], and a reference element, where feedback is provided digitally, as seen in fig 2. The advantage of this non-radiative calibration infrastructure is that it removes the need to have an external source or calibration system, so that calibration can be preformed dynamically.

This system provides a set of interconnecting reference elements, these reference elements provide at least one calibration path for each of the elements of the array, and in some cases, multiple calibration paths are provided.

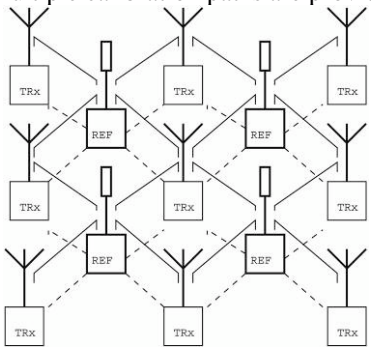

Figure 1: Distributed Transceiver System, with built in Calibration Infrastructure.

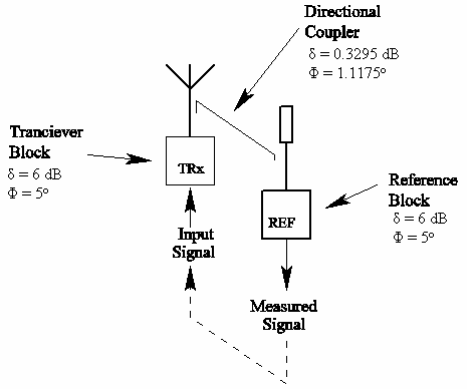

Figure 2: Calibration Path for an Antenna Element

Each of these calibration paths consists of the transceiver element, the interconnecting directional coupler path, the reference element and the digital feed back provided in the baseband. This is more clearly seen in fig 2. Calibration algorithms utilise this unique structure to calibrate the array.

III. Calibration Algorithms

This paper is going to compare two previously presented calibration algorithms with varying calibration accuracies, so that the effect on the radiation pattern can be compared. The two calibration algorithms are a middle reference calibration algorithm [4] and a dual path calibration algorithm [5].

The middle reference calibration algorithm is a comparison only algorithm. It selects a reference antenna element in the middle of the array. Then performs comparisons with the elements connected to the reference antenna element. The calibration progresses through the array using these one to one comparisons. It has an RMS standard deviation of 0.5472 dB and 1.8548° for a 5 by 5 planar array, calculated over 10,000 simulated array calibrations.

The dual path algorithm is another comparison based calibration algorithm, but it takes two paths to each element. The calibration is set up the same way as the middle reference algorithm, but instead of using only one to one comparisons. The algorithm takes two paths of identical length to the each element of the array from the reference antenna. These two paths are averaged to reduce the effect of outlying errors, to give overall consistency. It has an RMS standard deviation of 0.4716 dB and 1.6036° for a 5 by 5 planar array, calculated over 10,000 simulated array calibrations.

IV. Beamforming

The effectiveness of these calibration algorithms is considered in terms of their radiation pattern. This is because there is a clear connection between element errors and the effective radiation pattern [6-10].

The radiation pattern will be generated by using the beamforming equation of an ideal planar array, which is the ideal beamforming equation of two linear arrays oriented along different axis multiplied together [13]. The beamforming equation assumes omni-directional antenna elements.

$$AF = \sum_{n=1}^{N}\sum_{m=1}^{M} e^{j(n-1)kd_x \sin\theta\cos\phi+\beta_x} e^{j(m-1)kd_y \sin\theta\sin\phi+\beta_y} \qquad (1)$$

Where, $sin\theta cos\Phi$ are the 3D radiation pattern of the ideal linear array along the x – axis. $Sin\theta sin\Phi$ is the 3D radiation pattern of the ideal linear array along the y–axis, d_x and d_y is the element spacing of the x-axis linear array and the element spacing of the y-axis linear array, respectively. Finally β_x and β_y are the steering angles of the x-axis linear array and the y-axis linear array.

This equation is simplified for our purposes by assuming that each linear array can only steer in one direction only [14], and therefore the equation reduces to:

$$AF = \sum_{n=1}^{N}\sum_{m=1}^{M} e^{j(n-1)kd_x \sin\theta+\beta_x} e^{j(m-1)kd_y \sin\phi+\beta_y} \qquad (2)$$

The next step is to include the element variations, which can be done by multiplications, as shown in [6].

$$AF = \sum_{n=1}^{N}\sum_{m=1}^{M} A_{nm} e^{j(n-1)kd_x \sin\theta+\beta_x} e^{j(m-1)kd_y \sin\phi+\beta_y} e^{j\Delta\phi_{nm}} \qquad (3)$$

Where A_{nm} is each element's amplitude variation and $\Delta\Phi_{nm}$ is each element's phase variation.

V. Simulation Results

The beamforming equations *(2 & 3)*, were used in Matlab to simulate the effects of calibration on the radiation patterns of 4 by 4 antenna arrays. The simulations were set up by defining non-ideal arrays and calibrating them. A single array is selected randomly to be a representation of each case. The arrays were set up to have randomly varying component variations which are based upon the mean value (μ) and the standard deviation of the component value (σ) , which are presented in table 1.

The simulation results are presented in terms of their normalised 3D radiation pattern, where the array is centred at (0, 0) along the horizontal plane. The results are also presented in their component polar plots for clarity. The planar array is located along the 90° – 270° axis.

Four different cases are considered, an ideal array, a non-ideal array, and two non-ideal arrays each calibrated by a different calibration algorithm. The first case is that of a 4 by 4 ideal array. The radiation pattern of this array is generated by *(2),* and is shown in fig 3. The radiations patterns for the rest of the cases are generated from *(3)*. The second case is a non-ideal array that is uncalibrated, and is shown in fig 4. The third case is a non-ideal array calibrated by the middle reference calibration algorithm, which is shown in fig 5. The fourth and final case is a non-ideal array that is calibrated by the dual path calibration algorithm, which is shown in fig 6.

TABLE I
Component Imbalances

Component $_{(i,j)}$	$\mu_{(I,j)\,A}$	$\sigma_{(i,j)\,A}$	$\mu_{(i,j)\Phi}$	$\sigma_{(i,j)\Phi}$
Tx S21	50 dB	3 dB	10°	5°
Ref S21	60 dB	6 dB	85°	5°
Coupler S21	20.3295dB	0.3295dB	90.197°	1.1175°

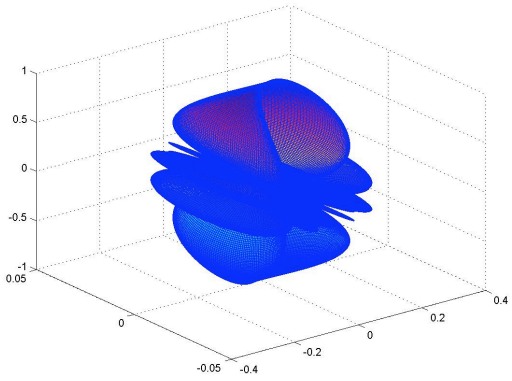

(a)

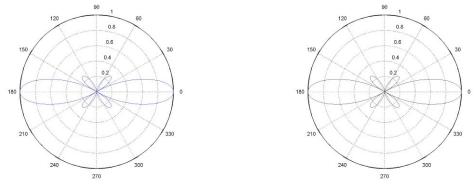

(b) (c)

Figure 3 : Normalised Radiation pattern for 4 by 4 ideal planar array, (a) 3D polar plot of the radiation pattern, (b) is the phi component and (c) is the theta component of the radiation pattern.

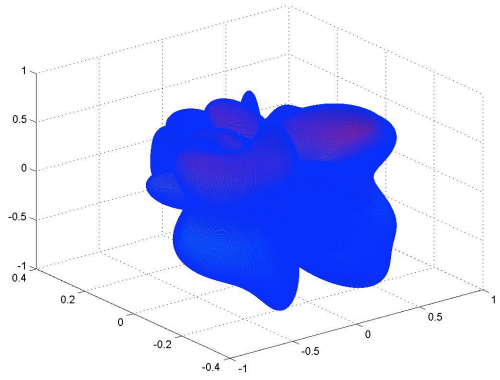

(a)

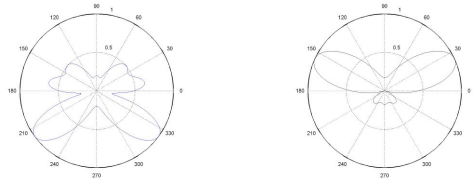

(b) (c)

Figure 4: Normalised Radiation pattern for 4 by 4 non-ideal planar array, (a) 3D polar plot of the radiation pattern, (b) is the phi component and (c) is the theta component of the radiation pattern.

From a comparison of figure 3 and 4, it is clear that calibration is needed to provide a desirable radiation pattern. Table 2 provides a more in depth comparison of all of the radiation patterns parameters. From this table it is clearer to see the extent of the effect of amplitude and phase variations of the non-ideal array.

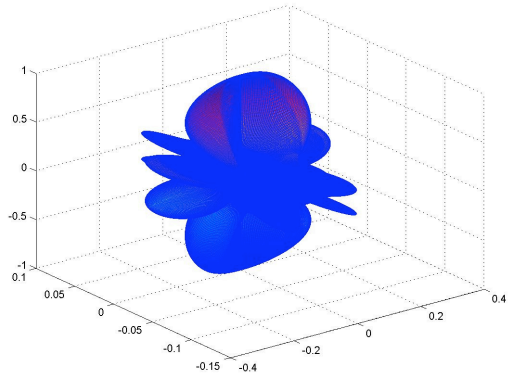

(a)

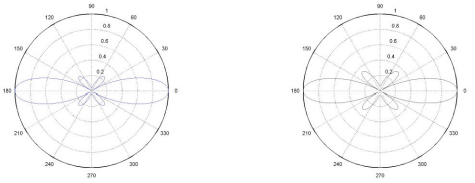

(b) (c)

Figure 5: Normalised Radiation pattern for 4 by 4 Middle Reference Calibrated planar array, (a) 3D polar plot of the radiation pattern, (b) is the phi component and (c) is the theta component of the radiation pattern.

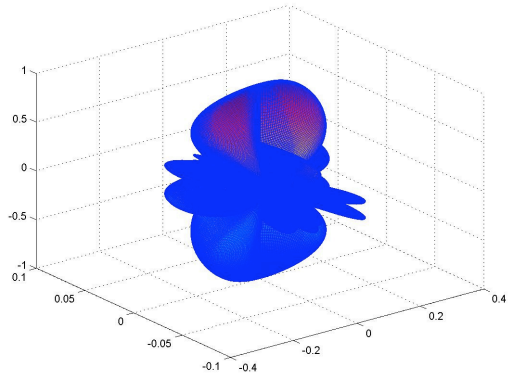

(a)

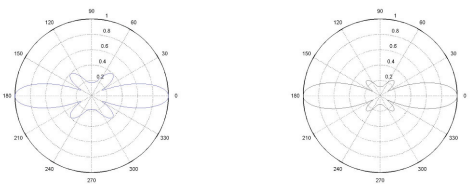

(b) (c)

Figure 6:Normalised Radiation pattern for 4 by 4 Dual Path Calibrated planar array, (a) 3D polar plot of the radiation pattern, (b) is the phi component and (c) is the theta component of the radiation pattern.

VI. Discussion

The radiation patterns are visually similar for the ideal (fig 3) and two calibrated arrays (fig 5 & 6). This is backed up by a comparison of the data in table 2. However, there are some differences between the calibrated arrays and the ideal array, due to their calibration errors. To consider these differences properly, each parameter is taken separately to compare the algorithms.

TABLE 2
Normalised Radiation Pattern Parameters

	Ideal Array	Non – Ideal	Middle Ref.	Dual Path
Beam Pointing Direction	Θ - 0^o, 180^0 Φ – 0^o, 180^o	Θ – 24.48^o, 155.52^0 Φ – 216.36^o, 323.64^o	Θ – 0.36^o, 179.64^0 Φ – 0^o, 180^o	Θ - 0^o, 180^0 Φ – 0^o, 180^o
Beamwidths	Θ – 26.64^o Φ – 26.64^o	Θ – 36^0 Φ – 30.96^o	Θ – 25.56^0 Φ – 26.64^o	Θ – 27.36^0 Φ – 25.56^o
Null Beamwidths	Θ – 60.12^0 Φ – 60.12^o	Θ – 106.92^0 Φ – 79.92^o	Θ – 61.92^0 Φ – 56.88^o	Θ – 55.08^0 Φ – 62.28^o
Null Depths	Θ – 0.004 Φ – 0.004	Θ – 0.113 Φ – 0.19 – 0.29	Θ – 0.015 – 0.031 Φ – 0.031 – 0.038	Θ – 0.1577 Φ – 0.1
Sidelobe Levels	Θ – 0.2722 Φ – 0.2722	Θ – 0.2047 Φ – 0.6324	Θ – 0.325 – 0.337 Φ – 0.325 – 0.337	Θ – 0.26 Φ – 0.39

The beam pointing error is high when you compare the ideal with the non-ideal, uncalibrated, array. This clearly shows that phase errors have a detrimental effect on the beam pointing angle. The beam pointing errors are only influenced by the phase errors and not the amplitude errors. This shows that the calibration algorithms are reducing the phase errors so that the beam pointing errors are significantly reduced or removed all together.

The beamwidth of the non-ideal array is much wider then the ideal or calibrated array. The calibrated arrays provide a closer match to the ideal array, but not a perfect one. Therefore, the calibration errors of the array are still affecting the beamwidth. Both of the calibrated arrays' beamwidth vary around the ideal value.

The sidelobe levels are reduced but also significantly increased for the non-ideal array. The calibrated arrays are also effected, but to a lesser extent. The reason for this detrimental effect of the calibration errors on the sidelobe levels is because the sidelobe levels are more susceptible to small errors. This is more clearly seen in the effect of quantization errors on sidelobe levels [10].

The first null beamwidths of the calibrated arrays also vary around the ideal first null beamwidth. The null depths of the calibrated arrays are, however, significantly shallower then that of the ideal case. Due to the single array representative, this could be an anomaly or could be a continuous effect. However for either case further analysis of the effectiveness of calibration needs to be done.

What is clear from these comparisons is that both of the calibration algorithms are effective. Neither of the calibration algorithms has a distinct advantage over the other. Apart from in the null depth, the middle reference calibration algorithm has a deeper set of nulls then that of the dual path calibration algorithm. These shallower null depths are significant in that they could limit the effectiveness of nulling of jammer signals in a communication system.

VII. Conclusions

The effectiveness of the calibration of a non-ideal array is significant. The calibration of an array reduces the affects upon the beam pointing error, the beamwidth error, the first null beamwidths and the sidelobe levels. However, when comparing the null depths, they are significantly shallower in both the calibrated arrays then in the ideal array, and even the non-ideal array.

This clearly shows the need for calibration of antenna arrays, so that the radiation patterns of the arrays are useable. Without such calibration, the pointing direction alone makes an uncalibrated array's radiation pattern unusable. The comparison of the two different calibration algorithms shows only one striking difference between them, and that is in the depth of the nulls, where the middle reference calibration algorithm actually provides a deeper null set. This shows the limitations of the comparison of the RMS standard deviations of the element variations which has previously been the figure of merit for the calibration of this system. Though these results must be considered as random representative cases and further analysis is needed.

Acknowledgment

Special thanks to Science Foundation Ireland (SFI) for their generous funding of this project through the Centre of Telecommunication Value Chain Research (CTVR).

References

[1] B. Schaer, K. Rambabu, J. Bornemann and R. Vahldieck, "A Simple Algorithm for the Control of Reactance in Beam Steering Applications with Parasitic Elements," *IEEE Topical Conferences on Wireless Communication Technology,*2003, Pp 394 - 395.

[2] N. Tyler, B. Allen and H. Aghvami. "Adaptive Antennas: The Calibration Problem", *IEEE Comms. Magazine Dec. 2004 Vol 42 Iss. 12*, pp. 114 – 122.

[3] R.E. Munson, "Conformal Microstrip Antennas and Microstrip Phased Arrays," *IEEE Trans. On Antennas and Propagation,* Vol. 22, No. 1, Jan 1974, Pp 74 - 78.

[4] J. Mc Cormack, T.S. Cooper and R. Farrell. "Tower Top Antenna Array Calibration Scheme for Next Generation Networks", *EURASIP Journal on Wireless Communication and Networking*, Vol. 2007, 2007.

[5] J. Mc Cormack, T.S. Cooper and R. Farrell. "A Multi-path Algorithmic Approach to Phased Array Calibration", *in 2nd European Conference on Antennas and Propagation EUCAP, Nov. 2007.*

[6] J.K. Hsiao, "Design of Error Tolerances of a Phased Array," *Electronic Letters, Vol. 21. No. 19*, 1985, Pp 834 – 836.

[7] K.R. Carver, W.K. Cooper, and W.L. Stutzman, "Beam-Pointing Errors of Planar-Phased Arrays," *IEEE Trans. On Antenna and Propagation,* Vol. 21, Iss. 2,March 1973, Pp199 - 202.

[8] N.K. Jablon, "Effect of Element Errors on Half-Power Beamwidth of the Capon Adaptive Beamformer," *IEEE Trans. On Circuits and Systems,* Vol. 34, No. 7, July 1987, Pp 743 - 752.

[9] R.S. Elliott, "Mechanical and Electrical Tolerances for Two-Dimensional Scanning Antenna Arrays," *IRE Trans. On Antennas and Propagation,* Vol. 6, No. 1, Jan 1958, Pp 114 - 120.

[10] M.S. Smith and Y.C. Guo, "A Comparison of Methods for Randomizing Phase Quantization Errors in Phased Arrays," *IEEE Trans. On Antennas and Propagation,* Vol. 31, No. 6, Nov. 1983, Pp 821 - 818.

[11] R.J. Mailloux, "Array Grating Lobes due to Periodic Phase, Amplitude and Time Delay Quantization," *IEEE Trans. On Antennas and Propagation,* Vol. 32, No. 12, Dec. 1984, Pp 1364 - 1368.

[12] T.S. Cooper, G. Baldwin and R. Farrell. "Six-port Precession Directional Coupler", *in Electronic Letters, Oct 2006*,Vol. 42, No. 21 pp. 1232 – 1234.

[13] C.A. Balanis, *Antenna Theory – Analysis and Design 2nd Edition*, John Wiley & Sons Inc., 1982*,* Pp 309 - 321.

[14] B. R. Mahafza, *Radar Systems Analysis and Design using Matlab,* Chapman & Hall / CRC, 2000, pp 350 - 371.

Experimental Results of Non-Radiative Calibration of a Tower Top Adaptive Array

Justine Mc Cormack, Gerry Corley and Ronan Farrell

Centre of Telecommunications Value Chain Research,

Institute of Microelectronics and Wireless Systems,

National University of Ireland, Maynooth,

Co. Kildare, Ireland.

jmccormack@eeng.nuim.ie

gcorley@eeng.nuim.ie

rfarrell@eeng.nuim.ie

***Abstract*— The need for calibration in antenna arrays is a persistent challenge and is one of the impediments to their widespread integration into communication infrastructures. The choice of antenna array structure dictates the means by which calibration can be achieved. The antenna structure used here is a distributed source array with an interconnected measurement structure for calibration. This non-radiative approach was taken to remove the need for external calibration sources, or computationally expensive modelling. This approach requires a calibration algorithm to utilise the measurement structure to get the best results. This paper will present a set of three such calibration algorithms used on an experimental setup to show the effectiveness of such calibration.**

I. INTRODUCTION

Antenna arrays provide a means of optimizing the radio links, by providing an increase in capacity, interference nulling and direction finding of users [1], [2]. These advantages assume that the elements of the array are amplitude and phase matched, or the differences to be known. However in a practical implementation, these amplitude and phase relationships are altered by finite manufacturing tolerances, path length mismatch, component aging, thermal effects, tower effects, element position variations and mutual coupling [3-16]. These imbalances are in some cases dynamic and angle of arrival dependent [17]. The dynamic nature of the array errors means that once off calibration, such as that done directly after manufacturing, is not sufficient to maintain performance.

These amplitude and phase imbalances or errors have an impact on the radiation pattern, which is to alter their beam pointing direction, sidelobe level, half power beamwidth and null depth [18]. There is a roughly linear relationship between amplitude and phase errors and beam pointing direction [19], the beamwidth [15], sidelobe levels [3], [20] and null depths of the radiation pattern.

The effect on the radiation patterns due to the imbalances in the amplitude and phase relationships make it very important to select an appropriate synchronisation or calibration method. There have been several different approaches taken in the past, such as creating fixed paths to each element of the array [5], [21], using calibration algorithms [11], which can be based upon array modelling [4], or measurements which is turn can be internal or external [5].

This paper presents a non-radiative approach to calibration. This choice was made because it offers a solution which does not require external sources, machined paths or extensive modelling of the array. The reasons for avoiding these approaches are that as the environment changes so will the performance of the array. Therefore dynamic calibration will be required. The non-radiative approach uses a distributed transceiver system which has an interleaved measurement structure for tower top implementation.

This paper is organised into six sections, the first of which presents the non-radiative measurement structure. This is followed by a section presenting the calibration algorithms that will be implemented on the system. The experimental structure is presented in the next section. The results are then presented and discussed.

II. NON-RADIATIVE TOWER TOP STRUCTURE

The non-radiative tower top structure is a distributed transceiver array, which consists of low power distributed transceiver elements, interwoven with reference elements, as is shown in fig 1. The non-radiative calibration is achieved by means of a measurement path for each array element. These measurement or calibration paths consist of the transceiver element, a directional coupler [22], and a

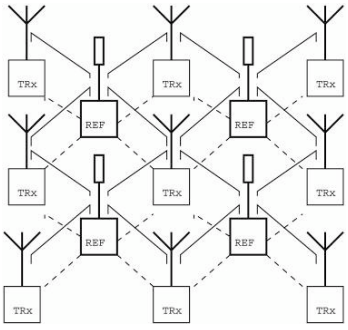

Figure 1: Distributed Transceiver System, with built in Calibration Infrastructure.

reference element, where feedback is provided digitally, as seen in fig 2. The advantage of this non-radiative calibration infrastructure is that it removes the need to have an external source or calibration system, so that calibration can be performed dynamically.

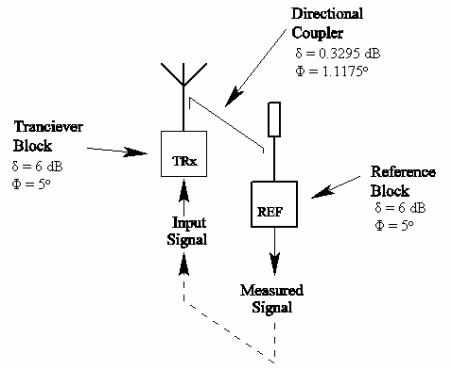

Figure 2: Calibration Path for an Antenna Element

This system provides a set of interconnecting reference elements, these reference elements provide at least one calibration path for each of the elements of the array, and in some cases, multiple calibration paths are provided. Each of these calibration paths consists of the transceiver element, the interconnecting directional coupler path, the reference element and the digital feed back provided in the baseband. This is more clearly seen in fig 2. Calibration algorithms utilise this unique structure to calibrate the array.

Another advantage of using this measurement structure is that it provides a rigid structure to the antenna array. This has the effect of removing element position errors from the calibration problem.

III. Calibration Algorithms

This paper compares three previously presented calibration algorithms with varying calibration accuracies, so that their effectiveness can be compared. The three calibration algorithms are a top left reference calibration algorithm, middle reference calibration algorithm [23] and a dual path calibration algorithm [24].

The top left reference calibration algorithm is a comparison only algorithm. It selects a reference antenna element in the top left corner of the array. Then performs comparisons with the elements connected to the reference antenna element. The calibration progresses through the array using these one to one comparisons. It has an RMS standard deviation of 0.6361 dB and 2.1418^{o} for a 5 by 5 planar array, calculated over 10,000 simulated array calibrations.

The middle reference calibration algorithm is a comparison only algorithm. It selects a reference antenna element in the middle of the array, and performs the same calibration process as top left calibration algorithm. It has an RMS standard deviation of 0.5472 dB and 1.8548^{o} for a 5 by 5 planar array, calculated over 10,000 simulated array calibrations.

The dual path algorithm is another comparison based calibration algorithm, but it takes two paths to each element. The calibration is set up the same way as the middle reference algorithm. Instead of using only one to one comparisons, the algorithm takes two paths of identical length to each element of the array from the reference antenna. These two paths are averaged to reduce the effect of coupler mismatch errors, to give overall consistency. It has an RMS standard deviation of 0.4716 dB and 1.6036^{o} for a 5 by 5 planar array, calculated over 10,000 simulated array calibrations.

IV. Experimental Setup

The experimental setup presented uses a 2 by 4 array, which is shown in fig. 3. The experimental setup is a representative structure as apposed to a full transceiver implementation. The transceiver elements are represented by voltage controlled attenuators (Mini-Circuits RVA-3000) and phase shifters (Mini-Circuits JSPHS-2484) to emulate the variations between each of the array elements. For the purposes of measurement, the antenna elements have been replaced by connections to a high speed scope (Agilent infiniium 54853A DSO 2.5GHz). The structure is fed by a signal generator, which supplies a single 2.46GHz signal. This signal is split into 8 signals. Each of these signals flow into each elements voltage controlled attenuators and phase shifters. These attenuators and phase shifters are set so that each path has a different amplitude and phase variation, which can be seen in fig. 4.

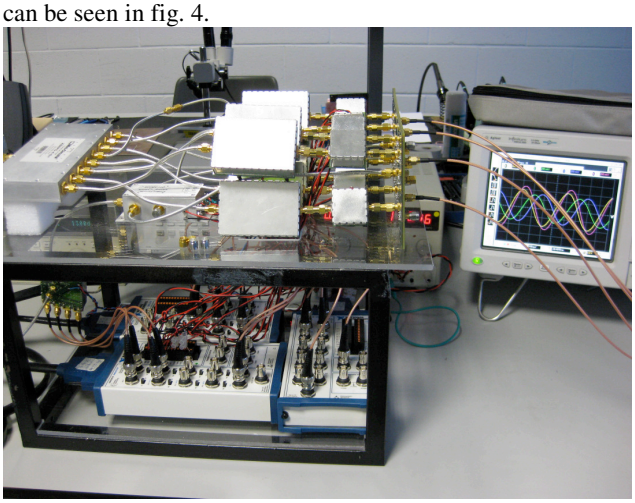

Figure 3: A photo of the 2 by 4 experimental array, where the antennas are replaced by a high speed scope.

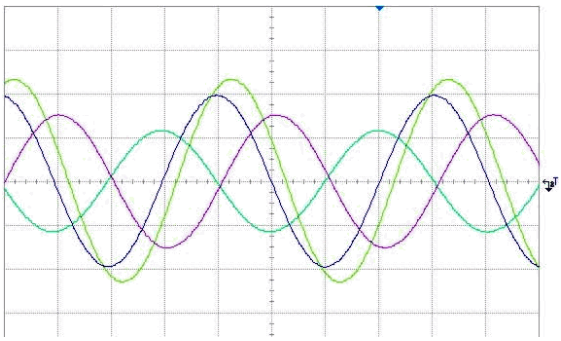

Figure 4: High Speed Scope Display of Uncalibrated Output Signals.

The calibration algorithms are implemented using Labview (National Instruments) via digital feedback provided by a set of two National Instruments PCI cards (6723 and 6251) and three breakout boxes (BNC-2110).

V. Experimental Results

As mentioned above, the top left reference calibration algorithm, the middle reference calibration algorithm and the dual path calibration algorithm need to be implemented upon the non-radiative measurement structure to achieve calibration. The experimental results from these calibration algorithms are presented in terms of the simulation predictions for a 2 by 4 array. The simulated probability density function (PDF) of the algorithm is determined from 1000 non-ideal arrays calibrated by the calibration algorithm under investigation. The non-ideal arrays are generated with randomly generated component variances, which are based upon the mean value (μ) and the standard deviation (σ) of the component value from this mean, these parameters are defined in table 1. The PDF of the experimental data is presented to highlight the performance of the array. This PDF has been centred at zero to by removing common offsets, for a clearer comparison of results.

TABLE I

Component Imbalances

Component $_{(i,j)}$	**$\mu_{(I,j)A}$**	**$\sigma_{(i,j)A}$**	**$\mu_{(i,j)\Phi}$**	**$\sigma_{(i,j)\Phi}$**
Tx S21	50 dB	3 dB	10^o	5^o
Ref S21	60 dB	6 dB	85^o	5^o
Coupler S21	20.3295dB	0.3295dB	90.197^o	1.1175^o

First we will consider the top left reference calibration algorithm. The sinusoidal waveforms measured by the high speed scope are presented in fig. 5, when compared to the uncalibrated signals shown in fig. 4; it shows the effectiveness of the calibration. However for a more detailed analysis the experimental results are compared to the simulated performance of the calibration algorithm. This comparison of the simulated probability density of the calibrated errors with the experimental results is shown in Fig. 6 and 7. The performance achieves the criterion of less than 1dB. However, the phase criterion of less than 5^o has been achieved for all but two of the phase values, 5.13^o and 5.7^o.

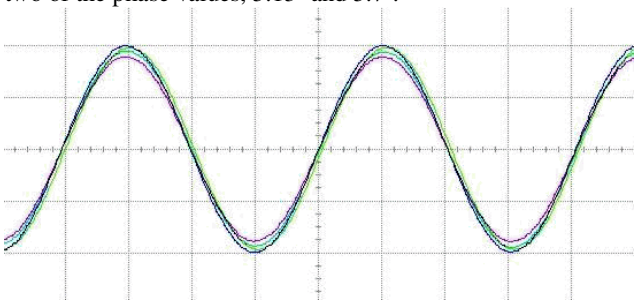

Figure 5: High Speed Scope Display of top left reference calibrated Output Signals.

Secondly, the sinusoidal waveforms measured by the high speed scope are presented in fig. 8, when compared to the

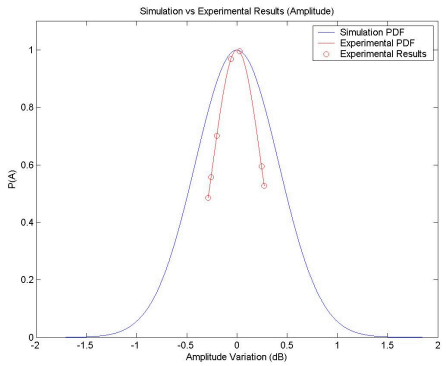

Figure 6: The Amplitude Simulation Results vs. Amplitude Experimental Results for the Top Left Reference Calibration Algorithm for a 2 by 4 array.

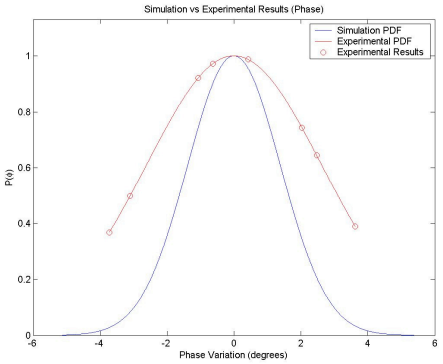

Figure 7: The Phase Simulation Results vs. Phase Experimental Results for the Top Left Reference Calibration Algorithm for a 2 by 4 array.

uncalibrated signals shown in fig. 4; it shows the effectiveness of the calibration. As before, a more detailed analysis of the experimental results is achieved when compared to the simulated performance of the calibration algorithm, which is shown in Fig. 9 and 10. The performance achieves the criterion of less than 1dB. It must be noted that the amplitude values from the experimental results have a narrower distribution than the top left reference calibration experimental results. However, the phase criterion of less than 5^o has been achieved for all but one of the phase values 5.7^o.

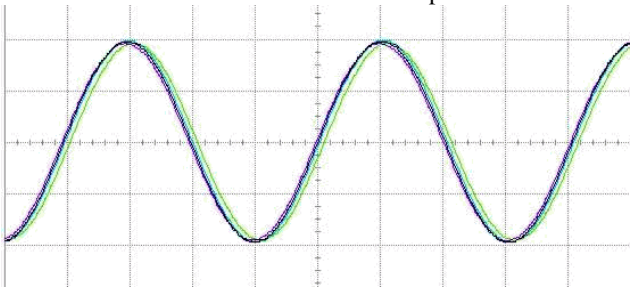

Figure 8: High Speed Scope Display of Middle Reference Calibrated Output Signals.

Finally, the sinusoidal waveforms measured by the high speed scope are presented in fig. 11. When compared to the uncalibrated signals shown in fig. 4; it shows the effectiveness

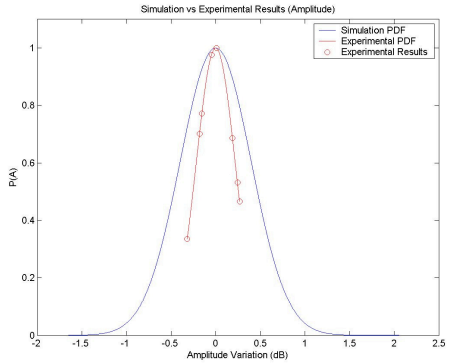

Figure 9: The Amplitude Simulation Results vs. Amplitude Experimental Results for the Middle Reference Calibration Algorithm for a 2 by 4 array.

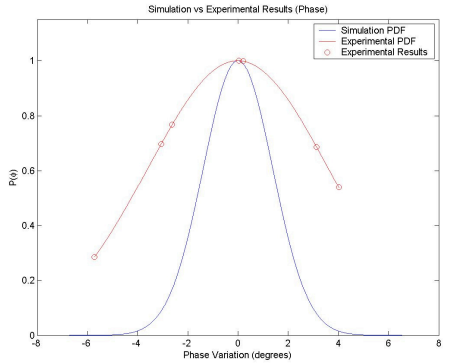

Figure 10: The Phase Simulation Results vs. Phase Experimental Results for the Middle Reference Calibration Algorithm for a 2 by 4 array.

of the calibration. The comparison of the simulated performance of the calibration algorithm with that of the experimental results gives a better comparison and is shown in Fig. 12 and 13. The performance achieves the criterion of less than $1dB$. It must be noted that the amplitude values from the experimental results have a narrower distribution then that of the middle reference calibration experimental results, except for a single outlier. The phase criterion of less than 5^o has been achieved for all element of the array, which surpasses either of the previous two algorithms.

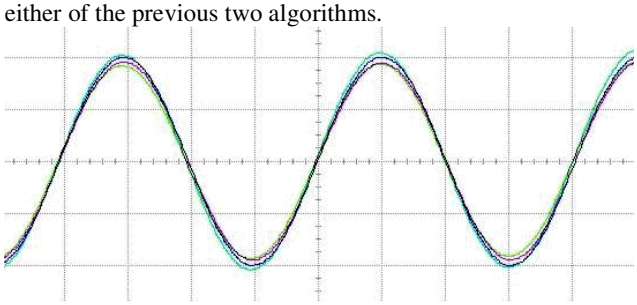

Figure 11: High Speed Scope Display of Dual Path Calibrated Output Signals.

VI. Discussion

The experimental results are consistent with the predicted performance from the calibration algorithms simulations. The

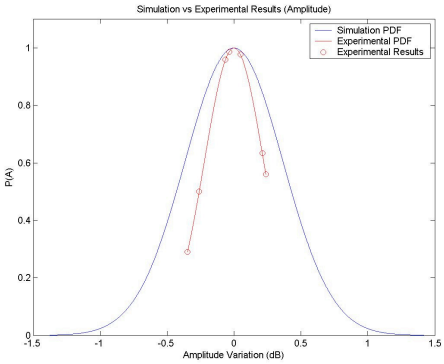

Figure 12: The Amplitude Simulation Results vs. Amplitude Experimental Results for the Dual Path Calibration Algorithm for a 2 by 4 array.

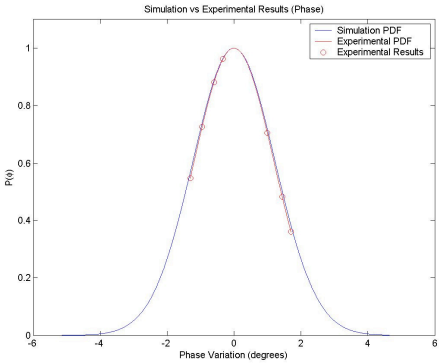

Figure 13: The Phase Simulation Results vs. Phase Experimental Results for the Dual Path Calibration Algorithm for a 2 by 4 array.

performance can be seen to gradually improve from the first calibration algorithm considered, top left reference calibration algorithm, to the final calibration algorithm that is considered here, dual path calibration algorithm. The reason for this gradual performance improvement is based on the fact that each of these algorithms is comparison based. The reason for this choice of calibration base technique is due to the fact that this non-radiative calibration structure is based on the sensor elements interleaved in the array. These sensor elements are not ideal and therefore will introduce calibration errors themselves. The effect of these errors can be reduced by using comparisons at each sensor elements; this prevents the sensor element errors propagating through the array.

The performance of the middle reference calibration algorithm is predicted to be better than the top left reference calibration algorithm as the reference antenna element is moved from the top left corner to the middle of the array, reducing the overall path length. The experimental data agrees with this prediction, the distribution of the values is wider for top left reference algorithm, and there are two phase outliers. There is however not a large improvement in our experimental setup array (2 by 4) as the reference antenna element in only moves in by one element due to the small size of the array.

The performance of the dual path calibration algorithm is predicted to have improved performance over the top left

reference calibration algorithm and the middle reference algorithm. The experimental results hold up this prediction, particularly in the phase results, as the dual path algorithm has met the less then 5^{o} criterion, when neither of the other two algorithms have. This improvement is due to the use of two paths to each element of the array instead of one. These comparisons are taken along paths of equal length from the reference antenna element to the calibrated element. The length criterion is used so that the number of coupler errors included in the comparisons is the same, so that there is not an increase in calibration errors from comparing two different path lengths. The two comparisons taken for each element are averaged. The reason for this averaging is to reduce the impact of coupler variations on the calibration performance, which has not been removed by the comparisons.

VII. CONCLUSIONS

This paper has presented a non-radiative calibration structure for an antenna array. This structure provides a rigid measurement structure which eliminates the position errors from the calibration problem as well as providing multiple measurement paths for all array elements except for the corner elements. These measurement paths are utilized by calibration algorithms. Three such calibration algorithms where implemented on a representative experimental setup, top left reference, middle reference and dual path calibration algorithms. These algorithms are all comparison based algorithms, to reduce the propagation of errors. The experimental performances of these algorithms were compared to Matlab simulations to show the effectiveness of this non-radiative calibration performance. The algorithms have shown their progressive performance improvement, so that the criterion of amplitude variance of less than 1 *dB* and phase variance of less that 5^{o}.

ACKNOWLEDGMENT

This material is based upon work supported by Science Foundation Ireland under Grant No. 03/CE3/I405 as part of the Centre for Telecommunications Value-Chain Research (CTVR) at the National University of Ireland, Maynooth.

REFERENCES

[1] B. Lindmark, S. Lundgren, J. R. Sanford, and C. Beckman, "Dual-polarized array for signal-processing applications in wireless communications," Antennas and Propagation, IEEE Transactions on, vol. 46, pp. 758-763, 1998.

[2] C. Passmann, F. Hickel, and T. Wixforth, "Investigation of a calibration concept for optimum performance of adaptive antenna systems," presented at Vehicular Technology Conference, 1998. VTC 98. 48th IEEE, 1998.

[3] R. Elliott, "Mechanical and electrical tolerances for two-dimensional scanning antenna arrays," Antennas and Propagation, IRE Transactions on, vol. 6, pp. 114-120, 1958.

[4] C. M. S. See, "A method for array calibration in parametric sensor array processing," presented at Singapore ICCS '94. Conference Proceedings, 1994.

[5] K. R. Dandekar, L. Hao, and X. Guanghan, "Smart antenna array calibration procedure including amplitude and phase mismatch and mutual coupling effects," presented at Personal Wireless Communications, 2000 IEEE International Conference on, 2000.

[6] W. H. Von Aulock, "Properties of Phased Arrays," Proceedings of the IRE, vol. 48, pp. 1715-1727, 1960.

[7] K. Yoon-Won and D. Pozar, "Correction of error in reduced sidelobe synthesis due to mutual coupling," Antennas and Propagation, IEEE Transactions on, vol. 33, pp. 1025-1028, 1985.

[8] P. S. Carter, "Circuit Relations in Radiating Systems and Applications to Antenna Problems," Proceedings of the Institute of Radio Engineers, vol. 20, pp. 1004 - 1041, 1932.

[9] B. Friedlander and A. J. Weiss, "Direction finding in the presence of mutual coupling," Antennas and Propagation, IEEE Transactions on, vol. 39, pp. 273-284, 1991.

[10] C. M. S. See, "Sensor array calibration in the presence of mutual coupling and unknown sensor gains and phases," Electronics Letters, vol. 30, pp. 373-374, 1994.

[11] N. Boon Chong and S. Chong Meng Samson, "Sensor-array calibration using a maximum-likelihood approach," Antennas and Propagation, IEEE Transactions on, vol. 44, pp. 827-835, 1996.

[12] A. L. Swindlehurst and T. Kailath, "A performance analysis of subspace-based methods in the presence of model errors. I. The MUSIC algorithm," Signal Processing, IEEE Transactions on, vol. 40, pp. 1758-1774, 1992.

[13] W. S. Youn and C. K. Un, "Eigenstructure method for robust array processing," Electronics Letters, vol. 26, pp. 678-680, 1990.

[14] R. Mailloux, "Array grating lobes due to periodic phase, amplitude, and time delay quantization," Antennas and Propagation, IEEE Transactions on, vol. 32, pp. 1364-1368, 1984.

[15] N. Jablon, "Effect of element errors on half-power beamwidth of the Capon adaptive beamformer," Circuits and Systems, IEEE Transactions on, vol. 34, pp. 743-752, 1987.

[16] W. Wasylkiwskyj, "Mutual coupling effects in semi-infinite arrays," Antennas and Propagation, IEEE Transactions on, vol. 21, pp. 277-285, 1973.

[17] C. Roller and W. Wasylkiwskyj, "Effects of mutual coupling on super-resolution DF in linear arrays," presented at Acoustics, Speech, and Signal Processing, 1992. ICASSP-92., 1992 IEEE International Conference on, 1992.

[18] J. K. Hsiao, "Design of error tolerance of a phased array," Electronics Letters, vol. 21, pp. 834-836, 1985.

[19] K. Carver, W. Cooper, and W. Stutzman, "Beam-pointing errors of planar-phased arrays," Antennas and Propagation, IEEE Transactions on, vol. 21, pp. 199-202, 1973.

[20] M. Smith and Y. Guo, "A comparison of methods for randomizing phase quantization errors in phased arrays," Antennas and Propagation, IEEE Transactions on, vol. 31, pp. 821-828, 1983.

[21] J. Andersen and H. Rasmussen, "Decoupling and descattering networks for antennas," Antennas and Propagation, IEEE Transactions on, vol. 24, pp. 841-846, 1976.

[22] T. S. Cooper, G. Baldwin, and R. Farrell, "Six-port precision directional coupler," Electronics Letters, vol. 42, pp. 1232-1233, 2006.

[23] J. McCormack, T. Cooper, and R. Farrell, "Tower-Top Antenna Array Calibration Scheme for Next Generation Networks," EURASIP Journal on Wireless Communications and Networking, vol. 2007, pp. 12, 2007.

[24] J. McCormack, T. Cooper, and R. Farrell, "A Multi-Path Algorithmic Approach to Phased Array Calibration," presented at Antennas and Propagation, 2007. EuCAP 2007. The Second European Conference on, 2007.

DEMONSTRATOR PLATFORM FOR ANTENNA ARRAY CALIBRATION

Gerry Corley, Justine Mc Cormack, Ronan Farrell
Centre for Telecommunications Value-Chain Research (CTVR),
Institute of Microelectronics and Wireless Systems,
National University of Ireland Maynooth,
Ireland.

***Abstract*-This paper presents a hardware platform for antenna array calibration research in tower top electronics. The platform has eight phase and amplitude controlled transmit channels and a novel antenna coupler array structure which provides non-radiative calibration capability. The phase and amplitude of each channel can be varied between 0 and 360° and over 25dB respectively under full software control. The platform has been used to test and develop array calibration routines which achieve amplitude variances of less than 1dB and phase variances of less than 5° measured between eight channels at the antenna connections.**

I. INTRODUCTION

In order to achieve accurate beamforming it is essential that the elements of an array are amplitude and phase matched or that the differences are known, in addition these relationships must be maintained in demanding environmental conditions such as a tower top over long periods of time. Traditionally this has been achieved through the use of tight tolerance components, phase matched cables and the use of factory measured calibration tables, however this is an expensive approach and offers little adaptation to the ambient environmental conditions.

Amplitude and phase errors between array elements distort the antenna radiation pattern in terms of beam pointing direction, sidelobe level, half power beamwidth and null depth [1] . The extent of the distortion has been well covered in antenna array literature [2], [3], [4].

There are several approaches to array calibration including tight tolerance design with factory determined calibration tables, calibration using internal and external radiating sources and non-radiative dynamic calibration [5]. The third approach was chosen as it does not require external radiators, high tolerance cables and components or extensive array modelling. In addition dynamic calibration allows continuous monitoring of the array status for network management purposes; this is a critical requirement for all cellular and wireless network operators.

Desirable features of any research platform are: that it be simple to use, that the controlling software be easy to modify and that the hardware be easily expandable, for example, through the addition of more array elements. In hardware, this was achieved through the use of off-the-shelf phase and amplitude adjustment components configured in a modular easily expandable fashion. As regards software it was decided to use Labview to control the system, implement the calibration algorithms and collect measurements. Labview is a graphical programming language aimed and test and control applications, it is easy to implement graphical user interfaces and can call both C and Matlab functions [6].

II. PLATFORM ARCHITECTURE

Effective non-radiative array calibration relies on the ability to measure the transmit or receive signals as close to their antennas as possible and to compare the measured signals with reference signals to ascertain the phase and amplitude relationship between the elements. The reference signal(s) can be the actual transmit signal in the case of live calibration or a pilot signal in the case of off-line calibration. A block diagram of a distributed transceiver array with integrated calibration/reference blocks is shown in Figure 1. This system consists of interconnected transceivers and calibration blocks where the calibration blocks provide at least one and in most cases multiple calibration paths to each transceiver, in addition every transceiver calibration path is linked to every other path through the tessellated transceiver and calibration block structure. This multiplicity and interdependence of calibration paths for each transceiver facilitates the development of powerful calibration algorithms [7].

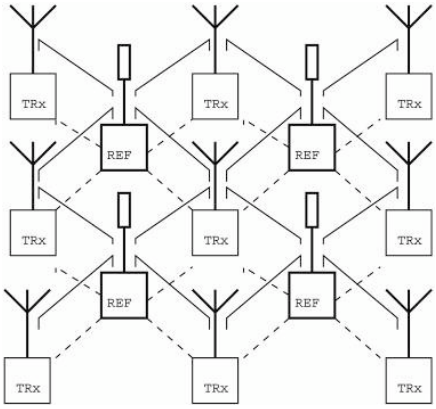

Figure 1: Distributed Transceiver System, with built in Calibration Infrastructure

A block diagram of the platform is depicted in Figure 2. The heart of the demonstrator is a 2x4 antenna coupler array; this novel design consists of an array of couplers where each coupler output provides coupling from the four surrounding transceiver through paths; a more detailed description of this coupler array and its operation is provided in [8] and [10]. In the case of transmission, the coupler outputs provide attenuated versions of the forward TX signals present at the through path inputs. The loss and phase shift between the through path input

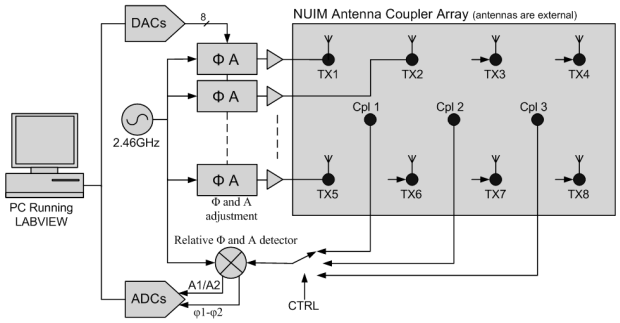

Figure 2: Block diagram of calibration and beamforming platform

and output is small, less than 1dB and the phase variation across all through paths is less than 2°. The coupler array variations can be included as a calibration offset table in the calibration algorithms.

The coupler outputs are connected through an RF switch to the vector voltmeter module which compares the coupled signal with a reference signal and produces DC outputs corresponding to the phase and amplitude difference between its inputs. The detector module is comprised of two Analog Devices AD8302 RF Gain and Phase Detector IC's configured to give I and Q outputs (cos φ & sin φ), from which it possible to generate a linear monotonic output for all angles between 0 and 360°.

$$I = A.\cos\varphi$$
$$Q = A.\sin\varphi$$

$$\varphi = \tan^{-1}(Q / I) \qquad (1)$$
$$\varphi` = \varphi \quad \text{for } I > 0, Q > 0 \qquad (1.1)$$
$$\varphi` = \varphi + 180° \quad \text{for } I < 0, Q > 0 \qquad (1.2)$$
$$\varphi` = \varphi + 180° \quad \text{for } I < 0, Q < 0 \qquad (1.3)$$
$$\varphi` = \varphi + 360° \quad \text{for } I > 0, Q < 0 \qquad (1.4)$$

The phase shift is described by equation (1) however this produces discontinuities at 90° and 270° so the response is modified according to equations (1.1 - 1.4). As regards relative amplitude, the AD8302 produces a linear output voltage for amplitude difference from -60dBm to 0dBm.

The phase and amplitude adjustment modules, one for each array element, allow the phase and amplitude of the RF signal to be varied from 0 to 398° and -7 to -32dB with respect to (wrt) the input by applying DC voltages to the phase and amplitude control inputs. The modules comprise continuously variable voltage controlled phase shifters (Mini-circuits JSPHS-2484) and a variable attenuator (Mini-circuits RVA-3000). These components are mounted on a printed circuit board with some control voltage level adjustment circuitry and the ensemble placed in a shielding can to minimise electromagnetic interference between array channels. Figure 3 shows a photograph of the phase and amplitude adjustment modules. An external amplifier was added in series with the phase and amplitude adjustment modules to compensate for their insertion loss and to ensure that the signal fed back to the phase and amplitude detector module would be at the input mid-range point.

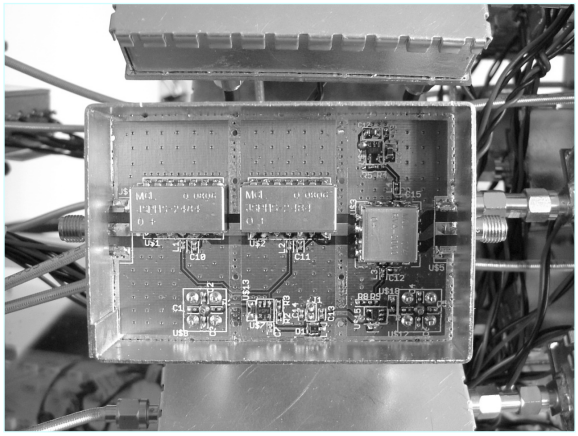

Figure 3: Phase and amplitude adjustment module

The control voltages for the phase and amplitude adjustment modules are generated by a National Instruments multi-channel 13 bit digital to analogue (DAC) card (NI PCI 6723); similarly the outputs of the vector voltmeter are digitised using a NI 16 bit analogue to digital (ADC) card (NI PCI 6251). The control of the ADC's and DAC's as well as the implementation of the control loop and the calibration algorithms were all done through Labview.

III. Platform Measurements

In the previous section the operation of the phase and amplitude adjustment and vector voltmeter modules was explained. In this section, measurements from these modules which are the core components of the platform are presented and discussed.

The phase and amplitude adjustment module was tested using a vector network analyser. By sweeping the module control voltages, the phase and amplitude of the RF signal at the output were plotted against the RF signal at the input, this is shown in figures 4 and 5. All RF

measurements were taken at 2.46GHz. The amplitude response is very non-linear but nonetheless monotonic. The phase response covers 398° and has some non-linearity at low voltages but again is monotonic. Non-linearity in the module's responses is not critical as phase and amplitude are set within a control loop which uses the vector voltmeter response to set reference points.

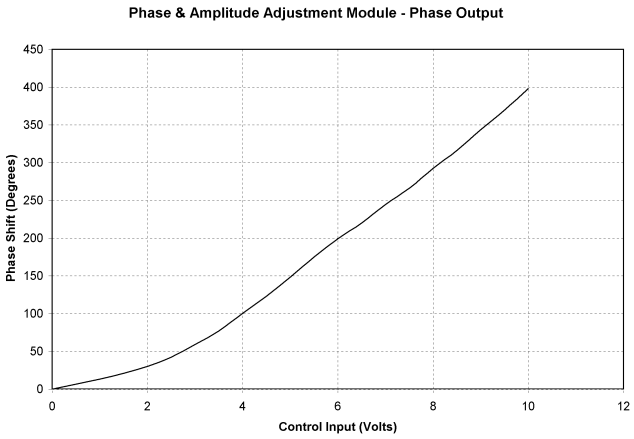

Figure 4: Phase and Amplitude Adjustment Module - Phase Output

The phase and amplitude adjustment module was reused to generate phase and amplitude differences between the RF inputs of the vector voltmeter module. The module DC output levels were recorded over the full platform phase and amplitude range between its RF inputs.

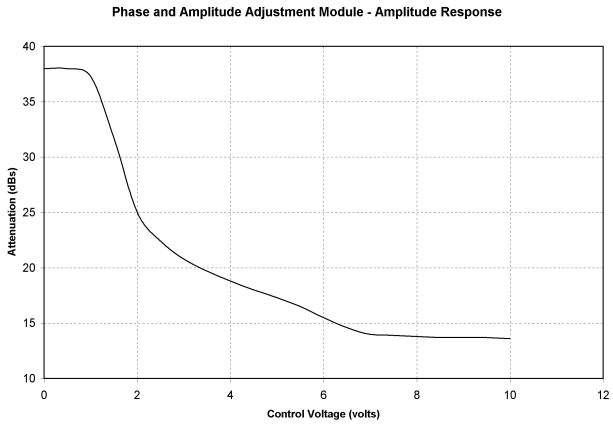

Figure 5: Phase and Amplitude Adjustment Module – Amplitude Output

Figures 6 shows the vector voltmeter phase output against phase input; the phase output is calculated from the I and Q outputs as described in the previous section. The response covers 360° before wrapping back to 0°, there is some non linearity but this could easily be adjusted for with a look up table. The relative amplitude plot in figure 7 shows a range of 25dBs for the platform; this is much greater than the expected amplitude mismatches in a beamformer.

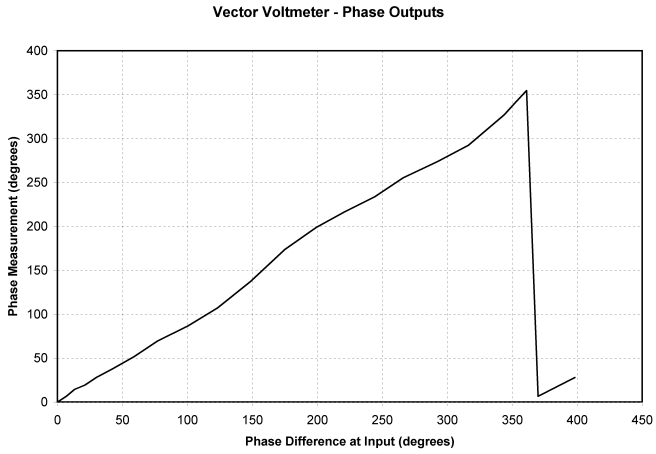

Figure 6: Vector Voltmeter - Phase Output

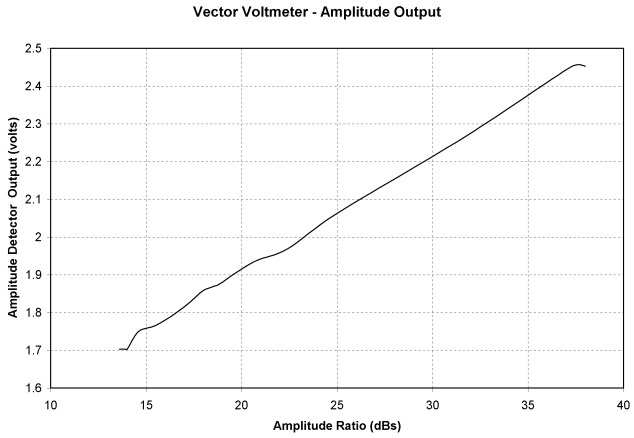

Figure 7: Vector Voltmeter - Amplitude Output

IV. Calibration Algorithm Demonstration

The initial application for the platform was to test calibration algorithms developed at the Institute. The calibration algorithms work by defining a single antenna element as a reference and calibrating all other antennas relative to that reference by following a particular route through the elements of the array. The choice of reference element and the path chosen determines the efficacy of the algorithm in terms of accuracy and speed. The results of testing on different algorithms have been presented in [9]. In this paper the measurements from testing one of these algorithms will be presented as an illustration of the capabilities of the platform.

The dual path algorithm is a comparison based calibration algorithm. It selects a reference element in the left hand corner of the array and then performs comparisons with the elements coupled to the reference antenna element; it takes two paths of identical length to each element of the array from the reference antenna.

These two paths are averaged to reduce the effect of coupler errors.

Figure 8 shows a photograph of the calibration algorithm test set-up. The antenna connections on the 2x4 coupler array were connected to the inputs of a high speed digital oscilloscope (Agilent Infinium 5483A DSO 2.5GHz); unused antenna connections were terminated with 50Ω loads. The oscilloscope offers resolutions of better than 1° in phase and better than 0.1dB in amplitude which is sufficient to verify the operation of the platform and algorithm.

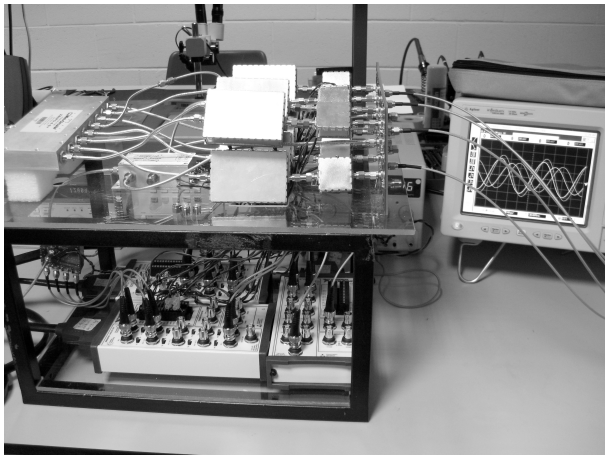

Figure 8: Calibration and beamforming platform with antennas replaced by a high speed digital oscilloscope

To represent an uncalibrated system, each channel was set to a random phase shift and amplitude attenuation by applying control voltages to the phase and amplitude adjustment modules. An oscillogram of the random phase and amplitude relationships on four of the antenna connections is shown in Figure 9. The dual path algorithm was then run in Labview on the platform PC and the phase and amplitude relationships were measured on the oscilloscope; Figure 10 shows an oscillogram of the signals at the antenna connectors after calibration.

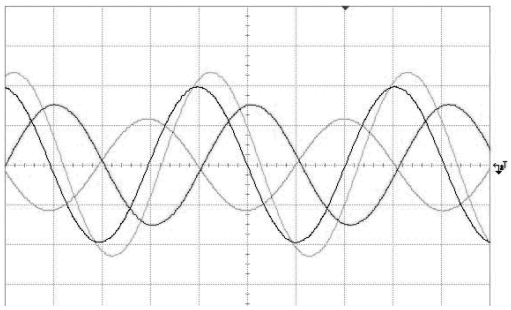

Figure 9: Oscillogram of uncalibrated output signals

From the oscillograms it is clear that after calibration there is no visible phase difference and a small visible amplitude difference between the channels. More precise measurements for each TX output of the array are presented in Table 1

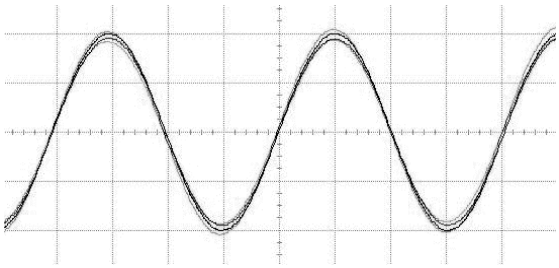

Figure 10: Oscillogram of antenna connections after calibration

Table 1: Transmit phase and amplitude measurements wrt TX1

	TX1	TX2	TX3	TX4	TX5	TX6	TX7	TX8
Phase wrt TX1 (°)	0	1.8	-2.2	-2.2	-1.6	0.l8	0.4	-0.4
Amplitude wrt TX1 dB	0	0.11	-0.27	-0.03	-0.49	-0.56	-0.22	-0.3

The results table shows that the maximum phase difference from the reference element (TX1) was 2.2° and between elements was 4°. The maximum amplitude difference between the reference and the other elements was 0.56dB and between all elements was 0.67dB.

V. CONCLUSIONS

This paper presented a test platform for the exploration and development of tower top antenna array calibration algorithms and technology. The platform operates at 2.46GHz and uses off-the-shelf components in a modular easily expandable architecture. The software, Labview, allows easy configuration of the hardware and implementation of calibration algorithms. Platform measurements were presented which showed a phase and amplitude control range of 0 to 360° and 25dB respectively for each array output. Additionally a calibration routine was run on an array with antenna outputs preset to random amplitudes and phases, the routine succeeded in reducing the phase and amplitude difference between outputs to less than 1dB amplitude and 5° phase.

ACKNOWLEDGMENT

The authors would like to thank Science foundation Ireland for their generous funding of this project through the Centre for Telecommunications Value Chain Driven Research (CTVR).

REFERENCES

[1] J. K. Hsiao, "Design of error tolerance of a phased array," Electronics Letters, vol. 21, pp. 834-836, 1985

[2] N. Jablon, "Effect of element errors on half-power beamwidth of the Capon adaptive beamformer," Circuits and Systems, IEEE Transactions on, vol. 34, pp. 743-752, 1987

[3] R. Elliott, "Mechanical and electrical tolerances for two-dimensional scanning antenna arrays," Antennas and Propagation, IRE Transactions on, vol. 6, pp. 114-120, 1958

[4] K. Carver, W. Cooper, and W. Stutzman, "Beam-pointing errors of planar-phased arrays," Antennas and Propagation, IEEE Transactions on, vol. 21, pp. 199-202, 1973.

[5] J. McCormack, T. Cooper, and R. Farrell, "Tower-Top Antenna Array Calibration Scheme for Next Generation Networks," EURASIP Journal on Wireless Communications and Networking, vol. 2007, pp. 12, 2007

[6] Y. Huang, "Design of a Dynamic Beamforming Antenna for Wimax Radio Systems", Aerospace Conference 2008 IEEE, pp.1 – 6, 2008

[7] J. McCormack, T. Cooper, and R. Farrell, "A Multi-Path Algorithmic Approach to Phased Array Calibration," presented at Antennas and Propagation, 2007. EuCAP 2007. The Second European Conference on, 2007

[8] T. S. Cooper, G. Baldwin, and R. Farrell, "Six-port precision directional coupler," Electronics Letters, vol. 42, pp. 1232-1233, 2006.

[9] J. McCormack, G. Corley, and R. Farrell, "Experimental Results of Non-Radiative Calibration of a Tower Top Adaptive Array", 3rd European Conference on Antennas and Propagation, EuCAP 2009. *Awaiting publication*.

[10] T. S. Cooper, J. Mc Cormack, R. Farrell and G. Baldwin. "Towards Scalable, Automated Tower–Top Phased Array Calibration", Vehicular Technology Conference, Dublin, Ireland April 23 – 25, 2007

References

[1] T. K. Sarkar, R. J. Mailloux, A. A. Oliner, M. S.-. Palma, and D. L. Sengipta, *History of Wireless*: John Wiley & Sons Inc., 2006.

[2] H. Friis, "A New Directional Recieving System," *Proceedings of the Institute of Radio Engineers,* vol. 13, pp. 685 - 708, Dec 1 1925.

[3] P. S. Carter, C. W. Hansell, and N. E. Lindenblad, "Development of Directive Transmitting Antennas by RCA Communication Inc.," *Proceedings of the Institute of Radio Engineers,* vol. 19, pp. 1773 - 1842, Oct 1 1931.

[4] H. H. Beverage, C. W. Rice, and E. W. Kellogg, "The Wave Antenna," *Journal of the American Institute of Electrical Engineers,* vol. XLII, pp. 258 - 269, Mar 1 1923.

[5] H. T. Friis and C. Feldman, "A Multiple Unit Steerable Antenna for Short Wave Reception," *Proceedings of the Institute of Radio Engineers,* vol. 25, pp. 841 - 917, Jul 1 1937.

[6] M. Fulilove, W. Scott, and J. Tomlinson, "The Hourglass Scanner - A New Rapid Scan, Large Aperture Antenna," *Institute of Radio Engneers, Internatioanl Convention Record,* vol. 7, pp. 190 - 200, Mar 1 1959.

[7] K. T. Button, "A Review of Microwave Ferrite Devices," in *PTGMTT National Symposium Digest*, 1963, pp. 167 - 170.

[8] W. F. Gabriel, "Adaptive Arrays - An Introduction," *IEEE Proceedings,* vol. 64, pp. 239 - 272, Feb 1 1976.

[9] B. Widrow, P. E. Mantey, L. J. Griffiths, and B. B. Goode, "Adaptive Antenna Systems," *Proceedings of the IEEE,* vol. 55, pp. 2143 - 2159, Dec 1 1967.

[10] R. M. Barrett, "Microwave Printed Circuits - A Historical Survey," *IEEE Trans. on Microwave Theory and Techniques,* vol. 3, pp. 1 - 9, Mar 1 1955.

[11] S. Applebaum, "Adaptive arrays," *Antennas and Propagation, IEEE Transactions on,* vol. 24, pp. 585-598, 1976.

[12] I. El - Azhary, M. S. Afifi, and P. S. Excell, "A Simple Algorithm for Sidelobe Cancellation in a Partially Adaptive Linear Array," *IEEE Trans. on Antenna and Propagation,* vol. 36, pp. 1482 - 1486, Oct 1 1988.

[13] B. Widrow, J. M. McCool, M. C. Larimore, and C. R. Johnson Jr., "Stationary and Non - Stationary Learning Characteristics of the LMS Adaptive Filter," *Proceedings of the IEEE,* vol. 64, pp. 1151 - 1162, Jan 1 1976.

[14] C. R. Baker and L. R. Chow, "Effect of Sampling Time Jitter on Array Performance," *IEEE Trans. on Aerospace and Electronic Systems,* vol. 14, pp. 780 - 788, Sep 1 1978.

[15] W. F. Gabriel, "Adaptive Processing Antenna Systems," *IEEE Antenna and Propagation Society Newsletter,* vol. 25, pp. 4 - 11, Oct 1 1983.

[16] W. F. Gabriel, "A Superresolution Traget - Tracking Concept," in *Antenna and Propagation Society International Symposium*, 1983, pp. 195 - 198.

[17] B. P. Ng, M. H. Er, and C. Kot, "A MUSIC Approach for Estimation of Direction of Arrival of Multiple Narrowband and Broadband Sources," in *IEEE Regions 10's Ninth Annual International Conference, Frontiers of Computer technology*, 1994, pp. 537 - 540.

[18] B. Ottersten, M. Viberg, and T. Kailath, "Performance Analysis of the Total Least Squares ESPRIT Algorithm," *IEEE Trans. on Acoustics, Speech and Signal Processing,* vol. 39, pp. 1122 - 1135, Mar 4 1991.

[19] P. Stoica and K. C. Sharman, "Maximum Likelihood Methods for Direction - of - Arrival Estimation," *IEEE Trans. on Acoustics, Speech and Signal Processing,* vol. 38, pp. 1132 - 1143, Jul 1 1990.

[20] J. Winters, "Propagation aspects for smart antennas in wireless systems," in *Antennas and Propagation Society International Symposium, IEEE*, 2000, p. 66 vol.1.

[21] Do-Hong, T. and P. Russer, "Signal Processing for Wideband Smart Antenna Array Applications," *IEEE Microwave Magazine,* vol. 5, pp. 57 - 67, Mar 1 2004.

[22] Z. Zhijun, M. F. Iskander, Y. Zhengqing, and A. Host-Madsen, "Hybrid smart antenna system using directional elements - performance analysis in flat Rayleigh fading," *Antennas and Propagation, IEEE Transactions on,* vol. 51, pp. 2926-2935, 2003.

[23] P. S. Carter, "Circuit Relations in Radiating Systems and Applications to Antenna Problems," *Proceedings of the Institute of Radio Engineers,* vol. 20, pp. 1004 - 1041, June 1932 1932.

[24] J. Andersen, H. Lessow, and H. Schjaer-Jacobsen, "Coupling between minimum scattering antennas," *Antennas and Propagation, IEEE Transactions on,* vol. 22, pp. 832-835, 1974.

[25] C. A. Balanis, *Antenna Theory - Analysis and Design*, 2nd ed.: John Wiley and Sons Inc., 1997.

[26] J. D. Kraus and R. J. Marhefka, *Antennas - for all applications*: McGraw-Hill Science, 2003.

[27] M. N. O. Sadiku, *Elements of Electromagnetics*: Oxford University Press, 2001.

[28] M. Andreasen, "Linear arrays with variable interelement spacings," *Antennas and Propagation, IRE Transactions on,* vol. 10, pp. 137-143, 1962.

[29] R. C. Hansen, A. Rudge, K. Milne, A. Olver, and P. Knight, "Linear Arrays," in *The Handbook of Antenna Design*. vol. 1 & 2: The Insitute of Electrical Engineers, 1986, pp. 695 - 834.

[30] R. W. P. King, M. Owens, and T. T. Wu, "Properties and Applications of the Large Circular Resonant Dipole Array," *IEEE Trans. on Antenna and Propagation,* vol. 51, pp. 103-109, Jul 31 2003.

[31] R. J. Mailloux, "Patterns of Nonplanar Arrays," in *Phased Array Antenna Handbook*: Artech House, 2005, pp. 185 - 221.

[32] D. Davies, A. Rudge, K. Milne, A. Olver, and P. Knight, "Circular Arrays," in *The Handbook of Antenna Design*. vol. 1 & 2: Institute of Electrical Engineers, 1986.

[33] S. Drabowitch, A. Paprernik, H. Griffiths, J. Encinas, and B. Smith, *Modern Antennas*: Springer, 1998.

[34] H. Nord, "Implementation of 8x8 Butler Matrix in Microstrip." vol. Diploma Stockholm, Sweden: Royal Institute of Technology, 2000.

[35] C. B. J. Dietrich., "Adaptive Arrays and Diversity Antenna Confirgurations for Handheld Wireless Communication Terminals," in *Electrical and Computer Engineering*. PhD Blacksburg, Virginia: Virginia Tech 2000.

[36] A. Villeneuve, "Taylor patterns for discrete arrays," *Antennas and Propagation, IEEE Transactions on,* vol. 32, pp. 1089-1093, 1984.

[37] W. White, "A flexible synthesis procedure for line source antennas," *Antennas and Propagation, IEEE Transactions on,* vol. 24, pp. 857-859, 1976.

[38] E. C. Dufort, "Pattern synthesis based on adaptive array theory," *Antennas and Propagation, IEEE Transactions on,* vol. 37, pp. 1011-1018, 1989.

[39] M. M. Dawoud, A. Tennant, and A. P. Anderson, "Null Steering in Adaptive Arrays using a Genetic Algorithm," in *European Microwave Conference, 1994. 24th*, 1994, pp. 1108-1114.

[40] M. Donelli, S. Caorsi, F. D. Natale, M. Pastorino, and A. Massa, "Linear Antenna Synthesis with a Hybrid Genetic Algorithm," *Progress in Electromagnetics Research PIER,* vol. 49, pp. 1 - 22, 2004.

[41] F. Ares, E. Villanueva, J. A. Rodriguez, and S. R. Rengarajan, "Application of genetic algorithms in the design and optimization of array patterns," in *Antennas and Propagation Society International Symposium, 1997. IEEE., 1997 Digest*, 1997, pp. 1684-1687 vol.3.

[42] M. Shimizu, "Determining the excitation coefficients of an array using genetic algorithms," in *Antennas and Propagation Society International Symposium, 1994. AP-S. Digest*, 1994, pp. 530-533 vol.1.

[43] A. Tennant, M. M. Dawoud, and A. P. Anderson, "Array pattern nulling by element position perturbations using a genetic algorithm," *Electronics Letters,* vol. 30, pp. 174-176, 1994.

[44] J. Bae, K. Kim, and C. Pyo, "Design of Steerable Linear and Planar Array Geometry with Non-uniform Spacing for Side-Lobe Reduction," *IEICE Trans Commun,* vol. E88-B, pp. 345-357, Jan 1 2005.

[45] R. Eberhart and J. Kennedy, "A new optimizer using particle swarm theory," in *Micro Machine and Human Science, 1995. MHS '95., Proceedings of the Sixth International Symposium on*, 1995, pp. 39-43.

[46] M. M. Khodier and C. G. Christodoulou, "Linear Array Geometry Synthesis With Minimum Sidelobe Level and Null Control Using Particle Swarm Optimization," *Antennas and Propagation, IEEE Transactions on,* vol. 53, pp. 2674-2679, 2005.

[47] K. Mahmoud, M. EL-Adary, S. Ibrahem, R. Bansal, and S. Zanul-Deen, "A Comparison between circular and hexagonal array geometries for smart antenna systems using particle swarm optimization," *Progress in Electromagnetics Research PIER,* vol. 72, pp. 75 - 90, 2007.

[48] A. M. Vural, "Effects of Perturbations on the Performance of Optimum/Adaptive Arrays," *Aerospace and Electronic Systems, IEEE Transactions on,* vol. AES-15, pp. 76-87, 1979.

[49] B. B. Kerim Guney, "Amplitude-only pattern nulling of linear antenna arrays with the use of an immune algorithm," *International Journal of RF and Microwave Computer-Aided Engineering,* vol. 18, pp. 397-409, 2008.

[50] M. Rattan, M. Patterh, and B. Sohi, "Antenna Array Optimization using Evolutionary Approaches," in *APEIRON*, 2008.

[51] A. J. Weiss, A. S. Willsky, and B. C. Levy, "Maximum likelihood array processing for the estimation of superimposed signals," *Proceedings of the IEEE,* vol. 76, pp. 203-205, 1988.

[52] T. K. Sarkar and N. Sangruji, "An adaptive nulling system for a narrow-band signal with a look-direction constraint utilizing the conjugate gradient method," *Antennas and Propagation, IEEE Transactions on,* vol. 37, pp. 940-944, 1989.

[53] L. C. Godara, "Application of antenna arrays to mobile communications. II. Beam-forming and direction-of-arrival considerations," *Proceedings of the IEEE,* vol. 85, pp. 1195-1245, 1997.

[54] M. Viberg and B. Ottersten, "Sensor array processing based on subspace fitting," *Signal Processing, IEEE Transactions on,* vol. 39, pp. 1110-1121, 1991.

[55] H. Krim and M. Viberg, "Two decades of array signal processing research: the parametric approach," *Signal Processing Magazine, IEEE,* vol. 13, pp. 67-94, 1996.

[56] J. B. Andersen, "Array gain and capacity for known random channels with multiple element arrays at both ends," *IEEE Journal on Selected Areas in Communications,* vol. 18, pp. 2172-2178, Sep 15 2000.

[57] Y. Wang and K. Roy, "A New Reduced-Complexity Sphere Decoder with True Lattice-Boundary-Awareness for Multi-Antenna Systems," *IEEE International Symposium on Circuits and Systems ISCAS,* vol. 5, pp. 4963-4966, Jan 14 2005.

[58] R. Yanhua, Z. Yan, L. Shanjian, and Z. Shidong, "3.52-GHz MIMO radio channel sounder," in *Communications, Circuits and Systems, 2008. ICCCAS 2008. International Conference on*, 2008, pp. 79-83.

[59] Q. H. Spencer, C. B. Peel, A. L. Swindlehurst, and M. Haardt, "An introduction to the Multi User MIMO Downlink," *IEEE Communications Magazine,* vol. October, pp. 60-67, Jul 31 2004.

[60] G. J. Foschini, G. D. Golden, R. A. Valenzuela, and P. W. Wolniamsky, "Simplified Processing for High Spectral Efficiency Wireless Communication

Employing Multi-Element Arrays," *IEEE Journal of Selected Areas in Communications,* vol. 17, pp. 1841-1852, Sep 15 1999.

[61] R. Spring, L. Zhou, N. Gogate, and A. S. Daryoush, "4 x 4 MIMO Experimental Test-bed using COTS at ISM Band," in *Radio and Wireless Symposium, 2007 IEEE*, 2007, pp. 173-176.

[62] S. Nanda, R. Walton, J. Ketchum, M. Wallace, and S. Howard, "A High-Performance MIMO OFDM Wireless LAN," *IEEE Communications Magazine,* vol. February, pp. 101-109, Jul 31 2005.

[63] K. Boyle, "Radiation patterns and correlation of closely spaced linear antennas," *Antennas and Propagation, IEEE Transactions on,* vol. 50, pp. 1162-1165, 2002.

[64] K. Carver, W. Cooper, and W. Stutzman, "Beam-pointing errors of planar-phased arrays," *Antennas and Propagation, IEEE Transactions on,* vol. 21, pp. 199-202, 1973.

[65] M. Feder and E. Weinstein, "Parameter estimation of superimposed signals using the EM algorithm," *Acoustics, Speech and Signal Processing, IEEE Transactions on,* vol. 36, pp. 477-489, 1988.

[66] A. Swindlehurst, "Synchronization and spatial signature estimation for multiple known co-channel signals," in *Signals, Systems and Computers, 1995. 1995 Conference Record of the Twenty-Ninth Asilomar Conference on*, 1995, pp. 398-402 vol.1.

[67] T. Chulajata, H. M. Kwon, and K. Y. Min, "Adaptive antenna array with no phase calibration for CDMA reverse link," in *Vehicular Technology Conference, 2000. IEEE VTS-Fall VTC 2000. 52nd*, 2000, pp. 127-134 vol.1.

[68] M. Wennstrom, T. Oberg, and A. Rydberg, "Effects of finite weight resolution and calibration errors on the performance of adaptive array antennas," *Aerospace and Electronic Systems, IEEE Transactions on,* vol. 37, pp. 549-562, 2001.

[69] H. Weiguang and H. M. Kwon, "Effect of mixer phase distortions on the DOA tracking algorithm for an adaptive antenna array," in *Vehicular Technology Conference, 2001. VTC 2001 Spring. IEEE VTS 53rd*, 2001, pp. 248-252 vol.1.

[70] N. Tyler, B. Allen, and H. Aghvami, "Adaptive antennas: the calibration problem," *Communications Magazine, IEEE,* vol. 42, pp. 114-122, 2004.

[71] M. Ganz and R. Compton, Jr., "A data-derived reference signal technique for adaptive arrays," in *Antennas and Propagation Society International Symposium, 1987*, 1987, pp. 58-61.

[72] F. Amoozegar, L. Paal, A. Mileant, and D. Lee, "Analysis of errors for uplink array of 34-m antennas for deep space applications," in *Aerospace Conference, 2005 IEEE*, 2005, pp. 1235-1257.

[73] S. D. Hayward and A. R. Beckett, "Bounding the angular scale factor error for adaptive arrays," *Radar, Sonar and Navigation, IEE Proceedings -,* vol. 151, pp. 71-75, 2004.

[74] L. Min and Y. Luxi, "Effect and calibration of mutual coupling in circular smart antenna applications," in *Microwave Conference Proceedings, 2005. APMC 2005. Asia-Pacific Conference Proceedings*, 2005, p. 4 pp.

[75] L. C. Godara, "Error Analysis of the Optimal Antenna Array Processors," *Aerospace and Electronic Systems, IEEE Transactions on,* vol. AES-22, pp. 395-409, 1986.

[76] M. Mowler and B. Lindmark, "Estimation of coupling, element factor, and phase center of antenna arrays," in *Antennas and Propagation Society International Symposium, 2005 IEEE*, 2005, pp. 6-9 vol. 4B.

[77] L. Yane, Y. Yuguo, Y. Jianguo, W. Dewei, D. Chuanjin, and Y. Huoping, "The Effect of Channel Mismatch and Mutual Coupling on GPS Adaptive Antenna Array," in *Radar, 2006. CIE '06. International Conference on*, 2006, pp. 1-5.

[78] G. Efstathopoulos, G. Elissaios, and A. Manikas, "The Effect of Uncertainties on the Performance of Array Systems," in *Personal, Indoor and Mobile Radio Communications, 2007. PIMRC 2007. IEEE 18th International Symposium on*, 2007, pp. 1-5.

[79] R. T. Compton, "Multiplier Offset Voltages in Adaptive Arrays," *Aerospace and Electronic Systems, IEEE Transactions on,* vol. AES-12, pp. 616-627, 1976.

[80] L. Godara, "The effect of phase-shifter errors on the performance of an antenna-array beamformer," *Oceanic Engineering, IEEE Journal of,* vol. 10, pp. 278-284, 1985.

[81] E. Lier, D. Purdy, J. Ashe, and G. Kautz, "An on-board integrated beam conditioning system for active phased array satellite antennas," in *Phased Array Systems and Technology, 2000. Proceedings. 2000 IEEE International Conference on*, 2000, pp. 509-512.

[82] S. C. Swales, T. Busby, D. J. Purle, M. A. Beach, and J. P. McGeehan, "A comparison of CDMA techniques for third generation mobile radio systems," in *Vehicular Technology Conference, 1993 IEEE 43rd*, 1993, pp. 424-427.

[83] G. V. Tsoulos, M. A. Beach, and S. C. Swales, "Sensitivity analysis of capacity enhancement with adaptive multibeam antennas for DCS1800," *Electronics Letters,* vol. 32, pp. 1745-1747, 1996.

[84] G. V. Tsoulos, M. A. Beach, and S. C. Swales, "On the sensitivity of the capacity enhancement of a TDMA system with adaptive multibeam antennas," in *Vehicular Technology Conference, 1997 IEEE 47th*, 1997, pp. 165-169 vol.1.

[85] I. J. Gupta, J. R. Baxter, S. W. Ellingson, P. Hyung-Geun, O. Hyun Seo, and K. Mun Geon, "An experimental study of antenna array calibration," *Antennas and Propagation, IEEE Transactions on,* vol. 51, pp. 664-667, 2003.

[86] P. N. Fletcher and M. Dean, "Derivation of orthogonal beams and their application to beamforming in small phased arrays," *Microwaves, Antennas and Propagation, IEE Proceedings -,* vol. 143, pp. 304-308, 1996.

[87] R. J. Mailloux, "Grating Lobes of a Linear Array and Planar Array," in *Phased Array Antenna Handbook*, 2nd ed: Artech House, 2005, pp. 27 - 30.

[88] R. Goossens and H. Rogier, "Optimal beam forming in the presence of mutual coupling," in *Communications and Vehicular Technology, 2006 Symposium on*, 2006, pp. 13-18.

[89] P. Darwood, P. N. Fletcher, and G. S. Hilton, "Pattern synthesis in small phased arrays using adaptive array theory," *Electronics Letters,* vol. 33, pp. 254-255, 1997.

[90] K. R. Dandekar, L. Hao, and X. Guanghan, "Experimental study of mutual coupling compensation in smart antenna applications," *Wireless Communications, IEEE Transactions on,* vol. 1, pp. 480-487, 2002.

[91] G. d'Elia, F. Soldovieri, and G. di Massa, "Mutual coupling compensation in a power synthesis technique of planar array antennas," *Microwaves, Antennas and Propagation, IEE Proceedings -,* vol. 147, pp. 95-99, 2000.

[92] P. Darwood, P. N. Fletcher, and G. S. Hilton, "Mutual coupling compensation in small planar array antennas," *Microwaves, Antennas and Propagation, IEE Proceedings -,* vol. 145, pp. 1-6, 1998.

[93] H. Rogier, "Mutual coupling compensation in uniform circular arrays with center element using a coupling matrix based on phase modes," in *Antennas and*

Propagation Society International Symposium 2006, IEEE, 2006, pp. 1133-1136.

[94] A. J. Weiss and B. Friedlander, "Mutual coupling effects on phase-only direction finding," *Antennas and Propagation, IEEE Transactions on,* vol. 40, pp. 535-541, 1992.

[95] P. N. Fletcher and M. Dean, "Application of retrodirective beams to achieve low sidelobe levels in small phased arrays," *Electronics Letters,* vol. 32, pp. 506-508, 1996.

[96] T. S. Bird, "Cross-coupling between open-ended coaxial radiators," *Microwaves, Antennas and Propagation, IEE Proceedings -,* vol. 143, pp. 265-271, 1996.

[97] C. Ruey-Shi, L. Kuan-Min, and W. Nam, "A network model of a feed through phased array lens of printed dipole elements," *Antennas and Propagation, IEEE Transactions on,* vol. 34, pp. 1410-1417, 1986.

[98] E. M. Friel and K. M. Pasala, "Effects of mutual coupling on the performance of STAP antenna arrays," *Aerospace and Electronic Systems, IEEE Transactions on,* vol. 36, pp. 518-527, 2000.

[99] J. Allen, "Gain and impedance variation in scanned dipole arrays," *Antennas and Propagation, IRE Transactions on,* vol. 10, pp. 566-572, 1962.

[100] S. Edelberg and A. Oliner, "Mutual coupling effects in large antenna arrays: Part 1--Slot arrays," *Antennas and Propagation, IRE Transactions on,* vol. 8, pp. 286-297, 1960.

[101] M. Malkomes, "Mutual coupling between microstrip patch antennas," *Electronics Letters,* vol. 18, pp. 520-522, 1982.

[102] R. Jedlicka, M. Poe, and K. Carver, "Measured mutual coupling between microstrip antennas," *Antennas and Propagation, IEEE Transactions on,* vol. 29, pp. 147-149, 1981.

[103] Y. Shiwen and N. Zaiping, "Mutual coupling compensation in time modulated linear antenna arrays," *Antennas and Propagation, IEEE Transactions on,* vol. 53, pp. 4182-4185, 2005.

[104] N. Amitay, J. Cook, R. Pecina, and C. Wu, "On mutual coupling and matching conditions in large planar phased arrays," in *Antennas and Propagation Society International Symposium, 1964*, 1964, pp. 150-156.

[105] M. Rammal, D. Eclercy, A. Reineix, and B. Jecko, "Study of mutual coupling effect on radiated patterns of antenna arrays," *Microwaves, Antennas and Propagation, IEE Proceedings -,* vol. 144, pp. 389-391, 1997.

[106] Y. Shiwen, N. Zaiping, and Y. Feng, "Mutual coupling compensation in small antenna arrays by the differential evolution algorithm," in *Microwave Conference Proceedings, 2005. APMC 2005. Asia-Pacific Conference Proceedings*, 2005, p. 4 pp.

[107] A. N. Lemma, E. F. Deprettere, and A. J. van der Veen, "Experimental analysis of antenna coupling for high-resolution DOA estimation algorithms," in *Signal Processing Advances in Wireless Communications, 1999. SPAWC '99. 1999 2nd IEEE Workshop on*, 1999, pp. 362-365.

[108] I. Gupta and A. Ksienski, "Effect of mutual coupling on the performance of adaptive arrays," *Antennas and Propagation, IEEE Transactions on,* vol. 31, pp. 785-791, 1983.

[109] N. Kojima, K. Hariu, and I. Chiba, "Low sidelobe pattern synthesis using projection method with mutual coupling compensation," in *Phased Array Systems and Technology, 2003. IEEE International Symposium on*, 2003, pp. 559-564.

[110] C. M. S. See, "A method for array calibration in parametric sensor array processing," in *Singapore ICCS '94. Conference Proceedings*, 1994, pp. 915-919 vol.3.

[111] B. Lindmark, S. Lundgren, J. R. Sanford, and C. Beckman, "Dual-polarized array for signal-processing applications in wireless communications," *Antennas and Propagation, IEEE Transactions on,* vol. 46, pp. 758-763, 1998.

[112] M. Bailey and C. Bostian, "Mutual coupling in a finite planar array of circular apertures," *Antennas and Propagation, IEEE Transactions on,* vol. 22, pp. 178-184, 1974.

[113] J. Blass and S. Rabinowitz, "Mutual coupling in two-dimensional arrays," in *WESCON/57 Conference Record*, 1957, pp. 134-150.

[114] C. B. Dietrich, Jr., K. Dietze, J. R. Nealy, and W. L. Stutzman, "Spatial, polarization, and pattern diversity for wireless handheld terminals," *Antennas and Propagation, IEEE Transactions on,* vol. 49, pp. 1271-1281, 2001.

[115] H. Rogier, "Spatial correlation in uniform circular arrays based on a spherical-waves model for mutual coupling," *AEU - International Journal of Electronics and Communications,* vol. 60, pp. 521-532, 2006.

[116] H. Rogier and E. Bonek, "Analytical spherical-mode-based compensation of mutual coupling in uniform circular arrays for direction-of-arrival estimation," *AEU - International Journal of Electronics and Communications,* vol. 60, pp. 179-189, 2006.

[117] H. Kitayoshi and K. Sawaya, "A study of a method of compensation for mutual coupling between multi-mode antennas and single-mode antennas," in *Antennas and Propagation Society International Symposium, 2003. IEEE*, 2003, pp. 713-716 vol.3.

[118] C. C. Yeh, M. L. Leou, and D. R. Ucci, "Bearing estimations with mutual coupling present," *Antennas and Propagation, IEEE Transactions on,* vol. 37, pp. 1332-1335, 1989.

[119] A. G. Demeryd, "Compensation of mutual coupling effects in array antennas," in *Antennas and Propagation Society International Symposium, 1996. AP-S. Digest*, 1996, pp. 1122-1125 vol.2.

[120] M. Kuipers, "Mutual coupling computation and effects in phased array microstrip antennas," in *Vehicular Technology Conference, 1998. VTC 98. 48th IEEE*, 1998, pp. 1181-1185 vol.2.

[121] R. Borowiec, R. Hossa, P. Slobodzian, and Z. Langowski, "Compensation of mutual coupling in small antenna arrays," in *Microwaves, Radar and Wireless Communications, 2002. MIKON-2002. 14th International Conference on*, 2002, pp. 894-897 vol.3.

[122] A. M. Wyglinski and S. D. Blostein, "Mutual coupling and scattering effects on cellular CDMA systems using smart antennas," in *Vehicular Technology Conference, 2000. IEEE VTS-Fall VTC 2000. 52nd*, 2000, pp. 1656-1662 vol.4.

[123] S. Sadat, C. Ghobadi, and J. Nourinia, "Mutual coupling compensation in small phased array antennas," in *Antennas and Propagation Society International Symposium, 2004. IEEE*, 2004, pp. 4128-4131 Vol.4.

[124] S. Stein, "On cross coupling in multiple-beam antennas," *Antennas and Propagation, IRE Transactions on,* vol. 10, pp. 548-557, 1962.

[125] W. H. Von Aulock, "Properties of Phased Arrays," *Proceedings of the IRE,* vol. 48, pp. 1715-1727, 1960.

[126] A. H. Mohammadian, L. M. Golovanevsky, S. S. Soliman, and M. A. Tassoudji, "Prediction of Mutual Coupling between Base Station Antenna Arrays," in *IEEE Radio and Wireless Conference RAWCON 2002*, 2002, pp. 153 - 156.

[127] K. M. Lee and R. S. Chu, "Analysis of mutual coupling between a finite phased array of dipoles and its feed network," *Antennas and Propagation, IEEE Transactions on,* vol. 36, pp. 1681-1699, 1988.

[128] N. Amitay, "Improvement of planar array match by compensation through contiguous element coupling," *Antennas and Propagation, IEEE Transactions on,* vol. 14, pp. 580-586, 1966.

[129] P. Hannan, D. Lerner, and G. Knittel, "Wide-angle impedance matching calculated for a phased array antenna," in *Antennas and Propagation Society International Symposium, 1963*, 1963, pp. 228-233.

[130] M. A. Ali and P. Wahid, "Analysis of mutual coupling effect in adaptive array antennas," in *Antennas and Propagation Society International Symposium, 2002. IEEE*, 2002, pp. 102-105 vol.1.

[131] R. Elliott and G. Stern, "The design of microstrip dipole arrays including mutual coupling, part I: Theory," *Antennas and Propagation, IEEE Transactions on,* vol. 29, pp. 757-760, 1981.

[132] H. Rogier and E. Bonek, "A model for describing mutual coupling in uniform circular arrays and its application to DOA estimation," in *Antennas and Propagation Society International Symposium, 2004. IEEE*, 2004, pp. 1251-1254 Vol.2.

[133] R. R. Ramirez and F. De Flaviis, "A mutual coupling study of linear and circular polarized microstrip antennas for diversity wireless systems," *Antennas and Propagation, IEEE Transactions on,* vol. 51, pp. 238-248, 2003.

[134] W. Kahn, "Ideal efficiency of a radiating element in an infinite array," *Antennas and Propagation, IEEE Transactions on,* vol. 15, pp. 534-538, 1967.

[135] W. Wasylkiwskyj and W. K. Kahn, "Mutual coupling and element efficiency for infinite linear arrays," *Proceedings of the IEEE,* vol. 56, pp. 1901-1907, 1968.

[136] J. Luo, J. R. Zeidler, and S. McLaughlin, "Performance analysis of compact antenna arrays with MRC in correlated Nakagami fading channels," *Vehicular Technology, IEEE Transactions on,* vol. 50, pp. 267-277, 2001.

[137] R. Bhagavatula, R. W. Heath, A. Forenza, D. Piazza, and K. R. Dandekar, "Impact of Mutual Coupling and Antenna Efficiencies on Adaptive Switching

Between MIMO Transmission Strategies," in *Vehicular Technology Conference, 2007. VTC-2007 Fall. 2007 IEEE 66th*, 2007, pp. 749-753.

[138] T. Svantesson and A. Ranheim, "Mutual coupling effects on the capacity of multielement antenna systems," in *Acoustics, Speech, and Signal Processing, 2001. Proceedings. (ICASSP '01). 2001 IEEE International Conference on*, 2001, pp. 2485-2488 vol.4.

[139] C. Krowne, "Dielectric and width effect on *H*-plane and *E*-plane coupling between rectangular microstrip antennas," *Antennas and Propagation, IEEE Transactions on,* vol. 31, pp. 39-47, 1983.

[140] J. Cook and R. Pecina, "Compensation coupling between elements in array antennas," in *Antennas and Propagation Society International Symposium, 1963*, 1963, pp. 234-236.

[141] P. J. B. Clarricoats, S. M. Tun, and C. G. Parini, "Effects of mutual coupling in conical horn arrays," *Microwaves, Optics and Antennas, IEE Proceedings H,* vol. 131, pp. 165-171, 1984.

[142] K. F. Warnick and M. A. Jensen, "Effects of Mutual Coupling on Interference Mitigation With a Focal Plane Array," *Antennas and Propagation, IEEE Transactions on,* vol. 53, pp. 2490-2498, 2005.

[143] K. M. Pasala and E. M. Friel, "Mutual coupling effects and their reduction in wideband direction of arrival estimation," *Aerospace and Electronic Systems, IEEE Transactions on,* vol. 30, pp. 1116-1122, 1994.

[144] T. S. Bird, "Modelling arrays of circular horns with choke rings," in *Antennas and Propagation Society International Symposium, 1996. AP-S. Digest*, 1996, pp. 226-229 vol.1.

[145] R. G. Vaughan, J. B. Andersen, and M. H. Langhorn, "Circular array of outward sloping monopoles for vehicular diversity antennas," *Antennas and Propagation, IEEE Transactions on,* vol. 36, pp. 1365-1374, 1988.

[146] T. S. Bird and D. G. Bateman, "Mutual coupling between rotated horns in a ground plane," *Antennas and Propagation, IEEE Transactions on,* vol. 42, pp. 1000-1006, 1994.

[147] R. G. Vaughan and J. B. Andersen, "Antenna diversity in mobile communications," *Vehicular Technology, IEEE Transactions on,* vol. 36, pp. 149-172, 1987.

[148] R. Mailloux, "Radiation and near-field coupling between two collinear open-ended waveguides," *Antennas and Propagation, IEEE Transactions on,* vol. 17, pp. 49-55, 1969.

[149] P. Hannan, "The element-gain paradox for a phased-array antenna," *Antennas and Propagation, IEEE Transactions on,* vol. 12, pp. 423-433, 1964.

[150] T. S. Bird, "Improved solution for mode coupling in different-sized circular apertures and its application," *Microwaves, Antennas and Propagation, IEE Proceedings -,* vol. 143, pp. 457-464, 1996.

[151] S. Edelberg and A. Oliner, "Mutual coupling effects in large antenna arrays II: Compensation effects," *Antennas and Propagation, IRE Transactions on,* vol. 8, pp. 360-367, 1960.

[152] D. D. Z. Hendrik Rogier, "Beamforming strategies for compact arrays in mobile terminals using the exact active element pattern method," *Microwave and Optical Technology Letters,* vol. 35, pp. 201-203, 2002.

[153] V. Galindo and C. Wu, "The relation between the far-zone pattern of the singly excited element and the transmission coefficient of the principal lobe in an infinite array," *Antennas and Propagation, IEEE Transactions on,* vol. 14, pp. 397-398, 1966.

[154] R. Mailloux, J. McIlvenna, and N. Kernweis, "Microstrip array technology," *Antennas and Propagation, IEEE Transactions on,* vol. 29, pp. 25-37, 1981.

[155] P. Hannan, "Proof that a Phased-Array Antenna can be Impedance Matched for all Scan Angles," *Radio Science,* vol. 2 (New Series), pp. 361 - 369, 1967.

[156] L. Lechtreck, "Effects of coupling accumulation in antenna arrays," *Antennas and Propagation, IEEE Transactions on,* vol. 16, pp. 31-37, 1968.

[157] C. Roller and W. Wasylkiwskyj, "Effects of mutual coupling on super-resolution DF in linear arrays," in *Acoustics, Speech, and Signal Processing, 1992. ICASSP-92., 1992 IEEE International Conference on*, 1992, pp. 257-260 vol.5.

[158] A. Fenn, G. Thiele, and B. Munk, "Moment method analysis of finite rectangular waveguide phased arrays," *Antennas and Propagation, IEEE Transactions on,* vol. 30, pp. 554-564, 1982.

[159] H. Steyskal and J. S. Herd, "Mutual coupling compensation in small array antennas," *Antennas and Propagation, IEEE Transactions on,* vol. 38, pp. 1971-1975, 1990.

[160] W. Wasylkiwskyj, "Mutual coupling effects in semi-infinite arrays," *Antennas and Propagation, IEEE Transactions on,* vol. 21, pp. 277-285, 1973.

[161] R. J. Mailloux, "Element Pattern Effects, Mutual Coupling, Gain Computued from Element Patterns," in *Phased Array Antenna Handbook*: Artech House, 2005, pp. 68 - 75.

[162] J. Allen and W. Delaney, "On the effect of mutual coupling on unequally spaced dipole arrays," *Antennas and Propagation, IRE Transactions on,* vol. 10, pp. 784-785, 1962.

[163] P. Hannan, "The ultimate decay of mutual coupling in a planar array antenna," *Antennas and Propagation, IEEE Transactions on,* vol. 14, pp. 246-248, 1966.

[164] J. Andersen and H. Rasmussen, "Decoupling and descattering networks for antennas," *Antennas and Propagation, IEEE Transactions on,* vol. 24, pp. 841-846, 1976.

[165] S. Hwang, T. K. Sarkar, and S. Best, "Direction of arrival (DOA) estimation using electrically small resonant dipole antennas," in *Radar, 2006 IEEE Conference on*, 2006, p. 8 pp.

[166] R. J. Garbacz, "Modal expansions for resonance scattering phenomena," *Proceedings of the IEEE,* vol. 53, pp. 856-864, 1965.

[167] R. Green, "Scattering from conjugate-matched antennas," *Antennas and Propagation, IEEE Transactions on,* vol. 14, pp. 17-21, 1966.

[168] W. Wasylkiwskyj and W. Kahn, "Theory of mutual coupling among minimum-scattering antennas," *Antennas and Propagation, IEEE Transactions on,* vol. 18, pp. 204-216, 1970.

[169] B. L. Diamond, "A generalized approach to the analysis of infinite planar array antennas," *Proceedings of the IEEE,* vol. 56, pp. 1837-1851, 1968.

[170] J. W. Wallace and M. A. Jensen, "The capacity of MIMO wireless systems with mutual coupling," in *Vehicular Technology Conference, 2002. Proceedings. VTC 2002-Fall. 2002 IEEE 56th*, 2002, pp. 696-700 vol.2.

[171] N. J. Kirsch and K. R. Dandekar, "Modeling effects of mutual coupling considered at both ends of a MIMO channel using computational electromagnetics," in *Vehicular Technology Conference, 2004. VTC2004-Fall. 2004 IEEE 60th*, 2004, pp. 4352-4355 Vol. 6.

[172] D. Pozar and D. Schaubert, "Analysis of an infinite array of rectangular microstrip patches with idealized probe feeds," *Antennas and Propagation, IEEE Transactions on,* vol. 32, pp. 1101-1107, 1984.

[173] D. M. Pozar, "Scanning characteristics of infinite arrays of printed antenna subarrays," *Antennas and Propagation, IEEE Transactions on,* vol. 40, pp. 666-674, 1992.

[174] W. Gregorwich, A. Hessel, G. Knittel, and A. Oliner, "A waveguide simulator for the determination of a phased-array resonance," in *Antennas and Propagation Society International Symposium, 1968*, 1968, pp. 134-141.

[175] H. A. Wheeler, "The Radiation Resistance of an Antenna in an Infinite Array or Waveguide," *Proceedings of the IRE,* vol. 36, pp. 478-487, 1948.

[176] H. Wheeler, "Simple relations derived from a phased array made of an infinite current sheet," in *Antennas and Propagation Society International Symposium, 1964*, 1964, pp. 157-160.

[177] E. DuFort, "Design of corrugated plates for phased array matching," *Antennas and Propagation, IEEE Transactions on,* vol. 16, pp. 37-46, 1968.

[178] N. Alexopoulos and I. Rana, "Mutual impedance computation between printed dipoles," *Antennas and Propagation, IEEE Transactions on,* vol. 29, pp. 106-111, 1981.

[179] G. H. Knittel, A. Hessel, and A. A. Oliner, "Element pattern nulls in phased arrays and their relation to guided waves," *Proceedings of the IEEE,* vol. 56, pp. 1822-1836, 1968.

[180] D. Pozar, "Input impedance and mutual coupling of rectangular microstrip antennas," *Antennas and Propagation, IEEE Transactions on,* vol. 30, pp. 1191-1196, 1982.

[181] D. Pozar, "General relations for a phased array of printed antennas derived from infinite current sheets," *Antennas and Propagation, IEEE Transactions on,* vol. 33, pp. 498-504, 1985.

[182] M. Davidovitz, "Extension of the *E*-plane scanning range in large microstrip arrays by substrate modification," *Microwave and Guided Wave Letters, IEEE,* vol. 2, pp. 492-494, 1992.

[183] P. Katehi and N. Alexopoulos, "On the effect of substrate thickness and permittivity on printed circuit dipole properties," *Antennas and Propagation, IEEE Transactions on,* vol. 31, pp. 34-39, 1983.

[184] H. Wheeler, "Simple relations derived from a phased-array antenna made of an infinite current sheet," *Antennas and Propagation, IEEE Transactions on,* vol. 13, pp. 506-514, 1965.

[185] L. Shen, S. Long, M. Allerding, and M. Walton, "Resonant frequency of a circular disc, printed-circuit antenna," *Antennas and Propagation, IEEE Transactions on,* vol. 25, pp. 595-596, 1977.

[186] Y. Takeuchi, H. Hirayama, K. Fukino, T. Murayama, Y. Notsu, and A. Hayashi, "Auto calibrated distributed local loop configuration of array antenna for CDMA cellular base station," in *Spread Spectrum Techniques and Applications, 2000 IEEE Sixth International Symposium on*, 2000, pp. 666-670 vol.2.

[187] H. Hirayama, T. Hada, K. Fukino, and Y. Takeuchi, "Full synchronized distributed array antenna for CDMA base stations," in *Radio and Wireless Conference, 2003. RAWCON '03. Proceedings*, 2003, pp. 131-134.

[188] S. Kobayakawa, M. Tsutsui, and Y. Tanaka, "A blind calibration method for an adaptive array antenna in DS-CDMA systems using an MMSE algorithm," in *Vehicular Technology Conference Proceedings, 2000. VTC 2000-Spring Tokyo. 2000 IEEE 51st*, 2000, pp. 21-25 vol.1.

[189] L. Wu, G. Liao, and L. Zhang, "A blind calibration method for smart antenna system," in *TENCON '02. Proceedings. 2002 IEEE Region 10 Conference on Computers, Communications, Control and Power Engineering*, 2002, pp. 1031-1034 vol.2.

[190] S. Tanaka, T. Ihara, and M. Sawahashi, "Optimum transmit antenna weight generation method for adaptive antenna array transmit diversity in W-CDMA forward link," in *Vehicular Technology Conference, 2001. VTC 2001 Spring. IEEE VTS 53rd*, 2001, pp. 2302-2306 vol.4.

[191] P. Hyeong Getin, P. Chul, O. Hyunseo, and K. Mun Geon, "RF gain/phase and I/Q imbalance error correction technique for multi-channel array antenna systems," in *Vehicular Technology Conference, 2001. VTC 2001 Spring. IEEE VTS 53rd*, 2001, pp. 175-179 vol.1.

[192] J. Jae Ho, P. Hyung Geun, and R. Deuk Su, "Calibration techniques of multi-channel transceiver using noninterfering calibration signals for CDMA smart antenna systems," in *Signal Processing, 2002 6th International Conference on*, 2002, pp. 1629-1632 vol.2.

[193] F. Ellinger, U. Lott, and W. Bachtold, "A calibratable 4.8-5.8 GHz MMIC vector modulator with low power consumption for smart antenna receivers," in *Microwave Symposium Digest., 2000 IEEE MTT-S International*, 2000, pp. 1277-1280 vol.3.

[194] F. Ellinger, R. Vogt, and W. Bachtold, "Calibratable adaptive antenna combiner at 5.2 GHz with high yield for laptop interface card," *Microwave Theory and Techniques, IEEE Transactions on,* vol. 48, pp. 2714-2720, 2000.

[195] F. Ellinger, U. Lott, and W. Bachtold, "An antenna diversity MMIC vector modulator for HIPERLAN with low power consumption and calibration capability," *Microwave Theory and Techniques, IEEE Transactions on,* vol. 49, pp. 964-969, 2001.

[196] K. Nishimori, K. Cho, Y. Takatori, and T. Hori, "Automatic calibration method of adaptive array for FDD systems," in *Antennas and Propagation Society International Symposium, 2000. IEEE*, 2000, pp. 910-913 vol.2.

[197] K. Nishimori, K. Cho, Y. Takatori, and T. Hori, "Automatic calibration method using transmitting signals of an adaptive array for TDD systems," *Vehicular Technology, IEEE Transactions on,* vol. 50, pp. 1636-1640, 2001.

[198] K. Nishimori, K. Cho, and T. Hori, "Automatic calibration method of adaptive array utilizing signal circulation for linear array," in *Vehicular Technology Conference, 2001. VTC 2001 Fall. IEEE VTS 54th*, 2001, pp. 1819-1823 vol.3.

[199] G. Tsoulos, M. Beach, and J. McGeehan, "Wireless personal communications for the 21st century: European technological advances in adaptive antennas," *Communications Magazine, IEEE,* vol. 35, pp. 102-109, 1997.

[200] P. A. Howard and C. M. Simmonds, "An evaluation of the range extension achieved by the TSUNAMI (II) adaptive antenna testbed," in *Vehicular Technology Conference, 1999 IEEE 49th*, 1999, pp. 443-447 vol.1.

[201] G. V. Tsoulos, M. A. Beach, and S. C. Swales, "Adaptive antennas for third generation DS-CDMA cellular systems," in *Vehicular Technology Conference, 1995 IEEE 45th*, 1995, pp. 45-49 vol.1.

[202] G. V. Tsoulos, M. A. Beach, and S. C. Swales, "Performance enhancement of DS-CDMA PCS cellular networks with smart antennas," in *Global Telecommunications Conference, 1995. GLOBECOM '95., IEEE*, 1995, pp. 213-217 vol.1.

[203] G. V. Tsoulos, G. E. Athanasiadou, J. P. McGeehan, and M. Beach, "Adaptive antennas for UMTS microcellular operational environments," in *Vehicular Technology Conference, 1998. VTC 98. 48th IEEE*, 1998, pp. 895-898 vol.2.

[204] M. A. Beach, H. Xue, R. Davies, J. P. McGeehan, and M. Barrett, "Adaptive antennas for third generation systems," in *Mobile Communications Towards the Year 2000, IEE Colloquium on*, 1994, pp. 10/1-10/6.

[205] M. A. Beach, H. Xue, and J. P. McGeehan, "Adaptive antenna technologies for third generation systems," in *Antennas and Propagation, 1995., Ninth International Conference on (Conf. Publ. No. 407)*, 1995, pp. 344-347 vol.1.

[206] S. C. Swales, M. A. Beach, D. J. Edwards, and J. P. McGeehan, "The performance enhancement of multibeam adaptive base-station antennas for cellular land mobile radio systems," *Vehicular Technology, IEEE Transactions on,* vol. 39, pp. 56-67, 1990.

[207] G. V. Tsoulos and M. A. Beach, "Calibration and linearity issues for an adaptive antenna system," in *Vehicular Technology Conference, 1997 IEEE 47th*, 1997, pp. 1597-1600 vol.3.

[208] C. M. Simmonds, M. A. Beach, M. Newman, and R. Arnott, "TSUNAMI (II)-initial field trial results [macrocellular radio]," in *Antennas and Propagation for Future Mobile Communications (Ref. No. 1998/219), IEE Colloquium on*, 1998, pp. 9/1-9/6.

[209] A. Agrawal and A. Jablon, "A calibration technique for active phased array antennas," in *Phased Array Systems and Technology, 2003. IEEE International Symposium on*, 2003, pp. 223-228.

[210] T. Brauner, R. Vogt, and W. Bachtold, "A versatile calibration method for small active antenna arrays," in *Microwave Conference, 2003. 33rd European*, 2003, pp. 797-800 vol.2.

[211] G. A. Hampson and A. B. Smolders, "A fast and accurate scheme for calibration of active phased-array antennas," in *Antennas and Propagation Society International Symposium, 1999. IEEE*, 1999, pp. 1040-1043 vol.2.

[212] K. M. Lee, R. S. Chu, and S. C. Liu, "A built-in performance monitoring/fault isolation and correction (PM/FIC) system for active phased array antennas," in *Antennas and Propagation Society International Symposium, 1993. AP-S. Digest*, 1993, pp. 206-209 vol.1.

[213] K. M. Lee, R. S. Chu, and S. C. Liu, "A performance monitoring/fault isolation and correction system of a phased array antenna using transmission-line signal injection with phase toggling method," in *Antennas and Propagation Society International Symposium, 1992. AP-S. 1992 Digest. Held in Conjuction with: URSI Radio Science Meeting and Nuclear EMP Meeting., IEEE*, 1992, pp. 429-432 vol.1.

[214] R. S. Chu and K. M. Lee, "Analysis and development of signal injection technique using transmission lines embedded at phased array aperture," in *Antennas and Propagation Society International Symposium, 1992. AP-S. 1992 Digest. Held in Conjuction with: URSI Radio Science Meeting and Nuclear EMP Meeting., IEEE*, 1992, pp. 433-436 vol.1.

[215] B. Smolders and G. Hampson, "Deterministic RF ing in phased arrays for the next generation of radio telescopes," *Antennas and Propagation Magazine, IEEE,* vol. 44, pp. 13-22, 2002.

[216] F. Amoozegar, L. Paal, J. Layland, R. Cesarone, V. Jamnejad, A. Silva, D. Losh, B. Conroy, and T. Cornish, "Uplink array system of antennas for the deep space network," *IEEE Aerospace Conference Proceedings,* vol. 2, pp. 1142-1160, Feb 26 2004.

[217] Q. Han, K. Inagaki, B. Hanna, and T. Ohira, "Evanescent Reactive-Near-Field Measurement for ESPAR Antenna Characterization," *IEEE Trans. on Antenna and Propagation,* vol. 54, pp. 2953-2961, Jun 23 2006.

[218] L. Duchesne, P. Garreau, N. Robic, A. Gandois, P. O. Iversen, and G. Barone, "Compact multi-probe antenna test station for rapid testing for antenns and wireless terminals," *5th International Symposium on Multi-Dimensional Mobile Communications and 10th Asia-Pacific Conference on Communications,* pp. 553-557, Jun 23 2004.

[219] L. Foged, B. Bencivenga, L. Durand, O. Breinbjerg, S. Pivnenko, C. Sabatier, H. Ericsson, B. Svensson, A. Alexandridis, S. Burgos, M. Sierra-Castaner, J. Zackrisson, and M. Boettcher, "Error Calculations Techniques and their Applications to the Antenna Measurement Facilities Comparison within the European Antenna Centre of Excellence," *Antennas and Propagation, 2007. EuCAP 2007. The Second European Conference on,* pp. 1-6, Jul 15 2007.

[220] V. A. Usin, O. D. Anohina, V. A. Kovalchuk, and A. V. Usina, "Application of linear phased antenna array for the antenna near field measurement," *5th*

International Conference on Antenna Theory and Techniques, Kyiv, Ukraine, pp. 405 - 407 Jun 23 2005.

[221] S. Dieter and W. Menzel, "High-Resolution Probes for Near-Field Measurements of Reflectarray Antennas," *IEEE Antennas and Wireless Propagation Letters,* vol. 8, pp. 157 -160, Jun 23 2009.

[222] M. H. A. Paquay, "STATE OF THE ART IN ANTENNA MEASUREMENTS IN EUROPE," *IEE Antenna Measurements and SAR, 2004. AMS 2004. ,* pp. 14-18, Jul 15 2004.

[223] B.-H. Wang, Y.-L. Wang, and H. Chen, "Array calibration of angularly dependent gain and phase uncertainties with instrumental sensors," in *Phased Array Systems and Technology, 2003. IEEE International Symposium on*, 2003, pp. 182-186.

[224] H. Pawlak, D. Notel, and A. F. Jacob, "Compact calibration scheme for planar DBF transmit antenna arrays using circular polarization at Ka-band," in *Antennas and Propagation Society International Symposium, 2005 IEEE*, 2005, pp. 752-755 vol. 2B.

[225] H. Pawlak, A. Charaspreedalarp, and A. F. Jacob, "Experimental Investigation of an External Calibration Scheme for 30 GHz Circularly Polarized DBF Transmit Antenna Arrays," in *Microwave Conference, 2006. 36th European*, 2006, pp. 764-767.

[226] R. Sorace, "Phased array calibration," *Antennas and Propagation, IEEE Transactions on,* vol. 49, pp. 517-525, 2001.

[227] D. L. Jones, "Weak-signal phase calibration strategies for large DSN arrays," in *Aerospace Conference, 2005 IEEE*, 2005, pp. 1150-1157.

[228] R. Lewenz, P. Filippidis, and S. Salous, "Antenna array calibration for a multi-channel direction of arrival sounder," in *High Frequency Postgraduate Student Colloquium, 2001. 6th IEEE*, 2001, pp. 119-124.

[229] C. Dau-Chyrh and J. Shin-Huei, "The study of Butler matrix BFN for four beams antenna system," in *Antennas and Propagation Society International Symposium, 2003. IEEE*, 2003, pp. 176-179 vol.4.

[230] B. Sheleg, "A matrix fed circular array for continuous scanning," in *Antennas and Propagation Society International Symposium, 1968*, 1968, pp. 7-16.

[231] B. Sheleg, "Butler submatrix feed systems for antenna arrays," *Antennas and Propagation, IEEE Transactions on,* vol. 21, pp. 228-229, 1973.

[232] J. Blass, "Multidirectional antenna - A new approach to stacked beams," in *IRE International Convention Record*, 1960, pp. 48-50.

[233] H. Zarei, A. Ecker, P. Jinho, and D. J. Allstot, "A full-range all-pass variable phase shifter for multiple antenna receivers," in *Circuits and Systems, 2005. ISCAS 2005. IEEE International Symposium on*, 2005, pp. 2100-2103 Vol. 3.

[234] R. A. York and T. Itoh, "Injection- and phase-locking techniques for beam control antenna arrays," *Microwave Theory and Techniques, IEEE Transactions on,* vol. 46, pp. 1920-1929, 1998.

[235] R. Adler, "A study of locking phenomena in oscillators," *Proceedings of the IEEE,* vol. 61, pp. 1380-1385, 1973.

[236] F. M. Gardner, *Phase Lock Techniques*, 3rd ed.: John Wiley and Sons Inc., 2005.

[237] R. N. Ghose, "Electronically Adaptive Antenna Systems," *IEEE Trans. on Antenna and Propagation,* vol. 12, pp. 161 - 169, March 1964 1964.

[238] V. F. Fusco, C. B. Soo, and N. Buchanan, "Constant phase IF self-tracking receiver analysis and characterisation," *Microwaves, Antennas and Propagation, IEE Proceedings -,* vol. 151, pp. 507-513, 2004.

[239] A. H. Al-Ani, A. L. Cullen, and J. R. Forrest, "A Phase-Locking Method for Beam Steering in Active Array Antennas," *Microwave Theory and Techniques, IEEE Transactions on,* vol. 22, pp. 698-703, 1974.

[240] K. Stephan and W. Morgan, Jr., "Analysis of interinjection-locked oscillators for integrated phased arrays," *Antennas and Propagation, IEEE Transactions on,* vol. 35, pp. 771-781, 1987.

[241] K. D. Stephan, "Inter-Injection-Locked Oscillators for Power Combining and Phased Arrays," *Microwave Theory and Techniques, IEEE Transactions on,* vol. 34, pp. 1017-1025, 1986.

[242] R. J. Pogorzelski, P. F. Maccarini, and R. A. York, "A continuum model of the dynamics of coupled oscillator arrays for phase-shifterless beam scanning," *Microwave Theory and Techniques, IEEE Transactions on,* vol. 47, pp. 463-470, 1999.

[243] R. J. Pogorzelski, "A 5-by-5 element coupled oscillator-based phased array," *Antennas and Propagation, IEEE Transactions on,* vol. 53, pp. 1337-1345, 2005.

[244] M. H. Er and B. C. Ng, "A self-steered array system for microwave communications," *Antennas and Propagation, IEEE Transactions on,* vol. 42, pp. 1192-1195, 1994.

[245] C. Gang, L. Wei, and L. Shiming, "Effects of Random Errors on the Sidelobe for a Linear Array," *Journal of Electronics,* vol. 19, Jan. 2002.

[246] E. Meng and A. Cantoni, "Derivative constraints for broad-band element space antenna array processors," *Acoustics, Speech and Signal Processing, IEEE Transactions on,* vol. 31, pp. 1378-1393, 1983.

[247] M. H. Er, "Adaptive antenna array under directional and spatial derivative constraints," *Microwaves, Antennas and Propagation, IEE Proceedings H,* vol. l35, pp. 414-419, 1988.

[248] B. D. Van Veen and K. M. Buckley, "Beamforming: a versatile approach to spatial filtering," *ASSP Magazine, IEEE,* vol. 5, pp. 4-24, 1988.

[249] O. L. Frost, III, "An algorithm for linearly constrained adaptive array processing," *Proceedings of the IEEE,* vol. 60, pp. 926-935, 1972.

[250] S. Applebaum and D. Chapman, "Adaptive arrays with main beam constraints," *Antennas and Propagation, IEEE Transactions on,* vol. 24, pp. 650-662, 1976.

[251] B. Friedlander, "A sensitivity analysis of the MUSIC algorithm," *Acoustics, Speech and Signal Processing, IEEE Transactions on,* vol. 38, pp. 1740-1751, 1990.

[252] A. Paulraj and T. Kailath, "Direction of arrival estimation by eigenstructure methods with unknown sensor gain and phase," in *Acoustics, Speech, and Signal Processing, IEEE International Conference on ICASSP '85.*, 1985, pp. 640-643.

[253] B. Friedlander and A. J. Weiss, "Eigenstructure Methods for Direction Finding and Sensor Gain and Phase Uncertainties," in *ICASSP - 88, International Conference on Acoustics, Speech and Signal Processing*, 1988, pp. 2681 - 2684.

[254] N. Jablon, "Effect of element errors on half-power beamwidth of the Capon adaptive beamformer," *Circuits and Systems, IEEE Transactions on,* vol. 34, pp. 743-752, 1987.

[255] T. Svantesson, "Mutual coupling compensation using subspace fitting," in *Sensor Array and Multichannel Signal Processing Workshop. 2000. Proceedings of the 2000 IEEE*, 2000, pp. 494-498.

[256] N. B. Shelton and B. D. Jeffs, "A robust iterative algorithm for wireless MIMO array auto-calibration," in *Acoustics, Speech, and Signal Processing, 2004.*

Proceedings. (ICASSP '04). IEEE International Conference on, 2004, pp. ii-341-4 vol.2.

[257] T. Brauner, R. Kung, R. Vogt, and W. Bachtold, "5-6 GHz low-noise active antenna array for multi-dimensional channel-sounding," in *Microwave and Optoelectronics Conference, 2003. IMOC 2003. Proceedings of the 2003 SBMO/IEEE MTT-S International*, 2003, pp. 297-301 vol.1.

[258] G. Conti and M. Mongiardo, "Network representation of multiple coupled nonconcentric circular and coaxial apertures," in *Antennas and Propagation Society International Symposium, IEEE, 1997 Digest*, 1997, pp. 464-467 vol.1.

[259] K. R. Dandekar, H. Ling, and G. Xu, "Effect of mutual coupling on direction finding in smart antenna applications," *Electronics Letters,* vol. 36, pp. 1889-1891, 2000.

[260] G. J. Burke, E. K. Miller, and A. J. Poggio, "The Numerical Electromagnetics Code (NEC) - a brief history," in *Antennas and Propagation Society International Symposium, 2004. IEEE*, 2004, pp. 2871-2874 Vol.3.

[261] S. Tao and L. Hao, "Array beamforming in the presence of a mounting tower using genetic algorithms," *Antennas and Propagation, IEEE Transactions on,* vol. 53, pp. 2011-2019, 2005.

[262] S. Yang, I. G. Gosling, S. H. Tan, and M. G. Sorwar, "TLM analysis of the mutual coupling of microstrip patch antenna arrays," *Microwaves, Antennas and Propagation, IEE Proceedings -,* vol. 147, pp. 207-210, 2000.

[263] M. Righi, J. L. Herring, and W. J. R. Hoefer, "Efficient hybrid TLM/mode-matching analysis of packaged components," *Microwave Theory and Techniques, IEEE Transactions on,* vol. 45, pp. 1715-1724, 1997.

[264] M. I. Sobhy, M. W. R. Ng, G. J. Langley, and J. C. Batchelor, "TLM analysis of microstrip patch antenna on ferrite substrate," in *Microwave Symposium Digest, 1999 IEEE MTT-S International*, 1999, pp. 1297-1300 vol.3.

[265] E. Van Lil and A. Van De Capelle, "Transmission line model for mutual coupling between microstrip antennas," *Antennas and Propagation, IEEE Transactions on,* vol. 32, pp. 816-821, 1984.

[266] J. A. Porti, J. A. Morente, H. Magan, and D. P. Ruiz, "RCS of low observable targets with the TLM method," *Antennas and Propagation, IEEE Transactions on,* vol. 46, pp. 741-743, 1998.

[267] W. Zhixiong and L. Ce, "An image reconstruction method using GPR data," *Geoscience and Remote Sensing, IEEE Transactions on,* vol. 37, pp. 327-334, 1999.

[268] P. Hammer, D. Van Bouchaute, D. Verschraeven, and A. Van de Capelle, "A model for calculating the radiation field of microstrip antennas," *Antennas and Propagation, IEEE Transactions on,* vol. 27, pp. 267-270, 1979.

[269] E. Penard and J. P. Daniel, "Mutual coupling between microstrip antennas," *Electronics Letters,* vol. 18, pp. 605-607, 1982.

[270] K. Kyungjung, T. K. Sarkar, and M. S. Palma, "Adaptive processing using a single snapshot for a nonuniformly spaced array in the presence of mutual coupling and near-field scatterers," *Antennas and Propagation, IEEE Transactions on,* vol. 50, pp. 582-590, 2002.

[271] K. Yoon-Won and D. Pozar, "Correction of error in reduced sidelobe synthesis due to mutual coupling," *Antennas and Propagation, IEEE Transactions on,* vol. 33, pp. 1025-1028, 1985.

[272] D. F. Kelley and W. L. Stutzman, "Array antenna pattern modelling methods that include mutual coupling effects," *Antennas and Propagation, IEEE Transactions on,* vol. 41, pp. 1625-1632, 1993.

[273] D. M. Pozar, "The active element pattern," *Antennas and Propagation, IEEE Transactions on,* vol. 42, pp. 1176-1178, 1994.

[274] K. R. Dandekar, L. Hao, and X. Guanghan, "Smart antenna array calibration procedure including amplitude and phase mismatch and mutual coupling effects," in *Personal Wireless Communications, 2000 IEEE International Conference on*, 2000, pp. 293-297.

[275] H. M. Aumann and F. G. Willerth, "Phased array alignment by the iterative sampling method," in *Antennas and Propagation Society International Symposium, 1991. AP-S. Digest*, 1991, pp. 1128-1131 vol.2.

[276] G. Tie, W. Jinyuan, G. Yanchang, and C. Xueli, "Large phased array antenna calibration using mutual coupling method," in *Radar, 2001 CIE International Conference on, Proceedings*, 2001, pp. 223-226.

[277] W. Yan and X. Shanjim, "Mutual coupling calibration of transmitting array," in *Antennas and Propagation Society International Symposium, 2003. IEEE*, 2003, pp. 928-931 vol.3.

[278] H. Gao, X. Zheng, and J. Li, "Estimation of mutual coupling coefficient by simulated annealing algorithm," in *Antennas, Propagation and EM Theory, 2003. Proceedings. 2003 6th International Symposium on*, 2003, pp. 275-278.

[279] L. Min and Y. Luxi, "Blind Calibration and DOA Estimation With Uniform Circular Arrays in the Presence of Mutual Coupling," *Antennas and Wireless Propagation Letters, IEEE,* vol. 5, pp. 315-318, 2006.

[280] Z. Xie and J. Wang, "The ability of blind calibration for the linear array," in *Antennas and Propagation Society International Symposium 2006, IEEE*, 2006, pp. 4565-4568.

[281] G. Feng, Z. Feng, and Z. Shi, "An on-line array calibration method for the DS-CDMA system," in *Antennas, Propagation and EM Theory, 2003. Proceedings. 2003 6th International SYmposium on*, 2003, pp. 307-310.

[282] B. Friedlander and A. J. Weiss, "Direction finding in the presence of mutual coupling," *Antennas and Propagation, IEEE Transactions on,* vol. 39, pp. 273-284, 1991.

[283] E. M. Friel and K. M. Pasala, "Wideband bearing estimation with compensation for mutual coupling effects," in *Antennas and Propagation Society International Symposium, 1994. AP-S. Digest*, 1994, pp. 1556-1559 vol.3.

[284] D. Kitchener, K. Raghavan, and C. G. Parini, "Mutual coupling in a finite planar array of rectangular apertures," *Electronics Letters,* vol. 23, pp. 1169-1170, 1987.

[285] R. Goossens and H. Rogier, "A Hybrid UCA-RARE/Root-MUSIC Approach for 2-D Direction of Arrival Estimation in Uniform Circular Arrays in the Presence of Mutual Coupling," *Antennas and Propagation, IEEE Transactions on,* vol. 55, pp. 841-849, 2007.

[286] A. C. Gately, Jr., D. J. R. Stock, and B. R. S. Cheo, "A network description for antenna problems," *Proceedings of the IEEE,* vol. 56, pp. 1181-1193, 1968.

[287] W. Wasylkiwskyj and W. Kahn, "An explicit relation between mutual coupling and the pattern of an antenna array," in *IRE International Convention Record*, 1966, pp. 167-171.

[288] W. Kahn and H. Kurss, "Minimum-scattering antennas," *Antennas and Propagation, IEEE Transactions on,* vol. 13, pp. 671-675, 1965.

[289] H. A. Abdallah and W. Wasylkiwskyj, "A numerical technique for calculating mutual impedance and element patterns of antenna arrays based on the

characteristics of an isolated element," *Antennas and Propagation, IEEE Transactions on,* vol. 53, pp. 3293-3299, 2005.

[290] H. A. Abdallah and W. Wasylkiwskyj, "Mutual impedance and element patterns of probe-fed patch antenna arrays based on the characteristics of an isolated element," in *Antennas and Propagation Society International Symposium, 2005 IEEE*, 2005, pp. 317-320 vol. 4A.

[291] O. E. Allen and W. Wasylkiwskyj, "Comparison of mutual coupling of blade antennas with predictions based on minimum-scattering antenna theory," *Electromagnetic Compatibility, IEEE Transactions on,* vol. 42, pp. 326-329, 2000.

[292] W. Wasylkiwskyj and W. Kahn, "Scattering properties and mutual coupling of antennas with prescribed radiation pattern," *Antennas and Propagation, IEEE Transactions on,* vol. 18, pp. 741-752, 1970.

[293] K. Sakaguchi, K. Kuroda, J. I. Takada, and K. Araki, "Comprehensive calibration for MIMO system," in *Wireless Personal Multimedia Communications, 2002. The 5th International Symposium on*, 2002, pp. 440-443 vol.2.

[294] R. Mailloux, "First-order solutions for mutual coupling between waveguides which propagate two orthogonal modes," *Antennas and Propagation, IEEE Transactions on,* vol. 17, pp. 740-746, 1969.

[295] P. Hannan, D. Lerner, and G. Knittel, "Impedance matching a phased-array antenna over wide scan angles by connecting circuits," *Antennas and Propagation, IEEE Transactions on,* vol. 13, pp. 28-34, 1965.

[296] B. Lindmark, "Comparison of mutual coupling compensation to dummy columns in adaptive antenna systems," *Antennas and Propagation, IEEE Transactions on,* vol. 53, pp. 1332-1336, 2005.

[297] A. J. Weiss and B. Friedlander, "Array shape calibration using sources in unknown locations-a maximum likelihood approach," *Acoustics, Speech and Signal Processing, IEEE Transactions on,* vol. 37, pp. 1958-1966, 1989.

[298] A. J. Weiss and B. Friedlander, "Array shape calibration using sources in unknown locations-a maximum likelihood approach," in *Acoustics, Speech, and Signal Processing, 1988. ICASSP-88., 1988 International Conference on*, 1988, pp. 2670-2673 vol.5.

[299] B. C. Ng and A. Nehorai, "Optimum active array shape calibration," in *Signals, Systems and Computers, 1991. 1991 Conference Record of the Twenty-Fifth Asilomar Conference on*, 1991, pp. 893-897 vol.2.

[300] A. J. Weiss and B. Friedlander, "Array shape calibration using eigenstructure methods," in *Signals, Systems and Computers, 1989. Twenty-Third Asilomar Conference on*, 1989, pp. 925-929.

[301] Y. Rockah and P. M. Schultheiss, "Array Shape Calibration using Sources in Unknown Locations - Part 1: Far - Field Sources," *IEEE Trans. on Acoustics, Speech and Signal Processing,* vol. 35, pp. 286 - 299, Mar 1 1987.

[302] M. Levi and H. Messer, "Sufficient conditions for array calibration using sources of mixed tapes," in *Acoustics, Speech, and Signal Processing, 1990. ICASSP-90., 1990 International Conference on*, 1990, pp. 2943-2946 vol.5.

[303] Y. Rockah and P. Schultheiss, "Array shape calibration using sources in unknown locations--Part II: Near-field sources and estimator implementation," *Acoustics, Speech and Signal Processing, IEEE Transactions on,* vol. 35, pp. 724-735, 1987.

[304] J. Lo and S. Marple, Jr., "Eigenstructure methods for array sensor localization," in *Acoustics, Speech, and Signal Processing, IEEE International Conference on ICASSP '87.*, 1987, pp. 2260-2263.

[305] N. Owsley, "Joint source and sensor location estimation," in *Acoustics, Speech, and Signal Processing, IEEE International Conference on ICASSP '84.*, 1984, pp. 190-193.

[306] B.-h. Wang, Y.-l. Wang, and H. Chen, "Array shape calibration using carry-on instrumental sensors," in *Radar Conference, 2003. Proceedings of the International*, 2003, pp. 636-639.

[307] V. Varadarajan and J. Krolik, "Sensor array shape estimation using active sonar clutter," in *Sensor Array and Multichannel Signal Processing Workshop Proceedings, 2002*, 2002, pp. 533-537.

[308] V. Varadarajan and J. Krolik, "Array shape estimation tracking using active sonar reverberation," *Aerospace and Electronic Systems, IEEE Transactions on,* vol. 40, pp. 1073-1086, 2004.

[309] Y. Weijun, W. Yuanxun, and T. Itoh, "A self-calibration antenna array system with moving apertures," in *Microwave Symposium Digest, 2003 IEEE MTT-S International*, 2003, pp. 1541-1544 vol.3.

[310] R. J. McGough, D. Cindric, and T. V. Samulski, "Shape calibration of a conformal ultrasound therapy array," *Ultrasonics, Ferroelectrics and Frequency Control, IEEE Transactions on,* vol. 48, pp. 494-505, 2001.

[311] A. Santori, J. Barrere, G. Chabriel, C. Jauffret, and D. Medynski, "Array Shape Self-Calibration for Large Flexible Antenna," in *Aerospace Conference, 2007 IEEE*, 2007, pp. 1-9.

[312] D. M. Pozar, "Characteristics of infinite arrays of subarrayed microstrip antennas," in *Antennas and Propagation Society International Symposium, 1992. AP-S. 1992 Digest. Held in Conjunction with: URSI Radio Science Meeting and Nuclear EMP Meeting., IEEE*, 1992, pp. 159-162 vol.1.

[313] R. B. Waterhouse and N. V. Shuley, "Scan performance of infinite arrays of microstrip patch elements loaded with varactor diodes," *Antennas and Propagation, IEEE Transactions on,* vol. 41, pp. 1273-1280, 1993.

[314] A. Zaghloul and R. MacPhie, "On the removal of blindness in phased antenna arrays by element positioning errors," *Antennas and Propagation, IEEE Transactions on,* vol. 20, pp. 637-641, 1972.

[315] Y. T. Lo and V. D. Agrawal, "A method for removing blindness in phased arrays," *Proceedings of the IEEE,* vol. 56, pp. 1586-1588, 1968.

[316] S. D. Targonski and D. M. Pozar, "Effect of random positioning errors on the input impedance of an infinite array of printed dipoles," in *Antennas and Propagation Society International Symposium, 1993. AP-S. Digest*, 1993, pp. 732-735 vol.2.

[317] Y. Kim and D. L. Jaggard, "The fractal random array," *Proceedings of the IEEE,* vol. 74, pp. 1278-1280, 1986.

[318] W. J. Hendricks, "The totally random versus the bin approach for random arrays," *Antennas and Propagation, IEEE Transactions on,* vol. 39, pp. 1757-1762, 1991.

[319] R. B. Waterhouse, "The use of parasitic elements to remove potential E-plane scan blindnesses in high dielectric substrate microstrip patch probe-fed phased arrays," in *Antennas and Propagation Society International Symposium, 1994. AP-S. Digest*, 1994, pp. 456-459 vol.1.

[320] D. Pozar and D. Schaubert, "Scan blindness in infinite phased arrays of printed dipoles," *Antennas and Propagation, IEEE Transactions on,* vol. 32, pp. 602-610, 1984.

[321] B. R. Mahafza, in *Radar Systems Analysis and Design using Matlab*: Chapman and Hall / CRC, 2000, pp. 350 - 371.

[322] J. K. Hsiao, "Design of error tolerance of a phased array," *Electronics Letters,* vol. 21, pp. 834-836, 1985.

[323] T. S. Cooper, G. Baldwin, and R. Farrell, "Six-port precision directional coupler," *Electronics Letters,* vol. 42, pp. 1232-1233, 2006.

[324] D. M. Pozar, *Microwave Engineering*: John Wiley & Sons, Hoboken, NJ, 1998.

[325] Dr. Francis Mullany, "Personal Comminucation," Alcatel Lucent, Bell Labs Ireland, 2005.